Alois Peter Schaffarczyk   *Editor*

Wind Power Technology

An Introduction

Second Edition

Springer

Green Energy and Technology

Climate change, environmental impact and the limited natural resources urge scientific research and novel technical solutions. The monograph series Green Energy and Technology serves as a publishing platform for scientific and technological approaches to "green"—i.e. environmentally friendly and sustainable—technologies. While a focus lies on energy and power supply, it also covers "green" solutions in industrial engineering and engineering design. Green Energy and Technology addresses researchers, advanced students, technical consultants as well as decision makers in industries and politics. Hence, the level of presentation spans from instructional to highly technical.

Indexed in Scopus.

Indexed in Ei Compendex.

Alois Peter Schaffarczyk

Editor

Wind Power Technology

An Introduction

Second Edition

🐎 Springer

Editor
Alois Peter Schaffarczyk 🔘
Department of Mechanical Engineering
Kiel University of Applied Sciences
Kiel, Germany

The translation of some chapters was done with the help of artificial intelligence (machine translation by the service www.DeepL.com). A subsequent human revision was done primarily in terms of content.

Preface

At the end of 2021 (2020), the installed capacity of wind turbines worldwide was 837 (733) GW. By the 2021 (2020) 98 (93) additionally GW were added. This amounts to 1814 (1590) TWh electricity produced in 2021 (2020).

Despite this uninterrupted growth, it is clear to all that this will contribute only partly to the envisaged decarbonisation World's targets for greenhouse gas reduction in industry by 2050. Further increased growth in the wind energy sector is therefore to be expected.

In the current war Russia is waging against Ukraine demonstrate yet again that a switch to (local) renewables is needed from a perspective of policies and to secure a more sustainable supply of energy.

Authors from the wind community in Schleswig-Holstein (a small state in the most northern part of Germany where most of the more modern German wind energy technology development started), Denmark and the Netherlands have collaborated to compile this introductory textbook on wind energy technology.

This textbook is intended for advanced undergraduate and first-year graduate students. Most of the chapters contain problems with solutions and/or hints how these problems have to be successfully solved.

Over 11 chapters cover all aspects of modern state of this technology. The book begins with a brief history and then supplements this with an explanation of the importance of wind energy in the international energy policy debate. Following chapters introduce the aerodynamic and structural aspects of blade design. Then the focus shifts to the flow of energy and loads through the wind turbine, through the powertrain and also the tower-foundation system, respectively. Next, the electrical components such as the generator and power electronics are discussed, including control systems and automation. Followed by an explanation of how wind turbines

are integrated into the electricity grid, despite the highly fluctuating nature of both this energy source and the grid load; this particular topic is especially relevant for Germany's transition to renewable energy. The final topic covers one of the youngest and most promising aspects of wind energy: offshore technology.

On behalf of the Authors.

Kiel, Germany   Alois Peter Schaffarczyk
June 2022

Acknowledgements

Contents

Editor and Contributors

About the Editor

Prof. Dr. Alois Peter Schaffarczyk has been working on the aerodynamics of wind turbines since 1997. He was a founding member and honorary board member of CEwind eG and teaches in the international Master of Science degree programme in Wind Energy Engineering.

For many years, Prof. Dr. Reiner Johannes Schütt was Head of Development and Technical Manager at of ENERCON NORD Electronic GmbH in Aurich. Today he teaches and researches in the field of Controls/Electrical Drives and Wind Energy Technology at the West Coast University of Applied Sciences in Heide.

Contributors

Jos Beurskens Schagen, The Netherlands

Torsten Faber Wind Energy Technology Institute, HS Flensburg, Flensbrug, Germany

Friedrich Wilhelm Fuchs Christian-Albrechts-University in Kiel, Kiel, Germany

Clemens Jauch Wind Energy Technology Institue, Flensburg University of Applied Sciences, Flensbrug, Germany

Christian Keindorf Kiel University of Applied Sciences, Kiel, Germany

Alexander Krimmer TPI Composites Germany GmbH, Berlin, Germany

Peter Krämer AEROVIDE GmbH, Rendsburg, Germany

Hans Kyling Fraunhofer Institute for Wind Energy Systems IWES, Bremerhaven, Germany

Wiebke Langreder EMD International A/S, Aalborg, Denmark

Klaus Rave Kiel, Germany

Malo Rosemeier Fraunhofer Institute for Wind Energy Systems IWES, Bremerhaven, Germany

Alois Peter Schaffarczyk Kiel University of Applied Sciences, Kiel, Germany

Reiner Schütt Heide, Germany

Sönke Siegfriedsen aerodyn engineering GmbH, Büdelsdorf, Germany

The History of Wind Energy

Jos Beurskens

Abstract Wind has probably been used as an energy source for more than 1500 years. In times when other energy sources were unknown or scarce, wind energy was a very successful energy source for industrial and economic development.

1 Introduction

Wind has probably been used as an energy source for more than 1500 years. In times when other energy sources were unknown or scarce, wind energy was a very successful energy source for industrial and economic development. Wind energy became a marginal source when inexpensive, easily accessible and abundant energy sources became available. From the point of view of wind energy's contribution to economic development, the history of wind energy can be divided into four, partly overlapping, periods. Except for the first period, the focus of the use of the wind is on the generation of electricity (Fig. 1).

600–1890: Classical period Classical windmills for mechanical drives more than 100,000 windmills in northwestern Europe. The period ends after the invention of the steam engine and due to abundant wood and coal resources.
1890–1930: Emergence of electricity-generating wind turbines The development of electricity into a source of energy accessible to everyone leads to the use of windmills as an additional means of generating electricity. Introduction of the theory of aerodynamics in the design of rotor blades. The period ends due to cheaper oil becoming available.

J. Beurskens (✉)
Schagen, The Netherlands
e-mail: hjmbeurskens@gmail.com

Fig. 1 Historical development of the use of wind as an energy The first and last periods have had the most significant impact on society. The years are indicative of the time periods of the respective development periods. *Photo* Jos Beurskens & Collection

> **1930–1960: First innovation phase** The need for electrification of rural areas and the energy shortage during World War II trigger new developments. Aerodynamic tools become much more advanced. The period ends due to cheaper gas and oil.
>
> **since 1973: Second innovation phase with commercialization** The energy crisis and environmental problems in combination with technological progress lead to the commercial breakthrough and the production of electricity in large quantities as well as hydrogen to substitute natural gas and other fossil fuels.

During the classical period, "wind devices" (windmills) converted the kinetic energy of the wind into mechanical energy. After electricity generators such as DC and AC generators were invented and used for public power supply, windmills were used to generate electricity. This development effectively began in the late nineteenth century and became a great economic success after the 1973 energy crisis.

In order to clearly distinguish between the different turbines, they are referred to as windmills or wind turbines in this book.

2 The First Windmills: 600–1890

Water mills are very likely to have paved the way for windmills. Water mills, in turn, evolved from devices driven by humans or animals. The devices known to us from historical sources had a vertical main shaft to which a crossbeam was attached vertically to drive the main shaft. The crossbeam was driven by farm animals such as horses, donkeys or cows. It seems logical that vertical windmills evolved from these devices. However, there are few historical sources to support this. More sources

Fig. 2 Schematic representation of the operation of a Chinese windmill. Solid lines represent blades, and dotted lines represent ropes [2]
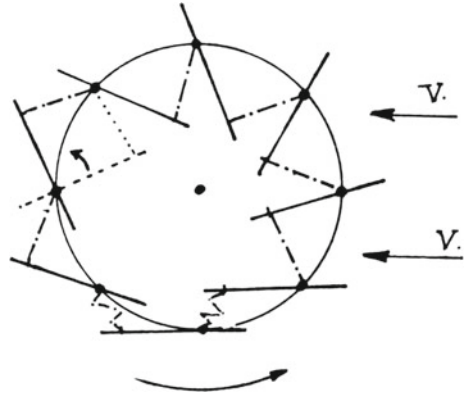
can be found about the "Nordic" or "Greek" water mills that evolved from animal-powered devices. Around 1000 BC, these types of water mills originated in the hills of the eastern Mediterranean and were also used in Sweden and Norway [9].

The first windmills with a vertical main shaft were found in Persia and China. In the middle of the 7-th century AD, the construction of windmills was a highly respected craft in Persia [8]. In China, vertical windmills were introduced by traders. The first European to report windmills in China was Jan Nieuhoff, who travelled to China in 1656 with one of the Dutch ambassadors. Until recently, similar windmills were still in use in China (see Fig. 2).

Another type of device was the treadmill, which was driven by the physical strength of people or animals. Paddles were arranged radially to the main shaft. By replacing the physical strength of men or animals with the strength of flowing water, the horizontal water mill developed from the treadmill. In this way, the so-called Vitruvian water mills, which were introduced by the Roman Vitruvius, were created in the first century BC. This water mill can be seen as the prototype for the undershot water wheel, which can be found all over Europe in rivers and streams with low differences in water level. It is widely believed that the Vitruvian wheel is the precursor of the horizontal windmill [9].

The first horizontal windmills were found during the Crusades in the Near East and later in Northwest Europe. These windmills had a fixed rotor construction that could not be turned into the wind (yaw). The rotor blades of these windmills were similar to those that can still be seen today, for example, on the Greek island of Rhodos. Around 1100, the first fixed trestle windmills, which stood on the city walls of Paris, were reported. It is unclear whether the windmills, which were widely spread, came to Europe via the Near East or were reinvented in Western Europe. Some authors even doubt the existence of horizontal windmills in the Ancient Near East during the Crusades [8, 28]. Others speak only of vertical windmills at that time [16, 17].

The assumption that the windmills of Western Europe were invented independently of those of the Near East is supported by documents found in archives in the Dutch province of Drenthe. In these documents, which date from 1040, the time

before the first crusades, two windmills (Deurzer Diep and Uf-felte) are mentioned. During the Renaissance, a number of vertical windmills were also built in Europe. Particularly famous was the windmill built by Captain Hooper in Margate London [25].

Technical development of the first horizontal windmills

The first windmills had no yaw mechanism and the blades consisted of a frame of longitudinal and transverse rods through which canvas was laced (see Fig. 3). The power output was controlled by winding the cloth either completely or partially by hand (see Fig. 3).

For static reasons, the main shaft was provided with an angle of inclination (dimensions of the mill building, the axial load on the thrust bearing, the possibility of constructing a supporting building or a conical tower for stabilisation).

Before examining the global evolution of windmills into wind turbines used to generate electricity today, the development of the classic windmill in Western Europe is described.

Although in the windy regions of Europe, the wind comes mainly from a certain direction; the wind direction varies so much that a yaw mechanism is useful in order not to lose too much energy when the wind blows sideways.

Fig. 3 "Power control" of a classical windmill. *Photo* Jos Beurskens

This requirement led to the first post windmills (see Fig. 4), which could be cast into the wind. These windmills were used for grinding grain. By means of a strong beam attached to the mill house, the entire house, which stood on a fixed substructure, could be turned until the rotor was perpendicular to the wind. Often the supporting beams of the substructure were covered with wooden planks in such a way that a storage room was created. The millstone and the gear wheels were located in the rotating mill house.

One of the first accounts of this type of windmill, dated 1299, comes from a monastery in Sint Oedenrode, in the Noord Brabant region of the Netherlands. Another attempt to turn the rotor into the wind was to build the windmill on a floating platform. The platform was attached by means of a joint to a pile driven into the bottom of a lake. Presumably due to the lack of stability of this windmill, which was built in 1594, north of Amsterdam, it was not possible to build a windmill on a floating platform and no such mill was ever built again. This concept, which can be considered the world's first offshore wind turbine, was not pursued further.

The so-called wip or hollow post windmill developed from the post windmill (see Fig. 5). After 1400, windmills were used in the flatter regions of the Netherlands not only for grinding grain, but also for draining lakes and swamps. The pumping device, usually a paddle wheel, was attached to a fixed point on the outside of the mill house. Only the transmission elements of the windmill were located inside, which

Fig. 5 Wip windmill from the province of South Holland. *Photo* Jos Beurskens

made the rotating part of the windmill noticeably smaller. With the beginning of the sixteenth century the need for a higher pumping capacity increased, so the post mill was replaced by a mill of which the only yawing part was the hood. Only the bevel gear was located inside the hood, with the result that this part weighed relatively little. When the need for higher power output increased, windmills were mainly built with rotating hoods. The machinery such as mill stones and hammering devices could be housed in the fixed mill house and no longer had to be placed in the moving part (as in the case of the post windmill) or in the open air (as in the case of wip windmills) (Fig. 6). See also

As the number of windmills increased, so did the pressure to operate them more efficiently. Innovations resulting from this motivation were integrated into the mills.

One innovation was the automatic yawing of the windmill rotor into the wind with the help of a wind rose: a rotor whose shaft was mounted perpendicular to the main shaft of the windmills. In England, Edmund Lee attached a wind rose to a windmill in 1745. The wind rose was a wooden structure mounted on the rotating part of the windmill to turn the rotor in the direction of the wind. John Smeaton, also

Fig. 6 The development of the classic "Dutch windmill". *Photos* Jos Beurskens

an Englishman, invented a wind rose that was mounted on the rotating hood of the windmill.

This innovation was so successful because it was used on a large number of windmills, especially in England, Scandinavia, northern Germany and the eastern part of the Netherlands. This concept was maintained into the era of electricity-generating wind turbines of the late nineteenth century and even into the late twentieth century. In the beginning, the transmission was fully mechanical and later the wind rose acted solely as a sensor to send a control signal to the yaw mechanism.

In the first phase of the classical period of windmills, they were mainly used for grinding grain and drainage. Gradually, wind was also used as a source of energy for all kinds of industrial processes. Especially in regions where no other easily manageable energy sources such as wood and coal were available, wind played a major role as a source of energy for industrial, economic development. This was especially the case in "de Zaanstreek" north of Amsterdam and in Kent, England. Windmills were used for sawing wood, producing paper, oil and paint, shelling rice and making mustard and chocolate. They were also used to ventilate buildings (England). The construction of windmills was mainly concentrated in suitable areas. The clustering of windmills, as in the windmill gallery, to drain swamps and lakes can be seen as a precursor to modern wind farms. See Fig. 7 [28].

Fig. 7 Cluster of windmills at Kinderdijk near Rotterdam. *Photo* Jos Beurskens
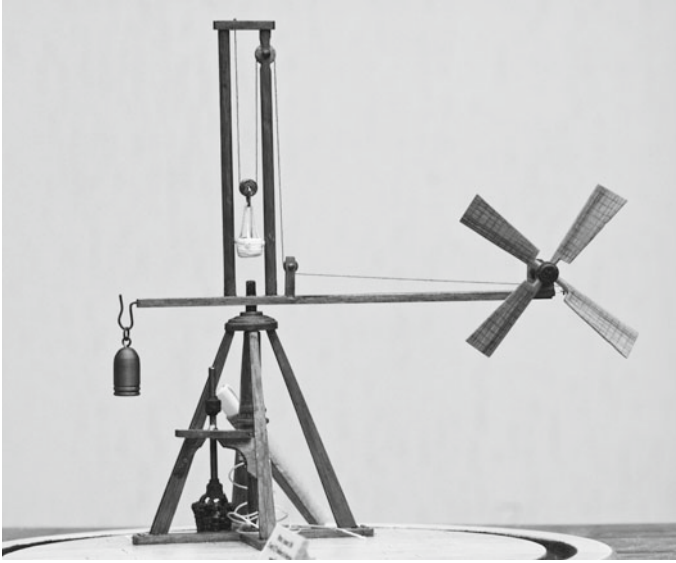
Fig. 8 Model of Smeaton's experimental setup, built by Arie Lamerée. *Photo* Jos Beurskens

Further innovations in the performance and control of the rotor were gradually introduced. The canvas that was looped through the sail beams was replaced by strips of cloth attached to the front of the wing. The negative pressure on the lee side held the cloth in place, giving it an aerodynamed profile. The power output was controlled by partially covering the wooden frame of the sail. To reduce maintenance, the wooden rods and frame were replaced with iron and steel components.

The path to a significant increase in aerodynamic efficiency is based on scientific research from the middle of the eighteenth century. Probably the most fascinating work was done by John Smeaton (1724–1792) and can be considered a precursor of modern research. Figure 8 is a model of Smeaton's experimental set-up. By pulling the rope, the vertical shaft begins to rotate, as does the arm to the end of which is attached to the model of a windmill rotor. The rotor is blown with a wind speed equal to the wing tip speed of the arm. During rotation, the rotor lifts a weight. By changing the rotor characteristics, the optimum "effective force" ("power" in modern physics) can be determined. Smeaton presented the results of his experiment "on the construction and action of windmill blades" in a classic treatise presented to the Royal Society in 1759. The "effective force" was equal to the product of the weight and the number of revolutions performed by the rotor in a given period of time, with friction losses on the apparatus to be compensated for.

Smeaton determined the best shape and "weather" of the blades. In classical windmill engineering, "weather" refers to the angle between the blade section and the plane of rotation. Today, "weather" refers to the twist of the rotor blades. Later, Maclaurin investigated the locally prevailing angle of attack using a distance function describing the angle between the cross section of the turbine and the axes of the rotor.

It is interesting to compare Smeaton's work with today's research, so his conclusions or "maxims" are reproduced verbatim in the following section [8]. His conclusions from the experiments:

Maxim 1: The velocity of mill blades, with the same shape and position, is nearly that of the wind. It is immaterial whether they are unloaded or loaded so as to produce a maximum.

Maxim 2: The maximum load is close to, but slightly less than, the wind speed squared, provided the shape and position of the wings are the same.

Maxim 3: The power of the same blades at maximum power output is close to but slightly less than the wind speed to the power of three (Fig. 8).

His conclusions from his theoretical considerations:

Maxim 6: For wings of similar shape and position, the number of rotations in a given period of time is antiproportional to the radius or length of the wings.

Maxim 7: The maximum load that wings of similar shape and position can withstand at a given distance from the pivot point has the value of the radius to the power of three.

Maxim 8: The effect of wings of similar shape and position has the value of the radius squared.

In addition to the automatic wind direction tracking yaw and the improved configuration of the blades, the efficiency of the windmills was improved by further innovations. For example, in 1772, Andrew Meikle was granted a patent for lamellas in the rotor blades to automatically regulate the power output. In 1787, Thomas Mead introduced the automatic regulation of these rotor blades by means of a centrifugal governor.

With the invention of the steam engine (Watt) came the possibility of being able to generate electricity at will. The supply of energy could be perfectly adapted to the demand for electricity. In addition, fuels such as coal and wood were relatively inexpensive. This had a devastating effect on the use of windmills. During the nineteenth century, the total number of windmills in northwestern Europe decreased from the initial number of 100,000 of windmills to 2000.

Thanks to the active conservation policy of the Verening de Hollandsche Molen (Dutch Windmill Association), 1,000 of the almost 10,000 windmills in the Netherlands have been preserved. These classic Dutch windmills are still operational.

3   Electricity Generation by Windmills: Wind Turbines 1890–1930

When the first electric dynamos and alternators were put into operation (see box "Dynamo", below), all kinds of energy sources were used to drive the generators. Generators were powered by treadmills, wood- or coal-fired steam engines,

water wheels, water turbines and wind rotors. In 1876, for example, Charles Brush's improved DC generator was powered by a treadmill, which in turn was driven by horses.

With the invention of the dynamo, it became possible to supply commercial consumers and individual households with energy from a distance by means of electricity. Electricity could be easily transported from a central generator to consumers. After the introduction of the first central electric plant, the demand for primary energy increased very quickly.

The development of electricity-generating windmills (hereafter called wind turbines) was not an independent process, but overlapped with the emergence of the first electric power plants and the first local electricity grids. The first person to use a windmill to generate electricity was James Blyth, a professor at Anderson College in Glasgow. He used his ten-metre-high vertical Finds turbine, built in 1887, to charge accumulators that supplied his holiday home with electric light.

In 1888, Charles Brush, the owner of a mechanical engineering company, constructed a 12 kW wind turbine with a diameter of 17 m at his home in Cleveland, Ohio (USA). Compared to its rated power, the turbine had a very large diameter. The rotor area was completely covered by the 144 narrow rotor blades, which is why the speed was low. This resulted in a very large transmission ratio from the rotor shaft to the generator. The power output was automatically controlled by a so-called "ecliptic regulator". The rotor was turned out of the wind to the increasing wind by a wind vane, which was positioned perpendicular to the main vane wheel, while the main vane wheel was attached to an oblique joint. This picture from *Scientific American*, 20 December 1890, shows many of the features of the turbine.

"Dynamo" was the original name for the direct current generator. It is contrasted with the alternator, which generates alternating current via a slip ring or a rotor magnet. The first operational public electric power station was built in New York in 1880. It consisted mainly of dynamos and operated arc lamps on a 2-mile circuit. There was a fierce competition between the proponents of the direct current systems under the leadership of the American inventor Thomas Alva Edison and the proponents of alternating current systems under the leadership of the American industrialist George Westinghouse. The direct current had the advantage that the electricity could be stored in electrochemical batteries. In contrast, the great advantage of alternating current was that the voltage could be easily converted to a higher voltage level to reduce transmission losses and then brought back to a lower voltage level at the electrical consumer. In the end, the AC systems won the competition.

Wind turbines were also used to generate electricity on board ships. The turbines were set up on deck and drove a dynamo via belt transmission. The electricity was then used to charge batteries on board. The rotors had wings covered with sailcloth.
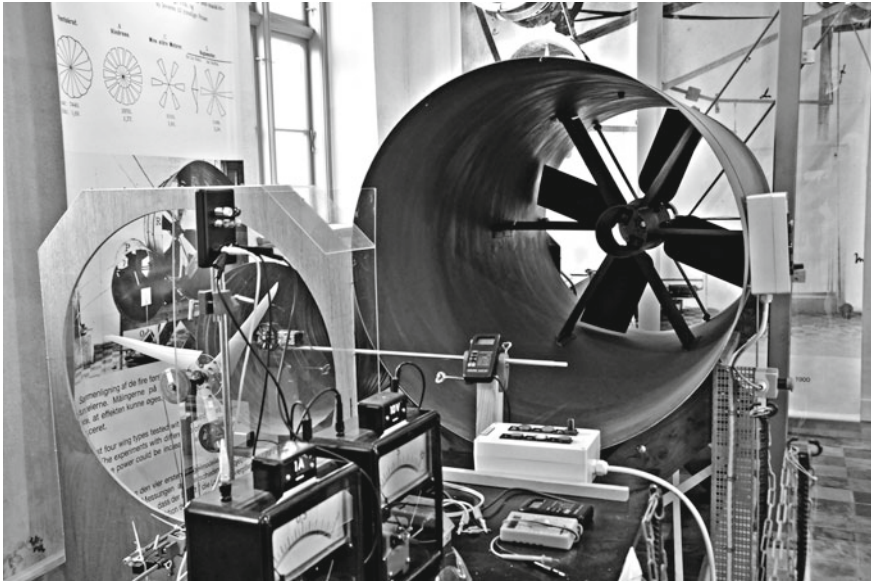
Fig. 9 Replica of the wind tunnel of Poul la Cours in Askov. *Photo* Jos Beurskens

Two examples of this are the *Fram*, the ship in which Fridtj of Nansen sailed to the Antarctic in 1888, and the *Chance* from New Zealand.

In 1891, Professor Poul la Cour constructed his first wind turbine in Askov, Denmark, to generate electricity that he used for various applications. He connected his wind turbine, which had four remote-controlled louvre blades, to two 9 kW dynamos. The electricity generated was used to charge batteries for Askov Folk High School and to produce hydrogen by electrolysis of water, which was used to power gas lamps. La Cour's designs were based on wind tunnel measurements at his school (see Fig. 9).

The louvre blades used by Poul la Cour were invented and applied in 1772 by Andrew Meikle in Great Britain. Meikle replaced the canvas with rectangular slats.

The slats opened automatically in gusts of wind against the force of steel springs. This was the first possibility of automatic regulation, which made the miller's job much more comfortable. However, the tension of the springs still had to be adjusted by hand. To do this, the windmill had to be stopped completely.

Later, the blades were controlled either automatically or manually by a rod running through the hollow main shaft of the mill. This allowed the mill to be controlled without having to stop it frequently. The system was patented by William Cubitt in 1807. The blades were controlled by a spider-like construction, which can still be found today in classical windmills, e.g. in Northern Germany, England and Scandinavia (see Fig. 10).

Although the blades of la Cours wind turbine had some innovations, the aerodynamic design was based on the classical windmills. Nevertheless, his rotor design

Fig. 10 Louvre blades of the *mill on the Wall in* the centre of Bremen. Photo Jos Beurskens

had an efficiency about three times too high as the previous ones. It took about two decades before efficient aerodynamic profiles developed from aviation were applied to wind turbines.

Based on the experiments that la Cour conducted in Askov, he made recommendations for practical implementation, from which the Danish manufacturers Lykkegaard and Ferritslev (Fyn), among others, developed commercial wind turbines. By 1908, Lykkegaard had built 72 wind turbines, and by 1928 the number had increased to about 120. The maximum diameter of the La Cour Lykkegaard wind turbines was 20 m. They were also equipped with 10–35 kW generators. The turbines generated direct current, which was transmitted to small direct current grids and batteries. As the price of fuel had risen dramatically, the development of wind technology in Denmark continued during the First World War.

Between the two world wars, attempts were made in the Netherlands to improve the performance of classical windmills. At the TU Delft, the helicopter pioneer Professor A. G. von Baumhauer and A. Havinga carried out measurements on 4-blade rotors of classical windmills [26]. However, the masonry of the classical windmills, which was supposed to support the improved rotors, would not have withstood the axial forces, as these also increased with the higher efficiency of the rotors. Further experiments were carried out in the 1950s and 1960s, but all failed due to lack of structural integrity of the windmill building or economic reasons (Prinsenmolen; de Traanroeier, Oudeschild, Texel).

In 1920 Albert Betz, head of the Göttingen Aerodynamic Research Institute, published in 1920, at the same time as Zhukowsky after Lanchester in 1916, a mathematical analysis of the theoretical maximum value of the power coefficient of a wind turbine rotor (this is usually called the Lanchester-Betz coefficient and equals $16/27 = 59,3$ %). It was based on the axial flow model. Betz also described wind turbines blades with improved aerodynamic efficiency.

The system had airbrakes on the low-pressure sides of the wings. Immediately after World War I, it was Kurt Bilau who wanted to further improve the efficiency of his 4-blade Ventimotor by giving the aeroprofile of the blades a streamlined shape. He even claimed a higher efficiency than Betz power coefficient. Bilau also built test facilities in East Prussia and in southern England.

After the First World War, the supply of fossil fuels increased considerably, which is why interest in wind energy declined. In the western industrial world, the further development of wind energy was continued on a very small scalet until the Second World War. However, this was not the case in the Soviet Union, where a large programme of electrification of remote areas was carried out under Stalin's regime. The little information available from this period shows that Soviet engineers took advantage of the latest developments in aerodynamics for their designs.

The rotor blades, designed by the Central Aerohydrodynamic Institute (TsAGi), can be pitched with a small auxiliary blade on the trailing edge of the main blade. In 1931, an experimental wind turbine was built near Sevastopol in the Crimea, operating in parallel with a peat-fired 20 MW electric power plant. The WIME D-30 turbine had a rotor diameter of 30 m and a rated power of 100 kW. It was in operation until 1942. Somewhat earlier, in 1923, a two-blade turbine with the same aerodynamic control system was tested at TsAGI (Tsentral'nyy Aerogidrodinamicheskiy Insitut) in Zhukovskiy, south-east of Moscow, see Fig. 11. This concept was relatively advanced for its time.

4   The First Innovation Period: 1930–1960

During and immediately after World War 2, various countries resumed the development of wind turbines. The reason for this was that strategic resources such as fossil fuels had become scarce. During this period, many innovations were introduced which probably enabled the widespread introduction of wind turbines for power generation in parallel with the power grid. The innovations, especially in the design of the rotor, mainly built on the innovations from the previous era (Fig. 12).

The most important developments took place in Denmark, the USA and Germany. During World War II, the company F. L. Smidth from Copenhagen developed wind turbines to generate electricity. As Denmark had no fossil fuels of its own, wind energy was one of the few ways to generate electricity. The Smidth turbines had 2-blade rotors, whereby the blades had a fixed angle of attack, were not adjustable and were stall-controlled. With these rotor blades, the power coefficient was relatively low, but the power curve was relatively wide. This meant that the efficiency of the

Fig. 11 TsAGI's experimental wind turbine at Zhukovskiy, near Moscow, 1923. Translation of text in Cyrillic script: Two-blade windmill-engine system (= wind turbine). TsAGi D = 6 m. At the 1923 agricultural fair in Moscow. Photo Jos Beurskens Collection

whole system, spread over a wide range of wind speeds, was relatively high. The Smidth aeromotors had a rotor diameter of 17.5 m (rated power was 50 kW) and were built on either steel lattice or concrete towers. After problems with the dynamic characteristics of the 2-blade rotors, Smidth introduced a larger turbine with a rotor diameter of 24 m (rated power 70 kW). A total of seven of these turbines were built. With one exception, they were all equipped with DC generators (see Fig. 13).

This type of turbine became the blueprint for the start of developments in modern wind energy after the first energy crisis in 1973. It was J. Juul who used Smidth's 3-blade design to build a 200 kW version with a diameter of 24 m in Gedser in 1957 (see Fig. 17). The machine had an asynchronous induction generator and was connected directly to the grid. It had three rotor blades, was stall controlled and had movable blade tips to prevent overspeeding when load was lost. The Gedser wind turbine became the archetype of the "Danish wind turbine", a generation of very successful wind turbines after the 1973 energy crisis.

After the publications of Betz in 1920 and 1925, Hermann Honnef designed a very large structure with several rotors based on the analytical results of Betz and others. This was possibly the first design based entirely on scientific findings. His

Ветроэлектрическая станция с ассинхронным генератором 100 кв.
Диаметр крыльев Д = 30 м. Высота башни 25 мм. Устанавливается
близ Севастополя в Крыму.
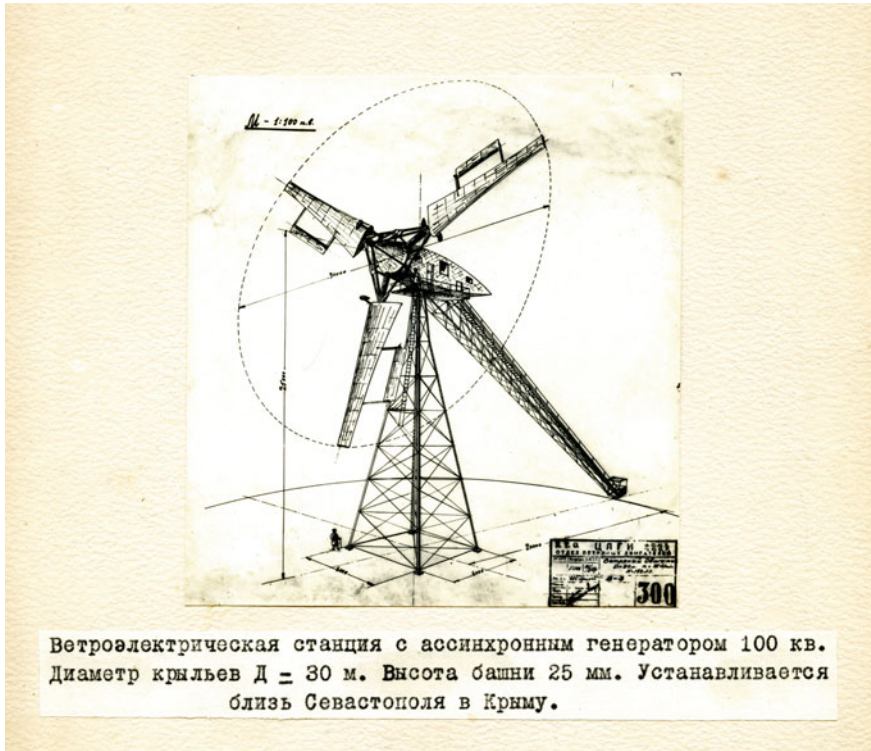
Fig. 12 100 kW wind turbine with rotor diameter of 30 m near Sevastopol, Crimea. Translation of the text in Cyrillic script: Wind turbine with asynchronous generator of power 100 kW. Diameter of the blades: D = 30 m. Tower height: 25 m. Located near Sevastopol, Crimea, USSR. Photo Jos Beurskens Collection

concept had 5 rotors, each with a diameter of 160 m and 6 blades. Each rotor was to power a 20 MW generator. The rotors consisted of two counter-rotating wheels. On 80% of the rotor diameter, a ring type generator was mounted. The ring-type generator were low speed direct drive generators which could be driven without a gearbox. The concept went far beyond what was technically feasible at the time. This becomes clear when one realises that only in 2012 turbines of similar size are being designed and built (see also Fig. 24).

With the support of the Kuratorium für Wind- und Wasserkraft (Board of Trustees for Wind and Water Power), which was founded in 1941 to support inventors in their search for energy sources, Honnef built a model of the multi-rotor wind turbine of two rotors on a test field on the Mathiasberg, northwest of Berlin. After the war the test field was destroyed by the Soviets and the equipment was melted in the blast furnace of Hennigsdorf.

With the collapse of the Third Reich, Honnef had to end its work in the field of wind energy in March 1945. The striving for independence in energy supply led to

Fig. 13 A decommissioned *Smidth aeromotor* in Denmark. Rotor diameter 24 m, rated power approx. 70 kW. The picture dates from 1972. Photographer Paul Smulders

the foundation of the Reichsarbeitsgemeinschaft Windkraft (RAW) in 1939, in which scientists, inventors and industry worked together. One project supported by the RAW was the 3-blade and 4-blade wind turbine planned by Franz Kleinhenz, which had a rotor diameter of 130 m and a rated output of 10 MW and was constructed in cooperation with the MAN company. However, the war prevented the construction planned for 1942. From the end of the war until the resumption of research and development on wind energy during the oil crisis in 1973 and beyond, Professor Ulrich Hütter was always a constant in Germany and managed a test facility of the company Ventimotor GmbH in Webicht, Weimar. There he gained a lot of practical experience in the design of small wind turbines. Hütter received his doctorate from the University of Vienna in December 1942 with a dissertation entitled *Beitrag zur Schaffung von Gestaltungsgrundlagen für Windkraft-werke (Contribution to the realisation of design conditions for wind energy systems)*. During his career, he worked alternately

in aircraft technology and wind energy technology. In 1947, Hütter built the first wind turbine after the end of the war.

In 1948, Erwin Allgaier wanted to build his wind turbine in series (3 rotor blades, 8 m rotor diameter, 13 kW rated power). Slightly larger turbines (11.28 m rotor diameter, 7.2 kW rated power) were exported to South Africa, Ethiopia and Argentina. The wind turbines were very light due to a relatively high tip speed ratio of 8. The installed power per unit swept rotor area was also very low, so that the wind turbine was suitable for low wind regimes and at the same time provided relatively high equivalent full load hours (capacity factor) (see Fig. 14).

In order to supply electricity to remote areas, the brothers Marcellus and Joseph Jacobs began to develop wind turbines for charging batteries in the USA in the early 1920s. After experimenting with 2-blade turbines, they introduced a 3-blade wind turbine with a rotor diameter of 4 m and a direct-drive DC generator one. Several thousand of these units were sold between the early 1920s and the first years after the 1973 oil crisis (see Fig. 15).

With the expansion of the power grid, rural power supply was no longer a major problem, and ever larger turbines were connected to power the grid. During the World War II, wind turbines appeared to be a potentially strategic technology for harnessing indigenous energy sources that could be used during times of crisis.

Fig. 14 Allgaier wind turbine WE 10 at the University of Stuttgart. *Photo* Jos Beurskens

Fig. 15 Wind farm with Jacobs wind turbines, Big Island Hawaii, 1988. *Photo* Jos Beurskens

The first megawatt turbine ever built was the Smith-Putnam wind turbine designed by Palmer C. Putnam and built by the S. Morgan Smith Company (York, Pennsylvania), which was erected on Grandpa's Knob, a 610 m hill near Rutland, Vermont [23]. This turbine had an downwind rotor with a diameter of 53.3 m. It was equipped with individually adjustable rotor blades. The rated power of the synchronous generator was 1.25 MW. The power output was controlled by means of hydraulically adjusting the blade angles. The rotor had no blade twist and had blades of constant cord. The plant operated from 1941 to 1945, feeding electricity into the Central Vermont Public Service Company grid during its 1000 h of operation. After losing a rotor blade on 26 March 1945, the plant was taken out of service due to lack of funds to repair the rotor [19]. It was not until the oil crisis of 1973 that Putnam's experience was used to build a whole series of large wind turbines in the USA.

Among the reasons that wind energy developments continued after World War II were [12]:

- the rapidly increasing demand for electricity, while in most places there was no local source of energy,
- post-war poverty and political conditions which forced countries to search for domestic energy sources instead of relying on imported fuels.

The knowledge of aerodynamics and materials provided by engineers employed in the military industry during the war and now in civilian industry favoured the conditions for continuing wind power development. The new technologies opened up the prospect of building more successful MW rated turbines than the one on Grandpa's Knob.

Later, in the 1950s, critical scientists and politicians realised that coal and oil should not be burned for the purpose of generating electricity, but were better suited as materials. Another fact caused concern: the notion of being dependent on only one source of energy (oil), which had to be imported from politically unstable regions. These concerns became the first signs of a political debate around de-democracy, limits to growth and consumption, diversity and environmental constraints on industrial development that began in the 1960s and culminated in the 1972 publication of the Club of Rome's study *The Limits to Growth* [14]. From the 1950s until the outbreak of the first energy crisis in 1973, not only Denmark, the USA and Germany contributed to further developments in wind energy, but also countries such as France and the UK. Surprisingly, the Netherlands, known as the land of windmills, did not participate in the development of modern wind energy, but tried to use classical windmills for electricity generation.

In 1950, the John Brown Company built a 3-blade turbine with a rated power of 100 kW and a rotor diameter of 15 m on the Scottish Orkney Islands for the North of Scotland Hydroelectric Board, which was operated in parallel to a diesel generator [8]. The rotor blades were attached to a hub using hinges. However, the complex rotor failed after a few months.

At the same time, the French engineer Andreau constructed a 2-blade turbine with a very unusual transmission system. The rotor blades were hollow and had openings at the tips. The rotor acted like a centrifugal pump, drawing air through the openings in the base of the tower, passing through an air turbine mounted at the base of the tower and drove a generator. This provided a smooth transmission which was an alternative to the stiff drive trains based on mechanically connected synchronous and induction generators. In 1951, De Havilland Propellers built a prototype unit for Enfield Cables Ltd. in St. Albans (Hertfordshire).

As it was impossible to operate the turbine economically due to the low wind speeds of the site and a low transmission efficiency of 20%, it was dismantled in 1957 and rebuilt in Grand Vent, Algeria, but after a short run it was taken out of service again. The concept seemed outlandish but it was not unique. As early as 1946, Ulrich Hütter presented a hollow 1-blade unit that was to function as a centrifugal pump. As a counterweight, the air turbine and generator were attached to the opposite side of the rotor blade (see Fig. 16). R. Bauer designed a 1-blade turbine with a rotor diameter of 3 m, which was operated by Winkelstraeter GmbH in 1952.

Besides Andreau, several other French engineers were involved in the design of wind turbines. In 1958, L. Romani built an 800 kW 3-blade test turbine with a rotor diameter of 30.1 m for the utility EDF (Electricité de France) in Nogent-le-Roi near Paris. The so-called Best-Romani turbine was equipped with a synchronous generator and was decommissioned in 1963 after the failure of a rotor blade.

In the same period of time, Louis Vadot designed two wind turbines with similar equipment to the Best-Romani turbine and built them for Neyrpic in Saint-Rémy-de-Landes (Manche). One of the turbines measured 21.1 m rotor diameter (132 kW), the other 35 m diameter (1000 kW); both had an induction generator. As EDF lost its interest in wind power, the turbines were decommissioned in 1964 and 1966 respectively.

Fig. 16 Hütter concept of
the single-blade rotor with
aerodynamic power
transmission. The blade
length is 6 m. Drawing Jos
Beurskens
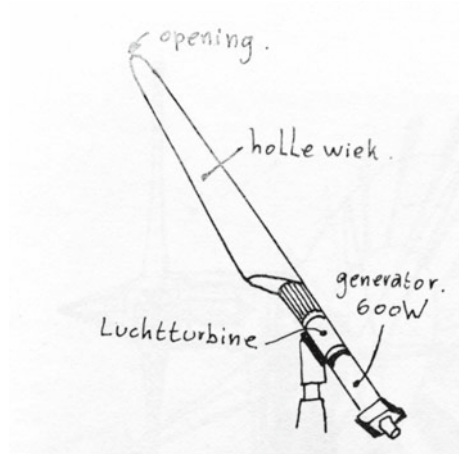
At the same time the technical developments were taking place, the research-based industrial communities of various countries were being called upon by international organisations to present results at international conferences. These institutions included UNESCO, the Organisation for European Economic Cooperation (OEEC) and the World Meteorological Organisation (WMO). The actions of these organisations (see [21, 22, 29]) provided an excellent overview of the progress of wind power technology from the end of the war to the beginning of the oil crisis. Interestingly, the use of wind power expanded from industrialised areas back to remote, arid areas and developing countries. The global potential of wind power was increasingly discussed alongside advances in theory and technology. These international conferences were the first modest steps towards the extensive international networks in the field of wind power that exist today.

From today's perspective, it is amazing how many modern inventions were made and tested in the period from 1930 to 1960. The developments were based less on analytical methods than on experiments. Not all experiments were successful; many technical mistakes were made. There were no funds available for repairs or the continuation of wind power technology development. Most of the experimental projects which were carried out in France, Great Britain, Germany, the USA and Denmark were stopped and the equipment was destroyed, with the exception of the wind turbine in Gedser, Denmark. Why this plant was so successful will be clarified in the following paragraph. One reason for stopping the further development of wind power was the fact that fossil fuels became cheap and nuclear power more and more popular. This optimistic scenario came to a sudden end with the publication of the study *The Limits to Growth* [14] and the outbreak of the oil crisis in 1973.

The table below gives a brief overview of the modern concepts that were developed during this period. The overview also includes an indicator of the success of the inventions.

5 The Second Innovation Period and Full Commercialisation: From 1960 Until Today

Almost all major technological developments in wind power were terminated by the mid-1960s. Fossil fuels were abundant and very cheap, and nuclear power was seen as the solution to all future energy problems. While there was little discussion among policymakers about both security of supply and environmental and safety concerns, societal concerns arose about limitless economic growth, its impact on developing countries and long term availability of fossil energy resources. The publication of the study *The Limits to Growth in* 1971/1972 on behalf of the Club of Rome [14], the subsequent discussions and the outbreak of the oil crisis in 1973 as a result of another Middle East conflict turned the assumed future problems into current, present problems.

The policy responses to the crisis resulted in a new energy policy, based on the following key issues.

- The dependency on energy monopolies (oil) should be limited by diversifying energy supply alternatives, including the use of domestic energy sources with a simultaneous increase in energy efficiency.
- Fossil energy sources should be reserved for the production of materials and should not be burned for energy faster than their regeneration rate.

About a decade later, environmental concerns (fossil fuels, nuclear waste) and safety concerns (nuclear energy; Three Miles Island, Chernobyl) became part of the political debate. As part of the new energy policy, many countries turned to renewable energy sources. These include solar energy and other energy sources such as wind energy, biomass and the extraction of energy from ocean heat. Research was also carried out into other sources such as geothermal and tidal energy. The first national research programmes were launched as early as 1973 and wind power played an important role in many of them. There were many similarities in the programmes: resource, siting, technological options, need for research and development, potential influences on the national energy balance, (macro) economic and social impacts and implementation strategies. However, the specific approaches and projects differed considerably from country to country. In retrospect, it can be said that where a balance was struck—in terms of time and financial sources—between technical developments, market development (both on the demand and supply side) and government policy (subsidies, regulations, infrastructure), the most successful projects were realised. However, this was not foreseeable in the mid-1970s. Some countries started to develop wind turbines from scratch and carried out analyses without paying attention to the market and infrastructure. Examples include the UK, the Netherlands, Germany, Sweden, the USA and Canada. Without exception, they all relied on large wind turbines as the basis for long-term energy scenarios.

However, based on past experience, this was not particularly surprising. Although not all of them were successful, the experiments and analyses of Hütter, Kleinhenz, Palmer Cosslett Putnam, Juul, Vadot, Honnef, Golding and others all pointed in

the same direction: the introduction of wind energy on a larger scale would only be economically feasible if very large wind turbines with an output of several megawatts each were used. The construction of such large plants was not only considered to be technically feasible, but also economically on the medium term. This becomes clear, among other things, from the session reports of the American Congress from 1971, which contain a reference to a corresponding study from 1964 [4]. A government-sponsored research group headed by Ali B. Cambel in the same year came to the following conclusions:

> "Sufficient knowledge is available to build a prototype with a capacity of 5,000–10,000 kW, which would allow a realistic assessment of wind energy utilisation. A design study of the turbines and a meteorological study of the possible sites would have to precede the actual construction. Such a programme would provide important information on the economic viability of wind turbines and their integration into the electricity grid [...] Even in the long term, wind energy is a reliable source of energy [...] It is inexhaustible and has no negative impact on the environment, as it does not produce any harmful or undesirable by-products."

Due to this, the multi-megawatt wind turbine was the technical basis of all state-supported developments. The only country that did not follow this general trend of focusing on large wind turbines was Denmark. There, risky technical experiments were avoided from the beginning, the market introduction was boosted and the policy supported the introduction of institutional framework conditions.

Independently of government-sponsored programmes, pioneering companies began developing and selling small wind turbines to supply water, charge batteries, and connect to the power grid. Many of these companies were inspired by E. F. Schuhmacher's "Small is Beautiful" vision from 1973. In the early 1980s, there were about 30 companies active in the market in Denmark alone, and about 20 in the Netherlands.

Non-governmental organisations (NGOs) also participated with the aim of using the wind to supply water to households, irrigate fields and water livestock in developing countries. Using their own source of energy to meet their main needs was important for further developments and required little outside capital. These organisations often had links with universities. Examples include the SWD/CWD in the Netherlands, ITDG in the UK, BRACE Institute in Canada, Folkecenter in Denmark, IPAT in Berlin, and several associations in different countries as well as the USA that were linked to universities.

The following section will take a closer look at the various technical developments. Since the developments that took place after the oil crisis were so far-reaching and diverse, it is not possible to describe them in as much detail as the developments in the earlier historical periods. The following description is limited to the general trends and presents the most important cases.

First, government-sponsored wind power developments are described. The best source for historical details is the IEA (International Energy Agency) Wind Energy Programme reports, issued annually since 1985. National projects often contributed to the IEA programme. Almost simultaneously with the government-sponsored development of large-scale wind turbines, small pioneering companies developed small-scale wind turbines. The consistent expansion and scaling up of these wind turbines formed the foundation of today's market (2023). In the following, more recent developments such as wind farms, offshore farms and the connection to the power grid will be discussed.

The state-subsidised development of large wind turbines

The first experiments were carried out in Denmark and formed a joint project between Denmark and the USA. As mentioned above, the wind turbine in Gedser was decommissioned in 1966, but not demolished. The first step towards a revival of wind energy development was the recommissioning of the Gedser wind turbine in 1977 (see Fig. 17).

The results of the joint Danish-American measurements and tests served as a starting point for both the research and development of NASA's wind energy research programme and Danish research and business activities. Ulrich Hütter's design philosophy was also an important part of the American development and research programme. In addition to Denmark and the USA, significant research and development programmes were also initiated in the Netherlands, Germany, Sweden, Great Britain, Canada and later in Italy and Spain during the late 1970s.

Smaller programmes, or rather projects, also existed in Austria, Ireland, Japan, New Zealand and Norway. The first group of countries took on the development of large wind turbines. The two main questions in the design of the first large test plants were the following:

Fig. 17 Gedser wind turbine in the early 1990s. *Photo* Jos Beurskens

- What is the potential of vertical axis wind turbines (Darrieus rotor) compared to horizontal axis wind turbines?
- Which strategy should be followed to develop low-cost wind turbines in the medium term?

Should we first go in the direction of light, high-speed turbines with corresponding rotor concepts, which is very risky but also holds a lot of potential? Or should we put reliability first and gradually improve the proven-and-tested designs from before 1960?

The USA, the Netherlands, the UK and Germany carried out a systematic analysis of the potential of horizontal axis plants compared to vertical axis plants. Canada focused on vertical axis turbines from the beginning, and Denmark was the only country to follow the second strategy. The first large wind turbines were commissioned in 1979 (Nibe 1 and 2 in Denmark) and the last purely experimental, non-economically operated wind turbine was completed in 1993. In total, about 30 experimental-only plants have been built in the various countries and have received strong government support.

Tables 1 and 2 provide an overview of a selection of these wind turbines. The commercial prototypes are also included. Figures 18, 19, 20, 21, 22 and 23 show some of these wind turbines, whose technical designs were very diverse. Many innovations of the past (Table 3) were redesigned and used. Significant upscaling (see Fig. 24) and technical improvements were achieved by incorporating glass fibre-reinforced plastics into the rotor structure and using new electrical conversion systems.

A notable exception to the state-sponsored developments is the Tvind wind turbine. Between 1974 and 1978, students and teachers at Tvind Højskole developed a wind turbine with a diameter of 54 m and a rated power of 900 kW. A large number of advanced features were introduced, such as variable speed electricity conversion system (implemented only later) and a (manually operated) pitch system. Although many modifications were made, this turbine is still in operation today (2016) (see Fig. 18).

The finite element method (FEM), although not as advanced as it is today, was used to improve the design of the sensitive components of the wind turbine, especially the structure of the hub. The basis for comprehensive design methods was highly incomplete. In aerodynamics, there were no or only inaccurate simulations of stalled flow, three-dimensional effects, aeroelastic modelling, etc. The same applied to characterization of the wind supply. The same was true for wind descriptions in the rotor plane, the effects of turbulence on performance and mechanical loading, and modelling and flow wake interactions.

Wind turbine concepts included:

- Rotors with 1–3 rotor blades for wind turbines with horizontal axis and 2 or 3 rotor blades for turbines with vertical axis,
- rigid hubs, pendulum hubs and movable hubs,
- rigid rotor, stall control and complete or partial control of the blade pitch angle,
- (nearly) constant and variable speed transmission systems.

Table 1 Selection of state-funded experimental plants

Wind turbine (country)	Rotor diameter (m)	Rated power (MW)	Year of commissioning	Commercial successor
Nibe 1 (Nibe, DK)	40	0,63	1979	No
Nibe 2 (Nibe, DK)	40	0,63	1979	No
25 m HAT (Petten, NL)	25	0,4	1981	No
5 × MOD-0 (Sandusky, Ohio; Clayton, New Mexico, Culebra, Puerto Rico Block Island, Rhode Island; Kuhuku Point, Oahu-Hawaii; USA)	38,1	0,1–0,2	Since 1975	No
WTS-75 (Näsudden, S)	38,1	0,1–0,2	Since 1975	No
WTS-3 (Marglarp, S)	75	2	1983	No
WTS-4 (Medicine Bow, Wyoming, USA)	78	3	1982	No
MOD-1 (Boone, North Carolina, USA)	61	1	1979	No
5 × MOD-2 (3 in Goodnoe Hills, Washington State; Medicine Bow, Wyoming; Solano, California, USA)	91	2,5	1980	No
MOD-5B (Kahuku Point, Oahu-Hawaii, USA)	97,5	3,2	1987	No
ÉOLE (Cap Quebec, CND)	100	4	1980	No
GROWIAN (Kaiser-Wilhelm-Koog, D)	100,4	3	1982	No

A spectacular range of installation techniques was also employed. The methods ranged from conventional installation using a crane to the use of the turbine's tower as a lifting device for platforms used to attach the rotor housing and blades.

After a modest start in terms of funding, the European Commission in 1988 began to increase R&D support for the development of large wind turbines. This change in policy was preceded by extensive discussions with scientists and industry representatives on optimal turbine size, industrial strategies and market potential.

The result of these discussions was that manufacturers who were already active in the production of smaller turbines and who had a serious interest in commercialising large wind turbines responded to the European Commission's initiative by closing agreements for the development and construction of the first commercial prototypes of megawatt rated wind turbines.

Table 2 First major European wind turbine development and test series

Wind turbine country	Rotor diameter (m)	Rated power (MW)	Year of commissioning	Commercial successor
European programme WEGA I				
Tjæreborg (Esbjerg, DK)	61	2	1989	No
Richborough (GB)	55	2	1989	No
AWEC-60 (Cabo Villano, E)	60	1,2	1989	No
European programme WEGA II				
Bonus (Esbjerg, DK)	54	1	1996	Yes
ENERCON E-66 (D)	66	1,5	1996	Yes
Nordic (S)	53	1	1996	No
Vestas V63 (DK)	63	1,5 ara>	1996	Yes
WEG MS4 (GB)	41	0,6	1996	No
WEST_GAMMA 60 (I)	60	1,5	1993	Yes
European demonstration programme THERMIE				
Aeolus II (D and S)	80	3	1993	No
Monoptoros	56	0,64	1990	No
NEWECS 45 (Stork, NL)	45	1	1991	No
WKA-60 (MAN, Helgoland, D)	60	1	1989	No
NEG-MICON (DK)	60	1,5	1995	Yes
NedWind (NL)	53	1	1994	Yes

The involvement of commercial companies in this programme changed the industry. The first testing and evaluation programmes, funded by individual governments and carried out by large construction and aerospace companies, slowly came to an end. The physical end of some wind turbines was quite spectacular: MOD 2, GROWIAN and Aelous II were blown up.

The design philosophy of the commercial prototypes was based on the gradual scaling up of smaller turbines developed and commercialised by some of the pioneering companies that had survived a severe crisis in the 1980s. However, the most successful wind turbines in the beginning were not the advanced, very fast running models, but those that had many of the features of the proven "Danish concept". This concept was based on the blueprints of the wind turbine in Gedser.

Fig. 18 Tvind wind turbine
in 1984. *Photo* Beurskens

With the WEGA and THERMIE programmes, the consistent expansion of the capacity of wind turbines began. Typical for this development phase was the consistent expansion of the smaller, successful commercial wind turbines. Many of the advanced, technical designs such as teetering hubs, down wind rotors and high-speed rotors with one or two blades were abandoned by the industry. Their first prototypes were rather "conservative", as customers were mainly interested in reliability and
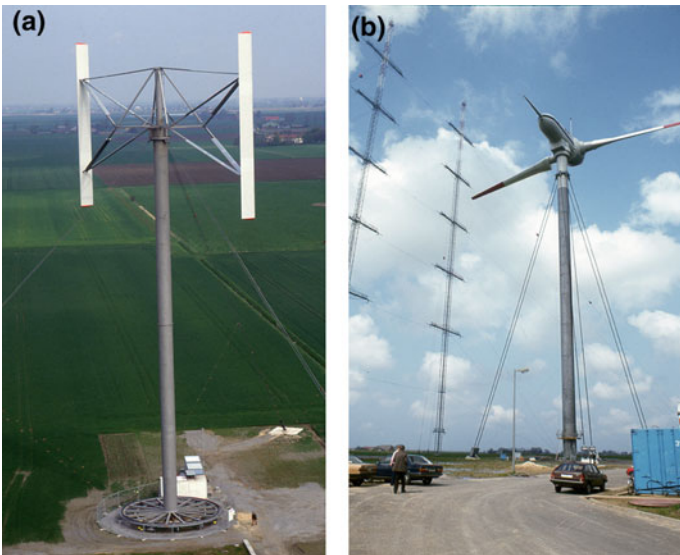

Fig. 19 Left: Heidelberg wind turbine with vertical axis of rotation in Kaiser-Wilhelm-Koog; right: GROWIAN wind turbine in Kaiser-Wilhelm-Koog. *Photo*: Jos Beurskens
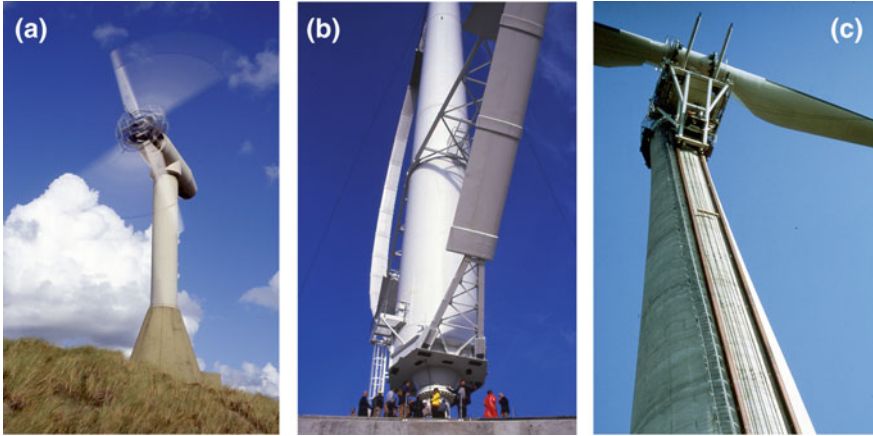
Fig. 20 Left: 25 m HAT wind turbine in operation in Petten, the Netherlands; centre: Canadian ÉOLE wind turbine with Darrieus rotor; right: WTS-75 wind turbine in Näsudden, Gotland, Sweden. Photo Jos Beurskens
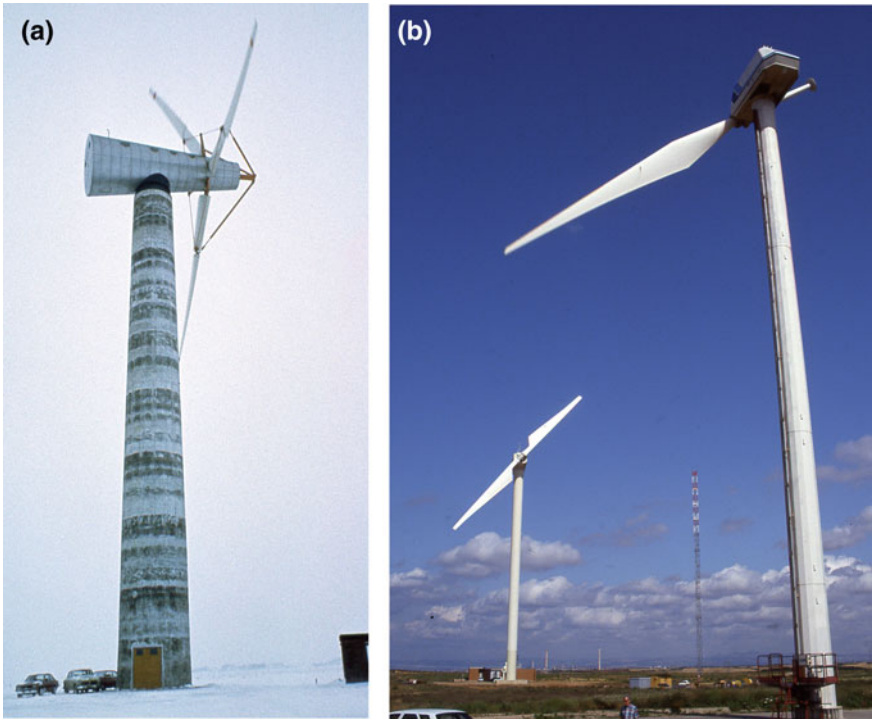
Fig. 21 Left: Nibe wind turbine in Jutland, Denmark; right: WEST Gamma 60 wind turbine with single-blade rotor in the foreground and two-bladed turbine in the background at the Alta Nurra test site, Sardinia, Italy. Photo Jos Beurskens

Fig. 22 MOD-2 wind turbine in Solano, California, USA. Photo Jos Beurskens

Fig. 23 Disassembled AWCS-60 in Kaiser-Wilhelm-Koog, Germany. Photo Jos Beurskens

not so much in advanced systems with potential for future cost savings. The innovations which were introduced later differed from the first generation of systems. The greatest advancement was the power electronic conversion, because it allowed variable rotational speed of the rotor and generator and greatly improved control of

Table 3 A selection of innovations from 1930 to approximately 1960

No	Description	Inventor/Developer	Country	Continued application
Rotor				
1	High-speed rotor: 3 rotor blades	Smidth Aeromotor	(1942)	Yes
		Jacobs (1932)	USA	Yes
2	High-speed rotor: 2 rotor blades	Smidth (1942)	DK	Yes
3	Stall control: 3 rotor blades	Smidth (Gedser; 19xx)	DK	Yes, medium-sized turbines
4	Blade tip brakes for stall control	Juul (Gedser)		
5	Stall control: 2 rotor blades	Smidth (1942)	DK	Yes, limited size
6	Single-sheet rotor	Farmer (1945)	D	Yes, limited
7	Complete blade angle adjustment, active	John Brown	GB	Yes
		Neyrpic-Vadot (1962–1964)	F	Yes
8	Complete blade angle adjustment control, assisted by auxiliary wings	WIME	USSR (1932)	No
		TsAGI	USSR (1930)	No
9	Flettner rotor on ships	Flettner (1925)	D	No (with the exception of Enercon experiments)
	Flettner rotor on rails [31]	Madaras (1932)	USA	No
10	Counterrotating rotor	Honnef (1940)	D	No
11	Introduction of GRP for rotor blade materials	Hütter	D	Yes
Capacity				
12	>1 MW nominal power, 4 rotor blades	Draft of MAN-Kleinhenz (1942)	D	No
13	>1 MW nominal power, 2 rotor blades	Smith-Putnam	USA (1.25 MW, 1945)	Yes
14	>1 MW nominal power, 3 rotor blades	Neypric-Vadot (1 MW, ca. 1960)	F	Yes
Draft				
15	Multirotor	Honnef (1932)	DK	Yes, very limited size in NL
16	Vertical axis rotor	Darrieus (Patent 1930)	F	Yes, limited size

Table 3 (continued)

| No	Description	Inventor/Developer	Country	Continued application
17	Down wind rotor	Kleinhenz (1942)	D	Yes, limited size
18	Concrete Tower	Smidth Aeromotor	DK	Yes
19	Rotor operates as a centrifugal air pump; Generates flow for the air turbine driven generator; 2 rotor blades	Andreau's Enfield	F, GB	No
20	Rotor operates as a centrifugal air pump; generates flow for the air turbine driven generator	Hütter	D	No
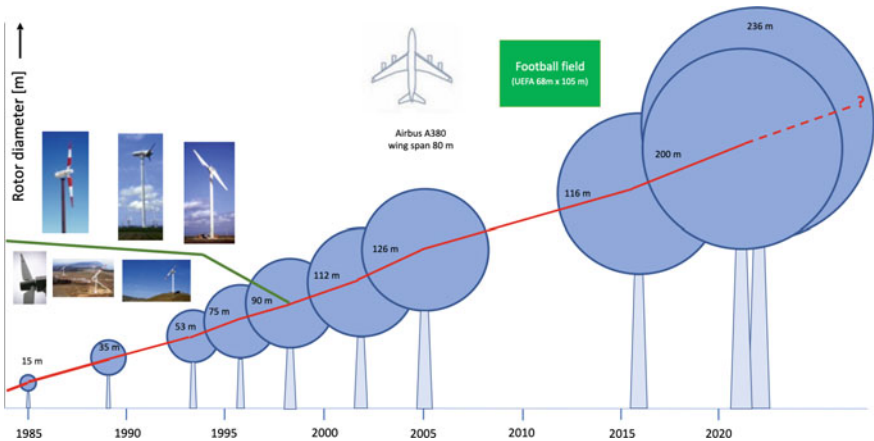
Fig. 24 Upscaling of modern wind turbines [Beurskens EWEA]

the turbines and combined with blade pitch angle control, resulted in an increase of energy efficiency.

With the use of progressive multi-parameter control strategies, the modern plants met the requirements of the power grid. Critical development/design procedures and the use of new materials led to a reduction in weight and thus also to a reduction in power generation costs.

Simultaneously with the increase in wind turbine size, the market volume of wind turbines also increased immensely. The product life of a certain type of wind turbine, based on turbine capacity, is usually six years and has been increasing with the growth of turbine size since 2002 [6].

The technical expertise increased impressively especially in the field of aero-dynamics, flow wake modelling in wind farms, aeroelasticity, FEM, structural

dynamics, measurement techniques, system modelling and control engineering. The purely analytical results had to be verified, which is why, in addition to laboratory facilities, experimental wind turbines were set up in the open air. The laboratory facilities included test rigs for rotor blades, test rigs for materials and test rigs for drive trains and wind tunnels.

Most of these research facilities originated from national initiatives and projects in European countries sometimes received support from the European Commission, all of which had special equipment. The most important test facilities for open-air wind turbines were as follows:

- MOD-0 (38 m in diameter, 1- and 2-blade rotors, USA): adjustable stiffness of the supporting structure.
- Uniwecs (16 m diameter, 2-blade rotor, idler, Germany): The configuration of the hub could be changed by a computer-controlled hydraulic system (single-pivoting rotor blades, pendulum hub, fixed hub) and damping and stiffness parameters were adjustable.
- 25 m HAT (25 m diameter, 2-blade rotor, windward rotor, Netherlands): The characteristics of the generator load are fully adjustable by using a DC generator and DC-AC converter.
- NREL, Phase II, III, IV Turbines (Boulder, USA).
- Risø, TELLUS Turbine (Denmark).
- TUD Open Air Facility (10 m diameter, 2-blade rotor, windward rotor, Netherlands): The fully equipped rotor blade for pressure distribution measurements could also be tested in a wind tunnel to enable a comparison with precisely defined flow conditions in a wind tunnel.
- Mie University (Japan).
- Imperial College and Rutherford Appleton (RAL) (United Kingdom).

The development of small wind turbines

In order to fully understand the development of modern wind energy technology and marketing success, the role of wind energy pioneers must also be considered. This refers to individuals as well as small companies.

Even before the oil crisis, pioneers built small wind turbines to power their own homes and small businesses (see Fig. 25). In a sense, these pioneers were following a craft developed during World War II. Many built wind turbines to provide electricity as the power grid was permanently collapsing. Various do-it-yourself instructions still exist from this time of war. Some of these do-it-yourself designs made it to industrial production. Examples for this are the Lagerwey turbine (see Fig. 27 [Henk Lagerweij & Gijs van de Loenhorst, Netherlands]), Enercon (Alois Wobben, Germany), Carter (see Fig. 29, Jay Carter, USA), Enertech (see Fig. 28 Bob Sherwin, USA). The Americans followed the tradition of Jacobs, but conceptwise the design was quite innovative. In Denmark, members of the Smedemesterforeningen built small turbines connected to the power grid mainly according to the proven "Danish design". From this pioneering work, companies such as Vestas, Bonus, NEG and Micon originated.

Fig. 25 Dutch do-it-yourself wind energy pioneer Fons de Beer with his passively controlled wind turbine. Photo Jos Beurskens

More than 30 small wind turbines from this period are in the German Wind Power Museum in Stemwede-Oppendorf [7] (See Fig. 26).

In order to support the efforts of small companies to improve their products and increase their economic success in the USA and the Netherlands, governments organised tenders for the development of low-cost small wind turbines. However, these were unsuccessful as demand for this type of small-capacity wind turbine slowly declined in favour of larger medium-sized grid connected turbines. It were the Danish manufacturers who started to sell their turbines on a large scale also on their own market and in various European countries. At the same time, they exported very successfully to the USA.

As demand for larger wind turbines increased, manufacturers gradually increased the capacity of their proven concepts. In the early 1990s, they reached the same size as the smaller, government-supported turbines from the 1980s. With the support of the European Commission (programmes: WEGA and THERMIE) and others, they were able to improve their designs, test their equipment and write success stories. This was a necessary condition for a successful market launch. At this point, the two originally separate development lines merged. The trend towards larger wind

Fig. 26 Wind turbine built by Martin Unger in 1973, Forstwolfersdorf, (GDR). In the German Wind Energy Museum. [Foto used with permission of Martin Unger]

Fig. 27 The early passively controlled wind turbine from Lagerwey van de Loenhorst with variable speed. Diameter: 10 m. *Photo* Jos Beurskens

Fig. 28 Enertech wind turbine at a California wind farm. *Photo* Jos Beurskens

Fig. 29 J. Carter's passively controlled down wind turbine. *Photo* Jos Beurskens

turbines continued due to the demand for very large wind turbines, as these seemed to be potentially more competitive in the offshore sector. See Fig. 24.

Almost none of the pioneering companies from the 1970s and 1980s emerged from this phase unchanged. Some went bankrupt, while others were successful.

They either remained entirely independent (ENERCON) or attracted the attention of foreign investors as independent companies (Vestas). Others merged or were acquired by larger companies. NEG and Micon can be cited as examples of better-known mergers.

Wind farms, offshore and grid connection

Along with the increasing capacity of wind turbines, wind energy projects (wind farms) also increased to such an extent that their total capacity increased from one megawatt to up to several hundred (See Fig. 30). In order to design wind farms efficiently, expertise was required in dealing with wake and flow conditions within wind farms. Research in these areas began in the early 1980s with physical analysis of wake flows and experimental studies in wind tunnels (see Fig. 31). Since the first investigations on flow conditions in wind farms, this field of research became more and more important. External influences, such as wind shear, the turbulence intensity and the stability of the atmosphere play a major role in the propagation of currents. Since these influences are very different onshore and offshore, the economic planning of offshore wind farms depends to a large extent on the results of investigations into the flow conditions in wind farms.

The importance of offshore wind energy in the development of wind energy increased, as the best sites for onshore wind energy production in Northwest Europe had already been used. Offshore is the only way for coastal states to significantly increase the contribution of wind energy to energy supply (>20%). Another reason for the growing importance of offshore wind energy is that public opposition to the

Fig. 30 Multimegawatt turbines from ENERCON, Northern Germany. *Photo* Jos Beurskens
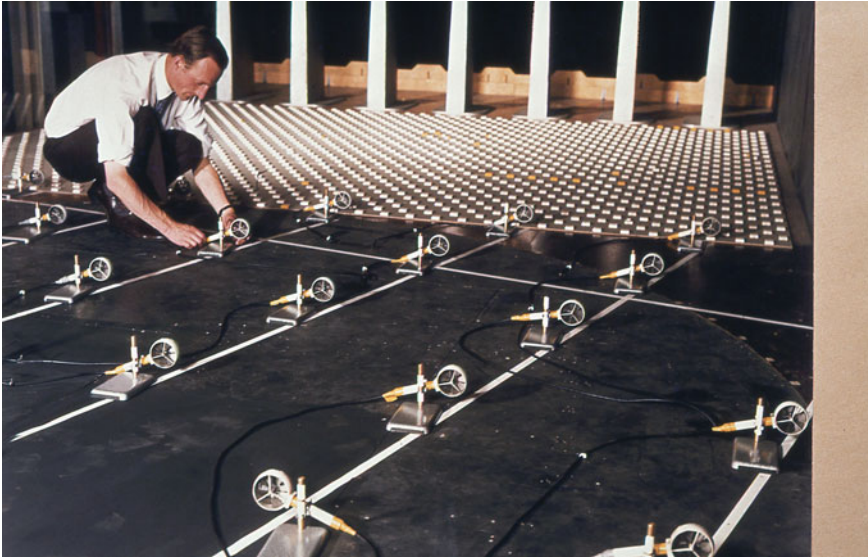
Fig. 31 Early wind farm measurements carried out by David Milborrow, Electrical Research Association, UK. *Photo* ERA (approved for free use)

erection of wind turbines in protected and ancient landscapes has arisen, especially in the UK and Sweden. The potential of offshore was recognised at the very beginning of the modern wind energy era. In 1973, Prof. Bill Heronemus, University of Massachusetts, USA, proposed what was then a very large floating foundation wind farm of 990 MW consisting of 165 turbines.

Each station consisted of a floating foundation supporting a three-rotor multi-rotor with 2 MW per turbine, see Fig. 32. The electricity generated was used to produce hydrogen by electrolysis, which was stored in submerged tanks to be transported ashore. The design of the wind turbine itself was based on a 1929 Soviet design built near Sevastopol, Crimea, see Fig. 12. Offshore wind energy has been studied since 1978 under the IEA Wind Energy Programme.

In 1991, the first large commercial offshore wind farm was built 2.5 km off the coast of Vindeby in Denmark, with a total capacity of 4.95 MW. This comprised 11 Bonus wind turbines of 450 kW each. The second Danish offshore wind farm, at Tuno Knob, was built in 1995. This wind farm has a total capacity of 5 MW and is composed of 10 Vestas wind turbines of 500 kW each. Both wind farms were built in sheltered and shallow waters. The first large offshore wind farm near Copenhagen, Middelgrunden, was built with the help of landscape architects and had a total capacity of 40 MW. It comprises 20 Bonus wind turbines, each able to generate 2 MW, arranged in an arc and built in a water depth of between 5 and 10 m.

The first step towards the use of wind energy in the harsh environment of the North Sea was taken in 2002 with the construction of the Horns Rev offshore wind farm. See Fig. 33. The installed capacity of the wind farm was 160 MW. This

Fig. 32 A wind power station of 3 × 2 MW, proposed by Prof. Bill Heronemus in 1973. *Photo* UMass (licensed for public use)

POLLUTION-FREE ENERGY
FROM OFFSHORE WINDS
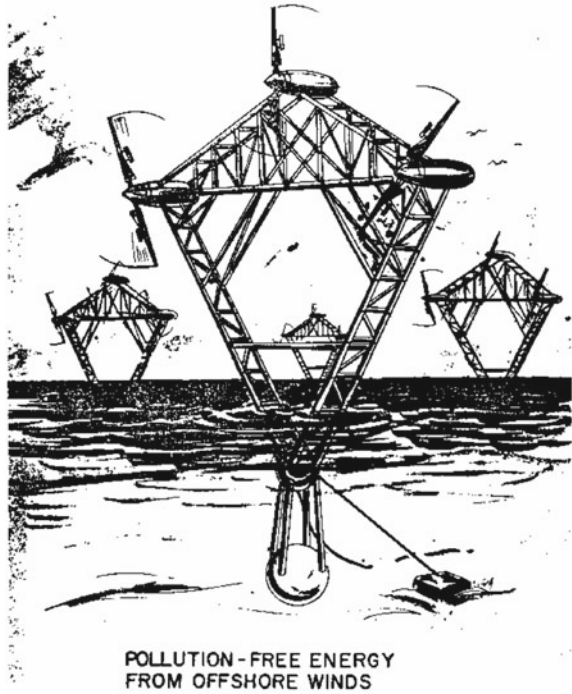
made it the first wind farm with a total capacity greater than 100 MW. The park comprises 80 wind turbines of 2 MW each, located between 14 and 17 km off the coast and in a water depth of between 6 and 14 m. Gradually, more countries joined the offshore community. By mid-2012, there were offshore plants with a total capacity of 4,100 MW. These were distributed among the following countries: Denmark, Sweden, the Netherlands, the UK, Ireland, Belgium, Germany and China. The list of countries that have or will have offshore wind farms in 2023 or earlier can be extended by Poland, Portugal, Spain, Finland, the USA, Taiwan, Japan, India and South Korea.

The rapid growth of wind farm capacities is illustrated by the following figures. Total installed capacity (mid-2021): 25 GW, generated by 5402 wind turbines, which in turn are distributed across 116 offshore wind farms.

Average capacity (2021)	708 MW/park
Average capacity (2015/2016)	43 MW/park
Average capacity of the 10 largest wind farms under construction	870 MW/park
Average capacity of the 10 largest projected wind farms	3200 MW/park

The majority of these offshore wind farms are located in relatively shallow water (up to 60 m water depth), many of which are only a short distance (up to 100 km) from the coast. Offshore turbines in shallow water have support structures that are
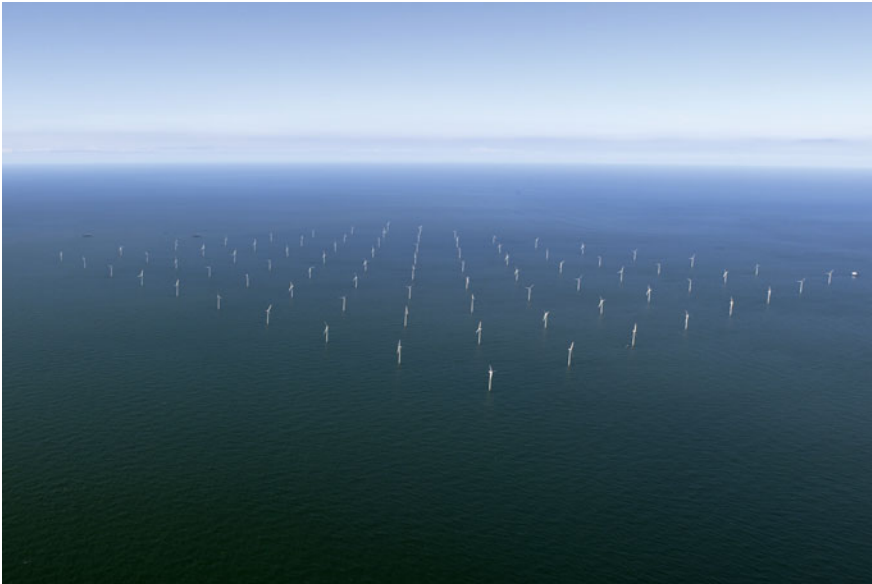
Fig. 33 160 MW Horns Rev offshore wind farm on the North Sea near Esbjerg, Denmark. *Photographer* ELSAM (approved for free use)

fixed to the seabed. The total potential of offshore wind, which also includes large water depths, is an order of magnitude higher than the potential of shallow water and coastal regions. Floating support structures are therefore necessary in these areas. The urgent need for large-scale action to limit global temperature rise, which was revived in the mid-2020s, has brought the use of offshore resources in deep seas by floating wind farms back into focus.

In 2021, there were five floating pilot wind farms in operation:

- Hywind, Scotland 2017, (5×6 MW)
- Hywind, Tampen, Norway 2019, (11×8 MW)
- Windfloat Atlantic, Portugal 2020 (3×8.5 MW)
- Koncardine, Scotland, 2021 (5×9.5 MW)

With the spectacular growth of offshore wind energy for more than a decade, aspects of implementation beyond the actual technology of wind energy systems have attracted the necessary attention in the fields of research and development, national and international policy and the wind industry. These aspects include wind resource assessment, transportation and installation vessels, operation and maintenance services, environmental aspects, morphology, risks and safety for shipping, morphology, energy collection and storage facilities, and last but not least, energy infrastructure (electricity and gas) infrastructure. Taking into account the capacities of offshore wind energy, European countries are planning more offshore wind farms, in an area without an existing electrical infrastructure. This highlights the need for a new approach to electricity grids. This need becomes more and more urgent

considering the variable power output of renewable energy sources. This mainly concerns wind power plants, solar power plants and hydropower plants. Since the lead time for grid expansion is very long, usually 10 years or more, grid expansion should have started 10 years ago to meet today's requirements. Grid expansion could and should have been part of these designs, but was not.

As mentioned earlier, early wind energy pioneers such as Poul La Cour and Bill Heronemus also considered the production of hydrogen by wind power plants. The replacement of fuels and gases of fossil origin with hydrogen produced by sustainable energy sources such as wind power became very urgent in the early 2020s. This was a direct consequence of the intense discussion on man-made climate change that started in the 2010s.

For wind energy, different options are considered. The direct generation of hydrogen by wind turbines, the generation of grid-connected electricity and the production of hydrogen in a substation, and finally the generation of electricity and hydrogen in a hybrid system, see Fig. 34.

For long transport distances at sea, the transport costs of electricity per unit of energy can be up to ten times more expensive than those of hydrogen. This underlines the need to produce hydrogen as close as possible to the wind turbines and not at the site of a distant end user. In 2021, the production of hydrogen using offshore wind energy has become an important part of the energy policy of many industrialised countries. Again, this is an old idea that will not be applied on a large scale until external conditions have changed significantly.

Translated with www.DeepL.com/Translator (free version).

International networks

In retrospect, the interesting question is whether the government-sponsored programmes of 1979 were of no use, since there were no commercial applications directly resulting from them.
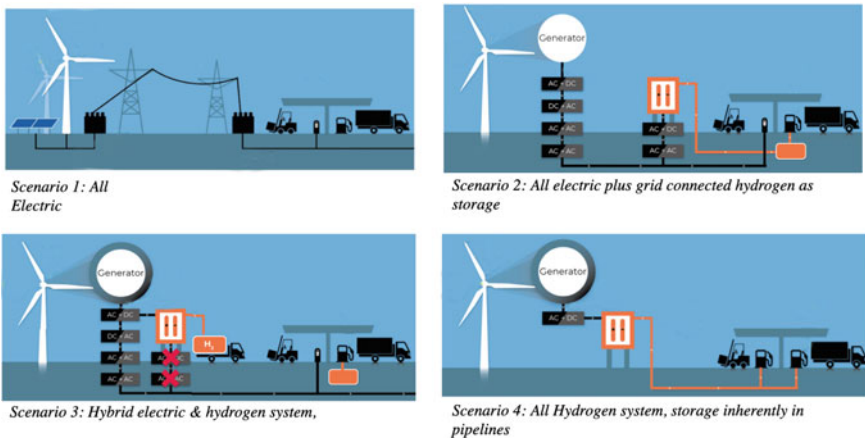

Fig. 34 Different ways to produce hydrogen from wind energy. *Photo* HYGRO

The answer would be "yes" if, between 1979 and 1985, there had been companies large enough to bear the risks involved in bringing large wind turbines to market. However, these companies did not exist at that time. The companies that would have been able to take such a risky path were not interested in the commercial introduction of large wind turbines at that time.

The answer would be "no", considering the enormous amount of accumulated data on design, operation and lessons learned from accidents and incidents. The way in which this knowledge contributed to the new generation of wind turbines is not directly traceable, as this development did not take place in a clear succession of steps. The learning process took place through experts who moved into the private sector and brought their knowledge with them. Conferences (e.g. organised by EWEA, the European Commission and AWEA) and technical meetings (e.g. organised by the IEA) were also held. The national research institutions created permanent facilities for the collection of expert knowledge on wind turbines. These institutions (initially Risø National Research Laboratory, ECN, SERI/NREL), universities and newer university networks such as ForWind and CEWind from Germany have been supported by national governments in the long term.

Without these institutions, access to the knowledge about wind turbines would have been blocked or even lost. The connection between the different aspects of this knowledge, such as resource management, structural dynamics, electrical and mechanical energy transmission and others, would also have been lost.

The fact that this knowledge is still coherent, up-to-date and accessible depends to a large extent on the degree of organisation of the scientific world and the intensive contacts between science and industry. Governments have had a smaller share in this. Although they and the European Commission have encouraged collaboration, it has been the wind energy sector itself that has launched or coordinated many initiatives, distributed tasks and developed and proposed strategic science programmes. Examples of these initiatives are the EWEA (European Wind Energy Association, 1982, now: WindEurope), the GWEC (Global Wind Energy Association 2005), the WWEA (World Wind Energy Association 2001), IMTS (Informal Meetings of Test stations, 1981, no longer active), the EUREC (European Renewable Energy Agency 1991), the EAWE (European Academy of Wind Energy 2003) and MEASNET (Measurement Quality Assurance Network 1997). These international networks represent an important dimension compared to today's national societies, which have existed for a long time.

In conclusion

Following the long path of history, from the beginnings of the practical use of windmills by the Persians to today's large-scale use of wind energy, two very successful periods can be distinguished: During the first period (1700–1890), the use of wind energy enabled the industrialization of parts of northwestern Europe, especially in the Netherlands. During the second period (after the 1973 oil crisis), wind began to play an important role worldwide [32]. The close integration of theory and practice in the development of the technology, the introduction of reliable market incentives

and political support proved to be the keys to the success of today's developments in the wind energy sector.

Literatures

1. Betz A (1925) Wind energy and its exploitation by windmills
2. Beurskens J, Houët M, van der Varst P, Smulders P (1974) Windenergie. Tech-nische Hogeschool Eindhoven, Afdeling Natuurkunde, Vakgroep Transportfysica. Eind-hoven 1974 (Dutch)
3. Beurskens HJM, Elliot G, Hjuler Jensen P, Molly JP, Schott T, de Wilde L (1986) Safety of small and medium scale wind turbines. Commission of the European Communities. DG for Energy
4. Congressional Record (1971) Proceedings and Debates of the 92d Congress, vol 117, no 190, Washington
5. Dörner H (2002) Three worlds—One life. Prof. Dr. Ulrich Hütter. ISBN 3-00-000067-4. Heilbronn
6. Ender C (2011) Wind energy use in Germany; Status 31-12-2010. DEWI Magazine
7. German Wind Power Museum. Mühlheide 14, Stemwede-Oppendorf. www.deutscheswindkraftmuseum.de
8. Golding EW (1955) The generation of electricity by wind power. E. and F.N. Spon, London
9. Greaves WF, Carpenter JH (1969) A short history of mechanical engineering. Longmans Green and Co, London
10. Hansen HC, Poul la Couren tidlig forkæmper for vedvarende energi. (Danish)
11. Harrison R, Hau E, Snel H (2000) Large wind turbines; design and economics. Wiley. ISBN 0-471-49456-9
12. Hau E (2000) Wind turbines. Fundamentals, technologies, application, economics. Springer, Berlin. ISBN 3-540-57064-0
13. Husslage G (1968) Windmolens. Keesing, Amsterdam
14. Meadows DH, Meadows DL, Randers J, Behrens III WW, The limits to growth. ISBN 0-87663-165-0. Universe Books 1972. a preprint was available as early as 1971. The report has been updated several times.
15. Molly J-P (1990) Wind energy; theory, application, measurement. Verlag C. F. Müller, Karlsruhe
16. Needham J (1965) Science and civilization in China, vol IV. Cambridge University Press, London, Section 27
17. Notebaart J, Windmills. Mouton Publishing House, The Hague, Paris
18. Oelker J (2010) Windgesichter. The dawn of wind energy in Germany. Sonnenbuch
19. Office of Production Research and Development (1946) War production board. Final Report on the Wind Turbine, Washington
20. Okulov V, van Kuik G (2009) The Betz-Joukowsky limit for the maximum power coefficient of wind turbines. Int J Altern Energy and Ecol
21. Organisation for European Economic Co-operation. Technical papers presented to the Wind Power Working Party
22. Procès Verbal des Séances du Congrès du Vent (1946). Carcasonne
23. Putnam PC (1948) Power from the wind. Van Nostrand Rein-hold Company, New York. ISBN 0-442-26650-2
24. Rave K, Richter B (2008) Im Aufwind. Schleswig-Holstein's contribution to the development of wind energy. Wachholz Verlag Neumünster. ISBN 978-3-529-05429-7
25. Reynolds J (1970) Windmills and watermills. Hugh Evelyn, London
26. Rijks-Studiedienst voor de Luchtvaart. Rapport A 258, A.G. von Baumhauer. Onderzoek van molen-modellen (Measurements on windmill models). Rapport A 269, Proefne-mingen met modellen van windmolens (Investigation of windmills).

27. Smeaton J (1759) On the construction and effects of windmillsails. Royal Society. London
28. Stokhuyzen F (1972) Molens. Unieboek, Bussum (Dutch)
29. UNESCO (1954) Wind and solar energy. In: Proceedings of the New Delhi symposium, vol I. Wind Energy. (English, Spanish, French)
30. Westra C, Tossijn H (1980) Wind Werk Boek. Ekologische Uitgeverij. Amsterdam. ISBN 906224-025-9 (Dutch)
31. Will towers like these dot the land? Electrical World (1932)
32. WindEurope (2020) Offshore Wind in Europe. Key trends and statistics

Dr. H. C. Jos Beurskens headed the Unit Renewable Energies and Wind Energy of the Energy Research Centre of The Netherlands (ECN, at present TNO) for more than 15 years. In 2008, he was awarded the Poul la Cour Prize by the European Wind Energy Association (EWEA) and received the degree of Doctor Rerum Naturalium Honoris Causa of the Carl von Ossietzky University of Oldenburg, Germany in 2009 for his life's work. He is now an independent consultant for technology development and research strategies.

The International Development of Wind Energy

Klaus Rave

Wind energy is a universal resource. It can serve as a solution to a multitude of global energy problems not only in theory but also in fact. It can be used to generate electricity, the leading energy of the twenty-first century. The finite nature of fossil resources and their geographically uneven distribution, the consequences of climate change due to their combustion, the dangers of the nuclear sector, most recently experienced dramatically in Japan and Fukushima, are increasingly finding answers and alternatives in the generation of electricity from renewable sources, above all through the use of wind energy. On a global scale, wind energy will form the backbone of a climate-friendly power supply.

1 The Beginning of the Modern Energy Debate

The international energy debate reached a new dimension with the publication of Meadow's *Limits to Growth*, the report of the Club of Rome. The shock of the first oil price crisis in 1973 hit the industrialized world hard: in Germany, there were even Sunday driving bans. Scarcity, distribution struggles: scenarios that called for a change of course.

The nuclear accidents at Harrisburg, but especially at Chernobyl (1986), marked a further dimension of the threat to and posed by energy supply. The so-called 'peaceful use of nuclear energy', as initiated by 'Atoms for Peace in response to the atomic bombs dropped on Hiroshima and Nagasaki in WWII, was increasingly questioned with regard to its risks (see [1–3]).

K. Rave (✉)
Hofbrook 29, 24119 Kiel, Germany
e-mail: drklausrave@gmail.com

Since the 1980s, the climate debate has emerged as the third major and currently dominant challenge to international energy supply, or, more precisely, the recognition that there are determining anthropogenic effects of a change in the earth's climate (see as an early popular science publication: [4]; also [5]; currently [6]). Security issues—both military and civilian, related to meeting demand and triggered by climate change—broadened the debate (see current and comprehensive [7]). The war that Russia waged against Ukraine demonstrates in a most dramatic way how energy supplies of oil and gas can be used—or rather abused—as an economic weapon.

Even if these three debates took place at different times and attempts were and are made, for example, to use the climate debate to accelerate the spread of nuclear energy as a supposedly CO_2-free form of electricity generation, the development of renewable energy sources, above all wind energy, was an essential and growing part of the chain of argumentation (see Table 1 on global growth). This connection was also made by the then UN Secretary-General Ban Ki-moon when he called for 'Sustainable Energy for All, target year 2030 (see *New York Times of* 11 January 2012 in the preliminary coverage of the Future World Energy Forum and the General Assembly of IRENA—see below—in Abu Dhabi). Otherwise, for the dangers from global warming, as for the nuclear risks, the formula applies: 'Avoid the unmanageable and manage the unavoidable'.

Table 1 Capacity of WTGs installed worldwide (in MW)

Year	Power	Increase
2000	17 400	3 760
2001	23 900	6 500
2002	31 100	7 270
2003	39 431	8 133
2004	47 620	8 207
2005	59 091	11 531
2006	73 938	14 703
2007	93 889	20 285
2008	120 624	26 872
2009	158 975	38 467
2010	198 001	39 059
2011	238 126	40 636
2012	283 048	45 169
2013	318 596	35 467
2014	369 553	51 477
2015	432 419	63 800
2016	486 749	54 900
2017	539 581	53 500

(continued)

Table 1 (continued)

Year	Power	Increase
2018	591 549	50 700
2019	650 550	60 400
2020	742 689	92 130

Two facts supported and strengthened this trend. On the one hand, the historical experience with the utilization of wind power for the development of mankind since the eighth century. On the other hand, in modern times there was a tradition of research and development in this field that had existed for decades, whether in the USA, Germany, Denmark, Holland or Great Britain (see Chap. 1 for more details).

In 1993, on the occasion of the European Wind Energy Conference held in Schleswig-Holstein, the breaking of barrier was celebrated: 1 000 MW had been installed. The year 2020 saw a new dimension: worldwide, more than 740 000 MW had been installed in over 90 countries, of which 24 countries had more than 1000 MW and 11 countries had more than 5000 MW (see Table 2).

Table 2 The wind countries worldwide

		End 2014	New 2015	End of 2015	End 2019	New 2020	End of 2020
Africa and Middle East							
	South Africa	570	483	1 053	1 980	515	2 465
	Morocco	787	–	787	–	–	–
	Egypt	610	–	610	1 452	13	1 465
	Tunisia	245	–	245	–	–	–
	Ethiopia	171	153	324		–	–
	Jordan	2	117	119	–	–	–
	Kenya	–	–	–	338		338
	Other[1]	151	–	151	2 684	295	3 009
	Total	**2 536**	753	**3 289**	**6 454**	**823**	**7 277**
Asia							
	China	114 604	30 500	145 104	236 320	52 000	288 320
	India	22 465	2 623	25 088	37 506	1 119	38 625
	Japan	2 794	245	3 038	3 857	551	4 373
	South Korea	610	225	835	1 493	160	1 651
	Taiwan	633	14	647	–	–	–
	Pakistan	256	–	256	1 239	48	1 287
	Thailand	223	–	223	1 538	–	1 538
	Philippines	216	–	216	427	–	427
	Vietnam	–	–	–	388	125	513

(continued)

Table 2 (continued)

		End 2014	New 2015	End of 2015	End 2019	New 2020	End of 2020
	Other[2]	167	–	167	2 114	566	2 670
	Total	**141 968**	**33 606**	**175 573**	**284 882**	**54 569**	**339 404**
Pacific							
	Australia	3 807	380	4 187	6 199	1 097	7 296
	New Zealand	623	–	623			
	Pacific Islands	12	–	12			
	Total	**4 442**	**380**	**4 822**	**6 199**	**1 097**	**7 296**
Europe							
	German-land	39 128	6 013	44 947	61 404	1 668	62 850
	Spain	23 025	–	23 025		–	–
	Great Britain	12 633	975	13 608	–	–	–
	France	9 285	1 073	10 358	16 643	1 318	17 946
	Italy	8 663	295	8 958	–	–	–
	Sweden	5 425	615	6 025	8 804	1 007	9 811
	Poland	3 834	1 266	5 100	–	–	–
	Portugal	4 947	132	5 079	–	–	–
	Denmark	4 881	217	5 063	1 703	0	1 703
	Turkey	3 738	956	4 694	8 056	1 224	9 280
	Netherlands	2 865	586	3 431	1 118	1 493	2 611
	Romania	2 953	23	2 976	–	–	–
	Ireland	2 262	224	2 486	–	–	–
	Austria	2 089	323	2 411	–	–	–
	Belgium	1 959	274	2 229	1 556	706	2 262
	United Kingdom	–	–	–	23 340	598	23 937
	Other[3]	6 546	833	7 387	81 928	6 735	88 512
	Total	**134 251**	**13 805**	**147 771**	**204 552**	**14 749**	**218 912**
	of which EU-28	129 060	12 800	141 578	–	–	–
Latin America and the Caribbean							
	Brazil	5 962	2 754	8 715	15 452	2 297	17 750
	Chile	764	169	933	2 145	684	2 829
	Uruguay	529	316	845	–	–	–
	Argentina	271	8	279	1 604	1 014	2 618
	Panama	35	235	270	–	–	–
	Costa Rica	198	70	268	–	–	–
	Honduras	126	50	176	–	–	–
	Peru	148	–	148	–	–	–
	Guatemala	–	50	50	–	–	–

Table 2 (continued)

		End 2014	New 2015	End of 2015	End 2019	New 2020	End of 2020
	Caribbean[4]	250	–	250	–	–	–
	Other[5]	285	–	285	3 817	823	3 920
	Total	**8 568**	**3 652**	**12 220**	**23 018**	**4 818**	**27 117**
North America							
	USA	65 877	8 598	74 471	105 466	16 205	122 317
	Canada	9 694	1 506	11 200	13 413	165	13 577
	Mexico	2 359	714	3 073	6 215	574	6 789
	Total	**77 930**	**10 818**	**88 744**	**125 094**	**16 944**	**142 683**
	Worldwide	**369 695**	**63 013**	**432 419**	**650 199**	**93 000**	**742 689**

(1) Algeria, Cape Verde, Iran, Israel, Kenya, Libya, Nigeria; (2) Bangladesh, Mongolia, Sri Lanka, Vietnam; (3) Bulgaria, Cyprus, Czech Republic, Estonia, Finland, Faroe Islands, FYROM; Hungary, Iceland, Latvia, Liechtenstein, Lithuania, Luxembourg, Malta, Norway, Romania, Russia, Switzerland, Slovenia, Ukraine (4) Caribbean: Aruba, Bonaire, Curacao, Cuba, Dominica, Guadalupe, Jamaica, Martinica, Granada, St Kitts and Nevis; (5) Bolivia, Colombia, Ecuador, Nicaragua, Venezuela	(1) Not specified (2) Not specified (3) Not specified (4) Not specified (5) Not specified		

Not only has the number of turbines and their scale has grown continuously but also the number of countries in which wind power is used to generate electricity commercially. The USA, Denmark, Germany and Spain can be named as pioneer countries where this development started in the 70s and 8os for the last century. For a long time, it was feared that these four would remain among themselves. The danger grew that political changes in just one country could trigger negative consequences for the entire development. Today, the use of wind energy is widespread in almost 100 countries. Growth is accompanied by technological and geographical diversification: for the first time, non-OECD countries led by China replaced OECD countries as growth drivers in 2010. The quantitative element is being supplemented and raised to a new level. In addition, generation costs are falling and availability is increasing. New wind farms produce more cheaply than coal-fired power plants.

2   On the Renewal of Energy Markets

The highly imbalanced regional and thus political distribution of conventional fuels was and is a defining cause of crises. Whether oil, gas, coal or uranium, the presence on national territory and the export potential or import dependence decided and still decide on prosperity, development and economic growth. The price cartel of

OPEC, the 'cheap' coal or the highly subsidized coal mining, the highly dangerous fuel cycle of uranium and the specific dependencies on gas supply each lead in different ways to foreign policy tensions up to wars as well as to domestic policy distribution disparities with momentous internal conflicts (see [7], p. 227 ff.). The Russian invasion of Ukraine is just the most recent and cruel example.

In modern history—the history of industrialization—energy markets have always been politically shaped or influenced. State-owned energy utilities, monopolistic or oligopolistic commodity producers shape the global energy economy. The ten largest (in terms of reserves) oil and gas companies in the world are state-owned (The Economist, January 21, 2012). Since the climate conference in Paris, the investment behaviour of international investors and capital providers has changed through a publicly declared retreat from fossil fuels.

The regulatory intensity of the energy markets is extremely differentiated: a scale of 0–100 would be used to the full. The correlation with Transparency International's global corruption index is striking. The spectrum of political influence ranges from 'Atoms for Peace' to the German 'coal penny' to the oligarchs of Gazprom, from research funding programmes to the German EEG. The regulatory shaping of the EU internal market is considered one of the most important and complex political processes of our time.

However, this is far outstripped by the protracted negotiations on an international climate protection agreement: the 2% target in Copenhagen just did not—yet—have any binding effect under international law. The Paris climate protection agreement with its 1.5° target by 2050 represents a breakthrough.

A global problem—the secure, environmentally and socially compatible meeting of energy needs—requires a framework of international law. The analogy to the situation of the financial markets suggests itself. Not only by the remark 'if the climate were a bank, it would already be saved', which was occasionally heard at the height of the crisis of the international financial markets in 2008. Binding agreements and regulatory standards are urgently needed in both fields. In both areas, the risk potential for the state, the economy and society is constantly growing. In both areas, only enforceable, internationally binding rules can have the lasting impact needed for long-term investment and stability. Climate protection and financial market regulation not only present the international community with new dimensions of cooperation but also are essential for the survival of mankind, (the ecology (for the terminology, see [8]) as well as the economy.

Change in the energy markets is currently taking place at various levels:

- At the level of the actors, new players are entering the field and traditional suppliers are changing. On the one hand, old monopolies are being broken up to create genuine markets through the separation of grid operation and generation, as in the EU; on the other hand, the number and weight of independent investors in energy generation is steadily increasing.

    New services are also emerging, such as electricity trading on the stock exchange and the provision of various types of storage capacity (pumped and compressed air storage, electromobility, the special role of Norway with the

companies Statoil and Statkraft and their strategy of becoming a 'Battery of Europe').

- At the level of raw material procurement of conventional energy sources, the offshore sector is continuously gaining in importance, or so-called unconventional sources such as shale gas are being developed and extracted in novel processes under environmentally questionable conditions.

1. Excursus: the reorganization of the use of the sea

Not only great opportunities but also risks are associated with the use of the offshore sector. The dangers posed by oil spills, such as those that recently became apparent in the Gulf of Mexico and off the coast of Brazil, are discussed time and again. To an even greater extent, this also applies to all developments in the Arctic and Antarctic regions, which are still protected by frozen claims and international treaties. The international community has a responsibility here.

This also applies to the world's oceans outside the 200-mile exclusive economic zone as defined in the United Nations Convention on the Law of the Sea. Following the USA, the EU Commission has presented a Green Paper—or rather a Blue Paper—from which an inclusive maritime policy is to be developed. The approval procedures for offshore wind farms in the North Sea and the Baltic Sea, as carried out in the most demanding manner by the Crown Estate of the UK and the German BSH, i.e. have set standards in planning law with regard to environmental impact assessments, etc., and are thus leading to a 'terranization' of the sea (see [9]). In this way, the use of the sea could be shaped responsibly, conflicts of interest resolved appropriately. Humanity would then, with regard to its treatment of this unique ecosystem of our blue (!) planet, finally have left the status of hunter-gatherers and arrived at a maritime industrial age in a quantum leap (see [10, 11]).

- At the level of final energy supply, electricity is systematically gaining market share and becoming the key energy of the twenty-first century (see [7], p. 714), not least due to its importance for the information technology sector both as an energy carrier and with regard to the technological interaction of ITC and energy supply, key words being 'smart grid', 'smart metering', 'smart home' and due to the strong increase in electromobility.
- On the level of energy transport, especially electricity transport, new dimensions open up with regard to distance and the resulting transport losses through HVDC technology, which entails only low (less than 5%) losses over thousands of kilometres.
- At the level of pricing, a high base can be assumed with prices rising in the medium to long term, both on the raw material side and in relation to end energy.

Electricity can be generated from diversified sources which puts it in a strategic place globally. provided interconnections operate.

3   On the Importance of Electricity Grids

Since the provision of electricity in secure networks is also essential for the growth of international communication channels, their specific strategic importance becomes even more evident (see [12]). The Internet and the power grid are each in their own right, and also through the emerging innovative symbiosis of both the strategic infrastructure investments, key to the modernization and sustainable development of economies from the local to the regional and national to the global level (see also [13]).

From the 'Super Grid (see Fig. 1) as conceived by Eddy O'Connor, founder of Airtricity, now Mainstream Renewable Power, to the 'Smart Grid' and 'Smart Metering' as currently conceived in Europe (Italy, Sweden, also Germany): Innovative technologies and cross-over applications lead to new dimensions (see [14]). Smart micro-grids offer a development perspective for emerging countries with low electrification levels.

The traditional supply-side is going to be replaced by optimized demand-side management according to the availability of renewable sources. This allows for renewable sources to develop their full potential. Less important is the number of levels at which the electricity is transported, distributed and delivered to the end customer, and by whom. Ultimately, this is a question of costs, since a margin must be earned at each level, e.g. at three levels in Germany, but only at one level in France or Italy.

The (US) National Academy of Engineering has rightly acknowledged large-scale electrification by means of power grid operation as the greatest engineering achievement of the twentieth century. The possibilities of information technology in conjunction with the power grid and electricity generation from renewable sources call for engineering achievements that can set standards for the twenty-first century.
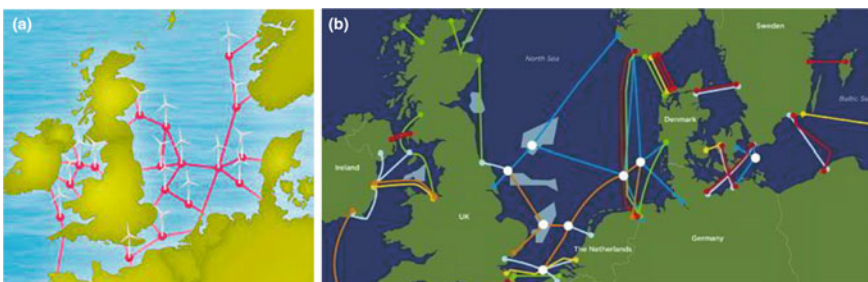
Fig. 1 European wind energy power grid (supergrid)

UN Secretary-General Ban Ki-moon pointed out in an article in the New York Times that, just 20 years ago, the global penetration of mobile phones was unimaginable (11 Jan. 2012). Creating new solutions by combining energy with information technologies something new will emerge. My thesis: analogous to the development of 'cloud computing' a kind of 'cloud generating. Supported by a worldwide network, the 'Global Link'. My formula: 'No communication without electrification'. The chairman of the State Grid Corporation of China, Liu Zhenya, in a remarkable speech in Houston, not only made a clear commitment to wind and solar power, but also outlined his plan for a 'global energy interconnection' (GEI) that would link China with Russia, Central Asia and Europe, while also benefiting from load shifts through time zones. This is to be achieved with existing technology, because, according to him, this is not a technical challenge: 'The only hurdle to overcome is mindset' [15].

In this way, the four megatrends are linked together: Globalization, Decentralization, Decarbonization and Digitalization. A further triad has also to be taken into account: scarcity, security and quality. And, there is one more: Finite resources, risks of nuclear power and dangers of climate change. Despite all the disparities in international development, especially the wide gaps in development levels and per capita income and CO_2 emissions, wind and solar energy, in addition to hydropower, geothermal energy and the potential of biomass, represent the overarching response within the framework of smart and long-distance grids.

Access to a power grid, the replacement of unstable island grids by interconnections, is a major challenge for developing economies. Not even a quarter of the 7 billion people currently living on our planet have such access. Yet in China, India, throughout Southeast Asia, in the former, now independent Asian Soviet republics, on the African continent and in Latin America, the use of information technologies is the key to economic and individual development: a secure power supply is thus also indispensable. Often enough there have been warnings about the 'digital divide', and often enough it has been disregarded that access to electricity and the security of access to an electricity grid represent an essential step in development (see [16], p. 3 f.).

In Europe, new forms of cooperation have to be tested 'top-down' within the framework set by the EU. In the USA and the North American continent at large, the challenge of East–West connections in addition to the modernization of the North–South axis pose a gigantic challenge. In the developing economies, it is necessary to achieve system integration and networking 'bottom-up' from decentralized approaches. What both developments have in common is that only technically sophisticated grid operation can ensure security of supply. Europe, and Germany in particular, has special know-how to contribute in this respect. Germany has been a transit state for a long time and a highly industrialized one as well. Its power grid is by far the best configured and operated in the world. Outage times are about 10 min in 2020, (a new record of stability and security of supply and a remarkable achievement given the ever-increasing number of decentralized feeds from wind and solar), while the next countries are already at over 4 h and the economic damage in the US is estimated to be about $150 billion caused by blackouts (see also [12]). The most

comprehensive account of power grid design can be found in the volume 'Renewable Energy Integration, edited by Lawrence E. Johns (see [17]).

Electricity generation will continue to be subject to change in the future. The electricity that comes out of the socket, on the other hand, must always have the same quality and be available at all times. The demanding task of modernizing and reconfiguring the grid is demanding but essential to the operation of electricity grids based on renewables.

The age of burning fossil fuels to generate energy is over. The vision of a perpetual nuclear fuel cycle no longer exists. Investors are concerned with preventing stranded investments, especially in relation to the high capital costs of nuclear power plants, whose processes are threatened by the non-commissioning of fast breeder reactors in Germany and France and by the unresolved question of final storage. If the transition to new energy sources and new ways of generating electricity is to be successful, the modernization of electricity grids is essential.

Hence, my formula: 'No transition without transmission'. It holds:

- to combine natural potentials with adapted technologies according to demand,
- to achieve cross-border security of supply,
- socially acceptable prices,
- to achieve price certainty and thus economic stability through the
- calculability of up-front costs, as made possible by wind energy and other renewable sources
- avoiding the volatile costs of finite fossil fuels.

In terms of its strategic importance for the twenty-first century, the expansion of the networks is comparable to the expansion of the rail and road networks and also the telephone networks in the late nineteenth and twentieth centuries. With regard to the latter, as is well known, a transatlantic cable was also considered illusory for a long time.

Without the vision of interconnection and networks, human history would have been different. But why should the trade in electricity not be globalized and physically transported on international routes? The history of the Silk Road or the Trans-Siberian Railway or the first cable from Ireland to the US may serve as a civilizational reference.

Questions of financing arise just as much as those of the form of organization—state, private and mixed economy. The return on investment is secured in the long term because it is regulated natural monoploy (see below). Investing into grids is therefore attractive investment for example for pension funds and insurance companies.

New opportunities can be offered by an energy policy that is not only politically but also financially participatory: Citizen wind farms were the pioneers. Offer investment opportunities to the local people and NIMBY (not in my backyard) just might go away.

In view of the plans to develop wind energy as the main energy source, the Danish government and parliament have integrated the grid operation of the entire country and then transferred them to a state-owned company. The Netherlands followed suit.

Grid operation is becoming technologically more demanding and the use of wind power is a decisive driver in this context. Initiated by the Fördergesellschaft Windenergie and scientifically supported by the Kassel-based ISET, the first special topic congress on the subject of 'Large Scale Integration was held in 2000. This was the beginning of a qualified and intensive debate in which the entire industry was involved. The organizer was the EWEA (now WindEurope), the oldest and largest industry association, which continued to work on this topic, cooperating closely with the Association of Electricity Grid Operators (ENTSO-E), which is now organized at the European level, and providing significant input, most recently at an international congress in Berlin in 2010 (see also [14], p. 173 ff., comprehensively also by EWEA, Powering Europe. Wind Energy and the Electricity Grid). This cooperation is urgently needed: networking for the networks. It is necessary to create the legal instruments that enable Europe-wide and global planning and investment.

As a natural monopoly, the grid-based energy source electricity requires stringent regulation so that, on the one hand, the right impulses for investments are set—through an adequate return on investment at the highest technical standard, and, on the other hand, no discriminatory market power is exercised, e.g. against independent electricity producers. The breakthrough of wind energy in Germany was achieved by the feed-in law of 1989, which came from the middle of the Bundestag and for the first time secured grid access as well as a defined remuneration. The 'unbundling, the separation of grid operation and electricity generation, as is standard in the EU today, is an essential contribution to the modernization of the energy markets.

4   The Renewed Value Chain

As the leading energy of the twenty-first century—so my thesis—electricity will therefore significantly change the market characteristics. A new global value chain will emerge:

- production from diversified renewable sources,
- transport as an independent service and a specific business model,
- storage as a strategic component of the value chain,
- trading to achieve the optimum of supply and demand and
- appropriate pricing including the integration of external effects (e.g. CO_2 pricing).

This new constellation of market players will take effect in all three currently defined marketplaces, not simultaneously and uniformly, but certainly in an overarching manner. Not only the mature onshore markets and the developing onshore markets, e.g. China, India and Brazil, but also the new offshore markets are already seeing the emergence of new players, or have announced this for the future. The traditional distinction, as formerly made (i.e. by BTM Consult), between markets that were driven by environmental policy and those that developed because of rising energy demand can no longer be maintained. Today investing in renewables is common and given priority whenever possible.

A careful risk assessment is indispensable for any investment in particular when it is long term. This applies especially to the energy sector, where the long-term nature of the investment and amortization is coupled with high political risks. The same applies to the use of capital as to the concrete planning or implementation of plans: Efficiency = Potential times Acceptance. According to various studies and surveys conducted over long periods of time, global approval for the increased use of renewable energies for power generation is overwhelming. Great hopes are placed on solar energy and wind power as their respective generation costs continue to decline. This broad acceptance, as well as the decentralized nature of electricity generation, therefore allows us to speak of a contribution by renewables to the democratic legitimacy of energy policy (see in detail [14], p. 399 ff.).

There are currently a large number of legal provisions and funding regulations. However, these are often only of short-term duration or are tied to the annuality principle of public budgets (see e.g. for the EU: [14], p. 231 ff.). In the context of this presentation, it is therefore not possible to provide a global overview that claims to be exhaustive.

The two main models, the fixed-price system and the system of quantity regulation (see in detail [18], p. 12 and 288 ff.), are to be highlighted. These systems are supplemented, for example, by trading in 'green certificates or emission rights such as the current CO_2 certificates or by tax incentives or specifications regarding the CO_2 content of an energy supplier's portfolio. Tendering models are becoming increasingly common. In particular, with regard to investment security and calculability, the fixed price systems influenced by the German Feed-in Law and the current Renewable Energy Act (EEG) have proven to be superior for a market opening. Incidentally, they have also proven to be court-proof: lawsuits brought by German energy suppliers before the EU Court of Justice failed. On the contrary, it is acknowledged that a higher remuneration than usual may be appropriate as the emission of CO_2 is avoided. (On the part of the EU Commission, a surcharge of 5 Ct. is recognized; Hohmeyer's study on the internalization of the external costs of energy production has achieved enormous practical relevance, see in depth [14], p. 370 ff, [19], p. 111 ff; [20], p. 213 ff).

The types and sources of financing are also diverse. However, project financing is globally dominant: 'Project financing is the financing of a project in which a lender initially focuses the credit assessment on the cash flows of the project as the sole source of funds through which the loans are serviced' (Nevitt, Fabozzi after [18], p. 14). The further procedure can be described in the variants BOT, BOOT and BLT (build, own, transfer; build, own, operate, transfer; build, lease, transfer). The ratio of debt to equity is risk-dependent. In developed onshore markets, it is usually 80:20; in the offshore sector, a higher equity ratio and a specific credit rating of the investors will be required.

There is a great deal of plurality on the part of both equity and debt providers. Farmers and closed-end funds, private and cooperative banks and savings banks and development banks with long-term favourable interest rates operate in this market with different shares depending on the country. Due to the ongoing crisis in the international financial market, the share of public sector or state lenders has increased

significantly in recent years. They range from the (US) Federal Financing Bank to the China Development Bank, the Brazilian BNDES, the IFC or the IDB and ADB to the EIB, the EBRD and KfW.

Hydrogen production by wind power by means of electrolysis is currently much debated. Strategies are being developed (e.g. National Hydrogen Strategy of the Federal Government of Germany, dating from 10 June 2020, see also the commentary 'Starting shot for the long haul' in Neue Energie 07/2020 as well as 'Another look in the toy box' The Economist 04/07/2020). Immense subsidies in the billions are being announced to convert industrial processes to this product, among other things. The high conversion losses are often just as little discussed as the increasing demand for electricity due to electromobility and digitalization. According to the Paris climate agreement, to achieve the 1.5° target, the power supply must be provided entirely from renewable sources—unless nuclear power plants are given longer operating times or new reactor types are introduced, as demanded by Bill Gates, for example, who is invested in such a company. In Europe, Green electricity will certainly not be available to cover that demand. Imports from Africa are being brought into play, thereby degrading a continent to the status of supplier, many states of which do not have a functioning power grid or in which less than 20% of the population has access to electricity. Australia is offering its potential, too. Care and caution are required if the niche applications for hydrogen are to be successful and do not harm the necessary transition of the electricity sector in accordance with climate change needs.

2. Excursus: plea for a new treaty

The political efforts to reach a follow-up agreement to the Kyoto Protocol are well known. As much as the expert opinion of the IPCC points to the dangers of climate change in an ever more reliable form, and representatives of the IEA such as Fatih Birol point to the narrow time window available for a change of course, the international process for reaching agreement on global climate protection targets is not accelerating. The significance of energy production and consumption is too wide-ranging, the economic situation and national per capita consumption as well as the CO_2 emissions triggered by these are too different to expect joint action quickly. A lack of courage and perspective is setting in, not only among environmental activists or progressive government representatives, but especially among the people who, like those of the Pacific island states or Bangladesh, would be particularly hard hit by accelerating climate change and the associated rise in sea level.

As a positive reference, the global problem of the hole in the ozone layer caused by the emission of CFCs should therefore be recalled. Here, a binding ban under international law has been introduced in a relatively short time. This geostrategic environmental threat was stopped. Substitutes were available. Damage to the growth of both developing and developed economies was avoided.

The substitute for coal, oil, uranium and gas is also ready: it is the renewables, wind power and solar energy as well as geothermal, biomass, of course also hydropower. (Solutions for the other causes of the climate problem, such as deforestation of rainforests or factory farming, must of course also be developed).

My proposal: Instead of relying on complex multidimensional agreements, an international treaty should initiate and secure global perspectives for investments in renewables. This would be a new kind of intergenerational contract: 'A renewable generation contract (for detailed information on the overall problem, see Lange, Internationaler Umweltschutz—Völkerrecht und Außenpolitik zwischen Ökonomie und Ökologie; 'Rethinkiung Social Contracts: Building Resilience in a Changing Climate' on the current debate on social contracts, O'Brien, Hayward, Berkes in Ecology and Society 14 (2) with interesting references to Norway, New Zealand and Canada). This label would also reflect the fact that there is another megatrend to which the international community must respond: demographic change, not only a European problem but also a challenge for Japan and China. Investments in wind and solar energy today secure future prosperity insofar as the higher up-front costs can be shouldered by the current generation, but the absence of burdens from expensive fuels compensates for rising pension and social costs. Investments in wind energy create a positive social balance.

5 International Perspectives

The potential for converting wind power into electricity has been described in a number of scenarios for Germany, the European Union and on a global scale. The target year for meeting almost 100% of electricity demand from renewable sources is 2050, with interim targets to be achieved in 2030.

Two keywords should be mentioned in advance which play an important role in the international debate. One is the discussion of the problem of 'local content, the other is the question of 'good governance. Local content, as will be shown, is always an issue for local acceptance and supportive policy decisions. However, there is no agreement on what is meant by such local value creation. In the political arena, reference is mainly made to the creation of jobs in industrial production (towers, generators, gearboxes and wings).

In economic terms, reference must be made to the entire value chain. The construction of the plant is always local, as is the subsequent service, which is indispensable for safe operation. Incentive systems such as those in the Canadian province of Ontario, which demand a certain 'local content', or the credit conditions of the Brazilian BNSDE, which ties the granting of its loans to 'local content', lead to

complaints by manufacturers at the WTO or have already led to the build-up of over-capacities with negative economic consequences for companies in the sector.

Some of the manufacturers are large corporations—such as GE and SiemensGamesa—while others are pure specialists—such as VESTAS and ENERCON. The TOP 3 had and have market shares of 12–14% each. Six Chinese companies are among the TOP 10, some of them state-owned or controlled. The world market leader (2020) is Goldwind, whose gearless turbine is equipped with German technology from the company Vensys. Technologically, gearless turbines compete with turbines with gearboxes. The supplier industry is also differentiated. The rapid growth of the industry is constantly placing new demands on them: New countries and climatic conditions from desert sands to ice storms, onshore and offshore technologies, large- and medium-sized turbine types must be tackled simultaneously. Sufficient equity capital and good creditworthiness when raising outside capital are prerequisites for being able to master this growth. The consolidation process is not yet complete.

'Good governance', i.e. the reliable translation of regulatory frameworks into good administrative practice, is the political foundation for a steady spread to further countries. Not only because energy markets have always been politically driven, as shown above. Rather, a reliable administrative culture is key to the implementation of investments in long-term assets and their trouble-free operation. The attractiveness of the investment location depends directly on this. Ensuring adequate public services is a relevant part of the risk trade-off in this context. Expert reports represent the wind conditions and thus the potential returns of a project, 'due diligence' assesses technical risks. 'Good governance' is difficult to capture as an assessment category, or is often not articulated clearly enough as a requirement by investors. Opportunisms sometimes stand in the way for a proper naming and shaming. A comparison between countries that have a legal instrument similar to the German feed-in law or the EEG and the installed plants alone shows the importance of practical implementation (see [18], p. 12). Although there are rating instruments in the context of granting loans to states, these do not go into the necessary depth and breadth to be able to take account of the problem of 'good governance'. Here, too, there is a need for action at the international level.

6 Expansion in Selected Countries

However, this special development should be placed in the context of the general and global expansion of wind energy. Beurskens has analysed this phase from a technological point of view and acknowledged it as the age of modern wind power utilization. The USA, especially California, was pioneer of this modern age. Even today—unfortunately—the turbines from these first boom years can be seen in the deserts near San Francisco, more at a stand-still than turning, depreciated in every sense of the word. For the boom was followed by the 'bust'. Tax incentives were discontinued, and, with them, further development came to an abrupt halt. Wind

companies such as VESTAS fell into insolvency, from which, however, they emerged restructured and strengthened thanks to the progressive Danish insolvency law. US Windpower, a dominant player in this market, had to bow out of it for good. It is all the more surprising that despite these negative experiences with tax-driven systems, they are still prevalent in the USA. For the first time, a 5-year term has now been introduced for the PTC, with positive effects on the US market.

Attempts to use wind energy in China were also made at a very early stage. As early as the 1980s, Germanischer Lloyd—now merged into DNV—operated a test field in Inner Mongolia with the support of the BMFT (see [21], p. 130 ff.). German and Danish wind pioneers set out for India to contribute to rural electrification. Through programmes of German development aid, MAN's twin-bladed turbine, the Aeroman with 50 kW output, was delivered to many developing countries (see the account of these beginnings in [21]). However, these approaches always remained selective or were regarded as a niche. They did not bring about relevant changes. The breakthrough in China (see below) was only achieved through own manufacturing and targets in the 5-year plan.

Great Britain was also a pioneering country in the field of research and development. Until the 1990s, there was a test field near Glasgow. The focus on the development of the financial centre in London and the accompanying trend towards de-industrialization put a stop to these approaches. Various policies to stimulate domestic use onshore failed. The most favourable prices could be realized near the coast at the highest points, and these met with the most intense resistance in planning terms, especially from influential landowners. The role of British scientists and entrepreneurs in the foundation and development of international associations such as the EWEA (today WindEurope) still has to be emphasized.

Germany also took a very special path in wind energy development. Initially, the focus was on R&D programmes. The GROWIAN was to overtake the Danish development without catching up with it. This twin-bladed turbine with a rotor diameter of 100 m was erected as the world's largest turbine in Kaiser-Wilhelm-Koog in Schleswig-Holstein in 1982. It was constructed by engineers from the DLR in Stuttgart: aircraft construction and aerospace entered into the development. This very costly experiment failed economically, but brought the industry numerous important insights for further development (see in detail in [21]). This was followed by the 100 MW programme, which promoted German turbines with a bonus of initially eight pfennigs on the generated kWh according to criteria such as diversity of manufacturer, location or operator. This government programme was declared as an R&D measure in the sense of a broad-based test (in order to avoid notification to the EU Commission). In reality, however, it served to reduce the lead of the Danish over the German manufacturers, who practised continuous technological up-scaling and were world market leaders (also including numerous components manufactured in Germany, experts assumed a value-added share of approx. 50%, see [21]). The result of this programme was the installation of a large number of wind turbines of the most diverse technologies: from single-wing to vertical-axis rotors, from setups such as 'Bush and Tree' to citizen wind farms. Although the programme also promoted turbine developments by large corporations, medium-sized firms profited

and entered the market. The breakthrough for the entire industry, however, came with the Electricity Feed Act, which guaranteed grid access and granted fixed compensation. This law (5 §§ on two pages!), initiated from the middle of the Bundestag by various Members of Parliament from a ross-soarer section of parties, started the system change in the energy industry: guaranteed access to the grid and a fixed price. Today's Renewable Energy Sources Act is based on it. In the international debate on energy policy, it has assumed a prominent position (see [7], p. 536 ff.).

The third European pacesetter for wind energy is Spain. Here, it was clearly an industrial policy that led the way. It was about creating new jobs in the country's regions. Manufacturing companies grew. Unlike in Germany, however, it was generally not 'independent power producers' that acted as investors, but energy suppliers, especially Iberdrola. Today, this company is one of the world's leading investors, along with the Danish company Oerstedt and the Italian Enel. They all have an excellent experience in wind farm monitoring and grid integration.

Until the takeover of the government by the extreme right-wing President Bolsanaro, Brazil underwent an independent development, characterized by strong economic growth, political stability and excellent energy resources (from hydropower to oil and gas reserves and biomass) as well as wind regimes. While a legal and support regime (Proinfa) modelled on the German feed-in law applied in the initial introduction phase, this was replaced by a strictly competitive regime based on tender rounds in 2010. The publicly quoted prices are very low in comparison, which is justified by high capacity factors: a challenging development.

7 The Role of the EU

The development of the European Union has been continuous. It was founded as the European Economic Community. The creation of common markets for coal and steel, and also agriculture, was the main focus. Separate treaties for the commercial use of nuclear power were concluded. In the meantime, accelerated by the fall of the Iron Curtain, the 6 founding countries France, Germany, Italy and the Benelux states have become a community of 27 countries including a EURO zone with 17 members. As a result of the financial and economic crisis, and also the sovereign debt crisis, this community of states is facing a historic test. It is to be hoped that it will be possible to overcome these weaknesses by mobilizing common strengths.

By these strengths are meant:

- a great deal of diversity,
- good experience in dealing with decentralization,
- the integration of different cultures,
- diverse experience in 'change management', be it through industrial change,
- be it through the change of the political and economic system after the fall of the iron curtain.

As early as the 1980s, the EU Commission began to promote wind energy within the framework of its research programmes and through European conferences (from which, among other things, the EWEA was founded, see below for the history of its origins). This decades-long tradition was then transferred to the Wind Technology Platform (TP Wind, see [14]) in 2005. In a second phase, the first Green Paper was drawn up in the 1990s, with significant input from Arthouros Zervos, a specialist from the Athens National Technical University who worked in the Directorate-General for Research and has been President of the EWEA and the EREC (European Renewable Energy Council) for many years, as well as co-founding the GWEC (see below for the history of its origins). Expansion targets were developed for the first time. In addition to the importance of research policies, the renewable energy industry also gained in importance, reinforced by the discussion on climate protection.

A further stage of development was reached with the 20-20-20 target. Such a target was first formulated at the EREC conference in Berlin in 2005, then taken up by the EU Commission and the European Parliament, and finally adopted by the Council of Ministers. 20% of energy requirements in 2020 to be met from renewable sources and, associated with this, a 20% reduction in CO_2 emissions. The question of the binding nature of targets had long been the subject of dispute between the Commission and Parliament, as well as the Council. A new instrument was the result of this dispute. Each Member State had to submit a 'National Renewable Energy Action Plan by autumn 2010 (see Table 3), demonstrating how this common target could be achieved at the national level. (Almost) all member states submitted their plans on time so that, for the first time in European history, a detailed and comprehensible framework for the expansion of renewable energies has been established. In the electricity generation sector, wind power is the main driver of the shift towards CO_2-free demand coverage, both through onshore and offshore expansion (see below).

Table 3 National Renewable Energy Action Plans		NREAP on	NREAP off	NREAP total
	Belgium	2 320	2 000	4 320
	Bulgaria	1 256	–	1 256
	Denmark	2 621	1 339	3 960
	Germany	35 750	10 000	45 750
	Estonia	400	250	650
	Finland	2 500	–	2 500
	France	19 000	6 000	25 000
	Greece	7200	300	7500
	United Kingdom	14 890	12 990	27 880
	Ireland	4 094	555	4 649
	Italy	12 000	680	12 680
	Latvia	236	180	416
	Lithuania	500	–	500

Table 3 (continued)

	NREAP on	NREAP off	NREAP total
Luxembourg	131	–	131
Malta	14,5	95	109
Netherlands	6 000	5 178	11 178
Austria	2 578	–	2 578
Poland	6 150	500	6 650
Portugal	6 800	75	6 875
Romania	4 000	–	4 000
Sweden	4 365	182	4 547
Slovakia	350	–	350
Slovenia	106	–	106
Spain	35 000	3 000	38 000
Czech Republic	4 365	182	4 547
Hungary	750	–	750
Cyprus	300	–	300
EU	17 0054	43 324	21 3378

The next development step was presented to the public by Energy Commissioner Oettinger in December 2011: a Roadmap 2050. This document presents various scenarios. Both a further expansion of nuclear energy and the large-scale use of CCS technology, which has so far only functioned on a laboratory scale, are considered. However, one scenario is also devoted to the increased expansion of renewables for electricity generation. In 2050, 97% is considered feasible. A dominant share of this is expected to come from the addition of wind farms. In 2021, the EU Commission offered a new dimension with the 'European Green Deal, which declared climate protection to be a central task of European policy.

8   International Institutions and Organizations

In addition to a large number of lobby and interest groups, two institutions play a prominent role in international communication on energy issues in general and the role and potential of renewables in particular:

- the International Energy Agency (IEA) and
- of the International Renewable Energy Agency (IRENA).

The International Atomic Energy Agency (IAEA), based in Vienna, is another specialized global institution.

The founding of the IEA in 1973 was an immediate and prompt reaction to the oil price crisis of that year. Sixteen industrialized countries took the initiative. As

an autonomous unit of the OECD, this institution was then based in Paris in 1974. Its executive director is Fatih Birol, the former chief economist. Despite regular and sometimes harsh criticism of assessments and forecasts, the annually published World Energy Outlook is the most influential global publication for the sector and thus also for the renewables industry (see below for the scenarios). Despite the influence of the conventional energy industry in the industrialized countries, the assessment of the potential of wind energy, for example, has gained considerable weight in recent years (see, for example, [22]).

One reason for this may have been the establishment of IRENA: competition between international institutions has a positive effect. The history of IRENA's development is much more long-winded than that of the IEA. The first suggestions can be found in the 'Brandt Report' (after former German Chancellor, Willy Brandt, who chaired the UN-initiated North–South Conference). At the following UN conference in Nairobi in 1981, this demand was included in the final document. A tireless advocate and propagator of this idea was Hermann Scheer, founder and long-time chairman of Eurosolar, who in his capacity as an SPD member of parliament also succeeded in having the demand for such an institution included in the first Red-Green coalition agreement. In Bonn in 2004, the demand was confirmed in the final resolution at the first 'International Conference for Renewable Energies'. This was followed by the first preparatory conference in Berlin in April 2008 and the founding conference in Bonn in January 2009. The statutes came into force in July 2010: the initial 75 signatory states became 86 plus the EU, with a total of 148 states plus the EU subscribing. The seat of the institution is Abu Dhabi. Three thematic areas have been defined as tasks for the work programmes:

- Knowledge management and technological cooperation;
- Policy advice and capacity building;
- Innovation and Technology.

REN 21: 'Renewable Energy Policy Network for the 21st Century' is the official title of this Paris-based network. It is sponsored by the German GIZ and the UNEP programme and supported by the IEA. Participants include governments, NGOs and international institutions. Inspired by the above-mentioned Bonn Conference in 2005, this network was mandated, among other things, to oversee international voluntary commitments. The 'Global Status Report on Renewable Energies', published annually in June, is regarded as the standard work for the sector (see also the interactive map).

Global Wind Day: 15 June has been 'Global Wind Day' since 2007. The EWEA took this initiative, which today Windeurope organizes together with GWEC. The aim is to raise public awareness of the importance of wind power. The forms of this public relations work are diverse: from photo competitions to tours and climbs, kite flying and painting competitions. The number of participating countries and organizations has increased steadily.

EWEA, AWEA, GWEC and Co.: EWEA, now WindEurope, is the oldest and largest association in the wind energy industry. Founded in 1982, this association today has over 700 members from more than 60 countries. A characteristic feature

of the association is that its membership includes all players in the industry. Manufacturers and suppliers, investors and project developers, almost all European associations and the most important research institutes. This 'Broad Church' therefore differs from other lobby groups and interest groups and has specific know-how due to its membership structure. In addition to the 'Wind Directions', background reports such as 'Wind in Our Sails', 'EU Energy Policy to 2050' or 'Pure Power-Wind Energy Targets for 2020 and 2030' are published regularly. Conferences and exhibitions are held annually.

The focus of the political work is essentially on four topics:

- the establishment of a genuine internal market for energy,
- the establishment of a stable regulatory framework,
- the achievement of a 'level playing field' for the use of wind power and
- the steady increase in the share of wind power in demand coverage.

AWEA—based in Washington—is the 2,500-member association representing the interests of the US wind industry and, as such, is an important driver of policy both centrally and locally. Its publications and events are in great demand and interest. CREIA stands for Chinese Renewable Industry Association, IWTA for Indian Wind Turbine Manufacturers Association, BWE for Bundesverband Windenergie and DWIA for Danish Wind Industry Association: all four national associations are very influential in their respective countries. The German association as well as its Danish counterpart have done pioneering work in their countries and beyond. In both countries, there are other associations, some with a long history in terms of technical standards, such as the Fördergesellschaft Windenergie in Germany or as a purely industrial association such as the VDMA or the Danish Association of Turbine Operators. This once again highlights the special importance of the WindEurope: only this association encompasses all the players in the industry. The associations of Brazil, Mexico, Canada, Japan and Korea are also constantly gaining influence and importance.

They are all members of the Global Wind Energy Council (GWEC). This was founded in 2006 as an international umbrella organization and is based in Brussels with representations in Singapur and Beijing. Since its foundation, Steve Sawyer, who came from Greenpeace, has been Secretary General, followed by Ben Blackwell. The members of GWEC are listed at www.gwec.net. In addition to national and continental associations, they include all major industrial players in the value chain.

Scenarios

Due to the long-term nature of investment cycles and the outstanding strategic importance of energy—especially electricity—for national economies, scenarios have traditionally been very important. In addition to forecasting price developments, the availability of raw materials—see, among others, the debate on 'peak oil'—and the strategic allocation of resources play a special role. The publications of the EU Commission have already been discussed. The fierce controversy surrounding the use of nuclear energy in Germany, resulting in the first decision by the Schröder/Fischer

government to phase out nuclear power, the revision of this decision by the Merkel government and the revision of this revision by the same government following the Fukushima super-GAU as a result of a seaquake and a tsunami triggered by it, have given rise to a particularly intensive preoccupation with scenarios. Mention should be made here of the SRU (German Advisory Council on the Environment), which considers it possible and feasible to meet energy needs only on the basis of renewable energies in 2050. The IPCC has also presented an extensive, 1,000-page study in which 164 scenarios were evaluated. In a consensus process, 194 country representatives agreed that renewables should account for 80% of global energy demand by 2050.

In order to make the voice of wind energy heard in the concert of scenario proclaimers, the EWEA went on the offensive in 2000 and, together with Greenpeace, published the first 'Windforce 10' report, which was updated in the following years as 'Windforce 12' and was replaced by the 'Global Wind Energy Outlook' of GWEC (Global Wind Energy Council) after its establishment.

The Global Wind Energy Outlook has examined the wind energy potential for the periods 2020, 2030 and 2050 in its scenarios. The publication is produced in collaboration with Greenpeace and DLR (German Aerospace Center, which was also active in the pioneering days of wind energy [21]). Three scenarios are considered:

- the assumptions of the IEA's World Energy Outlook (also extrapolated by DLR to the year 2050); this is considered the conservative scenario;
- in a second scenario, it is assumed—with reference to the support instruments already developed—that these will be implemented and that national expansion targets already defined will be achieved; this is regarded as the moderate scenario;
- thirdly, it is assumed that the most progressive expansion targets are achieved; this is the progressive scenario (see Table 4).

Table 4 Prospective market development: global (in MW)

Year	Conservative	Moderately	Ambitious
2007	93 864	93 864	93 864
2008	120 297	120 297	120 297
2009	158 505	158 505	158 505
2010	185 258	198 717	201 657
2015	295 783	460 364	533 233
2020	415 433	832 251	1 071 415
2030	572 733	1 777 550	2 341 984

9   Global Wind Energy Outlook 2010—The Global View into the Future

In retrospect, it has been possible to establish year after year that national targets have generally been exceeded or achieved ahead of schedule. This was already the case for the first targets set for Denmark and Schleswig-Holstein (see above). This was also the case for all EWEA forecasts for the EU Member States. However, this only applies to the development of the onshore market. Although the onshore market was and is decisive, it must be viewed in a different way today. There is no longer a uniform development, as was the case in the 1990s and the first half of the first decade.

As already highlighted above, three major trends can be distinguished: 1. the growth of the mature or maturing onshore markets. 2. the specific framework conditions for the development of offshore markets; not only is new ground being broken here in terms of planning and the need for adapted technologies, but financial factors are also decisive: the costs per turbine constructed are at least 2.5 times higher than for onshore wind turbines, the respective financing volume is generally in the upper three-digit million range, so that the consequences of the financial market crisis were clearly felt here. 3. meeting the needs of underserved economies and people, i.e. the fifth of humanity—1.4 billion—without access to electricity, who are also unable to pay for electricity because their incomes are on the poverty line: here, there is a need for instruments such as microcredits for small (wind) turbines and publicly financed projects (after careful evaluation of the 'rural electrification' programmes already implemented).

The global assessment of capacity growth in the Global Wind Energy Outlook is based on historical data. Current trends are taken into account, as are key market developments. For example, the IEA scenario assumed a decline in installed capacity to only 26.8 GW in 2010. In fact, more than 38 GW were installed. The moderate scenario is based on this order of magnitude. It assumes an annual addition of 40 GW, which could be increased to 63 GW from 2015.

10   Update on the Basis of 2015

China

China's development is particularly remarkable. For the third year in a row, the People's Republic achieved the leading position by a wide margin. More than 30 GW were reached in 2015. Four Chinese manufacturers are now among the global top ten (see above, for scenarios see Table 5). The strong home market serves as a basis for global market development with a focus on Africa and Latin America. A major advantage is that there is no lack of liquidity even for large projects. The China Development Bank is by far the largest wind power financier in the world. It also accompanies manufacturers on their way to internationalization. There is a

Table 5 Prospective market development: China (in MW)

Year	Conservative	Moderately	Ambitious
2009	25 805	25 805	25 805
2010	32 805	39 608	41 030
2015	45 305	115 088	134 712
2020	70 305	200 026	250 397
2030	95 305	403 741	513 246

clear expansion plan, anchored in the respective 5-year plans. The target for 2015—100GW—has been exceeded. The increasing political protests against the unbearable air pollution in the metropolises are at least partly answered by the large number of new wind power plants. 52GW in 2020 represents a new record for new construction. The targets of the 5-year plan are still ambitious.

The USA

The election of Joe Biden as President has given rise to optimism with regard to the development of the US market. An ambitious infrastructure programme has been drawn up, and the expansion of wind energy is to be accelerated, as is the urgently needed modernization of the electricity grid. In this way, growth impulses are to be provided even in the wake of the still rampant Corona pandemic (Table 6).

Canada

The North American neighbour Canada has also set out. In 2011, over 4 500 MW had been installed. While expansion is taking place in all provinces, Ontario (over 1 500 MW) is far ahead of Alberta and Quebec (Table 7).

The European Union

There are also uncertainties in the EU, especially with regard to the ambitious offshore targets. But the sovereign debt crisis is also leaving its mark, and the Spanish market came to a standstill. Grid expansion plans have been announced but await implementation. Minor dents in development should not overshadow the general trend. The EU Commission's cross-sector climate protection plan should provide new impetus (Table 8).

Table 6 Prospective market development: USA (in MW)

Year	Conservative	Moderately	Ambitious
2009	38 585	38 585	38 585
2010	45 085	49 329	49 648
2015	75 585	119 190	140 440
2020	106 085	220 041	303 328
2030	141 085	410 971	693 958

Table 7 New annual installed capacity in the EU (in MW)

Year	Offshore	Onshore
2001	4377	4
2002	5743	51
2003	5203	170
2004	5749	259
2005	6114	90
2006	7528	93
2007	8201	318
2008	7935	373
2009	9929	582
2010	8764	883
2011	8750	966
2012	1 200	11 700
2013	1 500	11 000
2014	1 500	11 700
2015	3 000	10 900
2016	1 600	12 300
2017	3 200	13 900
2018	2 700	9 400
2019	3 600	12 000
2020	2 900	11 800

Table 8 Share of EU countries (end 2011)

State	Power	Share (%)
Germany	29.1 GW	31
Spain	21.7 GW	23
France	6.8 GW	7
Italy	6.7 GW	7
United Kingdom	6.5 GW	7
Portugal	4.1 GW	4
Denmark	3.9 GW	4
Sweden	2.9 GW	3
Netherlands	2.3 GW	3
Ireland	1.6 GW	2
Other	8.3 GW	9

(continued)

Table 8 (continued)

State	Power	Share (%)
Shares of EU countries (as of end 2020)		
Netherlands	1 979 MW	13
Germany	1 650 MW	11
Norway	1 532 MW	10
Spain	1 400 MW	10
France	1 318 MW	9
Turkey	1 224 MW	8
Sweden	1 007 MW	7
Other	4 620 MW	32

Table 9 Prospective market development: Central and South America (in MW)

Year	Conservative	Moderately	Ambitious
2009	1 072	1 072	1 072
2010	1 522	1 956	2 082
2015	2 522	11 932	13 329
2020	4 772	28 004	42 224
2030	10 522	72 044	93 347

Central and South America

Positive things can also be said about the Latin American market. Brazil passed the 8 GW mark in 2015, and Mexico the 3 GW mark shortly before. Around 8 GW is expected by 2020 (see Table 9). Chile has a huge demand for electricity, but the regulatory framework is not yet in place. Argentina has excellent potential, but the south of the country is not connected to the grid. Political instability threatens these developments. These are the main reasons why this part of the world has so far fallen far short of its potential.

India

This also applies in a comparable way to India. Shortcomings in the power supply have long been recognized as a major obstacle to growth. It was not least industrial entrepreneurs who invested in the first wind farms in order to avoid power cuts through self-generation. The targets defined by the government to date have also fallen far short of the exploitable potential (see GWEC India Report). By contrast, the expansion of coal-fired power is taking place on a massive scale: $130 billion have been invested in this sector in the past 5 years (The Economist, January 21, 2012), making it all the more important for the Indian wind energy industry to be able to point to 2 years in a row in which it has been ranked third on the international list. Over 30 GW in 2015 indicates that a new momentum has been created. It can be assumed that the Delhi government is also revising its targets upwards (although there are fears of changes to the tax system with negative implications for the future).

Year	Conservative	Moderately	Ambitious
Table 10 Prospective market development: India (in MW)			
2009	10 926	10 926	10 926
2010	12 276	12 629	12 833
2015	19 026	24 747	29 151
2020	24 026	46 104	65 181
2030	30 526	108 079	160 741

The situation and potential of the subcontinent is described in detail in the 'Indian Wind Energy Outlook' (International Energy Agency) (Table 10).

South Korea

Over 400 MW were installed in South Korea in 2011. The national economy is beginning to see its potential for wind energy resulting from the experience of steel and shipbuilding. This is particularly true for the offshore industry. Here, the focus will be on the country itself. In this field, Korean corporations are beginning to become involved internationally. Government and industry are presenting scenarios that are aligned with the GWEC's approach (reference—moderate—ambitious). Target years are defined. For 2015, a minimum of 1.9 GW is expected, a maximum of 7.4. In 2020, the range is from 3 to 7.5, in 2030 from 7.4 to 23 GW. The latter is the target for industry. 10% electricity demand coverage would thus be achieved (see Korean Wind Energy Industry Association).

Africa

For a long time, Africa was considered to be an almost inaccessible market. Although the lack of a power supply is evident on this continent in particular, there were hardly any approaches to the use of wind energy. Not only was there a lack of a power grid or a legal basis but also a lack of skills and services pus the absence of good governance. State-owned monopolies stood in the way, too. And some countries were regarded as being just too small for any investment. It is therefore a particularly important signal that South Africa has now given the green light for the construction of several wind farms in two bidding rounds and is pushing ahead with the expansion. In this country, the strong lobby of the coal and uranium industry had to be politically contained in order to give renewables a chance. The country's industrial strength is expected to have particularly positive spillover effects on neighbouring countries. Kenya sees several new projects. Ethiopia has put itself on the wind map. Morocco not only has excellent resources due to its long Atlantic coastline but also the need to expand power generation capacity for the important tourism industry. Over 300 MW have already been installed. Further expansion is a government program. Egypt started very early with an initial test field and wind farms, reaching over 600 MW in 2011. However, especially the smaller states still suffer from their lack of attractiveness for investors. There is no electricity interconnection in sight.

Turkey

Turkey is by far the fastest-growing economy in the region. The demand for energy, especially electricity, is growing accordingly. This country is also a transit country for pipelines. The energy mix is coal-heavy. But people are starting to see and realize the opportunities of using wind power. By 2020, almost 10 GW had been installed.

Australia and New Zealand

The 2 GW mark was also reached in Australia in 2011. Despite the enormous coal reserves and the corresponding influence of this industry on the continent's national energy policy, the government has adopted ambitious climate protection targets at least on paper. Sone expansion can therefore be expected. South Australia and Western Australia are leading the way as states in this regard. New Zealand recorded growth of around 25% and passed the 600 MW hurdle (Table 11).

Table 11 Countries with more than 1 GW

		2011	2020
Asia-Pacific			
	China	145.1 GW	288.32 GW
	India	25 GW	38.625 GW
	Japan	3 GW	4,373 GW
	Pakistan	–	1.287 GW
	South Korea	–	1.515 GW
	Thailand	–	1.538 GW
Europe			
	Germany	45 GW	62.85 GW
	Spain	23 GW	27.1 GW
	United Kingdom	13.6 GW	23.94 GW
	France	10.4 GW	17.9 GW
	Italy	9 GW	?
	Sweden	6 GW	9.8 GW
	Poland	5.1 GW	6.6 GW
	Portugal	5 GW	5,917 GW
	Denmark	5 GW	6,128 GW
	Turkey	4.7 GW	9.28 GW
	Netherlands	3.4 GW	4,99 GW
	Romania	3 GW	?
	Ireland	2.5 GW	?

(continued)

Table 11 (continued)

		2011	2020
	Austria	2.4 GW	3.12 GW
	Belgium	2.2 GW	?
North America			
	USA	74.4 GW	122,317 GW
	Canada	11.2GW	13,577 GW
Latin America			
	Brazil	8.7 GW	17.75 GW
	Mexico	3 GW	6,789 GW
	Chile	–	2,829 GW
	Argentina	–	2,678 GW
Pacific			
	Australia	4.20 GW	7.296 GW
Africa and Middle East			
	South Africa	1 GW	2.465 GW
	Egypt	–	1.465 GW

Conclusion

1. The number of countries in which wind power is used to generate electricity has risen steadily to over 90. It is possible to speak of a worldwide spread of this technology.
2. At the same time, the proportion of countries in which installed capacity exceeded the critical 1 GW mark increased. In total, 24 countries have reached this installation figure, 15 European and another 9.
3. The formulation of targets is essential for the politically driven energy market. Never before have there been so many clearly defined targets as in 2015.
4. With the start of IRENA's activities, it can be assumed that the learning curve will become even steeper, i.e. the process will accelerate. For the first time, an international institution is focusing on the dissemination of knowledge about renewables.
5. The number and the economic as well as political weight of the players on the global wind energy market have reached a dynamic of their own.
6. The cross-sectional technologies of energy generation and information processing open up new perspectives and accelerate change.
7. The modern era of the energy age has begun.

Literatures

 1. Altenburg C (2010) Kernenergie und Politikberatung. Surveying a Controversy
 2. Aust S (1981) Brokdorf. Symbol of a Political Turn
 3. Traube K et al (1986) Nach dem super-GAU. Chernobyl and the Consequences
 4. Lyman F (ed) (1990) The greenhouse trap: what we're doing to the atmosphere and how we can slow global warming. World Resources Institute
 5. German Bundestag (ed), Erster Bericht der Enquete-Kommission "Schutz der Erdatmosphäre", 12. Wahlperiode
 6. Stern N, The economics of climate change. Stern Review, 2007, IPCC AR 6 Climate Change 2021
 7. Yerkin D (2011) The quest. engery, security and the remaking of the modern world
 8. Odum EP (1991) Principles of ecology—Habitats, material cycles, limits to growth
 9. Mann-Borghese E (1975) The drama of the seas
10. Runge K (ed) (2002) Coastal energy management. Integration of renewable energy generation on the coast
11. Zierul S (2010) The battle for the deep sea. Race Earth's Raw Mater
12. ders, Natural gas, electricity, broadband. Network infrastructures in Schleswig-Holstein in transition. In: Rave K, Schlie K, Schliesky U (eds) Working Paper 92, Lorenz-von-Stein-Institut
13. ders (2001) Information technology plus energy technology. A new approach. In: World market series, business briefing. World Bank
14. EWEA (2009) Wind energy: the facts. A guide to the technology, economics and future of wind power
15. E&E Reporter, 26. 02. 2016
16. ders (2003) Green power instead of blackout. In: Solarzeitalter, 15th volume, no 4
17. Johns LE (2014) Renewable energy integration
18. Böttcher J (ed) (2012) Handbook of wind energy. Onshore Projects: Realisation, Financing, Law and Technology
19. Cairncross F (1991) Costing the earth
20. Hohmeyer O, Ottinger R (eds) (1991) External environmental costs of electric power
21. Rave K, Richter B (2008) Im Aufwind - Schleswig-Holsteins Beitrag zur Entwicklung der Windenergie
22. IEA (2004) Renewable energy. Market & policy trends in IEA countries

Prof. Dr. jur. Klaus Rave headed the Department of Energy Economics in Schleswig-Holstein and was for many years a member of the board of the state's investment bank. For many years he has been active in international associations for wind energy, among others as President of the EWEA (European Wind Energy Association) and chairman of the GWEC (Global Wind Energy Council).

The Wind—From Theory to Practice

Wiebke Langreder

Abstract The understanding of flow models and their shortcomings requires an understanding of the drivers of wind. Therefore, the chapter starts by explaining the generation of global and local winds. Also, the generation of turbulence is covered since turbulence is the main driver for fatigue loads and is therefore one of the decisive factors for the lifetime of a wind turbine. The reader is introduced to mechanisms affecting the vertical wind profile, which play a role in flow modeling. Different scales of flow models are introduced. In the second part of the chapter, the reader is taken step by step through wind resource assessment. Additionally, the main technical risk factors, which are relevant to the choice of a suitable wind turbine, are explained.

1 Atmospheric Scales in Time and Space

1.1 Introduction

Variations in wind speeds in the atmosphere are caused by processes with time intervals ranging from less than one second to several months and spatial structures from a few millimetres to many hundreds of kilometres (Fig. 1). The scale analysis of meteorological motion systems originates from dynamic meteorology. By eliminating dispensable terms in the equations of motion (Navier–Stokes equations), scale analysis helps to simplify mathematical equations of numerical weather prediction for different scales. For wind energy, different scales play different roles: Microscale effects such as turbulence are important for the design of wind turbines as they influence the mechanical loads, while larger scales are important for the expected energy yield.

W. Langreder (✉)
EMD International A/S, Niels Jernes Vej 10, 9220 Aalborg, Denmark
e-mail: wl@emd.dk
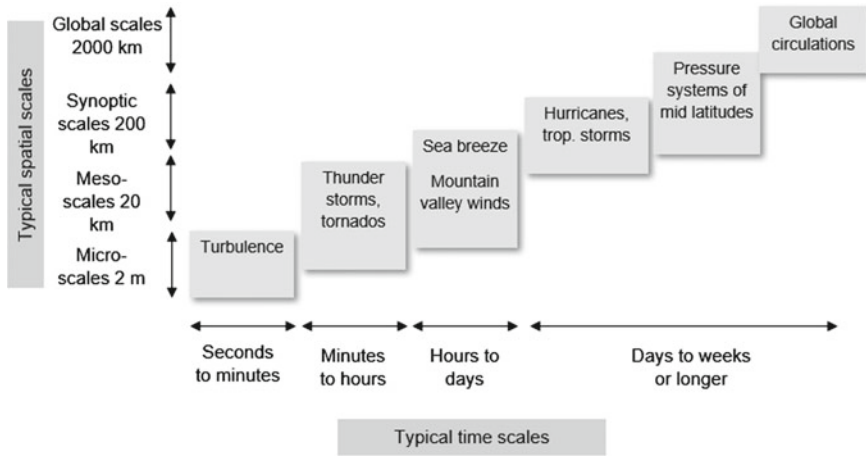
Fig. 1 Atmospheric scales

1.2 Global Scales—Formation of Global Wind Systems

Due to its spherical shape, the Earth experiences irregular solar radiation. This is accompanied by different degrees of warming, which is strongest at the equator and decreases towards the poles. The strong warming at the equator leads to the formation of low-pressure areas, while high-pressure areas form at the poles. The different pressures create a near-surface flow from the poles towards the equator. At higher altitudes, the airflow is oriented in the opposite direction. The Earth's rotation and the resulting Coriolis force cause the formation of three distinct circulations on each hemisphere, which are illustrated in Fig. 2.

In each hemisphere, tropical, mid- and polar latitudes can be identified. Europe is mostly located in the mid-latitudes. This area is characterized by cyclonic westerly winds. To the north, the mid-latitudes are bordered by the polar front, which is located around the 60th degree of latitude. The polar zone is dominated by a large low-pressure area over the polar region with easterly flows.

The tropical low-pressure belt at the equator is called doldrums. The subtropical high-pressure belt, also known as the horse latitudes, runs along the 30th degree of latitude. Like the middle latitudes, the tropical area is also interesting for wind energy: The Hadley circulation cells are formed by the air mass transport, which leads to the very constant and strong trade winds in the lower layers.

The position of global wind systems shifts with the seasons. During summer in the northern hemisphere, the earth's surface warms up most not directly at the equator, but further north at the 23rd degree of latitude, the Tropic of Cancer. Accordingly, the global wind systems shift towards the north.
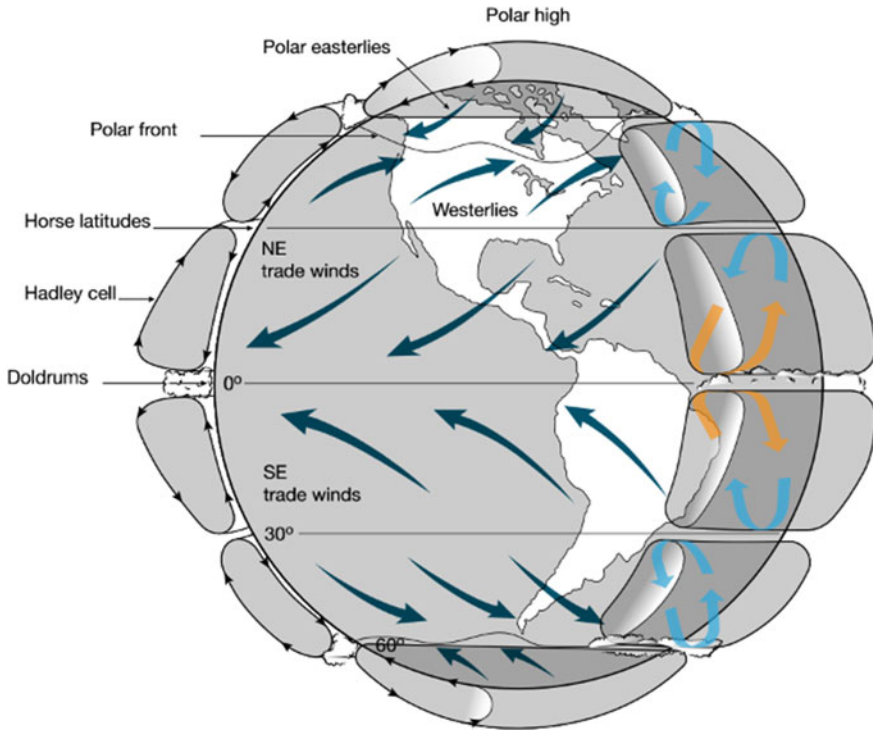
Fig. 2 Global wind circulation patterns

1.3 Mesoscale Phenomena—Formation of Local Wind Systems

Similar to the global wind systems, local compensating winds can also arise due to temperature differences. Knowledge of the formation mechanisms of these systems can be helpful in the search for suitable areas for wind energy.

The best known is probably the **sea–land circulation**, which is driven by differential warming of land and water coupled with their different heat capacities. During the day, land masses warm up more than the water surface. This differential warming causes a pressure gradient in the near-surface layer from sea to land (Fig. 3). This results in a cool and humid sea breeze that intensifies as the day progresses. In the late afternoon in clear weather conditions, the landmass begins to cool rapidly, while the high heat storage capacity of the water leads to comparatively negligible cooling. When the land mass is cooler than the water, the pressure gradient reverses and a land breeze develops. However, the land breeze is weaker than the sea breeze, since the temperature difference during night is much smaller than the temperature difference during the day.
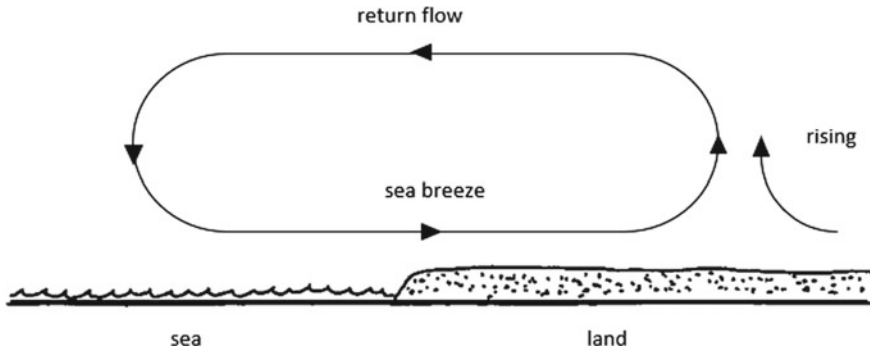
Fig. 3 Sea breeze, example daytime

How far inland the sea breeze is felt depends on many factors. These include, for example:

- What is the vegetation like? High surface roughness due to forests, for example, weakens the sea breeze.
- Is the sea breeze strengthened by the winds caused by pressure systems? If, for example, there is an area of high pressure over Poland, the resulting easterly winds from the area of high pressure will strengthen the sea breezes at the Baltic coast in northern Germany.

Circulations can also form in the mountains during radiation-intensive high-pressure weather conditions. The driver for the **mountain and valley winds** is again warming, in this case of the sunlit mountain slopes. The warming is accompanied by thermal upwelling, which causes an upwards flow on the slopes of the valley. The air rising on the slopes is replaced by the valley wind from below. At night, the process is reversed: the ground cools faster and more strongly than the air at the same altitude in the free atmosphere. This creates gravity-driven cold hillside winds that gather at the bottom of the valley and move towards the valley exit as mountain winds.

1.4 Microscale Phenomena—Turbulence

Turbulence is associated with the smaller scales (Fig. 1). While the expected wind energy yields can be determined from the larger scale diurnal and seasonal variations together with the mean wind speed of a site, the knowledge of the turbulence is primarily necessary for the load calculations of the wind turbine (Sect. 9.1).

The magnitude of turbulent fluctuations is typically expressed as the standard deviation σ_v of the velocity fluctuations. This is measured over a 10 min period, normalized to the mean wind speed V_{ave}, and referred to as turbulence intensity I_v.

$$I_v = \frac{\sigma_v}{V_{\text{ave}}} \qquad (1)$$

The turbulence intensity varies greatly. The variations are caused by natural fluctuations of the wind. However, to a certain extent, turbulence is also dependent on the averaging interval and the response behaviour of the measuring instrument used.

Two natural sources of turbulence can be identified: thermal and mechanical. Mechanical turbulence is caused by wind shear and depends on the surface roughness z_0. Often, the mechanically generated turbulence intensity I_v at a height z under neutral conditions, in flat terrain and infinite uniform roughness z_0 is calculated as a combination of Eqs. 1 and 4 simplified expressed as

$$I_v = \frac{1}{\ln\frac{z}{z_0}} \qquad (2)$$

From the equation, we see a decrease in turbulence intensity with increasing height above the ground. However, this expression is only valid as long as the profile is logarithmic and $\sigma = 2.5\ u^*$ holds. u^*, the friction velocity, as well as the relation between σ and u^* will vary with height, such that Eq. 2 should approximately be adjusted by an additional factor of 0.8 for the hub heights of 120–170 m, which are now more commonly used.

Thermal turbulence is caused by convection and depends mainly on the temperature difference between the ground and the air. In unstable conditions, i.e. when the ground is strongly heated, the turbulence intensity can reach very large values. Under stable conditions with very little vertical momentum exchange, the turbulence is typically very low.

The turbulence intensity varies not only with the height above ground (Eq. 2) but also with the wind speed. While the influence of mechanically generated turbulence dominates at higher wind speeds, thermally induced turbulence is dominant at low to medium wind speeds (Fig. 4, left). Onshore, the turbulence intensity is the highest at low wind speeds and shows an asymptotic behaviour towards a constant value at higher wind speeds (Fig. 5).

In offshore conditions, part of the wind energy is being used for the development of waves. This process leads to increasing turbulence (Fig. 4, right). Increasing turbulence is not only dependent on wind speeds but also on the sea fetch. Consequently, the sea surface roughness is time- and direction-dependent. Also, wind direction changes withdraw energy from the wind field in order to break up the existing wave field and generate a new one.

A similar phenomenon can be observed in or near forests, since here too the mechanically generated turbulence intensity increases at high wind speeds due to the increasing movement of the leaf canopy. Since the expected extreme gusts at a site depend on the turbulence at high wind speeds, the increasing turbulence offshore as well as in the forest is of great importance (Sect. 9.4).
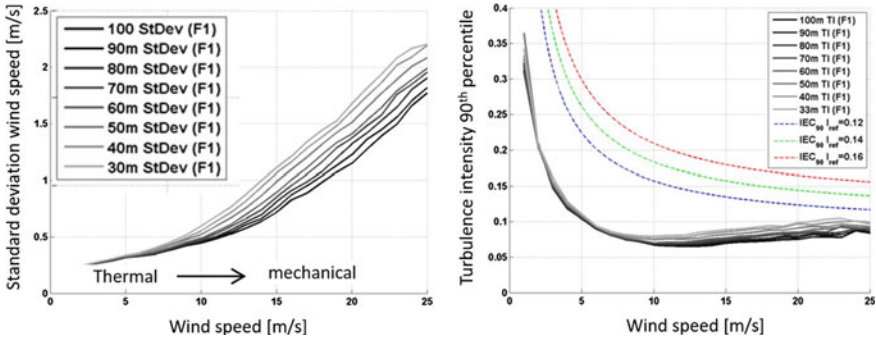
Fig. 4 Offshore standard deviation of wind speed (left) and turbulence intensity (right) at measurement heights from 30 to 100 m [1]
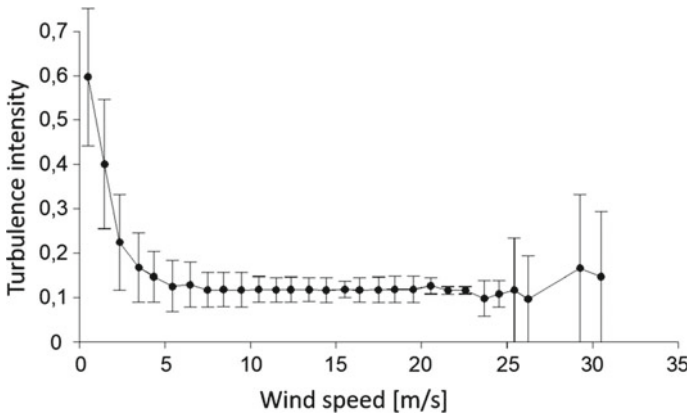
Fig. 5 Turbulence intensity I_v versus wind speed, for example, onshore conditions

Typical values of I_v in neutral conditions for different land cover at a height of 120 m a.g.l. are listed in Table 1.

Forests generally cause high ambient turbulence and therefore require special attention. The turbulence near the forest can be calculated with detailed models such as computational fluid dynamics (CFD) models. Various concepts are available for complex CFD codes. A common method for forest modelling is simulation via an

Table 1 Typical turbulence intensities at 120 m a.g.l. for different land covers

Land cover	Typical turbulence intensity (%)
Offshore	6–8
Open grass land	8–10
Agricultural area with hedges	10–12
Forest	>12

aerodynamic drag term in the momentum equations, parameterized as a function of tree height and leaf density.

Measured data show that the turbulence generated by the forest is significant in the range of five times the height of the forest in the vertical direction and up to 500 m from the forest edge in horizontal the direction. Outside these limits, the ambient turbulence intensity quickly approaches normal values, which no longer show the influence of the forest [2].

2 The Atmospheric Boundary Layer (ABL)

The lowest part of the Earth's atmosphere is called the atmospheric boundary layer (ABL). It is also known as the friction layer or planetary boundary layer (PBL). This part of the atmosphere is essentially responsible for weather patterns, as most of the turbulent vertical exchange of heat (energy) and water vapour takes place within it.

In contrast to the overlying free atmosphere, the atmospheric boundary layer is characterized by the influence of surface friction. The roughness of the ground draws energy from the airflow.

This creates a vertical wind speed gradient, also called wind shear. The shear causes turbulence, which transports the influence of surface friction to higher air layers through momentum and mass exchange. As a result, the surface friction influences not only the airflow but also the vertical distribution of temperature and pressure.

The height of the atmospheric boundary layer is linked to the spatial pattern of different roughnesses of the Earth's surface. It is smallest over the oceans and highest over mountains. In addition, the height varies with stability, ranging from a few metres' depth in stable stratification and several kilometres in unstable stratification. Typically, it varies between 100 and 2000 m, and the average depth of the atmospheric boundary layer is about 1000 m.

Above the atmospheric boundary layer is the 'free atmosphere', which is non-turbulent or only intermittently turbulent. In the free atmosphere, the wind is approximately geostrophic. The **geostrophic wind** is an idealized flow in which the wind blows parallel to the isobars on a pressure chart. This flow occurs when the pressure gradient force and the Coriolis force balance are in equilibrium. The pressure gradient force results from the pressure differences in the atmosphere and is always directed towards the low air pressure. In addition to the pressure gradient force, also the Coriolis force acts on the moving air mass: If air masses move from south towards north in the northern hemisphere, they are deflected to the right; if they move towards the south, they are deflected to the left. Thus, an equilibrium between the two forces can only be established if the geostrophic wind blows parallel to the isobars (Fig. 6). Although the geostrophic wind is an idealization, its concept plays an important role in numerical weather models.

In general, when moving closer to the ground, the atmospheric boundary layer is characterized by the increasing influence of surface friction, which leads to turbulence
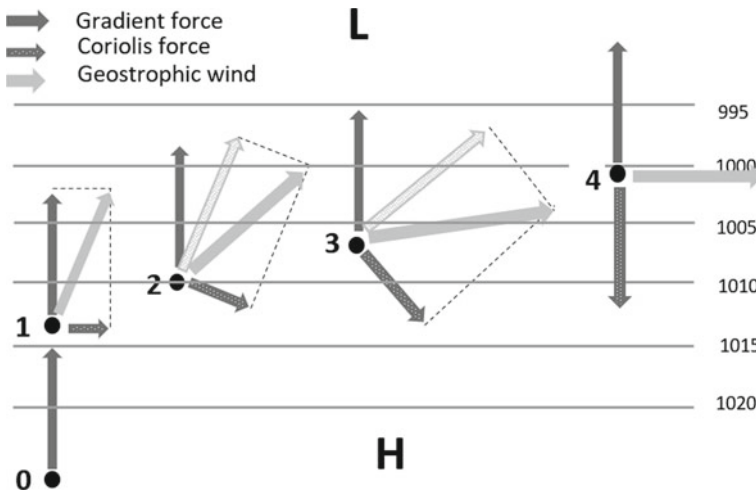
Fig. 6 Development of geostrophic wind in the northern hemisphere

and vertical mass and momentum exchange. The wind speed usually increases with altitude.

Within the atmospheric boundary layer, a further differentiation is made into the laminar sublayer, the Prandtl layer and the Ekman layer (Fig. 7). This differentiation is justified by the fact that the description of the physical processes can be simplified in the different layers. With increasing proximity to the ground, the surface friction gains more and more influence, and thus the dominance of the different physical processes determines the flow changes. Ultimately, therefore, the differentiation into different layers aids the solution of the Navier–Stokes equations.
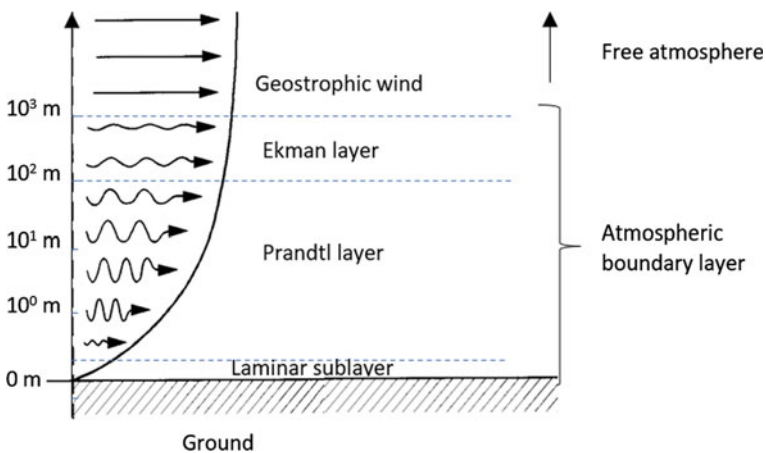
Fig. 7 Atmospheric boundary layer

In the upper part of the atmospheric boundary layer, the **Ekman layer**, the friction and the shear stress due to the Earth's surface become increasingly noticeable. In order to solve the Navier–Stokes equation, it is assumed that the change in turbulent shear stress with height is non-zero. The main characteristic of the Ekman layer is the wind direction rotation with height (termed the Ekman spiral).

While the geostrophic wind blows parallel to the isobars, the angle to the isobars increases with increasing proximity to the ground until—at the bottom of the Ekman layer—it blows into the low pressure at an average angle of 30° to the isobars. At the bottom of the Ekman layer, the wind speed is reduced by about 30–40% compared to the geostrophic frictionless wind.

Below the Ekman layer, there is the **Prandtl layer**. The Navier–Stokes equations in the Prandtl layer are solved by assuming that the turbulence does not change with height. Further, it is assumed that the wind direction is also constant with height. The height of the Prandtl layer is often expressed as a fixed percentage (about 10%) of the height of the atmospheric boundary layer. Its height would therefore depend on the vertical temperature profile, just like that of the atmospheric boundary layer. It is the lowest in cold, clear winter nights just before sunrise and the highest on sunny summer days in the early afternoon. On average, its height is 100 m. It should be remembered, however, that the Prandtl layer is based more on mathematical necessity than physics. Since early wind turbines did not exceed the height of the Prandtl layer, many flow models used in the wind energy sector are based on the physical assumptions made for the Prandtl layer.

The **laminar sublayer** (also called viscous sublayer) is only a few millimetres high and therefore irrelevant in the context of wind energy.

2.1 The Vertical Wind Profile

The vertical wind profile describes the increase of the wind speed with increasing height above ground. The assumptions used to describe the flow in the Prandtl layer result in a logarithmic wind profile that can be described as follows:

$$V(z) = \frac{u*}{\kappa}\left(\ln\left(\frac{z}{z_0}\right) - \Psi\left(\frac{z}{L}\right)\right) \tag{3}$$

The logarithmic profile is valid for flat terrain and uniform, infinite roughness and depends on the following quantities: the friction velocity $u*$, the height above ground z, the roughness length z_0 and the Von Kármán constant κ, for which a value of about 0.4 is usually assumed.

The empirical stability function Ψ corrects for the influence of temperature stratification. Ψ is positive for unstable stratification, negative for stable stratification and zero for neutral stratification (Sect. 2.3). The parameter L is the so-called Monin–Obukhov length and describes the vertical mass transfer as the ratio of frictional forces and buoyancy forces. The dimension is a length. Under neutral conditions,

when Ψ is zero, it can be Eq. 3 can be simplified to the following:

$$V(z) = \frac{u_*}{\kappa} \cdot \ln\left(\frac{z}{z_0}\right) \tag{4}$$

The wind speeds at two heights can be related to each other by applying this equation twice:

$$V_2(z_2) = V_1(z_1) \cdot \frac{\ln\left(\frac{z_2}{z_0}\right)}{\ln\left(\frac{z_1}{z_0}\right)} \tag{5}$$

If the roughness length z_0 is known, the velocity V_2 measured at height z_2 (e.g. hub height) can be derived from the wind velocity V_1 at height z_1 (e.g. measurement height). However, this equation is only valid for neutral stratification, flat terrain and infinite, uniform roughness.

Alternatively, the increase in wind speed with height is formulated using the exponential profile. According to this, two wind speeds at two heights have the following relationship:

$$\frac{V_1(z_1)}{V_2(z_2)} = \left(\frac{z_1}{z_2}\right)^\alpha \tag{6}$$

$V_1(z_1)$ and $V_2(z_2)$ are the wind speeds at heights z_1 and z_2, respectively.

However, this equation has no physical background and is based solely on empiricism.

The shear exponent α, which is also called Hellmann exponent, depends on the heights z_1 and z_2, the roughness, the atmospheric stratification and the terrain structure. Therefore, a measured height exponent is only valid for the respective location, the respective measurement heights z_1 and z_2 and the current stability. An application of the measured shear exponent in other states or a transfer to a different height ratio is not permitted. Equation 6 is therefore only of limited use.

It should be noted that the IEC 61,400-1 [3] defines a shear exponent of 0.2 for the determination of the design loads, while the 2017 EEG [4] defines a different value of 0.25. In reality, shear exponents vary over a wide range. As an example, Fig. 8 shows the frequency distributions of shear exponents measured at five different sites.

2.2 Influence of Roughness on the Wind Profile

Roughness is one of the key factors determining the wind profile. The roughness length z_0 describes the height above the ground at which the wind speed is zero. The unit of roughness length is metres. Roughness is often represented in the form

Fig. 8 Frequency distribution of shear exponent α [5]
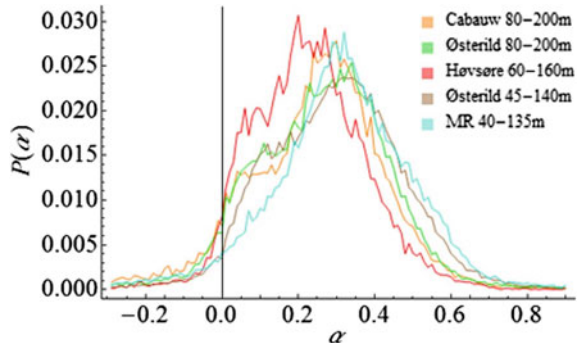
Table 2 Typical roughness length and corresponding classes based on [6]

Land cover	Roughness length z_0 (m)	Roughness class
Offshore	0,0002	0
Open agricultural area with very few obstacles	0,03	1
Low vegetation with a closed appearance, occasional obstacles	0,05	2
High vegetation, large obstacles	0,25	2,7
Many trees and/or bushes, numerous obstacles	0,5	3,2
Forest, towns	0,5–1,0	3,2–3,7

of roughness classes. Five classes are distinguished, from 0 to 4, whereby fractional classes are also possible, see Table 2.

The influence of roughness on the wind profile is shown in Fig. 9.

The vertical wind speed gradient generates mechanical turbulence. Consequently, many factors relevant to wind turbines are indirectly linked to surface roughness. This is, for example, the case for fatigue loads as well as the decay of the wake within a wind farm.

2.3 Influence of Atmospheric Stability on the Wind Profile

As can be seen from Eq. 3, the vertical wind profile depends not only on the roughness but also on the vertical temperature profile. The vertical temperature profile, which is also referred to as atmospheric stratification or stability, can be divided into three categories as follows (Fig. 10).

In **neutral** conditions, the temperature profile is adiabatic, i.e. there is an equilibrium between heating/cooling on one and expansion/contraction on the other side. As a result, no thermal energy is transported vertically. Therefore, the logarithmic
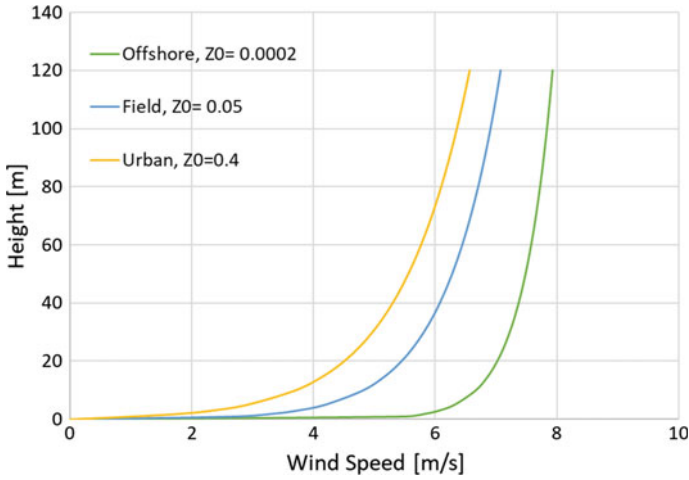
Fig. 9 Vertical wind speed profile for different roughness lengths assuming a geostrophic wind speed of 9 m/s

Fig. 10 Vertical temperature profile for different atmospheric stabilities
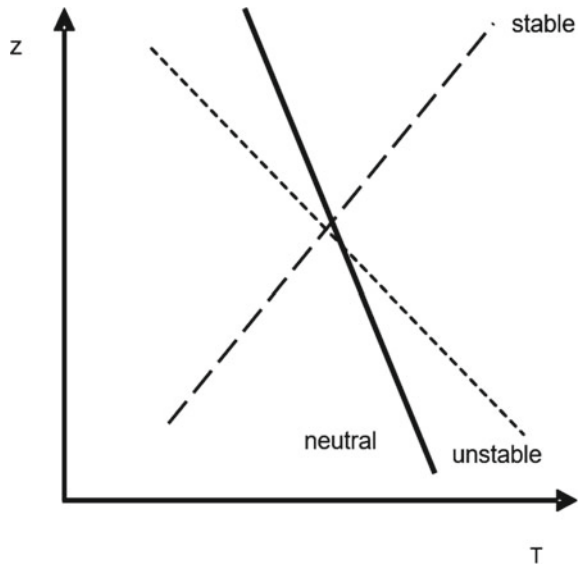
profile is solely influenced by the roughness (see Eq. 4). In neutral stratification, the temperature decreases by approximately 1 °C per 100 m. Neutral conditions occur typically at high wind speeds.

In the case of **unstable** stratification, the temperature decreases more strongly with altitude than in neutral conditions. This situation occurs, when the ground heats up considerably, and is thus typical for summer months during strong solar radiation.

The heating of the ground causes the air near the ground to rise because the air density in the layers above is lower (convection). Thus, a vertical mass exchange takes place, which leads to an increased thermally induced turbulence. The increase in wind speed with altitude is generally small.

In the case of **stable** stratification, the air near the ground is cooler than in the layers above.

Such a situation is typical for late-night hours in inland areas, especially in winter. Due to the higher air density of the layers near the ground compared to the air above, the vertical mass transfer and thus turbulence is suppressed. Due to the decoupling of the different air layers, the wind speed can change significantly with altitude. In some cases, significant changes in wind direction can occur with altitude.

Atmospheric stability can be determined in a number of ways. However, the accurate determination requires instrumentation that is often not used in the context of wind resource assessment. One of the most common scientific methods for determining the Monin–Obukhov length (see Eq. 3) is the measurement of all three wind components and the temperature fluctuations using an ultrasonic anemometer (see Sect. 6.2.2). Furthermore, the stability can be determined by measuring the temperature difference between two different heights. In this case, the stability is parameterized by the gradient Richardson number. Under offshore conditions, the stability can be determined by the temperature difference between water temperature and air temperature (Bulk Richardson number).

As a simplification, turbulence and shear can be considered as a proxy of atmospheric stability: In the case of stable stratification, turbulence is suppressed, resulting in high shear results. In the case of unstable stratification, thermal turbulence is induced, the shear is low (Fig. 11).
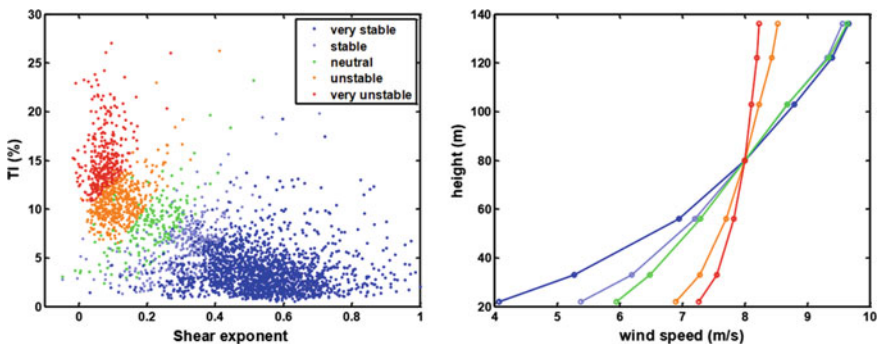
Fig. 11 Turbulence intensity versus shear exponent α (left) and vertical wind speed profile (right) for different atmospheric stabilities [6]
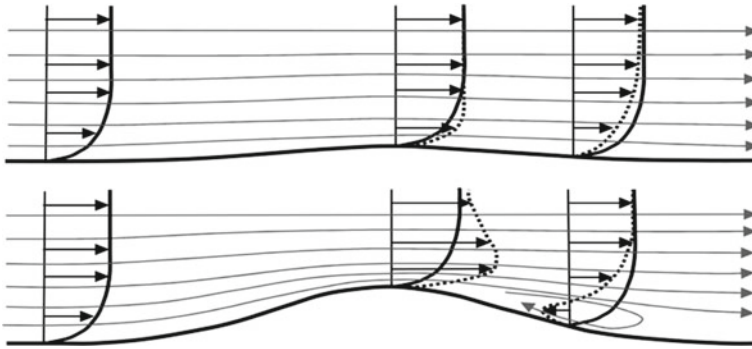
Fig. 12 Impact of orography on vertical wind speed profile for gentle hill (top) and steel hill (bottom)

2.4 Influence of the Orography on the Wind Profile

The term orography describes the differences in elevation in the terrain. In flat terrain, the influence of roughness on the vertical wind profile dominates. With increasing terrain complexity, the influence of shape of the terrain, i.e. orography, increases. The flow is generally accelerated over terrain elevations (speed-up), which leads to a deformation of the logarithmic wind profile. Depending on the height above ground, the profile becomes steeper in one area and flatter in another. The extent of deformation depends on the terrain slope, roughness and atmospheric stability. In very steep terrain, the flow can even separate and follows no longer the shape of the terrain. A turbulent separation bubble can form (Fig. 12, bottom). In the area of the separation bubble, the wind speed can decrease with increasing height leading to a negative shear exponent. As a rule of thumb, this occurs at terrain slopes greater than 30% or 17°. The location and extent of such a separation zone depend on the terrain slope, terrain curvature, roughness and atmospheric stability. In complex terrain, linearized flow models such as WAsP, which is often used to calculate wind yield (Sect. 4.3.1) cannot model separated flows, and therefore are only to a limited degree suitable for the calculation of the vertical wind profile. Higher fidelity models such as CFD models are often more suited in complex terrain (Sect. 4.3.2).

2.5 Influence of Obstacles on the Wind Profile

Local obstacles such as buildings influence the wind profile. These can partly shadow the lower parts of the wind profile and thus lead to a deformation of the wind profile. The extent of shadowing depends on the dimensions, position and porosity of the obstacle. Figure 13 shows the percentage reduction of the wind speed caused by a two-dimensional structure. The shaded zone describes the area directly at the obstacle,
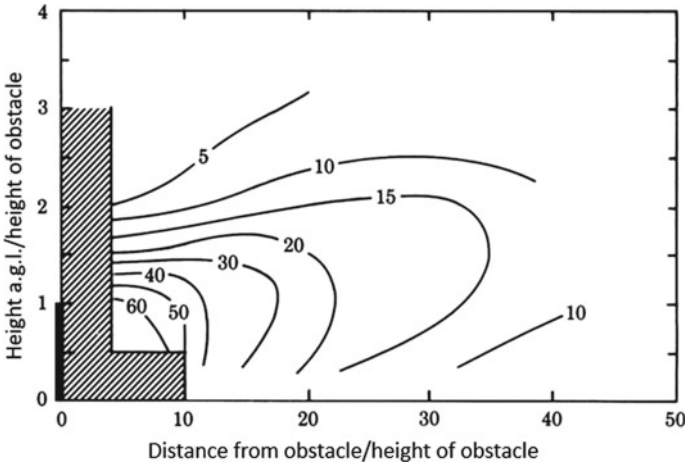
Fig. 13 Wind speed reduction in % behind an obstacle with the height '1' and depth '0', based on [7]

where the slowdown is strongly dependent on the detailed geometry of the obstacle. The flow in this area can only be described by more detailed numerical models such as CFD.

Figure 13 shows that an attenuation can only be detected up to three times the height of the obstacle. Influences of obstacles with limited heights such as houses on wind turbines with modern hub heights will therefore be negligible.

3 Statistical Representation of the Wind

3.1 The Power Spectrum

Observations of wind speed and direction show large variations over a variety of timescales. The longer the observed period, the larger the measured variance will be. This distribution of the variance over different temporal scales is illustrated by the power spectrum in Fig. 14. The representation as a power spectrum is particularly suitable for certain design calculations of the wind turbines, including fatigue loads.

The power spectrum is calculated by using a Fast Fourier Transform of a sufficiently long measured time series of wind speeds. The power spectrum in Fig. 14 was determined from a 1-year time series with a measurement frequency of 8 Hz. For illustration, the frequencies (x-axis) are labelled as time units. Due to the log-linear representation, the area under the curve reflects the energy content. This makes it possible to assign the energy components to the time units such as hours, days or seasons.

Fig. 14 Power spectrum of wind speeds measured over a flat homogeneous terrain in Denmark—the spectrum is shown in a log-linear, area-true representation, based on [7]
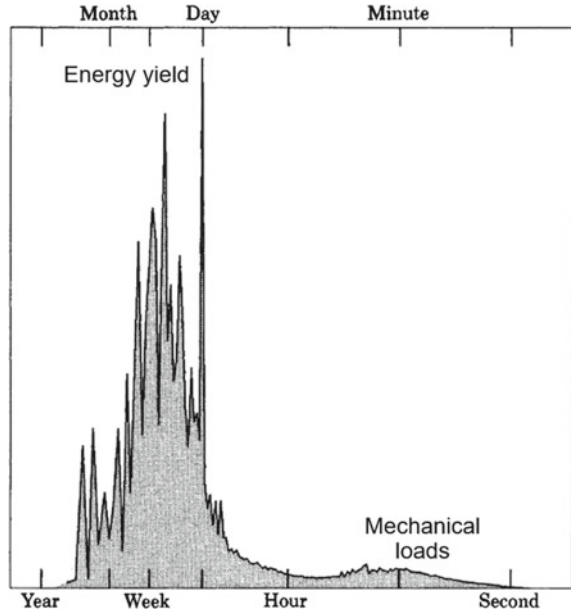
The power spectrum can be roughly divided into two sections. The energetically largest part lies in the range of temporal variations from hours to months and is thus relevant for energy yield calculations. The peak of the spectrum corresponds to temporal variations of one day and is caused by the diurnal wind speed variation at the specific location. The second largest maximum corresponds to temporal variations of a few days and is caused by synoptic variations such as the passage of low-pressure systems.

Variations with a time scale of less than one hour are associated with atmospheric turbulence (Sect. 1.4). This region of the spectrum is particularly relevant for determining the dynamic loads on the wind turbine. Numerous mathematical models have been developed to describe this part of the spectrum. Two spectral representations are often used: The Kaimal spectrum is an empirically developed model that agrees well with the observed spectra. The Von Kármán spectrum is less realistic for atmospheric turbulence but better describes the turbulence in tubes and wind tunnels.

These two turbulence spectra describe the temporal fluctuations of the turbulent component at a specific point of the area swept by the wind turbine rotor. However, since the rotor blades of the wind turbine sweep a turbulent field, the observation of the spectra at one point is not sufficient. The spatial change in lateral and vertical directions is also important because this spatial change is 'collected' by the rotating blade (rotational sampling). To reflect these effects, the spectral description of the turbulence must be extended through cross-correlation of the turbulent fluctuations of two points separated in lateral and vertical directions. The mathematical solution of the cross-correlation is considerably easier with the von Kármán spectrum, which

is why it is used more frequently than the Kaimal spectrum for the creation of 3D turbulence fields.

3.2 Frequency Distribution of the Wind Speed

While the power spectrum describes how much energy is associated with a certain temporal variation, the frequency distribution describes how often certain wind speeds occur. Generally, wind speeds are recorded for 10 min intervals. The graphical representation of the frequency of occurrence results in a histogram, typically in wind speed intervals (bins) of 0.5 or 1.0 m/s.

Histograms are often transformed into Weibull distributions as these often provide a good approximation to the actual observed frequency distribution of wind speeds (Fig. 15).

The mathematical expression of the Weibull distribution of the wind speed v is determined by two quantities, the shape parameter k, which is connected to the shape of the distribution, and the scale parameter A, which results with increasing magnitude into a shift of the curve to higher wind speeds and at the same time to a widened distribution.

$$f(v) = \frac{k}{A}\left(\frac{v}{A}\right)^{k-1} \exp\left(-\left(\frac{v}{A}\right)^{k}\right)$$
(7)

Both parameters are dependent on the local conditions and vary from place to place. Figure 16 shows a group of Weibull distributions for varying k parameters but constant mean wind speed v. Clearly, there is an increased frequency of high wind speeds in a distribution with a smaller k parameter. This is an important indication for the estimation of extreme wind speeds (see Sect. 9.4).
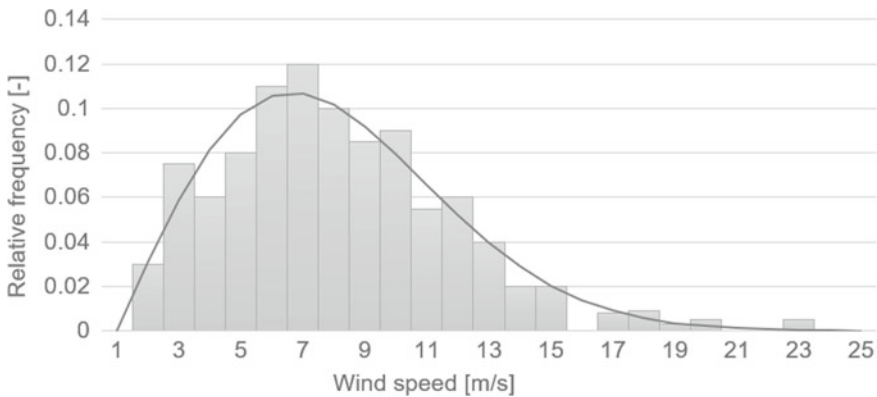
Fig. 15 Frequency distribution of wind speed shown as histogram and Weibull distribution
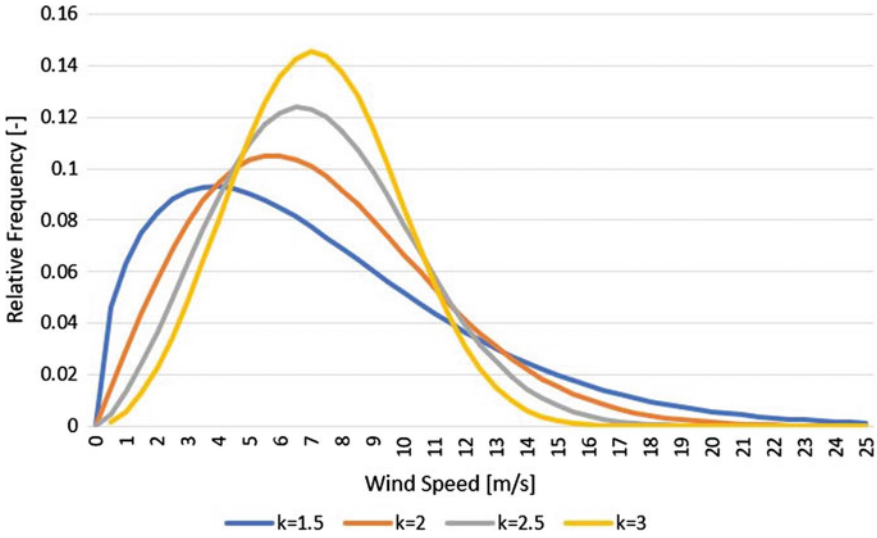
Fig. 16 Weibull distributions for constant mean wind speed but varying k parameter

The Weibull distribution is a probability density distribution. The median of the distribution corresponds to the wind speed bisecting the area under the curve. This means that half of the time the wind is blowing weaker than the median wind speed, and half of the time it is blowing stronger than the median wind speed. The mean wind speed is the average of the distribution. In a rough approximation, the relationship between the Weibull parameters A and k and the mean wind speed can be described as follows:

$$\overline{V} \approx A\left(0{,}568 + \frac{0{,}434}{k}\right)^{\frac{1}{k}} \tag{8}$$

Many different methods can be used for fitting the two Weibull parameters to a measured histogram. It is important that the fitting method focuses on the energetic part of the distribution which corresponds to the wind speed range most relevant for wind energy generation. Therefore, the fitting method of moments is most commonly used as it focuses on medium to high wind speeds but not on extreme wind speeds. Furthermore, the total energy content of the Weibull distribution should be identical to that of the observed distribution.

The possibility of describing the entire frequency distribution of the wind by two parameters saves computer resources for wind energy estimates. Today, the concept of the Weibull distribution is increasingly contested, firstly because, especially in the more exotic parts of the world, the wind speed distribution often does not sufficiently follow the shape of a Weibull distribution, and secondly, because the timeliness of the generated electricity is increasingly important when the traded directly on the electricity market. Thus, the economic success of a project is determined by

the temporal interaction of generation and electricity price. Therefore, energy yield calculations are increasingly carried out in the time domain, i.e. a time series of production is calculated.

3.3 Wind Direction Distribution

The energy yield of a wind farm depends both on the spatial distribution of the energy across the site and on a layout with the lowest possible wake losses between wind turbines (Sect. 10.2). Therefore, in addition to wind speed, the wind direction distribution must be known. A differentiation must be made between mean wind speed, frequency and energy rose (Fig. 17). These three representations can differ significantly since the energy is proportional to the cube of the wind speed.

The method described in the European Wind Atlas [7] presents a division into twelve 30° sectors to simplify the wind direction information, which is causally linked to the simplified representation of the wind speed as a Weibull function: To determine the Weibull distribution for a direction, the underlying histogram must be sufficiently filled. The smaller the sectors, the lower the probability of being able to create statistically significant histograms per sector.

It should be noted that the measurement of wind direction often has an uncertainty of up to 5°.

4 Flow Models

As explained in Sect. 1, meteorological phenomena are divided into different spatial and temporal scales to be able to simplify the equations of motion (Navier–Stokes equations) for the respective scale. This results in different types of flow models for different scales.
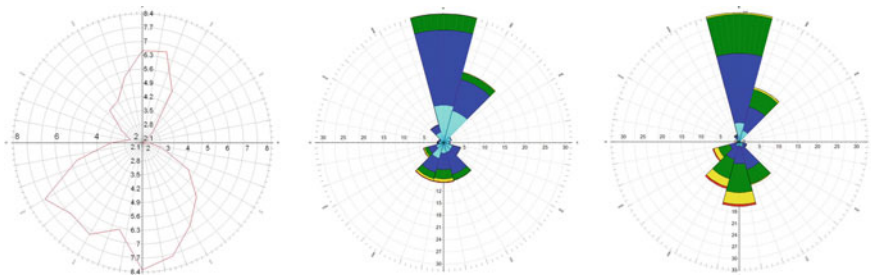
Fig. 17 Mean wind speed (left), frequency (centre) and energy rose (right)

4.1 Reanalysis Models

The so-called reanalysis models, which describe phenomena on the order of synoptic and global scales, assimilate millions of weather observations from synoptic weather stations, radiosondes, weather balloons, aircraft, ships, buoys and satellites into numerical weather models and compute a global, three-dimensional consistent description of the atmospheric state decades into the past. In this sense, this process combines the advantages of a model with the advantages of observations. Among the most common reanalysis data are ERA5 (produced by ECMWF, European Centre for Medium-Range Weather Forecasts) and MERRA2 (produced by NASA Global Modeling and Assimilation Office). Typically, the horizontal resolution of modern reanalysis data is 30–50 km, the temporal resolution is one hour.

On the one hand, these data sets are used for applications that rely on long-term meteorological data, for example, long-term corrections, and on the other hand, for the initialization of higher resolution models like mesoscale models.

For both applications, care has to be taken as both the composition of the assimilated data as well as the assimilation model as such may change over the years, which can lead to temporal inconsistencies.

4.2 Mesoscale Models

Reanalysis data are often used as boundary conditions for the next, higher resolution level of model, the so-called mesoscale models. These models add physical descriptions in the mesoscale range to the spatially and temporally coarsely resolved reanalysis data. They re-introduce atmospheric processes with spatial scales from about 2 km to several 100 km. Small-scale physical processes that are not resolved by the spatial and temporal discretization (mesh size and time step), such as boundary layer turbulence or convective exchange processes, are parameterized by ad hoc approaches, i.e. described approximately by resolved parameters. While generally the temporal resolution remains unchanged in the hourly range, and the horizontal resolution of mesoscale models is typically 1–3 km.

A commonly used mesoscale model is WRF (Weather Research and Forecasting Model), a modular numerical atmospheric model from the National Center for Atmospheric Research (NCAR).

The application of mesoscale models generally increases the correlation with local data compared to reanalysis data. Typically, the correlation coefficient R^2 is around 70% for data with a temporal resolution of one hour. For coarser temporal resolution, the correlation improves.

4.3   Microscale Models

4.3.1   Linearized Models—WAsP

Mesoscale model calculations are flanked by microscale flow models. These models often combine the determination of the spatial distribution of energy at the site with the modelling of the wake interaction between wind turbines. Once created for the specific site, these models allow rapid determination of energy production for different layouts, turbine types and hub heights.

The linearized flow model WAsP (Wind Atlas Analysis and Application Program), developed in the 1980s, has contributed significantly to the growth of the wind industry through its ease of use. WAsP belongs to the family of Jackson–Hunt models [9] like the MS3DJH model [8], both—in contrast to mass-consistent models—solve the linearized Navier–Stokes equation.

WAsP allows to determine the wind climate at any point of the site based on measured wind data. WAsP accomplishes this task by double vertical and horizontal extrapolations. The idea behind this is simple.

In the first step, the measured wind data are cleaned of local influences through obstacles, roughness and orography in order to calculate the geostrophic wind climate. Assuming that the geostrophic wind is valid for a larger area, the influences of local obstacles, roughness and orography on a nearby wind turbine site can be re-introduced in the next step by adding their local description. This principle is shown in Fig. 18 illustrated.

Since this procedure assumes the comparability of the measurement location with the future position of the wind turbine (the so-called similarity principle), the validity of the above assumption depends less on the distance but more on the similarity of the two positions. Therefore, it is extremely important to carry out wind measurements at a location that is representative of the future wind farm.

As already explained in Sect. 2.3, the vertical wind speed profile depends not only on orography, roughness and obstacles but also on atmospheric stability. During night-time, the cooling of the ground suppresses the development of a vertical exchange of momentum. Consequently, turbulence is suppressed, and high wind speed shear can be observed, sometimes accompanied by wind direction veer. Conversely, the heating of the ground during daytime causes increased turbulence through the vertical exchange of momentum. As a result, the wind speed increases less with increasing height above ground. To account for the effects of varying stability without having to model each wind profile, a simplified procedure was implemented in WAsP that requires only the climatological mean and the root mean square of the annual and daily variations in heat flux. This simplification allows a correction of the logarithmic profile for average stability effects.

Several studies have shown that using WAsP can lead to prediction errors in complex terrain [10]. This is caused by the linearization of the Navier–Stokes equations, which limits WAsP's functionality for complex sites where flow separation might occur. Figure 19 shows the separation of flow at a terrain slope of about 30%.

Fig. 18 Principle of European Wind Atlas [7]
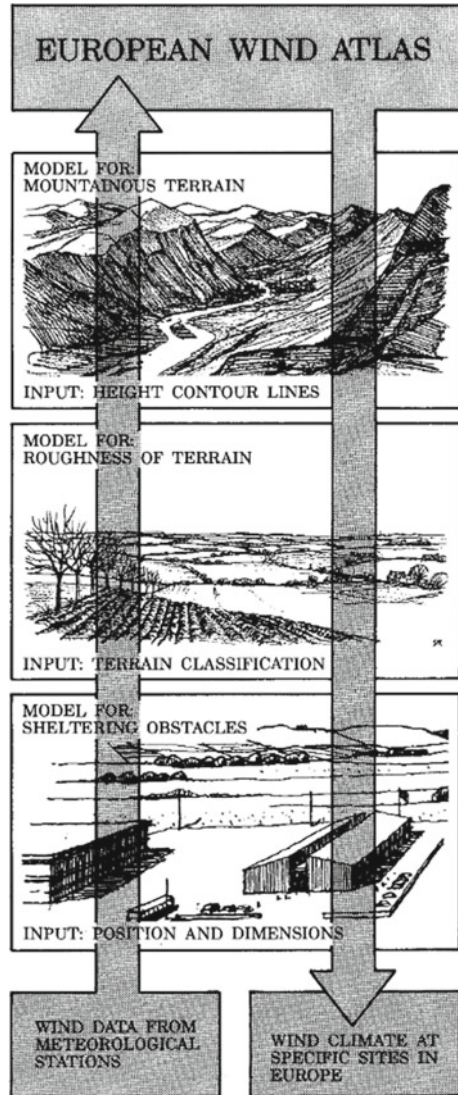
Rather than following the shape of the hill, the flow follows the shape of a virtual, flatter hill. However, WAsP uses the true terrain slope to calculate acceleration and thus overestimates wind speed. A partial correction of this model error is possible with help of the so-called Ruggedness Index (RIX). RIX is defined as the fraction of the area with a radius of 3 km around the site of interest, that exceeds a terrain slope of 30% and therefore violates the WAsP model assumptions of linear flow.

Figure 20 shows the relationship between the expected wind speed error and the difference in complexity between the position of the measuring mast and the position
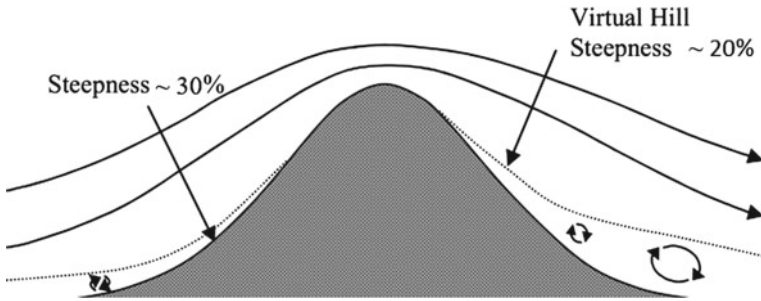
Fig. 19 Flow separation at a steep hill [11]

Fig. 20 Prediction error of wind speed as a function of the difference Δ-RIX between WTG position and reference [12]
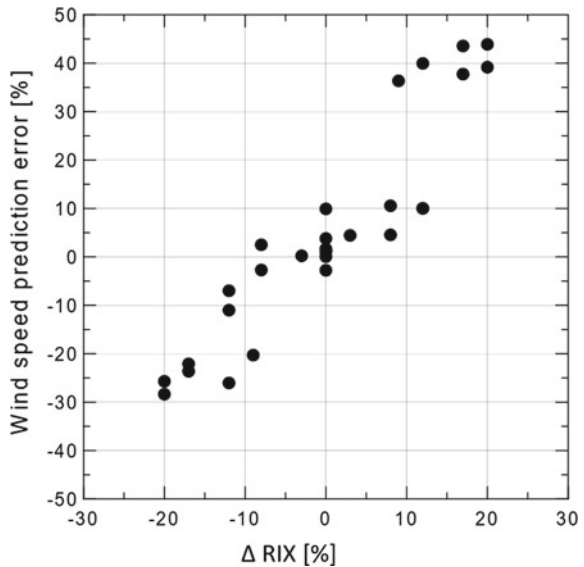
of the future wind turbine. Again, the similarity principle applies: if the complexity of the turbine position is comparable to the complexity of the measurement position, the prediction error is close to zero. If the reference site (measurement position) is less complex than the future turbine position, the difference Δ-RIX becomes positive, and thus an overestimation of the wind speed is to be expected. If the reference site is more complex than the future turbine position, the difference Δ-RIX becomes negative, and thus an underestimation of the wind speed is to be expected. It must be emphasized that the quantitative relationship between Δ-RIX and prediction error depends on the location.

Another challenge in WAsP is the modelling of forests. In order to model the wind speed correctly, a so-called displacement height combined with a high roughness must be used [13]. The flow across a forest is lifted as the forest acts partly as an artificial hill. Consequently, the flow is accelerated above the forest. The displacement
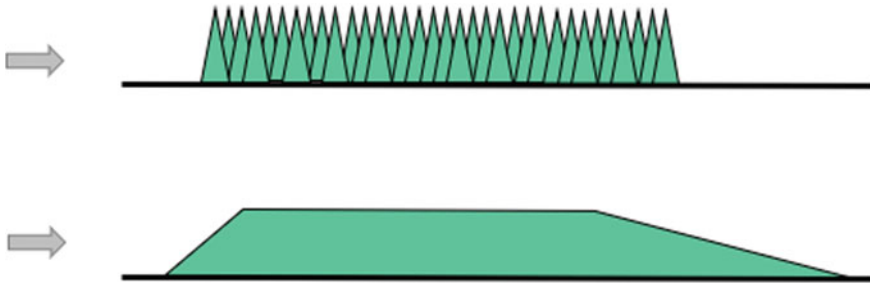
Fig. 21 Displacement height in WAsP caused by forest depending on wind direction

height is an artificial elevation of the terrain for the forested area, with the purpose of correcting the wind speed over the forest. The height of displacement depends on the density of the forest and the canopy and is often assumed to be between 0.9 and 1.1 times the tree height. At the forest edge, the displacement height should taper off. Depending on the wind direction it has been suggested to extend the displacement height up to a distance of 50 times the forest height [14] (Fig. 21). The roughness length to be applied for forest areas should be in the order of 0.4 m to more than 1 m. The increased roughness leads to a wind profile with a higher shear [13].

In summary, WAsP still plays an important role in determining wind resources, mainly because the calculations can be performed both quickly and easily. Its limitations resulting from the linearization of the flow model are known and well understood. Their consequences can be estimated and partially corrected.

4.3.2 Non-linearized Models

In recent years, the use of more complex models such as **CFD** (Computational Fluid Dynamics) has become more popular. CFD models are mostly used in a complementary way instead of replacing WAsP. The solution of the Navier–Stokes equations in CFD models is generally more complex than in linearized models such as WAsP. It has been shown that the performance of CFD models depends not only on the choice of parameterization but also on the skill and experience of the user, which makes it difficult to ultimately judge model performance [15].

Apart from re-estimating the local speed-up effects at the sites, CFD tools are frequently used to identify critical areas where wind conditions are particularly difficult to predict. Often CFD models are the only possibility to estimate turbulence, shear and inflow angle at the wind turbine's location which makes them a valuable tool for minimizing the technical risk of layouts at more complex sites.

Currently, the most widely used CFD tools are based on RANS solutions (Reynolds Averaged Navier Stokes). With ever-increasing computer power high-fidelity **LES** (Large Eddy Simulation) models are starting to be used for commercial applications.

5 The First Step: Site Identification

The wind resource is one of the most critical aspects in planning a wind farm. Different approaches are possible to obtain information about the wind climate. Wind atlases show colour-coded wind speed or energy for a given height above ground and are often used for the initial screening of suitable sites. The level of detail of the underlying flow model as well as its spatial resolution determines the quality of the atlas. One example is the Global Wind Atlas [16], which in its third version has a spatial resolution of 250 m. It is based on the mesoscale model WRF (Sect. 4.2) and initialized with the reanalysis data ERA5 (Sect. 4.1). For selected countries where this atlas has been validated with measurements, the mean absolute bias is given as 14% with an uncertainty of 10% [16]. The quality of a wind atlas can be improved by calibration with either measured wind or production data.

Hardly any other step in the process of wind farm development is as significant for economic success as the correct assessment of the wind regime at the future turbine site. Due to the cubic relationship between wind speed and energy content in the wind, the prediction of energy output is extremely sensitive to the accuracy of the wind speed and requires every possible attention.

6 The Second Step: Measuring the Wind Climate

6.1 Introduction

The measured wind climate is the main input for the flow models, which are used to extrapolate the measured wind vertically and horizontally to establish the spatial distribution of available energy across the site at hub height. The resulting resource map is the basis for the development of layouts.

The importance of wind speed measurements places very high demands on the quality of the instruments since the available kinetic power is proportional to the cube of the wind speed. Being exposed to harsh conditions, the measurement instruments must be robust and able to provide reliable data even during prolonged, unattended operation. Ideally, their power consumption should be low so that they can operate independently of the grid.

Any wind resource assessment requires a minimum measurement period of a full year to avoid seasonal bias. A shorter measurement duration leads to higher uncertainty [17]. If the instrumentation fails due to lightning, icing, vandalism or other reasons, and the failure is not quickly detected and rectified, data are lost. Often it is possible to compensate for the lost data, but the reduced data integrity will always lead to an increased uncertainty as potentially a bias can be introduced. In the worst case, the measurement period will have to start all over again; otherwise, the increased uncertainty could jeopardize the feasibility of the entire project.

The requirements for wind measurement are defined by the standard for power curve measurement, the IEC 61,400-12-1 [18]. In the context of power curve measurements, the standard describes the use of mast-mounted anemometers as well as remote sensing systems. Whereas the 2017 edition of IEC 61,400-12-1 does not allow a stand-alone use of remote sensing but requires the combination of remote sensing systems with a co-located measurement mast, today's reality is an increasing number of measurement campaigns based on stand-alone remote sensing systems.

The IEC standard describes suitable geometries and mounting arrangements for anemometer on the measurement mast which aims to minimize the influence of the mast's structure in the measurement. The measurement behaviour of the anemometers depends on several local climatic conditions such as turbulence, temperature and others. The impact of these factors is described through a so-called class number, which must be determined once for each anemometer model and describes its measurement uncertainty related to operational behaviour. The process is similar for remote sensing devices and involves the determination of the instrument's response to a range of climatic conditions compared to mast-mounted anemometers.

Great emphasis is placed on traceability of the instruments. This includes the calibration prior to and sometimes after the measurement campaign. Both cup anemometers and ultrasonic anemometers have to be calibrated in a MEASNET accredited wind tunnel [17–19]. Alternatively, the calibration can happen through comparison in situ with a reference anemometer [20]. Equally, the functionality of remote sensing systems has to be verified, where the behaviour of the individual system is ensured through comparison with a measurement mast.

In addition to wind speed and direction at several heights, other signals can be captured. These may include barometric pressure, relative humidity and temperature. All these parameters have an influence on the energy yield of the wind turbine. If additionally differential temperature measurements are performed, conclusions can be drawn about the atmospheric stability. Furthermore, in complex terrain [17] suggests the measurement of all three flow components (u, v & w) to determine the inflow angle.

The number and height of the measurements depend on the hub height of the planned wind turbines and the complexity of the site, since the uncertainty of the flow models increases with increasing complexity: The more complex the site, the more representative positions should be captured by the measurement campaign and the more important are hub height measurements to allow an accurate prediction of the wind resources.

Today (in 2022), there is no dedicated international standard for wind resource determination available, however, an international IEC standard for site assessment, IEC 61,400-15, is under development. Guidance can be found in the national Technical Guideline for Determination of Wind Potential and Energy Yields [19] issued by the Fördergesellschaft für Wind (FGW) as well as in the international Guideline for the Assessment of Site-specific Wind Conditions [17] issued by MEASNET. Both go beyond the IEC 61,400-12-1 in terms of content and describe procedures and the necessary documentation for calculating wind resources.

6.2 Anemometer

6.2.1 Cup Anemometer

Most onsite wind measurements use traditional cup anemometers. The cup anemometer has three cups, each mounted at the end of a horizontal arm, which in turn are arranged in a star shape on a vertical shaft. A cup anemometer rotates in the wind because the drag coefficient of the open cup is greater than the drag coefficient of the smooth back of the cup. Any horizontal flow will cause the anemometer to rotate proportional to the wind speed. Therefore, the rotational speed over a fixed period can be used to determine the average wind speed. The exact transfer function between the rotational speed and wind speed is best determined by calibration in a MEASNET accredited wind tunnel, which follows the s strict requirements as defined in [20]. MEASNET members regularly participate in round-robin tests to ensure comparability of results between different tunnels. The round-robin tests have significantly increased the quality of calibration. It should be noted that even calibrations to the highest standard have an uncertainty of about 1–2%.

In addition to the uncertainty related to calibration, further uncertainty arises due to the altered operational behaviour of the anemometer in the free atmosphere compared to the conditions in a wind tunnel, where the anemometer has been calibrated.

A distinction is made between static and dynamic effects. The description of the static behaviour includes the instrument's response to inclined flow, which can be caused either by terrain effects, thermal effects or mounting errors. According to IEC 61,400-12-1 [18], the anemometer should only measure the horizontal component of the wind, but not the vertical component. Furthermore, the friction in the bearing of the anemometer should be as independent of the temperature as possible.

The most relevant dynamic characteristic is the so-called over-speeding. Due to the aerodynamic properties of the cups, the anemometer tends to accelerate faster than it decelerates, which leads to an overestimation of the wind speed, especially in the medium wind speed range. Another dynamic property is described by the distance constant, which refers to the responsiveness of a cup anemometer following a step change in wind speed. The distance constant is the equivalent to the length of air stream which passes the anemometer during the time taken for it to respond to 63.2% of the step change. The distance constant should be as short as possible and is usually a few metres. Various methods for determining the distance constant are described in [21].

The individual response functions of the above-described static and dynamic behaviour are combined in the form of a class number. From this, the uncertainty of the operating behaviour for a specific anemometer brand can be determined as a function of the wind speed [18]. If the individual response functions were accessible by the anemometer manufacturer, the uncertainty of the operating behaviour could be determined specifically for the turbulence, inflow angle and temperature prevailing at the site. Unfortunately, only a few manufacturers currently provide this information.

The behaviour of the cup anemometer is well understood. Possible sources of error affecting the measurement include the effects of the measurement mast, boom and other mounting arrangements. Of course, proper maintenance of the anemometer is important. Problems can also occur due to icing of the sensor. By combining a heated and an unheated anemometer at the same measurement height, icing can be readily identified. Other climatic factors can affect the life of an anemometer such as corrosion near the sea or wear of the bearing in desert climates due to sand. Therefore, it is recommended to replace anemometers after 1 year.

6.2.2   Ultrasonic Anemometer

Ultrasonic anemometers, as the name implies, use ultrasonic signals to measure wind speed and direction. In addition, the sound virtual temperature can be determined, although this is dependent on the humidity of the air. The sound virtual temperature can be used to determine the Monin–Obukhov length (see Eq. 3). Ultrasonic anemometers have up to three transmitter–receiver pairs (sonotrodes). A three-axis sonic anemometer can provide a very high-resolution measurement of the three-dimensional wind vector (Fig. 22). The sonic anemometer operates on the principle of precisely measuring the time it takes an ultra-high frequency acoustic pulse (typically 100 kHz) to traverse a known path length in the direction of the wind and opposed to it. From the transit-time difference, the velocity of the flow can be determined. The wind measurement is independent of the air density and humidity.

Motionless ultrasonic anemometers have a number of advantages over mechanical anemometers and can provide measurements of turbulence, air temperature and

Fig. 22 Ultrasonic anemometer with three sonotrodes
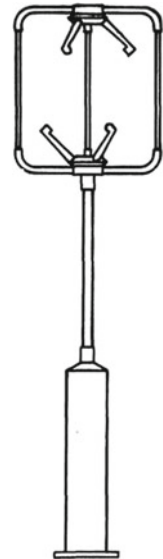
atmospheric stability. The measurement of all three wind components, the absence of moving parts and the high temporal resolution make the ultrasonic anemometer a very attractive wind speed-measuring instrument. In particular, the high temporal resolution makes ultrasonic anemometers more suitable for turbulence measurements than cup anemometers. In addition, the probe arms are easily heated, so that it can be used well in regions subjected to ice and snowfall.

However, ultrasonic anemometers also introduce new, less well-known sources of error. To ensure the necessary mechanical stability, the probe arms must be sufficiently robust in design, but at the same time, they should influence the airflow as little as possible. Due to the influence of the probe arms and the sensitivity of the measurement principle to small deviations in geometry, the absolute accuracy of ultrasonic anemometers is generally lower than that of high-quality cup anemometers [21]. Temperature variations can also affect the geometry. Less known is the fact that the sensors themselves are temperature sensitive. Furthermore, it should be considered that most ultrasonic anemometers have a higher power consumption than cup anemometers and can hardly be powered by batteries or solar-powered power supplies.

6.2.3 Measurement Mast Geometry

To perform accurate wind speed measurements, the instruments should be influenced as little as possible by the changing flow through and around the mast and the side booms. The influence of the mast can be minimized by sufficient distance between mast and instrument as well as the careful choice of the side boom's orientation with respect to the main wind direction. The influence of the mast on the measured wind speed should be less than 1% and the influence of the side boom less than 0.5% [18]. Other instruments, aviation lights and lightning protection should be mounted so as to minimize interference on the anemometer.

The influence of the mast on the flow depends on the type of mast. In front of tubular masts, the wind slows down and is accelerated around the sides (Fig. 23, left). Therefore, the least interference is achieved when mounting the side boom 45° to the main wind direction. The minimum distance from the centre of the mast should be 6.1 times the diameter of the tubular mast, but 8.2 times is better [18].

The flow conditions around a lattice mast are more complicated to determine. In addition to the orientation of the mast with respect to the wind, the distance of the anemometer to the mast centre, also the drag of the mast plays a role. Similar to the tubular mast, a deceleration in front of the mast can be observed, while an acceleration occurs at the flanks (Fig. 23, right). The least impairment is achieved when the side booms are mounted at 90° with respect to the main wind direction. The minimum distance from the centre of the mast should be 3.7 times the width of the lattice mast, but better 5.7 times [18].

Top-mounted instruments are generally less affected by the mast's structure than side-mounted instruments. Still, care has to be taken, as the support tube of the instrument has to be sturdy enough to avoid wind-induced vibrations. However, as a
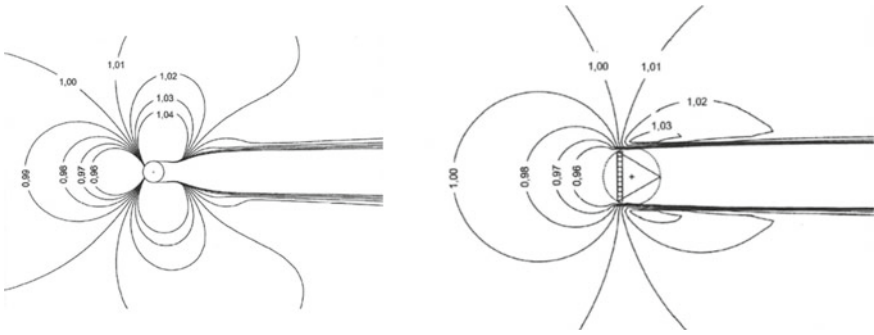
Fig. 23 Wind speeds around tubular mast (left) and lattice mast (right) normalized to free wind speed coming from left, based on [19]

consequence, the construction might become heavy, which can drive up the price of the mast. Additionally, top-mounted instruments are more susceptible to lightning strikes. Figure 24 shows possible arrangements of the top mounting.

Instruments at lower heights are obviously side-mounted. To minimize the influence of the side boom, the instrument should be mounted approximately 20 times the boom diameter above the boom. Further details on the determination of flow distortion can be found in [18, 21].

In general, redundancies should always be present. Mounting two opposing instruments at the same height allows correction of the mast influence.
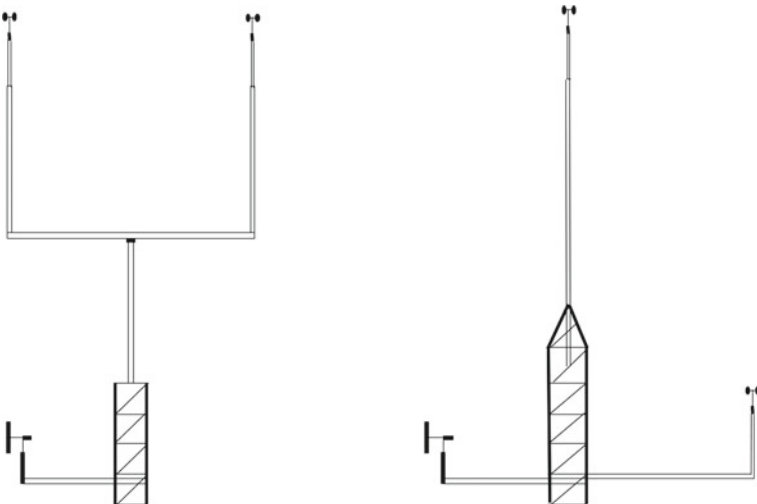
Fig. 24 Possible measurement geometries at the top of a mast

6.3 Remote Sensing Systems

Ground-based remote sensing systems are an alternative to mast-mounted anemometry. Two technologies have gained some acceptance in the wind energy community: LiDAR and SoDAR. Both LiDAR (Light Detection And Ranging) and SoDAR (Sound Detection And Ranging) use remote sensing techniques. Most systems are based on the Doppler effect. The signal emitted by a LiDAR is scattered by aerosols, while the signal emitted by the SoDAR is scattered by temperature fluctuations.

In many countries around the world, the process of obtaining a building permit for sufficiently tall measurement masts requires the involvement of, aviation or even military administrations. This often leads to disproportionately long planning periods and high costs, which do not occur when using remote sensing systems. According to IEC 61,400-12-1 [18], however, the use of remote sensing devices requires a co-located moderately high mast (e.g. 60 m). Such a hybrid system combines the high absolute accuracy and high availability of the cup anemometer with the greater vertical range of the remote sensing system. Like the anemometer, the operational behaviour of remote sensing systems depends on several conditions in the free atmosphere. This dependence of the behaviour is quantified by a class number, which has to be determined once for each model. The class number allows the determination of the measurement uncertainty.

As with anemometers, the measurement campaign using remote sensing should last at least one year, since the vertical profile varies greatly with different atmospheric stabilities, which are connected to seasonal and diurnal variations.

In contrast to the very small measurement volume of a cup or ultrasonic anemometer, both remote sensing technologies measure large volumes that change with altitude, which impacts direct comparisons to anemometer measurements. Both technologies require significantly more power than anemometers, making the use of a generator or fuel cell necessary.

While the precision of a LiDAR is superior to a SoDAR, and can approach that of cup anemometers [22], both instruments have an inherent weakness in complex terrain, as both measurement techniques assume homogeneity of the wind vector in the measurement volume, which is not the case for non-flat terrain (Fig. 25). There is evidence that errors of 5–10% in mean wind speed are not uncommon, e.g. [23]. Only a multiple remote sensing system, where several sufficiently separated units focus on the same volume, could eliminate this inherent error. Alternatively, the measurement error due to inhomogeneity can be reduced by numerical correction, e.g. through CFD models.

Another challenge is the interpretation of the measured turbulence intensity in connection with the verification of the turbine's suitability at the site according to IEC 61,400-1 [3], see Sect. 9.1. Since the measurement volume of remote sensing systems differs significantly from measurement volumes of traditional anemometry, the turbulence measured by remote sensing differs from that measured by a cup. This creates a deviation from the IEC 61,400-1. The industry initiative CFARS (Consortium for the Advancement of Remote Sensing) is currently working on a systematic

Fig. 25 Inhomogenous flow
in the measurement volume
[24]
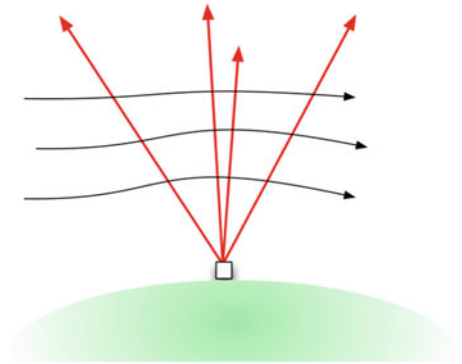
comparison and quantification of the influence of different measurement technologies on loads.

6.3.1 LiDAR

A LiDAR focuses on a specific distance and measures the frequency shift of the returning signal, which is scattered by the aerosols within the focal volume. Because light can be focused much more accurately and scatters much less in the atmosphere than sound, LiDAR systems have higher accuracy and a better signal-to-noise ratio than SoDAR. Most LiDARs can be divided into two categories.

The continuous wave LiDAR uses an optical system to focus on different heights (Fig. 26, right). Through a continuously rotating prism, the vertical laser beam is deflected 30° from the vertical. By adjusting the laser focus, the wind vector can be scanned along the circumference of a cone at different heights above the ground. The length of the measurement volume is defined by the optics of the device and the measurement height. Typically, it increases with the square of the measuring range.

The other system uses a pulsed signal with a fixed focus (pulsed LiDAR). In contrast to the continuous wave LiDAR, its prism does not rotate continuously (Fig. 26, left). Instead, the prism remains stationary, while the LiDAR sends a pulse in a specific direction and records the backscatter in a series of range windows (fixed time delays) triggered by the end of each pulse. In contrast to the continuous wave LiDAR, the probe length is constant with height.

LiDAR relies on the backscatter of aerosols carried by the wind to estimate wind speed. Variations in the vertical concentration of backscattering particles can lead to uncertainties in wind speed measurements. For example, if clouds or fog are present along the line of sight, there is a risk that strong reflections from the cloud or fog will swamp the Doppler signal, potentially resulting in a falsified wind speed estimate. Processing algorithms for cloud detection have been developed to identify, reduce or remove scatter from clouds and fog.
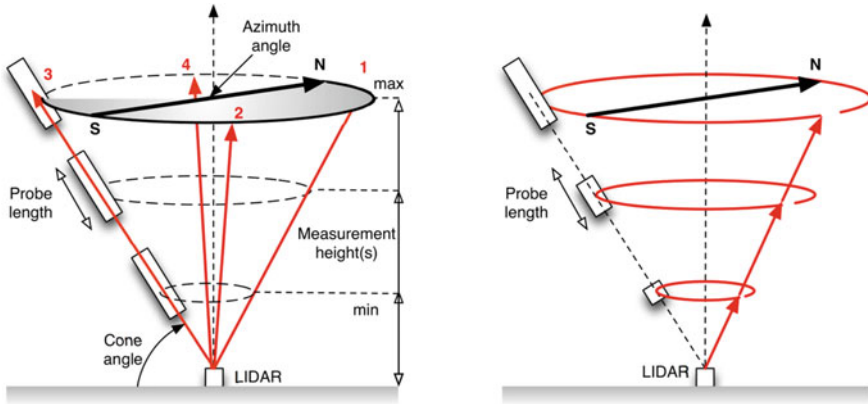
Fig. 26 Schematics of working principles of a pulsed lidar (left) and a continuous wave lidar (right) [24]

However, also an insufficient amount of particles, e.g. in very clean air, affects the functionality of the LiDAR. Other parameters that affect the measurement are errors in the vertical alignment of the instrument and uncertainties in the focusing height. The LiDAR, as an optical instrument, is also susceptible to the effects of dirt on the exit window, so there is a need for a robust cleaning device of the LiDAR window.

LiDARs have many different applications today: The vertical conical scan shown in Fig. 26 is used not only in the context of wind resource measurements but also for power curve measurements. In the offshore sector, LiDARs are installed either on platforms or on buoys, also here with a vertical, conical scan. Floating LiDAR technology reduces the need for meteorological measurement masts as the primary source of data to describe wind resources. The devices measure wind speed and direction at a fraction of the cost of conventional measurement masts. Savings of up to 90% are possible, based on a typical investment of 10 million euros for a measurement mast. To achieve commercial acceptance for investment decisions based on this relatively new technology, a roadmap has been formulated [25]. Through the definition of key performance indicators in terms of accuracy and availability, the roadmap provides a clear framework for floating LiDAR providers to reach full commercial acceptance.

LiDARs with conical scan patterns can also be mounted on the nacelle (Fig. 27). This mounting arrangement allows the measurement of the power curve according to IEC 61,400-12-2 [26]. In addition, the possibility of using knowledge of approaching gusts for active load control is currently being investigated.

Furthermore, through more complex control of the prism, LiDARs can also perform fan-shaped scans (Fig. 28). Often these scanning LiDARs have a longer range than the vertical scanning LiDARs, which can be in the range of several kilometres. Such measurements are used, for example, in complex terrain to locate flow separation, or to verify wake models. When positioned on existing offshore wind turbines or on the coast, scanning LiDARs can also be used to quantify wind resources in the vicinity.
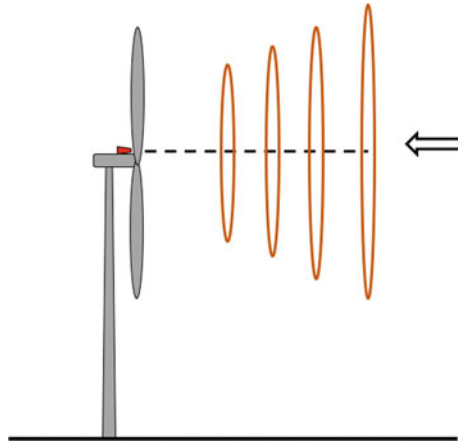
Fig. 27 Forward-looking nacelle-mounted lidar
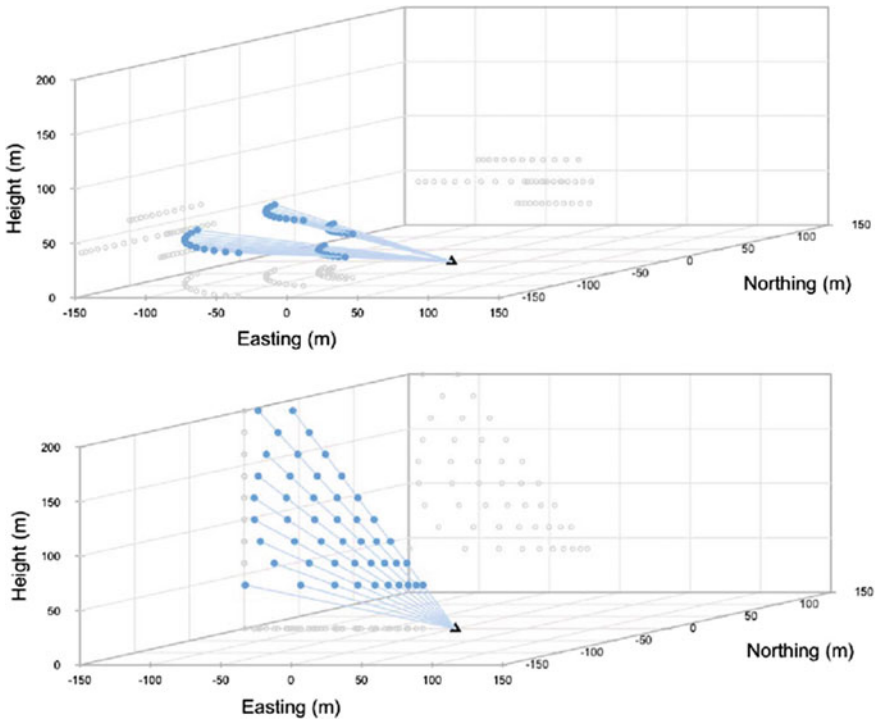
Fig. 28 Examples of different scan geometries of a scanning lidar [27]

6.3.2 SoDAR

There are different types of SoDARs with different arrangements of transmitter and receiver. A common variant is the phased array SoDAR, which consists of a combined transmitter–receiver array, i.e. it is monostatic. This array is electronically controlled to direct sound pulses in different directions, one in the vertical direction and two other directions at 90° to each other (Fig. 29). Assuming that the flow field in the volume covered by the three beams is homogeneous, the wind vector can be constructed from the three signals. Thus, in non-flat terrain, any measurement of a SoDAR is inherently error-prone just like that of LiDAR.

One of the disadvantages of a SoDAR is its dependence on temperature fluctuations, which is challenging under neutral and stable atmospheric conditions. Bistatic SoDARs, on the other hand, where the transmitter and receiver are spatially separated, are sensitive to inhomogeneities in wind speed and do not have this problem. However, bistatic SoDAR units are not currently commercially available.

Since the SoDAR is an acoustic system, the presence of ambient noise can affect the function of the SoDAR. The noise source can be rain, but also other noises, for example from animals, can have a negative effect. A particularly critical issue is the increase of noise in high wind speed situations. These situations are often associated with neutral stability and suffer from the lack of sufficient temperature fluctuations. False echoes from nearby objects such as house walls or trees can also

Fig. 29 Principle of a three-phased array SoDAR
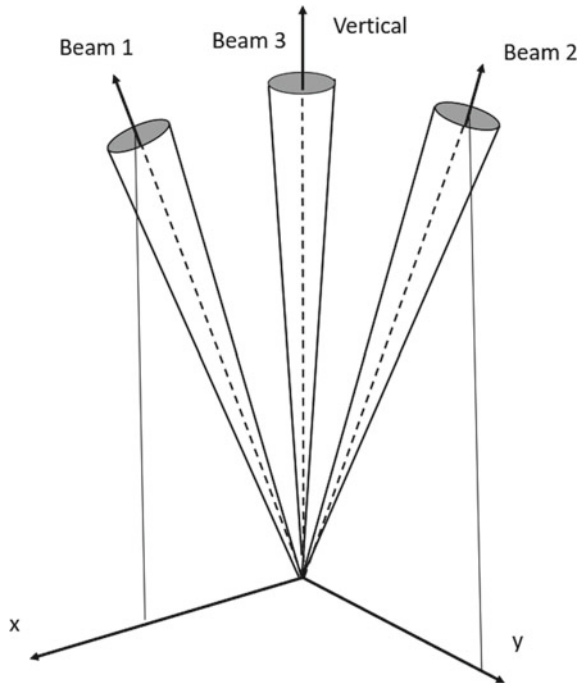
lead to a distorted signal. Other parameters that can affect the SoDAR measurement are errors in the vertical orientation of the instrument and temperature changes at the antenna. With an increasing altitude above ground, the signal-to-noise ratio of the SoDAR deteriorates, such that the data availability decreases.

For these various reasons, the measurement accuracy of SoDAR systems does not reach that of cup anemometers. At the same time, the measurement volume changes with altitude due to the aperture angle between the three beams. Therefore, a measured profile is difficult to interpret, since it can be based on a different number of measured values as well as a different measurement volume per height.

6.4 Production Data

Another very good source of information for the assessment of the wind regime are production data from nearby wind farms. These can be used to calibrate the flow model. However, production data are often only accessible on a monthly basis. In order to filter out months with unrepresentative production caused by issues such as grid curtailment or icing, these data are often checked for plausibility with a wind index. However, experience clearly shows that this method is not always sufficient, since periods with grid curtailment and other suboptimal performance cannot always be identified and thus lead to a contamination of the monthly production data. Consequently, this can then lead to an incorrect calibration of the flow model and ultimately falsify the result for the project under investigation.

In contrast to monthly production data the use of 10 min SCADA data allows precise identification and correction of non-optimal production periods and is thus preferable. If an existing wind farm is used to study a future project, analysis of SCADA data provides information not only from one position, but from several, and is consequently often superior to wind measurements, which are typically only available for a limited number of positions. Furthermore, the wake model can be calibrated for the existing wind turbines (Sect. 10.2). If the existing and planned wind farms are comparable with respect to terrain, size and layout, the found parameterization of the wake model can be assumed to be valid for the future turbines.

6.5 Measurement Period and Averaging Time

The energy yield is calculated based on the distribution of wind speeds at the site. However, the annual wind distribution varies considerably from year to year. Depending on the local climate, the annual mean wind speed values can vary by $\pm 15\%$ from one year to the next. To reduce the uncertainty of the interannual variability, a long-term correction of the measured data is performed (Sect. 7.3). However, on a monthly scale, the wind speed variability is much stronger, depending on the local climate—reaching variations of $\pm 50\%$. Therefore, it is of crucial importance
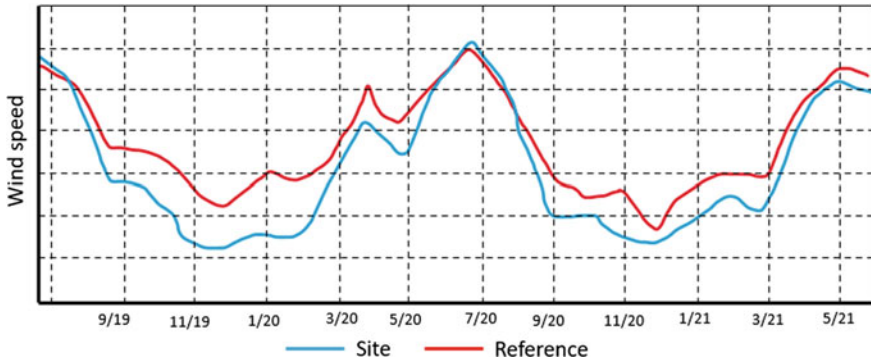
Fig. 30 Seasonal bias: example of deviation between onsite and reference data during winter

to measure whole years, because often the seasonal variations of the long-term reference data differ from those at the site. Figure 30 shows, for example, a significant difference between site and reference data in the winter months, while, in the summer months, the difference is negligible. A correction of a short-term measurement with less than 12 months using reference data would therefore be subject to error.

Normally, wind data are averaged over a period of 10 min. For this period, the standard deviation of the wind speed, which is necessary for the determination of the turbulence intensity, is calculated by the data logger. The averaging period of 10 min allows the data to be used directly for load calculations [3], as these also refer to 10 min averages.

7 The Third Step: Data Analysis

7.1 Quality Control

Both, the short-term and long-term, reference data should be subjected to rigorous quality control. This is mainly done manually but is supported by filter algorithms that flag unusual behaviour. The direct comparison of site data with long-term data can offer advantages here, for example, to check the wind direction measurements.

When using anemometers, special attention should be paid to possible signs of icing. Often heated instruments are combined with unheated ones as a deviation between the two sensors indicates icing. Wind vanes often ice up earlier than the rotating cup anemometers. Thus, a constant wind direction may also be an indication of ice. Such questionable periods should be excluded from further analysis.

Depending on the technology, low clouds and fog can affect the function of a LiDAR and lead to erroneous measurements. Furthermore, the quality of the signal can suffer in particularly clean air due to a lack of aerosols necessary to reflect the signal.

SoDARs require temperature fluctuations in the air to reflect the signal. Therefore, special attention should be paid to periods of stable or neutral stratification, as the functionality of the SoDAR may be impaired under these conditions.

7.2 Data Corrections

For further analysis, the highest possible data integrity is necessary. In general, at least 90% of the data should be available after filtering [17]. The data gaps caused by missing data or quality control can lead to systematic measurement errors, especially if the gaps are not randomly distributed but occur cumulatively in certain meteorological situations such as wintertime or certain times of the day. Therefore, data gaps of the relevant sensors such as wind speed and direction should be closed where possible by reconstructing the missing data from readings of other sensors to increase the data availability. For filling the data gaps, Measure-Correlate-Predict (MCP) methods are usually used to fill the data gaps (see next section).

7.3 Long-Term Correction

Weather, and therefore wind speeds, vary from year to year. Onsite data for the analysis of wind resources tend to cover a limited period, which in many cases is less than 5 years. The question therefore arises to what extent this measurement period is representative. Long-term measurements have shown that variations in wind energy beyond 20% occur [7]. For a proper assessment of the economic viability of a project, this variability must be considered. Each short-term measurement should therefore be corrected with long-term, reference data. This correction is based on the assumption that the short- and long-term data sets are well correlated. The coefficient of determination R^2 is used to quantify the quality of the correlation. R^2 of wind speed should not be less than 70% for a temporal resolution of 10 min [19]. In addition to the correlation of wind speed, the representativeness of wind directions should be checked. The k parameters of the frequency distributions should also be similar.

Today, reanalysis data (Sect. 4.1) are commonly used as long-term data, either directly or spatially refined through mesoscale models. Generally, weather stations are too strongly influenced by changes in their surroundings, such as growing vegetation or construction activity, and are therefore often inconsistent. However, even with reanalysis data, care must be taken in the choice of long-term period. Since both the composition of the input data of the reanalysis models as well as the assimilation models, can change over time, a reference period of 20 years is often chosen as a compromise, even though reanalysis data from longer periods might be available. In general, the interpretation of trends in long-term series is difficult because it is not possible to distinguish between natural trends and trends due to inconsistent input data or changes in the assimilation models. Only if there is absolute certainty, that

an observed trend is artificial and has no physical background, detrending of the long-term data can be considered.

Frequently, several long-term data sets are compared with each other. However, this has only a limited effect on the interpretation of trends since most reanalysis models are based on the same input data and are thus not statistically independent.

In principle, two different strategies for long-term correction can be distinguished.

The statistical method for correcting the short-term data is called **Measure-Correlate-Predict** or MCP. Here, for the concurrent period, a mathematical relationship is established between the short- and long-term data. The application of this mathematical relationship results in a synthetic long-term data series. Exemplary methods, which can be used to establish the relationship, are given below:

- Regression analysis: Here, the linear regression of the wind speeds of the short-term and long-term data is determined either omnidirectionally or by wind direction sector.
- Matrix method: The matrix method is based on the comparison of wind direction and wind speed frequency distributions to derive the statistical relationship between measured data and reference. A realistic estimation of distribution functions is important, also when data coverage is low. It should be noted that not every matrix method has sufficient conservation properties with respect to the statistical moments of the frequency distribution.
- Nonlinear methods such as neural networks.

In general, MCP methods require a high temporal data resolution and sufficient data coverage for all energy-relevant wind speeds. The chosen MCP method must be able to reproduce the original measured data without significant errors. Simple linear regressions of wind speed do not preserve energy, so additional measures are required to ensure energy conservation. However, such measures can reduce the quality of a correlation.

Instead of transposing the wind distribution from the reference station, **scaling methods** determine a correction factor for the short period data. For the short-term measurement period, the energy level of the reference data set is determined and compared with the energy of the total long-term period. The resulting ratio is then applied as a correction to the short-term onsite data. This procedure has the disadvantage that the wind rose measured onsite remains unchanged and should therefore only be used if the wind directions were representative during the measurement period.

8   The Fourth Step: Spatial Extrapolation

The analysis of the wind speed measurements results in a detailed description of the wind climate at several heights, but at one position only. To calculate the energy yield of the entire wind field across the site, the measurement results must be extrapolated vertically from measurement height to hub height and horizontally across the wind farm area.
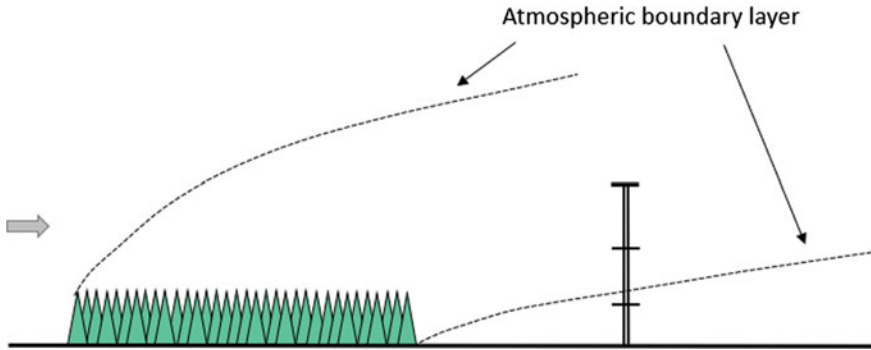
Fig. 31 Influence of internal boundary layer caused by a forest on a nearby measurement mast

The vertical extrapolation can be carried out either with the help of a flow model or by using the measured shear. The decision of which of the two methods is to be preferred depends on the conditions at the site and the geometry of the measurement.

Using measured shear for vertical extrapolation, has the advantage that the resulting time series of wind speed at hub height reflects varying atmospheric stability. It is thus preferable to the use of average atmospheric stability such as would be the case were WAsP to be used. However, if the measurement instruments are subjected to varying degrees of shadowing at different measurement heights, the measured shear will be falsified. This can be the case, for example, if the topmost instrument is placed at the tip (cf. Fig. 24, right), but the instruments at lower heights are mounted on side booms. Figure 31 shows another situation where the measured shear is distorted: The top two measurement heights are in the boundary layer caused by a nearby forest, while the lowest measurement height is free from the influence of the forest. The measured shear over all three heights is most likely not representative for the future positions of the wind turbines and should therefore not be used for vertical extrapolation.

For the horizontal extrapolation, microscale flow models are used (see Sect. 4.3). It is important to note that even advanced flow models have their limitations if the similarity principles are violated and the site characteristics of the proposed wind turbines deviate significantly from those at the measurement site.

9   The Fifth Step: Choosing the Wind Turbine

In the design of wind turbines, a number of assumptions are made that describe the wind climate on site. Since the robustness of a wind turbine is directly related to the cost of the machine, a system has been established to divide sites into different categories in order to optimize the costs of the wind turbines. The site class according to IEC Standard 61,400-1 [3] depends on the mean wind speed and the extreme wind

Table 3 Classification of WTGs according to IEC 61,400-1 [3]

Class	I	II	III	S
V_{ave} (m/s)	10	8.5	7.5	Manufacturer specified values
V_{ref} (m/s)	50	42.5	37.5	
Tropical V_{ref} (m/s)	57	57	57	

speed V_{ref} at hub height (see Table 3). The term extreme wind is used for the maximum 10 min average wind speed with a 50-year return period at hub height. For sites in areas with tropical cyclones, a design for particularly high extreme winds is required. A fourth class, the S class, allows manufacturers one or more deviations from the parameters of the first three classes.

In addition, three different turbulence classes for sites with low, medium and high turbulences were introduced. They are parameterized by I_{ref}, where I_{ref} represents the turbulence intensity at 15 m/s. I_{ref} has the values 0.12, 0.14 and 0.16 for the standard turbulence classes *A*, *B* and *C*, respectively. So, a site can be classified as I*A*, II*B*, III*C* or *S*, for example.

When selecting a suitable wind turbine for a specific site, this table can be used to determine the required wind class. At this point, it must be pointed out, that direct conclusions from the average wind speed to the extreme winds at hub height are not possible!

The mean wind speeds V_{ave}, the extreme winds at hub height V_{ref} and the turbulence I_{ref} are not the only relevant factors. In the context of certification of a proposed project, in addition to these parameters, the distribution of wind speed (*k* parameters, see Sect. 3.2), flow inclination (or inflow angle), shear (gradient) and turbulence are compared with the assumptions of the type certification of the wind turbine. The individual parameters, their cause and effect are explained below.

9.1 Turbulence

Section 1.4 describes ambient turbulence and its causes. In addition to ambient turbulence, turbulence is generated by neighbouring wind turbines, which also leads to increased mechanical loads.

Figure 32 shows the additional wake-induced turbulence intensity as a function of the distance between two wind turbines, expressed as a multiple of the rotor diameter [28]. These results are based on measurements at four sites of different complexity. The Frandsen model [28] defines the so-called effective turbulence, which is a combination of ambient and wake turbulence integrated over all directions and takes the accumulation of fatigue based on material properties into account. The calculated effective turbulence is based on the 90th percentile of the measured ambient turbulence and must be compared with the normal turbulence model (NTM) as a design limit according to IEC 61,400-1 [3] for a range of wind speeds. During the

Fig. 32 Wake-induced
turbulence intensity
according to Frandsen [28]
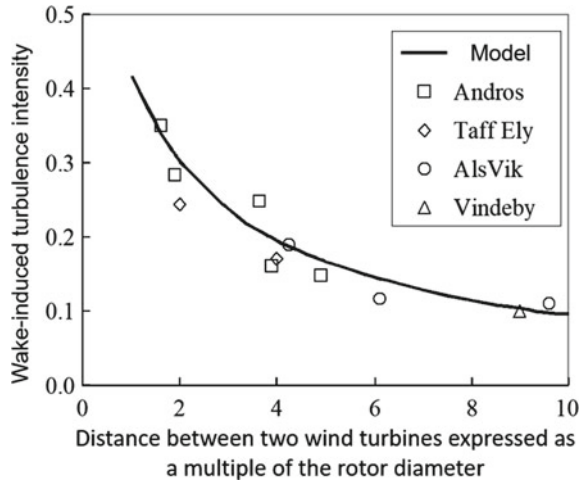
planning phase, it must therefore be ensured that the effective turbulence intensity
does not exceed the turbulence intensity assumed in the certification.

Turbulence is the main cause of material fatigue. In particular, turbulence causes
bending of the blade root. The turbulent wind field also causes alternating torsion of
the drive train. In addition, the tower is subjected to thrust (Fig. 33).

Fig. 33 Impact on loads due
to turbulence
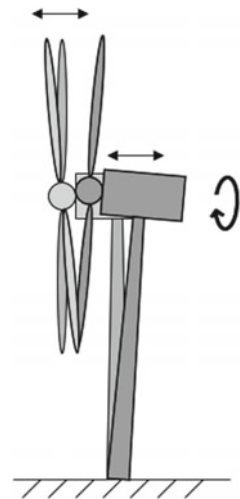
9.2 Vertical Gradient (Shear)

The wind speed difference between the top and bottom of the rotor is another wind load parameter, which has to be assessed when reviewing the turbine's suitability for the site. This difference is usually expressed as the height exponent α as used in the power law (Eq. 6). As a default value the IEC 61,400-1 assumes a shear exponent of 0.2 as the basis for the load calculations.

Since the blades experience a different angle of attack with each rotation due to wind speed differences at top and bottom of the rotor, alternating loads are caused on the blades. This leads to fatigue at the blade root. In addition, the rotating parts of the main shaft are subjected to bending (Fig. 34). It should be noted that not only high shear that causes excessive loads but also very small or negative shear. Therefore, locations with high as well as negative shear should be avoided.

A number of phenomena can cause large shear: In steep **terrain,** the flow might become separated. Consequently, the wind speed profile across the rotor might be distorted to such a degree, that parts of the rotor may even be subjected to negative shear (Fig. 12).

Similarly to steep terrain, large **obstacles** such as buildings or a forest can lead to distorted wind profiles as the wind speed at the lower part of the rotor can be strongly decelerated (Fig. 13). The degree of deceleration depends on the dimensions of the obstacle, its so-called porosity, and the distance of the turbine from the obstacle.

The **wake** behind a wind turbine is not only characterized by high turbulence (Fig. 32) but also by a clearly reduced wind speed compared to the surrounding area called the velocity deficit. The influence of a wake on the vertical wind profile is

Fig. 34 Impact on loads due to vertical shear
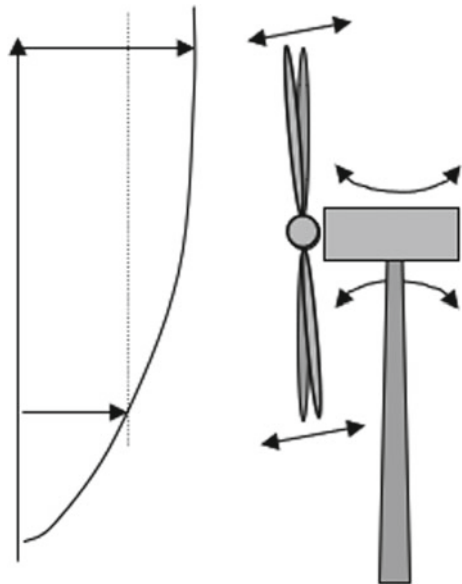
shown in Fig. 35. The dashed line shows the profile in front of the wind turbine, and
the solid line shows the profile behind the wind turbine. The deformed wind profile
clearly shows no only areas with negative gradients but also areas with very large
gradients.

In addition, partial shading of the rotor can also lead to strong horizontal wind
shear (Fig. 36). In this situation, the rotor experiences not only a vertical but also a
horizontal gradient, simultaneously with increased turbulence.

Finally, **atmospheric stability** is a driver for varying shear. As explained in
Sect. 2.3, higher shear exponents are to be expected, especially in winter months
and at night, while during summertime lower shear can be expected. Figure 8 docu-
ments the variation of shear exponents, ranging from negative shear up to values
around 0.8.

Fig. 35 Vertical wind
profile in front and in wake
of a WTG [29]
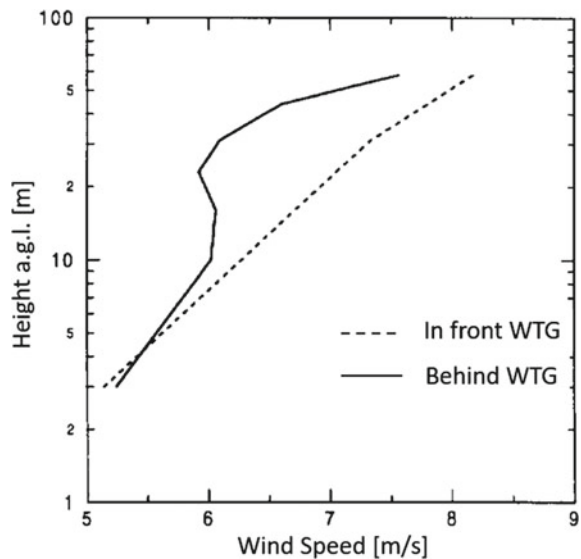
Fig. 36 Partial wake
situation
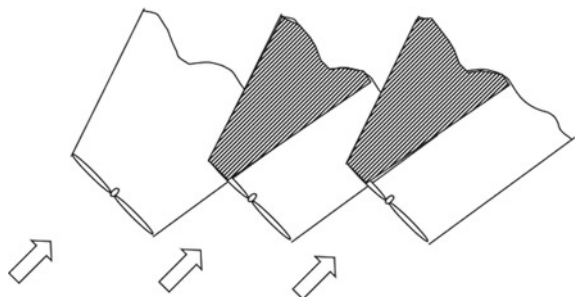
9.3 Inflow Angle

To benefit from the terrain-induced speed-up (Fig. 12), wind turbines are often installed at the point of greatest curvature of the terrain. An undesirable side effect of such a position is an inflow angle that deviates significantly from the horizontal. The inclined flow can lead to lower production, since the angular response of the wind turbine to inflow follows roughly a cosine and thus mainly the horizontal component of the wind contributes to the energy production.

In addition, the wind turbine is subjected to higher loads with increasing inflow angles. In particular, the fatigue loads on the blades increase as the blades are subjected to a constantly changing angle of attack. Also, the bending loads on the rotating parts of the drive train are increased. Finally, the uneven loading of the rotor causes additional loads on the yaw drive (Fig. 37).

As default, the IEC 61,400-1 [3] assumes an inclined flow of 8°. The inclined flow is naturally related to terrain slope. With increasing height above the ground, however, the influence of the terrain decreases. Especially in complex terrain, the limit value of 8° can quickly be exceeded. When placed in areas of flow separation, the flow can in the worst-case reverse and seriously damage the wind turbine.

A measurement of the inclined flow requires the measurement of all three wind components, for example, by using an ultrasonic anemometer at hub height. The measured inclined flow is only valid for the measurement position so that measurements can often only serve to verify a suitable flow model like CFD. However, scanning LiDARs can serve the purpose of identifying inflow across larger areas.

By optimization of the proposed layout, the technical risk due to flow inclination can often be controlled without significant loss of energy.

Fig. 37 Impact on loads due to non-horizontal inflow
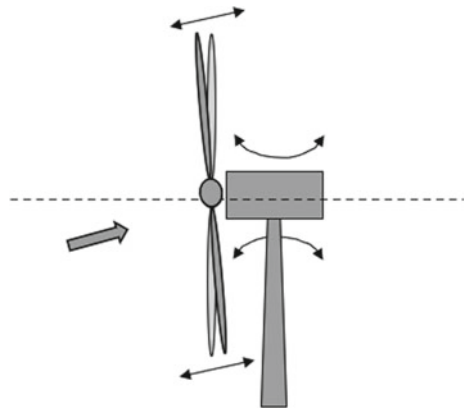
9.4 Extreme Winds

The selection of a suitable wind turbine for a site requires also knowledge of the expected maximum 10 min average wind speed V_{ref} with a return period of 50 years [3]. While local building codes often generalize the amplitude of extreme events over large areas, wind data measured on-site allows for a more accurate site-specific prediction of the expected 50-year event. Several methods allow to estimate the maximum 10 min wind speed at the site based on onsite data.

Like other climatic extremes, V_{ref} can often be described by a double-exponential Gumbel distribution [30]. The parameters describing the Gumbel-distribution are generally determined from plotting the measured extreme events against their rank. This so-called Gumbel plot ideally shows a linear relationship, the slope of this relationship is used to predict the 50-year event. Several methods are available to extract extreme events from a short-term data set and further fit the Gumbel distribution to these extremes [31]. However, all methods have one problem in common: the resulting 50-year estimate is strongly correlated with the highest measured wind speed event in the time series used for the analysis [32].

The European Wind Turbine Standard, EWTS [33], provides a way to estimate extreme wind based on the onsite wind speed distribution, rather than a measured time series. The EWTS provides a relationship between the shape of the wind distribution, described by the k-parameter, and the expected extreme wind (Fig. 16). The extreme wind is determined on the basis of the mean wind speed multiplied by a factor that depends on k. This factor is 5 for $k = 1.75$. For distributions with long tails (corresponding to a small k parameter), the factor is larger than 5. For distributions with a bigger k parameter, the factor is smaller than 5.

In addition to the maximum 10 min average wind speed at hub height with a return period of 50 years V_{ref}, the extreme 3 s gust V_{e50} has a critical influence on the wind turbine design and has to be established. The extreme 3 s gust is a function of V_{ref} and the turbulence intensity I_{ext}, which is the turbulence intensity that occurs during extreme winds.

$$V_{e50} = V_{ref}(1 + 2.8I_{ext}) \tag{9}$$

The relationship described in Eq. 9 is based on both experimental data and theoretical work. As mentioned in Sect. 1.4, caution is needed in offshore and forest situations because the turbulence intensity does not show an asymptotic behaviour but increases with increasing wind speed. It is therefore much more difficult to estimate I_{ext} under these conditions.

10   The Sixth Step: Energy Yield

10.1   *Energy Yield of the Individual Wind Turbine*

The estimate of annual electricity production is derived from the wind turbine hub height wind speed. The relationship between the generated electricity and the wind speed is described by the power curve.

Knowing the power curve of a wind turbine $P(v)$, the average electricity production can be estimated using the probability density function of the wind speed at hub height $f(v)$, typically expressed as a Weibull distribution (see Eq. 7).

$$P = \int_{0}^{\infty} f(v)P(v) \ dv = \int_{0}^{\infty} \frac{k}{A}\left(\frac{v}{A}\right)^{k-1} \exp\left(-\left(\frac{v}{A}\right)^{k}\right) P(v)dv \qquad (10)$$

This integral cannot be calculated analytically and must therefore be solved numerically. For this purpose, the power curve is divided into bins, typically in 0.5 m/s steps. The power output can now be calculated by summing the generated energy for each wind speed bin. As explained in Sect. 3.2, energy yield calculations are increasingly carried out in the time domain, i.e. a time series of production is calculated, as this approach is considered more correct and allows direct coupling to varying spot market prices.

Caution is advised as the energy contents of the wind are proportional to the air density. A power curve normally refers to an air density of 1.225 kg/m^3, which corresponds to a temperature of 15 °C at sea level. A higher altitude and/or a warmer location will result in a lower air density and thus a lower energy yield.

In addition to air density, a number of site-specific parameters influence the power curve and thus the energy yield. These parameters include turbulence, shear and the wind direction variation over the rotor surface (veer). IEC 61,400-12-1 [18] describes how these site-specific influence parameters can be taken into account in order to achieve comparability of power curves measured at different sites.

Figure 38 shows schematically the influence of turbulence: with increasing turbulence, the 'knee' of the power curve becomes flatter, but at the same time the power output increases for lower wind speeds. The overall influence of turbulence is therefore dependent on the wind speed distribution.

Shear also affects the power output. The simplification of the power curve referring to hub height wind speed becomes less and less suitable with increasing rotor size. Therefore, the so-called rotor equivalent wind speed (REWS) has been introduced, which accounts for the variation of wind speed across the rotor.
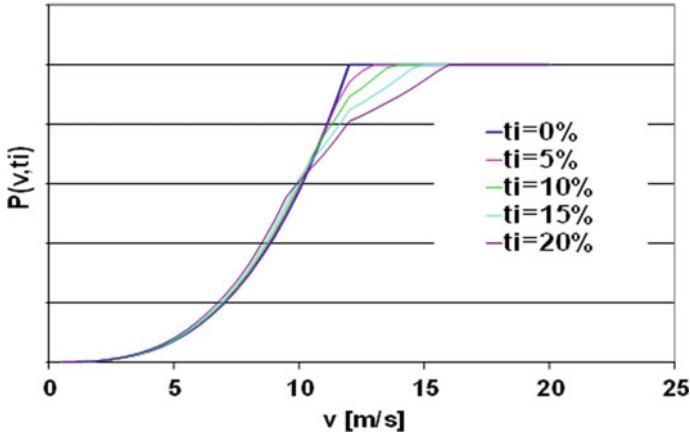
Fig. 38 Impact of turbulence intensity on the power curve

10.2 Energy Yield of the Wind Farm

Every wind turbine produces a wake. The wake describes the volume of reduced wind speed downstream of a wind turbine. If another nearby wind turbine is operating within this wake, the output of this downstream wind turbine is reduced compared to the wind turbine operating in the free wind. This power reduction depends on the wind turbine characteristics, the wind farm geometry and the wind climate. The wind turbines operating in the wake are not only subject to reduced wind speed (as shown in Fig. 35) but also to an increased dynamic load—due to the increased turbulence caused by the upstream wind turbines (Fig. 32). This increased turbulence must be taken into account when selecting a wind turbine class suitable for the wind turbine (Sect. 9.1).

Two models are commonly used in the industry to calculate the impact of upstream wind turbines on energy production, the N.O. Jensen model [34] and the eddy viscosity model of Ainslie [35].

The N.O. Jensen model is a simple kinematic model, which describes the speed reduction caused by a single turbine through a wake decay constant. The model is based on the assumption that the wake expands linearly as a function of the distance x to the rotor (Fig. 39).

The N.O. Jensen model describes the reduced velocity v_w (w for wake) in the rotor plane as follows:

$$v_w = v_0 \left[1 - \left(1 - \sqrt{1 - c_t} \right) \left(\frac{D}{D + 2kx} \right)^2 \right] \tag{11}$$

v_w wind speed in wake [m/s]
v_0 free wind speed in front of the wind turbine [m/s]
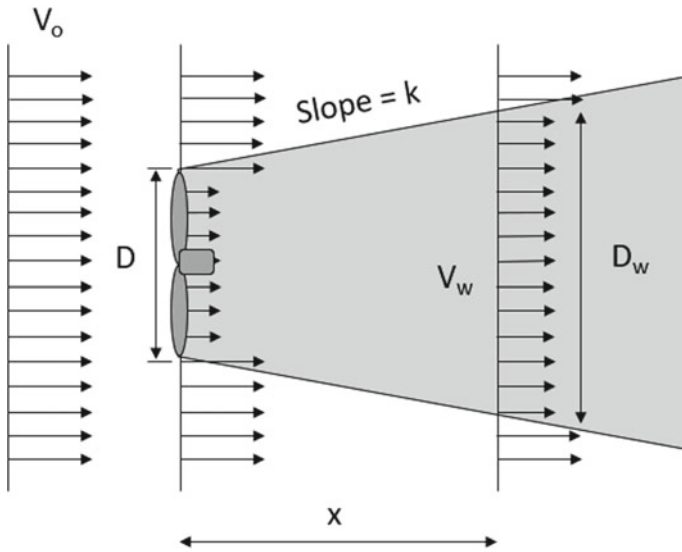
Fig. 39 Wake model according to N. O. Jensen

c_t thrust coefficient $[-]$
D Rotor diameter [m]
k wake decay constant $[-]$
x distance downstream [m]

The thrust coefficient c_t describes the horizontal thrust force on the rotor. This information is provided in form of the thrust curve by the manufacturer. The thrust curve has a great influence on the wake loss, but its validity is difficult to prove. The wake decay constant k is related to the opening angle of the conical wake. A high ambient turbulence intensity leads to increased mixing between the wake and the surrounding undisturbed flow causing the wake to be replenished with energy from the boundary layer. The opening angle of the wake increases, resulting in lower wake losses compared to situations with low turbulence. The effect of multiple wakes can be established through the square root of the sum of squares of the wind speed deficits [34].

The N.O. Jensen model was validated in the 1980s. Compared to today, the rotor diameters and the hub heights were small. Accordingly, the ambient turbulence at hub height was high, which resulted in a recommendation for the wake decay constant k of 0.075. From today's point of view, with considerably higher hub heights and a consequently lower ambient turbulence, this value is outdated and should be reduced. Investigations suggest connecting the wake constant k to the ambient turbulence at hub height [36]:

$$k \approx 0.4 \ \text{TI} \tag{12}$$

Although the N.O. Jensen model is somewhat crude, it is computationally very fast and useful for initial estimates of the wake losses of a wind farm. The performance of the above models has been evaluated through various blind tests [37].

The Ainslie model also dates from the 1980s, and is based on a numerical solution of the Navier–Stokes equations. The eddy viscosity is described by the turbulent mixing due to the induced turbulence generated in the shear layer of the wake and the ambient turbulence [35].

WakeBlaster belongs to the next generation of wake models, whose core is a parabolic three-dimensional RANS solver [38]. WakeBlaster solves the wake flow field for multiple turbines simultaneously rather than for a single turbine, eliminating the need for an empirical wake superposition model. It belongs to a class of mid-fidelity models designed for industrial use in wind farm design, operation and control.

10.3 Further Production Losses

In addition to wake losses, other sources of losses must be considered to determine the net yield (Fig. 40). Various guidelines [17, 19], as well as the working documents of the Technical Expert Group for the preparation of IEC 61,400-15 suggest lists of each item to be considered. Unfortunately, no consensus has yet been reached on which factors should be considered and how to categorize them. The most commonly used categories include:

- Internal wakes.
- External wakes caused by already existing as well as future wind farms.
- Availability
  - of the wind turbine,
  - of the infrastructure (balance of plant BOP), and
  - of the grid.
- Electrical losses
  - Electrical efficiency.
  - Parasitic consumption.
- Performance of the wind turbine
  - Suboptimal operation.
  - Generic and/or site-specific adjustment of the power curve.
  - High-wind hysteresis.
- Environmental conditions
  - Degradation without icing.
  - Degradation due to icing, shut down due to icing
  - Environmental loss e.g. shut down due to high temperature.
  - Site accessibility.
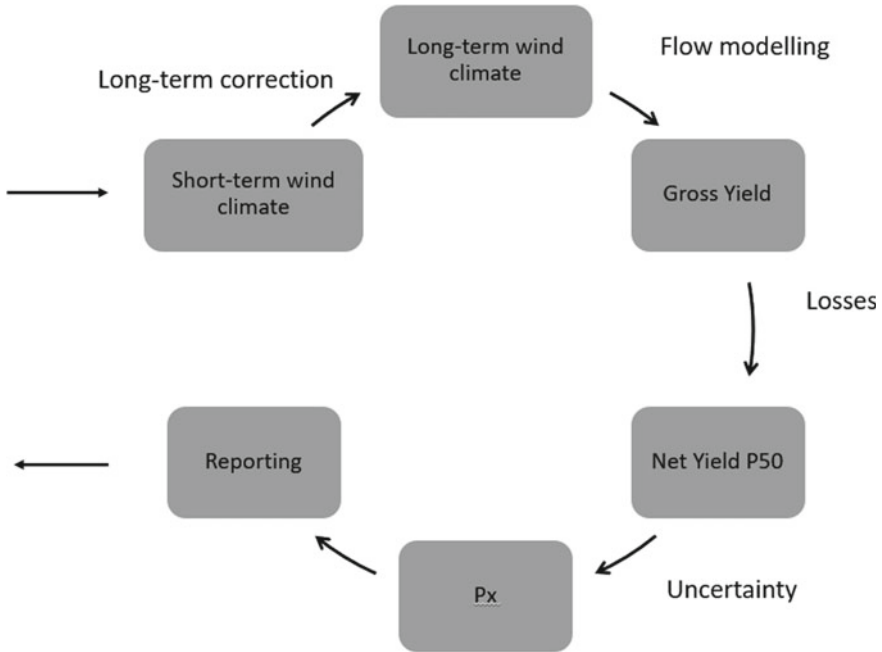
Fig. 40 Main steps of energy yield estimation

- Curtailments
  - Load-related curtailments (such as wind sector management).
  - Grid curtailment.
  - Permit curtailment (such as noise or shadow flicker).
  - Operational strategies.

Some of the loss factors can be calculated, often most accurately in the time domain. Bat curtailment, for example, requires the wind turbines to be switched off at a certain time of day and year, at certain wind speeds, and in certain weather conditions. A statistical determination of the resulting losses is possible, but less accurate than in the time domain.

A number of loss factors, such as availability, are typically covered by specific warranty agreements, so any consideration of uncertainty in these parameters requires a contract-specific review that is generally outside the scope of an energy analysis.

Since the late 2010s, another potential loss factor was cited, which is related to the upstream reduction of wind speed in front of a wind farm causing potentially a reduction of energy output. At the time this book was published, there was no industry-wide consensus on this effect, known as blockage [39]. The detection of blockage is extremely difficult because the effect to be measured is of the order of measurement uncertainty. Therefore, indirect attempts are made to detect blockage. Bleeg et al. [40] report a reduction in wind speeds in front of a wind farm, which

was detected by changed relationship of wind speed measured with multiple masts before and after the installation of wind farms. Furthermore, production differences along the front row of wind turbines in an offshore wind farm were referred to as evidence of blockage [41].

LES (large eddy simulation) models and simplified three-layer models of the atmosphere indicate a reduction in wind farm production on the order of 5% under stable conditions [42, 43], on average during the course of the year the losses would be significantly lower. There are indications that blockage might be connected to the size of the rotor and the turbine's hub height interacting with the atmospheric boundary layer (ABL).

Simpler engineering models as described in [44], describe how the thrust of the rotor slows down the flow in front of a wind turbine. This effect, called induction, is well known and understood. In the context of a wind farm a re-distribution of energy is expected through acceleration at the sides and the far depth of the wind farm, which partly offsets the reduced wind speed at the front row.

Some suggestions on the magnitude of losses can be found in [45]. Unfortunately, it is not always possible to verify the actual individual contributions once the wind turbine is operational. For one thing, the losses are so fragmented that the individual contributions are too small to be determined with certainty. For another, the error codes of SCADA systems rarely support the allocation of lost production to the categories assumed during the pre-construction process. Various blind tests attempt to identify the key challenges of pre-construction assessment and thereby improve accuracy [46, 47]. It often proves difficult to identify a clear pattern of behaviour in the method choices and loss assumptions.

When combining losses double-counting should be avoided. If, for example, turbines are bat-curtailed, they no longer generate a wake.

10.4   Uncertainty Analysis

In addition to the net yield P_{50} the uncertainty of the pre-construction assessment is key information when searching for finance. The gross energy yield as well as the individual loss factors are subject to uncertainties. A site-specific uncertainty analysis is an important part of any wind farm assessment. The most important contributions to uncertainty are:

- Historical wind resources including long-term correction
- Measurement uncertainty/wind data basis;
- Spatial extrapolation/Modelling wind field;
- Performance of the wind turbine:

  – Wake effects;
  – Loss factors.

For each element, the magnitude of the uncertainty is determined. Some suggestions on the magnitude of uncertainties can be found in [45].

Often, it is assumed that the individual uncertainties follow a normal distribution. Through use of a sensitivity factor, wind speed uncertainties can be translated into energy uncertainties. Once expressed as energy uncertainty, all individual uncertainties can be combined as total uncertainty. The total uncertainty can then be used to determine the AEP for different confidence levels, e.g. P_{90} being the production reached with 90% confidence.

It is common to present uncertainty results for different time horizons, from 1 to 20 years.

Literatures

1. Pollak D (2014) Characterization of ambient offshore turbulence intensity from analysis of nine offshore meteorological masts in Northern Europe. DTU Master thesis M-0056
2. Pedersen H, Langreder W (2007) Forest—Added turbulence: a parametric study. J Phys Conf Ser 75
3. IEC (2019) 61400-1 Wind energy generation systems part 1: design requirements, 4 edn, Geneva
4. *Erneuerbare Energien Gesetz (EEG)* (2017) BGBL I S. 2258
5. Kelly M, Larsen G, Dimitrov N, Natarajan A (2014) Probabilistic meteorological characterization for turbine loads. J Phys: Conf Ser 524. https://doi.org/10.1088/1742-6596/524/1/012076
6. Davoust S, Fric T, Shah M (2018) From real wind to actual power output. In: Power curve working group, Hamburg
7. Troen I, Petersen E (1989) European Wind Atlas, Roskilde, Denmark: Risø National Laboratory
8. Mason J, Sykes R (1979) Flow over an isolated hill of moderate slope. Quart J R Meteorol Soc 105:383–395
9. Jackson P, Hunt J (1975) Turbulent wind flow over a low hill. Quart J R Meteorol Soc 101:924–933
10. Mortensen N, Bowen A, Antoniou I (2006) Improving WAsP predictions in (too) complex terrain. In: European wind energy conference, Athens
11. Wood N (1995) The onset of flow separation in neutral, turbulent flow over hills. Bound Layer Meteorol 76:137–164
12. Mortensen N, Petersen E (1997) Influence of topographical input data on the accuracy of wind flow modelling in complex terrain. In: European wind energy conference, Dublin
13. Dellwik E, Jensen N, Landberg L (2004) Wind and forests—General recommendations for using WAsP. In: BWEA
14. Corbett J, Landberg L (2012) Optimising the parametrisation of forests for WAsP wind speed calculations: a retrospective empirical study. In: European wind energy conference, Athens
15. Bechmann A, Sørensen N, Berg J, Mann J, Réthoré P-E (2011) The bolund experiment, part II: blind comparison of microscale flow models. Bound-Layer Meteorol 141(245)
16. "Global Wind Atlas," DTU Wind Energy, Vortex, Nazka Mapps, World Bank Group, Søren Krohn Consulting, World in a Box. https://globalwindatlas.info/about/introduction
17. MEASNET (2022) Evaluation of site specific conditions v3
18. IEC (2017) 61400-12-1: power performance measurements of electricity producing wind turbines, 2nd edn

19. Technical Guideline TR6: Determination of Wind Potential and Energy Yield—Revision 11, Fördergesellschaft Windenergie FGW (2020)
20. MEASNET (2020) Anemometer calibration procedure v3
21. I. W. E. Group (1999) Recommended practices for wind turbine testing: 11—Wind speed measurement and use of cup anemometry
22. Lindelöw P, Courtney M, Mortensen N, Wagner R (2009) Are Lidars good enough? Accuracy of AEP predictions in flat terrain generated from measurements by conically scanning wind sensing Lidars. In: European wind energy conference, Marseille
23. Foussekis D, Georgakopoulos T (2009) Investigating wind flow properties in complex terrain using 3 Lidars and a meteorological mast. In: European wind energy conference, Marseille
24. IEA (2013) Recommended practices 15. Ground-based vertically-profiling remote sensing for wind resource assessment
25. C. T. O. W. Accelerator (2018) Roadmap for the commercial acceptance of floating LiDAR technology version 2, Carbon Trust
26. IEC (2013) Wind turbines—Part 12-2: power performance of electricity-producing wind turbines based on nacelle anemometry, Geneva
27. Clifton A (2015) Remote sensing of complex flows by Doppler wind Lidar: issues and preliminary recommendations, NREL
28. Frandsen S, Thøgersen M (1999) Integrated fatigue loading for wind turbines in wind farms by combining ambient turbulence and wakes. Wind Eng 23(6)
29. Petersen E, Mortensen N, Landberg L, Højstrup J, Frank H (1998) Wind power meterology part 1: climate and turbulence. Wind Energy 1:25–45
30. Gumbel E (1958) Statistics of extremes. Columbia University, Press
31. Palutikof J, Brabson B, Lister D, Adcock S (1999) A review of methods to calculate extreme wind speeds. Meteorol Appl 6:119–132
32. Langreder W, Højstrup J, Svenningsen L (2009) Extreme wind estimates with modest uncertainty—A contradiction? In: Windpower, Chicago
33. Dekker J, Pierik J (1999) European wind turbine standard II ECN-C-99-073. ECN, Netherlands
34. Katic I, Højstrup J, Jensen N (1986) A simple model for cluster efficiency. In: European wind energy conference, Rome
35. Ainslie J (1988) Calculating the flow field in the wake of wind turbines. J Wind Eng Ind Aerodyn 27:213–224
36. Peña A, Réthoré P, van der Laan M (2016) On the application of the Jensen wake model using a turbulence-dependent wake decay coefficient: the Sexbierum case. Wind Energy 19(4):763–776
37. Rodrigo JEA (2020) Validation of Meso-wake models for array efficiency prediction using operational data from five offshore wind farms. J Phys: Conf Ser 1618
38. Schlez W (2017) Virtual wind farm simulation. WindTech Int 9
39. Schlez W, Unlocking blockage—White paper on wind farm induction. https://zenodo.org/record/4288324
40. Bleeg J, Purcell M, Ruisi R, Traiger E (2018) Are wake losses enough? Additional energy losses associated with neglected wind turbine interactions. Energies. https://doi.org/10.3390/en11061609
41. Nygaard N, Steen S, Poulsen L, Pedersen J (2020) Modelling cluster wakes and wind farm. J Phys Conf Ser 1618(6)
42. Allaerts A, Meyers J (2017) Boundary-layer development and gravity waves in conventionally neutral wind farms. J Fluid Mech 814:95–130
43. Allaerts D, Meyers J (2018)Gravity waves and wind-farm efficiency in neutral and stable conditions. Bound-Layer Meteorol 166(2):269–299
44. Branlard E, Meyer Forsting A (2020) Assessing the blockage effect of wind turbines and wind farms using an analytical vortex mode. Wind Energy 23(11):2068–2086
45. Clifton A, Smith A, Fields M (2016) Wind plant preconstruction energy estimates: current practice and opportunities, NREL, US
46. Fields M, Optis M, Perr-Sauer J, Todd A, Lee J, Meissner J, Simley E, Bodini N, Williams L, Sheng S, Hammond R (2021) Wind plant performance prediction benchmark phase 1 technical report. NREL

47. Badger J, Cavar D, Nielsen M, Mortensen N, Hansen B (2021) CREYAP 2021. In: Wind Europe technology workshop

Wiebke Langreder, M.Sc., has been working in the international wind industry since 1996 in the field of wind resources and site assessment. Today she heads the consulting department for Wind and Energy Systems at EMD International A/S, Ålborg, Denmark.

Aerodynamics and Blade Design

Alois Peter Schaffarczyk

1 Summary

The aerodynamics of wind turbines as a quantitative description of the flow around parts of a or entire wind turbines or even wind farms is presented in outline. Since more comprehensive accounts of this field are now available [100, 107, 121], we content ourselves here with less space and refer for a more thorough study of these works and the Original literature, especially the final reports on the various MexNext phases [9, 103–105] This chapter is divided into three parts: Horizontal Axis Rotors, Vertical Axis Rotors and wind-powered vehicles. Figure 1 gives a first overview (without wind vehicles), where c_P a dimensionless (comparative) power and λ, Tip-Speed-Ratio, a dimensionless speed.

2 Introduction

At this chapter we introduce basic concepts of three-bladed rotors based on the classical rotor theory.

3 Wind Turbines with Horizontal Axis of Rotation

3.1 General

For the mechanical design of wind turbines, theoretical models must be used which, in the simplest form, can be traced back to the theories of Rankine [85] and Froude [30].

A. P. Schaffarczyk (✉)

Kiel Univeisity of Applied Sciences, Grenzstr. 3, D-24149 Kiel, Germany
e-mail: Alois.Schaffarcyzk@FH-Kiel.de
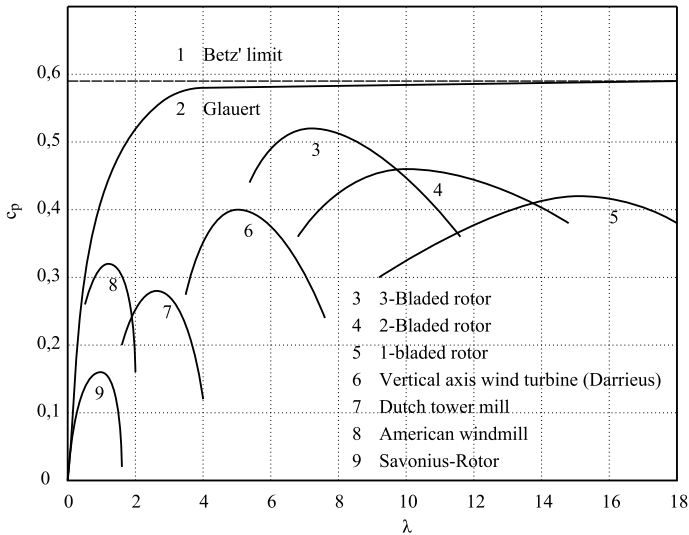
Fig. 1   Map of wind turbines

They were originally developed for ship and aircraft propellers, and then by Betz [6] and Glauert [33] to wind turbines. Despite all attempts to overcome the narrow limits (e. g. with CFD[1]) this Blade Element Momentum Method (BEM) is still the most widely used in practice today, since it provides very useful results in comparison to the low implementation and input effort, it provides very usable results.

In this respect, the development of the aerodynamic theory of wind turbines is proceeding in parallel to that of ship propellers [11] and helicopter [57] though of course quite large differences are present: In the case of ship propellers, for instance, cavitation and the associated much lower negative pressures on the suction side of the profile are of decisive importance, whereas with helicopter rotors the Mach number (= flow velocity/speed of sound) is close to one and thus the compressibility of the medium must be included.

3.2   Basic Aerodynamic Principles

2D-Aerofoils

If an aerodynamic profile (Fig. 2) of chord c, which is considered to be two-dimensional, is subjected to a flow of velocity v, there are two force components, one in the direction of (Fig. 2) (Drag – D) and one perpendicular to wind (Lift L)—per meter span wise extension and with coefficients:

---

[1] Computational Fluid Dynamics.
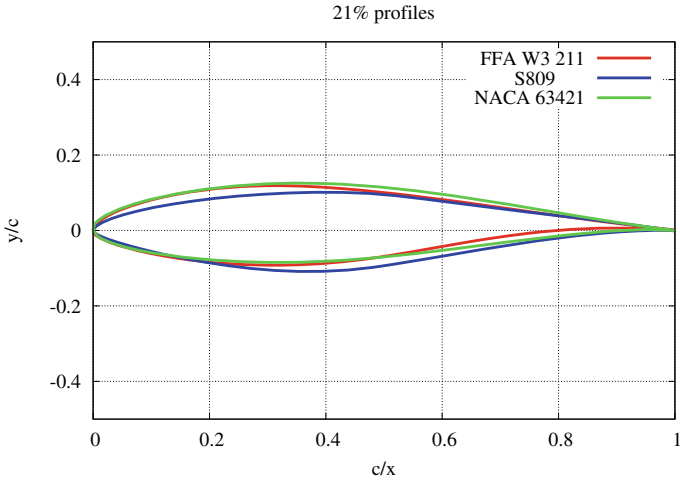
Fig. 2 Wind turbine aerodynamic profiles of 21% thickness

$$C_D = \frac{D}{\frac{\rho}{2}v^2 \cdot c \cdot 1}, \tag{1}$$

$$C_L = \frac{L}{\frac{\rho}{2}v^2 \cdot c \cdot 1}. \tag{2}$$

A typical polar curve (plotting these values against each other or relative to the angle-of-attack) is shown in Fig. 3 (AOA = Angle-of-Attack, α is the angle between the incident flow and the profile's chord). In practice, one usually uses tables (e.g., NACA by Abbot/Doenhoff [1] or University of Stuttgart's catalog [2]) or in some cases one has to make very elaborate measurements [28, 124] when their properties are not known.

We proceed step by step. Therefore, we first investigate systems that are purely be driven translationally. A sailboat or an ice glider can serve as an example (see Fig. 4).

Drag Forces

Let as above c_D and c_L from Eqs. 1 to 2 coefficient of drag resp. lift. If $A = c \cdot l$ is the area of the sail and U velocity of wind and v the corresponding one of the boat, then power can be calculated by

$$P = \frac{\rho}{2}(U - v)^2 \cdot C_D \cdot cl \cdot v. \tag{3}$$

Now defining an efficiency (by taking reference to the wind – per unit area – ($P_W = \frac{\rho}{2}U^3$) it follows:

NACA 63-421 - measurement(ME) vs. Boundary Layer Code(BL)
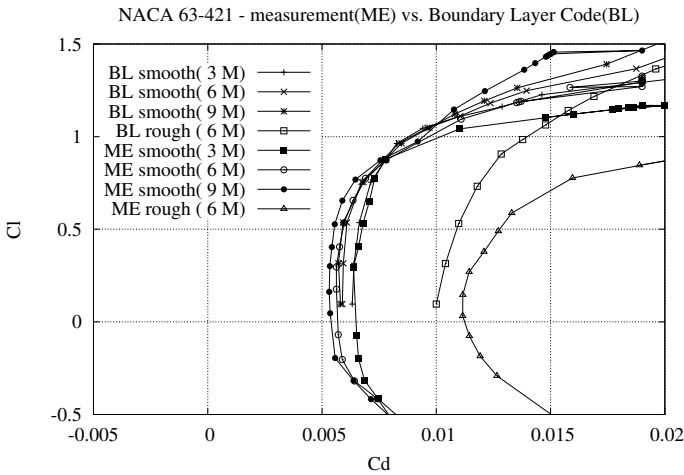
Fig. 3 Polar (c_L/c_D) of profile NACA 63 421

Fig. 4 Translational
propulsion via Drag or Lift
(D resp. L)
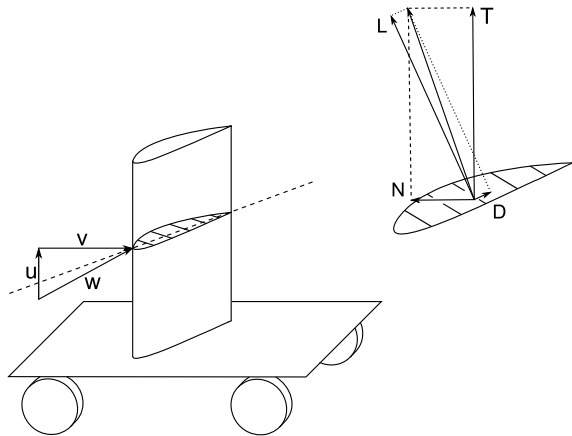
$$c_P = c_D(1 - v/U)^2(v/U) .\tag{4}$$

To maximize one takes the derivated to $a := v/U$, it can be seen that the maximum
power coefficient of such a drag-driven rotor is not greater than

$$c_P^{\max,D} = \frac{4}{27}c_D,\tag{5}$$

therefore $c_P^{\max,D} \approx 0,3$ at $v = 1/3U$. Such a sailboat sailing at wind force 7 (according
to Beaufort corresponding to 30 knots or 16.2 m/s) drives not faster than 10 knots.
If its sail has an area of 30 m^2 then its maximum power is about $P = 24$ kW.
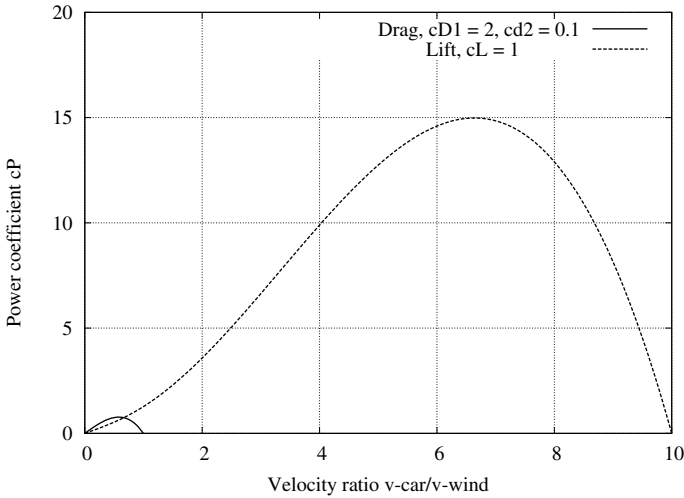
Fig. 5 Power coefficients of Drag and Lift driven vehicles in comparison

Lift Forces

In order to increase the efficiency of such vehicles, one uses lifting forces, which by themselves do not perform work, since they are perpendicular to the velocity.[2] However, the geometric relationships are a bit more complicated. The wind is now perpendicular to the direction of travel (half wind). The power is $P = N \cdot v$. N is the normal force perpendicular to the wind and parallel to v. The velocities U and v form a triangle and N is composed of:

$$N = N_L + N_D = L \cdot \cos(\phi) - D \cdot \sin(\phi) \tag{6}$$

By algebraic transformations (ϕ is the angle between wind and total relative velocity) this leads to:

$$c_P = a \left(\sqrt{1 + a^2} \right) \cdot (C_L - C_D \cdot a). \tag{7}$$

Maximum power coefficient now (see Fig. 5) is

$$c_P^{\max,L} = \frac{2}{9} C_L \left(\frac{C_L}{C_D} \right) \sqrt{1 + \frac{4}{9} \left(\frac{C_L}{C_D} \right)^2} \tag{8}$$

Note:

(a) Now the maximum velocity is greater than that of the wind and will be reached at

---

[2] $P = \dot{W} = \mathbf{F} \cdot \mathbf{v} = 0 \Leftrightarrow \mathbf{F} \perp \mathbf{v}$.

$$a = v/U = \frac{2}{3}\frac{C_L}{C_D} \tag{9}$$

in our example, $v_{\max} \approx 6U = 180$ knots.

(b) A (not insignificant) force T parallel to the wind must be compensated.
In Fig. 5 both cases for $C_D = 2$ resp. $C_L = 1$ and $C_L/C_D = 10$ are compared.
A somewhat more complete and comprehensive discussion of wind-powered
vehicles with rotor is carried out in Sect. 7.

4 Integral Momentum Methods

4.1 Momentum Theory of Wind Turbines: Betz' Limit

In the simplest case, a wind turbine extracts energy from the wind only by de-
accelerating it. which, because of mass conservation, must be accompanied by slip-
stream expansion (see Fig. 6). This results in a pressure drop behind the turbine, i.e.,
a thrust force **T** in wind direction. If one further assumes that only axial (i.e., in
the wind direction) velocity components are present, the following simple derivation
results:

$$\text{energy: } E = \frac{1}{2}mv^2 \tag{10}$$

$$\text{power: } P = \dot{E} = \frac{1}{2}\dot{m}v^2 \tag{11}$$

$$\text{power removed: } P_T = \dot{E} = \frac{1}{2}\dot{m}\left(v_1^2 - v_3^2\right) \tag{12}$$

$$\text{Froude's Law: } v_2 = \frac{1}{2}(v_1 + v_3) \tag{13}$$

$$\text{mass flow: } \dot{m} = \rho A v_2 \tag{14}$$

$$\text{therefore: } P_T = \frac{1}{2}\rho A v_1^3 \left(\frac{1}{2}\left(1 + \frac{v_3}{v_1}\right) \cdot \left(1 - \left(\frac{v_3}{v_1}\right)^2\right)\right) \tag{15}$$

Fig. 6 Idealized flow
conditions around a wind
turbine
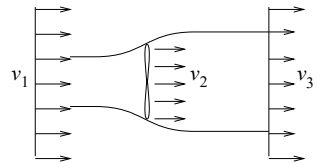
$$c_P(\eta) = \frac{1}{2}(1 + \eta) \cdot (1 - \eta^2). \tag{16}$$

$$\text{using: } \eta = \frac{v_3}{v_1} \tag{17}$$

$$\text{and: } a = \frac{v_2}{v_1} \tag{18}$$

$$c_T(a) = 4a \cdot (1 - a) \tag{19a}$$

$$c_P(a) = 4a \cdot (1 - a)^2 . \tag{19b}$$

Now we have more coefficients:

$$c_P = \frac{P}{\frac{\rho}{2} v^3 \frac{\pi}{4} D^2} \tag{20}$$

$$c_T = \frac{T}{\frac{\rho}{2} v^2 \frac{\pi}{4} D^2} \tag{21}$$

$$\lambda = \frac{\Omega R}{v} \tag{22}$$

and

$$\Omega = 2 \cdot \pi N / 60 \tag{23}$$

Thus, the maximum power coefficient, the (Betz limit) results:

$$c_P^{Betz} = \frac{16}{27} = 0,5926 \text{ at } a_{max} = \frac{1}{3}. \tag{24}$$

You can see that far downstream the wind is reduced by 2/3, i.e., to 1/3. Note furthermore, this derivation loses its validity when the air flow is completely diverted. (is braked, $a = 0.5$); and thus no slip-stream anymore exists behind the turbine.

Due to Newton's 3rd law, conservation of momentum in more modern terms—there is a back reaction on the turbine via $T = \frac{d}{dt}(m \cdot v) = \dot{m}v$ therefore a thrust force emerges

$$T = \dot{m}(v_1 - v_3). \tag{25}$$

Despite its simplicity this derivation gives a safe upper limit of the power capacity of a wind turbine, which cannot be exceeded despite persistent attempts by many inventors[3]

---

[3] Somewhat higher values—around 0.62—can be reached only if extended rotors, for example vertical axis wind turbines—*Darrieus*-Rotors—are regarded [98]. This was also recognized by Betz [6] (see Sect. 6.2).

4.2   Change in Air Density Due to Temperature and Altitude

Often it is necessary to convert standard density of air($\rho_0 = 1.225\,\text{kg/m}^3$) to other temperatures (ϑ) and other altitudes (H). For this purpose, you can use the auxiliary formulas:

$$\rho(p, T) = \frac{p}{R_i \cdot T},\tag{26}$$

$$T = 273, 15 + \vartheta,\tag{27}$$

$$R_i = 287,\tag{28}$$

$$p(H) = p_0 \cdot e^{-H/H_{\text{ref}}},\tag{29}$$

$$p_0 = 1\,015\,\text{hPa},\tag{30}$$

$$H_{\text{ref}} = 8\,400\,\text{m}.\tag{31}$$

4.3   Loss in Performance Due to Finite Number of Blades

A frequently asked question is on the number of blades. It should be noted at this point that the predominant trifolium is not due to exclusively aerodynamic reasons. The decisive factor is rather higher production costs (more than three blades) or increase in aeroelastic loads during yawing (less than three leaves). The lift L (here again per meter span) can be related to an important fluid-mechanical quantity, the circulation, by means of the theorem of Kutta-Joukovski to:

$$\Gamma := \oint \mathbf{v} \cdot \mathrm{d}s\tag{32}$$

$$L = \Gamma \cdot \rho \cdot v.\tag{33}$$

Further, this quantity is related to the local chord $c(r)$ and lift c_L:

$$\Gamma = \frac{B}{2} \cdot C_L c \cdot w.\tag{34}$$

Only the product of $c(r) \cdot C_L$ is determined by aerodynamic blade design.[4] However, the blade element or actuator-disk method (see below) implicitly assumes, that there is no pressure equalization at the tip of the wing, and so a constant circulation ($\simeq$ lift $\simeq$ driving torque) may remain. This is strictly valid only the case with B(number of blades) $\rightarrow \infty$. For the case of a finite number of blades Prandtl [84] has already given

---

[4] Recently a more complete open-source aerodynamic blade design code has been published [52].

an approximation for the corresponding loss in circulation. It is based on potential theoretic considerations, according to which the vortex-induced flow around a B-bladed rotor can be conformally mapped to a stack of B plates.

Let F (the reduction factor of the circulation at the blade tip) be given by

$$\Gamma = F(B) \cdot \Gamma_\infty, \tag{35}$$

it follows:

$$F = \frac{2}{\pi} \arccos\left(\exp(-f)\right) \tag{36}$$

$$f = \frac{B}{2} \cdot \frac{R - r}{r \cdot \sin(\phi)} \tag{37}$$

Here ϕ flow angle (see Eq. (52)). The losses are particularly high for $B = 1$ and $B = 2$.

Case $B = 1$, for example built as Monopteros (see Fig. 7) has been highly controversial for a long time Only Okulov [77] succeeded with the help of new analytical approaches in a cohesive solution that blends harmoniously into the overall picture. Recently [37, 110] flow simulation (CFD) methods have also been applied, to examine the overall validity of these assumptions. There are indications that the loss of circulation is greater than estimated by Prandlt's approximation. However,

Fig. 7 One-bladed wind turbine monopteros on the DEWI-test field near Wilhelmshaven. *Photo Alois Schffarczyk*

the caveats that we have discussed in Sect. 5.5 on the basis of comparisons with measurements will be explained in more detail there.

4.4 Swirl Losses and Local Optimization of the Wing According to Glauert

In order to include the rotating motion of the rotor, analogously to the case of purely axial flow balancing angular momentum is used to determine power according to: $P = M \cdot \omega$

$$M = \dot{m} \cdot r v_t \text{ globally and} \tag{38}$$

$$\mathrm{d}M = d\dot{m} \cdot r v_t \text{ locally} \tag{39}$$

Now, if the rotor is divided into circular rings of thickness dr and area $dA = 2\pi r \, dr$, it follows:

$$\mathrm{d}M = 4\pi r^3 v_1 (1-a) a' \omega \, dr. \tag{40}$$

Here $a' := \omega/2\Omega$ is a corresponding induction factor for the tangential velocity component. For the total power results by integrating over all rings (annular element in Glauert's terms):

$$P = \int \omega \cdot \mathrm{d}M. \tag{41}$$

This can be expressed again in terms of a power coefficient:

$$c_P = \frac{8}{\lambda^2} \int_0^\lambda (1-a) a' x^3 \, dx \tag{42}$$

with $x = \omega r/v_1$ being the local tip-speed-ratio. In comparison to Betz's 1D model, one now has two parameters a, a' to be optimized, both of which are depending on x. Another equation, the so-called Glauert's orthogonality condition (see [19, 133]),

$$a'(1-a') \cdot x^2 = a(1-a) \tag{43}$$

is necessary to close the system of equations.[5] According to Glauert the rotor is now (locally) optimal, if the function

$$f(a, a') = a'(1-a) \tag{44}$$

becomes extreme under constraint Eq. (43).

---

[5] Again, it can be shown that this model is valid only fot $c_T \to 0$ (see [115]).

Taking the derivative of Eq. (44) to a leads to:

$$(1 - a)\frac{\mathrm{d}a'}{\mathrm{d}a} = a' \tag{45}$$

or the same from Eq. (43):

$$(1 + 2a')x^2 \frac{\mathrm{d}a'}{\mathrm{d}a} = 1 - 2a. \tag{46}$$

Together thus:

$$a' = \frac{1 - 3a}{1 + 4a}. \tag{47}$$

As a' has to be ≥ 0 (if not we would not have a turbine but a propeller) therefore $0.25 < a < 0.33$. Equations (43) and (47) now determine $a(x)$ and $a'(x)$ (see Talbe 1). In order to perform integration radial extension of the blade (i.e., over x, see Eq. (42), one only has to invert the function $x(a)$, i.e., $x(a) \rightarrow a(x)$, after a' has been inverted by means of Eq. (43) which is quite some trouble. The results summarized in Table 1 and Fig. 8. Recent investigations (see, for instance [16]) show that these relations strictly apply only in the limiting case of lightly loaded rotors, i.e $C_t \rightarrow 0$. For wind turbines, however, typically $c_T \approx 0.7 \ldots \approx 1$.

Thus, Glauert's analysis [33] (see Table 1) shows that the power coefficient is only affected by swirl losses when λ falls below 2. The integration over x (dimension less radial distance) already indicates that a transition to blade elements has to be performed. For a further study, we refer to [117] for a new and very readable account and critique of the Glauert's theory.

Table 1 a, a' as function of $x = \omega r/v$ from Glauert's optimum wind turbine

a	a'	x
0.25	∞	0.0
0.26	5,500	0.073
0.27	2,375	0.157
0.28	1,333	0.255
0.29	0.812	0.374
0.30	0.500	0.529
0.31	0.292	0.753
0.32	0.143	1,15
0.33	0.031	2,63
0.333	0.003	8,58
1/3	0.00	∞
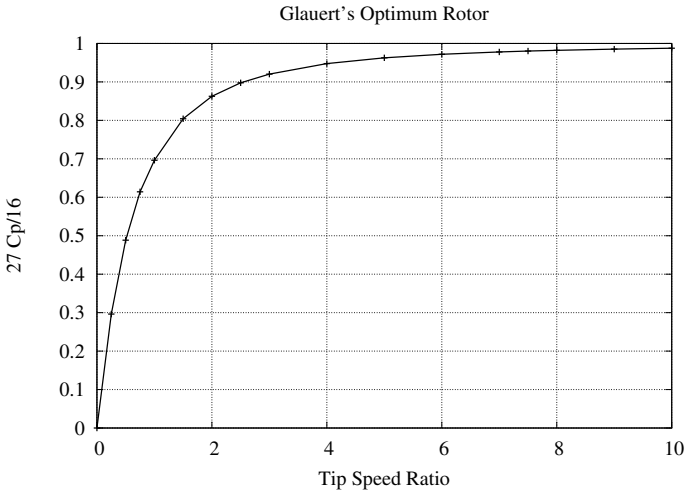
Fig. 8 Optimal wind turbine rotor according to Glauert, including only swirl losses

4.5 Aerodynamic Loss Due to Profile Drag

The last, essential mechanism for reducing the output of a wind turbine is the so-called profile loss. A summary of all contributions is shown in Fig. 9. E1 and E2 are two systems from a German manufacturer and are intended to visualize to progress made within 10 years.
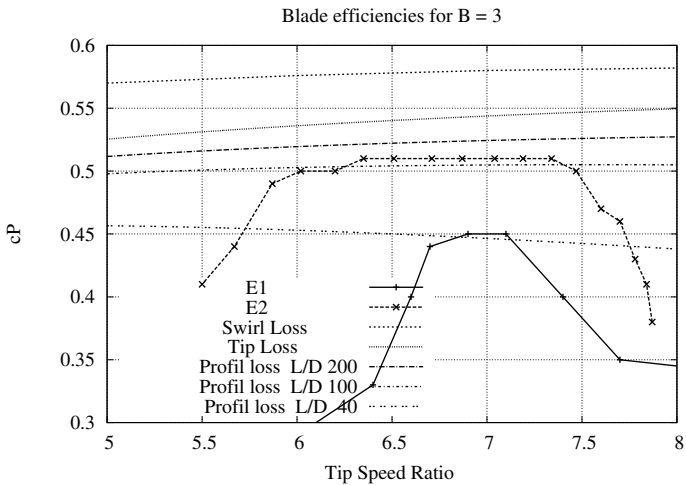
Fig. 9 Comparison of the aerodynamic loss mechanisms for blade number $B = 3$

5 Momentum Theory of Blade Elements

5.1 Formulation

The actual blade element method [90, 117] (Fig. 10) in conjunction with the differential momentum method is a suitable procedure to make measurable statements about the performance of rotors (propeller like impeller) and loads. The assumptions of the momentum theory are exceeded insofar as now lift and drag—described by the parameters C_L, C_D (see above)—are used. The increments of moment (dQ) and axial force (thrust, dT dT) are given as:

$$dT = d\dot{m}(v_1 - v_2) = 4a(1 + a)2\pi r \, dr \cdot \frac{\rho}{2}v_1^2 \qquad (48)$$

$$dQ = d\dot{m}(v_1 \cdot r) = 2\pi r \, dr \cdot \rho v_2 \cdot 2\omega r^2 = 4\pi r^3 \rho v_1 \Omega(1 - a)a' \qquad (49)$$

Here r is the considered distance from the hub and v_1 is the axial incident (far down stream) flow velocity. and $v_2 = (1 - a) \cdot v_1$ the value in the propeller plane. Overall, this gives (Fig. 11) for the velocity and force triangles. They are:

$$C_n = C_L \cdot \cos(\varphi) + C_D \cdot \sin(\varphi) \qquad (50)$$

$$C_{\tan} = C_L \cdot \cos(\varphi) - C_D \cdot \sin(\varphi) \qquad (51)$$

with

$$\tan(\varphi) = \frac{1 - a}{1 + a'} \frac{v_\infty}{r\Omega} \qquad (52)$$

and

$$\varphi = \alpha + \theta \qquad (53)$$

with flow angle φ and θ twist of the blade. This method has been completed in many details by supplementary assumptions. They are, e.g., the above-mentioned losses due blade tip effects F and an empirical extension of $c_T(a)$ for $a > 0.5$ (Glauert

Fig. 10 Blade elements
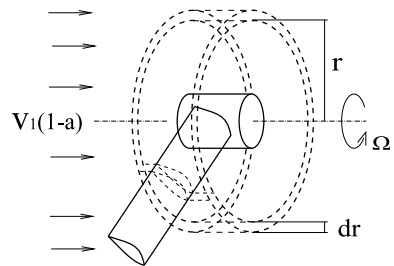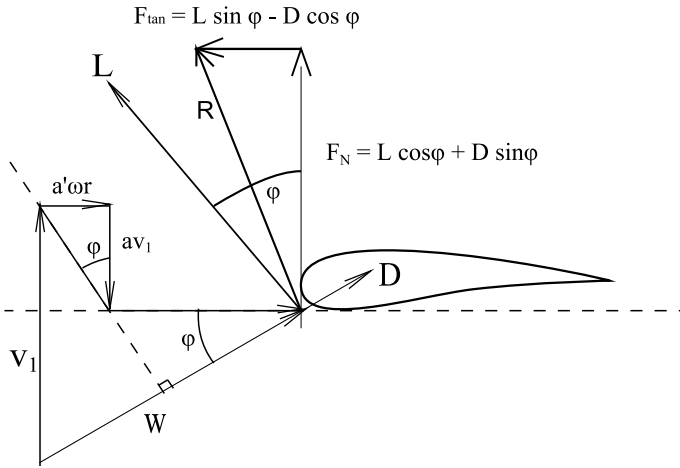
$V_1(1-a)$

Fig. 11 Velocity and force triangles

extension, see Eq. 58 Thus, then (w is the total incident flow velocity):

$$dT = Bc \frac{\rho}{2} W^2 C_n \cdot dr \tag{54}$$

$$dQ = Bc \frac{\rho}{2} W^2 C_t \cdot r \, dr \tag{55}$$

$$w^2 = (v_1 \cdot (1 - a))^2 + \left(\omega r \cdot (1 + a')\right)^2 \tag{56}$$

Analogous to a (axial induction) we already mentioned that $a' := 2\omega/\Omega$. Also for a' an analogous Froude's theorem is assumed, according to which the induced components in the propeller plane are half as large as in the far wake. Equation (48) applies for the thrust only as long as a is $< 1/3$ (or at least < 0.5), otherwise one must use empirical extrapolations like the above-mentioned Glauert extension

$$c_T = 4a(1 - a)F, \ a \leq \frac{1}{3} \tag{57}$$

$$c_T = 4a(1 - 0.25 \cdot (5 - 3a)a)F, \ a > \frac{1}{3}. \tag{58}$$

Re-arranging Eqs. (48) and (49) for a resp. a', it follows:

$$\frac{a}{(1 - a)} = \frac{Bc F_t}{8\pi r F \cdot \sin^2(\varphi)} \tag{59}$$

$$\frac{a'}{(1+a')} = \frac{Bc F_n}{4\pi r F \cdot \sin(\varphi)\cos(\varphi)} \tag{60}$$

Overall, then, the iteration scheme is as follows:

- Estimate a and a' (initially: $a = a' = 0$),
- (*) determine φ from Eq. (52),
- determine AOA α from Eq. (53),
- determine C_L and C_D from a table Tabelle (see Sect. 3.2),
- determine C_n and C_t from Eq. (53),
- determine a and a' from Eqs. (60) and (60),
- goto (*) and iterate below a pre-defined error.

Remarks

1. F may be expressed as:

$$F = \frac{2}{\pi}\arccos\left(\exp\left[-\frac{B/2(1 - r/R_{\text{tip}})}{r/R_{\text{tip}}\sin(\varphi)}\right]\right). \tag{61}$$

2. Handling F within the BEM is not unique. An alternative may be defined by replacement of $a \to a \cdot F$ and $a' \to a' \cdot F$ in Eqs. 60 and 37.
3. Simple fixed-point iteration may not converge or may take too much iterations.
4. A recent review [58] in which many of the numerical peculiarities (see Sect. 5.2, multiple solutions, [52]) are mentioned discusses these subjects in much more rigor and detail.
5. Accuracy of wind tunnel measurements and its extension to real 3D atmospheric flow on wind turbine blades is subject of ongoing discussion [102].
6. Estimating mechanical loads demands for more realistic inflow conditions. This is closely related to modeling turbulent flow. See [49, 100] for more details.

5.2 Specific Implementations: Wt-Perf, CCBlade and FAST

Wt-Perf used to be a FORTRAN implementation of M. Buhl, National Renewable Energy Laboratory (NREL), Golden, Colorado, USA, based on legendary PROP-Code of Walker [132] which is not supported anymore.

Instead, OpenFAST code [76], which contains a full structural (BEAM) model or python-based CCBlade code [74] should be used. As larger parts are still written in FORTRAN(90) a suitable compiler (for example GNU) is necessary.

5.3   Optimization and Blade Design

The outer shape of a blade is geometrical (aerodynamic), determined by the chord
distribution $c(r)$, the twist distribution $\vartheta(r)$ and the cross-sections (= aerodynamic
profiles). From the above considerations many so-called optimal designs have been
derived [31, 33, 133]. In the simplest case for relative chord c/R:

$$c(r)/R = 2\pi B \, \frac{8}{9} \, \frac{1}{C_L} \, \frac{1}{\lambda^2 \cdot \left(\frac{r}{R}\right)} \tag{62}$$

(see for example [31]) and for twist:

$$\theta = \arctan\left(\frac{3}{2} \, \lambda \, \frac{r}{R}\right) \tag{63}$$

 Results of a local aerodynamic optimization according to Wilson [133] and de
Vries [19] are shown in Fig. 12 and compared to realized bladed. The implementation
of further constraints, such as loads and other factors for optimizing the overall costs
of the energy generated in this way are presented in a large number of publications.
As a recent example, we refer to [137]. In [91] an attempt is made to describe
commercial blade designs on which these approaches are mirrored. Finally, [52]
gives a full account on aerodynamic blade design.
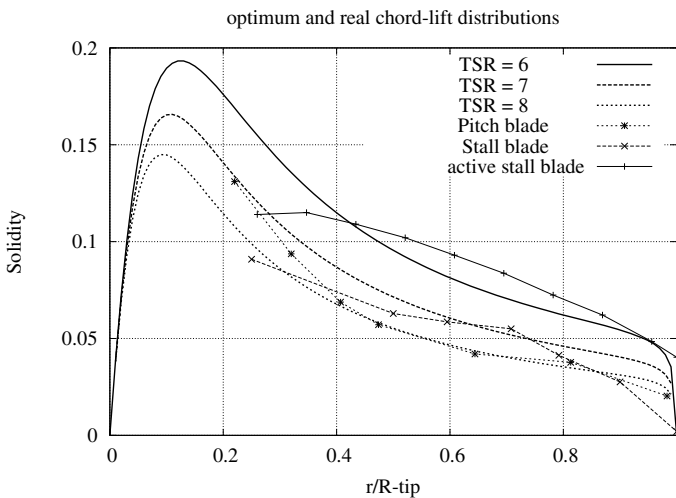
Fig. 12 Optimum blade design ($B = 3$) according to Wilson/de Vries; in comparison with realized
blades

5.4 Extensions, Differential Formulations, Actuator-Line Method

Including radial velocity components

A major deficit in Actuator-Disk models is the neglect of radial velocity components which—at least—are appearing in the vicinity of the rotor. One way to overcome is the use a suitable distribution vortex rings and a vortex cylinder as some kind of a far-field boundary condition. Schaffarczyk et al. [101] gives an overview about the approach, an independent implementation and a comparison to a specific propeller and wind turbine case.

Implementation inside CFD(RANS) models

The blade element method is very much based on integral energy and momentum balances, which are statements only at three locations (far upstream of the rotor, at the rotor itself and far downstream). Since it is assumed that at the first and last position no radial variations of velocities take place, this is a one rather than two-dimensional method. A full 2D extension is provided by the so-called actuator-disk methods. They can be solved semi-analytically (see [16]). It should be noted at this point that one can simplify full 3D methods to some extend (see Sect. 5.5) in order to achieve a some kind of a middle way that requires much lesser computational effort.

The implementation in CFD is essentially carried out via an additionally introduced volume forces. For this purpose, lift and drag are divided in the axial and circumferential directions and applied to the area element $2\pi r \, dr$. As a volume force, this pressure jump must then still be corrected to the thickness of the plane which it refers to. We give below a few examples of the effectiveness of the method.

Validation and sample active stall blade

A so-called active stall sheet (ARA48, [93]) was used to compare both methods (see Fig. 13). Deviations in the vicinity of the blade tip are clearly visible, since no Prandtl correction is included in the CFD formulation.

Wind turbine with Diffusor

Hansen et al. [34] present the effect of a wind concentrator consisting of a NACA 0015-(ring) profile. Our method [94] could be used for the selection of a suitable blade shape for this combined system, since there was a very strong interaction between the rotor and the diffuser and therefore a separate design was not possible.

Phillips [83] examined in great detail many other approaches and parameters. We were able to show that an integral BEM procedure is unsuitable. van Bußel [128] gives a current summary on the state of theory and experiment.

Counter-rotating tandem wind turbine

An interesting variant, which makes perfect sense for ship propellers and helicopters consists in the so-called contra-rotating wind turbine. Two close-by rotors are rotation in opposite directions so that—at least—swirl losses are reduced.
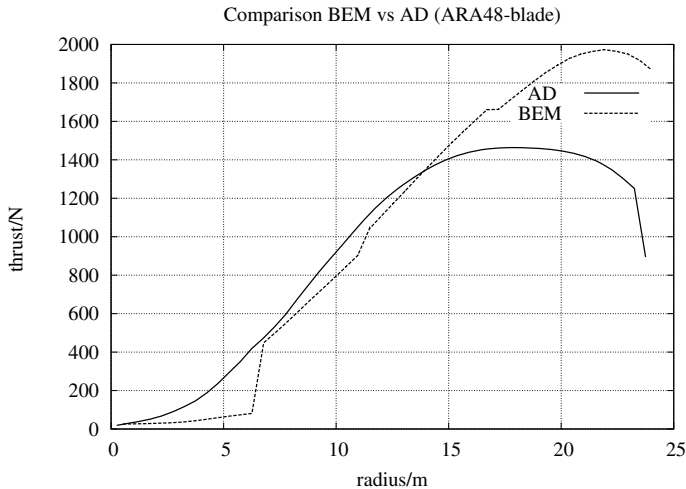
Fig. 13 Validation using the example of an active stall blade (ARA48). Comparison of integral (BEM) and differential (CFD-BEM) method for thrust

However, studies [97] show that the expected gain in yield (approx. 5–10%) may be by too great an additional effort—especially in the design of the blade—could be nullified.

Actuator-Line Method

A now widely used method, which combines 3D CFD (see Sect. 5.5) and BEM, represents the so-called Actuator-Line method [126].

Elegance of this method, however, is somewhat relativized by the fact that an additional parameter ϵ, the width of the spatial smearing of the loads, the precise determination of which is still the subject of of much ongoing research [62].

5.5   3D Flow Simulation—CFD—RANS

The use of effective numerical methods for the investigation of wind turbines is always been advanced in parallel with the general development of aerodynamic theories. Since about twenty years, numerical methods for solving the full three-dimensional Navier-Stokes equations—together with empirical turbulence models such as the k-ε or k-ω-model also commercially available. Unfortunately, these turbulence models not yet sufficiently mature to make sufficiently accurate statements. Results of many However, studies on various detailed issues seem to suggest that CFD (in the in this sense of the numerical solution of the 3D Navier-Stokes equations) is the only possibility-consistent extension of the aerodynamic description of wind turbines. seems to be. As an impressive example of the results that can only be
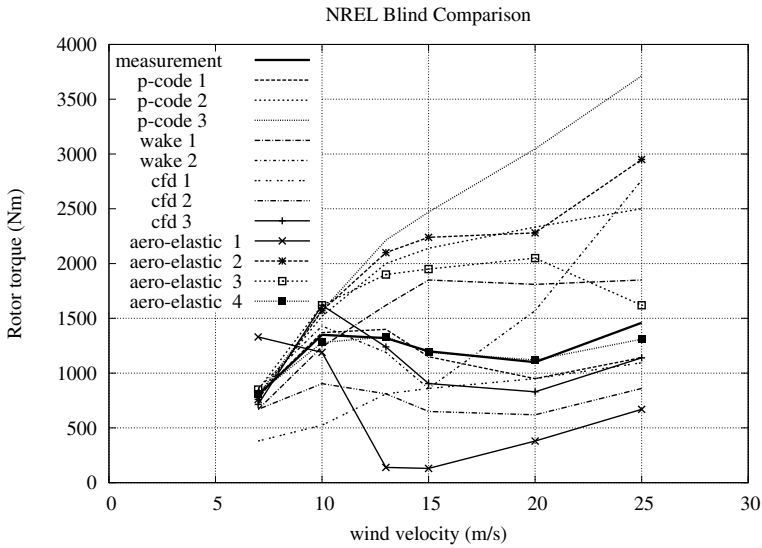
Fig. 14 Blind comparison of measurements within the NASA-AMES wind tunnel in 2000. from [111]

achieved with 3D CFD, a compos-blind comparisons of the NASA Ames wind tunnel tests. from the year 1999/2000 are compiled in Fig. 14. The data series C1 to C3 represent the CFD calculations. CFD3 is the study of Risø. Further benchmarks are available in the already mentioned MexNext reports [9, 103–105]. Although there are differences even between different CFD codes but in general these methods tend to be more accurate than blade element or vortex methods. This can also be seen in Fig. 15. Apart from a few outliers, the agreement even within a group is only around 10%.

5.6 Summary: Horizontal Axis Wind Turbines

In this chapter, we have presented the main findings and results of aerodynamics applied to wind turbines with horizontal axis. Even though work has been carried out in this field for more that 150 years there still seem to be no final answers to many questions in detail. However, the BEM (Blade Element Momentum Method) presented in much detail is sufficient in many respects, if one does not disregard their validity limits
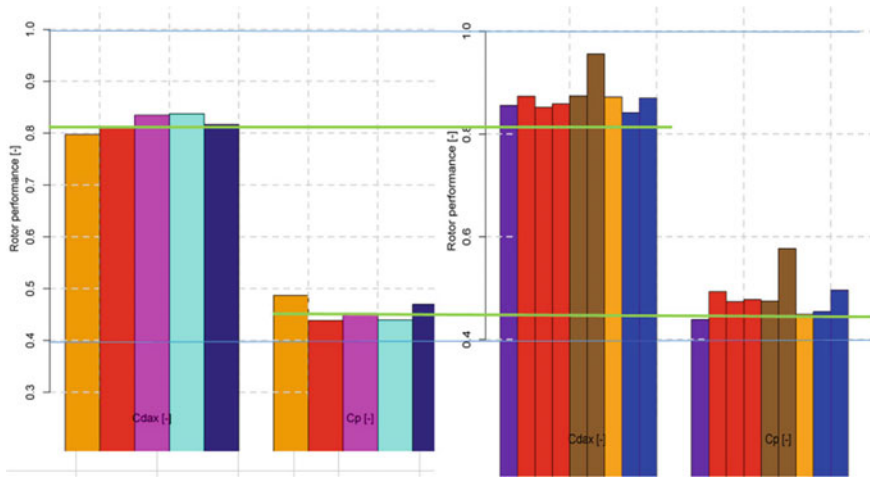
Fig. 15 Blind comparison for DANAero case 1.1, 2021, from [105]. To the left: CFD, To the right: BEM and Vortex-Codes. Larger values correspond to thrust c_T, lower ones to c_P. Additionally lines drawn inside roughly indicate an average value

6 Vertical Axis Wind Turbines

6.1 General

Wind turbines with a vertical axis of rotation (VAWT) (Fig. 16) are an alternative to the conventional wind turbines with a horizontal axis. They also offer the possibility of application of methods of unsteady (transient) fluid mechanics. Due to their independence from the wind direction practical realizations—if compared to HAWT—had some advantages, however, many plants—up to the 4 MW power plant and more than 100 m high ÉOLE-Cat Cap-Chat, Canada, [87, 88]—failed, (see Fig. 17a)—most likely due to the inadequately taken into account fatigue loads. Figure 17b shows a 3-bladed machine with 50 kW rated power (HEOS Energy GmbH, Germany) and Fig. 17c a more recent one from Agile Wind Power of year 2021.

In this part essential models and methods shall be presented as they are used in contrast to the aerodynamics of the horizontal turbines. Map (Fig. 1) clearly shows the difference of lift driven rotors compared to drag-driven rotors also with VAWT (Darrieus or Savonius type). However, it is also clear that in the last thirty years, horizontal machines have undergone an enormous leap forward in development, which did not benefit the vertical machines, so that currently only small systems below 100 kW are developed or manufactured [67, 113]. In Germany, the development was mainly carried out by the companies Dornier [5, 24, 29, 44, 59] and Heidelberg-Motor [42]. In the USA, the Sandia National Laboratory has developed a large number of studies have been carried out, the reports of which are available on the Internet [26, 112]. A good overview of all these projects is given in [81]. Worth mentioning is a plant of

Savonius-Rotor   Darrieus-Rotor   H-Darrieus-Rotor
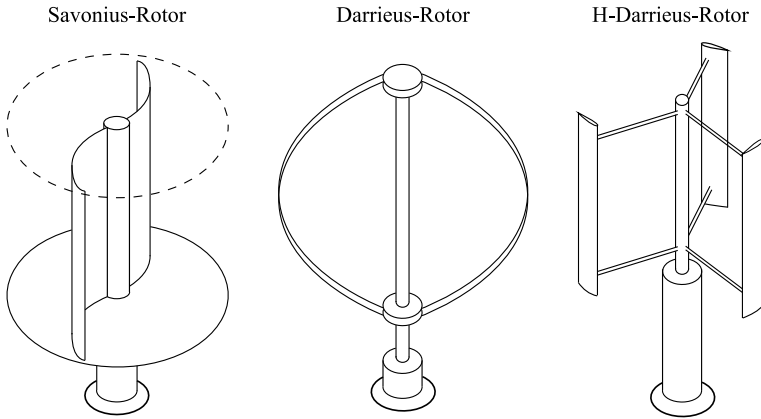
Fig. 16 Wind turbines with vertikal axis
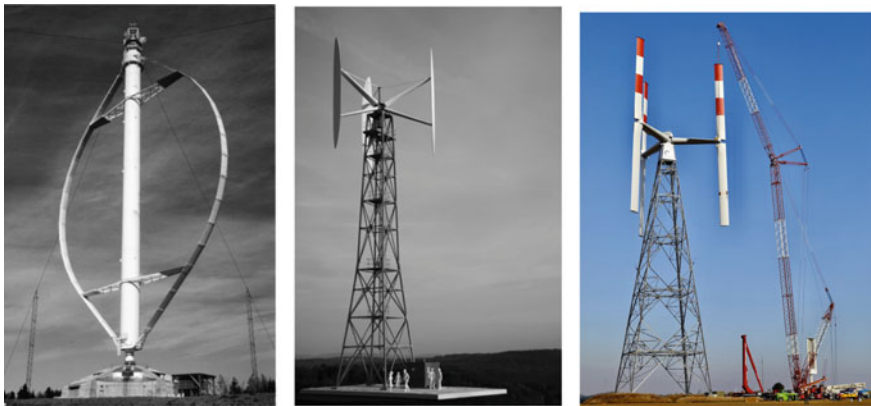
Fig. 17 Left; So far largest VAWT ÉOLE-C at Cap-Chat, Canada, $A = 4000 \, \text{m}^2$, 1988, $P = 4 \, \text{MW}$, used with permission of Prof. Dr.-Ing. Tamm, Nordakademie Elmshorn, Germany. Middle: one 75 kW turbine, 2010 used with permission of HEOS Energy GmbH, Chemnitz. Right: Agile A32 with approximately 750 kW rated ppwer and avout $1700 \, \text{m}^2$ rotor swept area. ©Agile Wind Power, 2021

the company Heidelberg-Motor, which has been in operation in the Antarctic since the beginning of the 90s until 2008 was used for power generation [138]. In 2022, a vertical turbine is to be erected there again. Only recently have new studies been started on optimization [60, 82]. Paulsen et al. [82] describes the results of a project to develop a 20 MW VAWT for the deep sea.

In the usual way, let v_1 be the wind speed, $\omega = 2\pi RPM/60$ be the angular velocity derived from RPM Thus $\lambda = \omega R/v_1$, the tip-speed ratio, is a important parameter. As A. Betz already showed in 1926, his model only applies to a wind turbine with horizontal axis, the effect of which on the air flow through an (infinitely thin) disk of swept area $= 2\pi R_{tip}^2$ is modeled. In order to reach or even exceed

$c_P^{\text{max,Betz}} = 16/27 = 0.593$ (Eq. (24))a lso for VAWT many efforts have been made to achieve this goal.

Main questions in the design of such rotors are thus:

- How close can you get to that value?
- What operating and fatigue loads does such a turbine experience?
- Can it compete with systems with a HAWT?

The last question can of course only be decided together with cost models [38, 39].

6.2 Aerodynamics of H-Rotors

Momentum Theory 1: Single Streamtube model of Wilson et al. [133]
In order to determine and discuss the power coefficient c_P of a VAWT analogously to that of a HAWT ting, Wilson [133] assumes $c_L = 2\pi \sin(\alpha)$[6] representing as bound circumferential circulation, attached to the wings. If one averages over a period, then one arrives in a first approximation at [134]:

$$c_P(x) = \pi \cdot x \left(\frac{1}{2} - \frac{4}{3\pi} x + \frac{3}{32} x^2 \right) \tag{64}$$

with

$$x = \lambda \cdot \frac{Bc}{R}. \tag{65}$$

This model thus gives the maximum power coefficient of $c_p^{\text{max}} = 0.554$ at

$$a_{\text{max}} = \frac{1}{2}\sigma \cdot \lambda = 0.401. \tag{66}$$

Here $\sigma = B \cdot c/R$ with B number of blades and c their chord, is called solidity of the profile. Remarkably important conclusions can be drawn from this comparatively simple model. In the case of high solidity (e.g., in the case of self-starting systems such as the DAWI-10- plant and others) is the optimal tip-speed-ratio determined from Eq. (66) $\lambda_{\text{opt}} = 0.8/\sigma$, seems to be too small by a factor of 2[7] so that very probably further, e.g., Dynamic-Stall effects (see Sect. 6.2) have to be taken into account, since the angles of attack (AOA) in this case become so large that the relation $c_L = 2\pi\alpha$ is no longer considered valid.

However, from Fig. 18 we see that profile drag increases $\lambda(c_p^{\text{max}})$ considerably.

---

[6] Also in this case α represent the angle-of-attack. Strictly speaking it can only be properly defined (and measured) in an ideal 2D flow environment.

[7] The authors thanks Mr. Goerke, Weserwind AG, Germany for this information.
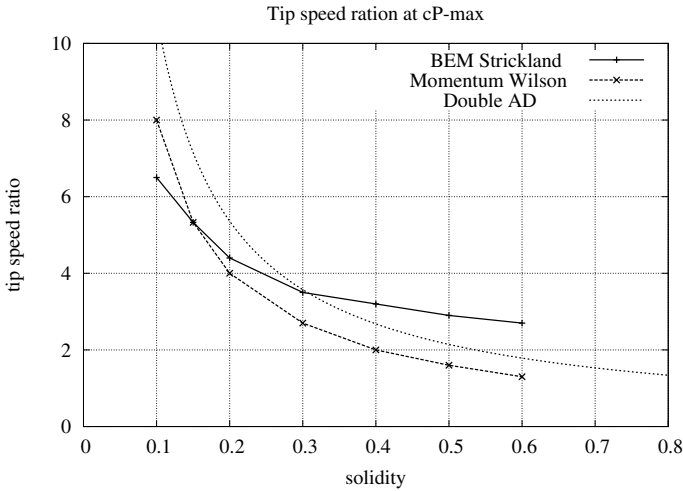
Fig. 18 Tip-speed-ratio for maximum C_P from Wilson (inviscid) Strickland (BEM) and Loth and McCoy (Double Actuator Disk)
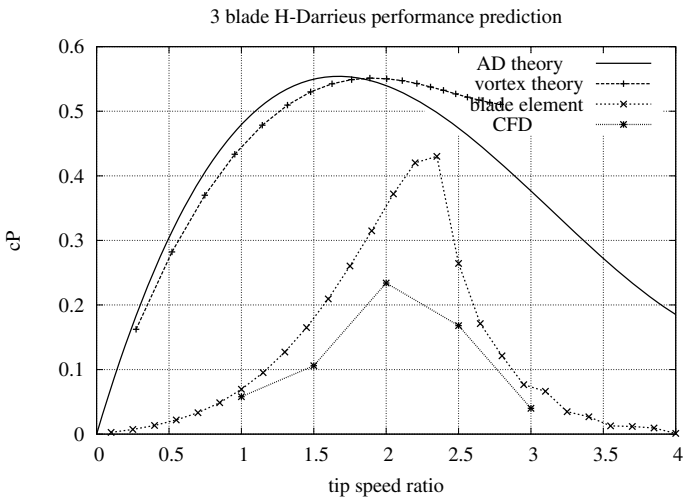
Fig. 19 Various methods used for performance prediction of a VAWT-Rotor of solidity $\sigma = 0.48$

Momentum Theory 2: Multiple Streamtube Model nach Strickland [119]
Compared to Wilson, Strickland specifies a blade element method, i.e., measured (2D, see above) polars can be included in the determination of the power coefficients. If one applies this model to a realized small wind turbine, one obtains the results from Fig. 19.

One can clearly see a reduction of $c_P^{\max}$ by profile drag. Reasons which lead to even a further decrease of $c_P^{\max}$-value are further discussed below within the CFD part Sect. 6.2

However, it is important to note that with all three approaches, the optimal λ is approximately around the same value.

Multiple Streamtube Models

In 1927, Betz already noted that the limit value named after him could be exceeded. If, instead of a disc assumed to be infinitely thin structures are considered. This idea was developed in detail by Loth und McCoy. They used a so-called double Actuator-Disk model and showed $c_P^{max,Loth} \approx 0.62$. Problem 5 discussed this in more detail. However, it has to be said that up to now no prototype could be built that would have explicitly shown these c_P-values.[8] Nevertheless, this model and its extension seems to be the *work horse* [81] of VAWT analysis.

Vortex Models

(a) **Models with steady flow conditions** There are a number of approaches to the description of the flow field which, instead of the flow-field, use the vorticity ($\omega = \nabla \times \mathbf{v}$) as the principal field quantity, since it is possible to use (at least in 2D) ω instead of the more common velocity-pressure formulation of Fluid Mechanics. These approaches are also able to handle the transient character of the flow field [47, 123, 131]. Models are of particular importance in this respect, as they the change in the main flow due to generation, shedding, and convection of vortices (vorticity) at the edges of the blades. Pioneering here was the work of Holme [46], which distributes the bound vortices along a circle ($B \to \infty$) to reach for an asymmetric but stationary model. It is further interesting that Holmes' approach was able to describe a slip-stream-deflection perpendicular to the inflow. As a first step we translated this approach within an Actuator-Disk model. Within that framework, Holme's model can be easily implemented in CFD systems, so that beyond the linearization which was used by Holme to make extraction of numbers easier a more complete and accurate non-linear approach was possible [98].

(b) **Time dependent methods** A fundamental difference in the treatment of vertical rotors is the strong, periodical change of many—if not all—quantities during one revolution. If the number of blades is less than 3, then a simple transient vortex model [120] can properly be used for modeling. It could be shown [20, 135], that rotational-averaged quantities can well be reproduced. Figure 20 shows the flow field of a three-bladed H-rotor with the solidity of $\sigma = 0.3$ und $\lambda = 2$ after two revolutions.

The interest in such vortex methods has recently been rekindled [17, 69]. Furthermore this identicates the load variations effective per rotation, which are used

---

[8] ÉOLE-C reached $c_P^{\max} \approx 0.42$; another well-documented VAWT (SANDIA, 34 m diameter, 260 kW) reached $c_P = 0.41$ at TSR $= 6$ and RPM $= 28$
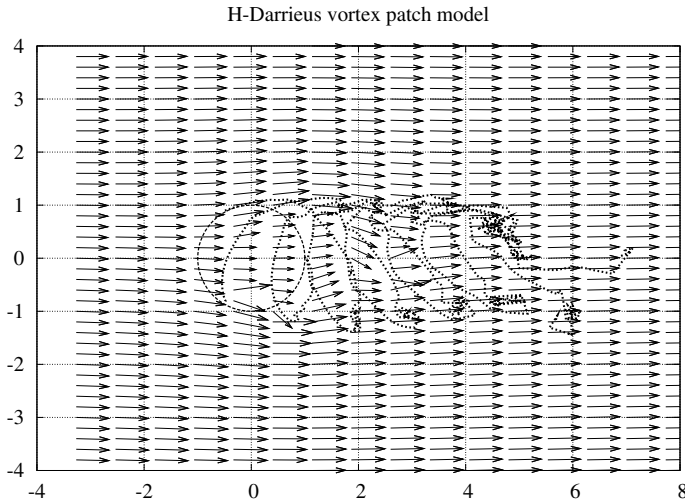
Fig. 20 Snapshot of the flow field of a trifoliate *H* Darrieus-Rotor after two revolutions

for the load spectra for. This is important for the determination of the fatigue strength [18, 25, 72]. More up-to-date overviews are provided by [18, 25, 72]

(c) **Dynamic-Stall** The phenomenon of the dynamic stall is understood as the quite striking change of the Polars due to dynamic inflows, e.g., when the wing oscillates. A detailed discussion with respect to VAWT is given in Oler et al. [78]. We only note here that this effect with large solidity as well as small TSR—and thus large AOA-changes—is particularly pronounced.

(d) **3D CFD** Because of the complicated flow conditions in VAWTs, 3D CFD seems to be the best solution offering method. Bangga et al. [4] compare different measured plants of varying solidity $\sigma = 0.25$ bis 1.3. Prediction of position and value maximum power are in-accurate even with highest spatial resolution (meshes) especially in comparison to the much greater effort required in comparison to analogous BEM approaches.

(e) **Remarks on selection rules for the aerodynamic profiles** In contrast to the horizontal machines in which circulation $\Gamma \approx c \cdot C_l$ is an important parameter determining blade design this function takes on the solidity $\sigma = B \cdot c/R$. For this reason C_l—and thus the whole profile—is included only implicitly as in all other concepts either ideally $C_l = 2\pi\alpha$ is to be set or otherwise polar tables have to be used.

If we consider the tangential force generating the driving moment in its details, the following applies:

$$C_t = C_l \cdot \sin(\alpha) - C_D \cdot \cos(\alpha) \tag{67}$$

$$= C_L \left(\sin(\alpha) - \frac{1}{GZ} \cdot \cos(\alpha) \right) \tag{68}$$
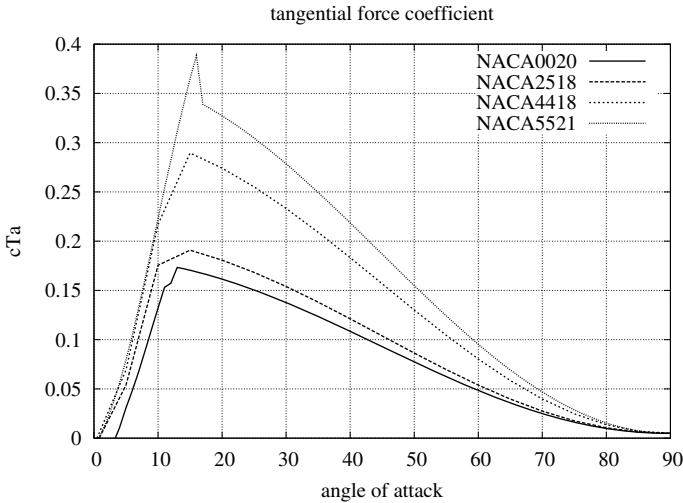
Fig. 21 Comparison of profiles for use in VAWTs: $C_t(\alpha)$

with $GZ = c_L/c_D$. Therefore local optimization would lead to high c_L constraint to high L2D ratio.[9] Therefore instead of a local optimization a global one (i.e., for the whole blade) is much more meaningful:

$$\frac{1}{2\pi}\langle C_t \rangle := \int\limits_{0}^{2\pi} C_t/\varphi) \cdot \mathrm{d}\varphi \to \max. \tag{69}$$

where by one is confronted with a so-called variational problem.

Figure 21 shows the dependence of the tangential force from the angle-of-attack for different four-digit NACA profiles.

It is clearly visible that symmetric profile at small AOAs ($<7°$) and sub-critical ($RN < 500k$) Reynolds numbers can develop negative tangential forces (up to $40°$) of the a full revolution.

Paraschivoiu [81] as Duetting [23] and Kirke [48] in their investigation are more detailed on this question, whereby [23] focuses on the important starting behavior.

Experimental investigations for a so-called DAWI-10 machine were carried out by Meier et al. [65] DAWI-10 possesses a comparable large solidity $\sigma = 0.69$. As a result measured C_t as a function of azimuthal angle shows a strong deviation from the measured values.

We would like to conclude this section with the following recommendations for profile selection:

---

[9] Paraschivoiu references in [81], p. 248, a specific profile which at a L2D ratio of 75 has a $c_L = 1.0$ almost doubled as other profiles, Reynolsnumber = 3M.

- The effect of camber and increased AOA (nose turned out) is equivalent to an increase of chord.
- The effects of the dynamic stall are to be included in the aerodynamic modeling, when small tip-steed-ratios occur due to large solidity.
- Modern symmetrical (see [68] and for discussion of NACA 00tt versus NACA 63ctt[10]) can be developed, for example using EPPLER's code or generic optimization algorithms (compare to [10]).

Application of Computational Fluid to VAWT

Finally a few words should be spent to the application of CFD methods for analysis and performance prediction of VAWTS. As the flow is much more complex than for HAWTs it is no surprise that this is reflected in a CFD model and case set-up as well. Bangga et al. [4] give a recent review of what can be reached by today's capabilities.

6.3 Aero-Elastics of VAWTs

The structural design of a wind turbine is determined by the aerodynamic loads originating from the wind. Both extreme (gust of the century) and operational loads (nominal wind incl. turbulent fluctuations) determine the dimensioning of the material. The specific aerodynamic modeling thus has an effect far beyond pure aerodynamics. Unfortunately, there are currently no or only a few systems available that can model VAWTs in that respect. An exception is the system developed by Vollan [129, 130] GAROS.

In [50] we have modeled a sample-turbine (intended to use for a wind-driven vehicle, see Sect. 7). As a typical output a stability diagram (Campbell-Diagram) was generated, see Fig. 22.

It can be seen that below the rated speed (in this case 120 RPM = 2 Hz) and between the 1P- and 3P- (nP = n-times rotor speed) excitation a number of Eigen-frequencies can be found. However, the total damping of the system is always negative, so that no aerodynamic divergence is to be expected. Especially the large tower head mass of approx. 650 kg (corresponding to 130 kg/kW) seems to be responsible for the relatively small values of these Eigen-frequencies However, one has to consider that because of $\nu \sim m^{-1/2}$ a halving of the tower head mass is accompanied by only a 30% increase in frequencies. It should be further noted at this point that the so-called simplified load diagram of IEC 61400-2 for small wind turbines with swept area $< 200\,\mathrm{m}^2$ can also be transferred to VAWT [45, 99].

As already noted, large (>5 MW rated power) offshore VAWTs are potentially to be through-from more favorable energy prices if, for example, the aeroelastic insta- and the additional aerodynamic fatigue loads in the lee-side circulatory half can be predicted with certainty. The former is investigated in [79].

---

[10] Miglore [68] talks of 20% increase of yield.
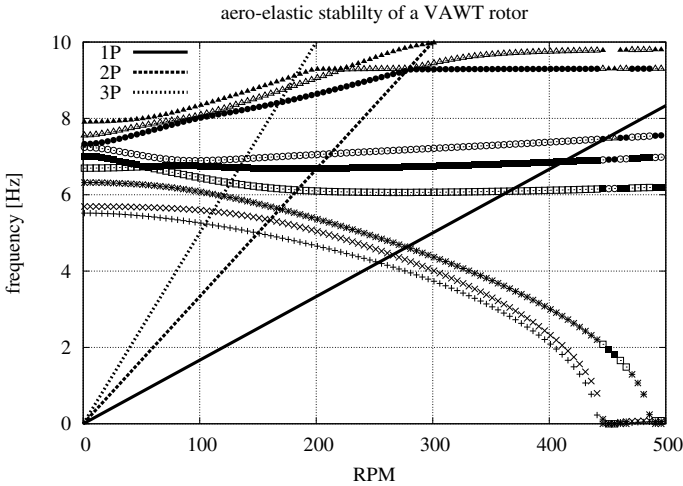
Fig. 22 Campbell-diagram of a small VAWT

6.4 A 50 kW Sample-Rotor

This machine (see Fig. 17b) of blade length $H = 10,21$ m and rotor diameter $2 \cdot R = 10$ m, e.g., swept area $A = 100$ m^2, has $(B = 3)$ solidity of $\sigma = 0.68$ an a maximum chord of $c_{max} = 1.31$ m. However, the blades taper noticeably toward the tip so that this value -if regarded as an representative one - is somewhat overestimated. Figure 23 shows measured power-date and prediction by Strickland's cdode [119]. As one can see there is a pronounced variation in the location of the power maximum as well as a large miss match in the maximum power itself. Due to the relatively low wind speeds, only a few measured values in the range of significant electrical power are available. Through suitable averaging (binning) the dispersion can be significantly reduced, however, a large, so far unexplained difference to the power curve with the leaf intersection method.

6.5 Design Rules for Small Wind Turbines of H-Darieus Type

- An overall concept must be drawn up prior to any design.
- If the machine is to be self-starting, i.e. $c_m(0) > 0$, the torque curve of the electric generator must fit to the aerodynamic design.
- A trifoliate rotor with a cambered profile that is not too thick often seems suitable.
- It is possible to design and use new families of profiles [15]. They seem to represent an improvement over the four-digit profiles of the NACA family
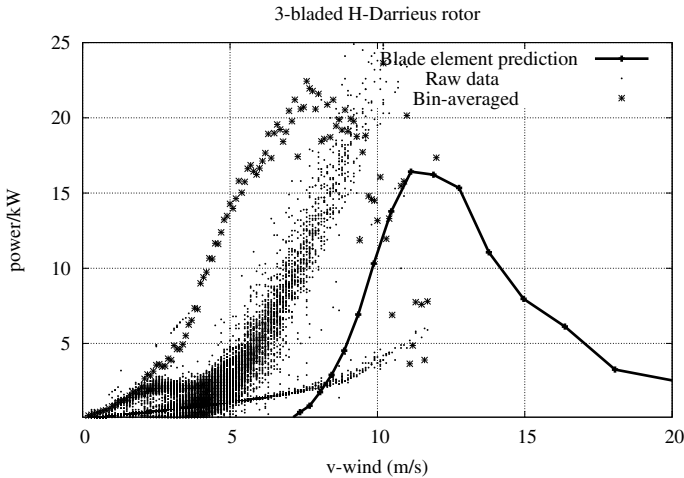
Fig. 23 Measured and predicted power of a 50 kW-VAWT

- Optimum TSR is determined by solidity $\sigma = Bc/R$. It should not take values below 3.[11] So that the maximum angles of attack do not become too large and Dynamic-Stall effects must be taken into account.
- An aeroelastic simulation model (e.g., with GAROS or CACTUS) must be used in the early stages of development, so that the specific tower head masses can be kept in a sensible region clearly below 100 kg/kW can be achieved.
- A type certification to be aimed at and should show the seriousness of the undertaking.

6.6 Summary: VAWT

Basics
First, a brief overview of the aerodynamic models developed so far was given given. It turns out that many of the older semi-analytical methods (e.g., the vortex-ring [Cylinder] Model) can be easily integrated into existing CFD systems. Thus stationary, i.e., comprehensively averaged, examinations can be carried out in a short time. As important results can be noted: It does not seem to be impossible to Betz's limit (= 0.59), an optimal fast running number can be obtained from Eq. (66) or Fig. 18. Criteria for aerodynamic profile selection were benamed. In [71] the historical development up to 2019 is summarized very nicely.

Profiles
Machine-optimized aerodynamic profiles are available from VAWT in by far not as high a volume. number as is the case with HAWT. This is reflected not least in the

---

[11] Paraschivoiu ([81], p. 177) even assumes dynamic stall for $\lambda < 4$!

Fig. 24 Principle of a wind car
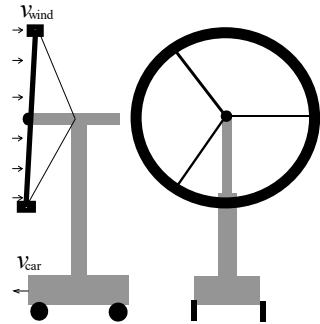
still customary the use of four-digit NACA profiles, which were introduced in the 1930s, is still a problem. The development of stand-alone profiles, as was the case for HAWT in Delft or at Risø is still completely pending. A remarkable exception to this is [15].

Starting behavior

The possibility of self-starting VAWTs (which is difficult using blades with high aerodynamic efficiency, $c_m(\lambda = 0) > 0$) was already investigated int the 1980ies in various PhD theses[15, 23]. The results of these investigations was a design with high solidity (>0.4) using cambered profiles, e.g., NACA 4418. Matching the torque characteristics (mechanical and electrical rotor) is important and it should be examined whether an alternative rotor design with smaller solidity and a generator switchable to motor-mode represents an alternative.

7 Wind Driven Vehicles with Rotor

7.1 Introduction

In Sect. 3.2 we briefly discussed vehicles with a rigid sail and showed that it is advantageous to use lift forces for propulsion. In this context, it is interesting to take a more general look at so-called headwind vehicles. The concrete reason for that is that in 2008 an international competition *Racing Aeolus*, was proposed and held in Den Helder, The Netherlands, for the first time. This was continued in 2009 and 2010 in Stauning, Denmark, and took place since 2011 in Den Helder again. In 2020 and 2021, the competition could because of the COVID-19 pandemic not be carried out. From the group of participants the Danish [32], the Stuttgarter [55, 56] and that from The Netherlands [8] details of their design methodology are published, so that it seems advisable to do so also for the wind-cars from Kiel [90] in some detail. Figure 24 shows the principle of the wind car. A wind turbine converts kinetic energy of the wind into one that can be used by the drive train to power the vehicle to move

forward. However, in contrast to a stationary wind turbine a large force, thrust, has to be transported and this spends the majority of the power generated.

7.2 On the Theory of Wind-Driven Vehicles

The concepts for verting the kinetic energy of the wind by means of a wind turbine into mechanically useful energy are discussed in detail in Sect. 3 More can be found, for example in [19, 91]. The essential criterion in this case is that the rotor is designed in such a way that it should be that, as stated

$$c_P := \frac{P}{\frac{1}{2}\rho v^3 \frac{\pi}{4} D^2}$$

(70)

is maximized. It is easy to show that then the thrust (= force on the turbine in wind direction) by

$$c_T := \frac{T}{\frac{1}{2}\rho v^2 \frac{\pi}{4} D^2}$$

(71)

with $c_T^{\text{Betz}} = 8/9 = 0.89$.

A wind turbine optimally designed for power extraction thus suffers large thrust, which must be transported continuously. The dimension- less ratio c_P/c_T is 2/3.

7.3 Numerical Example

In competition, the swept rotor area is limited to $2 \times 2 = 4\,\text{m}^2$. If a rotor with a horizontal axis is used, the area is reduced to $\pi = 3,14\,\text{m}^2$. If one assumes a wind velocity of 7 m/s and a vehicle velocity of 3.5 m/s then numerically we have $P = 1\,320\,\text{W}$ and $T = 188\,\text{N}$. If there were no other forces to overcome, it would take the transport of the thrust alone the power of $P_{\text{thrust}} = 660\,\text{W}$.

This is the idealized case. In reality, a well-designed rotor has a $c_P = 0,36$ only about 60% of the mentioned power (= 780 W). A vehicle with assumed 50 N rolling resistance needs additionally a power of $50N \cdot 3.5\,\text{m/s} = 175$ W. This means that this vehicle does not drive against the wind at all. Therefore, it makes sense to lay out the blade so that $v_{\text{car}}/v_{\text{wind}} \to \text{max}$. This is achieved with the help of the BEM method (see Sect. 4).

Two optimization strategies for the design of an optimal blade geometry have been already described:

- Chose an conventional (i.e., wind turbine like) $c(r)$ and optimize local flow angle ϕ(Stuttgart).

- Chose AOA that the local profile work at maximum c_L/c_D and optimize $c(r)$ (Copenhagen).

The Stuttgart design (from 2008, called *Ventomobil*) is so detailed that comparisons can be made. From [55, 56] one sees $\lambda = 5$, $c_P = 0.24$ and $c_T = 0.23$. At $v_{\text{wind}} = 8$ m/s this then results in $v_{\text{car}}^{\text{max}} = 5$ m/s and a driving power of $P = 250$ W.

In contrast Denmark's design *WinDTUrbineracer* [138] may be summarized in the following equation:

$$C_{\text{PROPF,loc}} = \eta_P \eta_T \left(1 + \frac{1}{V/V_{\text{wind}}}\right) C_{\text{P,loc}} - C_{\text{T,loc}} \rightarrow \max. \tag{72}$$

7.4 The Kiel Design Method

W start from an approach from de Vries [116] and begin with

$$C_T = \frac{8}{\lambda^2} \int_0^\lambda (1 - aF)aF \left(1 + \frac{\tan(\varphi)}{L2D}\right) x \, dx \tag{73}$$

$$C_P = \frac{8}{\lambda^2} \int_0^\lambda (1 - aF)aF \left(\tan(\varphi) - \frac{1}{L2D}\right) x^2 \, dx \tag{74}$$

Here $L2D$ is the lift-to-drag ration, $x = \lambda r/R$ local TSR and and F Prandtl' tip-loss factor [91], see Eqs. (61) and (35)–(37) for the complete BEM-Algorithm The optimization problem, Eq. (72):

$$C_{\text{PROPF,loc}} \rightarrow \max \tag{75}$$

we solve within a short FORTRAN program using a double binary Search Procedure.

7.5 Evaluation

The output of the results of the above optimization task is done appropriately as is usually done in mechanics in the form of a (modified) dimensionless drag coefficient of the vehicle.

$$K := C_D \cdot \frac{A_V}{A_R} \tag{76}$$
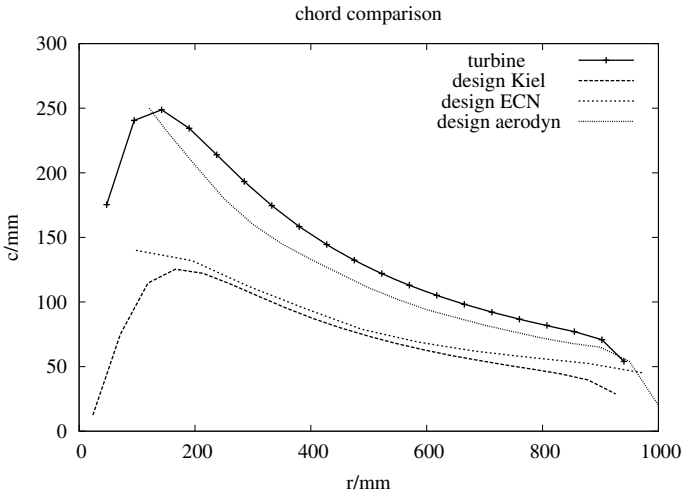
Fig. 25 Optimum chord distribution for blades of wind-driven vehicles
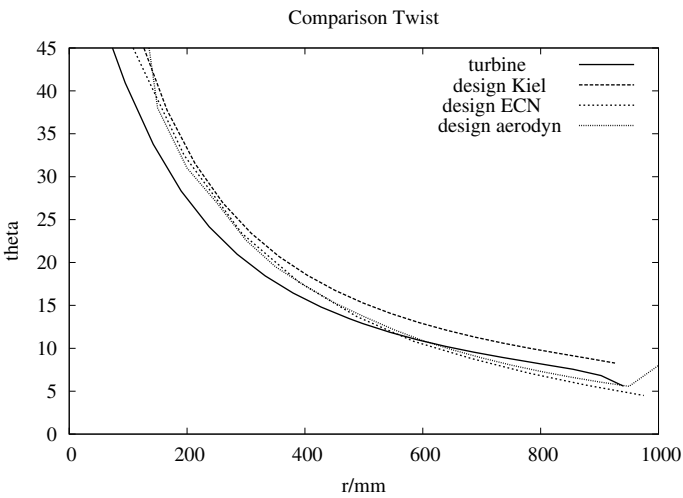
Fig. 26 Optimale Verwindungsverteilungen fuer Blaetter von Windfahrzeugen

C_D is the intrinsic drag coefficient of the vehicle, defined via $D := c_D \cdot \rho/2v^2 \cdot A_V$. A_V and A_R are the projected areas of the rotor and the vehicle (see Fig. 24). The problem with this approach is the inclusion of a constant rolling resistance. As an important result it can be stated that there is basically no upper limit on the driving speed there. Special blade geometries (chord and twist distribution) can also be derived (see Figs. 25 and 26).

Table 2 Results of the optimization for a wind-powered vehicle

K	a	v_c/v_{wind}	c_P	c_T	c_P/c_T	$\eta_{\text{Drivetrain}}$
0.013	0.05	2,0	0.16	0.18	0.89	>0.8
0.06	0.1	1,0	0.29	0.35	0.83	0.7
0.14	0.13	0.75	0.37	0.47	0.79	0.7
0.33	0.18	0.5	0.44	0.60	0.73	0.7
1,0	0.24	0.25	0.50	0.74	0.68	0.7
3,1	0.29	0.1	0.51	0.82	0.62	0.7
36	0.31	0.01	0.52	0.86	0.60	0.7

Design parameters for our car are: $B = 3$, $\lambda = 5.5$, Design-lift $c_L = 1.0$ and lift-to-drag ration = 80. Rotor radius is equal to 900 mm drive train efficiency is assumed to be 70% (Table 2).

It seems not to be excluded to use the results of this special blade geometry also by pitching commercially available (for example by Wind Dynamics AS, Denmark) blades. Figure 27 compares our results with the optimization of Sørensen [116]. It should be noted that our values are not exact because of additionally included variables (c_D and tip-loss correction) and should basically result in lower velocities. In Fig. 27, two additional upper K-boundaries are drawn, which are unrealistically exclude high c_P values. Furthermore, it can be seen that the published values from [55] can be realized with K-values below 0.005.

If in 2009 a vehicle with $v_{\text{car}}/v_{\text{wind}} \geq 0.5$ is separately awarded (and achieved, see Fig. 29). Now the condition for this set to $v_{\text{car}}/v_{\text{wind}} \geq 1$ Our analysis (Fig. 27) shows that this places high demands on all components.
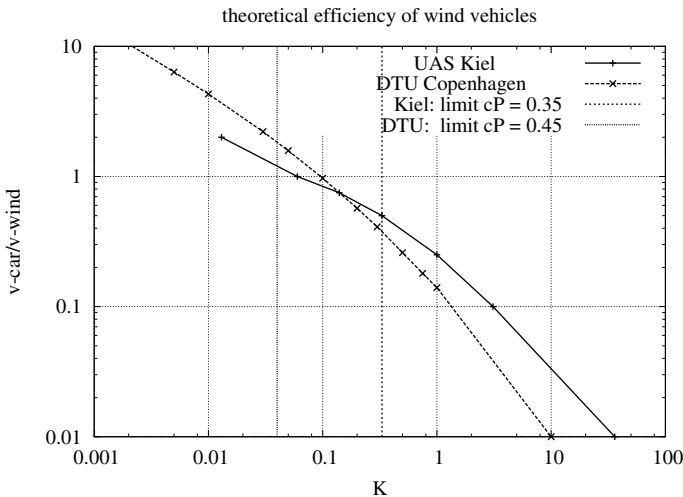
Fig. 27 Optimum layouts for wind-powered vehicles from Copenhagen and Kiel

7.6 Completed Vehicles

The first vehicles with a VAWT rotor and an electric drive train did not bring any satisfactory results. Therefore, since 2009, a radically simplified concept has been created and also realized. A diffuser ring made of GRP was constructed and could be very light (12 kg mass). The yaw and pitch system was dispensed with and a single four-speed moped transmission (ratios 6, 8, 10 and 17 to 1) is used. The rear axle has two cardan shafts with freewheel and a chain. Since 2012, various own drive trains have been designed and built [90]. The first success was achieved in 2010. Kiel took second place in the overall standings at the weak winds around 5 m/s 2019 as well, but with a fundamentally changed approach, the Twin Thunder, a double rotor, see Fig. 28. In 2018 and 2019, the Canadian ETS team from Montreal achieved a speed ratio of 1.15 and 1.14 respectively. An overview for the results from the year 2019 is given in Table 3.

The speed ratios achieved are shown in Fig. 29 are compared with the best values achieved by other vehicles and forecasts.

Fig. 28 Kiel's wind vehicle *Baltic Twin Thunder*, 2019. *Photo* Alois Schaffarczyk

Table 3 Results from racing Aeolus 2019

Vehicle	Rank	Endurance %	Drag race	Fastest %	Innovation
Chinook	1	105.5	1	114.8	2
BTT	2	59.2	2	78.4	1
Wind turbine racer	3	72.9	3	103.3	8
NeoVento	4	27.3	4	47.7	4
Spirit of Amsterdam					
DTU E	5	20.9	–	40.4	7
Stormy Sussex	6	–	–	–	2
REK Yildiz	7	–	–	–	5
Fibershark-Alkmaar	8	–	–	–	6
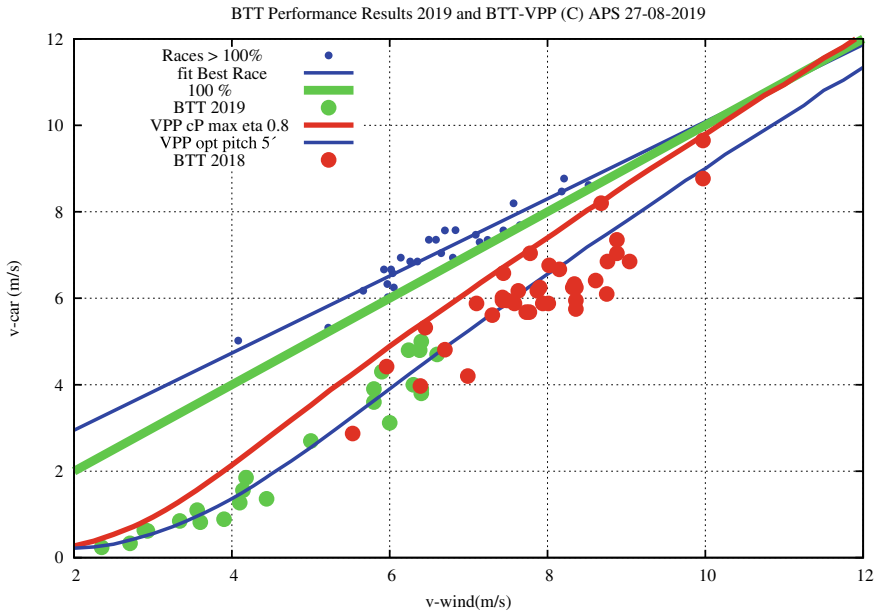
Fig. 29 All results obtained with Baltic Thunder vehicles until 2019

7.7 Summary: Wind Vehicles

In order to maximize the power available for the propulsion of a wind-driven vehicle, a different optimization criterion has to be applied than for the design of a classical wind turbine optimized for power extraction. In any case, the load on the wind turbine, whether it is described by a or c_T has tob decreased further, interesting discussion about differences and similarities between propeller and turbine operation (i.e., with tailwind) can be found in [32].

It can be seen that competitive speeds ($v_{car}/v_{wind} > 1.0$) are only achieved if the K-value has values significantly less than ($K = 0.1$) and the drive train must have an efficiency of more than 80%. The Kiel-based wind car Baltic Thunder *Baltic Thunder* has so far been the best place-The teams have achieved second place in both 2010 and 2019. Other teams now reach a speed ratio greater than 1. The current record is for a speed ratio of almost 1.15 (team chinook, 2018). This was achieved by minimizing all parasitic resistances and a significant reduction of the mass(<150 kg) is achieved An independent blade development, as also carried out by other groups (cf. Figs. 25 and 26) has been carried out since 2011, but with limited success.

8 Homework Problems

1. What is the annual yield of a wind turbine with $D = 120$ m, $c_P = 0.5$, $v_{nenn} = 11$ m/s and 2 500 full-load hours? How high is the annual yield (in euros) with a remuneration of 5 Eurocent per kWh?

2. Using Eqs. (62) and (63) derive the maximum relative thickness c/R of a blade at $r/R = 0.25$ and $C_L = 1.0$. many meters is this for a blade from problem 1?

3. How big is the (relative) in yield for the turbine from problem 1 if it is operated) in winter ($\vartheta = -20°C$) at sea-level and) in summer ($\vartheta = 30°C$) in the mountains ($H = 1500$ m)?

4. Show: If one assumes a Rayleigh distribution of wind speed:

$$P(v) = \frac{\pi}{2} \frac{v}{\bar{v}} \exp\left(-\frac{\pi}{4}\left(\frac{v}{\bar{v}}\right)^2\right)$$

then the maximum annual energy yield still can be described by a *1-2-3 equation*:

$$\overline{P} = \rho^1 \cdot \left(\frac{2}{3}D\right)^2 \cdot \bar{v}^3.$$

What average $\bar{c}_P$ does this correspond to? Compare this with Problem 1!

5. Consider a double Actuator-Disk as a model of a wind turbine with a two contra-rotating rotors or as that of a Darrieus rotor. Show under the assumption of a fully developed slip-stream from the disk 1 as an inflow condition to the disk 2 ($v_2^{in} := v_1 \cdot (1 - 2a)$):

$$c_{P2} = \frac{16}{27} \cdot (1 - 2 \cdot a)^3,$$

and

$$c_P^{\max} = c_{P1} + c_{P2} = \frac{64}{125} + \frac{16}{125} = 0.512 + 0.128 = 0.64 \ .$$

Also determine the respective thrust coefficients c_{T1}, c_{T2} and c_T.

6. Design a wind vehicle for $v_{\mathrm{wind}} = 8$ m/s and $v_{\mathrm{car}} = 4$ m/s. Swept rotor area is assumed to be 3 (2,5) m^2 and K (Eq. 76) is 0.1. Discuss your results as a function of the drive train efficiency and in light of the diagram Fig. 27, and Table 2, resp.

References

1. Abbot IH, von Doenhoff AE (1959) Theory of wing sections. Dover Publications Inc., New York (USA)
2. Althaus D (1996) Niedriggeschwindigkeitsprofile. Vieweg, Braunschweig
3. Ashwill TD (1992) Measured data for the 34 m vertical axis wind-turbine, Sandia National Laboratories, SAND91-2228. Albuquerque, NM
4. Bangga G, Dessoky A, Wu Z, Rogowski K, Hansen MOL (2020) Accuracy and consistency of CFD and engineering models for vertical axis wind turbines. Energy 206. https://doi.org/10.106/j.energy.2020.118087
5. Bankwitz H, Fritzsche A, Schmelle J, Welte D, Swamy C (1975, 1978 und 1982) Entwicklung einer Windkraftanlage mit vertikaler Achse (Phase I–III), Friedrichshafen
6. Betz A (1926) Wind-Energie und ihre Ausnuetzung durch Windmuehlen. Vandenhoeck & Ruprecht, Goettingen
7. Boettcher J (ed) (2020) Green banking realizing renewable energy projects. De Gruyter, Berlin, Germany
8. Boorsma K, Machielse L, Snel H (2010) Performance analysis of a shrouded rotor for a wind powered vehicle. In: Proceedings of the TORQUE 2010. Crete, Greece
9. Boorsma K, Schepers JG, Gomez-Iradi S, Herraez I, Lutz T, Weihing P, Oggiano L, Pirrung G, Madsen HA, Shen WZ, Rahimi H, Schaffarczyk AP (2018) Final Report of IEAwind Task 29, MexNext, Phase 3, ECN-E-18-003, Patten, The Netherlands
10. Bourguet R, Martinat G, Harran G, Braza M (2007) Aerodynamic multi-criteria shape optimization of VAWT blade profile by viscous approach. In: Proceedings of the Oldenburg i. O, Euromech Colloquium Wind Energy
11. Breslin JP, Andersen P (1986) Hydrodynamics of ship propellers. Cambridge University Press, Cambridge, UK
12. Burton T, Sharpe D, Jenkins N, Boßanyi E (2021) Wind energy handbook, 3rd edn. Wiley, Chichester
13. Carli R (1986) Design, construction, installation and results of initial trials of a vertical axis variable geometry windenergy converter. In: Proceedings of the EWEA conference and Expo, Rome, Italy
14. CFX 4.2 (1997) Solver AEA technology. Harwell, Oxfordshire, United Kingdom
15. Claeßens MC (2006) The design and testing of airfoils in small vertical axis wind turbines. M.Sc. thesis. Technical University of Delft, Delft, The Netherland
16. Conway JT, Schaffarczyk AP (2003) Comparison of actuator disk theory with Navier-Stokes calculation for a yawed actuator disk. In: Proceedings of the 8th CASI meeting, Montreal, Canada
17. Corporation FloWind (1996) Final project report: high-energy rotor development, test and evaluation, Sandia National Laboratories, Sand96-2205. Albuquerque, NM

18. De Tavernier D, Sakib M, Griffith T, Pirrung G, Paulsen U, Madsen HÅ, Keiher W, Ferreira C (2020) Comparison of 3D aerodynamic models for vertical axis wind turbines H-rotor and Φ-rotor TORQUE 2020. J Phys: Conf Ser 1618:052041

19. de Vries O (1979) Fluid dynamics aspects of wind energy conversion. AGARDograph, No. 242, Neuilly-sur-Seine, France

20. de Vries O (1979) Fluid dynamic aspects of wind energy conversion; Chap. 4.5: vertical-axis turbines, AGARD-AG-242, Neuilly-sur-Seine, France

21. de Vries O (1983) On the theory of the horizontal-axis wind turbines. Ann. Rev. Fl. Mech 77–96

22. Dumitrescu H, Alexandrescu M, Alexandrescu A (2005) Aerodynamic analysis of a straight-bladed darrieus rotor including dynamic-stall effects. Rev Roum Sci Technol 99–113 (Bucarest, Roumania)

23. Duetting J (1987) Untersuchungen ueber das Startverhalten von Windrotoren mit vertikaler Achse. Dißertation der Universitaet Bremen, Germany

24. Eckert L et al (1990) Analyse und Nachweis der 50 kW-Windenergieanlage (Typ Darrieus), Interner Bericht, Dornier GmbH, MEB 55/90

25. Ferreira CS, Madsen HÅ, Barone M, Roscher B, Deglaire P, Ardiun I (2014) Comparison of aerodynamic models for vertical axis wind turbines TORQUE 2014. J Phys: Conf Ser 524:012125

26. Ferreira CS (2009) The near wake of the VAWT. Ph.D. thesis. Technical University Delft, The Netherlands

27. FLUENT Inc. (1998) FLUENT 5 user's guide. Fluent Inc., Lebanon, NH

28. Freudenreich K, Kaiser K, Schaffarczyk AP, Winkler H, Stahl B (2004) Reynolds-number and roughness effects on thick airfoils for wind turbines. Wind Eng 5:529–546

29. Fritzsche A et al (1991) Auslegung einer Windenergieanlage mit senkrechter Drehachse im Leistungsbereich 350–500 kW. Dornier GmbH, Friedrichshafen

30. Froude RE (1889) On the part played in propulsion by differences in fluid pressure. Trans Inst Nav Arch 390

31. Gasch R, Twele J (eds) (2016) Windkraftanlagen, 9th edn. Springer, Heidelberg

32. Gaunå M, Stig Øye, Mikkelsen R (2009) Theory and design of flow driven vehicles using rotors for energy conversion. In: Proceedings of the EWEC, Marseille, France

33. Glauert H (1993) The elements of airfoil and airscrew theory, 2nd edn. Cambridge University Press, UK

34. Hansen MOL, Srensen NN, Flay RGJ (1999) Effect of placing a diffuser around a wind turbine. In: Proceedings of the EWEC, Nice, France

35. Hansen MOL (2015) Aerodynamics of wind turbines, 3rd edn. Earthscan, Oxon (UK)

36. Hansen MOL, Srensen DN (2001) CFD model for vertical axis wind-turbine. In: Proceedings of the EWEC, Kopenhagen, Denmark

37. Hansen MOL, Johannson J (2004) Tip studies using CFD and comparison with tip loss models. In: Proceedings of the EAWE conference the science of making torque from wind, Delft, The Netherlands

38. Haris A (1991) The variation in cost of energy with size and rated power for vertical axis wind-turbine. In: Proceedings of the British wind energy conference

39. Harrison R, Hau E, Snel H (2000) Large wind turbines—Design and economics. Wiley

40. Hau E (2016) Windkraftanlagen, 6th edn. Springer, Berlin

41. Healey JV (1981) Tandem-disk theory—With particular reference to vertical axis wind turbines. J Energy 4:251–254

42. Heidelberg G, Kroemer J (1993) Windkraftanlage H-Rotor: Erfahrungen. Aktuelles und Ausblick, Husumer Windenergietage, Husum, Germany

43. Heier S (2018) Windkraftanlagen, 6th edn. Springer, Heidelberg

44. Henseler H (1990) Eole-D Abschlußbericht, Friedrichshafen

45. Heym C (2010) Entwicklung eines Berechnungsprogramms fuer den allgemeinen Sicherheitsnachweis von Kleinwindanlagen mit vertikaler Rotorachse nach IEC 61400-2:2004, Masterthesis, FH Kiel, Kiel

46. Holme O (1976) A contribution to the aerodynamic theory of the vertical-axis wind turbine. In: Proceedings of the international symposium on wind energy systems. Cambridge, England

47. Katz J, Plotkin A (2001) Low-speed aerodynamics. Cambridge University Press

48. Kirke BK (1988) Evaluation of self-starting vertical axis wind turbines for stand-alone applications. Ph.D-thesis. Griffith University, Australia

49. Kleinhans D, Friedrich R, Schaffarczyk AP, Peinke J (2009) Synthetic turbulence models for wind turbine applications. In: Peinke J, Oberlack M, Talamelli A (eds) Progress in turbulence III. Springer proceedings in physics, vol 131. Springer, Berlin, Heidelberg. https://doi.org/10.1007/978-3-642-02225-8_26

50. Kleinmann D (2007) Aeroelastische Analyse einer 5 kW H-Darrieus Anlage mit GAROS. Studienarbeit, FH Kiel

51. Klimas PC, Sheldahl RE (1978) Four aerodynamic prediction schemas for vertical axis wind-turbines: a compendium, Sandia National Laboratories, Sand78-0014. Albuquerque, NM

52. Korjahn M, Schaffarczyk AP, Schlipf D (2022) Kiel Univ Appl Sci. Kiel Germany. https://doi.org/10.13140/RG.2.2.18455.04009

53. Lakshminarayana B (1996) Fluid dynamics and heat transfer of turbomachinery. Wiley, New York

54. Lapin EE (1975) Theoretical performance of vertical axis wind-turbine. In: Trans ASME Winter Meeting Houston, Texas, USA

55. Lehmann J, Miller A, Capellaro M, Kuehn M (2008) Aerodynamic calculation of the rotor for a wind driven vehicle. In: Proceedings of the DEWEK, Bremen, Germany

56. Lehmann J, Kuehn M (2009) Mit dem Wind gegen den Wind. Das Windfahrzeug InVentus Ventomobil, Physik in unserer Zeit, pp 176–181

57. Leishman JG (2006) Principles of helicopter aerodynamics, 2nd edn. Cambridge University Press, Cambridge, UK

58. Ledoux J, Riffo S, Salomon J (2021) Analysis if the blade element momentum theory. SIAM J Appl Math 81(6):2596–2621

59. Lieferung und Montage einer 2,25 MW Darrieus-Windenergienanlage EOLE-D (1990) Interner Bericht, Dornier GmbH

60. Lobitz DW, Ashwill TD (1986) Aeroelastic effects in the structural dynamic analysis of vertical axis wind-turbine, Sandia Report, SAND85-0957. Albuquerque, NM, USA

61. Loth JL, McCoy H (1983) Optimization of Darrieus turbines with an upwind and downwind momentum model. J. Energy 313–318

62. Martinez-Toßas LA, Menneveau C (2019) Filtered lifting line theory and application to the actuator line model. J Fluid Mech 863:269–292

63. Maßé B (1986) A local-circulation model for Darrieus vertical-axis wind turbine. J Prop 135–141

64. Mays ID, Clare R (1986) The U.K. vertical axis wind-turbine programme experiences and initial results. In: Proceedings of the EWEA conference and expo, Rome, Italy

65. Meier H, Schneider J-D, Richter B (1988) Meßungen an der Windkraftanlage DAWI 10 und Vergleich mit theoretischen Untersuchungen, Germanischer Lloyd, WE-4/88, Hamburg

66. Melzer R (2006) Konstruktive Entwicklung eines Vertikalrotors fuer Kleinwindkraftanlagen. Studienarbeit, TU Chemnitz

67. Mertens S, van Kuik G, van Bußel G (2003) Performance of an H-Darrieus in the skewed flow on a roof. J Sol En Eng 433–440

68. Migliore PG (1983) Comparison of NACA 6-series and 4-digit airfoil for Darrieus wind turbines. J Energy 4:291–292

69. Mikkelsen R (2005) Private communication. In: Clausen RS, Snderby IB, Anderkjær JA (eds) Eksperimentel og Numerisk Undersgelse af en Gyro Turbine, Master-thesis, DTU, Lyngby

70. Molly J-P (1990) Windenergie - Theorie, Anwendung, Meßung, 2nd edn. C. F. Mueller, Karlsruhe

71. Moellerstroem E, Gipe P, Beurskens J, Ottermo F (2019) A historical review of vertical axis wind turbines rated 100 kW and above. RenSus En Rev 105:1–3

72. Murray JC, Barone M, The development of CACTUS, a wind and marine turbine performance simulation code, AIAA 201-147. https://doi.org/10.2514/6.2011-147
73. Newman BG (1983) Actuator-disc theory for vertical-axis wind turbines. J Wind Eng Ind Aero 347–355
74. Ning SA (2013) CCBlade documentation release 0.1.0. NREL/TP-5000-58819, Golden, CO, USA
75. Nitzsche F (1994) Dynamic aeroelastic stability of vertical-axis wind turbines under constant wind velocity. J Prop Power 3:348–55
76. NREL. nrel.gov/wind/nwtc/openfast.html
77. Okulov VL (2007) Optimum operating regimes for the ideal wind turbine. In: Proceedings of the the science of making torque form wind, Lyngby, Denmark
78. Oler JW, Strickland JH, Im BJ, Graham GH (1983) Dynamic stall regulation of the Darrieus turbine, Sandia Report, SAND83-7029. Albuquerque, NM, USA
79. Owens BC, Griffith DT (2014) Aeroelastic stability investigations for large-scale vertical axis wind turbines TORQUE 2014. J Phys: Conf Ser 524:012092
80. Paraschivoiu I, Desy P (1986) Aerodynamics of small-scale vertical-axis wind turbines. J Prop 282–288
81. Paraschivoiu I (2002) Wind turbine design—With emphasis on Darrieus concept. Polytechnic International Press, Montreal, Canada
82. Paulsen US et al (2015) Outcomes of the DeepWind conceptual design. In: Proceedings of the 12th DeepSea Workshopt, Trondheim, Norway
83. Phillips DG (2003) An investigation on diffuser augmented wind turbine design. Ph.D. thesis. The University of Auckland, Auckland, New Zealand
84. Prandtl L (1919) Zusatz zu: A. Betz: Schraubenpropeller mit geringstem Energieverlust, Nachrichten der Kgl. Ges. d. Wiß. Math-phys Klaße (Berlin)
85. Rankine WJ (1865) On the mechanical principles of the action of propellers. Trans Inst Nav Arch 13
86. Rao HV, Perera GEL (1988) Modified Betz-type limit for optimization of vertical axis wind turbines. In: Proceedings of the BWEA conference, pp 213–220
87. Richards B (1986) Design, fabrication and installation of project EOLE 4MW prototype vertical axis wind turbine generator (VANTG). Proc. EWEC, Rome, Italy
88. Richards B (1987) Initial operation of project EOLE 4MW vertical axis wind turbine generator. In: Proceedings of the wind power 22–27
89. Rohrbach C, Wainauski H, Worobel R (1977) Experimental and theoretical research on the aerodynamics of wind driven turbines, ERDA Contract No. E(11-1)-2615
90. Rohwer B, Schaffarczyk AP (2021) On the aerodynamics design of Kiel's wind cars *Baltic Thunders* Report No. 66 CFD Lab. Kiel University of Applied Sciences, Kiel Germany (in German)
91. Schaffarczyk AP, Aerodynamics and aero-elastics of wind turbines, Chapter 3 of [121]
92. Schaffarczyk AP (1998) CFD Investigations for a wind turbine inside a solar chimney. In: 12th IEA expert meeting on aerodynamics for wind-turbines. Lyngby, DK
93. Schaffarczyk AP (1998) Vergleich verschiedener Numerischer Stroemungßimulationsver-fahren an einem Aktiv-Stall-Blatt und Schlußfolgerungen fuer eine aerodynamische Opti-mierung, 4. Deutsche Windenergiekonferenz. Wilhelmshaven, pp 356–360
94. Schaffarczyk AP, Phillips D (2001) Design principles for a diffusor augmented wind-turbine blade. In: Proceedings of the EWEC, Copenhagen
95. Schaffarczyk AP, Conway JT (2003) Analytical and numerical actuator disk theories for yawed rotors, Bericht Nr. 37 des Labors fuer numerische Mechanik, Kiel
96. Schaffarczyk AP, Winkler H, Freudenreich K, Kaiser K, Rebstock R (2003) Reynolds number effects on thick aerodynamic profiles for wind turbines. In: Proceedings of the EWEC, Madrid, Spain
97. Schaffarczyk AP, Actuator disk modelling of contra-rotating wind-turbines, Bericht Nr. 32 des Labors fuer numerische Mechanik Kiel

98. Schaffarczyk AP (2006) New aerodynamical modeling of a vertical axis wind-turbines with application to flow conditions with rapid directional changes. In: Proceedings of the Dewek, Bremen, Germany
99. Schaffarczyk AP, Kemena T (2010) A simplified model for fatigue load calculation of small wind turbines with vertical axis of rotation. In: Proceedings of the DEWEK, Bremen, Germany
100. Schaffarczyk AP (2020) Introduction to wind turbine aerodynamics, 2nd edn. Springer Nature, Berlin
101. Schaffarczyk AP (2021) An open source FORTRAN90 code using vortex rings and a vortex cylinder for a constantly loaded actuator disk. Kiel University of Applied Sciences, Kiel Germany https://doi.org/10.13140/RG.2.2.23065.13925
102. Schaffarczyk AP (2021) Corrections and uncertainties. In: Stoevesandt B, Schepers G, Fuglsang P, Yuping S (eds) Handbook of wind energy aerodynamics. Springer, Cham. https://doi.org/10.1007/978-3-030-05455-7_32-1
103. Schepers JG, Boorsma K, Cho T, Gomez-Iradi S, Schaffarczyk AP, Jeromin A, Shen WZ, Lutz T, Meister K, Stoevesand B, Schreck S, Micallef D, Pereira R, Sant T, Madsen HA, Sørensen N (2012) Final Report of IEAwind Task 29, MexNext, Phase 1, ECN-E-12-004, Patten, The Netherlands
104. Schepers JG, Boorsma K, Gomez-Iradi S, Schaffarczyk AP, Madsen HA, Sørensen N, Shen WZ, Lutz T, Schulz C, Herraez I, Schreck S (2014) Final Report of IEAwind Task 29, MexNext, Phase 2, ECN-E-14-060. Patten, The Netherlands
105. Schepers JG, Boorsma K, Madsen HA, Pirrung GR, Bangga G, Guma G, Lutz T, Potentier T, Braud C, Guilmineau E, Croce A, Cacciola S, Schaffarczyk AP, Lobo BA, Ivanell S, Asmuth H, Bertagnolio F, Sørensen NN, Shen WZ, Grinderslev C, Forsting AM, Blondel F, Bozonnet P, Boisard R, Yaßin K, Hoening L, Stoevesandt B, Imiela M, Greco L, Testa C, Magionesi F, Vijayakumar G, Ananthan S, Sprague MA, Branlard E, Jonkman J, Carrion M, Parkinson S, Cicirello E (2021) Final Report of IEAwind TCP Task 29, detailed aerodynamics of wind turbines. https://doi.org/10.5281/zenodo.4925963
106. Schatter W (1987) Windenergiekonverter. Fr. Vieweg, Braunschweig
107. Schmitz S (2020) Aerodynamics of wind turbines. Wiley
108. Sheldahl RE, Klimas PC, Feltz LV (1980) Aerodynamic performance of a 5 m diameter darrieus turbine with extruded aluminium NACA-0015 blades, Sandia National Laboratories, Sand80-179. Albuquerque, NM
109. Sheldahl RE (1981) Comparison of field and wind tunnel Darrieus wind turbine data. Sandia National Laboratories, Sand80-2469. Albuquerque, NM
110. Shen WS, Srensen JN, Bak C (2005) Tip loß corrections for wind turbine computations. Wind Energy 4:457–475
111. Simms DA, Schreck S, Hand M, Fingersh LJ (2001) NREL unsteady aerodynamics experiment in the NASA-ames wind tunnel: a comparison of predictions to measurements, NTEL/TP-500-29494. Golden, CO, USA
112. Soler A, Clever HG (1991) Bau, Aufstellung und Erprobung einer 50 kW-Darrieus-Windkraftanlage, Friedrichshafen
113. Solum A, Deglaire P, Erikson S, Ståberg M, Leijon M, Bernhoff H (2006) Design of a 12 kW vertical axis wind-turbine equipped with a direct driven PM synchronous generator. In: Proceedings of the EWEC, Athens
114. Srensen DN, Srensen JN (1998) Towards improved rotor-only axial Fans. In: Part I: a numerical efficient aerodynamic model for arbitrary vortex flow Danish Center for applied mathematics and mechanics report, Lyngby, Denmark
115. Srensen JD, Srensen JN (2011) Wind energy systems. Woodhead Publishing Ltd, Oxford
116. Srensen JN, Aero-mekanisk model for vindmlledrevet kretj, unveroeff. Bericht, Kopenhagen, Daenemark, ohne Jahr
117. Srensen JN (2016) General momentum theory for horizontal axis wind turbines. Springer, Cham, Heidelberg, New York, Dordrecht, London
118. Spera DA (ed) (2009) Wind turbine technology, 2nd edn. ASME Press, New York

119. Stickland JH (1975) The Darrieus turbine: a performance prediction model using multiple Streamtube, Sandia National Laboratories, Sand75-0431. Albuquerque, NM
120. Stickland JH, Webster BT, Nguyen T (1979) A vortex model of the Darrieus turbine: an analytical and experimental study. In: Proceedings of the annual winter meeting, ASME, New York
121. Stoevesandt B, Schepers G, Fuglsang P, Yuping S (eds) (2021) Handbook of wind energy aerodynamics. Springer, Cham. https://doi.org/10.1007/978-3-030-05455-7_32-1
122. Templin RJ (1974) Aerodynamic performance theory for the NRC vertical axis wind turbine, LTR-LA-160. Canada, Ottawa
123. Thwaites B (ed) (1960) Incompressible aerodynamics. Oxford University Press
124. Timmer WA, Schaffarczyk AP (2004) The effect of roughness on the performance of a 30% thick wind turbine airfoil at high Reynolds numbers. Wind Energy 295–307
125. Tong W (ed) (2010) Wind power generation and wind turbine design. WIT Press, Southampton, UK
126. Troldborg M (2009) Actuator line modeling of wind turbine wakes. Ph.D. thesis. Technical University of Denmark, Lyngy, Denmark
127. Ushijama I (2004) Wind energy research at AIT. Presentation at the Hamburg Wind-Energy Fair, Hamburg, Germany
128. van Bußel GJW (2007) The science of making more torque from wind: diffuser experiments and theory revisited. In: Proceedings of the the science of making torque form wind, Lyngby, Denmark
129. Vollan A (1977) Aeroelastic stability analysis of a vertical axis wind energy converter, Bericht EMSB-44/77. Dornier System, Immenstaad
130. Vollan AJ (1978) The aeroelastic behaviour of large Darrieus-type wind energy converters derived from the behaviour of a 5,5 m rotor. In: Proceedings of the international symposium on wind energy systems, Amsterdam, The Netherlands, p C5
131. White FM (1991) Viscous fluid flow, 2nd edn. Mc GrawHill, New York
132. Walker SN (1976) performance and optimum design analysis/computation for propeller type wind turbines. Ph.D. thesis. Oregon State University, OR, USA
133. Wilson RE, Lissaman PBS, Walker SN (1976) Aerodynamic performance of wind turbines. Oregon State University Report
134. Wilson RE, Lissaman PBS, Walker SN (1976) Aerodynamic performance of wind turbines, Chap. 4: aerodynamics of the Darrieus rotor, Corvallis, Oregon, USA
135. Wilson RE, Walker SN (1983) Fixed wake theory for vertical axis wind-turbines. J Fl Eng 389–393
136. Worstell MH (1978) Aerodynamic performance of the 17 m diameter Darrieus wind-turbine. Sandia National Laboratories, Sand78-1737. Albuquerque, NM
137. Xudong W, Shen WZ, Zhu WJ, Soerensen JN, Jin S (2009) Shape optimization of wind turbine blades. Wind Energy 12:781–803
138. Zastrow F (1992) Entwicklung von Windkraftanlagen fuer den Einsatz in der Antarktis, Abschlußbericht, BMFT, POL 0041, Bremerhaven

Prof. Dr. A. P. Schaffarczyk has been working on the aerodynamics of wind turbines since 1997. He was a founding member and honorary board member of CEwind eG and teaches in the international Master of Science degree programme in Wind Energy Engineering.

Rotor Blade Structure

Malo Rosemeier and Alexander Krimmer

Abstract The rotor blade is the key component of a wind turbine generator (WTG) and converts the energy of the wind into a mechanically useful form of energy. It represents a significant cost factor in the overall context of the turbine and at the same time has an enormous impact on the yield of the turbine. This chapter deals first with the normative requirements for the development and the verification of the serviceability and operational reliability of rotor blade structures. It then considers the loads acting on the rotor blade and the properties of the materials used. Furthermore, it addresses structural models for the analysis of blades and moreover discusses the design criteria for the topology and conventional manufacturing processes as well as deviations which occur. In addition, it considers the costs as part of the design process and their impact on the form of the blade structure, since the minimisation of the Levelised Cost of Energy is the main optimisation target when designing WTGs. Finally, it discusses blade materials from a sustainable development point of view. The chapter aims to provide a well-founded overview of a range of topics which are of relevance for the engineer working with the blade.

1 Introduction

The rotor blade is the key component of a wind turbine generator (WTG) and converts the energy of the wind into a mechanically useful form of energy. It represents a significant cost factor in the overall context of the turbine and at the same time has an enormous impact on the yield of the turbine.

M. Rosemeier (✉)
Fraunhofer Institute for Wind Energy Systems IWES, Bremerhaven, Germany
e-mail: malo.rosemeier@iwes.fraunhofer.de

A. Krimmer
TPI Composites Germany GmbH, Berlin, Germany
e-mail: a.krimmer@tpicomposites.com

Designing a rotor blade is a complex, iterative process which presents the design engineer with several challenges because of the overall structural concept of the rotor blade. For the development process to be successful, it is essential that the design engineer has sufficient understanding of the system, and hence the inclusion of the rotor blade chapter in this book is extraordinarily helpful. Starting from the system under consideration, it is possible to introduce simplifications which facilitate a mathematical-physical understanding and description of the problem, thus making the design problem amenable to a solution.

The main consideration in this chapter is the rotor blade structure for WTGs with horizontal axis (HAWT). This allows the rotor blade to be viewed as a cantilever beam which is fixed to the rotor hub via the blade bearing, also called pitch bearing. Here, it is subjected to aerodynamic loads on the one hand and to mass-induced loads, on the other. The second set of loads in particular means that strengthening the structure is generally accompanied by an increase in the mass and hence the load. Lightweight construction is thus necessary to counteract this so-called snowball effect.

To present a suitable approach to this problematic aspect, this chapter deals first with the normative requirements for the development and the verification of the serviceability and operational reliability of rotor blade structures. It then considers the loads acting on the rotor blade and the properties of the materials used. Furthermore, it addresses structural models for the analysis of rotor blades and moreover discusses the design criteria for the topology and conventional manufacturing processes as well as deviations which occur. In addition, it considers the costs as part of the design process and their impact on the form of the rotor blade structure, since the minimisation of the Levelised Cost of Energy (LCoE) is the main optimisation target when designing WTGs. Last but not least, it discusses rotor blade materials from a sustainable development point of view.

The chapter aims to provide a well-founded overview of a range of topics which are of relevance for the engineer working with the rotor blade. Those seeking more detailed information are referred to the literature referenced.

2   Normative Requirements

For construction approval, the release of the investment loan and the insurance of a WTG or a wind farm, the end customer/operator must have a type certificate. Section 2.1 begins by describing the route to the certificate for the key component, the rotor blade. Certification schemes relate to the standards and guidelines, which are based on a safety concept. Particular emphasis is placed on the Limit-State-Design concept, which is discussed in Sect. 2.2. Finally, an overview of the development cycle of a rotor blade is given in Sect. 2.3.

2.1 Certification

A type certificate confirms that a product (WTG) and its components (e.g. rotor blade or tower) have been assessed as being compliant with defined requirements regarding design and manufacture, for example. In Germany, the German accreditation body (DAkkS) qualifies accredited companies to issue these certificates in accordance with specific certification schemes, and technical standards and guidelines [64]. Examples of certification authorities, called IECRE Certification Bodies (RECBs) according to the IEC System for Certification to Standards Relating to Equipment for Use in Renewable Energy Applications (IECRE System), which hold an accreditation for schemes, standards and guidelines which are used for the certification of WTGs, especially for the rotor blade component [18], are: Det Norske Veritas (DNV) (operated separately until 2012 as DNV and Germanischer Lloyd (GL) and until 2021 combined as DNV GL), TÜV Nord, TÜV Süd, TÜV Rheinland, DEWI- OCC as part of Underwriters Laboratories (UL) and Bureau Veritas.

The WTG manufacturer decides for one of the following certification schemes, each of which represents a consistent system of guidelines and technical standards, either according to the preference of the end customer or the economic aspects:

- GL 2010: "Guideline for the Certification of Wind Turbines" [42].
- DNVGL-SE-0441: "Type and component certification of wind turbines" [27] in conjunction with DNVGL-ST-0376 "Rotor blades for wind turbines" [26].
- IEC 61400-22: "Conformity testing and certification" [55] in conjunction with recognised standards and guidelines such as [26, 42, 60]. This scheme was replaced by IECRE System in 2018.
- IECRE OD-501: "IECRE System—Type and Component Certification Scheme" [57] in conjunction with OD-501-1 "Conformity assessment and certification of Blade by RECB" [58] and IEC 61400-5 "Wind energy generation systems—Part 5: Wind turbine blades" [60].

National requirements must also be fulfilled, if applicable. In Germany, for example, a WTG is deemed to be a building and must undergo type testing according to the guidelines of the German Center of Competence in Civil Engineering (DIBt) [24], see Chap. 7 of this book. This also includes an expert report for the rotor blade.

Depending on the scheme, the requirements for the design and manufacture of rotor blades are defined by one of the following standards and guidelines: GL 2010 [42], DNVGL-ST-0376 [26] or IEC 61400-5 [60]. What these fundamentally have in common is that they are based on the Limit-State-Design concept, see Sect. 2.2. The older GL 2010 differs from the latter two in the composition of the partial safety factors (PSFs), among other things. The latter two allow the PSFs to be reduced when detailed structural analyses or comprehensive validation tests on the full-scale blade test level of the testing pyramid (Fig. 1) or a level between coupon tests and full-scale blade tests are carried out.

Finally, a full-scale blade test is required for the component certificate of the rotor blade. This serves to validate the design assumptions on the one hand and to
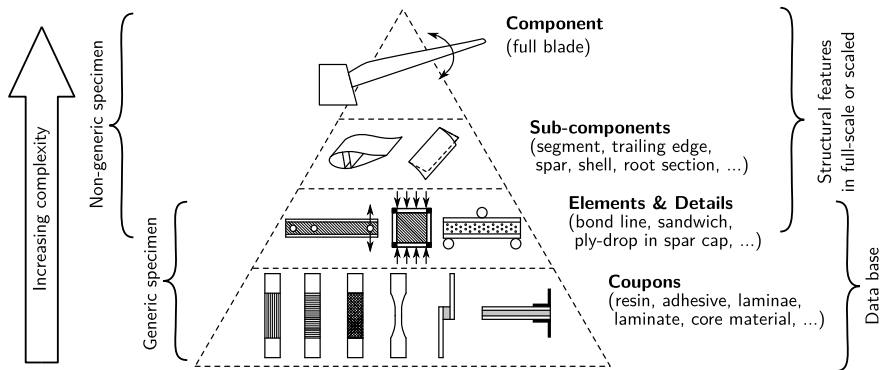
Fig. 1 Testing pyramid; based on [60]. Copyright © 2020 IEC Geneva, Switzerland. www.iec.ch

identify relevant failure modes or critical manufacturing details on the other [26]. In the full-scale blade test, the rotor blade is subjected to a testing program comprising static and cyclic tests, if applicable [56]. Test institutions which are accredited to test rotor blades in accordance with the IECRE System, so-called IECRE Test Laboratories (RETLs), include the following independent test institutes [61]: FRAUNHOFER INSTITUTE FOR WIND ENERGY SYSTEMS IWES, BLADE TEST CENTRE (BLÆST), OFFSHORE RENEWABLE ENERGY (ORE) CATAPULT, MASSACHUSETTS CLEAN ENERGY CENTER WTTC and SGS.

2.2 Safety Concept

In engineering, three concepts exist to verify that a structure is safe against technical failure [92]: (i) the deterministic safety concept, also called Permissible Stress Design (PSD) or Allowable Stress Design (ASD), which is used in mechanical engineering; (ii) the semi-probabilistic safety concept widely used in construction engineering, also called Limit State Design (LSD) or Load and Resistance Factor Design (LRFD) and (iii) the probabilistic safety concept. In PSD, the resistance, i.e. the material limit value or the strength, is simply reduced by means of a global safety factor and compared to the internal load, i.e. the stress or strain present [143]. In LSD, in contrast, PSFs are applied to each action/load (external force or moment) or their effects and the resistance. An effect can be an existing load, deformation or stress resultant (internal force or moment), for example. A resistance can be a tolerable load, strength, deformation or stress resultant. The structural safety, also called failure probability, which is often expressed by the reliability index, plays a key role here. Probabilistic methods are frequently used to calibrate the PSFs to a target reliability index for a standard or guideline [63]. With LSD, it ultimately has to be shown that none of the crucial Limit State (LS) is exceeded in all relevant design situations [13].
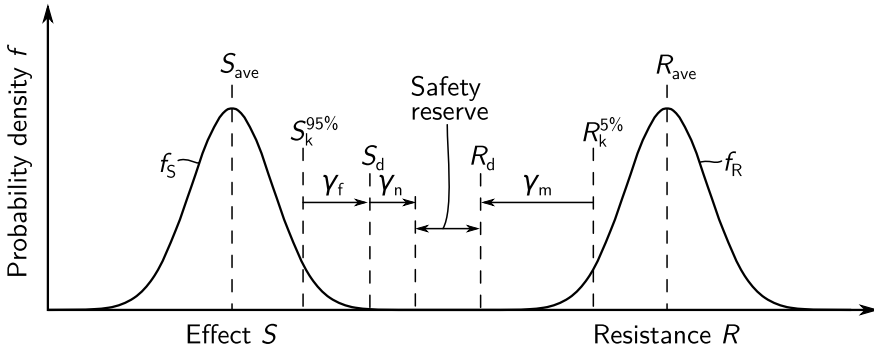
Fig. 2 Probability density functions of effect and resistance; based on [60]. Copyright © 2020 IEC Geneva, Switzerland. www.iec.ch

The standards and guidelines listed in Sect. 2.1 are based on the LSD. They state that for the rotor blade of a WTG in the ultimate limit states (ULS), the verifications must be provided for:

- strength failure,
- stability failure and
- fatigue failure.

In the serviceability limit states (SLS), the following must be provided:

- verification of the deformation limit.

For every limit state, a limit state equation can be formulated such that the resulting design value of the resistance R_d, for example a strength, is greater than or equal to the actual design value of the effect S_d, for example an existing stress, as a function of an action/load F_d [59]:

$$\gamma_n \cdot S_d\,(F_d) \leq R_d \tag{1}$$

Here, S and R are not quantities which can be measured directly, but variables which are subject to variance. Figure 2 shows the corresponding probability density function f_S and f_R about the average S_{ave} and R_{ave}. The characteristic values of the probable effect are therefore determined as a function of the characteristic action $S_k\,(F_k)$ as well as the expected resistance R_k of the rotor blade with the aid of methods based on probability theory, e.g. by considering the 95 % quantile of the effect and the 5 % quantile of the resistance. The corresponding design values R_d and S_d result from the application of PSFs to the characteristic values [23].

The PSF for the action/load γ_f, also called load factor [26], takes account of possible unfavourable deviations and uncertainties of the load as well as inaccuracies of the computational model [59]. Multiplying γ_f by the characteristic value of the action F_k gives the design value:

$$F_\text{d} = \gamma_\text{f} \cdot F_\text{k}. \tag{2}$$

The PSF for the resistance γ_m, also called the reduction factor [26], can take account of unfavourable deviations caused by adverse environmental conditions, temperature effects, manufacturing effects, the accuracy of calculation and validation methods as well as the resolution and combination of applied loads [60]. Dividing the characteristic resistance R_k by γ_m gives the design value:

$$R_\text{d} = \frac{R_\text{k}}{\gamma_\text{m}}. \tag{3}$$

Furthermore, a PSF γ_n is defined to take account of the severity of the consequences of a potential failure. Here, the components are classified into component classes 1–3, and different values for γ_n are specified for each of them [59]:

(1) Fail-safe structural components whose failure does not lead to a failure of another main WTG component and does not adversely affect the safety of the system as a whole. This requires a design with alternative load paths, so-called redundancy. Such a WTG component can be a replaceable main bearing, for example.
(2) Structural components with a safe life whose failure leads to the failure of another main component. The structure is designed such that no failure occurs during its service life. This means that the structures have a tendency to be heavier and must be replaced at the end of their service life. This WTG component class includes the rotor blade. The rotor blade may also be designed to be damage tolerant, however [60]. This concept allows damage to occur on components or structures that can be inspected well so that it is possible to notice the damage. The growth of cracks or damage is included in the calculation and the intention is for operation to continue from the point in time at which the damage occurs until the damage has reached a magnitude where it can be detected during an inspection. Critical growth of the crack which leads to a static fracture or excessive deformation, for example, does not happen during this phase between two inspections and the operational safety of the structure is maintained.
(3) Mechanical components with safe life which connect the actuators and brakes with main structural components for the purpose of non-redundant safety systems.

The safety reserve with respect to the target failure probability of the rotor blade in a limit state can then be expressed as the ratio of the design values, given by [25]:

$$\text{Safety Reserve Factor (SRF)} = \frac{R_\text{d}}{\gamma_\text{n} S_\text{d}}. \tag{4}$$

If the SRF ≥ 1, the verification was successful.
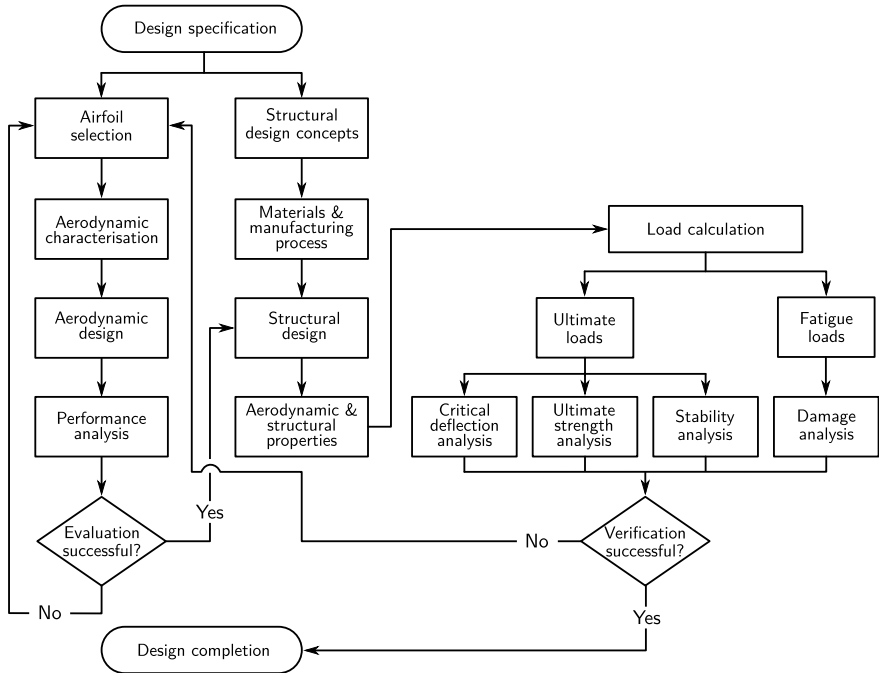
Fig. 3 Design process for WTG rotor blades; based on [60]. Copyright © 2020 IEC Geneva, Switzerland. www.iec.ch

2.3 Development Cycle of the Rotor Blade

The design process of a rotor blade from specification to completion is shown in Fig. 3. Fundamentally, two main development lines can be identified: (i) aerodynamic design and (ii) structural design. The two lines are conditional on each other and form a cycle, which is repeated several times. The objective is to optimise the rotor blade as the component and the WTG as the complete system so as to achieve maximum energy yield with minimum material usage and thereby realise the lowest possible LCoE. The mutual conditionality is discussed in detail in the sections below.

3 Loads

When a WTG is operating, different types of load act on its rotor blades and these are discussed in Sect. 3.1. Furthermore, the possible ways of calculating loads are illustrated in Sect. 3.2. Section 3.3 then goes on to describe the design load cases which are relevant for the verification. Finally, the effect of the dimensional scaling of blades is explained in Sect. 3.4.

3.1 Types of Load

The loads on a rotor blade of a WTG are subdivided into external and internal actions. The external actions/loads include the gravitational load, the aerodynamic loads induced by the wind and the rotation, and the inertial loads generated by the rotational acceleration and rotation. The internal actions/loads include residual stresses caused by a change in temperature.

Figure 4a depicts a schematic of the wind field acting on the WTG. This wind field can be split up into a deterministic component, which is generated by wind shear and is described as a function of the height $v(h)$, and a stochastic component $v(t)$, which arises as a result of (i) the turbulence as a consequence of the ground unevenness at the site and also the wake of other WTGs in a wind farm situation, which is characterised by the effective turbulence intensity [59]; (ii) changes in wind direction or (iii) gusts, see Chap. 3 of this book. It becomes clear that the rotor blade is exposed to a different wind load situation depending on the azimuth angle position of the rotor.

The gravitational force F_g acts on the centre of mass, which is at around 1/3 of the blade length (Fig. 4b), and causes an alternating bending moment in the sweep direction (lead-lag) M_x (Fig. 4d) as a consequence of the rotation.
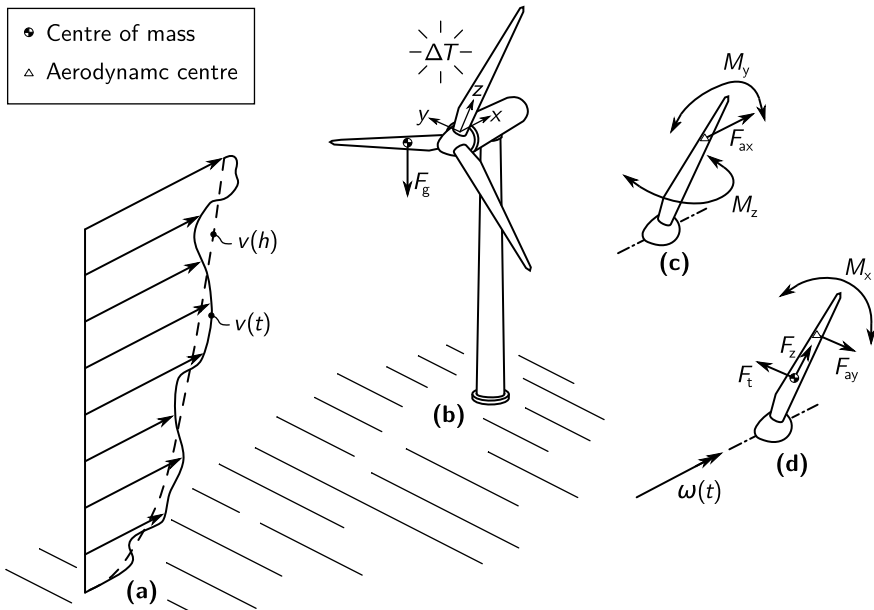
Fig. 4 Loads acting on the rotor blade: wind field (**a**), gravitational load and temperature change (**b**), aerodynamic load component, flapwise bending moment and twisting moment (**c**), aerodynamic load component and inertial force and lead-lag bending moment and rotor acceleration as well as centrifugal force (**d**); based on [103]. Copyright © 2013 Malo Rosemeier

In the speed-controlled partial load regime, the aerodynamic load acts on the aerodynamic centre, which is at around 2/3 of the blade length. It is generated by lift and drag on the airfoil (see Fig. 11 in Chap. 4 of this book), which can be split up into a drive component in the sweep direction F_{ay} (Fig. 4c) and a thrust component in the flap direction F_{ax} (Fig. 4d). These force components then correspondingly cause a lead-lag bending moment M_x and a flapwise bending moment M_y (Fig. 4c). In the full load regime, the power of the WTG is controlled with the blade pitch angle, which reduces the aerodynamic load. If the blade pitch angles of the three rotor blades are not synchronised with each other, for example, because they are installed incorrectly, this situation leads to an aerodynamic imbalance, whose impact for the non-rotating components, such as the tower, can be crucial [112]. Conventional practice is to mount the rotor blades in a cone angle with respect to the rotor plane to increase the tower clearance. When the blade is thought of as a rigid body, the aerodynamic load would generate a twisting moment M_z (Fig. 4c) at the blade root because of the cone angle and also because of the geometric flapwise pre-bend of the blade. In reality, however, the blade is flexible so that, especially in rated operation, the aerodynamic load component F_{ax} bends the blade back into the direction of the rotor plane, which in turn reduces the twisting moment M_z at the blade root. A pre-bend of the blade in the sweep direction, particularly in the direction of the blade trailing edge, has a similar effect. Here, the aerodynamic load generates a twisting moment M_z, which twists the blade at the tip and thus leads to a locally smaller blade pitch angle, which in turn reduces the aerodynamic load and thus the bending moment at the blade root [9]. Aerodynamic instabilities such as flutter can occur in an overspeed situation, in which aerodynamic forces couple the torsional resonance mode with a flapping resonance mode [47]. The flutter resonance thereby produced results in a twisting moment M_z and a flapwise bending moment M_y.

Inertial forces F_t (Fig. 4d) arise when the rotor is accelerated or decelerated ($\omega(t)$), and result in a lead-lag bending moment M_x. In the idling or stationary situation with lateral inflow, the rotor blade can be excited in its resonance mode in the sweep direction when the excitation frequency resulting from vortex-induced lateral vibrations and the resonance frequency of the blade couple in resonance [51]. The vibration generates an inertial force F_t which acts on the centre of mass and then causes a lead-lag bending moment M_x.

Furthermore, the rotation generates a centrifugal force F_z in the rotor plane (Fig. 4d). This can induce an aerodynamic and mass imbalance when the blade masses are not balanced, as can occur as a result of ice accretion, for example. With the rigid blade, the cone angle would cause a portion of F_z to produce a bending moment in the flap direction M_y. As described above, this is reduced again by the actual flexibility of the blade in rated operation. The centrifugal force has a stiffening effect with increasing rotor speed and thus has an impact on the blade resonance frequencies [39].

A temperature change to the blade structure produces intrinsic mechanical loads. These build up during the cooling process of the rotor blade after the materials have cured because the materials have very different thermal expansion coefficients.

Depending on the operating temperature of the WTG, significant residual stresses can be generated, for example in the adhesive joints [108].

3.2   Load Calculation

For the aero-servo-elastic simulation of the loads, the aerodynamics are modelled with the aid of Blade Element Momentum Theory (BEM), Vortex Methods or Computational Fluid Dynamics (CFD). They are coupled to the WTG structure, which is either discretised by spring-mass damper systems, finite element (FE) systems or modally modified beams. The WTG states are adjusted by a speed and blade pitch angle controller. The structural model of the WTG is thereby subjected to so-called Design Load Cases (DLCs). These not only consider situations which occur in operation, but also extreme situations such as gusts, emergency stops and grid loss [59]. Commonly used simulation environments for the time as well as for the frequency domain include HAWC2/HAWCStab2 [20], OpenFAST [87], Bladed [22], MoWiT [36], Adams/AdWiMo [84], Flex [90], ADCoS [1], Cp-Lambda [95], alaska/Wind [62] and Simpack [21]. A comparison of different simulation environments can be found in [66, 96], for example.

In particular, the mass-load-induced fatigue load spectrum as the crucial load in the blade root region can already be estimated with little simulation effort [110]. To this end, the number of rotations during the total life and the static mass moment, which results from the product of the total mass and the lever arm between blade root and centre of mass (Fig. 4b), is considered.

3.3   Design Load Cases

The mechanical loads from the simulations are summarised in the design load cases for the rotor blade, which are explained below. These design loads can be specified either for an individual type of WTG or as a broad design load envelope for several versions of a WTG type [59].

3.3.1   Load Case of Minimum Tower Clearance

For this load case, the simulation time series are examined for the minimum distance between tower surface and blade tip. The load state along the blade, particularly flapwise, dimensions the maximum permissible blade tip deflection.

3.3.2 Extreme Load Envelope

This load case involves a load envelope, and means that the simulation time series are examined for their maximum and minimum values for every cross section along the rotor blade. In general, the load vector components of an envelope do not occur at one and the same time. The extreme loads, which are extracted as point clouds, are therefore enveloped and projected into the four main directions, for example, and also in more than four sectors. At least 12 sectors are required for the blade root, for example, [60]. A projection method is illustrated in [26].

3.3.3 Fatigue Load Spectra

For this load case, the simulation time series are processed with the aid of load cycle counting methods, for example, Rainflow Counting [77], see Fig. 4 in Chap. 7 of this book. This results in load spectra, also called Markov matrices or range-mean matrices. A collective consists of a number of cycles n_i, a mean stress S_{mi} and a stress amplitude S_{ai}. The usual procedure is to add the total damage of all collectives together using the linear damage accumulation hypothesis according to Palmgren [91] and Miner [82]. The use of load spectra for the structural analysis can become relatively computationally intensive when high sectoral resolution is desired. For this reason, load spectra of force or moment time series are also used, and then Damage Equivalent Loads (DELs) for a reference number of cycles to failure n_{ref} and a material-specific negative inverse exponent of the fatigue life curve m [52] are derived therefrom, see Fig. 5 in Chap. 7 of this book. One disadvantage of using DELs is that it is almost impossible to take the influence of the cycle means into account. This appears to be critical since the matrix materials of fibre-reinforced polymer (FRP), in particular, are extremely sensitive to mean stress [122]. However, when the DELs have high sectoral resolution within a blade cross section, it does seem possible to take mean stress effects into account nevertheless [97].

3.3.4 Loads from Changes in Temperature

This load case results from the boundary conditions of the rotor blade manufacturing process. In the simplest case, the temperature difference ΔT between curing and operating temperature can be used here, cf. [3, 108, 109]. Internal loads caused by stresses from temperature changes and the different thermal expansion coefficients of the individual materials can be added to the extreme loads and taken into account in the fatigue load spectra as a static average [74].

3.4 Effects of Scaling

GALILEO's square-cube law [38] applies to the scaling of WTG rotor blades as it does to all other three-dimensional (3D) bodies, and is referred to below as the scaling law. It states that for the linear scaling of a body, its surface area increases as the square of its length and its volume increases as the cube of its length. Consider a cube with edge length L_1 as shown in Fig. 5. If the cube is scaled such that the edge length doubles to L_2, then the base area A_1 in the figure scales by a factor 4 to the base area of the scaled cube A_2. In this process, the volume of V_1 increases by a factor of eight to the value V_2. This means that when the length of the rotor blade is doubled, its mass increases eightfold according to the scaling law.

A selection of different structural concepts for rotor blades is plotted in Fig. 6 and shows rotor blade mass as a function of the rotor diameter. The selection includes all wind classes, material combinations and generations of the last 30 or so years. The regression took account of all blades made from glass fibre (GF) in epoxy resin (EP) and this results in an exponent of approx. 2.2. When the regression is carried out separately for different structural concepts for rotor blades, the exponents lie between 1.9 and 2.8 [72]. Hence, the structural masses of rotor blades do not in fact increase proportional to the third power, as expected according to the scaling law, but roughly proportional to the 2.4th power of the rotor blade length.

The reason for the exponent in the scaling must be sought in the type of loading of the rotor blade. As has been described above, rotor blades are mainly exposed to two types of loads: gravitational loads from their own mass on the one hand and loads from the aerodynamic action on the other.

The mass loads of a rotor blade depend directly on its mass and thus its volume, while the aerodynamic loads are determined by the aerodynamic surface of the blade. Like the surface area of the rotor blade and thus the aerodynamic loads, the cross-sectional areas of the rotor blade increase as the square of its length. These cross-sectional areas form the resistances against the loads. This means the aerodynamic loads do not lead to a disproportionate increase in mass. As shown, the volume and therefore the mass loads increase as the third power of the length, however, which means that the cross-sectional areas have to increase disproportionately. This explains first of all why the mass of the rotor blade structure which has to withstand these loads increases by a value which lies between the two powers 2 and 3, i.e. around 2.4.

Fig. 5 Scaling using the example of a cube; based on [73]. Copyright © 2017 Alexander Krimmer

$$L_2 = 2 \cdot L_1$$
$$A_2 = 4 \cdot A_1$$
$$V_2 = 8 \cdot V_1$$
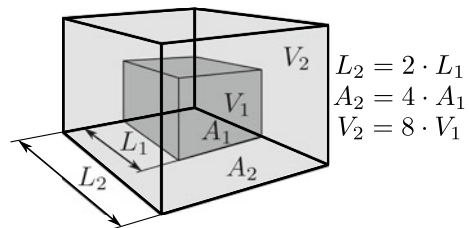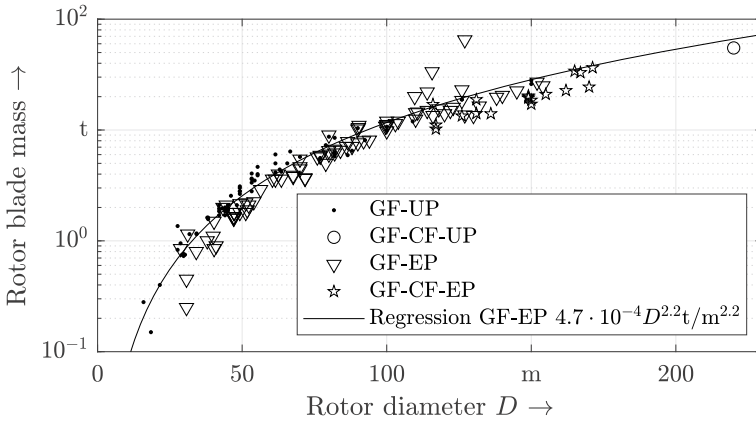
Fig. 6 Masses of various structural concepts for rotor blades: Glass fibre (GF)-reinforced unsaturated polyester resin (UP) (GF-UP); GF-reinforced skin laminate and carbon fibre (CF)-reinforced spar cap with unsaturated polyester resin (UP) (GF-CF-UP); GF-reinforced epoxy resin (EP) (GF-EP); GF-reinforced epoxy resin (EP) (GF-EP); GF-reinforced skin laminate and CF-reinforced spar cap with epoxy resin (EP) (GF-CF-EP); based on [72]. Copyright © 2014 Alexander Krimmer

Furthermore, the aerodynamic loads of a rotor blade in the lee direction, the downwind direction, cause a more quasi-static deformation, while the rotation of the rotor leads to a cyclically changing bending load of the rotor blade with each revolution resulting from its own mass. It thus becomes clear that it is primarily the service loads which increase disproportionally when scaling rotor blades and greater consideration will have to be given to these loads in the future.

4 Materials

The rotor blades of WTGs are composed of a large number of different materials. The main components are fibre-reinforced polymer (FRP), whose composition, properties and processing are discussed in Sect. 4.1. Core materials are also used to guarantee stability in the thin-walled rotor blade structures, and their properties and modes of action are presented in Sect. 4.5. Furthermore, rotor blades usually contain structural adhesives, whose properties and tasks are documented in Sect. 4.6. A frequently underestimated task concerns the coating materials, which can be found in Sect. 4.7. Moreover, various metals are used in the lightning protection system, at the blade connection and at a segmented-blade joint. They are presented in Sect. 4.8.

4.1 Fibre-Reinforced Polymers

FRPs have largely become established as the main structural material in the manufacture of rotor blades. Blades manufactured nowadays consist primarily of glass fibres (GFs) in an epoxy resin (EP) matrix. A smaller number are likewise constructed from GF, but embedded in unsaturated polyester resin (UP). Furthermore, there is an increasing tendency to strengthen the main reinforcing elements of rotor blades with carbon fibres (CFs). For the main spar caps, the use of pultruded unidirectional (UD) plates has become established. These are also manufactured with CFs in various resin matrices such as EP, UP and vinylester (VE).

There are a variety of reasons for using FRPs, the most important ones being:

- high strength,
- high stiffness,
- low density,
- advantageous fatigue strength properties,
- ease of manufacture and
- simple production of the components in freeform surfaces.

Figure 7 shows the structural principle of FRPs with their important components. The laminate (Fig. 7a) is composed of laminae or plies, as they are shown in Fig. 7b with information on the fibre orientation, for example, when one of the plies is a UD fibre-reinforced single ply. Furthermore, core materials in a sandwich laminate or adhesive layers between two substrate laminates, which are the bonded elements, can also be considered as single ply. The fibre-reinforced UD single ply, as shown in Fig. 7c, is composed of

- fibre,
- sizing and
- resin matrix.

The fibre itself, as illustrated in Fig. 7d, is usually surface coated with sizing, which bonds chemically with the resin matrix.

The question is why fibres in particular have such excellent mechanical properties. The observations by GRIFFITH [44] are the simplest way to explain this. Figure 8 shows the results of his experiments. It is clearly evident that the strength of the GF considered increases disproportionally when their diameter is decreased. This is because the probability of damage becomes lower with decreasing fibre cross section, an effect which is known as the fibre paradox.

To make these properties available for use in structural mechanics, the fibres are embedded in a so-called matrix. In the case of rotor blades, this nowadays consists of polymers such as EP and UP, but researchers are also experimenting with polyurethane (PU) and polymers with thermoplastic properties [85] as well. The task of the matrix is to transfer the forces acting on the structure into the fibres. These forces are primarily transferred via shear. Furthermore, the matrix provides the dimensional stability of the basic textile framework and guarantees that the fibres are protected from external influences.
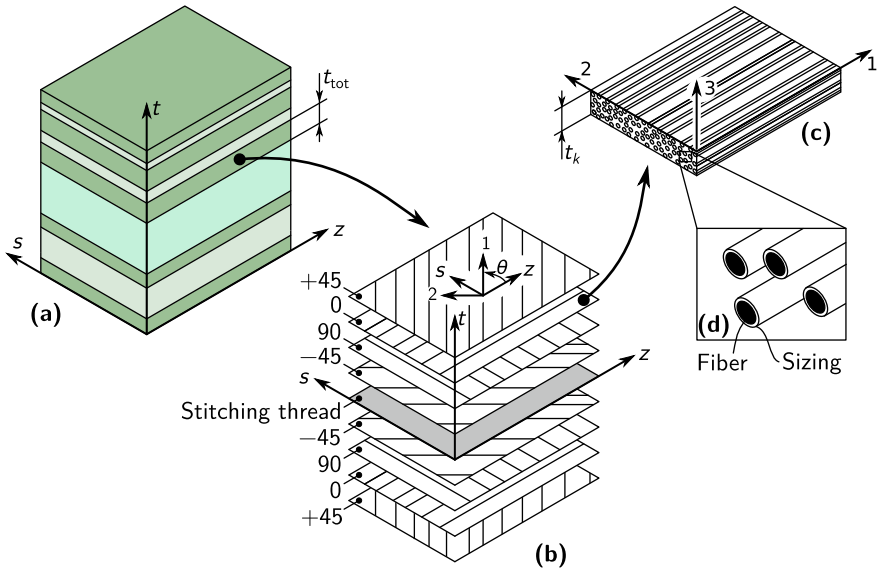
Fig. 7 Layup stacking with various laminates (**a**); fibre-reinforced polymer (FRP) laminate (**b**); lamina (**c**); fibre and sizing (**d**); based on [111]. Copyright © 2020 Malo Rosemeier
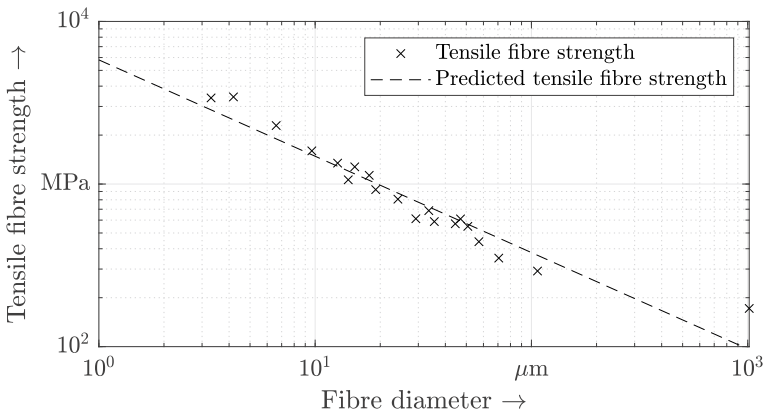
Fig. 8 Tensile strength of glass fibre (GF); data from [44]. Copyright © 2021 Alexander Krimmer

Table 1 Conventional mechanical properties of materials

Property	E-glass	HT carbon	EP matrix
Young's modulus longitudinal/transverse in GPa	80	240/15	3.00
Shear modulus transverse/longitudinal in GPa	32	45	1.07
Poisson's ratio transverse-longitudinal	0.25	0.3	0.4
Tensile strength in MPa	2000	4000	70
Strain at fracture linearised in %	2.5	1.67	2.3
Negative inverse stress-life curve exponent	10	14	10
Density in kg/m^3	2600	1800	1150
Coefficient of thermal expansion long./trans. in 10^{-6}/K	5.3	-0.6/20	60
Price in €/kg (in 2021)	1.00	15.00	4.00

The most important mechanical properties for the most important materials which form the FRP are given in Table 1. The properties for orthotropic high-tenacity (HT) CF are stated in the fibre direction (longitudinal) as well as orthogonal to it. The mass-related prices given must be understood as rounded guide values, while the actual prices are naturally subject to market fluctuations.

Other materials such as R-GFs are also suitable for use in rotor blades. They have a modulus of elasticity (Young's modulus) which is 10 % higher than that of E-GFs. Since only an introduction to the topic is provided here, the selection is limited to the materials most frequently used.

4.2 Semi-Finished Textile Products

The FRP used in the rotor blade structures is usually non-crimped fabrics (NCFs) in the form of semi-finished textile products. These fabrics are characterised by the fact that several fibre plies in the form of GF rovings are laid one on top of the other with different orientations by machine before being stitched together. This increases the number of raw materials involved by the stitching thread, which usually consists of polyethersulfon (PES). A tri-axial (TX) NCF is depicted in Fig. 9.

Woven fabrics can also be used for the manufacture, for example. Their disadvantage is that the waviness or undulation of the fibres is greater because the plies are interwoven, and it is thus not possible to exploit the mechanical properties of the fibres to the same extent. Further details can be found in [116].

The text below is therefore based on NCFs for the manufacture of WTG rotor blades. A so-called non-crimped fabric composite (NCFC) is thus produced in the manufacturing process, which then requires that different NCFs have to be characterised in the composite. The types of NCFs usually used in rotor blades are UD, bi-axial (BX) and TX NCFs.
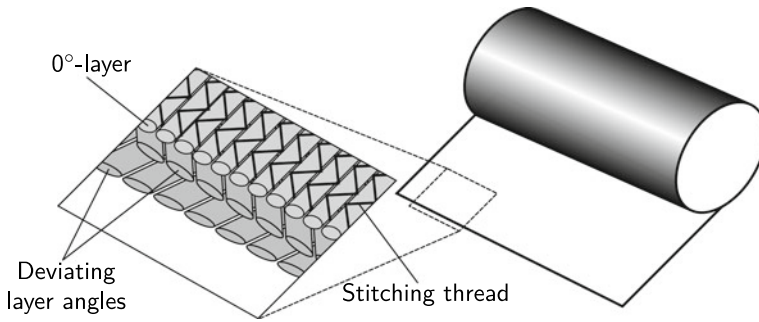
Fig. 9 Schematic diagram of tri-axial non-crimped fabric [72]. Copyright © 2014 Alexander Krimmer

4.3 Materials Testing

To now make rotor blade structures predictable, the mechanical properties of the materials and of the FRP in particular must be known. These can be determined by means of materials testing on the coupon level of the testing pyramid (Fig. 1). Corresponding normative stipulations for this are given in [60]. Materials testing can be carried out at different levels of the testing pyramid involving different amounts of effort and with varying levels of validity. The main challenge consists in the fact that the properties of the rotor blade materials evolve only during the manufacturing process of the rotor blade structure. They are affected significantly by the process parameters during rotor blade manufacture and also by the properties of the semi-finished fibre material and the matrix. The most important ones are

- manufacturing methods (hand layup (HL), vacuum infusion (VI) or others);
- accuracy during layup of the material;
- process pressure;
- consequential compaction and fibre volume fraction (FVF) and
- temperature profile during processing and curing.

To be able to determine the properties accordingly, these process parameters have also to be set as best as possible during the production of the material samples. This naturally means that the same semi-finished products and resins as in the rotor blade must be used for the testing.

Since FRPs are orthotropic materials, i.e. materials with anisotropic properties, at least three tests must be carried out on each semi-finished product to characterise the elastic properties. These are tensile tests in the main reinforcement direction and at right angles to it, as well as a test to determine the shear properties. It is thus possible to determine the required tensile and shear strengths. If it is additionally desired to determine the required compressive strengths as well, then compression tests in the main reinforcement direction and at right angles to it are also required.

More tests or fewer tests have to be carried out on the different NCFs used depending on the complexity of the material model used. Materials testing is usually associated with high costs, which have to be kept low. An effective way of keeping the number of tests as small as possible is to use Extended Inverse Laminate Theory (EILT) [72]. This allows a generic material model to be parametrised right down to the elastic and strength properties of fibre and matrix.

4.4 Elasticities of the Unidirectional Single Ply

EILT is based on the inverse execution of classical laminated plate theory (CLPT) [101, 135]. It is an established and effective tool for predicting the properties of layered FRPs.

To carry out CLPT, all that is required is the two-dimensional (2D) compliance matrix which describes the planar stress state. If the intention is also to determine the elastic properties of a laminate expressed in three dimensions (3D), then it is necessary to already establish the properties of the single ply in 3D. Inverting the matrices leads in each case to the elasticity matrices of the single ply. For the 2D case, all further steps are described in [101, 135]. For the 3D expression of the laminate properties, reference is made to the work of CHOU [16]. He formulates a suitable method to calculate them.

Starting from the expression of the compliances and stiffnesses of the individual ply, an inverse calculation right down to the properties of the individual components, fibre and matrix, is performed using micromechanical rules of mixture as part of EILT. If these properties are known, the micromechanical rule of mixtures can again be used to predict the properties of UD single plies.

Software is available from different institutions and with different capabilities which can rapidly and simply generate predictions for mechanical properties of FRPs. Mention is made here of two of them, which are available for free and provide a simple introduction to the topic.

AlfaLam Advanced Layerwise Failure Analysis of Laminates (AlfaLam) is a program based on CLPT which is made available by the Leichtbau und Bauweisen (KLuB) Institute at the TU Darmstadt. It can be found on the KluB download page [125]. The program versions deposited there date from 2009, however.

eLamX^2 is likewise based on CLPT and is made available by the Institute of Aerospace Engineering at the TU Dresden [50]. eLamX^2 likewise provides a user forum and is regularly updated. Moreover, an impressive overview of the capabilities and possibilities of the software is provided at [50].

eLamX^2 also includes micromechanical rules of mixture, but their forecasting accuracy is limited. To achieve better results, attention is drawn to HASHIN and ROSEN [49], whose procedure is likewise used in [135] as well as the micromechanical equations in [74]. The latter were used to provide an overview of the mechanical behaviour of a GF-EP-UD single ply as a function of the FVF in Fig. 10.
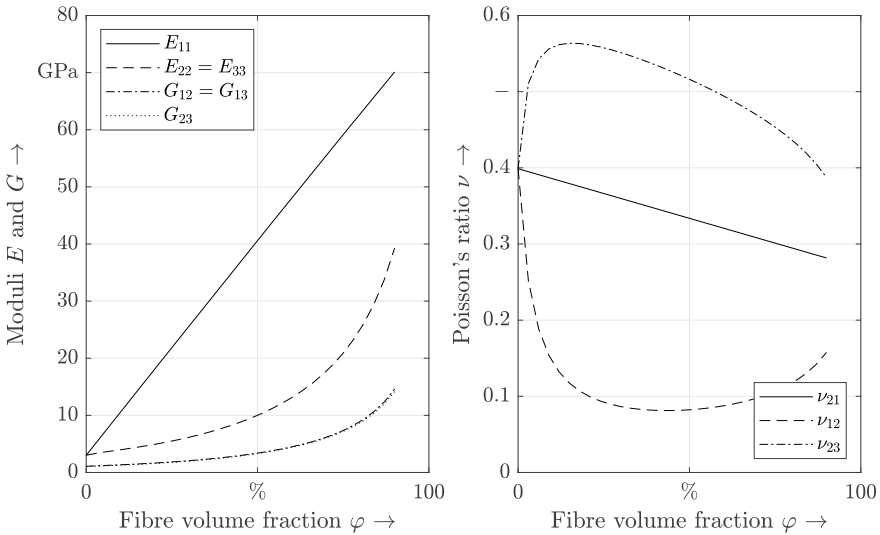
Fig. 10 Mechanical properties of a glass fibre-epoxy resin unidirectional (GF-EP-UD) single ply. Copyright © 2021 Alexander Krimmer

If a more detailed examination of the topic of FRPs is to be conducted, it is recommended that you program the CLPT yourself in accordance with [101, 135], for example. A good introduction is provided by the Python implementation compmech [12].

4.5   Core Materials

Rotor blades for WTGs are thin-walled structures in the best sense of the word. Such structures are usually prone to buckling, which is a stability failure phenomenon of planar load-bearing structures. Under in-plane compressive loading, the load-bearing structures give way from the load direction and consequently do not absorb additional forces [141]. In the rotor blade, this applies to the skin laminate sections of the rotor blade structure. They are the easily recognisable sandwich sections in Fig. 16.

To prevent this stability failure, the skin sections of the rotor blade are built as sandwich structures. In the rotor blade, they consist of the outer and inner skin laminates or skins, which are kept apart by a core to increase the parallel-axis component of the area moment of inertia and thus the bending stiffness of the sandwich cross section. This core is usually flexible and has comparatively high shearing rigidity. In order not to significantly increase the structural mass of the rotor blade at the same time, materials are used which comply with this requirement and have a low density. In the rotor blade, these are predominantly:

- polyvinyl chloride (PVC) foam,
- polyethylene terephthalate (PET) foam,
- PU foam and
- end-grain Balsa wood.

The core materials are usually supplied as sheets. If they are orthotropic materials, as is the case with PET foam and end-grain Balsa wood, the directions of the highest elastic modulus are oriented in the thickness direction of the plates. This explains why end-grain Balsa wood is used, for example, which is characterised by the fact that its direction of growth points into the thickness direction of the plate.

The core materials mentioned here are not flexible enough to follow the contours when they are laid into the rotor blade mould, however. Therefore, if a curvature has to be introduced into the core material plates, a fabric is bonded on one side and slots are made in the other side of the plate with a saw or a knife. This process allows the plates to be draped along the contours. Furthermore, the plates are partially perforated to ensure that the resin flows through the thickness of the plate. A perforated and slotted PVC foam plate is depicted in Fig. 11a.

The fact that resin of very low viscosity is used in the VI process has a disadvantageous effect. It fills the cavities which are present in the dry stack-up, and thus the perforations and slots described above are filled with resin, for example. Furthermore, open cells at the surface of the core material fill as well. The resulting resin intake of the core is described in [88, 107] and made amenable to a calculation. This is absolutely essential for a reliable prediction of the mass for the rotor blade structure.

Figure 11b shows cross sections through corresponding sandwich plates.
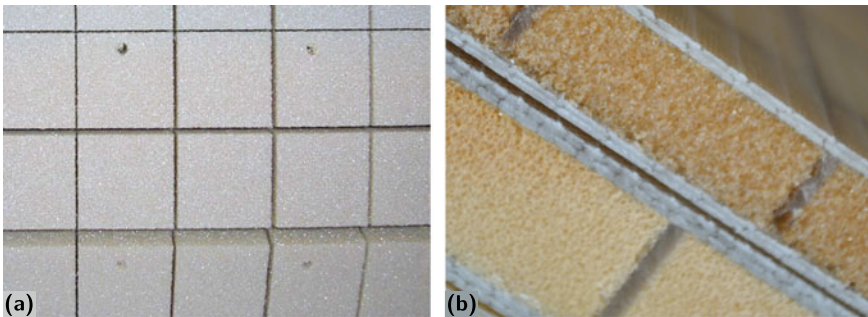
Fig. 11 Top view (**a**) of a PVC foam plate with a density of $60 \, kg/m^3$, slotted and perforated, and sectional view (**b**) of sandwich plates with different thicknesses with GF-EP skins and PVC core; top 10 mm, bottom 15 mm thickness with partially filled slots; Copyright © 2021 Alexander Krimmer

4.6 Adhesives

The majority of the rotor blades manufactured nowadays are produced as two skin laminates. This means that the aerodynamic suction-side skin laminate and the aerodynamic pressure-side skin laminate are prefabricated separately. The shear webs which are needed are glued into one of the skin laminates and then the two skins are bonded together. The dimensions of the bonding partners mean that the bonding gaps which have to be bridged with an adhesive are large. In today's rotor blades, they are nominally specified to be around 5 mm, but can reach thicknesses of up to 30 mm. If they are to become structurally effective, the adhesive joints must not exceed a thickness of 10 mm. The adhesive exudes into empty spaces with thicknesses of up to the stated 30 mm in the region of so-called blind bonded joints as well.

Since the adhesives are usually exothermic-reaction resin materials, there is a risk of a significant local temperature increase, which can ultimately lead to the surrounding structure being damaged. Hence, the adhesive must also be kept as thin as possible even in regions which have no structural effect.

To be able to bridge thick bonding gaps as well, however, fillers are added to the adhesives. This increases the viscosity of the adhesives significantly. Depending on the type of filler selected, e.g. GF in the form of short fibres, the adhesive additionally becomes more or less abrasive during delivery and when mixing resin and curing agent. Finally, to simplify the workability during the process, thixotropic additives are admixed to the adhesives. Thixotropy describes the so-called shear-thinning behaviour. Shearing of the substance leads to a decrease in viscosity here. After a rest period, the viscosity increases again, however. This is important so that the adhesive does not slide off vertical surfaces again once it has been applied. One example for a thixotropic agent is pyrogenic silicon dioxide, also called pyrogenic silicic acid.

Further detailed information on adhesives and bonds can be found in [45].

4.7 Coating

A surface coating is applied to the rotor blade to protect its surface structure against weathering phenomena such as rain, ultraviolet (UV) light, sand storms, snow and ice. This coating usually consists of many different layers and can include the following:

- gel coat,
- putty,
- pore filler,
- finishing coat and
- erosion protection.

The gel coat is usually applied to the negative mould (see Sect. 8) of the rotor blade. The rotor blade structure is then stacked up inside this mould and bonds with

the gel coat layer during the manufacturing process. This provides the basis for the further surface processing of the rotor blade after it has been removed from the mould on the one hand; on the other, the gel coat forms a protection for the mould. Since the resin matrix has very low viscosity as a rule, it will also fill small depressions, defects and holes in the surface of the mould during the VI. After the curing, the resin is adhesively and mechanically bonded to the surface. Demoulding the rotor blade will then cause further damage to the surface of the mould. These mould surfaces must then be repaired on a regular basis. If the first layer in the mould is a gel coat, this bonding does not take place as just described and the mould surface is protected and accordingly has a longer life.

After the rotor blade has been demoulded, the surface is sanded to remove residues of the mould release agent from the production process and activate the surface for the application of the surface coating. Afterwards, any depressions are evened out with the putty and surface finished by sanding. The surface is then skimmed with the filler to fill the remaining pores. Lastly, the finishing coat is applied. The number of coating layers depends on the coating system used and the layer thickness to be achieved. The next step is to apply the erosion protection for the leading edge of the rotor blade. This can be an adhesive film or also a coating. Finally, aerodynamic aids such as vortex generators and trailing edge serrations are bonded to the surface.

Conventional gel coats consist of PU or EP. In general, PU in liquid form or in the form of a paste is used for the subsequent coating components, since it is characterised by good UV light resistance.

4.8 Metals

Metals are used in rotor blades for the lightning protection system, for the connection of the rotor blade root to the blade bearing of the rotor hub, and also at segmented-blade connections.

For the lightning protection system, a distinction is usually made according to the material used for the main reinforcements or spar caps of the rotor blade. GF composites act as a dielectric and therefore do not have to be protected separately. In these blades, the lightning protection system is limited to inserting contacted lightning receptors in the vicinity of the blade tip. The tip is especially endangered by potential lightning strikes because of its exposed position. The receptors to be inserted and the connecting lightning protection cable are made of aluminium because of its low specific mass. Since aluminium has comparatively poor fatigue strength, the aim is to lay the lightning protection cable along the lines of the elastic centres of the blade cross sections as far as possible (see Fig. 13).

If CF is used in the main spar caps (see Fig. 16a), solving the lightning protection problem becomes more difficult. The conductivity of the spar caps and their flammability means they have to be protected against lightning strikes in particular. Aluminium should not be used for this purpose, however, because contact corrosion can occur between CF and aluminium. Copper is therefore preferred here.

Furthermore, the lightning protection system is connected to the rotor hub via a slipring in some cases. This is then usually manufactured from stainless steel, for example, V4A.

Finally, high-strength tempered steels are used for the rotor blade connection to the blade bearing. The materials used for the expansion bolts achieve strength values in the region of 1000 MPa. Examples are 30CrNiMo8, 34CrNiMo6, 42CrMo4, 42CrMoS4 or 32CrB4.

5 Structural Models

Structure and substructure models of the rotor blade with various degrees of detail are used on the one hand to compute cross-sectional properties which are then used to parametrise beams for the load simulation, and on the other to carry out structural analyses with the computed loads. Since the design process and the optimisation are done iteratively, the computational efficiency of the models is particularly important. In a subsequent development stage, models which are more complex and hence more computationally intensive are relevant for detailed analyses.

The computationally efficient models include analytically based descriptions, and also semi-analytical descriptions with a relatively small number of variables to be determined. The computationally intensive models include detailed representations of the structure as shell and solid models, discretised with the aid of FE.

5.1 Geometry and Structure

The external geometry of the rotor blade, also called planform, results from aerodynamic and also structural requirements. Airfoils which are relatively thin have better aerodynamic properties than relatively thick airfoils. On the other hand, relatively thick airfoils allow more economical use of material, since the parallel-axis component in the geometric moment of inertia comes into play here. A challenge with the structural design is the transition from the airfoil of relatively long chord lengths to the cylindrical blade root at the connection. This is down to the large three-dimensional change of the rotor blade surface which leads to effects which cannot be described sufficiently well with first-order approaches. The changes in the cross sections along the longitudinal axis lead to so-called "pumping" or "breathing", where the cross section deforms and it can no longer be assumed that the planarity of the cross section is maintained.

The rotor blade planform can be described by a family of airfoils, a chord length distribution, an aerodynamic twist distribution, a thickness distribution and a thread point distribution (Fig. 12). The airfoils are then usually characterised with respect to their aerodynamic lift and drag factors as a function of the angle of attack, see Fig. 3 in Chap. 4 of this book. Panel codes such as XFOIL [28] and its extension
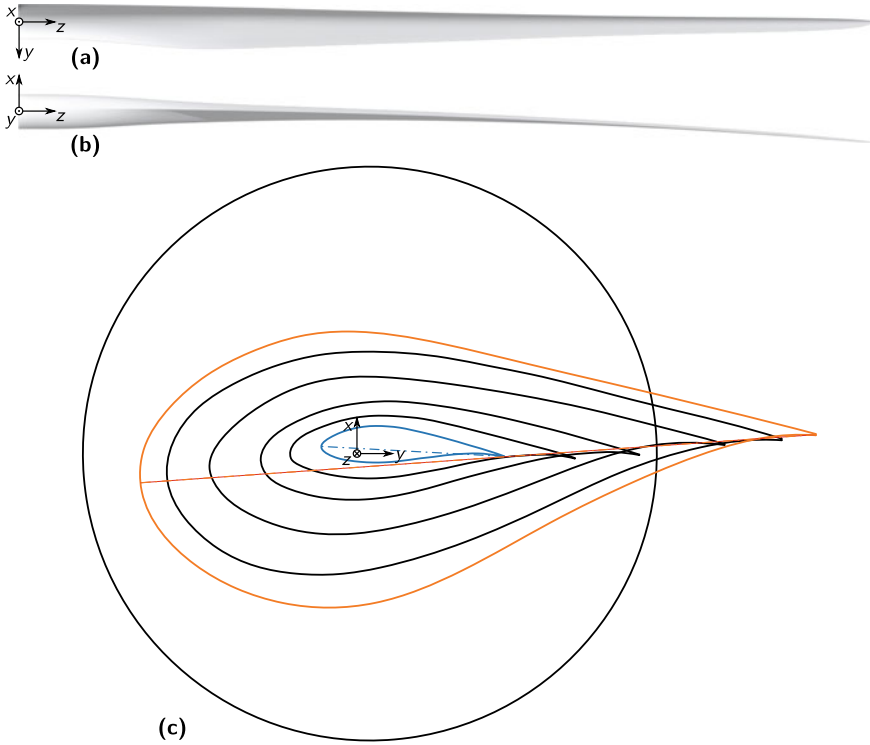
Fig. 12 Planform of a modern rotor blade of an onshore WTG: View onto the suction side (**a**), the trailing edge (**b**) and from the root into the inside of the blade (without pre-bend) (**c**); *z*-axis of the coordinate system marks the pitch axis; dash-dot line shows a chord of an airfoil close to the blade root and to the blade tip. Copyright © 2021 TPI Composites Inc.

RFOIL [10] or CFD codes such as OpenFOAM [30] or EllipSys [19] are used for this purpose. The aerodynamic performance is then analysed with the aid of BEM codes such as CCBlade [86, 89], QBlade [124] or FOCUS6 [145].

Load-bearing spar caps and webs are positioned within this geometric shell. Panel sections are built in sandwich construction, see Fig. 16. The manufacturing process is taken into account here.

5.2 Cross-Sectional Properties

When the distribution and positioning of materials within the blade cross section and in the longitudinal blade direction are known, the cross-sectional properties can be determined.

The structural properties of a cross section are described by a stiffness matrix and a mass matrix. Typically, the cross-sectional stiffness is given as a 6×6 matrix in accordance with Timoshenko beam theory [129]. For balanced laminates, this results in the following structure of the stiffness matrix $[S]$ in relation to a reference point in a reference coordinate system (CoS) (see Fig. 12) within the cross section:

$$\vec{F} = [S]\,\vec{u} \quad \Rightarrow \quad \begin{Bmatrix} F_x \\ F_y \\ F_z \\ M_x \\ M_y \\ M_z \end{Bmatrix} = \begin{bmatrix} k_x GA & k_{xy} GA & 0 & 0 & 0 & S_{16} \\ k_{xy} GA & k_y GA & 0 & 0 & 0 & S_{26} \\ 0 & 0 & EA & S_{34} & S_{35} & 0 \\ 0 & 0 & S_{34} & EI_{xx} & EI_{xy} & 0 \\ 0 & 0 & S_{35} & EI_{xy} & EI_{yy} & 0 \\ S_{16} & S_{26} & 0 & 0 & 0 & GJ \end{bmatrix} \begin{Bmatrix} \gamma_x \\ \gamma_y \\ \varepsilon_z \\ \kappa_x \\ \kappa_y \\ \theta_z \end{Bmatrix},$$

(5)

where $\vec{F}$ contains the forces F and moments M acting on the cross section and $\vec{u}$ the shear strain γ, strain ε, curvatures κ and twisting θ. The shear centre relative to the reference point is given by [34]:

$$x_s = -\frac{C_{26}}{C_{66}} \quad \text{and} \quad y_s = \frac{C_{16}}{C_{66}}, \quad \text{where} \quad [C] = [S]^{-1}.$$

(6)

The elastic centre or centroid relative to the reference point is given by [34]:

$$\begin{Bmatrix} y_e \\ -x_e \end{Bmatrix} = -\begin{bmatrix} C_{44} & C_{45} \\ C_{45} & C_{55} \end{bmatrix}^{-1} \begin{Bmatrix} C_{34} \\ C_{35} \end{Bmatrix}.$$

(7)

The structural twist angle between the elastic axes and the reference CoS is given by [40]:

$$\nu = \frac{1}{2} \tan^{-1}\left(-\frac{2EI_{xy}}{EI_{xx} - EI_{yy}}\right).$$

(8)

To populate the stiffness matrix, the axial stiffness AE, the shear stiffnesses kGA, the bending stiffnesses EI and the torsional stiffness GJ are calculated. If structural couplings exist, e.g. between bending and torsion, these need to be determined as well. The fully populated stiffness matrix results only when unbalanced laminates are used. For the fully populated stiffness matrix, the shear centre additionally depends on the bending torsional compliances C_{46} and C_{56} [34], for example.

To consider the simplified concept it is often sufficient to determine the 3x3 sub-stiffness matrix comprising tension (AE) and bending components (EI) according to Euler-Bernoulli [31].

The populated mass matrix $[M]$ is then:
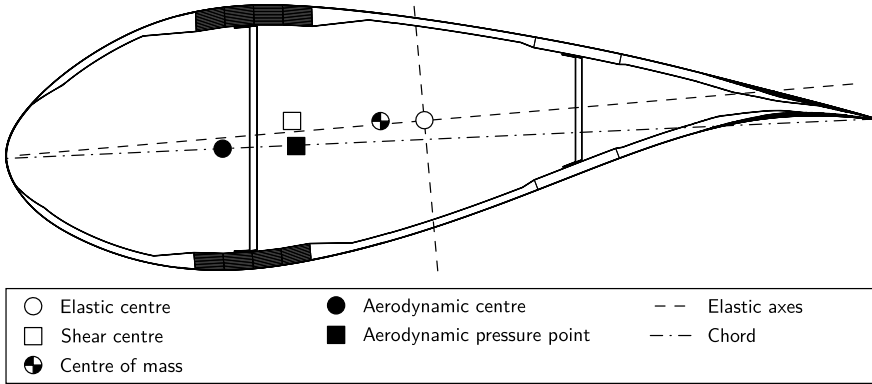
Fig. 13 Blade cross-sectional properties. Copyright © 2021 TPI Composites Inc.

$$
\overrightarrow{F} = [M]\, \overrightarrow{\ddot{u}} \quad \Rightarrow \quad
\begin{Bmatrix} F_x \\ F_y \\ F_z \\ M_x \\ M_y \\ M_z \end{Bmatrix}
=
\begin{bmatrix}
m & 0 & 0 & 0 & 0 & M_{16} \\
0 & m & 0 & 0 & 0 & M_{26} \\
0 & 0 & m & M_{34} & M_{35} & 0 \\
0 & 0 & M_{34} & J_{xx} & J_{xy} & 0 \\
0 & 0 & M_{35} & J_{xy} & J_{yy} & 0 \\
M_{16} & M_{26} & 0 & 0 & 0 & J_{zz}
\end{bmatrix}
\begin{Bmatrix} \ddot{u}_x \\ \ddot{u}_y \\ \ddot{u}_z \\ \ddot{\theta}_x \\ \ddot{\theta}_y \\ \ddot{\theta}_z \end{Bmatrix}, \quad (9)
$$

where $\overrightarrow{\ddot{u}}$ contains the accelerations $\ddot{u}$ and angular accelerations $\ddot{\theta}$. The location of the centre of mass is given by

$$
x_{\mathrm{m}} = \frac{M_{34}}{m} = -\frac{M_{16}}{m} \quad \text{and} \quad y_{\mathrm{m}} = \frac{C_{35}}{m} = -\frac{M_{26}}{m}. \quad (10)
$$

To populate the mass matrix, the masses are m and the moments of inertia J.

The stiffness and mass matrix elements are computed on the basis of a 2D discretisation of the cross section with arbitrary degree of detail (Fig. 13). The resulting grid can then be analysed with the aid of analytical methods [70, 140, 147] or numerically based methods, such as Variational Asymptotic Beam Sectional analysis (VABS) [14], BEam Cross section Analysis Software (BECAS) [8], Sonata/ANBA4 [32], PreComp [7] or Farob/FOCUS6 [76, 145]. The methods have different requirements regarding the grid quality.

5.3 Beam Models

When modelled as a beam, the rotor blade allows for a computationally efficient analysis of global properties such as resonance frequencies (also called natural frequencies or eigenfrequencies) and modes, determination of total mass and the overall

centre of mass as well as the analysis of the deformation response to arbitrary external load cases.

The classic beam according to Euler-Bernoulli [31] uses only the tension and bending components of the stiffness matrix. An implementation can be found in [48]. Such a beam is implemented in ElastoDyn as part of OpenFAST, for example. For computationally intensive processes, the degrees of freedom of the beam are significantly reduced by using modal correction methods. This method is clearly illustrated in [37]. The theory according to Timoshenko [129] additionally takes account of shear and torsion components as well. Extended beam models take account of all structural couplings, i.e. a full 6x6 stiffness matrix (Eq. 5) as well as geometric non-linearities. Such a beam is implemented in Geometrically Exact Beam Theory (GEBT) [53], BeamDyn [137–139] as part of OpenFAST or in the form of an anisotropic beam element [69] in HAWC2, for example. The implementation of the beam in the form of FE in environments such as Ansys APDL [2] has turned out to be beneficial for the design of full-scale blade tests [81]. Modal correction methods can no longer be applied to geometrically non-linear considerations.

A comparison of different degrees of detail for beam models with impact on the WTG loads resulting from aero-servo elastic simulations can be found in [102].

5.4   Models for Thin-Walled Structures

Rotor blades are thin-walled structures, i.e. the wall thickness or skin thickness is relatively small compared to the thickness of the rotor blade. The elongation across the skin thickness can therefore be assumed to be constant. Simply supported or clamped plate or sandwich models [141] are therefore suitable for the stability analysis of parts of the cross section such as shear webs, spar caps or panel sections, and also for the strength analysis of adhesive joints. The stiffnesses of a structural part are described using CLPT, see Sect. 4.4. The total cross section can also be modelled as the chain-linking of plate and sandwich elements, however, so that a stability analysis on the cross-sectional level becomes possible. In so-called finite strip models, a thin-walled cross section is modelled with prismatic discretisation. A rotor-blade-specific implementation is known as FINSTRIP [133].

A comparison of different models for the stability calculation can be found in [105].

5.5   Full-Blade and Detailed Models

Beam models based on structural properties that are uniform across a beam element and prismatically discretised are sufficient for less detailed estimates of the structural response, such as elongations along the blade trailing edge. When, for example, planar elongation states are of interest, however, FE models are indispensable. This

is particularly relevant in the tapering and geometrically twisted section inside the blade which transitions from a circular cross section to an airfoil and whose cross-sectional deformation can no longer be described with beam models.

FE models of the full blade are often based on shell elements which are based on first-order shear deformation theory [101]. This makes it possible to consider shear stiffnesses in the thickness direction and turns out to be advantageous in the stability analysis of local effects in sandwiches [107]. Solid elements which are coupled to the shell can be used for the analysis of adhesive joints [109]. The use of solid elements allows normal stress components in the thickness direction to be considered in addition. This can be helpful in the analysis of thick laminates, particularly near the blade root. To avoid the enormous increase in computational effort [106] when modelling the full blade as a solid model [93, 94], it is worthwhile creating detailed substructure models. In submodelling, node displacements and rotations of the full-blade shell or solid model are transmitted to the cutting interfaces of the submodel.

A detailed model is often used for the analysis of the blade root connection or segmented-blade connections, to include the eccentric loading of the expansion bolt and the laminate, for example, see Sect. 6. The same applies to adhesive joints which are subjected to a multi-axial internal load.

6   Blade Root Connection Concepts

Two concepts have essentially been successful for the blade root connection: the joint with bushing (or insert) and with T-bolt, see Fig. 14.

In the bushing joint, an expansion bolt clamps the inner ring of the blade bearing to a bushing bonded to the blade root laminate. The axial longitudinal force of the bolt is transferred from the outside of the bushing to the inner and the outer root laminate via shear forces. The bushing is accordingly designed to be long so that sufficient surface area is available for the shear force transfer.

With the T-bolt joint, the expansion bolt clamps the inner ring of the bearing to the root laminate. The axial longitudinal force of the bolt is transferred from the barrel nut to the pre-tensioned laminate through a positive mechanical and frictional engagement. The laminate section between two adjacent barrel nuts (not shown in the figure and subsequently referred to as the net section) then transfers the longitudinal force to the root laminate.

The cross-sectional view leads one to suspect that the connection is subject to eccentric loading. In the bolt in particular, this causes a bending load in addition to an axial one. The form of this internal load in the longitudinal direction, and also along the circumference of the root, depends on the compliance of the hub, the blade bearing and the concept for the blade root connection [15, 113].

The use of bushings in the root tends to allow the root region to be designed with thinner walls than for roots with T-bolt design. A motivation for the structural preference of bushings could therefore be a lower blade mass, which would then be reflected in a reduction of the loads in blade bearing, hub and tower. The complexity
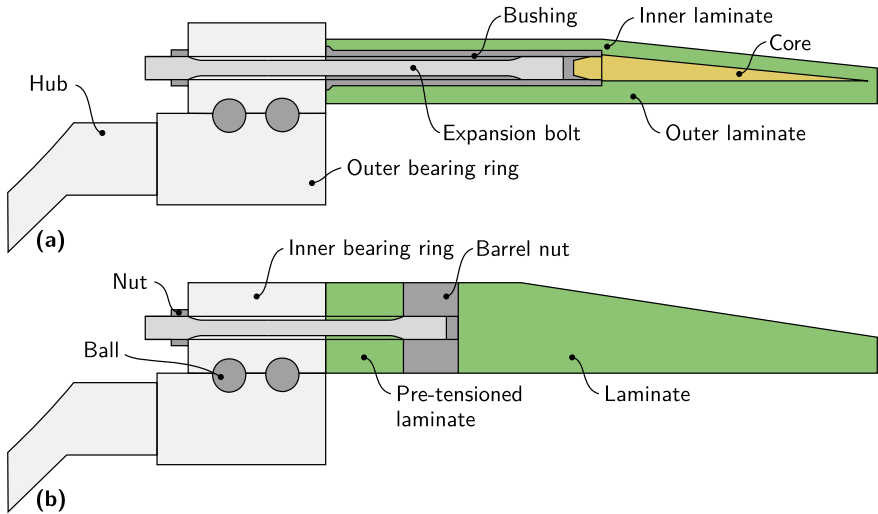
Fig. 14 Cross-sectional view through the blade root connection, constructed using a bushing (**a**) and a T-bolt (**b**). Copyright © 2021 Malo Rosemeier

of the bushing connection means that a computational structural analysis is associated with a great amount of modelling and validation effort. In practice, the permissible extraction force is often determined experimentally with an axial extraction test of a unit cell. This has the disadvantage that a design of a bushing connection is usually retained for each new blade design and accordingly only the root diameter and hence the number of bushings is adjusted. When the wall thickness remains constant, the relative wall thickness decreases, which favours cross-sectional deformations such as the so-called "breathing". This "breathing" can cause unfavourable internal loads in sandwich panels and in the blade bearing.

Analytical models to assess the limit states of the T-bolt connection, such as net section failure, bearing failure, shear-out failure and cleavage failure [26, 116] are established, however, as is the CLPT for thick laminates in particular [16]. The advantage here is that the T-bolt connection can be optimised in detail for every new blade design, see also Sect. 9.4.

7 Structural Design Verifications

The ultimate and fatigue strength verifications for the structural members subjected to the design load cases are conducted in accordance with the certification scheme selected, i.e. the partial safety factors to be used. In addition, further verifications which affect the serviceability of the WTG have to be conducted in relation to the rotor blade structure.

7.1 Strength Verifications for Fibre-Reinforced Polymers

To assess the load-bearing capacity of rotor blades for WTGs, it is first necessary to know the strengths of FRPs. The materials testing (Sect. 4.3) usually provides this information only for UD-NFC composites or for UD single plies, however. The orthotropy of FRPs means that a direct assessment of the load-bearing capacity is not possible. Hence, the use of failure criteria and failure functions has become normal practice. For the ultimate strength verification of rotor blade structures, the procedure according to PUCK [98, 135] is now established.

The strength hypothesis according to PUCK is an action-plane-based failure model. It is based on the COULOMB-MOHR strength hypothesis, which was originally developed for geodetic materials and heaps of material. It produces realistic strength predictions especially for the quasi-static compressive load transverse to the fibre direction. To this end, the failures are first categorised into fibre-dominated (fibre fracture (FF)) and matrix-dominated failures (inter-fibre fracture (IFF)). Furthermore, a distinction is made between the fracture modes A, B and C of the IFF.

- FF: Failure caused by a tensile or compressive stress in the fibre direction.
- IFF Mode A: Failure caused by a combined tensile and shear stress which acts in the direction of the tensile stress perpendicular to the fibre direction.
- IFF Mode B: Failure caused by a combined compressive and shear stress which acts in the direction of the compressive stress perpendicular to the fibre direction, where the absolute value of the shear stress is greater than the absolute value of the compressive stress.
- IFF Mode C: Failure caused by a combined compressive and shear stress which acts in the direction of the compressive stress perpendicular to the fibre direction, where the absolute value of the shear stress is less than the absolute value of the compressive stress.

When used as part of the structural optimisation, this has the advantage that it is possible to identify the stress or load state which was the original cause of the failure as well as the component, fibre or matrix which failed. In addition, the expression according to Puck is homogeneous of degree one. This means that stress exposures can be stated in the form

$$e = \frac{[\sigma]}{[R]}. \tag{11}$$

The stress exposure e is then linearly dependent on the stress vector $[\sigma]$ of the single ply. $[R]$ is a strength vector. An actual division only works in the uni-axial case, however, while the mathematical effort is higher for complex stress states. Details are given in [98]. The consequence of the linear dependence is that for a stress exposure of $e = 0.5$, a load precisely twice as large would lead to failure.

Moving on to the fatigue strength analysis, it turns out that predictions are not possible without further ado with PUCK's failure hypothesis, since a superposition of the stress exposures from different fracture modes and fibre stress exposures is

not covered. Hence the fatigue strength verification is frequently based on results of fatigue strength tests on the coupon level of the testing pyramid (Fig. 1).

A WTG easily experiences load cycle numbers of around $n = 10^8$, which already originate simply from the number of revolutions of the rotor as a consequence of rated operation. This load cycle range is the so-called Ultrahigh-Cycle Fatigue (UHCF) regime.

The fatigue strength properties of FRPs depend on many parameters. The first step is to describe their phenomenological behaviour under service loads in the different phases.

It is observed that FRPs initially have no macroscopically visible damage under this type of load when the loads are sufficiently small. This phase ends when the first crack occurs in the FRP as a consequence of the load, usually in the matrix or the fibre-matrix interface. At the same time, this point in time marks the transition to the phase of crack density growth. In this phase, the mechanical properties of the FRP degrade to a greater or lesser extent. The incidence of the initial damage and the crack density growth are affected significantly by the stacking of the semi-finished textile materials, for example, by the crossing points of fibres lying on top of each other as well as the arrangement of the stitching threads, for example [146]. The total failure of the composite ends this phase as well as the fatigue process overall.

Depending on the size of the load and the orientation of the reinforcing fibre in the composite in relation to the load direction, the overall process proceeds with different speeds [78]. It can lead to failure within only a few thousand load cycles or last for millions of load cycles.

It is easy to understand that the sizing, whose purpose is to ensure the bonding between fibre and matrix, has a significant effect on the point in time of, and the stress level at damage initiation, and thus on the fatigue strength behaviour [127]. In consequence, the matrix also has a substantial influence on the damage initiation in FRPs, especially when the load direction is arranged transverse to the fibre direction [78].

In addition to the mechanical properties, also as a function of temperature and the degree of curing [3, 33], the visco-elastic behaviour, such as the strain rate dependence, creep behaviour and relaxation behaviour [79, 83] and the fracture toughness [123] of the matrix also have an influence on their fatigue strength behaviour. A matrix-based procedure therefore works quite well, at least to predict the initiation of matrix-dominated damage [74]. In this procedure, a comparison stress is formed on the component level, which makes the consideration independent of the reference planes used by PUCK.

The fatigue strength behaviour of polymers can be quite simply expressed using the equation according to BASQUIN [4]. The results of changing tensional-compressive loads with the load ratio of $R = -1$ are quite well simulated by this at least. The load ratio is defined by

$$R = \frac{\sigma_l}{\sigma_u}, \tag{12}$$
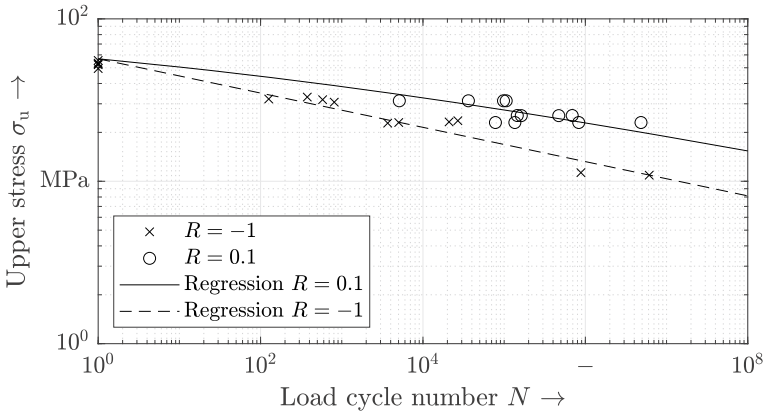
Fig. 15 Results of the cyclic test and regression according to BASQUIN-GOODMAN for an EP adhesive. Copyright © 2021 Alexander Krimmer

where the index u stands for the upper and the index l for the lower stress of a sinusoidal internal load.

Further detailed information on the fatigue strength test and the fatigue strength in general can be found in HAIBACH [46] and SURESH [121]. In combination with the equation according to GOODMAN [43], load conditions deviating from $R = -1$ can be described as well. Corresponding experimental results and regressions for the approaches given are shown in Fig. 15 for an adhesive. The test results for $R = -1$ and $R = 0.1$ were evaluated in their entirety here. The corresponding curves shown are based on the same parameter set with the negative inverse stress-life exponent $m = 9.48$ and the strength $R_t = 56.8$ MPa. The graphs presented can be generated with [104]:

$$N = \left(\frac{2R_t}{(1 - R)\,\sigma_u} - \frac{|1 + R|}{1 - R} \right)^m . \tag{13}$$

With some restrictions, the approaches can be transferred to FRPs as well. An isotropic adhesive was used here to make the illustration clear and intelligible. Moreover, further approaches to the description are conceivable [104].

7.2 Stability Verifications

The stability of a structure is essentially determined by its stiffness and slenderness. If a load-bearing structure becomes unstable, this leads to a sudden deformation, which then usually leads to a strength failure. For rotor blades, a distinction is made between global and local stability failure (also called buckling failure). Global buckling takes

place when, for example, a sandwich becomes unstable in its entirety, comprising the skins and the core. In practice, the sandwich then behaves like a plate made from a single laminate ply. Local buckling is when the skin becomes unstable because of skin wrinkling, for example, or the core becomes unstable because of core shear crimping, for example [107]. Details of various stability failure modes can be found in [141]. Local modes can be described well with analytical models, see Sect. 5.4. Within limits, the frequently used FE shell model with adequate element types is used for this purpose as well, however, see Sect. 5.5.

For the verification, the solutions of a linear eigenvalue problem, i.e. the buckling resistances and their buckling modes, are compared to an applied extreme load distribution and expressed with the safety reserve factor (Eq. 4). Since rotor blades are thin-walled on the one hand and slender, strongly deforming structures on the other, a computationally much more complex geometric non-linear stability analysis which takes account of geometric imperfections, i.e. the application of stress-free pre-deformations, can be carried out, where the load vectors follow the deformation step by step [106].

7.3 Verifications of the Adhesive Joint

Adhesive joints in rotor blade structures are subjected to both mechanical internal loads caused by gravitational loads and aerodynamic actions as well as internal loads caused by a change in temperature. In addition, these loads are multi-axial, comprising linear expansion, shear and peeling. In principle, the ultimate strength verification as well as the fatigue strength verification for the adhesive joint can be carried out along the lines of the IFF of FRPs on the basis of stress-based methods [109], see Sect. 7.1. For the purpose of model validation, tests can be carried out on the coupon level, and also on the full-blade level or an intermediate level of the testing pyramid (Fig. 1).

At first sight, the frequently observed transverse cracks in rotor blade adhesive joints do not seem to have any effect on the integrity of the blade structure and a damage-tolerant design could be discussed here, cf. [67]. However, since the consequences of initiated transverse cracks, such as crack propagation into the load-bearing structures [109], can lead to an increased failure probability, a safe-life design seems to be the right approach to achieve reliable operation.

7.4 Verifications of the Sandwich Core

Relatively wide and thin-walled sandwich panels, particularly inside the blade near the root, are exposed to the so-called "breathing", a deformation within the cross section. This means that bending takes place in the sandwich in addition to the axial tension. Here, the core is subjected to a shearing load in a plane of the plate across

the thickness and a compressive load out of the plane of the plate. The verifications are provided with suitable plate or detailed models, see Sects. 5.4 and 5.5.

7.5 Verifications of the Expansion Bolt

The preloaded expansion bolt at the blade root connection or at a segmented-blade joint is one of the few replaceable load-bearing structural members of the rotor blade. The eccentric load situation at the blade root connection (see Sect. 6) causes a bending stress of the bolt as well as the purely axial load. As a machine element, the verifications for the expansion bolt are provided on the basis of recognised mechanical engineering guidelines such as [134], for example.

7.6 Serviceability Verifications

In addition to the verification of critical deformation, i.e. the tower clearance between blade tip and tower surface in particular, verification must be provided that the resonance frequencies of the rotor blade are not excited by the rotor frequency and its harmonics which arise in operation. For this purpose, the rotor blade can no longer be considered separately from the WTG system, since the resonance modes between the blades occur in so-called coupled rotor modes, cf. [117]. Such a verification is provided with the aid of a Campbell diagram, see Fig. 7 in Chap. 7 of this book. In addition, mention is also made here of the verification of aero-elastic instabilities, such as flutter [47] and vortex-induced vibrations of the rotor blade [51].

8 Manufacturing

Rotor blades for WTGs are usually manufactured in negative moulds for the rotor blade skins. These moulds define the aerodynamic skin of the rotor blade for the manufacturing process, which is then filled with the rotor blade structure during the manufacturing process.

Most rotor blades manufactured today are produced as two skins. These blades therefore comprise two load-bearing skins for the aerodynamic suction side and pressure side, into which the main reinforcement is integrated. The two skins are joined together by means of structural adhesive joints and via shear webs to form the final rotor blade structure. A corresponding rotor blade cross section is depicted in Fig. 16a. The adhesive joints of the leading edge, the trailing edge and the shear webs in the aerodynamic pressure side are marked accordingly. In the aerodynamic suction side, the connections of the shear webs were carried out as HL in this case.
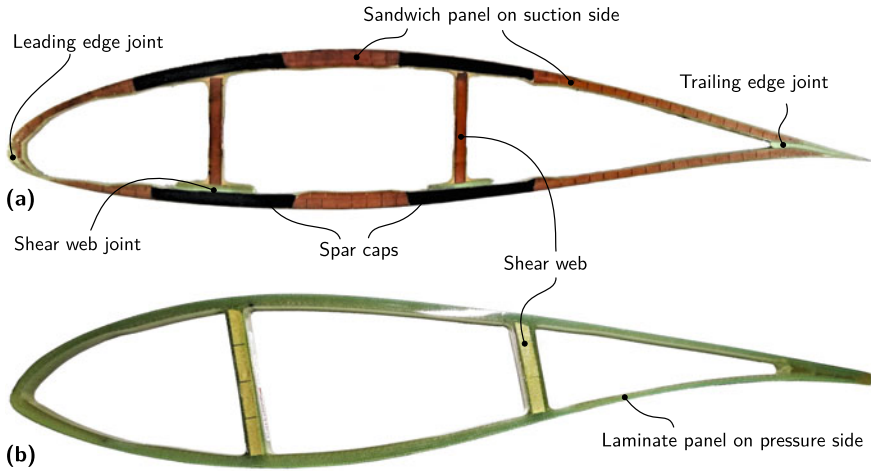
Fig. 16 Blade cross section from a rotor blade in half-shell construction with four spar cap system and CF-reinforced spar caps (**a**) and from a One-Shot blade manufactured by means of integral construction by CARTFLOW (**b**). Copyright © 2021 Alexander Krimmer

Furthermore, it is possible to identify the spar caps, which are shown in black because of the CF reinforcement and arranged here in a four spar cap system.

Deviating from the half-shell construction, rotor blades are in some cases manufactured by means of so-called integral construction. Siemens Gamesa Renewable Energy (SGRE) in particular developed the IntegralBlade® technology [120], as it called it, and established it even for rotor blades on large offshore WTGs. Another manufacturer which pursues a similar approach is CARTFLOW. A rotor blade cross section of a blade from this manufacturer is illustrated in Fig. 16b. Here, the lack of a structural bond is particularly conspicuous.

In Sect. 8.1, the discussion first addresses the most important manufacturing processes used in rotor blade manufacture. Sect. 8.2 provides an overview of possible constructional deviations and their consequences.

8.1 Methods

For rotor blades, a fundamental distinction is made between the manufacture of rotor blades with the HL method, with the method using pre-impregnated fibres (prepreg), and the VI method. In all cases, single-sided moulds are used, which are sealed in different ways. Essentially, these three methods differ in the way the resin matrix is introduced.

In VI manufacture, which covers many different methods such as Vacuum-Assisted Resin Infusion Moulding (VaRIM) and Seaman's Compound Resin Infu-

sion Moulding Process (SCRIMP), a vacuum bag is applied onto the dry stacked-up semi-finished fibre material. This is then evacuated with vacuum pumps before the low-viscosity resin matrix, which follows the largest pressure gradient, is pressed into the component.

If the manufacturing process still uses the HL method, these steps are mainly limited to overlaminates, which are usually applied throughout the finishing process or in the course of repairs if manufacturing deviations have to be corrected. However, it is essential here that a predefined quantity of resin is applied to the semi-finished fibre material outside the mould. This can also be done with an automated impregnating machine.

After impregnation, the work steps in the prepreg and HL methods are nearly the same. The work sequence for the VI method is now briefly described.

Even today, the manufacture of rotor blades for WTGs is still largely a manual process. The layup of the non-crimped textiles and the core material is usually done by hand. Prefabricated components are placed into the rotor blade mould with the aid of hoists or cranes. The flow media, feed lines and suction hoses as well as the vacuum bag are again arranged by hand. The vacuum is produced by vacuum pumps to a differential pressure of approximately atmospheric pressure. The stacked setup is then checked for leaks. Once this has been done, the infusion can commence.

Before the infusion, the heater, which is usually integrated in the rotor blade mould, is brought to a predefined processing temperature. After the infusion is completed, the temperature is increased to a material-dependent value and maintained at this value to ensure the resin matrix is cured. During curing, the resin matrix undergoes volumetric shrinkage. The more the viscosity of the resin material increases, the more it is able to transfer shear forces. The shrinkage component, which can transfer forces, is called polymer-physical shrinkage. This causes internal stresses, which are comparable to thermal residual stresses [115].

Blades manufactured in integral construction are removed from the mould and after curing, they are practically ready for the surface finishing and post-processing of the blade root connection. In contrast, the two blade skin laminates and the prefabricated shear webs are joined by bonding, trimmed, overlaminated and then subjected to surface finishing as well as post-processing of the blade root connection. The process of half-shell manufacture is nicely illustrated in a video [130].

8.2 Deviations

Within the processes described, the structural properties can naturally deviate from the desired state. A distinction must be made according to whether these are deviations which lie within the tolerances specified or outside them. When they lie within the tolerances, then the effect of the deviation on the serviceability and operational safety of the rotor blade structure is taken into account in its design and is acceptable. If a deviation is outside the tolerances specified, then the serviceability and operational safety of the structure may possibly be compromised. The design engineer

can examine this by computation. If the structure is not operationally safe and not sufficiently load-bearing, the deviation must be remedied. In general, this means a repair of varying degrees of complexity.

Examples of these deviations are

- air inclusions (finely dispersed air bubbles, local accumulations of air or even dry spots in the laminate);
- undulations (angle errors, waviness or wrinkles in the laminate);
- misalignments (insufficient overlaps, gaps between plates of core material);
- cracks caused by internal (for example, temperature-related) stresses;
- uncured material (caused by mixing errors or insufficient heat input during curing) and
- discolourations or changes to the mechanical properties caused by local overheating especially of the core material.

If a repair is not carried out, the consequences for the support structure can sometimes be disastrous. The consequences of the deviations are presented in brief here.

Air inclusions primarily affect the matrix-dominated properties of the composite. This means the matrix-dominated moduli and strengths decrease with increasing porosity, for example. This is particularly critical for the compressive strength in the fibre direction, since the matrix provides less support to the fibres.

Undulations right through to waviness and wrinkles primarily affect the compressive strength of the laminate in the fibre direction. A misalignment of the fibres causes the stresses to transfer from the fibres into the matrix. The stresses which a matrix can tolerate are much lower than those which the fibres can tolerate. Hence undulations sometimes cause drastic decreases in the compressive strength in the fibre direction. Undulations, especially in main reinforcement elements such as spar caps, are generally extremely critical deviations.

Misalignments usually lead to excessive stresses at overlaps or in the adjacent structural members. They can occur in all parts of the structure and are to be assessed as being critical.

Cracks are not always directly critical for the operational safety. They do lead to the formation of voids in the structure, however. These can fill with moisture, for example, under certain weather conditions and frost can then aggravate the damage, for example. In any case, they form the starting point for damage growth.

Uncured material is extremely critical to the operational safety of FRP structures. The transfer of forces from fibres to matrix and vice versa is only possible to a limited extent. This means that the fibre-dominated and the matrix-dominated strength is compromised.

Discolourations indicate a change in the chemical and therefore potentially the mechanical properties. In the case of core materials, the buckling stability of sandwich structures may be compromised here.

9   Topology Optimisation

Now that all the important components of the rotor blade and their mechanical properties are known, a structural optimisation is possible. For the optimisation, a quantity needs to be specified which can be used to assess the quality of the design. This is then minimised or maximised during the optimisation. In a lightweight construction such as a rotor blade, the mass is an obvious optimisation target, which of course has a crucial impact on the loads of a WTG since it is a cantilever beam structure.

The usual procedure is to carry out a load simulation with an initial model draft of a rotor blade. In relation to the wind turbine, the rotor blade is described by its stiffness distribution, its mass and its static moment. The objective is to demonstrate by means of computation the load-bearing capacity and operational safety of the rotor blade in all aforementioned verifications with the loads determined from the load simulation.

For a WTG, costs, yield and the LCoE are assessment parameters of overriding importance. Since the rotor blades account for between 15 and 25 % [99] of the wind turbine costs, the rotor blades have a significant influence on the aforementioned assessment quantities. It is difficult to optimise the WTG as an overall system, however, since the rotor blade designer often does not have all the necessary information about the turbine at their disposal. For simplicity, the optimisation is therefore restricted to a rotor-blade-related optimisation.

When, in the course of the optimisation, the mass and the static moment of the rotor blade deviate from the rotor blade model initially used for the load simulation, a new load simulation must be carried out. According to [60], tolerances of $\pm 3\%$ and $\pm 4.5\%$ apply to the mass and the static moment of the rotor blade, respectively.

An overview of possible optimisation targets and their interaction is given below. Guidance is given for taking aero-elastic effects into account. Greater emphasis is nowadays being placed on optimisation of design for manufacture in particular, since it has a significant influence on the quality and the manufacturing cycle time.

9.1   Optimisation Targets

As already mentioned, the optimisation targets according to which the rotor blade is optimised may differ or supplement each other. These targets can be

- energy yield,
- costs,
- mass,
- loads and
- power.

The primary objective of the design is naturally the generation of a high yield. Hence material which is as low cost as possible should be used. Basically, the topology of a structure is therefore optimised until it is no longer possible to achieve the

optimisation target with the given set of materials. Only at this stage does the change to a higher quality material take place, since this is generally accompanied by higher costs.

To be able to constructively assess these relationships, the important structural properties must be monitored during the optimisation. It is therefore advisable to create a mass model and a cost model for the rotor blade structure. This should include, for example, Capital Expenditures (CapEx) for material, production equipment and tools, staff, transport and in the best case even Operating Expenditures (OpEx) for maintenance and repair, for example, as well as Disposal Expenditures (DispEx) which are incurred by the rotor blade for the whole turbine. The yield model is usually provided by the aerodynamicists. They also answer questions regarding power and loads, cf. [65].

It is not always possible to directly assess the mass and cost impacts of adjustments on the structure. When changes are made to the structure, their consequences for the mass (Fig. 6) and the costs should therefore always be considered. With the structural and topological optimisation, it can be assumed that the yield initially remains the same. The steps mentioned mainly cover the issues of yield, costs, loads, mass and power.

Further boundary conditions may possibly also have to be taken into account in the optimisation. These can be

- time to market,
- manufacturing cycle time,
- quality,
- number of main moulds and additional moulds,
- recyclability,
- space required in production and
- transport restrictions (bridge height, radii of road bends and rail tracks).

All these topics should be considered when designing and optimising the rotor blade structure.

9.2 Aero-Elastic Properties

The blades become more slender with increasing rotor blade length. This can be attributed to the tip-speed ratios (TSRs) of the turbines on the one hand. They are sometimes simply equipped with longer blades, while the other turbine characteristics remain the same. This means that the tip-speed ratio in rated operation increases, which leads to more slender rotor blades, see Fig. 12 in Chap. 4 of this book. Furthermore, transport restrictions lead to slender blades, since the maximum chord length and the root diameter, for example, are restricted by boundary conditions for road or rail transport.

More slender blades are more susceptible to aero-elastic instabilities, since the enclosed area of a cross section has a significant influence on its torsional stiffness

and decreases from cross section to cross section in relation to the length of the rotor blade. This relationship is described by the second BREDT-BATHO formula and is a consequence of the first BREDT-BATHO formula, which assumes a constant shear flux in the cross section caused by the torsion [141]. For cross sections with inhomogeneous properties, the relationship is more complex [144], but the difference is small in the first approximation [5].

To counteract the tendency to aero-elastically unstable behaviour, it is primarily necessary to ensure that the shear centre (Fig. 13) of the cross section is located in the edge direction in front of the pressure point of the aerodynamic force at around 1/3 of the airfoil chord length so that the aerodynamic load causes a twisting of the cross section towards the feathering position, i.e. towards a smaller angle of attack. A twist towards a larger angle of attack has an unfavourable impact on the loading, for example, through stall-induced vibrations [47].

A further issue which can affect the aero-elasticity is the changing structural twisting angle along the rotor blade (Eq. 8). This is mainly caused by the fact that rotor blades have an aerodynamic twist, which means that the airfoils are arranged along the blade axis so that they always have the most favourable aerodynamic angle of attack. In Fig. 12b, the airfoil chords of the largest and the smallest airfoils are marked by dot-dashed lines. This makes it easy to see the different angles of attack. In Fig. 13, the main axes of inertia are furthermore marked by dashed lines. It is easy to imagine that the twist of the main axes of inertia roughly moves with the twisting of the airfoil chord, naturally influenced by the position of the main spar caps. This basically illustrates that a pure bending moment in the flapwise direction, for example, always causes a lead-lag bending as well.

9.3 *Design for Manufacturing*

Optimisation of the manufacturing cycle time, quality, number of main and additional moulds, space required for manufacturing and recyclability touches on the field of Design for Manufacturing (DfM). Here, the assessment is not as easy as for the pure structural optimisation, since the advantages and disadvantages in the manufacturing process are often not as easy to assess. It may be the case that a specific process can proceed faster, but that more staff need to be involved. Such a step would only be advantageous when the cost savings resulting from the shorter processing time overcompensate the higher staffing costs.

It is possible to formulate some rough guidelines, however. To keep the manufacturing cycle time short, a proven method is

- to keep the ply book simple;
- avoid local reinforcements, if possible;
- keep the number of prefabricated components low;
- keep the number of additional moulds correspondingly low and
- carry out manufacturing steps in the main mould, coordinated where possible.

Since main spar caps are usually manufactured in additional moulds, for example, it would therefore be favourable to decide for a two spar cap concept instead of a four spar cap concept, since fewer components will have to be manufactured in an additional mould. A structural comparison of the two concepts is provided by [105]. This means in practice that the main spar cap pair must be arranged where the airfoil is thickest, where the parallel-axis contribution to the flapwise bending stiffness is optimum. A less pronounced trailing edge spar cap pair, as shown in Fig. 13, provides lead-lag bending stiffness.

Attention is currently also being paid to the recyclability of rotor blade structures. To facilitate this, recyclability must already be taken into account when designing the rotor blade structure, in the selection of the materials and manufacturing processes, see Sect. 10.

9.4 Blade Root Connection

As has already been indicated in Sect. 6, as far as the blade root connection is concerned, the optimisation of the bushing connection is often limited to the adjustment of the diameter of the root circle and thus to the number of bushing segments over the root circle, because of the analysis effort involved. When upscaling, the wall thickness thus remains constant. This can lead to unfavourable cross-sectional deformations and thus internal loads, which cannot be counteracted in the construction without complex further development of the bushing connection. If the expansion bolt is the dimensioning element of the connection, however, the bushing connection allows a larger number of connection segments to be accommodated over the root circle than does the T-bolt connection, thus relieving the load on the expansion bolt.

It is comparatively easy to verify the failure modes of the T-bolt connection, in contrast. The essential parameters therefore remain available to influence the mechanical properties. These are, for example, laminate thickness, fibre angle, barrel nut diameter, net section fraction in the barrel nut circle, expansion bolt length, flange separation of the barrel nut bore and others. All these parameters can and must be optimised to guarantee the load-bearing capacity of the connection.

As already mentioned, the price is an important optimisation target. Here, the T-bolt connection has significant advantages over the bushing connection because the material costs are already much lower. The increased effort required to manufacture the bushing connection increases this advantage further. A disadvantage in this consideration is that the manufacture of the T-bolt connection requires a separate workstation for the rotor blade, which is situated between the main mould area and the area for the post-processing and the surface finishing of the rotor blade. Moreover, the drilling machine for the T-bolt connection has higher initial capital expenditure than the milling cutter for the milling finish of the bushing flanges once the rotor blade has been manufactured.

Especially because of the significantly lower costs for the T-bolt connection, it is necessary to make a well-justified decision for one or the other type of connection.

9.5 Blade Segmentation

Blade segmentation is a topic which is discussed time and again as a way to react to restrictions on the blade lengths to be transported. Blade segmentation means that the rotor blade is manufactured in two segments and provided with a connection at its separation point in a similar way and with similar versions as the root connection. The two segments are then joined together on the WTG construction site.

Blade segmentation is rarely used, however. Segmented blades were the standard design at ENERCON for a long time, but have been replaced by one-piece manufacturing despite the blades increasing in length. Other manufacturers also repeatedly experiment with the concept. If one type of rotor blade is manufactured for a large number of WTG types or sites, it can be worthwhile to produce various blade tip lengths which are then individually combined with a root segment to suit the requirement. It must be noted here that this procedure is not established practice as yet. Until now, the segmented manufacture of rotor blades has been more frequently used to solve logistical problems, at GENERAL ELECTRIC (GE) and SGRE, for example.

Disadvantageous is particularly the mass of the joint. It is smaller, the more the position of the segmentation joint is shifted towards the tip, since the forces and moments to be transferred decrease. Here they have a greater leverage with respect to the root, however, so that the mass of the joint is unfavourable for the static moment of the rotor blade.

It must be stated in general that the segmented manufacture of rotor blades primarily affects the logistics of the rotor blade. This normally comes before the actual service life of the rotor blade and only takes a few weeks of the rotor blade life. The compromise which has to be made for this has a negative impact on the structure in the form of additional forces and moments for the remaining service life of the rotor blade, which is between 20 and 30 years in operation. This must be counteracted with an additional support structure, which in turn increases the masses and thus the loads of the rotor blade. It therefore makes sense to consider whether it is not more favourable to find the technical solution in transport technology, since logistical solutions can be reused for many blades, while blade segmentations have to be built into each individual rotor blade.

10 Sustainability

"…to make development sustainable [is] to ensure that it meets the needs of the present without compromising the ability of future generations to meet their own needs" [131]. To safeguard sustainable development in this way, 195 countries have undertaken to limit the global temperature rise to significantly below $2\,°C$ and to strive to keep it below $1.5\,°C$ [132]. This limit allows the emission of only a limited amount of CO_2. According to the "budget approach" [100], this means a complete decarbonisation for Germany, i.e. CO_2 or climate neutrality by 2035 [100]. Climate

neutral here means that all fossil fuels have to be replaced with renewable energy sources by then.

As engineers working with wind energy, we are frequently confronted with the question as to whether wind energy can actually be converted with a smaller CO_2 footprint than energy from other sources of energy. Reference is made first to [114], which states that the CO_2 footprint for onshore wind energy is $11\,gCO_2eq/kWh$ in the median. For offshore wind energy, the value is given as $12\,gCO_2eq/kWh$ and is thus equal to the CO_2 footprint of nuclear energy. All other commercially available technologies are at least a factor of 2 higher. It must be stated, however, that the issues of the treatment of the waste from the nuclear energy conversion and repositories for this waste have still not been solved, even 70 years later [11], which is not compatible with sustainable development.

It is now possible to compare the above-mentioned values for the CO_2 equivalent of the energy sources with the CO_2 footprint of the current energy mix. For 2018, this has been given as $475\,gCO_2eq/kWh$ [54]. It is clear that wind energy is currently the most favourable source of energy as far as the CO_2 footprint is concerned, and is significantly better than the current energy mix, but it does not yet achieve CO_2 neutrality.

More interesting is the consideration of the so-called ecological amortisation. This describes how long a turbine has to operate before it has generated the energy which is required to manufacture and operate it. The assumption for WTGs is 6 to 24 months [128] depending how high its capacity factor is. These values are so impressive because ecological amortisation for conventional power stations is not possible. They have to be continually fed with energy in the form of fuels, for example, to achieve an energy yield.

The design CO_2 footprint of a rotor blade is defined by the energy yield which it could theoretically produce under design conditions. WTGs and the rotor blade component in particular are often not subjected to the design loads during their planned lifetime so that the blades can continue to be operated either on the WTG at the site, or, if another component, e.g. the main shaft, limits the residual lifetime, on a different WTG at a site which may have lower wind speeds until the design loads are exploited, cf. [110]. The actual CO_2 footprint of a rotor blade is therefore usually larger than the design CO_2 footprint. Continued operation thus reduces the CO_2 footprint which then approaches the design CO_2 footprint. The unplanned removal and re-installation at a different site increases the CO_2 footprint again, however, because of the emissions from fossil fuels.

The question is therefore how WTGs can accomplish climate-neutral energy conversion particularly in respect of the rotor blade. This means in practice that the CO_2 footprint must be reduced in a first step and neutralised in a second.

The raw resources for the rotor blade materials are currently crude oil, sand, wood and to a lesser extent metals. To ideally reduce the CO_2 footprint of the materials to zero, this especially means not emitting the bound carbon compounds, which originate from the crude oil used as the basic resource, into the atmosphere by burning, for example, but keeping them in circulation.

This particularly concerns actions which take place after the end of the design life of the rotor blade. One option for neutralisation is to reuse structural elements of the blade, for example, in the form of support structures such as bridges. In the European Union, around 570 Mt of rotor blade waste is expected between 2020 and 2030 [118]. It is easy to imagine that, for various reasons, this amount cannot be used for bridges or other support structure alone.

An alternative is to deposit it in landfills, but this is already banned in some European countries. Although this does not release the carbon compounds of the fossil materials into the atmosphere, it does mean that the other valuable raw materials such as glass and wood are not returned to the cycle either. Several recycling methods are available to regenerate the bound raw materials as well as the bound energy.

One possibility is pyrolysis [17, 41], whereby the raw materials such as GF and CF as combustion residues can be reused in degraded form, i.e. as short fibres. The problem is that the crude-oil-based carbon compounds from the resin matrix are released in this process, because the matrix is burnt. Since the fibres cannot be reused in the same quality and with the same functionality as for the original material, this form of recycling corresponds to degraded recovery or downcycling.

With co-processing [119], the rotor blades are mechanically crushed and used as fuel for the production of cement, for example. Although this adds combustion residues from fossil materials to the atmosphere, the conventional fossil fuels used in cement manufacture are saved. The GF contained replaces sand fractions in the cement clinker. CF-reinforced EP composites are not suitable for cement co-processing. Co-processing is currently one of the few commercially available recycling options for rotor blade structures.

Further recycling options which are not yet commercially viable are mechanical grinding [136], solvolysis [75] and fragmentation by means of high-voltage pulse technology [80].

To reduce the CO_2 footprint further, organic-based raw materials can also be used as an alternative or in addition. EP resins which are produced partially on the basis of regenerative raw materials, for example, are already commercially available. Here the attempt is being made, among other things, to replace crude-oil-based raw materials such as bisphenol A (BPA). For the CF, 95 % of the total amount is currently manufactured on the basis of crude-oil-based polyacrylonitrile (PAN) precursors [35]. Research and development on alternatives for the crude-oil-based production of CF is currently underway as well [35]. Natural fibres such as flax, for example, initially have a smaller CO_2 footprint than CF or GF [6]. Since the mechanical properties of natural fibres are on the one hand worse and on the other subject to a larger statistical variability than industrially manufactured fibres, a higher mass of materials must accordingly be used in the blade to achieve the required stiffnesses and strengths. Whether this reduces the CO_2 footprint of the rotor blade must be answered on an individual basis. When the materials used are based completely on renewable raw materials, then even burning the components would be climate neutral.

Other options to meet the challenges of recycling can be preventative measures. For the current generation of rotor blades, use is sometimes already being made of

special EP curing agents which have been developed for a simplified solvolysis [29]. The residues can be admixed to thermoplastic matrix materials and used again in FRPs, while the fibre materials can be recovered. Whether these can be returned to a full use in structural materials is a research topic which is being investigated.

Furthermore, thermoplastic matrix materials can be used instead of polymer matrix materials. Pyrolysis is not necessary here because the composite can continue to be used, albeit it in lower quality applications of structural materials, since the structure is mechanically fragmented and converted into a thermally workable material. The advantage is that the carbon compounds in the matrix are not released. It goes without saying that this recycling option must already be planned during rotor blade development. Separating the thermoplastics matrix from the fibre materials simply by increasing the temperature is not possible without further ado since the viscosity of the matrix in the molten state is usually comparatively high.

At present, end-grain Balsa wood in particular is becoming scarce because of the globally increasing installed wind power [126]. The manufacturers are being forced to change to alternative core materials so as not to endanger supply chains. Alternative types of wood and also non-renewable raw materials based on conventional materials can be used as a fall-back here. The latter can even increase the CO_2 footprint of blades, when rotor blades are burnt or co-processed, for example. If recycled PET is used as the alternative, for example, it is removed from closed recycling loops, for example, for bottles [68] or in the textile industry for clothing, not simply for the service life of the rotor blade. The bonding with EP created in the manufacturing process, for example, means it can no longer be used in recycling, because the PET used can no longer be recycled in the same quality and fed into the recycling loops stated.

Finally, sustainable development also includes the fact that the natural regenerative ability of the systems involved (mainly living beings and ecosystems) is maintained [142]. In respect of the rotor blade, it should be mentioned that erosion can result in matrix and fibre materials getting into the ecosystem and thus into the food chain of organisms as well in the form of micro-particles or nano-particles. Especially when the EP matrix is based on BPA, ingesting the materials with food can be harmful to health [71].

This demonstrates that the materials used in rotor blades can currently not be recycled to a sufficient degree. Work is being done on promising approaches, however, to further improve the sustainability of the wind energy conversion. At this point it again becomes clear that the rotor blade must be considered and optimised in the context of the WTG system, and also in the context of the resource-efficient supply of energy for our society. As engineers, our task is to take up this challenge for the benefit of future generations. This is the only way that an energy supply based on equitable access to resources is possible for all humankind.

Literatures

1. Aero Dynamic Consult: ADCoS. https://www.aero-dynamik.de/Simulation_82.html
2. Ansys: Mechanical APDL. https://www.ansys.com/
3. Antoniou A, Rosemeier M, Tazefidan K, Krimmer A, Wolken-Möhlmann G (2020) Impact of site-specific thermal residual stress on the fatigue of wind-turbine blades. AIAA J 58(11):4781–4793. https://doi.org/10.2514/1.J059388
4. Basquin OH (1910) The exponential law of endurance tests. In: Proceedings of the thirteenth annual meeting, vol 10. American Society for Testing Materials, Atlantic City, New Jersey, USA, pp. 625–630. https://pdfcoffee.com/basquin-the-exponential-law-of-endurance-testspdf-pdf-free.html
5. Beelitz T, Hadzhiyski A, Kenfack R, Marzik J, Popiela B, Sahr R, Blümel T, Krimmer A (2021) Untersuchung des Torsionsverhaltens dünnwandiger, geschlossenzelliger Profilträger mit inhomogenem Querschnitt. In: Deutscher Luft- und Raumfahrtkongress 2021. Deutsche Gesellschaft für Luft- und Raumfahrt - Lilienthal-Oberth. https://doi.org/10.25967/550319
6. de Beus N, Carus M, Barth M (2019) Carbon footprint and sustainability of different natural fibres for biocomposites and insulation material. Tech. rep., Nova-Institute GmbH, Hürth, Germany. http://eiha.org/media/2019/03/19-03-13-Study-Natural-Fibre-Sustainability-Carbon-Footprint.pdf
7. Bir GS (2001) Computerized method for preliminary structural design of composite wind turbine blades. J Solar Energy Eng 123(4):372–381. https://doi.org/10.1115/1.1413217
8. Blasques JP, Stolpe M (2012) Multi-material topology optimization of laminated composite beam cross sections. Compos Struct 94(11):3278–3289. https://doi.org/10.1016/j.compstruct.2012.05.002
9. Bortolotti P, Bottasso CL, Croce A, Sartori L (2019) Integration of multiple passive load mitigation technologies by automated design optimization-the case study of a medium-size onshore wind turbine. Wind Energy 22(1):65–79. https://doi.org/10.1002/we.2270
10. Bosschers J (1996) Modelling of rotational effects with a 2-d viscous-inviscid interaction code. Tech. Rep. 96521. NLR—Netherlands Aerospace Centre, Amsterdam, the Netherlands
11. Bundeszentrale für politische Bildung: Auf Endlagersuche. Der deutsche Weg zu einem sicheren Atommülllager (2020). https://www.bpb.de/gesellschaft/umwelt/endlagersuche/315473/einleitung
12. Castro SGP, Rosemeier M (2019) Comput Mech (Compmech). https://github.com/mrosemeier/compmech
13. CEN: Eurocode: basis of structural design; EN 1990:2002 + A1:2005 + A1:2005/AC:2010. European Committee for Standardization (2010)
14. Cesnik CE, Hodges DH (1997) VABS: a new concept for composite rotor blade cross-sectional modeling. J Am Helicopter Soc 42(1):27–38. https://doi.org/10.4050/JAHS.42.27
15. Chen G, Wen J (2012) Load performance of large-scale rolling bearings with supporting structure in wind turbines. J Tribol 134(4):041105. https://doi.org/10.1115/1.4007349
16. Chou P, Carleone J, Hsu C (1972) Elastic constants of layered media. J Compos Mater 6(1):80–93. https://doi.org/10.1177/002199837200600107
17. Cunliffe A, Jones N, Williams P (2003) Pyrolysis of composite plastic waste. Environ Technol 24(5):653–663. https://doi.org/10.1080/09593330309385599
18. DAkkS: Datenbank der akkreditierten Stellen (2021). https://www.dakks.de/de/akkreditierte-stellen-suche.html
19. Danmarks Tekniske Universitet (DTU): Ellipsys. https://the-numerical-wind-tunnel.dtu.dk/EllipSys
20. Danmarks Tekniske Universitet (DTU): HAWC2. https://www.hawc2.dk
21. Dassault Systèmes: Simpack. https://www.3ds.com/products-services/simulia/products/simpack/product-modules/wind-modules/
22. Det Norske Veritas (DNV): Bladed. https://www.dnv.com/services/renewables-engineering-software-138662

23. DGfM: MauerWerk - Das Lehrportal - 3.1 Sicherheitskonzept. https://www.mauerwerksbau-lehre.de/vorlesungen/3-sicherheitskonzept-und-einwirkungen/31-sicherheitskonzept/311-allgemeine-grundlagen

24. DIBt: Richtlinie für Windenergieanlagen - Einwirkungen und Standsicherheitsnachweise für Turm und Gründung - Stand: Oktober 2012 - Korrigierte Fassung März 2015. Mitteilungen des DIBt, Technische Regel, Referat I 8, Bautechnisches Prüfamt, Grundlagen der Standsicherheit (2015). https://www.dibt.de/fileadmin/dibt-website/Dokumente/Referat/I8/Windenergieanlagen_Richtlinie_korrigiert.pdf

25. DNV: DNV-DS-J102 (2010) Design and manufacture of wind turbine blades, offshore and onshore wind turbines. https://rules.dnv.com/docs/pdf/dnvpm/codes/docs/2010-11/DS-J102.pdf

26. DNV GL: DNVGL-ST-0376 (2015) Rotor blades for wind turbines. https://www.dnv.com/energy/standards-guidelines/dnv-st-0376-rotor-blades-for-wind-turbines.html

27. DNV GL: DNVGL-SE-0441 (2016) Type and component certification of wind turbines. https://www.dnv.com/energy/standards-guidelines/dnv-se-0441-type-and-component-certification-of-wind-turbines.html

28. Drela M (1989) XFOIL: an analysis and design system for low Reynolds number airfoils. In: Mueller TJ (ed) Low Reynolds number aerodynamics. Springer, Berlin, Heidelberg, pp 1–12. https://doi.org/10.1007/978-3-642-84010-4_1

29. Dubey PK, Mahanth SK, Dixit A, Changmongkol S (2020) Recyclable epoxy systems for rotor blades. In: IOP conference series: materials science and engineering, vol 942. IOP Publishing. https://doi.org/10.1088/1757-899X/942/1/012014

30. ESI Group: Openfoam. https://www.openfoam.com/

31. Euler L (1744) Methodus inveniendi lineas curvas maximi minimive propietate gaudentes, Additamentum I, De curvis elasticis. Bousqet & Socios, Lausanne, Geneva, Switzerland. https://mdz-nbn-resolving.de/urn:nbn:de:bvb:12-bsb10053439-8

32. Feil R, Pflumm T, Bortolotti P, Morandini M (2020) A cross-sectional aeroelastic analysis and structural optimization tool for slender composite structures. Compos Struct 253:112755. https://doi.org/10.1016/j.compstruct.2020.112755

33. Fiedler B (2009) Hochleistungs-Faserverbundwerkstoffe mit Duroplastmatrix. Werkstoffe Struktur Eigenschaften Modellierung. TuTech Innovation GmbH, Hamburg, Germany

34. Fink R (2018) Einfluss der Materialkopplungen der klassischen Laminattheorie auf die Lage des Schubmittelpunktes mehrzelliger, dünnwandiger Profilquerschnitte. Technische Universität Berlin, Masterarbeit

35. Fraunhofer IAP (2019) Bio-based carbon fibers-high-performance and sustainability for light-weight applications. https://www.iap.fraunhofer.de/en/press_releases/2019/biobased-carbon-fibers.html

36. Fraunhofer IWES, MoWiT—Modelica for wind turbines library. https://www.iwes.fraunhofer.de/en/research-spectrum/entry-oem-supplier/aerodynamics-for-wind-turbines/Load-Calculations.html

37. Freymann R (2011) Strukturdynamik: Ein anwendungsorientiertes Lehrbuch. Springer, Berlin, Heidelberg, Germany (2011). https://doi.org/10.1007/978-3-642-19698-0

38. Galilei G (1638) Discorsi e dimostrazioni matematiche intorno à due nuoue scienze. Elsevier, Leiden, Netherlands. https://doi.org/10.3931/e-rara-3923

39. Gasch R, Knothe K, Liebich R (2012) Strukturdynamik: Diskrete Systeme und Kontinua, chap. 18–Bewegungsgleichungen von rotierenden elastischen Strukturen. Springer, Berlin, Heidelberg, Germany, pp 599–614. https://doi.org/10.1007/978-3-540-88977-9_18

40. Gere JM, Goodno BJ (2012) Mechanics of materials, 8th international edn. Nelson Education

41. Ginder RS, Ozcan S (2019) Recycling of commercial e-glass reinforced thermoset composites via two temperature step pyrolysis to improve recovered fiber tensile strength and failure strain. Recycl 4(2):24. https://doi.org/10.3390/recycling4020024

42. GL (2010) Guideline for the certification of wind turbines. Germanischer Lloyd Industrial Services, Hamburg, Germany

43. Goodman J (1899) Mechanics applied to engineering. Longmans, Green and Co., London, England. https://archive.org/details/mechanicsapplie03goodgoog
44. Griffith AA (1921) VI. The phenomena of rupture and flow in solids. Philos Trans R Soc London Ser A Contain Pap Math Phys Character 221(582–593):163–198. https://doi.org/10.1098/rsta.1921.0006
45. Habenicht G (2009) Kleben: Grundlagen, Technologie, Anwendungen, 6 edn. Springer, Berlin, Heidelberg, Germany. https://doi.org/10.1007/978-3-540-85266-7
46. Haibach E (2006) Betriebsfestigkeit, 3 edn. Springer, Berlin, Heidelberg, Germany. https://doi.org/10.1007/3-540-29364-7
47. Hansen MH (2007) Aeroelastic instability problems for wind turbines. Wind Energy 10(6):551–577. https://doi.org/10.1002/we.242
48. Hansen MOL (2015) Aerodynamics of wind turbines, 3rd edn. Routledge, London, UK
49. Hashin Z, Rosen B (1964) The elastic moduli of fiber-reinforced materials. J Appl Mech 31(2):223–232. https://doi.org/10.1115/1.3629590
50. Hauffe A (2020) Elamx^2. https://tu-dresden.de/ing/maschinenwesen/ilr/lft/elamx2/elamx
51. Heinz JC, Sørensen NN, Zahle F, Skrzypiński W (2016) Vortex-induced vibrations on a modern wind turbine blade. Wind Energy 19(11):2041–2051. https://doi.org/10.1002/we.1967
52. Hendriks H, Bulder B (1995) Fatigue equivalent load cycle method. A general method to compare the fatigue loading of different load spectrums. Tech. Rep. ECN-C-95-074. Energy research Centre of the Netherlands (ECN). https://www.ecn.nl/publicaties/PdfFetch.aspx?nr=ECN-C--95-074
53. Hodges DH (2006) Nonlinear composite beam theory. Am Inst Aeronaut Astronaut. https://doi.org/10.2514/4.866821
54. IEA (2019) Global energy & CO2 status report—The latest trends in energy and emissions in 2018. Tech. rep., Int Energy Agency. https://iea.blob.core.windows.net/assets/23f9eb39-7493-4722-aced-61433cbffe10/Global_Energy_and_CO2_Status_Report_2018.pdf
55. IEC (2010) IEC 61400-22—Wind turbines Part 22: conformity testing and certification. International Electrotechnical Commission, Geneva, Switzerland
56. IEC (2014) IEC 61400-23—Wind turbines Part 23: full-scale structural testing of rotor blades. International Electrotechnical Commission, Geneva, Switzerland
57. IEC (2018) IECRE OD-501—IEC system for certification to standards relating to equipment for use in renewable energy applications (IECRE System): type and component certification scheme. International Electrotechnical Commission, Geneva, Switzerland
58. IEC (2018) IECRE OD-501-1—IEC system for certification to standards relating to equipment for use in renewable energy applications (IECRE System): conformity assessment and certification of blade by RECB, 2 edn. International Electrotechnical Commission, Geneva, Switzerland
59. IEC (2019) IEC 61400-1—Wind energy generation systems—Part 1: design requirements, 4 edn. International Electrotechnical Commission, Geneva, Switzerland
60. IEC (2020) IEC 61400-5—Wind energy generation systems—Part 5: wind turbine blades. International Electrotechnical Commission, Geneva, Switzerland
61. IECRE (2021) RE testing laboratories (RETLs). https://test.iecre.org/dyn/www/f?p=110:7:::::P7_ORG_TYPE:RETL
62. Institut für Mechatronik in Chemnitz: alaska/Wind. https://www.ifm-chemnitz.de/produkte/alaskamultibodydynamics/alaskawind
63. ISO (1998) ISO 2394—General principles on reliability for structures. International Organization for Standardization, Geneva, Switzerland
64. ISO (2012) ISO/IEC 17065—Conformity assessment—Requirements for bodies certifying products, processes and services. International Organization for Standardization, Geneva, Switzerland
65. Jamieson P (2020) Top-level rotor optimisations based on actuator disc theory. Wind Energy Sci 5(2):807–818. https://doi.org/10.5194/wes-5-807-2020

66. Jonkman J, Musial W (2010) Offshore code comparison collaboration (oc3) for iea wind task 23 offshore wind technology and deployment. Tech. Rep. NREL/TP-5000-48191. National Renewable Energy Laboratory (NREL), Golden, Colorado, USA. https://doi.org/10.2172/1004009

67. Jørgensen JB, Sørensen BF, Kildegaard C (2018) The effect of buffer-layer on the steady-state energy release rate of a tunneling crack in a wind turbine blade joint. Compos Struct 188:64–71. https://doi.org/10.1016/j.compstruct.2017.12.081

68. K-ZEITUNG (2020) Das Branchenblatt der Kunststoffindustrie: Mit PET-Recycling zum geschlossenen Kunststoffkreislauf. https://www.k-zeitung.de/mit-pet-recycling-zum-geschlossenen-kunststoffkreislauf/

69. Kim T, Hansen AM, Branner K (2013) Development of an anisotropic beam finite element for composite wind turbine blades in multibody system. Renew Energy 59:172–183. https://doi.org/10.1016/j.renene.2013.03.033

70. Kollár LP, Springer GS (2003) Mechanics of composite structures. Cambridge University Press. https://doi.org/10.1017/CBO9780511547140

71. Konieczna A, Rutkowska A, Rachon D (2015) Health risk of exposure to Bisphenol A (BPA). Roczniki Państwowego Zakładu Higieny 66(1)

72. Krimmer A (2014) Mikromechanische Modellierung von Fasergelege-Kunststoff-Verbunden auf Basis von Normprüfungen unter Berücksichtigung der in-situ-Eigenschaften der Matrix. Ph.D. thesis, Technische Universität Berlin. https://doi.org/10.14279/depositonce-3869

73. Krimmer A (2017) Ermüdungsbewertung von Faser-Kunststoff-Verbunden am Beispiel von Rotorblättern. Lightweight Des 10(4):28–33. https://doi.org/10.1007/s35725-017-0037-0

74. Krimmer A, Leifheit R, Bardenhagen A (2016) Assessment of quasi-static and fatigue performance of uni-directionally fibre reinforced polymers on the basis of matrix effort. In: 6th EASN international conference on innovation in European aeronautics research. Porto, Portugal. https://doi.org/10.5281/zenodo.3878156

75. Kumar S, Krishnan S (2020) Recycling of carbon fiber with epoxy composites by chemical recycling for future perspective: a review. Chem Pap 74:3785–3807. https://doi.org/10.1007/s11696-020-01198-y

76. Lindenburg C, de Winkel G (2005) Buckling load prediction tools for rotor blades. Tech. Rep. ECN-C–05-103, Energy research Centre of the Netherlands ECN Wind Energy, Patten, the Netherlands. https://publicaties.ecn.nl/PdfFetch.aspx?nr=ECN-C--05-103

77. Madsen P, Dekker J, Thor S, McAnulty K, Matthies H, Thresher R (1990) Recommended practices for wind turbine testing, 3. fatigue loads, 2. edition. Tech. rep., International Energy Agency Programme for Research and Development on Wind Energy Conversion Systems

78. Mandell JF, Ashwill TD, Wilson TJ, Sears AT, Agastra P, Laird DL, Samborsky DD (2010) Analysis of SNL/MSU/DOE fatigue database trends for wind turbine blade materials. Tech. Rep. SAND2010-7052, Sandia National Laboratories, Albuquerque, New Mexico, USA. https://doi.org/10.2172/1034894

79. Mandell JF, Miller D, Samborsky D (2013) Creep/fatigue behavior of resin infused biaxial glass fabric laminates. In: 54th AIAA/ASME/ASCE/AHS/ASC structures, structural dynamics, and materials conference. American Institute of Aeronautics and Astronautics, Boston, Massachusetts, USA. https://doi.org/10.2514/6.2013-1630

80. Mativenga PT, Shuaib NA, Howarth J, Pestalozzi F, Woidasky J (2016) High voltage fragmentation and mechanical recycling of glass fibre thermoset composite. CIRP Annals 65(1):45–48. https://doi.org/10.1016/j.cirp.2016.04.107

81. Melcher D, Rosemann H, Haller B, Neßlinger S, Petersen E, Rosemeier M (2020) Proof of concept: elliptical biaxial rotor blade fatigue test with resonant excitation. In: IOP conference series: materials science and engineering, vol 942. IOP Publishing, p 012007. https://doi.org/10.1088/1757-899x/942/1/012007

82. Miner MA (1945) Cumulative damage in fatigue. J Appl Mech 12(3):A159–A164. https://doi.org/10.1115/1.4009458

83. Movahedi-Rad AV, Keller T, Vassilopoulos AP (2018) Fatigue damage in angle-ply GFRP laminates under tension-tension fatigue. Int J Fatigue 109:60–69. https://doi.org/10.1016/j.ijfatigue.2017.12.015

84. MSC Software: Adams/AdWiMo—Advanced wind turbine modeling. https://hexagon.com/support-success/manufacturing-intelligence/design-engineering-support/toolkit-solutions

85. Murray RE, Swan D, Snowberg D, Berry D, Beach R, Rooney S (2017) Manufacturing a 9 m thermoplastic composite wind turbine blade. In: 32nd technical conference on proceedings of the american society for composites (ASC). https://doi.org/10.12783/asc2017/15166

86. National Renewable Energy Laboratory (NREL) (2021) CCBlade. https://github.com/WISDEM/CCBlade

87. National Renewable Energy Laboratory (NREL) (2021) OpenFAST. https://github.com/OpenFAST/openfast

88. Nickel A (2011) Optimierung der Designparameter von GFK-Kern-Verbunden unter Berücksichtigung der Harzaufnahme des Kerns. Diplomarbeit, Technische Universität Berlin

89. Ning SA (2014) A simple solution method for the blade element momentum equations with guaranteed convergence. Wind Energy 17(9):1327–1345. https://doi.org/10.1002/we.1636

90. Øye S, Flex

91. Palmgren A (1924) Die Lebensdauer von Kugellagern. Zeitschrift des Vereins Deutscher Ingenieure 68(14):339–341

92. Pech A, Kolbitsch A, Zach F (2008) Tragwerke. Springer, Wien, Österreich. https://doi.org/10.1007/978-3-211-33032-6

93. Peeters M, Santo G, Degroote J, Van Paepegem W (2018) Comparison of shell and solid finite element models for the static certification tests of a 43 m wind turbine blade. Energies 11(6):1346. https://doi.org/10.3390/en11061346

94. Peeters M, Santo G, Degroote J, Van Paepegem W (2018) High-fidelity finite element models of composite wind turbine blades with shell and solid elements. Compos Struct 200:521–531. https://doi.org/10.1016/j.compstruct.2018.05.091

95. Politecnico di Milano: Cp-Lambda. http://www.poliwind.polimi.it/

96. Popko W, Huhn ML, Robertson A, Jonkman J, Wendt F, Müller K, Kretschmer M, Vorpahl F, Hagen TR, Galinos C, Le Dreff JB, Gilbert P, Auriac B, Víllora FN, Schünemann P, Bayati I, Belloli M, Oh S, Totsuka Y, Qvist J, Bachynski E, Sørum SH, Thomassen PE, Shin H, Vittori F, Galván J, Molins C, Bonnet P, van der Zee T, Bergua R, Wang K, Fu P, Cai J (2018) Verification of a numerical model of the offshore wind turbine from the alpha ventus wind farm within OC5 phase III. In: 37th international conference on ocean, offshore and arctic engineering. American Society of Mechanical Engineers. https://doi.org/10.1115/OMAE2018-77589

97. Previtali F, Eyb E (2021) An improved approach for the fatigue calculation of rotor blades based on sector loads. Wind Eng. https://doi.org/10.1177/0309524X20985320

98. Puck A (1996) Festigkeitsanalyse von Faser-Matrix-Laminaten: Modelle für die Praxis. Hanser, Munich, Germany

99. Quaschning V (2021) Erneuerbare Energien und Klimaschutz: Hintergründe–Techniken und Planung–Ökonomie und Ökologie–Energiewende, 6 edn. Hanser, Munich, Germany. https://doi.org/10.3139/9783446468689

100. Rahmstorf S (2019) Wie viel CO2 kann Deutschland noch ausstoßen? https://scilogs.spektrum.de/klimalounge/wie-viel-co2-kann-Deutschland-noch-ausstossen/

101. Reddy JN (2003) Mechanics of laminated composite plates and shells: theory and analysis, 2 edn. CRC Press, Boca Raton, Florida, USA. https://doi.org/10.1201/b12409

102. Rinker J, Gaertner E, Zahle F, Skrzypiński W, Abbas N, Bredmose H, Barter G, Dykes K (2020) Comparison of loads from HAWC2 and OpenFAST for the IEA Wind 15 MW reference wind turbine. J Phys: Conf Ser 1618:052052. IOP Publishing. https://doi.org/10.1088/1742-6596/1618/5/052052

103. Rosemeier M (2013) Non-linear ultimate limit state analysis of a wind turbine blade. Master's thesis, Hochschule Bremerhaven, Munich, Germany. https://www.grin.com/document/211296

104. Rosemeier M, Antoniou A (2021) Probabilistic approach for the fatigue strength prediction of polymers. AIAA J 60(2):951–961. https://doi.org/10.2514/1.J060444

105. Rosemeier M, Bätge M (2014) A concept study of a carbon spar cap design for a 80m wind turbine blade. J Phys: Conf Ser 524:012039 (IOP Publishing). https://doi.org/10.1088/1742-6596/524/1/012039

106. Rosemeier M, Berring P, Branner K (2016) Non-linear ultimate strength and stability limit state analysis of a wind turbine blade. Wind Energy 19(5):825–846. https://doi.org/10.1002/we.1868

107. Rosemeier M, Buriticá P, Antoniou A (2018) Impact of resin uptake of core materials on buckling of wind turbine blades. J Phys: Conf Ser 1037:042001 (IOP Publishing). https://doi.org/10.1088/1742-6596/1037/4/042001

108. Rosemeier M, Krimmer A, Antoniou A (2020) Development of thermal residual stresses during manufacture of wind turbine blades. J Phys: Conf Ser 1452:012060 (IOP Publishing). https://doi.org/10.1088/1742-6596/1452/1/012060

109. Rosemeier M, Krimmer A, Bardenhagen A, Antoniou A (2019) Tunneling crack initiation in trailing-edge bond lines of wind-turbine blades. AIAA J 57(12):5462–5474. https://doi.org/10.2514/1.J058179

110. Rosemeier M, Saathoff M (2020) Assessment of a rotor blade extension retrofit as a supplement to the lifetime extension of wind turbines. Wind Energy Sci 5(3):897–909. https://doi.org/10.5194/wes-5-897-2020

111. Rosemeier M, Saathoff M (2020) Impact of manufacture-induced blade shape distortion on turbine loads and energy yield. https://doi.org/10.5281/zenodo.4058566

112. Saathoff M, Rosemeier M, Kleinselbeck T, Rathmann B (2021) Effect of individual blade pitch angle misalignment on the remaining useful life of wind turbines. Wind Energy Sci 6(5):1079–1087. https://doi.org/10.5194/wes-6-1079-2021

113. Schleich F, Stammler M (2019) Realitätsgetreue Abbildung von Rotorblattlagerbelastungen durch Berücksichtigung der Anschlusssteifigkeiten. In: VDI-Berichte 234813. VDI-Fachtagung Gleit- und Wälzlagerungen 2019. Gestaltung - Berechnung - Einsatz: Schweinfurt, vol 2348. Verein Deutscher Ingenieure, pp 209–220. https://doi.org/10.51202/9783181023488-209

114. Schlömer S, Bruckner T, Fulton L, Hertwich E, McKinnon A, Perczyk D, Roy J, Schaeffer R, Sims R, Smith P, Wiser R (2014) 2014: Annex III: technology-specific cost and performance parameters. In: Edenhofer O, Pichs-Madruga R, Sokona Y, Farahani E, Kadner S, Seyboth K, Adler A, Baum I, Brunner S, Eickemeier P, Kriemann B, Savolainen J, Schlömer S, von Stechow C, Zwickel T, Minx JC (eds) Climate change 2014: mitigation of climate change. Contribution of working group III to the fifth assessment report of the intergovernmental panel on climate change. Cambridge University Press. https://www.ipcc.ch/site/assets/uploads/2018/02/ipcc_wg3_ar5_annex-iii.pdf

115. Schümann JP (2019) Zur zeit-, temperatur- und umsatzabhängigen Entwicklung polymerphysikalischer Vernetzungsschwindung aminisch vernetzender Epoxide. Ph.D. thesis, Technische Universität Clausthal, Clausthal, Germany. https://doi.org/10.21268/20190306-0

116. Schürmann H (2007) Konstruieren mit Faser-Kunststoff-Verbunden, 2 edn. Springer. https://doi.org/10.1007/978-3-540-72190-1

117. Skjoldan PF (2011) Aeroelastic modal dynamics of wind turbines including anisotropic effects. Ph.D. thesis, Danmarks Tekniske Universitet, Risø Nationallaboratoriet for Bæredygtig Energi. https://backend.orbit.dtu.dk/ws/portalfiles/portal/5509069/ris-phd-66.pdf

118. Sommer V, Stockschläder J, Walther G (2020) Estimation of glass and carbon fiber reinforced plastic waste from end-of-life rotor blades of wind power plants within the European union. Waste Manag 115:83–94. https://doi.org/10.1016/j.wasman.2020.06.043

119. Sommer V, Walther G (2021) Recycling and recovery infrastructures for glass and carbon fiber reinforced plastic waste from wind energy industry: a European case study. Waste Manag 121:265–275. https://doi.org/10.1016/j.wasman.2020.12.021

120. Stiesdal H, Enevoldsen PB, Johansen K, Kristensen JJ, Noertem M, Winther-Jensen M (2001) Verfahren zur Herstellung von Windmühlenflügeln. https://worldwide.espacenet.com/patent/search/family/026069092/publication/DE60210729T2?q=pn%3DDE60210729T

121. Suresh S (2003) Fatigue of materials, 2 edn. Cambridge University Press, Cambridge, UK. https://doi.org/10.1017/CBO9780511806575

122. Sutherland H, Mandell J (2005) Optimized goodman diagram for the analysis of fiberglass composites used in wind turbine blades. In: 43rd AIAA aerospace sciences meeting and exhibit. American Institute of Aeronautics and Astronautics. https://doi.org/10.2514/6.2005-196

123. Tareq MS, Jony B, Zainuddin S, Al Ahsan M, Hosur MV (2021) Fatigue analysis and fracture toughness of graphene reinforced carbon fibre polymer composites. Fatigue Fract Eng Mater Struct 44(2):461–474. https://doi.org/10.1111/ffe.13371

124. Technische Universität Berlin - Institut für Strömungsmechanik und Technische Akustik - Fachgebiet Experimentelle Strömungsmechanik: Qblade (2016). http://www.q-blade.org

125. Technische Universität Darmstadt - Fachgebiet Konstruktiver Leichtbau und Bauweisen (KLuB): Alfalam (2009)

126. The Economist—The Americas: a worrying windfall—The wind-power boom set off a scramble for balsa wood in Ecuador (2020). https://www.economist.com/the-americas/2021/01/30/the-wind-power-boom-set-off-a-scramble-for-balsa-wood-in-ecuador

127. Thomason JL (2019) Glass fibre sizing: a review. Compos Part A: Appl Sci Manuf 127:105619. https://doi.org/10.1016/j.compositesa.2019.105619

128. Thomson C, Harrison G (2015) Life cycle costs and carbon emissions of wind power: executive summary. Tech. rep., University of Edinburgh, Edinburgh, Scotland. https://www.climatexchange.org.uk/media/1459/life_cycle_wind_-_executive_summary_.pdf

129. Timoshenko SP (1921) LXVI. On the correction for shear of the differential equation for transverse vibrations of prismatic bars. London Edinburgh Dublin Philos Mag J Sci 41(245):744–746. https://doi.org/10.1080/14786442108636264

130. TPI Composites (2019) TPI composites blade manufacturing process. https://youtu.be/jpRudTUIyfM

131. UNO (1987) Report of the world commission on environment and development: our common future. Organisation der Vereinten Nationen. https://www.are.admin.ch/dam/are/de/dokumente/nachhaltige_entwicklung/dokumente/bericht/our_common_futurebrundtlandreport1987.pdf.download.pdf

132. UNO (2015) TREATIES-XXVII.7.d Paris agreement. Organisation der Vereinten Nationen. https://treaties.un.org/doc/Treaties/2016/02/20160215%2006-03%20PM/Ch_XXVII-7-d.pdf

133. Varik MV (2013) FINSTRIP: theoretical reference. Knowledge Centre WMC

134. VDI (2003) VDI 2230 Part 1—Systematic calculation of high duty bolted joints Joints with one cylindrical bolt. Verein Deutscher Ingenieure, Düsseldorf, Germany

135. VDI (2006) VDI 2014 Part 3 development of FRP components (fibre-reinforced plastics) analysis. Verein Deutscher Ingenieure, Düsseldorf, Germany

136. Vincent GA, de Bruijn TA, Wijskamp S, Rasheed MIA, van Drongelen M, Akkerman R (2019) Shredding and sieving thermoplastic composite scrap: method development and analyses of the fibre length distributions. Compos Part B: Eng 176:107197. https://doi.org/10.1016/j.compositesb.2019.107197

137. Wang Q, Sprague MA, Jonkman JM (2014) Nonlinear Legendre spectral finite elements for wind turbine blade dynamics. In: 32nd ASME wind energy symposium, p. 1224. American Institute of Aeronautics and Astronautics, National Harbor, Maryland, USA. https://doi.org/10.2514/6.2014-1224

138. Wang Q, Sprague MA, Jonkman JM (2016) Partitioned nonlinear structural analysis of wind turbines using Beamdyn. In: 34th wind energy symposium. American Institute of Aeronautics and Astronautics, San Diego, Kalifornien, USA, p 0753. https://doi.org/10.2514/6.2016-0753

139. Wang Q, Yu W (2017) Geometrically nonlinear analysis of composite beams using wiener-milenković parameters. J Renew Sustain Energy 9(3):033306. https://doi.org/10.1063/1.4985091

140. Wang S, Zhang C (2014) Structure mechanical modeling of thin-walled closed-section composite beams, part 2: multi-cell cross section. Compos Struct 113:56–62. https://doi.org/10.1016/j.compstruct.2014.03.002

141. Wiedemann J (2007) Leichtbau: Elemente und Konstruktion, 3 edn. Springer, Berlin, Heidelberg, New York. https://doi.org/10.1007/978-3-540-33657-0
142. Wikipedia (2021) Die freie Enzyklopädie: Nachhaltigkeit. https://de.wikipedia.org/wiki/Nachhaltigkeit
143. Wittel H, Jannasch D, Voßiek J, Spura C (2019) Roloff/Matek Maschinenelemente, 24 edn. Springer Viewer. https://doi.org/10.1007/978-3-658-26280-8
144. Wlassow WS (1959) Dünnwandige elastische Stäbe, vol 1, 2 edn. Staatsverlag für physikalisch-mathematische Literatur, Moscow, Soviet Union
145. WMC Technology Center Netherlands: FOCUS6
146. Zangenberg J, Brøndsted P, Gillespie Jr JW (2014) Fatigue damage propagation in unidirectional glass fibre reinforced composites made of a non-crimp fabric. J Compos Mater 48(22):2711–2727. https://doi.org/10.1177/0021998313502062
147. Zhang C, Wang S (2014) Structure mechanical modeling of thin-walled closed-section composite beams, part 1: single-cell cross section. Compos Struct 113:12–22. https://doi.org/10.1016/j.compstruct.2014.03.005

M.Sc. Malo Rosemeier has been working as a research assistant at the Fraunhofer Institute for Wind Energy Systems IWES since 2013. In the Rotor Blades department, he is responsible for applied research on blade structures. The focus is on the development of validation tests and structural analysis methods, among other things.

Dr. Alexander Krimmer works as Senior Engineer Composite Materials and Structures at TPI Composites Germany GmbH. There he is responsible for qualification, specification, evaluation and preparation for certification of structural materials for wind turbine rotor blades. In addition, he teaches at the Department of Aircraft Construction and Lightweight Design at the Institute of Aeronautics and Astronautics at the TU Berlin in the modules of fibre composite lightweight construction as well as production and design of fibre-reinforced plastic composites.

The Drivetrain

Hans Kyling, Sönke Siegfriedsen, and Peter Krämer

1 Introduction

The systems referred to as wind turbine generators (WTG) or simply wind turbines in this chapter serve to convert the kinetic energy of the wind into electrical energy. They are driven by a rotor which acts as a repeller to extract kinetic energy from the wind. As is the case with any conventional power plant, this mechanical energy or power is made up of a rotary motion with rotational frequency ω, rotational speed n and the force of this motion, the torque M.

$$P_{\text{Mech}} = M \cdot \omega = M \cdot 2 \cdot \pi \cdot n$$

The basic structure of a wind turbine is as follows: The rotor blades are driven by the wind and the resulting torque causes the rotor hub to rotate. The rotor hub is connected to the rotor shaft. The rotor shaft and a suitable mount separate the torque desired from the so-called parasitic loads (bending moments, lateral forces and thrust). The parasitic loads are transferred from the rotor bearing assembly via the main frame and a yaw bearing into the tower. The torque is converted either directly (gearless wind turbine) or in a downstream gearbox into a faster motion with reduced torque, and then converted into electric power by means of a generator. The discussion in this chapter follows the load flow and starts at the blade angle adjustment, better known as blade pitch systems, and ends at the yaw bearing in the

H. Kyling (✉)
Fraunhofer Institute for Wind Energy Systems IWES, Am Seedeich 45, 27572 Bremerhaven, Germany
e-mail: hans.kyling@iwes.fraunhofer.de

S. Siegfriedsen
aerodyn engineering GmbH, Hollerstraße 122, 24782 Büdelsdorf, Germany

P. Krämer
AEROVIDE GmbH, Provianthausstraße 9, 24768 Rendsburg, Germany

case of parasitic loads and at the generator in the case of the torque. The nacelle accommodates the drivetrain components required for the energy conversion.

The diverse technical (e.g. onshore and offshore site) and market demands placed on a wind turbine and the possibility of using various component arrangements and versions mean that a large variety of drivetrain concepts exist. The concept selected has a significant impact on the so-called tower head mass (sum of the masses of rotor and nacelle) and also on the costs (approx. 30% of the total costs) of a wind turbine, and also a direct impact on the development via the dimensioning of components. Depending on the concept chosen, it is possible to use more or less standard mechanical components in a drivetrain. Many of the components in the drivetrain of a wind turbine are subjected to large alternating loads which have to be taken into account when dimensioning the components.

As already described in earlier chapters, it is possible in principle to use different types of rotor to generate the torque, but at this point we would like to stress that only horizontal axis wind turbines are considered here.

2   Blade Pitch Systems

In wind turbines with a horizontal rotor axis, especially those in the multi-megawatt class, rotor blade adjustment according to the pitch principle has been used for decades for power control. Compared to the situation in the past, when it was normal for the rotor blades to be fix-mounted and the power was restricted with the aid of the stall effect, the technically more complex pitch system offers various advantages whose effect overall is cost reduction with increasing turbine dimensions. In addition to turbine operation adapted to different wind conditions by means of power and speed control which are both optimised to generator type and grid code, it is also possible to use suitable control algorithms to keep any load peaks which occur, particularly in extreme wind situations, at a much lower level. This in turn has an impact on the dimensioning of various cost-relevant components such as rotor bearing assembly, main gearbox, tower and foundation structures.

In grid operation, the pitch angle is varied between 0° and around 30° for power control (Fig. 1, left). Furthermore, the slow idling of the drivetrain when decoupled from the grid, which is favourable for the mount and the lubrication, can be effected by a pitch angle of around 70° (Fig. 1, right). In addition, it is possible to stop the rotor including the drivetrain within seconds by adjusting the pitch angle to around 90° into the so-called feathering or feathered position (aerodynamic brake).

The section below deals exclusively with the fundamental design of the pitch system to adjust the whole rotor blade about its pitch axis and the different technical designs of the drive required. Neither the design of the pitch system nor its operation and control is considered in more detail.

Every pitch system regardless of the design and type of the drive requires the rotor blade to be connected to the rotor hub by means of a rotating bearing. The blade bearing used here is usually a double-row four-point contact ball bearing (Fig. 2,
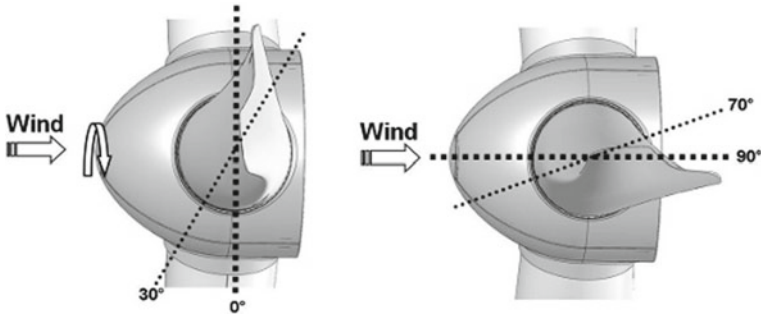
Fig. 1 Pitch angle between 0° and 30° for grid operation, 70° for grid-decoupled idling and 90° as feathered position for complete stop [aerodyn]
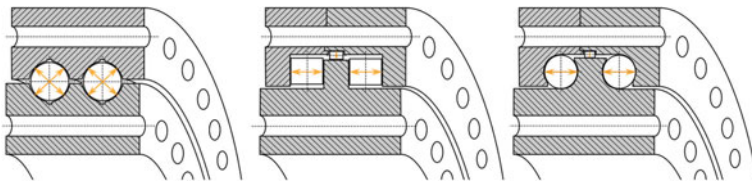
Fig. 2 Double-row four-point contact ball bearing (left), triple-row roller bearing (centre) and T-Solid® (right) [Stammler]

left), whose design allows it to transfer the radial, as well as the large axial and bending load components which are introduced. Bearing designs comprising triple-row roller slewing rings (Fig. 2, centre) as well as a combined version in the form of the T-Solid® bearing from IMO (Fig. 2, right) are also commercially available [1]. Whether the inner or outer ring is fixed to the rotor hub, while the other one in each case can rotate and hold the rotor blade depends, amongst other things, on the preferred design and positioning of the drive (Fig. 5). More important for the decision, however, is the size of the blade connection which is chosen, and the market has already established specific sizes for rotor blades to match the turbine size (power class) and wind conditions (wind class). This makes it possible to use rotor blades from different manufacturers without changing the dimensions of the connection. The loads determine the design specification with the requisite bearing raceway diameter and a cast rotor hub which is as light as possible.

Three concepts for triple-bladed and double-bladed rotors have developed over time one after the other for the adjustment or specific setting of a pitch angle.

In the simplest concept, an actuator synchronised via a mechanical linkage adjusts all blades simultaneously. To be able to stop the rotor when this actuator fails, this concept requires a separate, mechanical rotor brake which brings the drivetrain to a halt from the maximum speed against the maximum rotor torque. The loads acting in the drivetrain in this situation and the sudden large peak in dissipated heat at

the brake would mean that turbines of the multi-megawatt class needed components whose dimensions made them economically unviable.

A concept has thus become established whereby each rotor blade is equipped with its own actuator including all the system components required for the one-time movement of the blade into the feathering position. In power-regulated grid operation, all rotor blades are set to the same pitch angle, synchronised solely via the control. Should one actuator fail, the remaining actuators can independently bring the rotor blades connected to them into the feathering position. The load on the turbine and the mechanical rotor brake can thus be sufficiently restricted and economically viable dimensioning achieved. Even without the mechanical brake coming into play, the rotor speed can be kept below a critical value in every conceivable case.

For some years now, efforts have been underway to develop this concept further. The wind conditions across the swept area formed by the rotating rotor are not homogeneous. As turbine sizes and rotor diameters increase, the difference in wind speeds and turbulences within the swept area is becoming ever larger. This means that each rotor blade on the rotor experiences a different load at a specific point in time. The idea is now simple: The pitch angle of each rotor blade is individually controlled (Individual Pitch Control—IPC) such that the load on each rotor blade is the same regardless of position, and overall, the rotor is kept at rated power or maximum partial power. Important challenges lie on the one hand in the reliable measurement of the loads in the long term as well, and in the development of control algorithms which allow sufficiently rapid pitch angle adjustment on the other. In particular, the rapid rotation of the rotor blade over its whole length, which can amount to around 110 m nowadays, without any appreciable twisting, and the resulting shortfall in the aerodynamic effect accompanied by the simultaneous introduction of parasitic oscillations makes the design of the structure, drive and control very difficult. Moreover, there is no straightforward answer to the question as to whether the gain in service life through the prospect of load reduction on the rotor blades and a potential increase in the energy yield of the wind turbine justifies the disadvantages arising from the continuous necessity to adjust the pitch angle (pitch bearing and pitch systems).

Systems with only one actuator primarily have one hydraulic cylinder arranged in the stationary nacelle. The stroke of the piston is transferred via a rod through the hollow shaft of the rotor and gearbox, if applicable, into the rotating rotor hub, where it is converted into the same pivotal movement via coupling rods on all connected rotor blades.

The systems used in today's multi-megawatt turbines can be divided into those with electric and those with hydraulic actuators (Fig. 3). The transmission of the supply power and the signals between the stationary nacelle and the rotating rotor hub is carried out via a slipring unit alone or a slipring unit combined with a hydraulic rotary feedthrough (Fig. 4). Depending on the design of the drivetrain, this interface is located at the front or rear end of the hollow rotor shaft or the free end of the gearbox input shaft.

To ensure that the above-mentioned aerodynamic brake works and can safely bring the turbine to a halt should this non-redundant interface fail, the pitch system
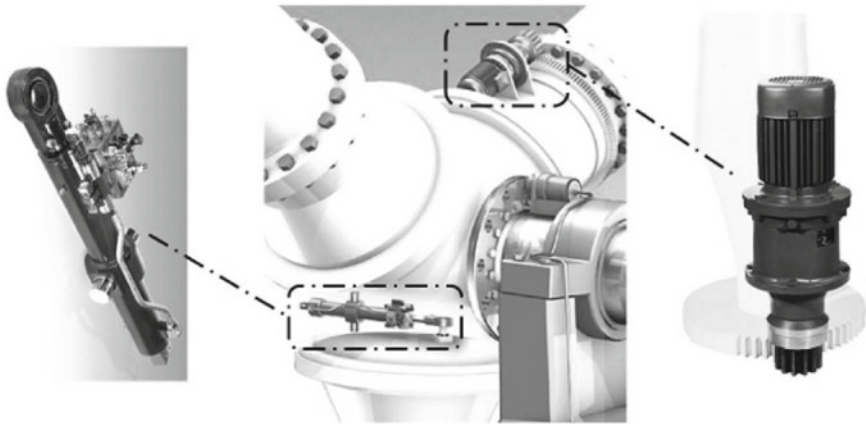
Fig. 3 Pitch system with hydraulic (left) or electric (right) actuators [Bosch Rexroth]
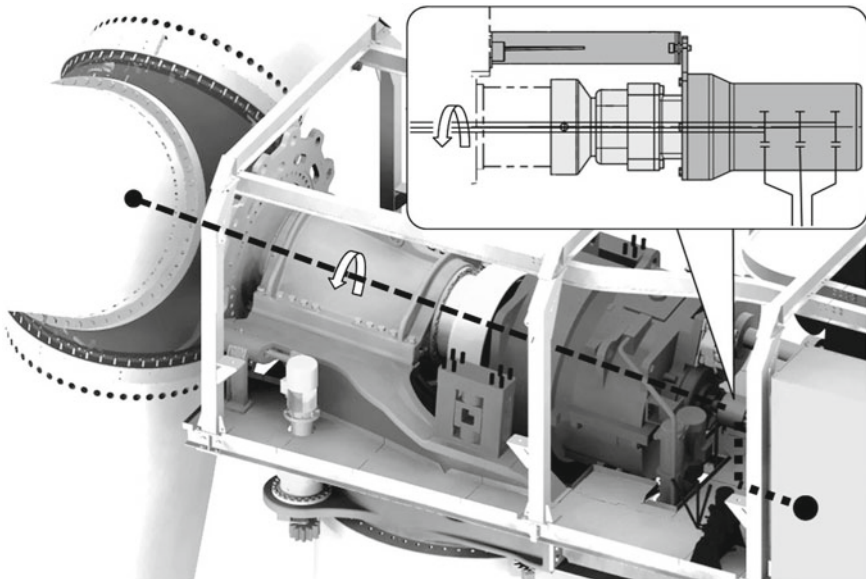
Fig. 4 Transfer of supply power and communication between stationary nacelle and turning rotor [aerodyn]

must safeguard the availability of the complete system necessary for at least a full pivotal movement of 90° in the rotor hub. This accommodates not only the control system for the actuator but also suitable energy storage devices. An energy storage device is also necessary to be able to stop the turbine in the event of a grid failure.

The energy storage systems used for electric systems are electro-chemical lead-gel batteries, and more recent concepts are increasingly using ultra-capacitors too.
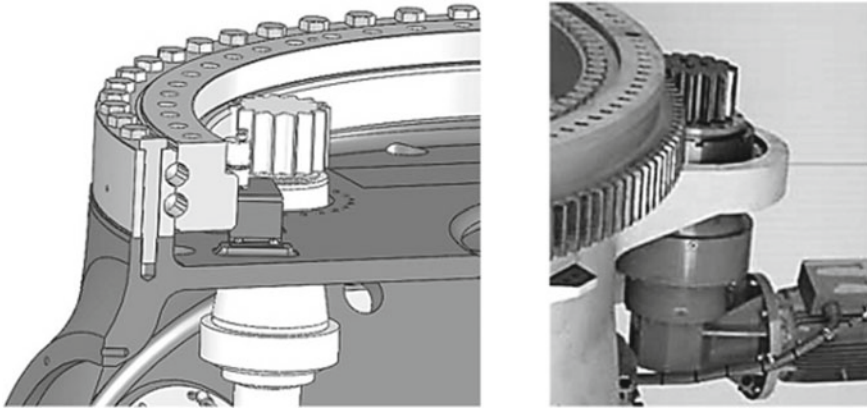
Fig. 5 Motor-gear combination connected to rotor hub turns inner ring of the blade bearing [aerodyn]

These are comparable with bladder accumulators or piston accumulators as far as their properties are concerned:

- Charge capacity guarantees full pivotal movement,
- Fast charging and operational readiness,
- Adequate service life even when frequently discharged.

In their most common basic design, electric systems comprise a motor-gearbox combination with a 3- to 5-stage planetary gearbox (Fig. 5).

The gear pinion on the output side either engages directly with the teeth on the inner or outer ring of the blade bearing (Fig. 6) or is coupled to it via a toothed drive belt. This drive is usually fix-mounted onto the rotor hub and turns the blade bearing ring connected to the rotor blade.

In some designs, the drive is fixed to the rotary blade bearing ring and runs along the toothed, stationary blade bearing ring. The disadvantage of this arrangement is that mounting, maintenance and power supply are more complex, but it also has the advantage that, in conjunction with the base plate required for the drive, it can significantly increase the stiffness against so-called ovalisation (a load-based deformation of the structure from a circle into an oval) in the blade connection region. With this arrangement and the arrangement with outside drives, the inner ring of the bearing is bolted to the hub, thus facilitating smaller and lighter hub designs.

The hydraulic systems usually contain double-acting cylinders, which are articulated to the rotor hub and the rotary blade bearing ring. The piston stroke is converted into a pivotal movement of the blade bearing ring with connected rotor blade. The stroke necessary for a 90° pivotal movement requires an overall cylinder length which cannot be accommodated within the boundaries of the rotor blade connection when a single cylinder is used. In most known designs, the cylinder therefore protrudes from the front of the rotor hub.
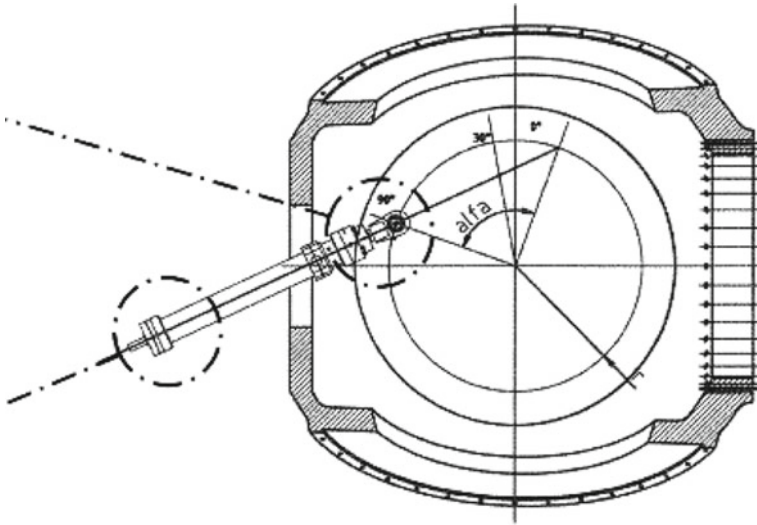
Fig. 6 Arrangement of a single cylinder in hydraulic pitch systems

In an alternative design, the pivotal movement is executed via two small cylinders which are arranged in series, via an intermediate pivoted lever, or two small cylinders are used which are operated in parallel on opposite sides. This arrangement can be accommodated wholly within the blade connection diameter (Fig. 7).

A common feature of all hydraulic designs is that the basic supply needed to operate the cylinders must be provided by hydraulic power units in the stationary nacelle and thus via a hydraulic rotary union. The technically tried and tested power units with reservoir are not suitable to be accommodated in the rotating rotor hub.

An innovative step could be the electro-hydrostatic actuator (EHA), a hybrid drive which combines an electric servomotor with a hydraulic gear and control valve system and which has been used in aviation engineering for two decades. To the outside, the actuator has only electric interfaces; the hydraulics are completely integrated so as to be autonomous.

The perfect concept for a pitch system...

... does not exist. The question as to whether to use electric or hydraulic actuators, chemical or static energy storage devices, or blade bearings with teeth on the inner or the outer rings, for example, must always be answered anew and individually to suit the overall concept of a WTG. For the operator of a wind turbine, what ultimately counts is the return on their investment.

At installation sites with very frequent grid fluctuations and failures, considerable strain is put on the energy storage devices. In such cases, static storage methods such as ultra-capacitors or pressurised oil accumulators have technical advantages over electro-chemical lead-gel batteries. Since ultra-capacitors are only now becoming
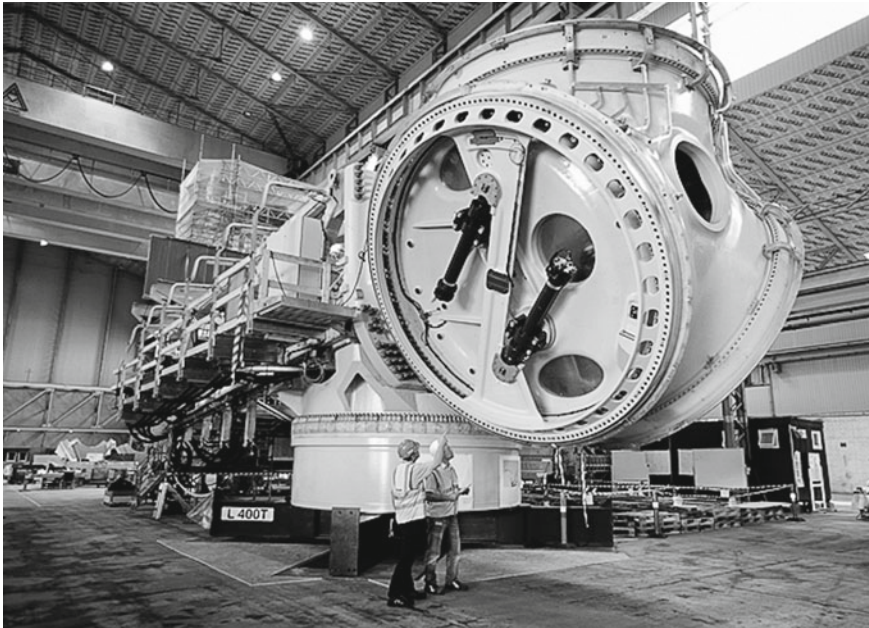
Fig. 7 Two pitch cylinders on the MHI Vestas V164 [MHI Vestas]

attractive in electrical systems, turbines in such regions have usually had hydraulic systems.

At installation sites which frequently experience very low ambient temperatures, it is much easier to use a purely electric system to supply the heating needed by the system components. Oil pipes, valves and pressurised oil accumulators, in particular, are very problematic here.

At installation sites which frequently experience very high ambient temperatures, it is simpler to cool hydraulic systems by means of recirculating oil cooling in the stationary nacelle. At present, the only way to cool converters and motors of electrical systems in the rotating rotor hub is with ambient air ventilation.

Depending on the design, this type of cooling can be much more complex to realise when the goal is to seal the interior of the rotor hub against contaminated ambient air (offshore, desert, steppe, etc.). For an alternative fluid cooling circuit, the same conditions as for the supply of a hydraulic pitch system have to be taken into account.

3 Rotor Hub

The rotor hub connects the rotor blades to the rotor shaft. In the early years of industrial wind power and for smaller turbines as well, rotor hubs were also designed

as welded structures. For WTGs in the multi-megawatt range, only cast hubs have been used for decades because this production method imposes far fewer restrictions as far as the shape is concerned, and the material can be used more efficiently or the stress on the component can be made more uniform. The rotor hub must be very rigid close to the blade bearing connections to minimise load-induced ovalisation of the bearings when the turbine is in operation. The loads emanating from the rotor blades must be deflected within a very constrained space and transferred in their entirety into the rotor shaft. The region connected to the rotor shaft must be adapted to suit the local stiffness. The design must also take account of additional asymmetric loads and further connections for the pitch systems, manholes, etc. The hub can execute around 100 million revolutions over the lifetime of the turbine. The fatigue strength thus required places further demands on the design of the rotor hub. The key design criterion for the components of a WTG is the resulting costs. Casting can provide the most efficient compromise given the large number of requirements which have to be met. The casting materials used can create additional site-specific challenges such as sufficient resistance to brittle fracture at low temperatures, however. Weight savings at the rotor hub have a very positive impact on the mass of the tower head. Figure 7 shows a modern rotor hub.

4 Drivetrain Components

The following section describes the classical components of a drivetrain. They are considered independently of different drivetrain concepts.

4.1 Rotor Locks and Rotor Turning Devices

The rotor lock has no direct function when a WTG is operating and is only used when maintenance or repairs to the drivetrain are being carried out. The turbine must first be stopped before work can be undertaken on the rotating components. The rotor can be stopped by means of an aerodynamic braking process (see Sect. 2) on the one hand or a mechanical brake on the other (see Sect. 4.5). The latter is designed more for emergencies and as a holding brake, however.

Service staff needs to be protected from any rotary motion of the drivetrain when carrying out maintenance work on the drivetrain or the hub of the rotor. Even with the mechanical brake, its operating principle (frictional contact) means slight slippage cannot be excluded, and the rotor blades can generate torque even in the "feathered position"; hence the so-called rotor lock is integrated into the drivetrain. It establishes a positive mechanical engagement between a rotating component and a non-rotating component, usually the main frame. The simplest principle, which is frequently used in practice, provides for a hydraulic or electric bolt to be inserted into a perforated

disc which is integrated into the drivetrain. With smaller turbines, the bolt is often inserted directly by hand or with the aid of a thread.

The perforated disc is often located in the direct vicinity of the rotor hub. This arrangement maximises the number of fixed components and has the advantage that it is possible to safely replace a suitably mounted gearbox in an emergency. In this case, however, the rotor subjects the device to extreme loads and the device must therefore be dimensioned accordingly.

In addition to the locking device directly on the rotor, consideration is also being given to performing the locking downstream of the transmission gearing. One example here is engagement by means of a toothed brake disc in combination with a rotor turning device located there. This has the advantage that the torque-induced loads would be correspondingly reduced by the transmission ratio. However, one must also be aware that all loads also act on the gearbox. Moreover, locking would no longer be possible if the gearbox failed.

Since it is difficult to manually rotate the rotor to the locking position via a braking manoeuvre with a defined stop, and manual rotation (only possible with turbines in lower level power classes with transmission gears) harbours the risk of injury, a method of adjusting the angle of rotation, a rotor turning device or a turning drive should be incorporated. Various approaches can be adopted to realise such a drive. Apart from additional drives which engage in the above-mentioned toothed brake disc by means of a pinion (Fig. 8), solutions which are integrated into the gearbox can be procured from suppliers, or hydraulic linear actuators can be used. Using the generator as a motor, or automatic braking with a defined stop with the aid of the aerodynamic and mechanical brake are also done in practice.
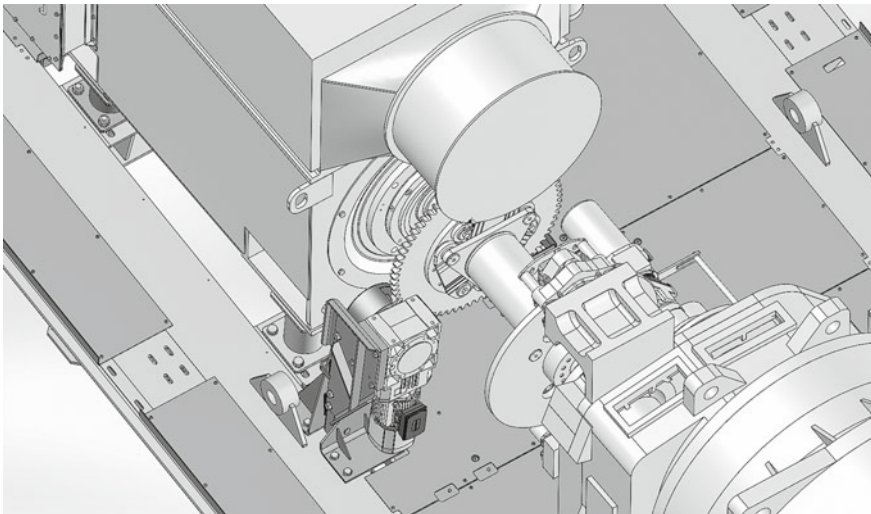
Fig. 8 Drivetrain with rotor turning device [aerodyn]

Rotor turning devices are not used solely to adjust the angle of rotation when locking the rotor, but also when mounting individual blades. The large static loads resulting from the eccentricity of the centre of gravity of the rotor mean that the devices here have a much more robust design and are usually used as mobile units only for the assembly.

4.2 Rotor Shaft

The rotor shaft and its mounting serve to connect the rotating rotor with the rest of the drivetrain, and also the stationary main frame of the wind turbine, also called the nacelle baseplate. The rotor shaft transfers the torque generated to the downstream drivetrain. It is also called the main shaft, since many drivetrain concepts additionally have a smaller, faster rotating shaft to connect the gearbox output to the generator input.

The structural dimensions of the rotor shaft depend primarily on the rotor mounting chosen as part of the drivetrain concept. This mounting can take the form of an elongated component like a conventional shaft (see Fig. 11) through to a short shaft stub (see Fig. 15). In the hub, the pipes and cables to supply the operating media (e.g. voltage, measurement signals, hydraulics) are laid through the shaft. The demands placed on a rotor shaft are similar to those listed in Sect. 3 Rotor Hub. Both forged as well as cast rotor shafts are available nowadays. The forged materials used are stronger, and so the shafts can be constructed with smaller diameters. This in turn means that smaller bearings can be used. Hence the shaft–bearing system generally has a cost advantage despite the higher specific costs of a forged shaft. The advantages of cast rotor shafts are that they require less mechanical finishing, allow a relatively unconstrained design (can be designed as distinctly hollow shafts) and are therefore lighter and less expensive than a forged shaft. The economical aspect of the two competing types of shaft is governed mainly by the quantities to be produced. The lower material strength of the materials used for casting nowadays means that cast shafts have to have larger diameters by comparison. Higher strength materials for casting such as EN-GJS-600 in combination with the so-called chill-casting method will be able to remedy this in the future and demonstrate a potential for use in light-weight construction (Fig. 9). In general, we need to further improve our knowledge of materials and components and to transfer this knowledge into the relevant guidelines and standards in order to exhaust the technical potential [1–3].

Further challenges lie in so-called bearing creep (creeping of the bearing ring in the circumferential direction for shaft–hub connections subjected to high bending loads) and, for cast shafts, in the risk of brittle fracture and the associated fracture mechanical strength verification (Fig. 10).

A bolted joint is typically used to connect the rotor shaft to the hub, sometimes designed with several rows. Achieving the pre-stress specified is a challenge which is sometimes underestimated, as is the case with many other aspects of wind energy, and requires detailed knowledge of the mating of bolt and nut and the methods and

Fig. 9 Experimental setup at Fraunhofer IWES to investigate the fatigue strength of a cast shaft [Fraunhofer IWES]

Fig. 10 Traces of bearing creep on contact surface to the bearing seat of a main bearing inner ring [Fraunhofer IWES]

tools used for tightening. The rotor shaft is connected to the gearbox or the generator either via a bolted joint or a shrink-fit disc joint.

4.3   Rotor Bearing Assembly

The rotor loads are transferred via the rotor bearing assembly, the connection between rotating and stationary components of the drivetrain, into the main frame of the nacelle. When selecting a suitable solution, an important criterion is thus an efficient load path. The degree of compactness is also a decisive factor for the structural design, however, and depends on the philosophy of the developer. The mounting concept selected has an impact on the overall length of the drivetrain and thus on the length of the nacelle. In addition, the main frame is essentially determined by the mounting concept. These aspects have a direct impact on the tower head mass and the associated costs.

The rotor bearings, also called main bearings, are machine parts which are subjected to high loads. To increase the service life of these bearings and facilitate low-friction and low-wear operation, a central lubrication system is usually provided for the rotor bearings, and also for the blade bearings, the yaw bearing and the bearings in the generator. The type of lubrication depends on the mounting concept and the sealing system used. When the rotor bearing assembly is integrated into the gearbox, it often shares the oil lubrication of the gearbox, whereas grease lubrication is usually used when the bearings of the rotor bearing assembly are located in separate housings. Nowadays, automatic grease lubrication pumps are used, which supply the bearing with fresh lubricating grease at fixed intervals. The old grease is then pushed through the seal, often a labyrinth seal, and out of the bearing and collected in a waste container. Oil lubrication in the compact design described is always designed as a loop. The sealing system of the bearing is more complex, however. In addition to an oil tank and an oil filter, there is also a cooler, which can cool the hot oil if necessary.

Two-Point Mount

The designation two-point mount, or two-point bearing assembly, stands for a concept in which two rolling bearings are arranged on the rotor shaft. These transfer all rotor loads via the main frame into the tower. Downstream of the rotor shaft, the torque needed to convert the energy acts on the next drivetrain component. Depending on the drivetrain concept, this component can be a gearbox (see Fig. 11) or a generator. In the case of a shaft with two-point mount, the gearbox or the generator (with gearless turbines) is in the first approximation loaded not by forces or bending moments from the rotor but only with the torque. This also applies to the moment bearing solution described below. It is possible to replace the gearbox on the turbine without removing the rotor, which is normally not possible with the three-point mount. With a two-point mount or a moment bearing as well, constraining forces can be generated which are introduced by the mounting of the torque supports in the event of deformations or misalignment. These forces can be minimised by special elastomer mounts on the torque supports of the gearboxes.

The fact that there are two bearings which are separate from each other means that the rotor shaft in this solution is very long and thus heavy. In many developments,
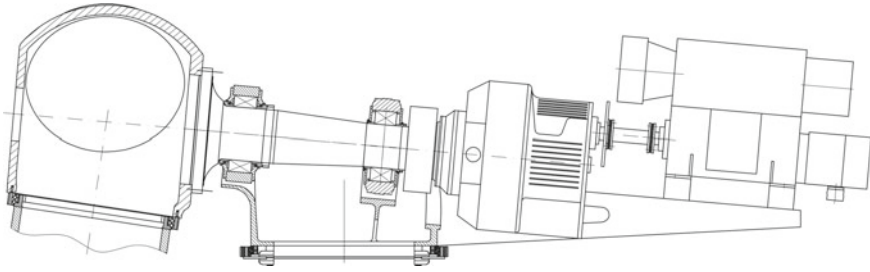
Fig. 11 Rotor shaft with two individual bearings [aerodyn]

the shaft is designed as a forged shaft because of the strength advantages. The rotor shafts have a large bore in the centre for the power supply lines of the pitch system. Cast hollow shafts are also used for large turbines.

With this mounting version, a distinction is made between a two-point mount with separate housing (Fig. 11) and a two-point mount with a shared housing (Fig. 12). The latter solution is much more compact. With two individual bearing housings, a self-aligning bearing (Fig. 13, right) in combination with a cylindrical rolling bearing is normally used so as to be able to compensate the misalignment of the housings with respect to each other and the deformations of the shaft without any reaction. The same type of bearing is also used in the three-point mount described below. For a two-point shaft mounting and a one-piece housing, an adjusted tapered roller bearing is usually used.

Mounting the rotor on a protruding shaft journal can be considered as a kind of special solution of the two-point mount. The two bearings are arranged directly on the journal in the hub and transfer the loads directly from the rotor into the shaft journal of the main frame (Fig. 15). In this solution, the sole task of the rotor shaft is to transfer the torques to the gearbox or the generator.
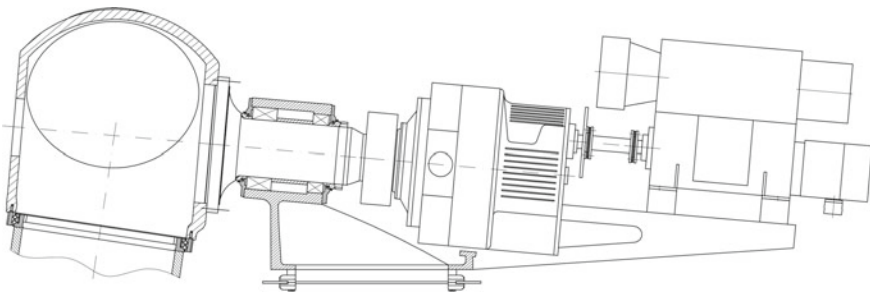
Fig. 12 Bearing assembly in a closed housing [aerodyn]
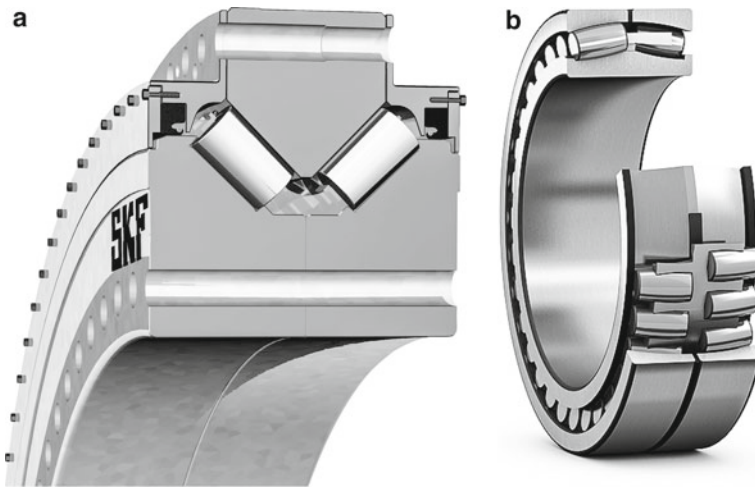
Fig. 13 Types of bearings: Double-row tapered roller bearing Nautilus Plus (left), self-aligning rolling bearing (right) [SKF]

Three-Point Mount

With a three-point mount, also called a three-point bearing assembly, the rear rotor shaft bearing is integrated into the gearbox when viewed from the hub (Fig. 14). The mounting concept is characterised by the fact that there is no rear bearing housing and the shaft is much shorter. The three-point mount derives its name from the connection points to the main frame. In addition to the front rotor shaft bearing, which is arranged directly at the main frame, the lateral gearbox supports are included as well. The complete assembly is thus highly compact but the components are easily accessible nevertheless. A further advantage with the three-point mount is that the three points make the system statically determinate to the outside and thus no unforeseeable additional constraining forces can be generated, as can arise with the two-point mount. This solution has disadvantages as well, however: Apart from the load acting on the gearbox, replacing a damaged gearbox is a much more complex operation. The three-point mount is nevertheless a widely known concept which is frequently used.

Moment Bearing

This concept uses a so-called moment bearing, usually a double-row tapered roller bearing nowadays (Fig. 13, left), as the sole mounting of the rotor shaft. In addition to the acting forces, the bearing must primarily absorb the pitching and yawing moments of the rotor. This characteristic gave this type of bearing its name. It is currently the most compact bearing design, primarily due to its very short rotor shaft. In addition, this concept is suitable for integrating further functions in the drivetrain assembly (see Sect. 5.4).
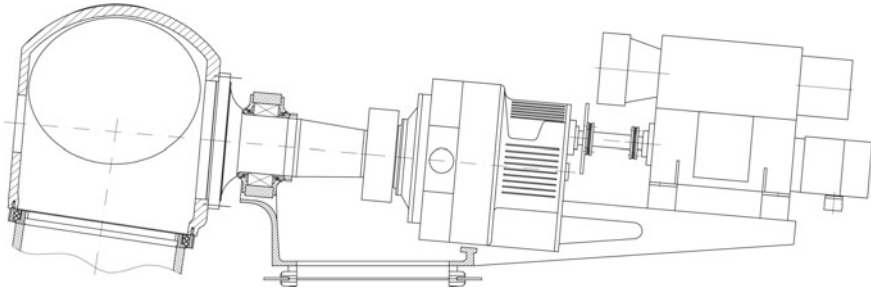
Fig. 14 Drivetrain with three-point mount [aerodyn]
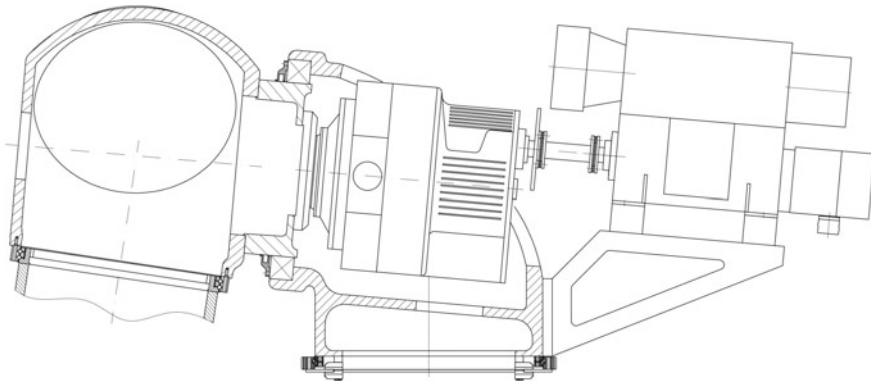
Fig. 15 Drivetrain concept with moment bearing [aerodyn]

A solution which uses moment bearings places high demands on the main frame. This basic structure, which is nowadays generally constructed as a cast body, must be designed to enclose the bearing so as to be able to conduct the large loads into the tower. The concept also provides for a mounting concept without a rotor shaft, where the inner ring of the bearing is bolted directly to the hub or the rotor of the generator (direct drive) (Fig. 15).

4.4 Gearbox

Gearboxes can be thought of as the heart of wind turbines with a conventional drivetrain with separate systems. Since gearboxes are components which result in very long turbine downtimes when they fail, and account for a very large proportion of the total turbine costs, there have been many innovations and developments in this field. The primary objective here was to improve the reliability and ease of maintenance

Hohlrad I   Hohlrad II   Ritzelwelle

Sonne I

Stirnrad
Sonne II

Planeten I

Planeten II
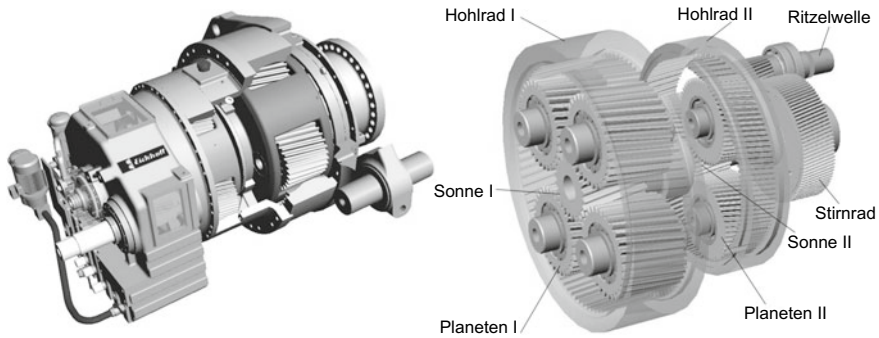
Fig. 16 3.6-MW gearbox with two planetary stages and one spur gear stage [Eickhoff]

of the gearboxes, and this has led to many concepts which have become commercially established with varying degrees of success. This section aims to provide an overview of today's gearboxes and the fundamental considerations for several types of gearbox.

WTG gearboxes usually have several stages and serve to convert the large torque originating from the rotor into a smaller torque with higher rotational speed at which the generator is operated.

While smaller WTGs up to 100 kW are mainly equipped with pure spur gears, gearboxes for turbines in higher power classes have the first transmission stage as a planetary stage. From a power of approx. 2.5 MW upwards, the second stage is likewise built as a planetary stage (Fig. 16).

Whereas spur gear stages have only one engagement, which transfers the torque in its entirety, planetary gear stages have several engagement points corresponding to the number of planets used, and the input torque is distributed thereover. This relieves the load on the components and leads to much more compact designs.

In today's gearboxes, the number of planets used varies between three and five. In the planetary gear stages, the planets are driven and the sun is the output in most gearboxes, while the ring gear is stationary. The individual planets therefore always engage with the ring gear in addition to engaging with the sun, which serves to support the torque.

Many manufacturers are moreover pursuing the concept of power splitting with gearbox types which distribute the input torque directly across several stages simultaneously and thus ramify the powertrain (Fig. 17). The advantages of this concept include the fact that the individual stages are subjected to a lower, more uniform load and a more compact design can be achieved. It is thus also possible to create designs where the planets are only rotating around themselves and drive the ring gear.

A spur gear stage is used as the last stage to produce an axial offset between input and output shaft. This offset is necessary because gearboxes are designed with a central hollow shaft which is used as the feedthrough to supply the hub with operating media. A so-called slipring feedthrough is mounted at the end of the gearbox housing facing the generator. It has sliding contacts which facilitate the transmission of signals
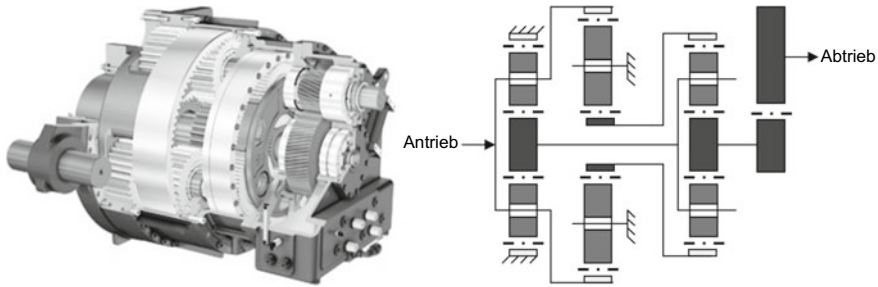
Fig. 17 Gearbox with power splitter [ZF Industrieantriebe Witten GmbH]

and electric power from the rotating drivetrain (e.g. hub) into the stationary system of the nacelle. Hydraulic pitch systems also have a hydraulic rotary feedthrough in the hollow shaft.

This creates a problem with gearboxes which have only planetary stages (so-called concentric gearboxes). If one looks along the direction of the load, the generator is located directly behind the gearbox output of the generator, and hence there is no room to accommodate a corresponding feedthrough, and so other, more complex solutions have to be found in this case. One solution can be to likewise build the generator with a hollow shaft.

Concentric gearboxes are used for so-called hybrid drives, for example, where the gearbox has only two planetary gear stages and is connected directly to a generator. Consequently, this is operated at a lower speed and is accordingly bigger (for the same rated power) (see Sects. 5.3 and 5.4). The gearing for spur gear and planetary gear stages can be a spur-toothed gearing as well as a helically cut gearing. The advantages of a helically cut gearing lie in the more uniform power transmission and the better running smoothness. These advantages have to be weighed against the greater complexity of their manufacture and mounting and the generation of axial forces.

Modern gearboxes are developed with the aim of producing large quantities and manufactured by mass production, which is why it is beneficial to use large numbers of cast parts. This means that the planet carriers and gearbox housings, for example, are almost always cast components nowadays. They are sometimes subjected to high loads since, depending on the drivetrain concept (for example when a three-point mount is used), not only the torque but also a fraction of the rotor loads or the resulting deformations of the drivetrain act on them. Although the maximum load for the gearbox is usually the drive moment, bending moments can also lead to extremely high loads and deformations of the housing. Since the ring gear of the planetary stages is at the same time part of the gearbox housing or rigidly joined to it, this can cause nonuniform engagements and loads on the teeth and bearings, which can thereby be damaged.

An interesting concept in relation to gearboxes is the so-called flexpin mounting. This is an alternative way of mounting the planets which has been used by various

manufacturers for several years. The planets are mounted on a flexible bolt and are able to pivot their axis slightly, while the bolt is supported by the gearing at the same time. This concept facilitates a more uniform load distribution to all the planets and better engagement with the teeth, even when taking into account the unavoidable manufacturing tolerances and deformation of the periphery when in operation.

The large deformations mentioned have made the use of the finite element method (FEM) an indispensable tool in gearbox development. In addition, dynamic aspects have increasingly been taken into consideration over the years. Since the bearings have large numbers of gearings and ball-pass frequencies, the gearbox represents the greatest potential for resonant excitations in the drivetrain. Special software is used to determine these excitations and detailed analyses are part of the gearbox certification.

The gearbox is usually connected to the WTG structure via two lateral housing supports, which transmit the forces via elastic elements into the main frame. These supports absorb only torques, the dead weight of the gearbox itself is borne by the connection to the rotor shaft.

In addition to the conventional, aforementioned types of gearbox, turbine and gearbox manufacturers are pushing ahead with the development of various alternative concepts. One example of a gearbox design with variable transmission ratio and a constant rotational speed to the generator is the Voith WinDrive (Fig. 18). This is a combination of a planetary gearbox and a hydrodynamic converter, which is located between the main gearbox and the generator. The planetary gearbox of the Voith WinDrive is a superposition gearbox, where only a fraction of the input power is transmitted directly to the generator and the remaining power acts onto the pivot-mounted ring gear of the first stage with variable speed via the converter and via the second planetary stage. The transmission ratio control is achieved by adjustable guide vanes in the hydrodynamic converter.

The advantage of this concept is that load peaks are damped by the dynamic coupling and the frequency converter is no longer needed.

An important trend over recent years has been the increase in the so-called torque density, i.e. the ratio of rated torque and the installation space required. Onshore WTGs are subject to narrow constraints as far as the logistics are concerned. By increasing the torque density, more rated power can be accommodated in the limited installation space available. At the same time, the specific weight and the costs resulting therefrom are reduced. To increase the torque density, engineers are working on gearbox types with a higher number of planets, optimised materials, and a more in depth understanding of the (design) model, amongst other things.

4.5 Brake and Coupling

A coupling generally connects two shafts with each other. In a conventional geared wind turbine, a coupling is used as the connecting member between gearbox and generator. This drivetrain concept is the basis of the explanations below. There are
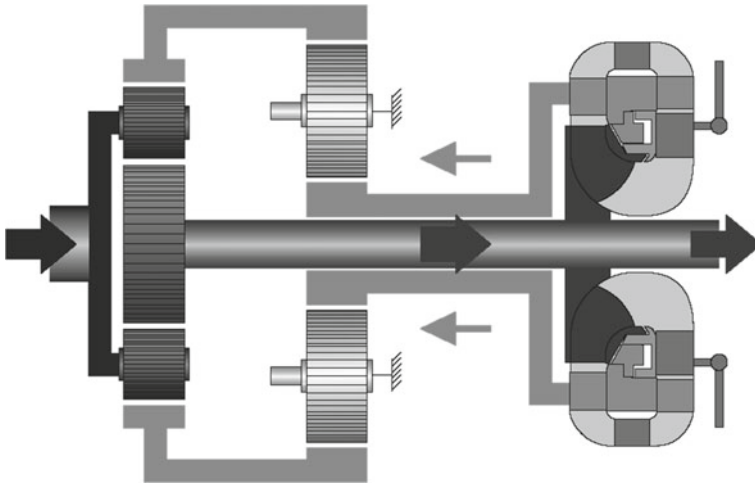
Fig. 18 WinDrive [Voith]

also wind turbine concepts where a coupling is used directly behind the rotor shaft to bring about a defined load separation. The coupling performs further functions in addition to the pure transmission of the torque. Tensioning elements are usually used to connect the coupling to the gearbox and generator.

The flexible mounting of generator and gearbox means that the coupling must be able to compensate the movements of the two components with respect to each other. In addition, it must be able to compensate for a certain misalignment between gear shaft and generator shaft caused by the mounting or also the operating load. Double-jointed torsionally rigid couplings are usually used.

Moreover, couplings have an overload protection, whose purpose is to protect the gearbox against high torques which can act in the generator for a short period. These torques are primarily generated when the generator short circuits, and the generator jams while the driving torque continues to be introduced from the rotor. Without the overload protection, very large forces would then act on the bearings and teeth in the gearbox, which could damage the components or cause them to fail. Overload protection usually takes the form of a slip clutch, which is set to a maximum torque and slips when the torques are excessive. In normal operation, the moments are transferred by frictional contact.

A further property of couplings is their electric insulation. In the event of a lightning strike, the lightning, coming from the blade, would run through the whole drivetrain, damaging the generator in particular. Most couplings are therefore equipped with a spacer shaft which is usually made from fibreglass-reinforced plastic. There are also alternative versions which have a centre tube made of carbon fibre composite or steel, whereby the flexible elements take on the role of the electric insulation in the steel version (Fig. 19).
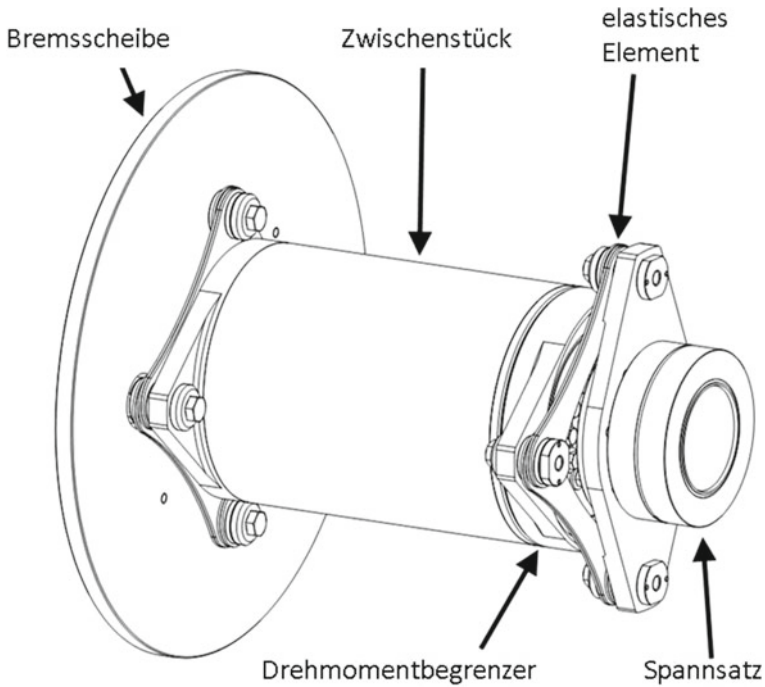
Fig. 19 Coupling [KTR Kupplungstechnik GmbH]

A further function of the coupling is to transfer the braking power via a brake disc to the drivetrain. The brake is usually located directly at the gearbox output and is bolted to the gearbox housing. The brake disc is usually made of steel.

In large WTGs with three independently operating pitch systems, the brake is not used to decelerate the turbine from full speed. It is used only when the turbine has been largely decelerated by pitching the blades, to then bring the drivetrain to a complete standstill. To achieve braking system redundancy for stall WTGs or turbines with a central pitch cylinder, the mechanical rotor brake must be able to decelerate the rotor from all operating modes (emergency stop). Accordingly, the brakes are bigger or more brakes are required.

The lack of a transmission means that rotor brakes for direct-drive turbines are likewise bigger. The structure of direct-drive turbines, which have a larger nacelle diameter because of the generator dimensions, means that the brakes here can usually be mounted on a larger diameter, although these turbines fundamentally require much higher numbers of brake callipers.

For the most part, two brake callipers are used for turbines with gearbox and a power >2 MW, whereas a single brake is still sufficient for smaller turbines.

There are two types of brakes: fixed-calliper and floating-calliper brakes. With floating-calliper brakes, the braking pressure is applied by one of the two friction linings. The other friction lining is connected directly with the calliper, which is
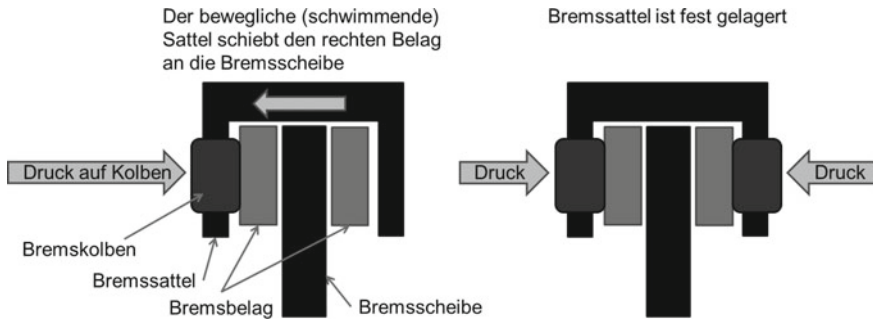
Fig. 20 Principle of the floating-caliper brake (left) and fixed-caliper brake (right) [aerodyn]

floating and can move freely on a guide pin. With the fixed-calliper brake, the two calliper jaws are rigidly joined to each other and have two hydraulic pistons (Fig. 20).

The advantage of the floating-calliper brake is that it can be self-aligning, and therefore no axial forces are introduced into the coupling and hence into gearbox and generator. A floating-calliper brake is thus less demanding as far as mounting accuracy is concerned. In line with their concept, fixed-calliper brakes must be mounted with much greater accuracy to ensure that the brake disc really is precisely in the centre between the two friction linings. The advantage of the fixed-calliper brake is that much larger forces can be applied. The fixed-calliper brake is usually less expensive, but cannot be used when an axial movement of the gear shaft is to be expected.

Rotor brakes are either hydraulically or electrically driven. Electric brakes became commercially available much later than hydraulic brakes and are not yet so widespread. Electric brakes are advantageous when the intention is to use no hydraulic unit at all and thus avoid the problem of possible oil leaks. In addition, lower maintenance costs are to be expected when electric brakes are used.

The high temperatures generated with geared WTGs during braking place particular demands on the brake lining. The most common brake linings here are organic brake linings or sintered metal linings. Organic brake linings consist of a binding agent and various materials such as metal, glass, rubber, resin and different reinforcing fibres. Compared to sintered metal linings, they function better as a holding brake (so-called static brake) because they have a higher friction value in this case. The sintered metal linings have better temperature resistance. The decision as to which lining to use must be made on the basis of a detailed consideration of the turbine design, the load cases and the turbine control. Issues to be considered here include the specified maintenance wind speed, which dimensions the maximum holding moment of the brakes, and the maximum brake speed, which results from the specified maximum rotational speed for the brake activation.

The obvious thing is to select an organic brake lining for direct-drive turbines since the thermal load is low.

4.6 Generator

The generator represents a key component of the drivetrain since it is responsible for converting the mechanical energy into electrical energy. It is dealt with in detail in Chap. 8. There are numerous designs for direct-drive WTGs with a high number of poles or geared WTGs with a low number of poles. With the direct-drive drivetrain concepts, the generator is usually mounted via the existing rotor bearing assembly, although separately mounted systems exist here as well. Conventional electric generators with two bearings are usually used for high-speed systems. The mechanical connection of the various generators to the particular drivetrain can be seen in Sect. 5. Of the high-speed generators, the doubly-fed asynchronous generator is the most widespread. Today's WTGs have permanent-magnet excited synchronous generators as well as asynchronous squirrel cage generators, which have the advantage that they do not require sliprings, and the associated full-scale converter makes it easier to comply with the grid connection conditions. A disadvantage, however, is that the costs are much higher, since with the doubly-fed generator, only around a third of the current has to flow through the converter and thus the costs for the converter are lower. High-speed generators are usually built as four-pole generators. The nominal speed of these generators is 1500 rpm (synchronous) or around 1650 rpm (asynchronous). For generators with higher rated power (>3 MW) or for 60 Hz grid frequency, six-pole generators (1000 rpm synchronous at 50 Hz) are often used. The mounting is a weak point with high-speed generators. Although the rolling bearings are designed for a lifetime of 20 years, it turns out in practice that the actual lifetime is much shorter. The reasons for this have not been unequivocally identified. The manufacturers are meanwhile excluding bearing currents as the cause, since earthing brushes are being used as a countermeasure. The lubrication is usually provided via an automatic relubrication system mounted on the generator. Lubrication is often cited as the reason for the damage nevertheless. Many generators have recently been retrofitted with ceramic bearings (rolling elements made from ceramic material) to ensure the bearings have a longer service life. They have better properties should starved lubrication occur, and also better insulation properties, but are more expensive than conventional steel bearings. The high-speed systems are frequently cooled by air-to-air heat exchangers (Fig. 21, right). In the generator, fans generate an internal airflow, which in turn dissipates the heat to an external airflow via a heat exchanger.

For a closed, sealed nacelle, a generator with air-water heat exchangers can also be an option.

With water jacket cooling (Fig. 21, left), it is often not possible to cool the inside of the generator so uniformly, whereas the disadvantage with solutions using air-water heat exchangers is the lower temperature gradient compared to air-air heat exchangers. This is down to the additional heat transfer which this concept needs.

The low-speed and medium-speed generators with large numbers of poles have fewer problems with the service life of the bearings. Direct-drive turbines frequently use the rotor bearing assembly as the generator bearing as well. These turbines use
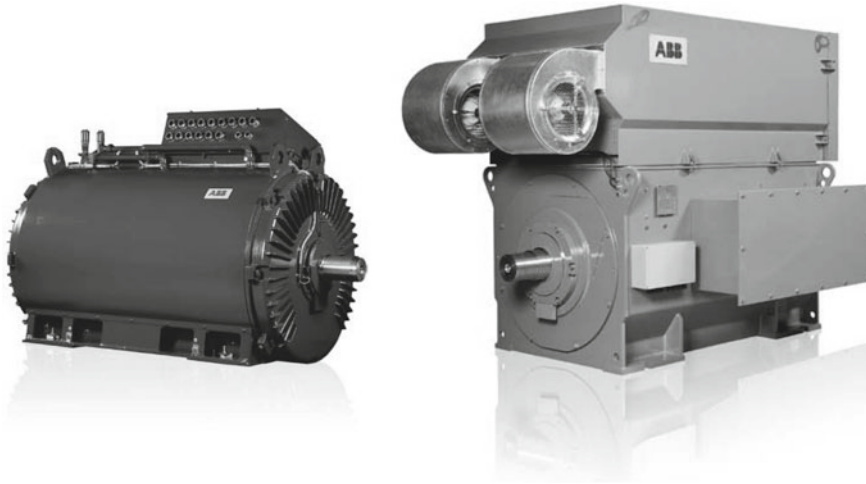
Fig. 21 Permanent-magnet generator with water jacket cooling (left) and generator with top fan (right) [ABB]

permanent-magnet excited or electrically excited generators (Fig. 22). With electrically excited generators, the sliprings can be dispensed with when a pilot generator mounted on the same shaft is used for the excitation. Since the costs for the magnets required are high and difficult to plan, electrically excited systems continue to generate interest, although they are not as compact to build. The generator rotor can also take the form of an external rotor, which has a positive effect on the external diameter.
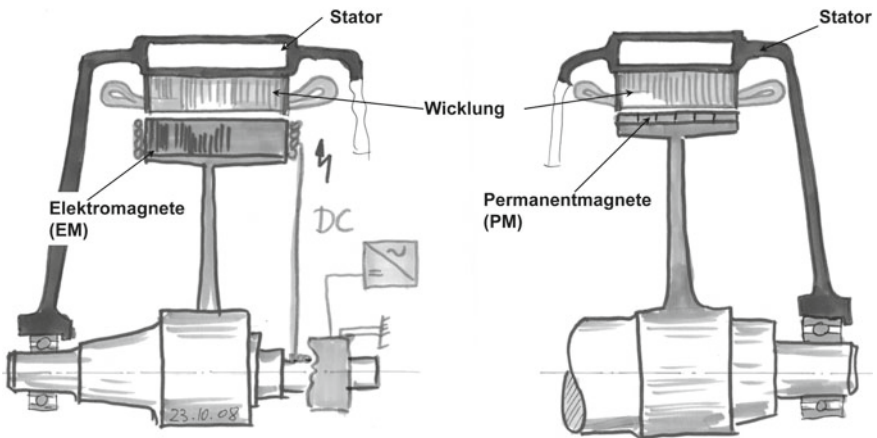
Fig. 22 Excitation of direct-drive generators [F. Klinger]
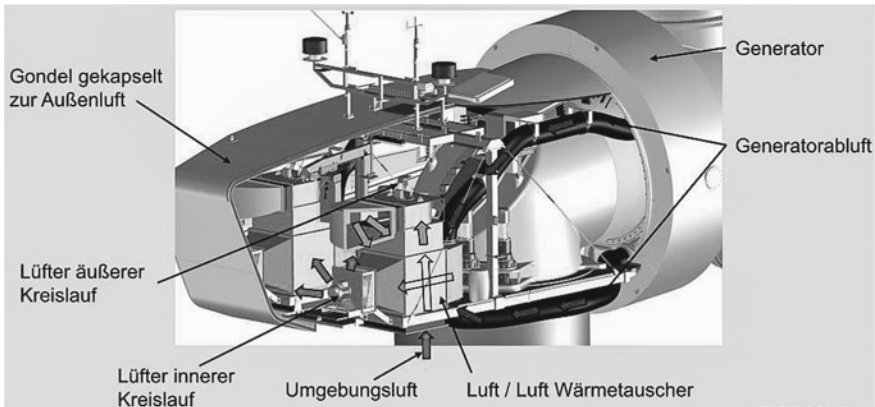
Fig. 23 Cooling system of a Vensys WTG [Vensys]

The cooling and the air gap stability are the design challenges with the low-speed generators. The effect of the drivetrain concept and the mounting on the air gap is described in Sect. 5. The cooling can be effected in manifold ways, many of which are patent protected (water cooling, air cooling, etc.). The compactness of the generator is determined by the cooling efficiency and also by the flux density in the air gap brought about by the excitation system. The costs involved mean the direct-drive generators are not as efficient as the high-speed ones, and the cooling system must accordingly be bigger. Figure 23 shows a schematic for the cooling system of a Vensys WTG as an example.

Chapter 8 discusses the electrical design of the generators and converters in detail.

4.7 Yaw System

Yaw systems, also known as wind direction alignment systems, ensure that the nacelle always faces into the prevailing wind and the loads arising are safely transferred into the tower. The nacelle is, therefore, pivot mounted on the tower head. Large, modern WTGs are equipped with an electric or hydraulic drive for the yawing (or tracking). Small WTGs have a wind vane, which automatically keeps the nacelle in the wind (Fig. 24).

A wind vane can be dispensed with when it is a small downwind turbine (rotor downwind of the tower). Old designs of small or medium-sized turbines and traditional windmills have a fantail to drive the wind tracking automatically (Fig. 25). This section describes the various options for arranging yaw components and their function.

Their main task consists in keeping the nacelle facing into the wind. The drives do not track every change in wind direction directly. The control only starts tracking

Fig. 24 WTG with wind
vane [Leading Edge
Turbines Ltd]
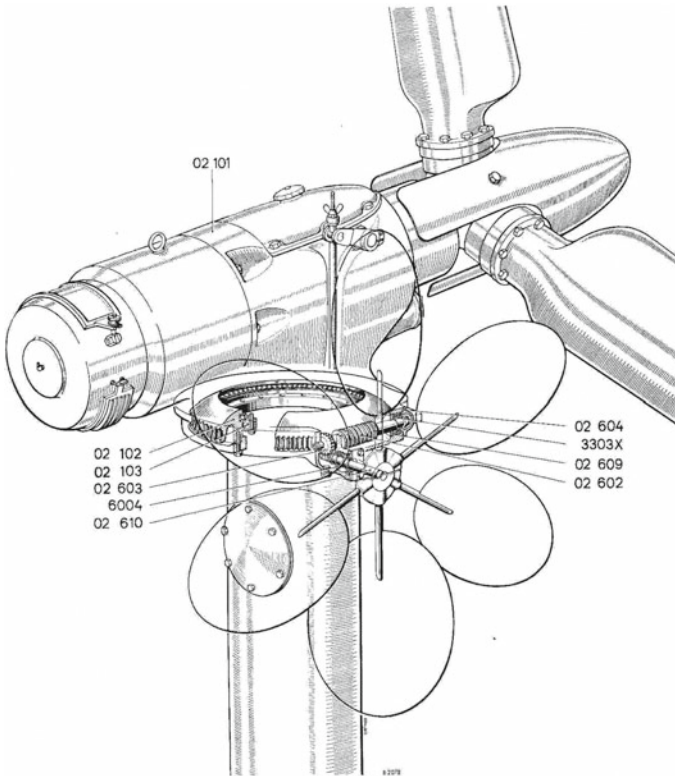
Fig. 25 WTG with fan tail [Allgaier]

when a certain oblique incoming flow has become established on average over a specific time interval. If this were not the case, the yaw system would execute small movements too frequently. The deviation of the wind direction from the longitudinal axis of the turbine is measured using a wind vane on the nacelle. The drive is usually executed via several gears (pinions) which engage with a gearing on the yaw bearing. The number and size of the drives depends on the size of the wind turbine. During yawing, the rotary motion must be damped by means of a brake or preloaded journal or plain bearings, since otherwise the tower head could rock to and from within the gearing and the service life of the components would thus be significantly reduced. The yaw brakes also ensure that the nacelle still faces into the wind when the yaw drives are idle. The drives themselves normally also have brakes, which help bring the nacelle to a halt. A further function of the yaw drives is to untwist the cables. A cable loop is located in the upper part of the tower, which allows the WTG to execute no more than two or three complete turns. The number of revolutions of the tower head is monitored with respect to its original orientation via appropriate sensors and the WTG control. The yaw drives initiate the untwisting of the cables at a suitable point in time.

4.7.1 Yaw Bearing

The yaw bearing or tower head bearing is usually a large diameter rolling bearing with external or internal teeth, designed as a four-point contact bearing, single row (Fig. 26) or double row. A journal bearing (Fig. 27) is a special form of yaw bearing which has the damping function integrated. The disadvantage here is that more drive power is required because of the increased friction.
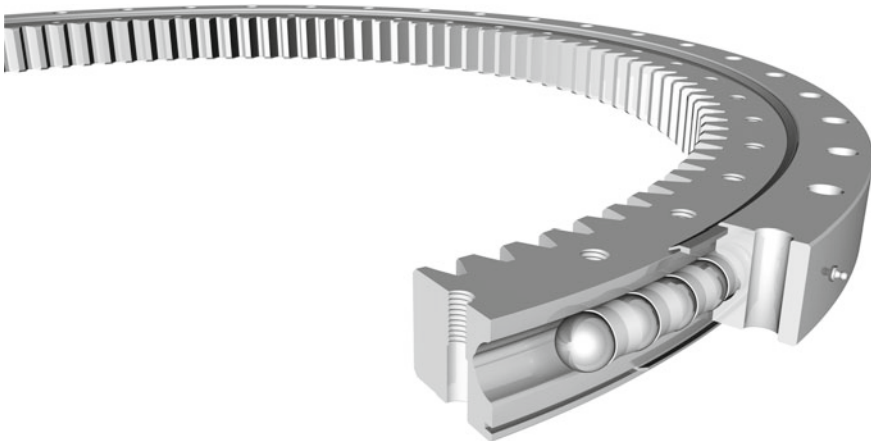
Fig. 26 Single-row four-point contact bearing [Thyssen Krupp Rothe Erde GmbH]

Fig. 27 Journal bearing
[aerodyn]
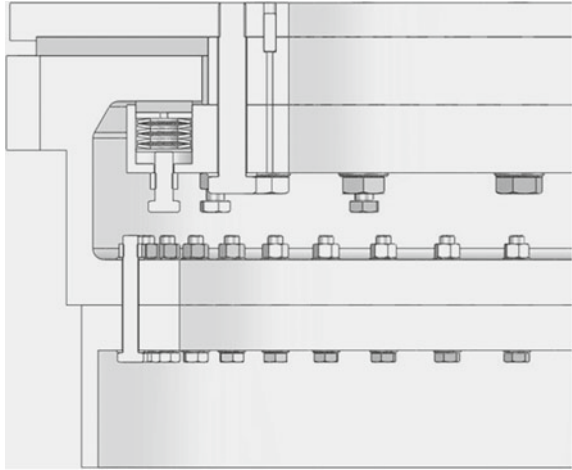
4.7.2 Drives

In most cases, a gear motor with a pinion on the output, several concentric planetary gear stages and a flange-mounted AC motor is used as the drive. An immobilisation brake is usually integrated into the AC motor as well. Other types of drive, e.g. with worm gear or with hydrostatic motors, are used less frequently. The characteristic that the AC motor has a specific stalling torque is used as overload protection for the gearing (Fig. 28).

4.7.3 Brakes

The yaw brake normally consists of a brake disc and several hydraulic fixed-calliper brakes which are controlled via an appropriate hydraulic unit (Fig. 29, right). Two pressure levels are typically used: a low pressure for damping during a yaw motion (tower head rotation) and a high pressure for braking. Other systems operate with electric braking systems (Fig. 29, left) or can dispense with disc brakes completely, e.g. when a journal bearing is used and the brakes are integrated into the drive.

4.7.4 Sensors

A variety of sensors are used to detect the position of the nacelle and initiate an untwisting of the cables in due time. In most cases, a cam switch is used to detect the position for the untwisting of the cables. In addition, an absolute encoder (Fig. 30) is used to detect the absolute position of the nacelle. The sensors usually engage with the bearing teeth via a pinion.

Fig. 28 Drives for wind direction tracking (Yawing) [Bonfiglioli]
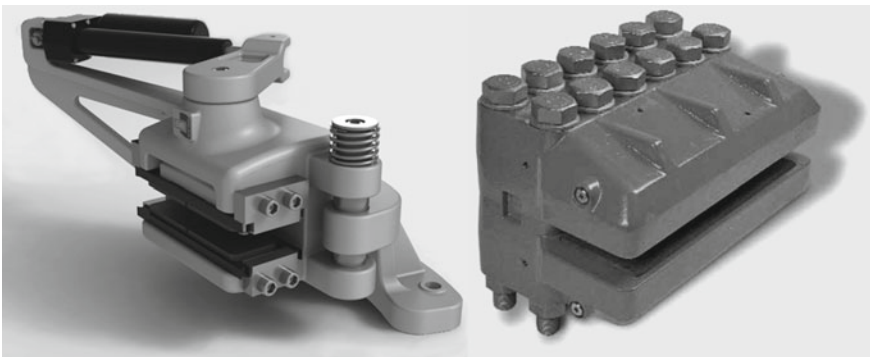
Fig. 29 Brake calipers: electric [KTR Kupplungstechnik GmbH], hydraulic [Svendborg Brakes]

4.7.5 Central Lubrication

A central lubrication system is normally also used for the yaw system to supply the bearing raceways and the teeth with grease when the turbine is in operation. Suppliers in this field have developed systems especially for the wind industry (Fig. 31).

Fig. 30 Absolute encoder [aerodyn]

4.7.6 Arrangements for Yaw Systems

If we consider the rolling bearing systems which are normally used, yaw systems can be arranged in four different ways:

1. Yaw bearing with internal teeth and internal yaw brake,
2. Yaw bearing with internal teeth and external yaw brake,
3. Yaw bearing with external teeth and internal yaw brake,
4. Yaw bearing with external teeth and external yaw brake.

With the first arrangement, the nacelle is turned via a yaw bearing with internal teeth (Fig. 32). The yaw disc brakes and the yaw drives are located inside the tower in this case. The advantages of this arrangement are that this version can be well protected against ambient conditions (contamination, humidity, transport damage) and the load path through the bearing is also very favourable. The disadvantages are that very little space is available for the components, the bolts of the outer ring of the yaw bearing are located outside the tower and are thus more difficult to access, and lubricating grease can deposit on the yaw brake disc.

The second type also has a yaw bearing with internal teeth, but here the yaw disc brakes are outside the tower (Fig. 33). The yaw drives are still located inside the tower. With this arrangement, the load path through the bearing is likewise very favourable, and thus an advantage of this version. Further advantages result from the larger diameter of the brake disc, which means a smaller braking force is required. In addition, the lubricating grease for the teeth can no longer deposit on the yaw brake discs. In this version, the bolts of the outer ring of the yaw bearing are likewise located outside the tower, which is a disadvantage. The total width of the main frame is necessarily larger than when the brakes are inside.

The third version consists of a yaw bearing with external teeth and internal yaw brakes. The yaw drives are therefore located outside the tower and the yaw disc brakes
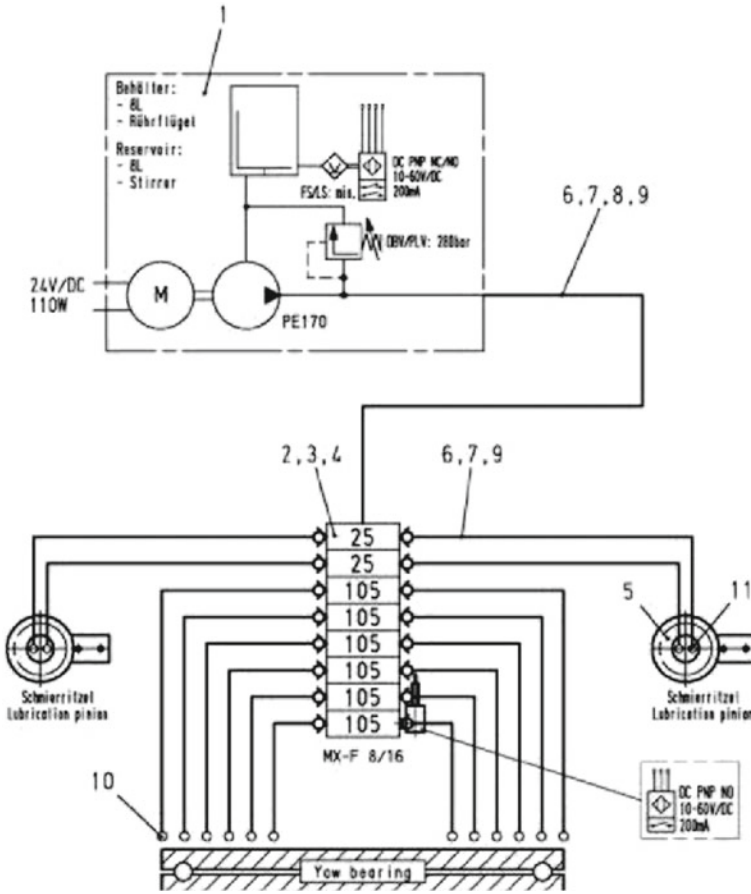
Fig. 31 Central lubrication [aerodyn]

are inside (Fig. 34). The advantages of this arrangement are more space to access the nacelle inside the tower, good siting options for the yaw drives, the lubricating grease on the teeth does not get onto the yaw brake discs, and there is a larger pitch circle on the bearing, which results in a smaller torque on the drives.

The overall width of the main frame is very large and therefore a disadvantage of this version. In addition, the load path through the bearing tends to be more unfavourable, which means the tower flange must be thicker.

The fourth arrangement with external teeth and external brake has not yet been realised to the best of the authors knowledge.
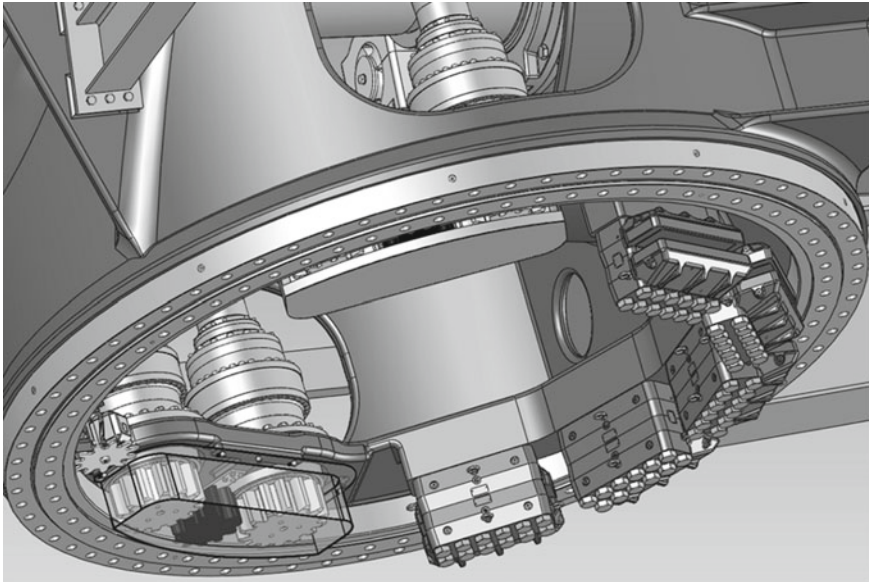
Fig. 32 Internal teeth of the yaw bearing with internal yaw brakes (brake disc not shown) [aerodyn]

Fig. 33 Internal teeth of the yaw bearing with external yaw brakes [aerodyn]
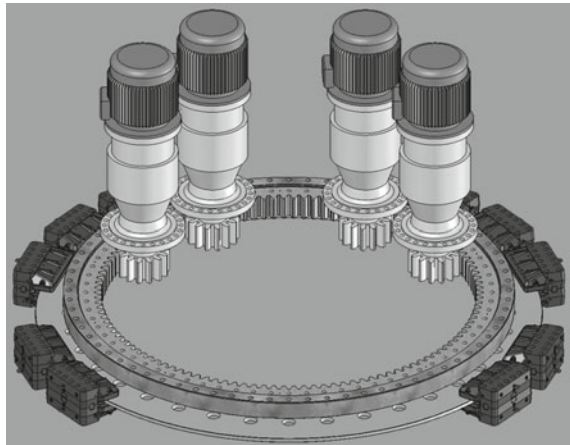
5 Drivetrain Concepts

This section presents and considers different drivetrain concepts on the basis of their rotor bearing assembly and the gearbox/generator concept. Since a great many combinations are possible, this book limits itself to projects which have actually been realised. Table 1 provides basic information on the possible options in a summary drivetrain concept matrix.
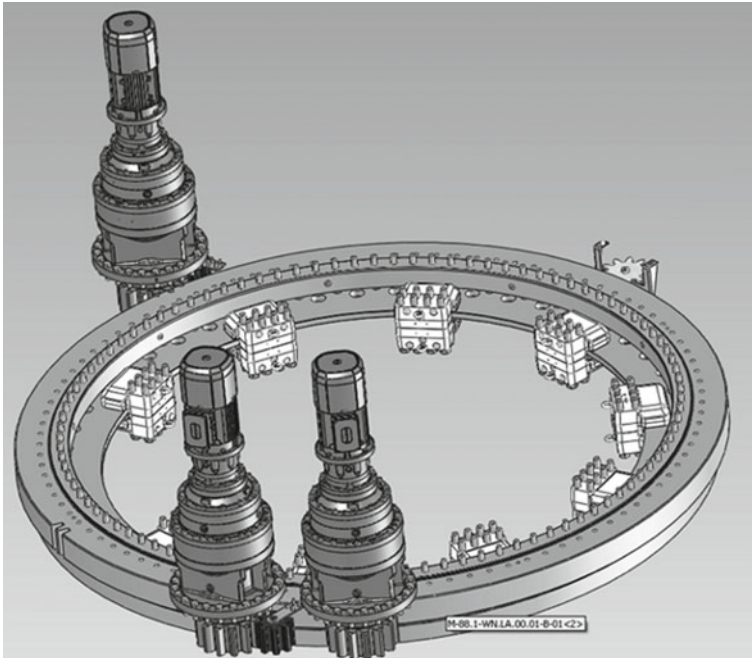
Fig. 34 External teeth of the yaw bearing with internal yaw brakes [aerodyn]

Table 1 Drivetrain concept matrix

Mounting concept	Type of gear: direct	Type of gear: 1–2 stages	Type of gear: 3–4 stages
Two-point mount	Section 5.1	Section 5.3	Section 5.5
Three-point mount			Section 5.6
Moment bearing	Section 5.2	Section 5.4	Section 5.7

On closer examination of the matrix, it is clear that two possible combinations with three-point mount (direct-drive concept and drivetrain with 1–2 stage gearboxes) have been omitted. Although these versions would be possible in theory, the authors are not aware of any instances where they have been implemented in practice. Moreover, a direct-drive drivetrain based on a three-point mount cannot be realised so as to be economically competitive because of the high loads on the generator housing.

5.1 Direct Drive—Two-Point Mount

Gearless WTGs, also called direct-drive WTGs, are characterised by greater reliability and lower maintenance costs. Their disadvantages are their large dimensions and the comparatively high cost of constructing such turbines. A well-known manufacturer which used to have comparatively large market shares is the German company Enercon. Enercon has so far used electrically excited generators which are very heavy and have a very large installation footprint. More modern types of generator, e.g. those from Vensys or SGRE, use permanent magnets and often no longer have a weight disadvantage when compared to geared WTGs. The problems with these are the high costs and the cost fluctuations for the raw material, so-called rare earths, needed to manufacture the permanent magnets.

The mounting concept of the rotor for the Enercon WTG is based on two bearings which are arranged on a protruding shaft journal (see Fig. 35, top). The hub is connected directly to the rotor of the generator which is located inside the generator. The generator stator is arranged in the housing, which in turn is flange-mounted on the main frame. The offshore wind turbine manufactured by GE (formerly ALSTOM), a 6 MW turbine with a rotor diameter of 150 m, follows the concept described.

The advantages of the two-point mount described in Sect. 4.3 have to be weighed against the disadvantages, however. On the one hand, the bending of the shaft journal affects the air gap of the generator so that the main frame and the shaft have to be designed with the appropriate stiffness and are therefore heavy. On the other, it is more difficult to access the hub and the generator is also difficult to access. The GE Haliade 150–6 MW (see Fig. 35) uses the so-called "PureTorque®" concept whereby the mounting minimises the effect on the air gap. The torque is transferred from the rotor to the generator via elastic elements.

The arrangement depicted in Fig. 36 can be considered to be similar to the Enercon concept. This drivetrain, which is built by Vensys, has an external generator rotor, however. The stator is inside the generator and connected to the main frame.

Since the shaft with the two bearings does not pass through the whole hub, as is the case with the Enercon concept, the hub is accessible with this arrangement. Furthermore, the rotating generator housing is not subjected to the rotor loads.

The air gap is affected by the bending deformations of the shaft journal in this concept as well, however, and the resulting design is likewise very heavy.

A further example for the mounting concept with two separate bearings in conjunction with a direct-drive WTG is shown in Fig. 37. The concept of the mTorres TWT 1500 and TWT 1.65 is based on a longer, highly integrated generator which is arranged directly above the tower.

This version has the advantage of a smaller generator diameter and a smaller supporting main frame, but the disadvantage that up to 90% of the rotor loads act on the generator housing. Here as well, this has an impact on the generator air gap.

The solution realised by Scan Wind (now likewise GE) is based on a very long rotor shaft which is mounted with two separate small-diameter bearings (Fig. 38). Not only the rotor but the generator with stator and rotor as well is mounted on the
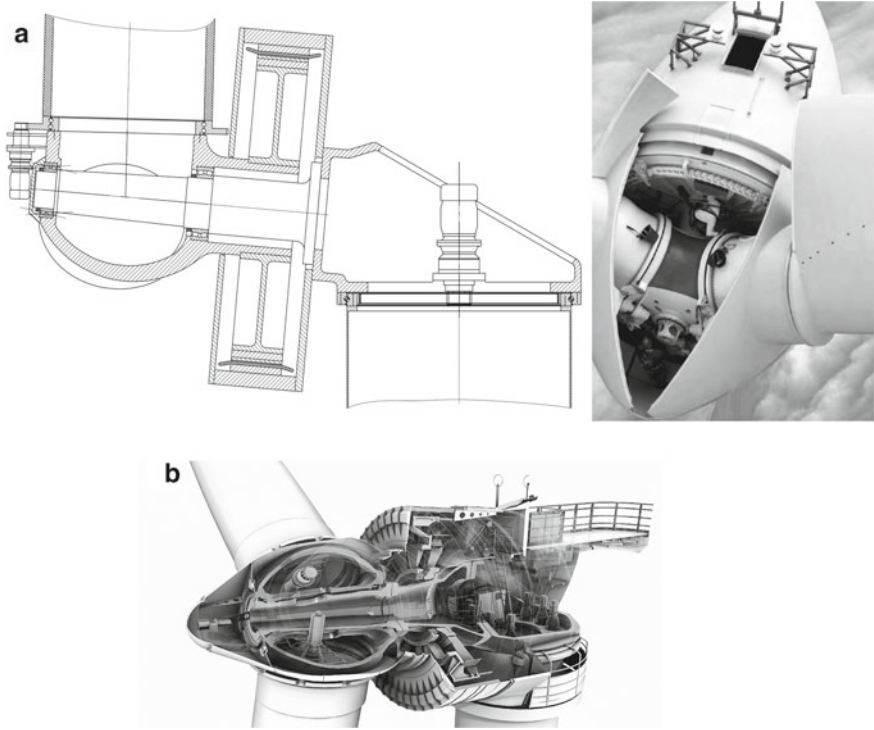
Fig. 35 Drivetrain concept similar to that of Enercon [top, aerodyn], drivetrain of the GE Haliade 150–6 MW [bottom, GE Renewable Energy]
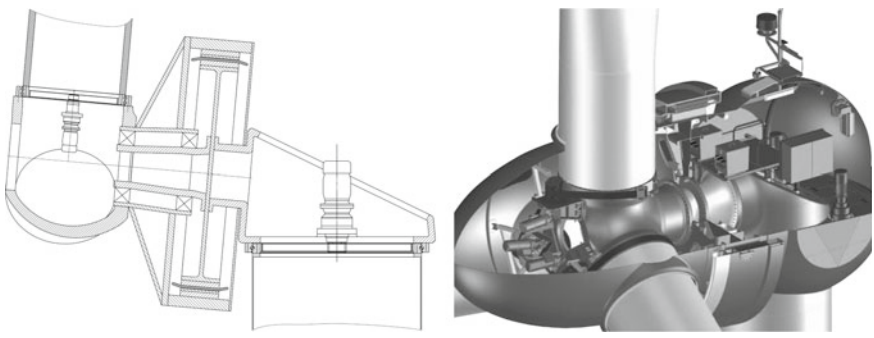
Fig. 36 Drivetrain concept [left; aerodyn] and nacelle [right, Vensys] of Vensys 1.5 MW WTG

shaft. This mounting concept has the great advantage that the generator is loaded only by the torque, leading to small deformations of the generator and its housing, which means that the air gap of the generator is not affected either. Since the rotor shaft and the main frame in this rotor and generator arrangement depend on the diameter
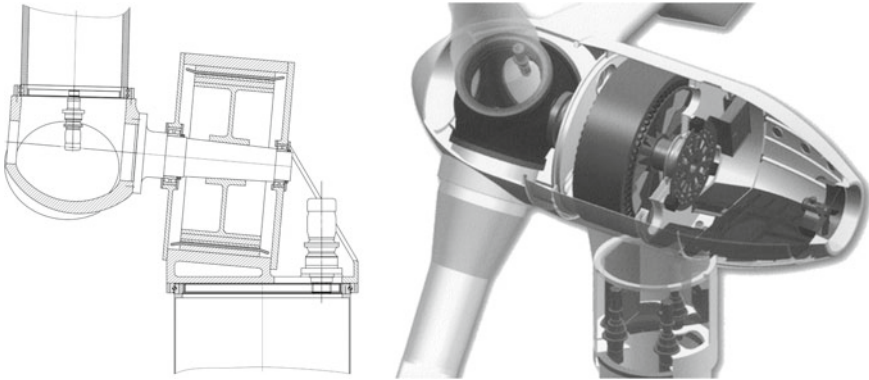
Fig. 37 Drivetrain concept [left, aerodyn] and nacelle of United-Energies.es 1.5 MW [right, United-Energies.es]

of the upper tower, this can result in very large and heavy support structures. This solution also has the disadvantage that the generator needs its own mounting.

A variation of this concept can be seen in Fig. 39. The two-point mount of the extremely long rotor shaft has remained the same. With the Heidelberg Motor HM 600, the generator housing with the stator is not mounted on the rotor shaft, but is flange mounted directly onto the main frame.

This design has the advantage that the generator housing is subjected to very low loads. Moreover, no bearings are needed for the generator housing. The air gap of the generator is affected by the flexing of the rotor shaft, however, which must therefore be designed with the appropriate stiffness. This requirement in conjunction with the length of the shaft is a challenge which is not to be underestimated.

Considering both the onshore and the offshore market in 2021, the only one of the 10 WTG manufacturers with the largest shares of global sales (referred to as the TOP10 OEM 2021 below) to pursue this concept is GE with the Haliade and a
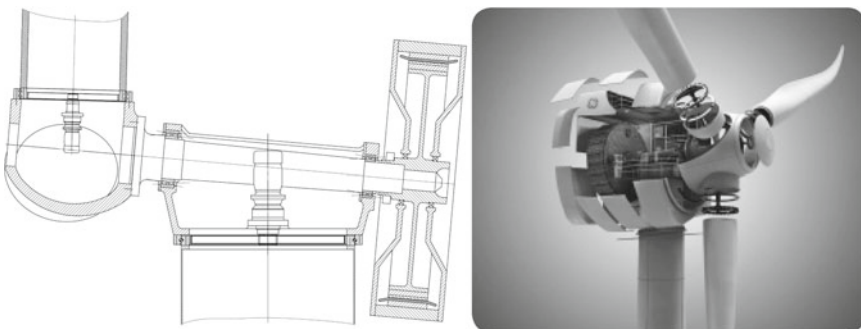
Fig. 38 Drivetrain concept [left, aerodyn] and nacelle of GE 4.1-113 [right, GE Renewable Energy]
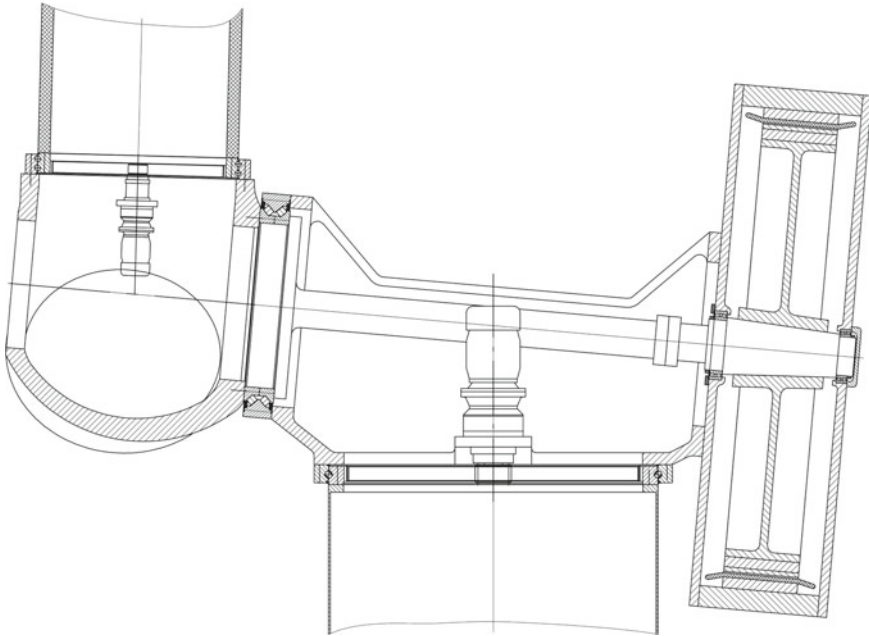
Fig. 39   Drivetrain concept of Heidelberg Motor HM 600 [aerodyn]

nominal power of up to 14 MW. Although Enercon continues to pursue this concept, it is no longer amongst the 10 largest WTG manufacturers in global terms.

5.2   Direct Drive—Moment Bearing

This section resembles Sect. 5.1 in that it considers a gearless drivetrain concept, although the advantages and disadvantages of the direct drive are not repeated.

The discussion below therefore concentrates on direct-drive drivetrain concepts with moment bearing and starts with a drivetrain concept which Lagerwey has implemented in various WTGs. The rotor hub is mounted on the main frame by means of a moment bearing, which is usually a two-row tapered roller bearing. This transfers the torque to the inner rotor of the generator. The stator is fixed to the main frame inside the generator housing (see Fig. 40).

Although the structure of this version affords direct access to the hub, it has disadvantages in respect of the dimensions and the weight of the support structure required because of the large bearing diameter and the effect of the deformation on the air gap of the generator.

The design of the 2.5 MW turbine from Vensys differs from that of its 1.5 MW turbine in that it has a drivetrain with only one main bearing. Figure 41 shows that
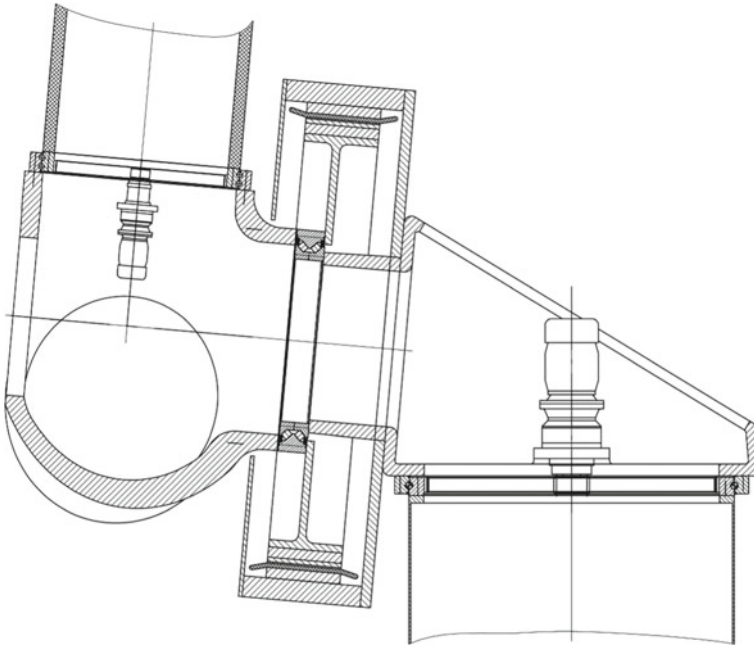
Fig. 40 Drivetrain concept similar to Lagerwey [aerodyn]
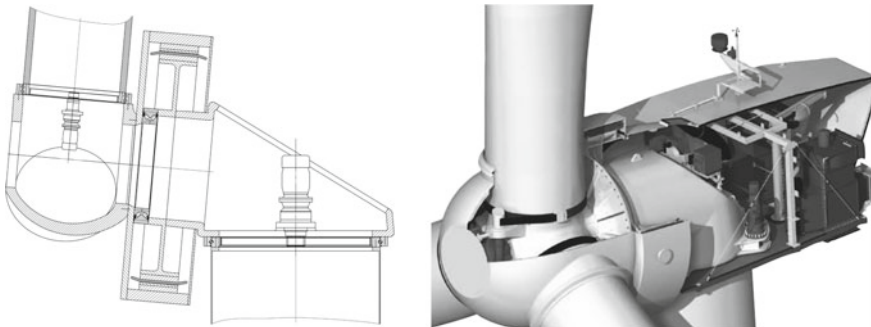
Fig. 41 Drivetrain concept [left, aerodyn] and nacelle of Vensys 2.5-MW WTG [right, Vensys]

the generator concept has not changed, however. In this WTG as well, the generator rotor is designed as an external rotor and the stator is located inside and connected to the main frame. The drivetrain concepts of SGRE in the offshore segment and Goldwind look similar to this.

Since the setup differs from the Lagerwey concept only in the rotor–stator arrangement, the same advantages and disadvantages can be considered to apply.
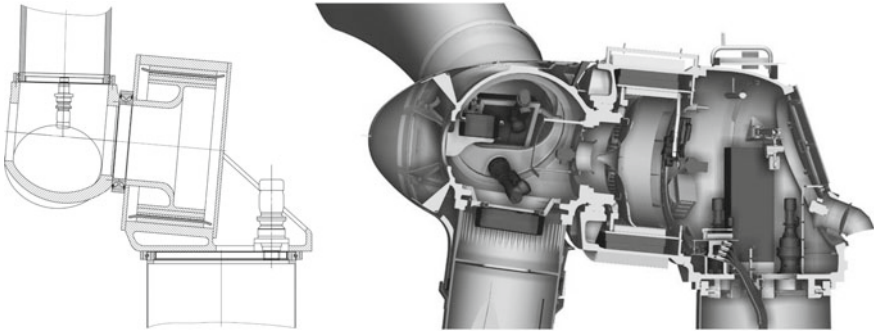
Fig. 42 Drivetrain concept [left, aerodyn] and sectional view of a nacelle from LEITWIND [right, LEITWIND]

LEITWIND pursues the drivetrain concept depicted in Fig. 42 in its products. The turbines with rated powers of 1–3 MW use a moment bearing and a generator with relatively small diameter. The resulting main frame, therefore, has smaller dimensions than the above approaches to a solution. This advantage can be put into perspective by the fact that the hub is accordingly larger because of the large bearing diameter, however. The other disadvantages of the direct drive with moment bearing have also to be taken into account here.

Amongstthe TOP10 OEM 2021 SGRE and Goldwind rely on this drivetrain concept.

5.3 1–2 Stage Gearboxes—Two-Point Mount

The drivetrain concept presented in this and the following paragraphs is based on a 1–2 stage gearbox and a medium-speed generator. This version, which is also known as a hybrid drivetrain, attempts to combine the advantages of the direct drive (see Sects. 5.1 and 5.2) with those of the classic drivetrain concept with multi-stage gearbox (see Sects. 5.5 and 5.7). The result is a gearbox which is smaller than that of the classic 3–4 stage gearbox concepts, and a generator which is more compact than in the gearless drivetrain concept, so that overall lower tower head weights can be achieved. The hybrid solution is the most recent drivetrain version, which explains why it is not as widespread as the other concepts.

The complete integration of the drivetrain components into the main frame (see Multibrid M5000, Adwen AD-5 or aerodyns SCD) which often goes hand in hand with this supports the successful implementation of this objective. On the other hand, one has to consider that the repair possibilities with these concepts without dismantling the tower head are extremely limited.

In this section, we first turn our attention to the hybrid designs with a two-point mount. The Clipper Liberty 2.5 MW WTG can be presented as a solution which has
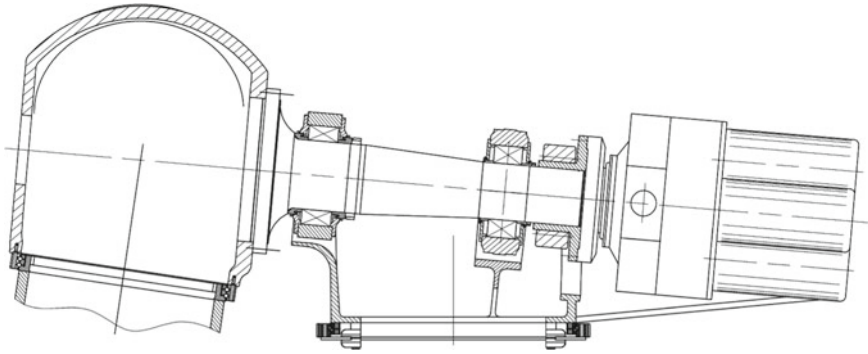
Fig. 43 Drivetrain concept [aerodyn]

been implemented. This turbine design is similar to the one shown in Fig. 43. The gearbox has 4 outputs, a generator being attached to each one.

The good isolation of the components from the rotor loads and the resulting simpler design can be considered as advantages of this design. A further advantage is the fact that a generator is easy to replace in the event of failure because the individual generators are small. As far as the bearing concept is concerned (this applies to all drivetrain concepts with two-point mount), the supplier situation is favourable.

This solution has disadvantages as well. Apart from the long and heavy rotor shaft, the actual construction of the mechanical rotor brake also presents a technical challenge. And there is also the custom-made gearbox, which creates a dependence on the supplier.

Gamesa (now SGRE) has developed a 5 MW turbine with two-stage gearbox and medium-speed generator. A special characteristic here is the linkage of the components (see Fig. 44). The front of the rotor bearing assembly housing is connected directly to the main frame. The gearbox is flange-mounted behind it, and the generator is mounted behind this. A tubular spacer is used here, which also accommodates the coupling. The complex part of this solution is the realisation of the signal and electric power connection of the components located in the hub.

This concept is gaining in popularity especially for large offshore turbines, since an increase in reliability is expected because the third gear stage is not required and the generator speed is lower. Vestas has likewise put its faith in the two-point mount, medium-speed concepts with the V164, its 8 MW offshore turbine.

Amongst the TOP10 OEM 2021, this drivetrain concept is used by Vestas, Shanghai Electric and CRRC.
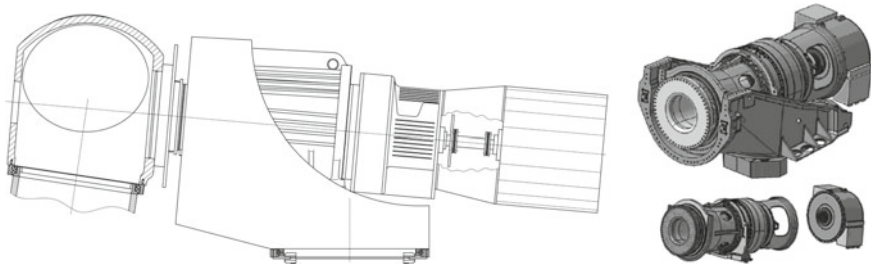
Fig. 44 Drivetrain concept [left, aerodyn] and mounting concept with drivetrain of the Gamesa 4.5 MW [right, by courtesy of Gamesa Adwen]

5.4 1–2 Stage Gearbox—Moment Bearing

The WTG Adwen AD-5 (formerly Multibrid, now SGRE) has an integrated hybrid drivetrain with moment bearing. It resembles the drivetrain concept in Fig. 45, which depicts a gearbox integrated into the yaw bearing and a medium-speed generator with the corresponding diameter.

The mount of the extremely compact drivetrain of the Adwen AD5 consists of a two-row tapered roller bearing, into which a special form of a planetary gearbox has additionally been integrated (see Fig. 45, right).

Not only the bearing and the gearbox but the generator as well is integrated into the main frame. The drivetrain of this WTG has very small dimensions due to the high level of function integration and the short rotor shaft, and is therefore very light.

The construction of this design also presents a technical challenge, however. Both the gearbox and the generator are subjected to the rotor loads because of the function integration discussed. While in the case of the generator it is mainly the air gap which is affected, the engagement of the teeth can be impaired in the gearbox. Furthermore, a design solution needs to be found for the access to the nacelle. Since most components are custom-made developments, problems with suppliers can emerge here as well.
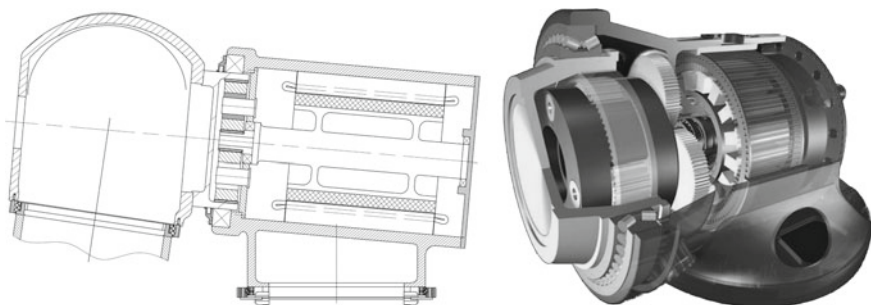
Fig. 45 Drivetrain concept [left, aerodyn] and head support of Multibrid M5000 [right, aerodyn]
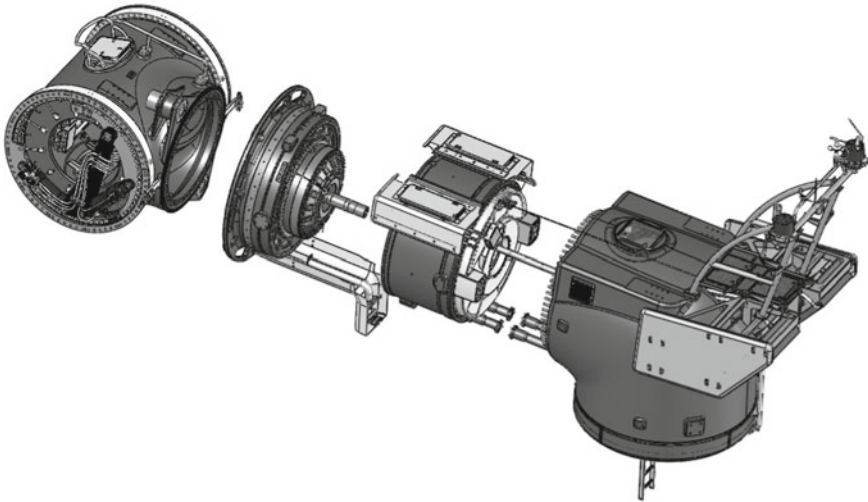
Fig. 46 Nacelle of the SCD 3.0 MW [aerodyn]

The SCD (Super Compact Drive) concept is a design from aerodyn with a two-blade rotor, which is being built by a Chinese manufacturer as a 3 and 6 megawatt turbine. The concept uses a modular arrangement whereby the tubular gearbox and generator are bolted one behind the other onto the head support. All components stated have almost the same diameter and are bolted together at the outer ring. The load path of the rotor loads, therefore, runs through the housings of the drivetrain components via the head support into the tower.

The head support looks basically like a tubular elbow section, where the drivetrain is connected at the side with nearly horizontal axis and the head of the WTG is mounted on the tower on the other side with a vertical axis. This concept thus no longer has a nacelle with casing in the conventional sense. All peripheral devices are arranged in two storeys in the head support and tower (Fig. 46).

Such fully integrated systems are advantageous when the WTG manufacturers have high vertical integration and large quantities are built. The FWT 3000 (formerly Fuhrländer) WTG can be given as a further development with moment bearing and two-stage gearbox (Fig. 47). The gearbox and generator are realised as an integrated solution, but are not fully integrated. The advantage here is that the gearbox and generator can be replaced without having to dismantle the rotor. Amongst the TOP10 OEM 2021, MingYang uses this concept with its MySE11-203.
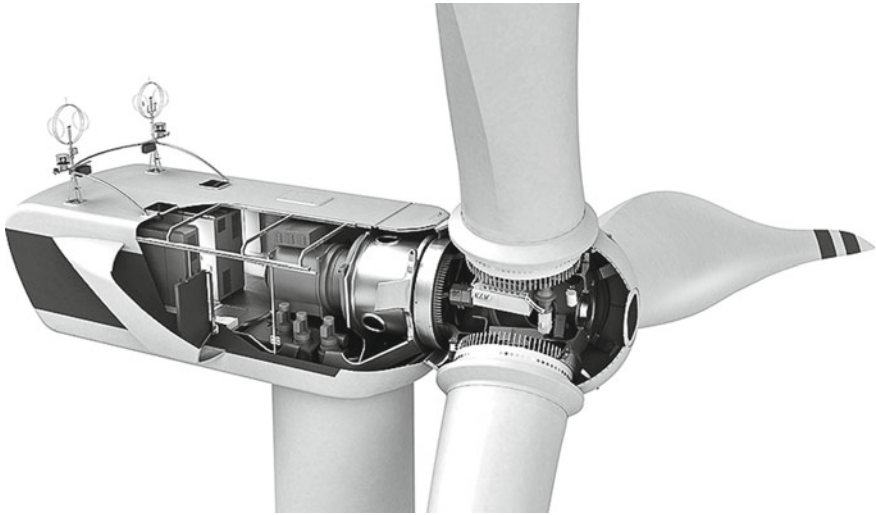
Fig. 47 FWT 3000 [FWT]

5.5   3–4 Stage Gearbox—Two-Point Mount

The two-point mount with multi-stage gearbox represents the classical design of a drivetrain with separate systems. The solutions known as standard constructions and most frequently implemented in practice have already been presented in Figs. 11 and 12 and described in Sect. 4.3.

Both versions conduct the greater part of the rotor loads directly into the main frame via the mount so that the gearbox and the generator are exposed only to the torque. The supplier situation is accordingly good because of the large number of turbines developed on the basis of these concepts.

To provide only a few examples for this type of WTG, the Vestas V80, Siemens (now SGRE) SWT 3.6-107 or the Senvion (formerly Repower) 5 M can be given as well-known representatives of the version with separate bearings.

The version with a sealed bearing housing is mainly represented by WTGs from GE, SGRE (Onshore, formerly Gamesa), Vestas or the aeroMaster family (1.5, 2.5, 3.0, 5.0 MW) from aerodyn Energiesysteme GmbH. As has already been described in Sect. 4.3, the advantage of the arrangement is the use of zero-clearance bearings. This increases their reliability. The most important aspect here is the fact that the axial movement of the drivetrain is eliminated, which ultimately benefits the gearbox as well (Figs. 48 and 49).

As has already been mentioned in Sect. 5.1, ALSTOM (now GE) uses a rotor bearing assembly where the rolling bearings are arranged on a shaft journal. The goal of conducting the bending moments of the rotor directly into the tower and transferring only torque to the drivetrain (Fig. 50) is the same here as in the case of the direct drive offshore turbine. The only special feature of the otherwise conventional
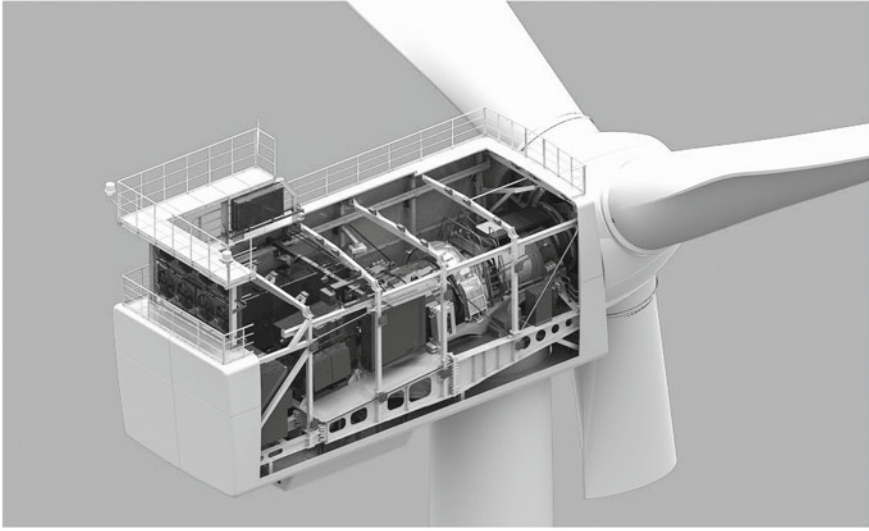
Fig. 48 Nacelle of the aeroMaster 5 MW from aerodyn Energiesysteme GmbH [aerodyn]
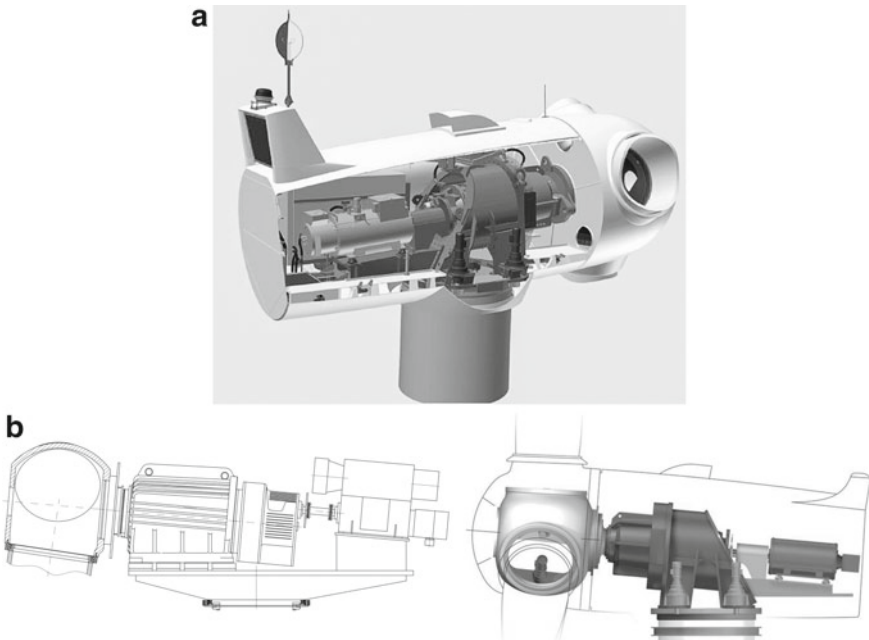
Fig. 49 Drivetrain concept [right, aerodyn] and implementation with the 1–65 MW turbine of AMSC [left, AMSC]
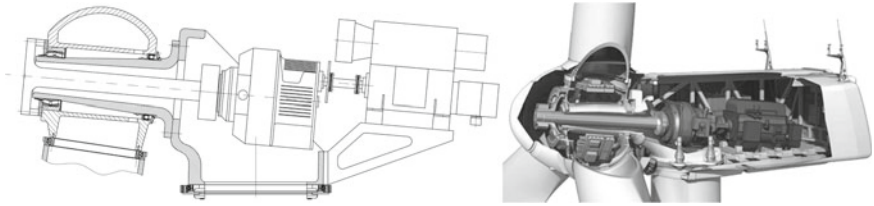
Fig. 50 Drivetrain concept [left, aerodyn] and nacelle of ALSTOM ECO 100 with Pure-Torque®technology [right, GE Renewable Energy]

drivetrain is the rotor shaft which runs in the shaft journal. It exits the shaft journal at the front where it is flange-mounted to the hub.

A further drivetrain configuration based on a two-point mount is presented in Fig. 51 and is mainly to be found in older WTGs.

In this concept, the generator is arranged on the housing of the rotor bearing assembly and the gearbox is used to realise the axial offset. Since the drivetrain runs in a kind of U-shape, it is relatively short and high so that an additional generator support is not required.

Considering the TOP10 OEM 2021, the drivetrain concept described above consisting of a two-point mount and a gearbox with more than 2 stages is actively being developed by SGRE in the onshore segment and Windey from China.
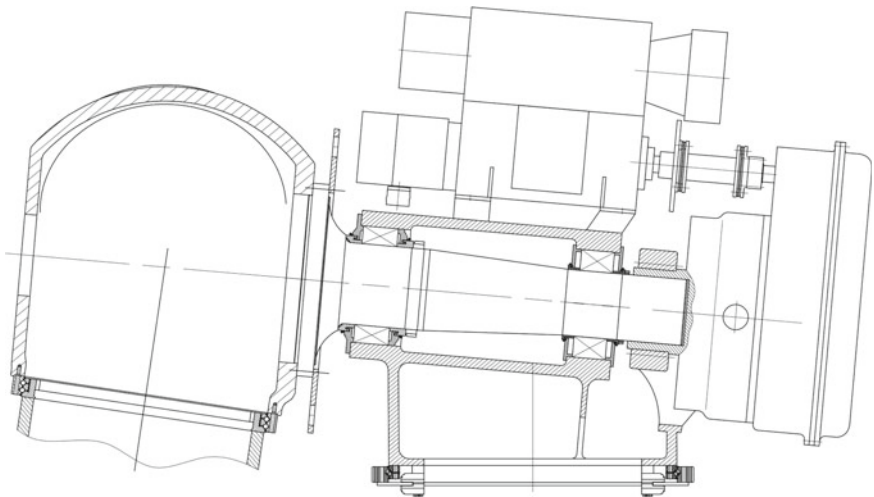
Fig. 51 Drivetrain concept of the Komai KWT 300, the HSW 1000 and the Dan-Win27 [aerodyn]

5.6 3–4 Stage Gearbox—Three-Point Mount

The three-point mount concept has already been described in detail in Sect. 4.3. Many of the established market leaders use this concept. It can be found in the onshore designs of GE, Nordex, SGRE and Vestas, for example. Some of the manufacturers also use other concepts in parallel. The three-point mount has turned out to be reliable and low cost, and is probably the concept which has been built most frequently to date.

As is the case with every standard construction, favourable supplier situations regarding the components can be expected for this version as well (Fig. 52).

A drivetrain concept with a very similar arrangement is shown in Fig. 53. Here, only a variable torque converter is introduced into the drivetrain between gearbox and generator. Its task is to keep the speed on the output shaft towards the generator constant and thus simplify the grid connection of the wind power turbine. The objective is to do without the frequency converter, which is needed with turbines with

Fig. 52 Nacelle of the Vestas V136-3.45-MW WTG [c Vestas Wind Systems A/S, by courtesy of Vestas]
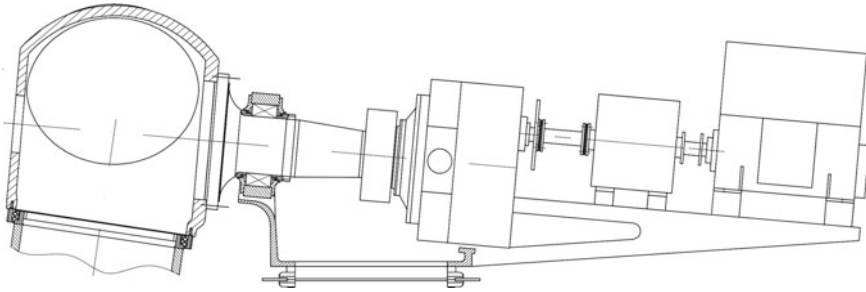
Fig. 53 Drivetrain concept [aerodyn]

fixed transmission ratios and variable generator speed. Since the structure of the actual drivetrain remains unchanged here, i.e. a gearbox with high transmission ratio is required here as well, the advantages and disadvantages of the previous structure apply to this solution as well. In the DeWind example, a hydrodynamic converter is used, as described in Sect. 4.4.

Amongst the TOP10 OEM 2021, this drivetrain concept is in widespread use with GE, Vestas, SGRE, Envision, Windey and CRRC.

5.7   3–4 Stage Gearbox—Moment Bearing

In the last position of the drivetrain matrix we continue with our considerations of drivetrains which use a gearbox with large transmission ratio and high-speed generators. The mounting concept used here is the moment bearing described in Sect. 4.3 (Fig. 15).

First, we consider a solution whereby the drivetrain with separate systems is combined with the said moment bearing. This results primarily in a short drivetrain but standard components can still be used. Availability problems can arise only in respect of the moment bearings because they are custom made.

This drivetrain has been realised in the 5 MW offshore WTGs from Bard, Mitsubishi (MWT 92/95), Fuhrländer (FL 2500) Fig. 54 and Unison (U 88/93), for example.

Vestas also uses this concept for the V90-3.0 MW. To minimise the drivetrain even further, however, function integration is used in accordance with the Multibrid concept (see Sect. 5.4) and the rotor bearing assembly is arranged in the gearbox. In contrast to the Multibrid concept, the generator is arranged separately, however, and the turbine has a three-stage gearbox which is only partially enclosed by the main frame.

None of the TOP10 OEM in 2021 is actively pursuing this concept now.
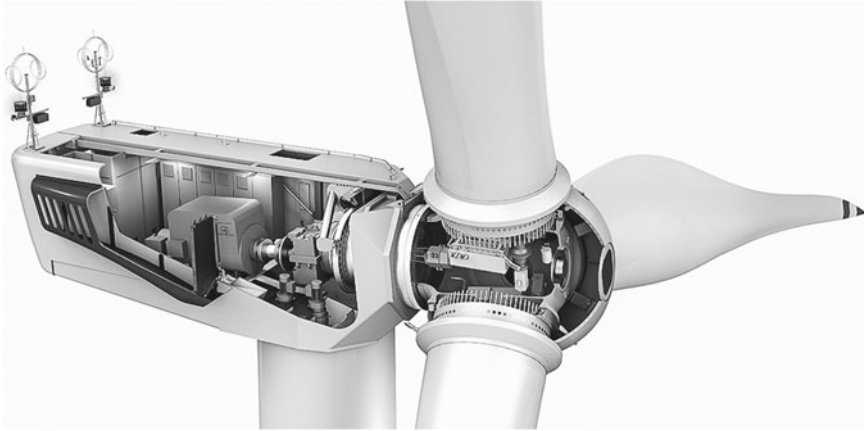
Fig. 54 Drivetrain with moment bearing FWT 2500 – formerly Fuhrländer [FWT]

6 Damage and Causes of Damage

Damage and the associated costs to repair a WTG can represent a significant proportion of the electricity production costs. The resulting risks for the operator of a wind farm can be mitigated by appropriate types of insurance or by directly commissioning the WTG manufacturer with maintenance and repair. In the early years of industrial wind energy at the end of the 1980s/beginning of the 1990s, the design methods were still inadequate so that much of the damage was caused by design faults. In general, it has been possible to significantly improve turbine reliability, even if there is still a need for improvement. One of the main challenges is the short development times of bigger and bigger turbines with sometimes very short testing times. The mass production of several new types of turbine starts even before it has been possible to identify technical deficiencies and remedy them by means of an appropriate modification. The two graphs below (Figs. 55 and 56) give an overview of the causes of damage and the resulting downtime categorised according to the components or sub-systems of a WTG.

Main causes of damage:

- Design faults,
- Quality defects during manufacturing,
- Wind events at the site for which the turbines was not designed,
- Inadequate maintenance.
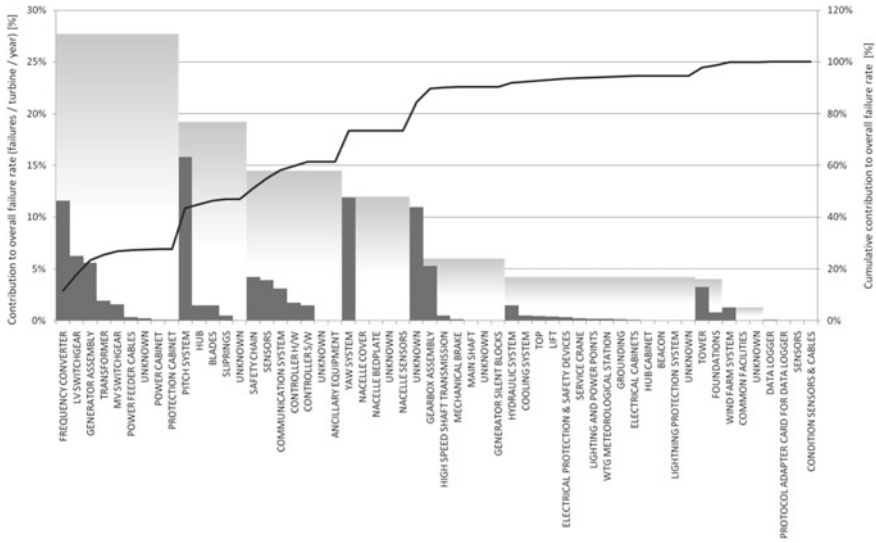
Fig. 55 Failure rate as per Reliawind study of the European Union [DNV GL]
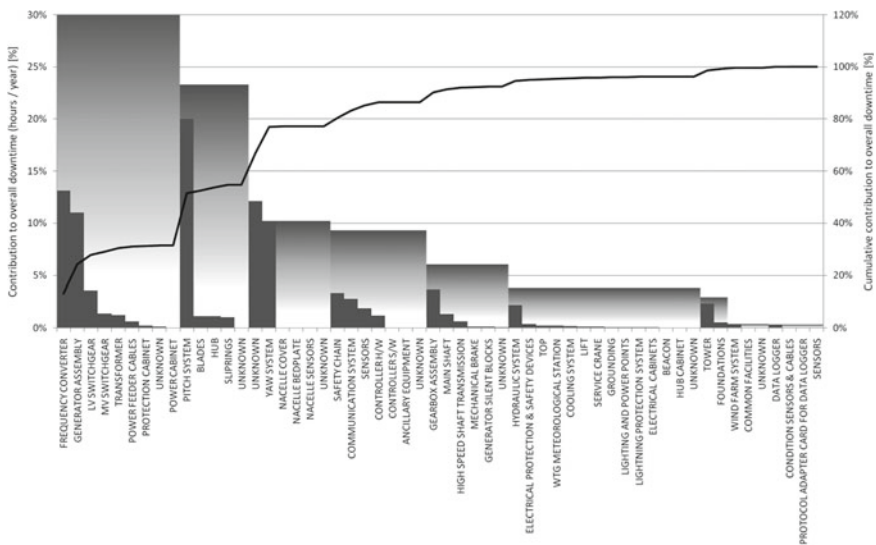
Fig. 56 Downtime as per Reliawind study of the European Union [DNV GL]

7 Design of Drivetrain Components

The design of WTG drivetrain components is characterised by the fact that the wind industry is a relatively young sector, which is why the design verification

uses modern approaches. Tools such as the finite element method (FEM) and simulations of dynamic processes have long been part of the standard repertoire of WTG developers.

The design of the structural components is mainly done by the turbine manufacturers, whereas the outsourced parts such as gearboxes or rolling bearings, for example, are predominately designed by the suppliers.

User requirement specifications and functional specifications are usually used for the coordination between turbine manufacturer and supplier, in which turbine developers specify the requirements for the components very precisely.

Guidelines and standards, which form the basis of the WTG certification, play a major role in the design of the WTG and its components. They specify which verifications have to be provided and the safety factors which the developments must comply with. The *Guideline Zertifizierung von Windenergieanlagen (Certification of wind turbine generator systems)* from DNV GL and IEC 61,400 are internationally recognised guidelines which are often used to design WTGs. The guidelines themselves place special demands on the components with regard to the safety factors and the verification, and close reference is made to existing component-specific standards from DIN, EN, ISO and IEC.

The development of every turbine design starts with a load calculation which is based on the statistical analysis of wind data. These data are used to simulate the loads acting on the turbine. The blade design is very important here. In addition to the blade length and the blade area, the blades can have many more characteristics which have a crucial impact on the loads occurring (stiffness, mass inertia etc.). The blade development and the load calculation are therefore two processes which usually take place in parallel at the beginning of the turbine development and have a big impact on each other.

The rough dimensions of the turbine are already specified in the load simulation. Several sectional planes are determined along the load flow which are used to define coordinate systems according to a standard. The resulting loads are determined for the individual sectional planes. Each component design refers to a specific coordinate system. Distinctions are made between coordinate systems such as blade root, tower head or rotor shaft. The hub-rotor shaft coordinate system is of main relevance for the design of the drivetrain. A possible coordinate system is depicted in Fig. 57. For a better understanding of what follows, all loads stated in this section refer to this coordinate system.

WTGs are usually designed for a service life of 20 years, the load calculation being based on statistical and stochastic evaluations to determine the loads for such a period. The above-mentioned Guidelines define precise load cases from which time series are generated which in turn contain information on the duration and characteristics of the ambient turbine conditions under specific operating conditions. In addition, they provide information about how often the time series occur over the whole service life of a turbine.

When evaluating the loads, a distinction must be made between service loads, which occur during normal turbine operation, and extreme loads, which occur under

Fig. 57 Coordinate system hub-rotor shaft [aerodyn]
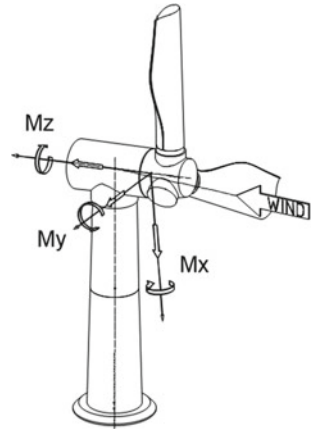
special conditions such as the failure of a component and are not included in the fatigue strength verification.

For the evaluation and utilisation for the verifications, the service load time series are aggregated to load collectives with the Rain-Flow-Count method, and the time durations of specific load levels are aggregated in LDDs (Load Duration Distribution).

Load Duration Distribution (LDD)

For the LDDs, the loads are subdivided into several levels and the length of time the particular load level occurs during the time series (load duration) is evaluated. Multiplying this by the frequency of occurrence of the particular time series during the total service life of the turbine gives a specific number of hours for this particular load level, which can then be used to determine the damage for a component. The frequency of occurrence results from the statistical distribution of the individual load cases, which are assigned to specific wind speeds.

When designing a drivetrain, the LDDs of the torque are used to design the gearbox gearing, for example. Figure 58 (left-hand side) shows by way of example how the LDD of a load component is derived from a time series.

Rainflow Counting (RFC)

The load collectives are determined by counting the load changes which a component experiences during its lifetime. Since these cannot simply be added together as in the case of LDDs, a special way of counting must be used, so-called rainflow counting.

Here, the load cases are examined in respect of the course of the load cycles, and the load changes which occur for each load case are evaluated. Multiplying by the frequency with which the load cases occur over the total life of the turbine, it is also possible to determine how frequently the components have to bear the load changes. After all load time series have been processed with the rainflow counting method, the height (amplitude) and frequency (number of cycles) of all load changes
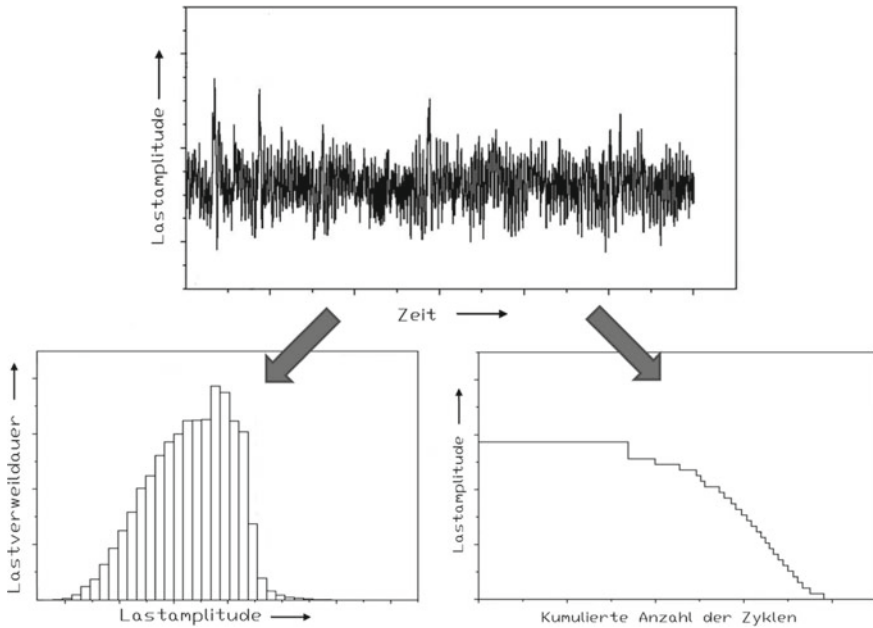
Fig. 58 Time series in LDD and RFC representation

are available. When the impact of the average stress is important for the verifications, so-called Markov matrices are used, where the collectives are additionally classified according to an average stress impact. The number of load change levels selected has an effect on the accuracy of the computed results. The use of load collectives in the verification is ultimately only a simplification to shorten the computation processes. More exact results are achieved when the time series are used directly. This is used nowadays in the fatigue strength calculations of large structural components. Suitably specialised software is used for this purpose. Figure 58 (right-hand side) shows by way of example how an RFC of a load component is derived from a time series.

In addition to the pure input torque (Mz), forces and bending moments also act on the drivetrain, whereby it is primarily the bending moments that are important for the drivetrain dimensions. A distinction is made here between pitching moments (My) and yawing moments (Mx), which pivot around the horizontal axis and the vertical axis respectively (see Fig. 57). These moments lead to the largest drivetrain deformations, which are determined by means of FEM. Both the extreme loads and the service loads have to be taken into account when designing the drivetrain components. WTGs have comparatively high numbers of load changes. According to the requirements of the Guidelines, they are calculated for a service life of usually 20 years. The high-cycle fatigue calculation is carried out according to modern computation methods, which use fatigue damage calculations (finite-life or high-cycle fatigue strength) with different Wöhler curves. This chapter does not discuss the details of these computations.

The detailed design of the functional components such as the pitch system or the yaw system involves the use of special programmes to evaluate the loads. The results can then be used to dimension the drives.

For better determination of the dynamic effects and to avoid overloading components through local resonances, simulation programmes are now used which either analyse the resonances within the drivetrain or are even used as the complete load calculation software to determine all loads within the drivetrain with greater accuracy. Setting up a model of such a detailed simulation is very complex, since in addition to all mass and stiffness data, decisions must be made as to the numbers of teeth, clearance or ball-pass frequencies of the bearings, for example.

The first software solutions for the detailed investigation of the dynamics of drivetrains was only able to simulate the torsional behaviour of the drivetrains. The best known software for this is the torsional vibration simulation software DRESP, which is still widely used. Modern simulation software can take account of several degrees of freedom for the components, and is known as multi-body simulation software (MBS software). Figure 59 shows the model of a drivetrain derived by means of such software.
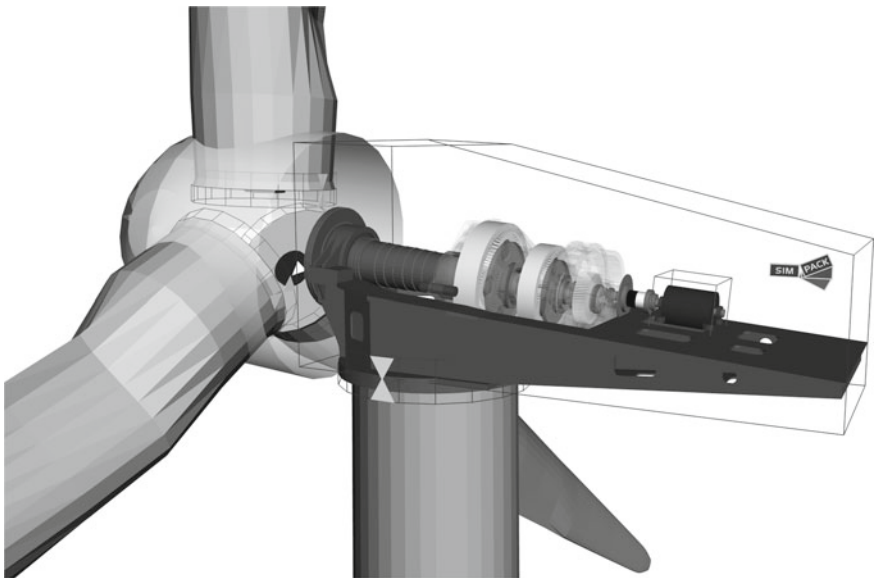
Fig. 59 Model 5 MW drivetrain resonance analysis [SIMPACK GmbH, TU Dresden IMM]

8 Validation

Validation provides the assurance that the properties of the product allow it to be used for its intended purpose. Section 6 discusses WTG damage and causes of this damage. Section 7 explains the fundamentals of WTG design. This section is concerned with validation, and supplements the two preceding sections in as far as validation improves our understanding of the model, and this can then be applied to the design, thus allowing damage to be minimised. The overriding intended purpose of a WTG is to convert mechanical into electrical energy. Validation provides the assurance that this objective has been achieved. A common methodological approach to conducting the validation is the so-called V-model according to VDI Guideline 2206 [4]. Figure 60 shows what an excerpt from the V-model can look like using the example of a WTG.

According to the methodology described in VDI 2206, the principal intended purpose(s) is/are converted into detailed product requirements during the system design of a product (in this case a wind turbine). This creates a large number of requirements for the particular levels of consideration (e.g. whole system, sub-system, component and material). The product development according to the V-model includes the verification that all these requirements are complied with. The verification can be carried out on the virtual, partially real or completely real prototype.

The validation activities can have very different objectives here. Typical validation objectives can be function test, robustness verification, lifetime verification or model validation. The accuracies required for the validation measures depend crucially on the costs associated with them and the risk considered.
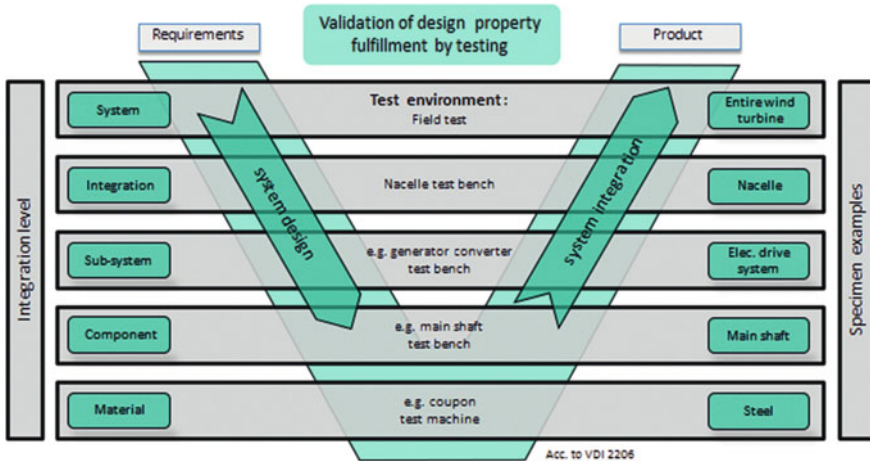
Fig. 60 Illustration of the application of the V-model to a WTG
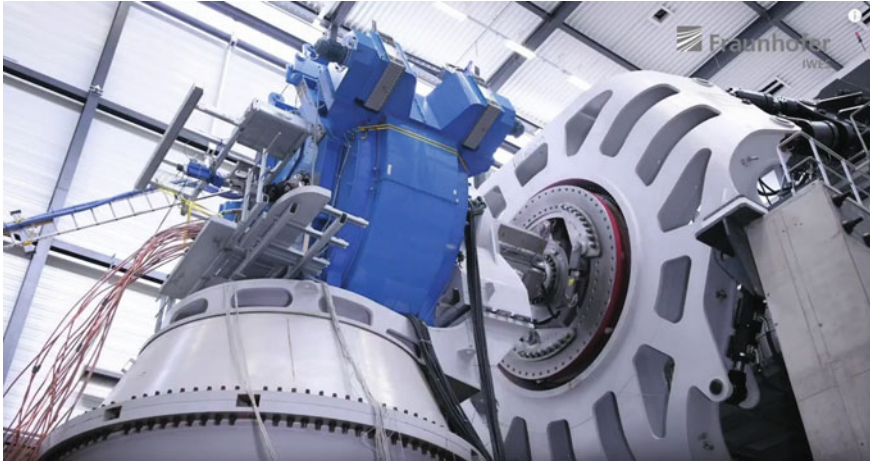
Fig. 61 Gearless HTS generator (blue) on the nacelle test rig [Fraunhofer IWES]

One interesting example of the application of a validation project is a nacelle test campaign. The development of suitable system test rigs means it is now possible to undertake experimental examinations of complete nacelles, drivetrains and generators of gearless turbines. The preparations for such a campaign to integrate the test specimen can take up to one year. The work which needs to be carried out includes the design and procurement of the necessary mechanical adaptors and the cooling. Furthermore, the test specimen must be integrated into the electrical system and the control system and the metrological concept must be planned. It takes around 3 to 12 months to carry out a nacelle test campaign, depending on the objective and scope. Some of the tests which can be performed are: model validation, modal analysis, heat runs, ramp up, lubrication, isolated operation, fault ride through, frequency variations, flicker, grid impedance, etc. Figure 61 shows the test setup of such a test campaign using the example of a high-temperature superconducting (HTS) generator for future use in a gearless WTG. This test campaign was carried out as part of the EcoSwing project, which was funded by the EU.

9   Intellectual Property Rights in Wind Energy

In wind energy, the importance of intellectual property rights has increased significantly over the last 20 years. The number of patent applications in Germany in the patent subclass F03D Wind Motors increased to a maximum in 2012, for example, and has remained on a similarly high level ever since.

Those wanting to develop, build, sell or operate wind turbine generator systems must critically examine this large number of patents which have been granted or applied for. The intellectual property rights must be analysed and evaluated for

possible conflicts with one's own design solutions or methods. This is particularly difficult in the case of intellectual property rights which have not yet been granted because at that point in time, it is not yet clear how large the scope of protection will be when they are granted. This process is made more difficult by the fact that a new application is only published after 18 months. If any intellectual property rights are particularly troublesome for one's own venture, or maybe there has even been a violation, it is then necessary to investigate whether the intellectual property right can be circumvented by other technical solutions or can be nullified. It is thus necessary to determine the prior art before the application date which conflicts with the patent claims and was not available to the examiner at the patent office.

An overview of all published intellectual property rights can be obtained from various Internet databases, some of which have good search tools. Patent databases are furthermore an excellent tool to generate one's own ideas or further developments. To examine whether your own good ideas can be protected, a comprehensive search regarding the degree of novelty and the non-obviousness must likewise be carried out.

Approx. 90% of the technical know-how subject to intellectual property rights is published only in patent specifications and not in other publications. Patent specifications with their full text can be downloaded from the Internet portal of the European Patent Office (https://worldwide.espacenet.com/).

Figure 62 shows the graph of global patent applications for the years 1970–2008. Before the 1970s, there was hardly any activity as far as applications for wind energy patents were concerned. It was not until the first oil crisis in 1972 that people started to give more thought to wind energy utilisation. This also coincided with the first patent applications. Over the next 25 years or so, the number increased by approx. 200 applications per year. At the turn of the century, there were approx. 5,000 patents worldwide. The numbers of patent applications then increased drastically so that today, approx. 5,000 documents are added every year.

Figure 63 shows how the patents overall are distributed over the individual countries, whereby the first application and any national versions in other countries are counted as one. It can be seen that countries where wind energy utilisation is of significant importance are most active in respect of patent applications. The leading countries include China, the USA and Germany. Despite low levels of wind energy utilisation, countries such as Japan, Korea and Australia have a large number of applications.

Figure 64 shows the distribution of patent applications categorised according to applicant until 2012. The information is arranged according to WO applications (international applications) and not national first applications, because a WO application is much more important due to the large number of national applications which may possibly be derived from it. General Electric led the field at that time for national first applications with around 660, but less than 10% were transferred into global applications. Vestas, the global market leader, transferred approx. 370 of approx. 450 first applications into the international process. Other top-ranked applicants included companies such as Mitsubishi, Enercon, Siemens, LM Glasfiber and Gamesa.
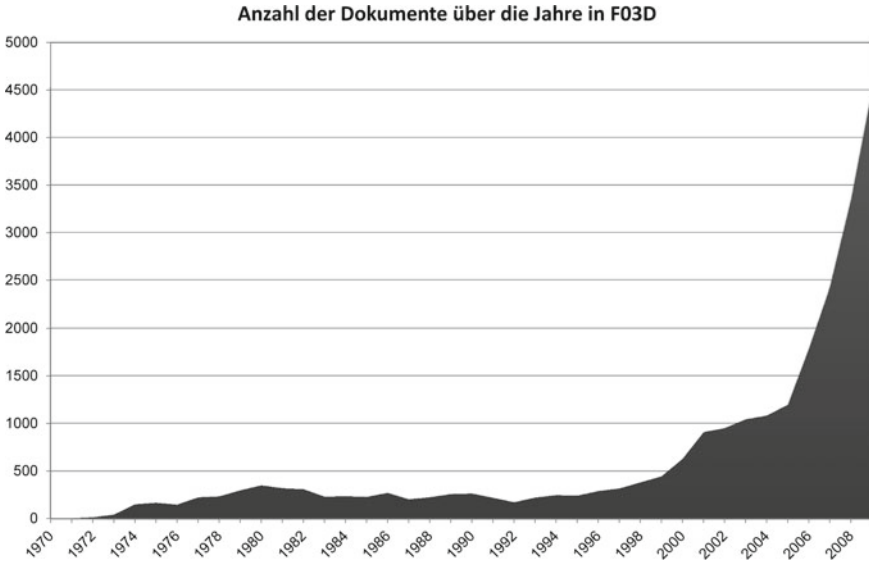
Fig. 62 Annual new applications
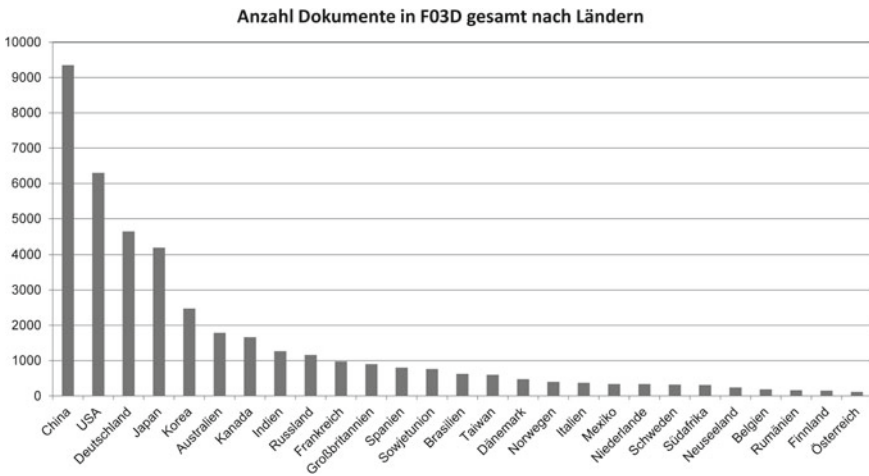
Fig. 63 Distribution of the patents according to countries (last update 2012)

Exemplary Patents for Drivetrains

Excerpts of three patent applications for different drivetrain designs are presented by way of example. A gearbox system with high transmission ratio, a direct-drive system, and a hybrid solution with only two gear stages were selected at random. Globally, there are more than 1,000 patent specifications relating to very

Gegenüberstellung der Anmeldungen WO und Gesamt
Top 25 der Wettbewerber
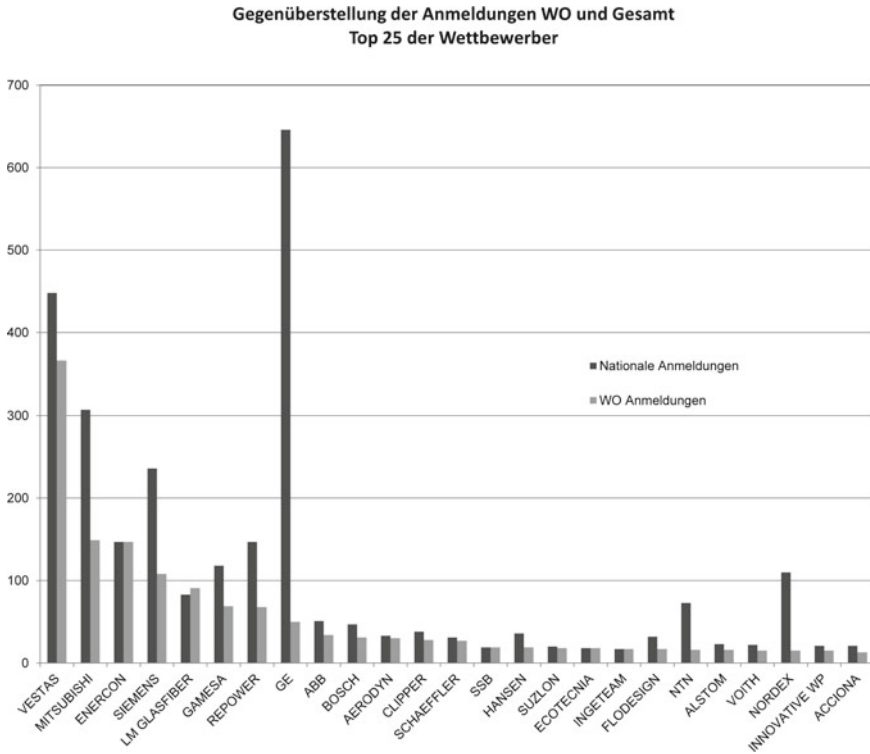
Fig. 64 Top-25 applicants (last update 2012)

different drivetrains, whereby all solutions have their own specific advantages and
disadvantages.

**Electrical energy generating installation driven at variable rotational speeds,
with a constant output frequency, especially a wind power installation WO
2010/121783 A1**

The invention relates to an energy generating installation, especially a wind power
station, comprising a drive shaft connected to a rotor, a generator and a differential
transmission provided with three drives or outputs. A first drive is connected to the
drive shaft, an output is connected to a generator, and a second drive is connected
to an electrical differential drive. The differential drive is connected to a network
by means of a frequency converter. The objective of the invention is to reduce the
harmonics.

According to the invention, this objective is solved by the fact that the frequency
converter for the active filtering of harmonics of the energy generating installation,
in particular the generator, can be controlled. This means that when designing the
generator, less or no consideration at all must be given to harmonics reduction.
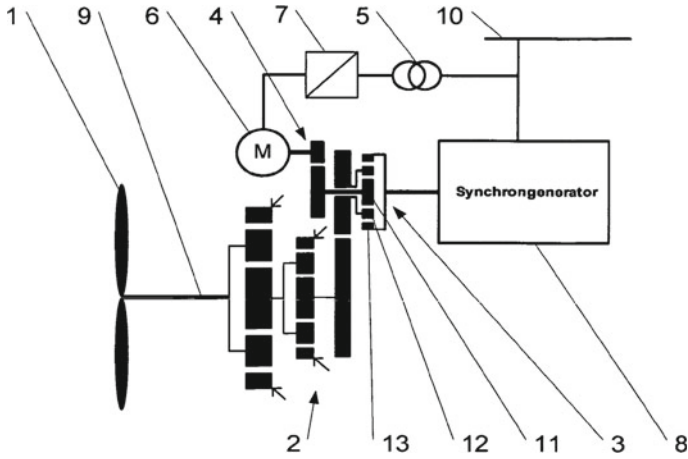
Fig. 65 Variable-speed gearbox

Patent claim 1

Energy-generating installation, especially a wind power installation, with a drive shaft connected to a rotor (1), a generator (8), and with a differential transmission (11–13) with three drives and outputs, a first drive being connected to the drive shaft, an output to a generator (8), and a second drive to an electrical differential drive (6, 4), and the differential drive (6, 4) being connected to a network (10) via a frequency converter (7, 5), characterised in that the frequency converter (7, 5) can be controlled for active filtering of harmonics of the energy generating installation, especially of the generator (8) (Fig. 65).

Wind turbine generator system DE 102 39 366

The present invention is based on the objective to create a new wind turbine which allows a reduction of the construction length of the rotor/generator assembly which protrudes laterally from the carrier tower by means of a constructional simplification and reduction of the mass. The wind turbine generator system according to the invention which solves this objective is characterised by the fact that the vanes of the wind rotor are arranged on the rotor ring or/and an axial extension of the rotor ring.

Advantageously, this solution to the invention allows the rotor to be moved back towards the support tower so that a central middle piece of the rotor, which holds the rotors in the extreme case that the rotor ring alone forms a hub of the wind rotor, protrudes from the support tower no further than the generator towards the axis of rotation of the rotor. In a particularly preferred embodiment of the invention, the rotor or the rotor ring, with the extension, if applicable, is mounted on a tubular support structure which holds the stator windings, whereby, compared to conventional wind turbine generator systems, a particularly large material and weight reduction can be achieved when the radius of the support structure or of the bearings is almost the same as the air gap radius of the generator. In this case, the air gap geometry of the generator

is sufficiently constant even if the generator parts have a weak, material-saving design. The possibly extended rotor ring can pivot on several bearings, which are arranged on an axis and separated from each other, or on a single bearing, preferably arranged at the transition to the extension. If the rotor ring alone forms the hub of the rotor or a part thereof, it is expedient to support it with two bearings, the stator windings being arranged between the two bearings.

Patent claim 1

Wind turbine generator system, particularly for rated powers in the megawatt range, whose wind rotor (4) is directly connected to a magnet-bearing (22) rotor ring (21) of a generator (5), wherein the vanes (26) of the wind rotor (4) are arranged on the rotor ring (21) or/and an axial extension (31) of the rotor ring (21) (Fig. 66).

Wind turbines with load-transmitting components DE 10 2007 012 408

The objective of the invention is to create a drivetrain which allows a very compact, light-weight and thus low-cost overall design, and integrates the main components such as rotor bearing, gearbox, generator and wind direction tracking device into the load path from the rotor to the tower. This is to ensure that the individual components, in particular gearbox and generator, can be mounted separately and handled individually for repair work as well (Fig. 67).

Fig. 66 Direct-drive wind turbine generator system
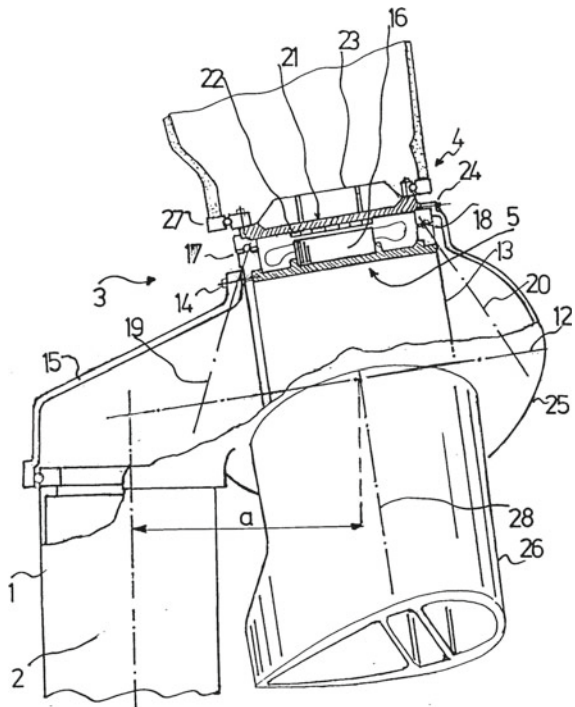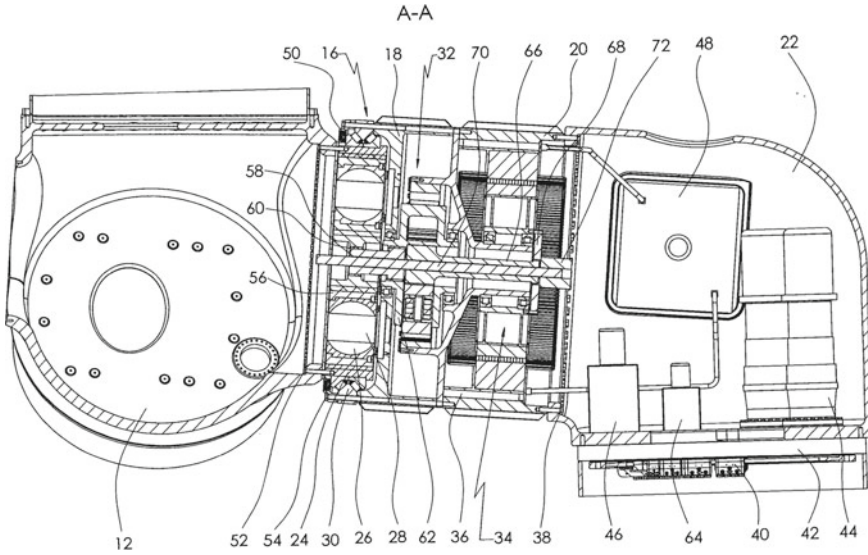
Fig. 67 Wind turbine generator system with load-transmitting components

In this invention, the components gearbox, generator and wind direction tracking are arranged in separate housings which are bolted together. Each housing is designed as a load-bearing structure to transfer the maximum static and dynamic rotor loads. The rotor bearing is also bolted to the gearbox housing and transfers the rotor loads into the gearbox housing. This housing transfers the loads to the generator housing. The generator housing in turn transfers the loads into the main frame, which in turn transfers the loads via the yaw bearing into the tower. This structure means the housings of the components take over the dual function of load transfer element and mounting element for the individual parts of the components. This design allows the machine to be very light-weight and thus low cost, and additionally obviates the need for a nacelle casing, because all components are designed such that they can be exposed to weathering. For ease of mounting, it makes sense to design the gearbox housing and the generator housing as two separate housings, but they can also be designed as one unit.

Patent claim 1

Wind turbines with at least one rotor blade (10), a hub (12), a gearbox housing (18) accommodating a gearbox (32), a generator housing (20) accommodating a generator (34), a head support (32), a tower (14), and an azimuth bearing (42) rotatably supporting the head support on the tower (14), characterised in that the rotor bearing (16), the gearbox housing (18) and the generator housing (20) are arranged between the hub (12) and the head support (22) and designed as load-transmitting components and joined together by means of bolted connections (54, 38).

Literatures

1. Stammler M (2020) Endurance test strategies for pitch bearings of wind turbines
2. Kyling H (2017) Präsentation: "Full scale main shaft fatigue testing" auf dem "Wind Power Monthly Drivetrain Component Optimisation Forum"
3. Rauert T et al (2014) Fatigue life of rotor shafts in theory, practice and in a full scale testing environment
4. VDI (2004) Richtlinie 2206, Entwicklungsmethodik für mechatronische Systeme

Dipl.-Ing. Hans Kyling is head of the department System Validation Mechanical Drive Train department at the Fraunhofer Institute for Wind Energy Systems IWES. For more than a decade, he has been involved in both numerical and experimental investigations of complete drive trains as well as individual subsystems and components of wind turbines.

Tower and Foundation

Torsten Faber

1 Introduction

Today's wind turbines (WTGs) reach to incredible heights. In 2020, the average turbine configuration in Germany reached a hub height of 135 m and a total height of approximately 196 m (including the rotor blades) [1]. The currently highest onshore turbine reaches a height of approximately 178 m using a hybrid tower and, with a total height of approximately 246 m, joins the league of the highest skyscrapers in Germany.

These impressively large structures are generally designed for a design lifetime of at least 20 years. Due to continuous further developments, the design lifetime of newer types has already been increased to 25 years and more. The turbine manufacturers guarantee technical availabilities of approx. 98%. The structure of a wind turbine is subjected to up to one billion load changes during its design lifetime.

The standard tower nowadays is a tubular steel tower and is formed by individual tower sections, which in turn are made of welded tower segments. A frictional connection is achieved by means of ring flanges with pre-tensioned bolts (see Fig. 1). Depending on the type of embedment, the foundation is connected to the tower by up to 240 pretensioned bolts.

The stresses acting on a wind turbine tower are demonstrated by the following example. For example, the wind impacting on the rotor at a WT with 2 MW and a tower height of 80 m, resulting in a horizontal thrust force of approx. 1500 kN at the tower top. This corresponds to the weight force of almost 100 cars of 1.5 each (100 * 1500 kg * 9.81 m/s^2 = 1472 kN). This thrust force pushes the tower top in the direction of the wind and generates a bending moment of approx. 110 000 kNm, which has to be absorbed via the tower, as a lever on the bearing (foundation).

T. Faber (✉)
Wind Energy Technology Institute, HS Flensburg, Kanzleistrasse 91-93, 24943 Flensbrug, Germany
e-mail: faber@hs-flensburg.de
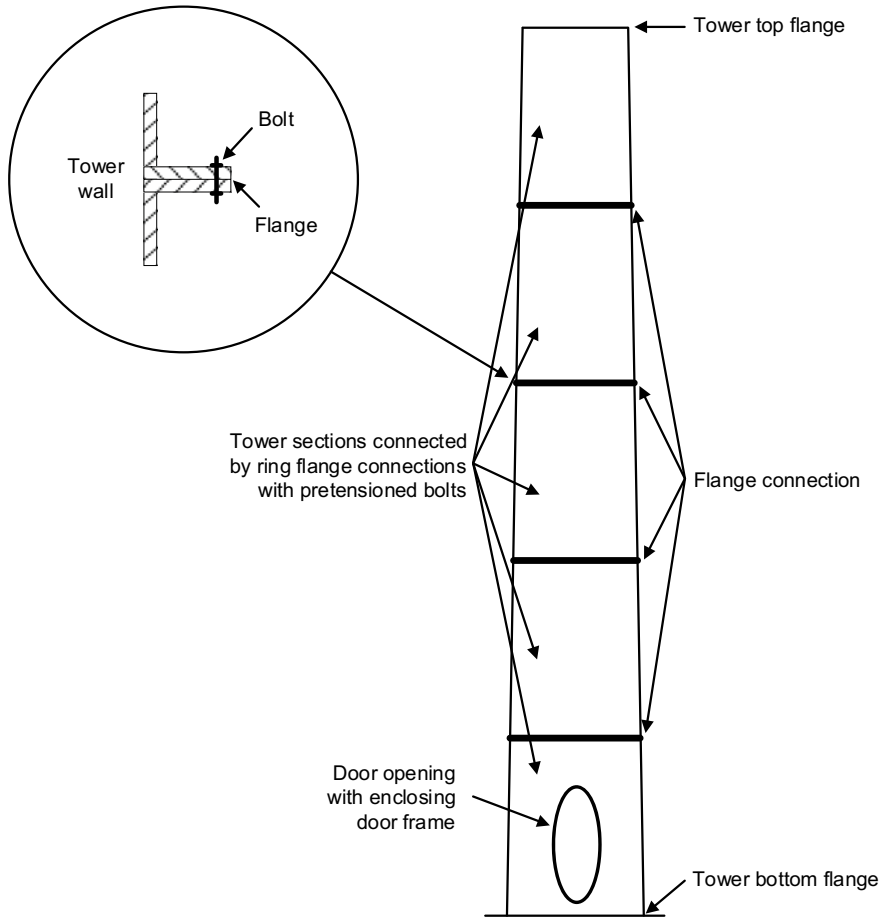
Fig. 1 Structure of a classic tubular steel tower [WETI]

The fatigue stress which the tower has to resist are up to one billion load cycles ($n = 10^9$) with an associated bending moment amplitude of about 15 000 kNm (considered simplified with a damage-equivalent collective). Following the example above, this moment at the tower bottom is then comparable to the weight force of 11 cars moving the tower head horizontally back and forth (see Fig. 2).

The manufacturing costs of the tower can account for up to one third of the total costs of a standard WTG. This is followed by the rotor blades with a share of approx. 20%. The foundation contributes only 5–10% to the costs and therefore plays a subordinate role.

The WTG is defined as a structure according to the "Guideline of the German Institute for Structural Engineering (DIBt)" from the tower head flange (without the bolts) downwards. The subsystem tower concerns the upper part down to the base flange without anchor bolts. The tower top bolts belong to the main frame and are

Extreme load:
Here pulls the weight of
100 cars.

Fatique load:
The weight of 11 cars pulls
back and forward.
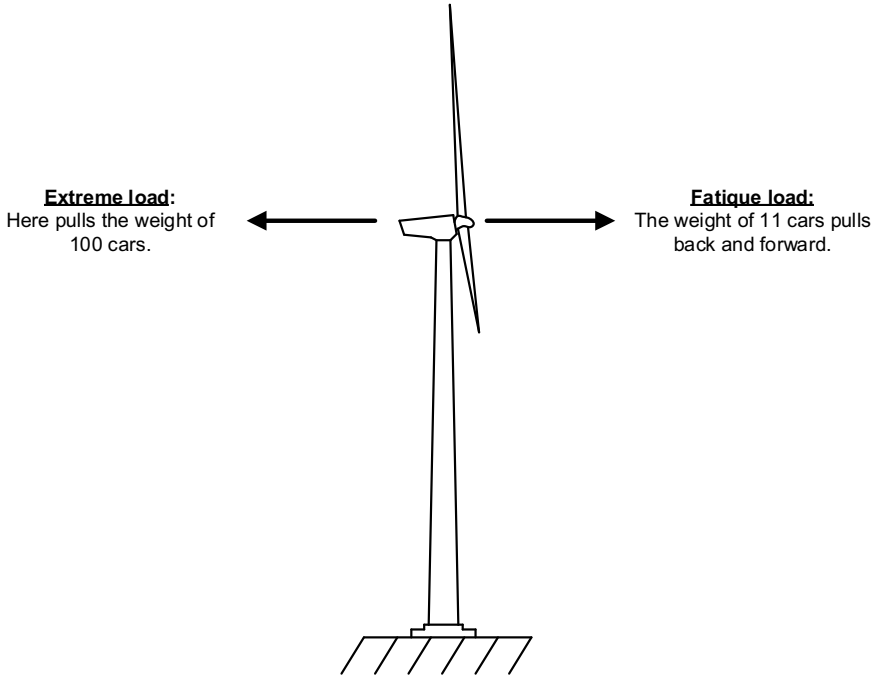
Fig. 2 Forces at the tower top of a wind turbine [WETI]

therefore verified with mechanical engineering standards (e.g. ISO). The anchor bolts at the bottom are usually calculated in the statics for the foundation.

Tasks for 1

- What is the height of the highest wind turbines today, including the rotor?
- What percentage of the total production costs of a wind turbine is accounted by the tower?

2 Guidelines and Standards

In Germany, the relevant standards for certification include the "Guideline for Wind Turbines" from the German Institute for Building Technology (DIBt) [2]. This guideline was developed in the project group "Wind Turbines" by engineers from the areas of research and industry. It concerns the verification of the stability of the wind turbine structure and special impacts on the same.

DNV provides extensive specifications, guidelines and recommendations. These guidelines deal with the entire WTG and can be seen as a common thread, which in turn refers in detail to other standards, e.g. the Eurocodes (EC) and standards from the German Institute for Standardization (DIN). An important standard for the steel

construction of a wind turbine is EC 3, which covers topics such as fatigue, material load capacity and crack propagation of steel structures.

The internationally recognized standard for wind turbines is provided by the International Electrotechnical Commission (IEC). IEC 61400 consists of several parts, each covering a specific topic. For example, part IEC 61400-1 specifies the design requirements of wind turbines [3].

Tasks for 2

Name three important standards, guidelines and specifications for wind turbines!

3   Stresses on Towers

In case of a WTG, in contrast to conventional structures, the static weight is relatively low in the ultimate limit state design and serviceability limit state design. In contrast, the load caused by the wind is the major stress component. As a rule, a wind turbine must withstand these dynamic fatigue loads at least for 20 years. To ensure that a wind turbine can withstand these loads, an accurate dynamic simulation of the extreme loads and fatigue loads on the entire system is required.

The basic requirement for availability is that the turbines or their components withstand the external stresses to which they are subjected during their design lifetime.

In current practice, the internal forces for the design of the individual components of a wind turbine are determined with the support of computer-based simulations in which stochastic load events of variable intensity as well as turbulent and laminar wind speed and direction are acting on an idealized wind turbine structure (see Fig. 3).

Thereby, the specific operation and control of the turbine is considered. Thereby, the specific operation and control of the turbine is taken into account. In the case of a stochastic load event, the internal forces are determined as a result of the turbulent
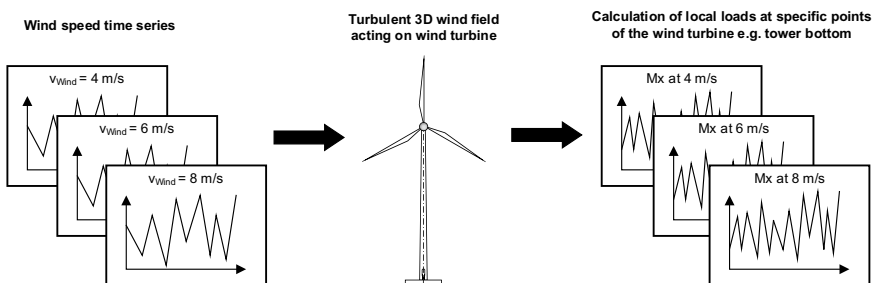
Fig. 3 Exemplary schematic load simulation for an onshore wind turbine [WETI]

wind and, if applicable, due to the irregular sea state prevailing offshore. In a deterministic load event, the internal forces are determined as a result of a discrete gust and, if required, a discrete regular wave.

The calculation requires an extensive amount of time and effort, which means that it is not possible to simulate the entire intended service life of the turbine. Instead, small time series (usually 10 min) are considered, each reflecting individual events according to the applied framework (standard, guideline) within the scope of so-called load cases.

These include start and stop events, grid failures, gusts, inclined flows, normal operation as well as combinations of these. The time series generated in these time intervals are extrapolated for the entire design lifetime. Statistical methods are used to calculate a time series for the design lifetime for each of the local forces to be considered, taking into account the probabilities of occurrence of the individual events. This is done for various previously defined (up to several hundred) design sections. The extreme and structural loads of the various load cases that are relevant for the structural design can also be extracted from the generated time series. For the design as well as for the potential lifetime extension consideration, it must always be kept in mind that the actually occurring loads can differ from the simulated loads depending on the location, therefore the wind class for the WTG is defined in advance.

3.1 Fatigue Loads

For the verification of fatigue, the potential loads for the entire lifetime are determined as time series. Since the further calculation with time series is only realized in very rare cases due to the high effort required, the load ranges for the design sections are usually classified using a suitable counting method (Rainflow—Count), which results in the so-called Markov matrices. These are generally easier to handle with sufficient information content (see Fig. 4).

For the fatigue analysis of e.g. steel components with linear relation between external loads and internal forces or stresses, the Markov matrices can be reduced
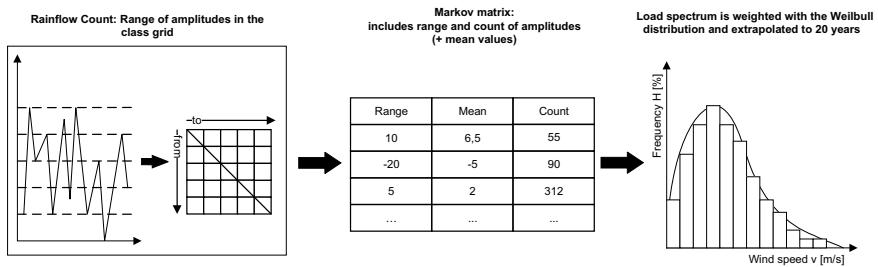
Fig. 4 Rainflow classification and extrapolation of load time histories to 20 years [WETI]

Load collective for 20 years   **Damage calculation with**
                                        material dependent Wöhler curves
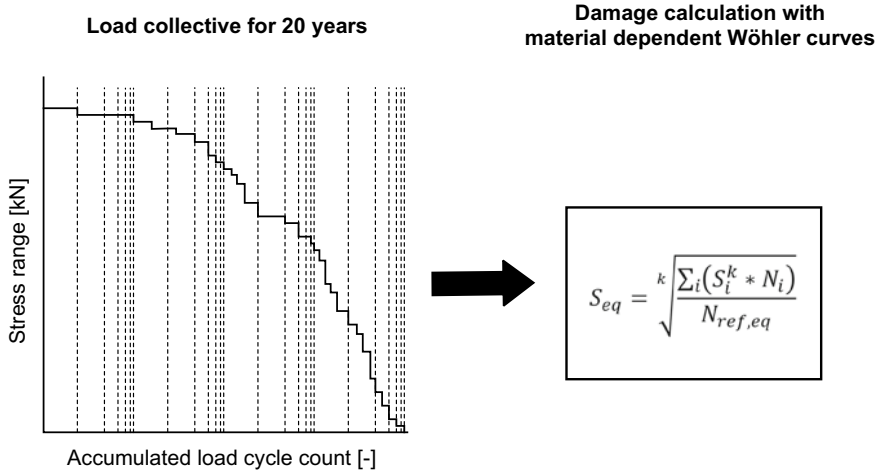
Fig. 5 Lifetime estimation [WETI]

in a further step directly to amplitude collectives with cycle counts assigned to each cycle range (see Fig. 5).

For structural components such as the tower top flanges, for example, the non-linear transfer function needs to be determined first by using FE calculations and then considered in the analysis. A further difficulty occurs if the material resistance is also mean-dependent, as is the case with reinforced concrete.

3.2 Extreme Loads

In addition to fatigue loads, a wind turbine must withstand extreme loads over short periods of time. For example, the bending moment at the tower base usually increases initially with wind speed. After a certain wind speed, however, it can decrease again, as the rotor blades are increasingly pitched out of the wind by the control. If the wind speed becomes too high, the WTG shuts down. The bending moment also decreases.

The event of a 50-year wind gust is rarely relevant for design. Much more critical is a combination of different extreme wind events. For this purpose, extreme wind events are combined with regard to their probability and the resulting load is calculated. This calculation is very complex and can vary in the result due to the simulated wind fields.

4 Verification for the Tower

The purpose of the load calculation is mainly to match the actual loads of a WT with the simulation. A lot of experience and understanding of the entire WT system are required for this. The verification concepts of structural engineering usually apply the beam or shell membrane theory. These theories do not initially consider local construction details such as the connectors or openings.

Up to two decades ago, the state of the art was to calculate the local forces at the tower using the loads at the tower top. A few years later, linear interpolation between the tower top and the tower bottom was used, and today the internal forces at all relevant points are calculated individually.

As in Fig. 6, the loads acting on the tower result in a simplified way from the machine at the tower top (mainly due to the rotor thrust), the self-weight of the tower and the wind load on the tower.
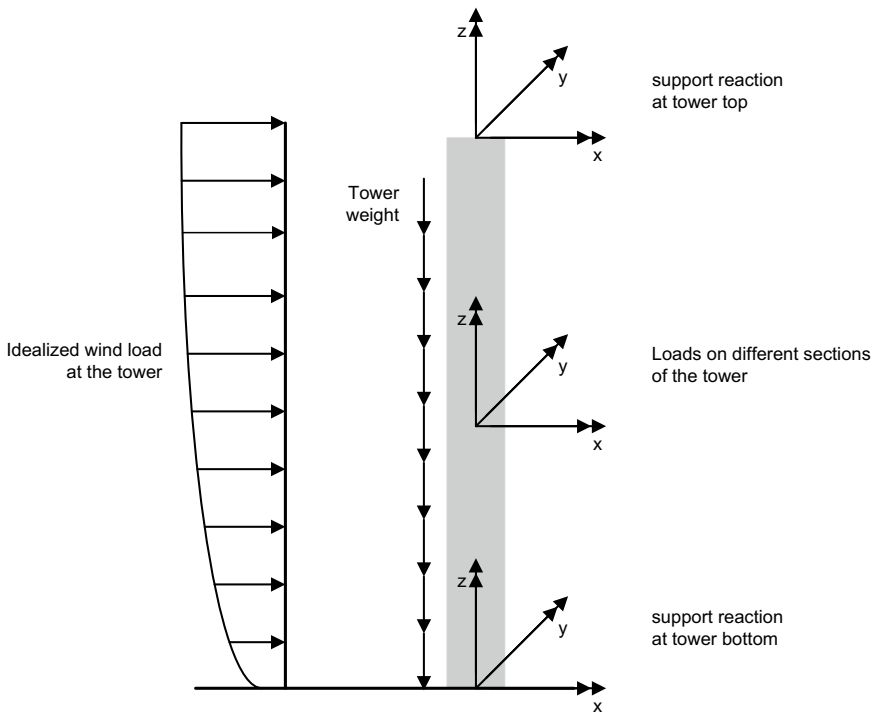
Fig. 6 Loads on the tower of a wind turbine [WETI]

4.1   Ultimate Limit State Capacity

For the verification of the ultimate limit state against material damage, the maximum stress is determined statically with the help of the transformation equations; this maximum existing stress covers all load cases. This side is called the loading side σ Fd. On the other side is the acceptable stress, the resistance side σ Rd where the proof of the resistance of the material is obtained considering the geometry (structure and cross section) and the material. It is necessary to apply σ Fd $\leq$ σ Rd, i.e. to exclude damage, the resistance side always has to be at least equal to or greater than the load side.

In civil engineering, there is the analysis concept with partial safety factors on the loading side and on the resistance side. On the resistance side, the partial safety factors depend on the material γ_m and the manufacturing accuracy of the geometry.

For fatigue loading, the partial safety factors are furthermore dependent on the detectability and the consequences of damage. For the fatigue loads, γ_m is, e.g., in the range of 0.9–1.25 depending on good or bad detectability, respectively, with accessibility and the consequences following the damage.

When the damage only leads to an interruption of operation, γ_m is in the range of 0.9–1.0. If the damage has more wide-ranging consequences as a result, γ_m is larger. In case of a total loss of the WT or hazard to people, γ_m is set to the highest.

In addition to material and cross-section, thickness also contributes greatly to the stability analysis. The stress verification is based only on the law: stress = load with respect to cross-sectional resistance. Depending on the stress, the material is either compressed or stretched. Stability failure is defined as buckling. As a consequence, the system deflects from the system planes or axes and abruptly fails.

For the design of the tower in the ultimate limit state, all stress verifications, the stability verifications against buckling and the fatigue strength verifications for fatigue are carried out. Details to be investigated separately are, for example, the flanges and the door opening on the tubular tower.

For the tower top flange, the excentric load application and the associated carding moment usually have to be verified with FEM calculations, and local excess stresses have to be investigated in the case of the door opening.

In the case of lattice towers, special attention has to be focused on the torsional softness and the connecting means of the individual beams, which are often manufactured as slip-resistant prestressed bolted connections. Very short clamping lengths should be avoided, since even slight settling leads to large prestressing losses.

4.2   Serviceability Limit States

In addition to the ultimate limit state, the serviceability limit state has to be verified. This includes specifications for the limitation of crack widths and deformations. The

last one requires, among other aspects, whether the clearance between the rotor blade and the tower is sufficient, considering the imperfections and deformations.

The partial safety factor for the resistance side is $\gamma_m = 1.0$.

4.3   Frequencies Calculations (Natural Frequencies)

The natural frequencies have to be determined for the entire structure and each individual component. Usually, the Campbell diagram is used to check whether the natural frequencies are outside the operating range of the excitation frequency. If this is not the case, dampers can be used if necessary.

The natural frequencies of a wind turbine tower are of major importance. If the system is excited at its natural frequency, resonance occurs. The tower oscillates and this can lead to damage or even complete failure of the tower.

The first and the second natural frequency of the tower are usually relevant, for lattice towers also the torsional natural frequency. The exciting frequencies result from the rotor speed of the WTG with its multiple depending on the number of rotor blades.

To prevent resonance, the excitation frequencies have to be at least a distance of plus/minus five percent from the natural frequencies of the tower. Operation close to the resonance range is only permitted in exceptional cases when using, for example, an operational monitoring system.

Figure 7 shows a Campbell diagram. This diagram is a method of eliminating overlap between the stimulating frequency and the natural frequencies of the individual components. The x-axis plots the speed of the operating range in revolutions per minute (rpm). The y-axis maps the natural frequency of the components in Hertz (Hz). Here the natural frequency of the component is plotted with a safety margin of $\pm 5\%$. For comparing the rotational speed n with the natural frequency f, the rotational speed must be converted into the frequency. This is done by the linear equation: $y = \frac{n}{60}$. This function is also called 1P or rotor frequency. This graph is plotted in the diagram including two graphs with $\pm 5\%$ deviation, which provide a further safety margin. Since a total of three rotor blades excite the system in most WTGs, the same is done for the triple value, resulting in a graph with the following equation: $y = \frac{n}{60} \cdot 3$. This straight line is called 3P and describes the blade passing frequency (Fig. 8).

The grey area in the diagram, where the excitation frequency and the natural frequency would overlap, should not cross the two lines 1P and 3P.

For towers with a low stiffness, the first natural frequency is below the 1P line. These are soft, mainly tall and slender towers. This is referred to as a soft-soft design. Most common are towers with a medium stiffness, so that the first natural frequency lies between the 1P and the 3P line (soft-stiff). Very stiff towers are unusual, they are above the 3P line (stiff-stiff) in the diagram.

In most cases (soft-stiff), the excitation frequency passes through the first natural frequency of the tower when the WTG starts in operation. The second natural
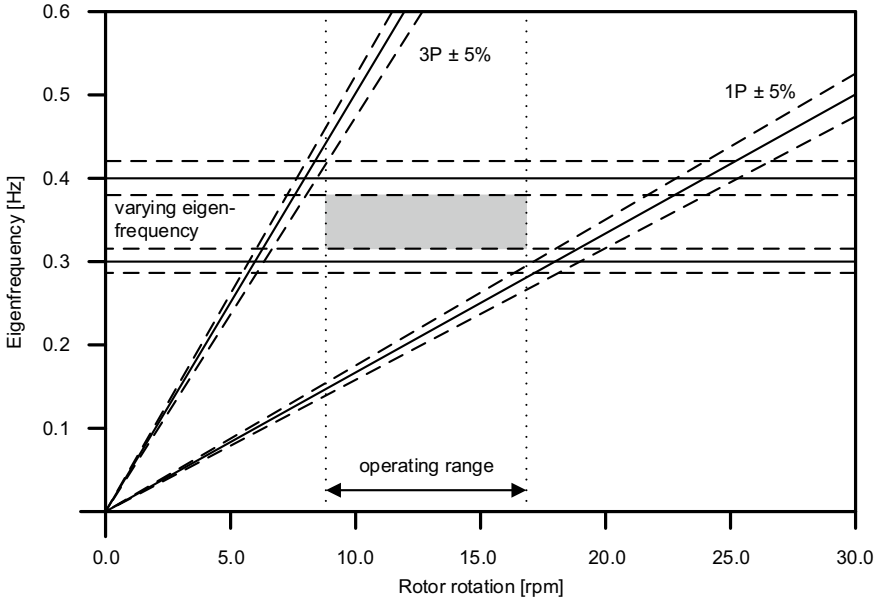
Fig. 7 Campbell diagram [WETI]

frequency of the tower and the first natural frequency of the rotor blade are usually greater than the 3P frequency located in the operating range.

Tasks for 4

The following WTG is given:

Given values:

- Tower system:
    - Wall thickness: $t = 8$ cm
    - Diameter: $D = 4$ m
    - Hub height (in this example equal to the tower height): $h = 80$ m
    - Aerodynamic drag coefficient: $c_W = 1.17$

- Material data:
    - Young's modulus: $E_{St} = 210000$ N/mm^2
    - Density of steel: $\rho_{St} = 7750$ kg/m^3

- forces and moments:
    - Wind pressure: $w_T = 2\frac{kN}{m^2}$
    - Self weight of the nacelle: $G = 1000$ kN
    - Thrust force: $F = 2000$ kN
    - Moment: $M = 40000$ kNm
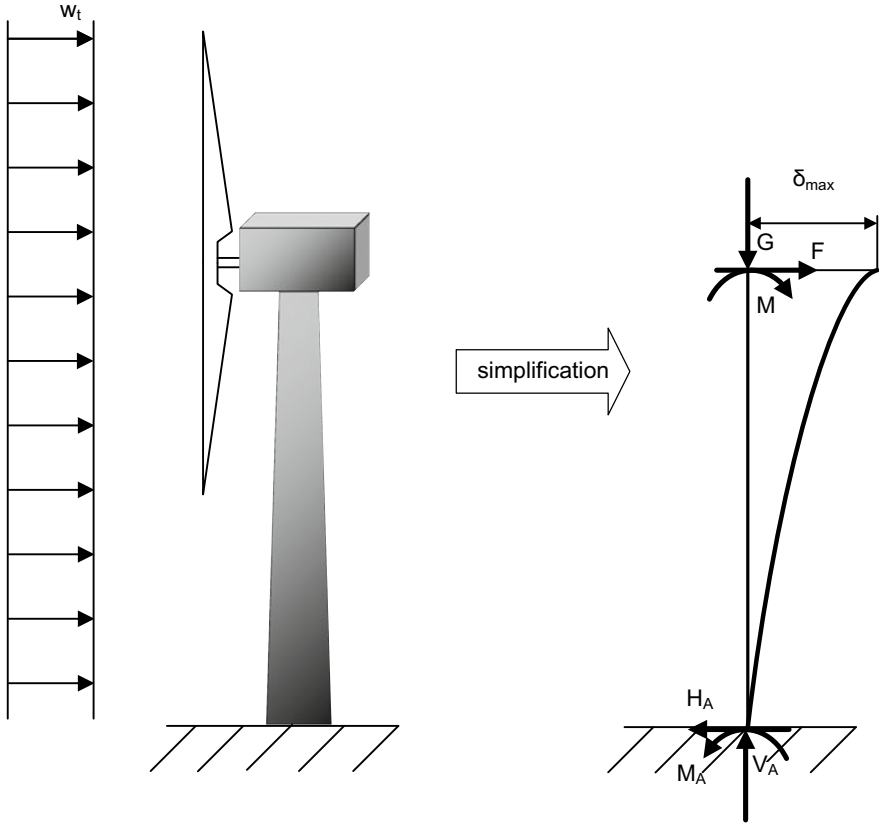
Fig. 8 Forces acting on a wind turbine [WETI]

- Calculate the resulting forces H_A, V_A and M_A at the tower bottom, as well as the moment of inertia I and the maximum deflection of the tower δ_{max}!
- What happens when a system is excited at its natural frequency and what does this mean for the WTG?
- Draw the Campbell diagram for a 3 blade wind turbine with the following values. Energy production in the speed range $n = 7.5–17.5 \ \text{min}^{-1}$

  1. Natural frequency tower $f_{ET1} = 0.4$ Hz
  2. Natural frequency tower $f_{ET1} = 0.9$ Hz

- Which parameters can be varied if the ranges overlap? How would the parameters have to be changed in this case?

5   Construction Details

Relevant design details have to be calculated separately using suitable simplified methods, e.g. the finite element method (FEM). Relevant design details of a wind turbine include openings of the tower shell, flange connections with eccentrically prestressed bolts, and welded joints.

5.1   Openings in the Wall of Tubular Steel Towers

Openings in the tower shell result in local load concentrations, so why complex geometries can only be calculated using FEM. The load concentration factor is a value of 1 at nominal load for an undisturbed tower shell, and 3 for a circular unstiffened opening.

Figure 9 shows the various openings in the wall of tubular steel towers.

5.2   Ring Flange Connections

The standard flange is connected with excentric pretensioned bolts. The nonlinear force flow of the bolts requires special calculation methods. The verification against extreme loads can be carried out without including the prestressing. The verification against fatigue loads, on the other hand, requires complex calculations based on the nonlinear force flow of the bolts.

Deviations of the ring flanges lead to a significant increase of the bolt force and can therefore result in damage. A perfect flange has no deviation, the maximum deviation must not exceed three millimetres. For the FEM calculations, the deviations must be included. Examples of different failure points of a flange connection are shown in Fig. 10.

5.3   Welded Joints

For welded joints, the permissible stress of the base material is reduced. For fatigue loads, the nominal load is determined in a simplified way using detail categories. The behaviour of welds to fatigue loads is unfavourable due to the notch that occurs in a weld. This means that welded joints are assigned to unfavourable notch classes.

When calculating the structural load, the geometry of the connections, but not the weld geometry, must be considered (e.g. finite element calculation).
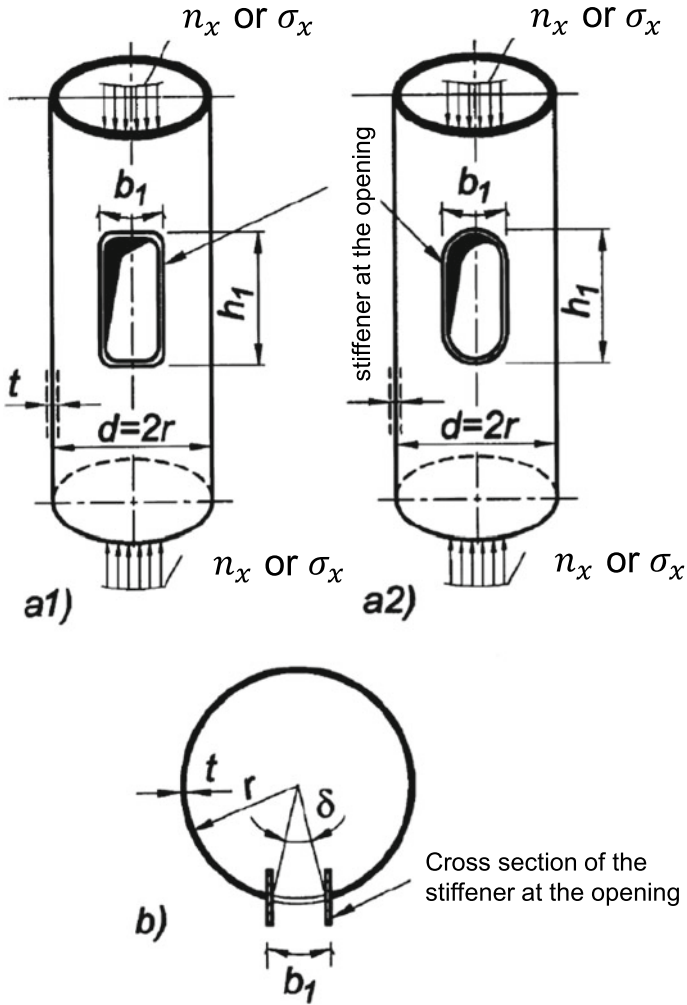
Fig. 9 Examples of different door openings [2]

6 Materials for Towers

Towers for wind turbines can be made of different materials. The materials must be able to withstand fatigue loads in particular. The modulus of elasticity, i.e. the stress-strain behaviour, is relevant in this context. Materials have very different properties in this respect (see Fig. 11 and Table 1). The common materials are listed below.
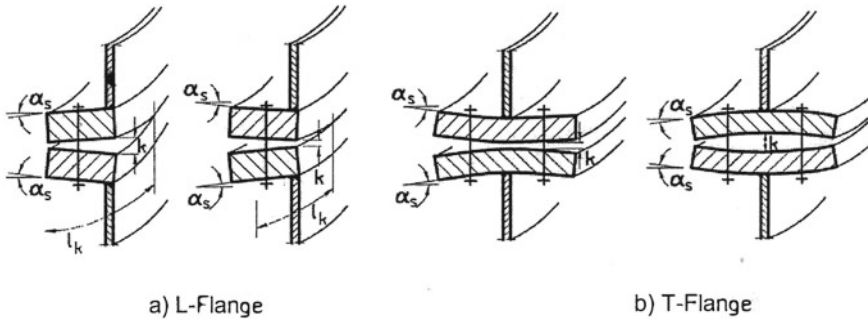
Fig. 10 Faulty flange connections at **a** a L-Flange and **b** of a T-Flange [2]
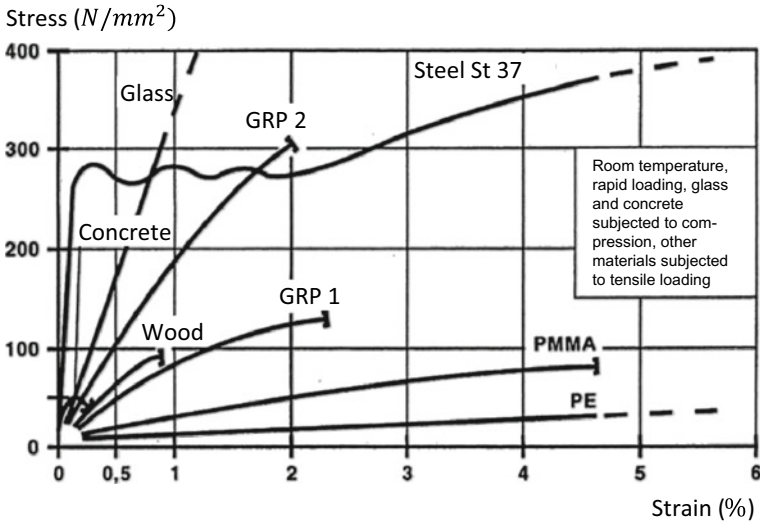
Fig. 11 Stress-strain curves of different materials [according to Wesche: Baustoffe für tragende Bauteile, Bauverlag 1996]

Table 1 Young's modulus E and thermal expansion coefficient αT for different materials

Material	Young's modulus E (Mpa)		Temperature expansion coeff. αT (1/K)
Glass		70 000	9×10^{-6}
Steel		210 000	12×10^{-6}
Stainless steel		170 000	$10 \ldots 16 \times 10^{-6}$
Aluminium		70 000	24×10^{-6}
Concrete	20 000…	40 000	10×10^{-6}
Wood parrallel to the grain	10 000…	17 000	$4 \ldots 6 \times 10^{-6}$
Wood perpendicular to the grain	300.	1 200	$25 \ldots 60 \times 10^{-6}$

6.1   Steel

The tubular steel tower is the standard structure for hub heights up to 100 m and is one of the most commonly installed types in the wind energy sector so far. This is partly due to the fact that the fatigue behaviour of steel, a homogeneous and isotropic material, is well researched. Steel has the highest level of automation and prefabrication and is relatively economical to manufacture. On-site erection is simple and quick. However, welding steel segments and flanges degrade the fatigue.

The tubular tower consists of several tower sections connected by flanges through pretensioned bolts at the construction site. The individual tower sections are made up of tower segments which are welded together from separate cylinders. These cylinders are made from flat steel plates by a forming process (round rolling). Figure 12 shows a classic 3-rollers round bending machine. Through this plastic forming process, residual stresses are selectively applied to the material. The resulting radius of the tube wall depends essentially on the applied pressure.

The flanges are usually formed from out of a steel block. The steel grade and quality used depends on the thickness and the application requirements such as the component category, the steel strength class and the onshore or offshore application.

6.2   Concrete

Concrete towers especially in hybrid construction (steel above, concrete below) are increasingly used for hub heights above 100 m in the last years, because they have no transport limitation in diameter and less corrosion or stability problems in contrast to steel towers. They are either precast reinforced concrete elements connected on site, usually by prestressing, or manufactured on site by means of in-situ concrete. The last, however, could only very rarely be used. Cracking and fatigue characteristics are disadvantageous with this type of construction.

6.3   Wood

In the history of wind energy, wood was the predominant material. It was at the beginning of the 20th century that wood was replaced more and more by steel and now it does not have a significant role as a material for wind energy. The company TimberTower, however, has specialized in the construction of wooden towers and uses the advantages of the natural material wood.

This wooden tower consists of a composite system of cross-laminated timber panels glued together one on top of the other. The individual components are assembled on site to form a hollow structure with a diameter of 7 m at the tower base and
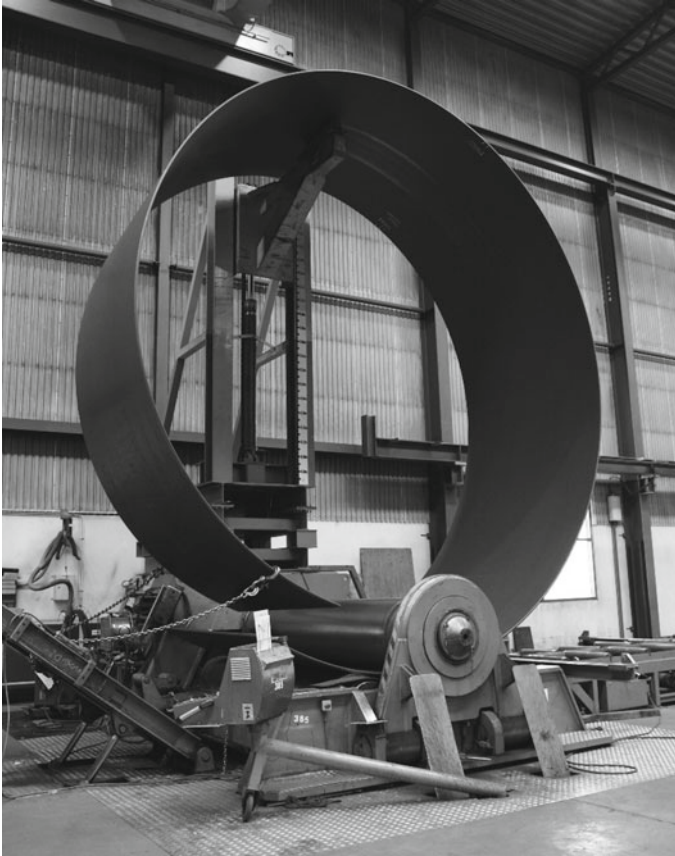
Fig. 12 Forming process of a steel plate to a tower segment with a classic 3-rollers round bending machine [WETI]

2.40 m at the tower top. The tower structure can consist of a hexagon, octagon or dodecagon.

Technical advantages include easy transport in 40-foot containers without the need for a heavy transporter. So far, hub heights of up to 200 m are planned.

The use of wood for the tower of a wind turbine has not yet been widely researched. This lack of experience is evident, for example, in the connecting materials.

As a natural product, wood is CO_2 neutral and can be recycled without major difficulties after the lifetime of a wind turbine has expired.

Since social acceptance and the associated CO_2 balance are becoming increasingly important, the author expects a renaissance of this material in the future.

6.4   Glass Fibre Reinforced Plastic

Glass fibre reinforced plastic (GRP) is used as a standard for rotor blades of WGTs. There is no experience yet with the use of GRP for the tower of a WTG.

GRP is a versatile material with very good ultimate limit properties. It has a high strength with relatively low weight. Disadvantages are the high costs, the complex production and the unfavourable CO_2 balance.

Tasks for 6

What are the advantages and disadvantages of the different materials steel, concrete, wood and GRP when used for the tower of a wind turbine?

7   Designs of Towers

There is a wide variety of towers for wind turbines. They differ in cross-section, material and structural concept. A selection of tower structures is presented in the following.

7.1   Tubular Towers

The standard and most common tower for wind turbines is the tubular tower. The main advantage here is the point-symmetrical cross-section. Therefore, the resistance to stress is the same in all directions. Furthermore, the circular cross-section is the most torsionally stiff cross-section.

The tubular tower has a high degree of prefabrication. For transport reasons, the tower usually consists of several tower sections that are connected by connection elements. The erection on site is easy and fast to realize. A disadvantage is the limitation of the diameter due to the transport under bridges (between 4.20 and 4.50 m).

7.2   Lattice Towers

Lattice towers are not no common, even this form of construction offers a number of advantages. Like tubular steel tower, a high degree of prefabrication is also possible. Due to the lightweight construction and the final structure, which can be assembled from small parts, there are no transport limitations due to size. The disadvantage is the relatively large amount of work involved in erecting the structure on site due to the large number of components that have to be assembled. In addition, there is a high

maintenance work due to the large number of components as well as connections. The resistance of the tower in relation to the torsional moment can also be critical.

7.3 Guyed Towers

The tower of the first large wind turbine in Germany at the beginning of the 80 s called GroWian ("Große Windenergieanlage") was a guyed tower. Due to numerous material problems and a lack of experience at the time, the turbine could only be operated for a few hours. Nevertheless, important research results could be obtained.

The greatest advantage of a guyed tower, as with sailboat masts, is the reduced bending moment due to the anchoring, which allow a smaller diameter of the tower cross-section in the lower area. This saves material and simplifies the transport.

The anchoring of the tensioning cables in the ground is usually problematic, since large prestressing forces and thus tensile forces are generated at the support.

7.4 Comparison of Different Tower Concepts

In the following, six different tower types are compared with regard to tower mass, tower costs and the cost ratio of the tower to the total costs of a WTG (see Fig. 13).

For this purpose, a 100 m and a 125 m high tower were assumed. The data for the results presented are taken from the study "Tall Towers for Large Wind Turbines" by
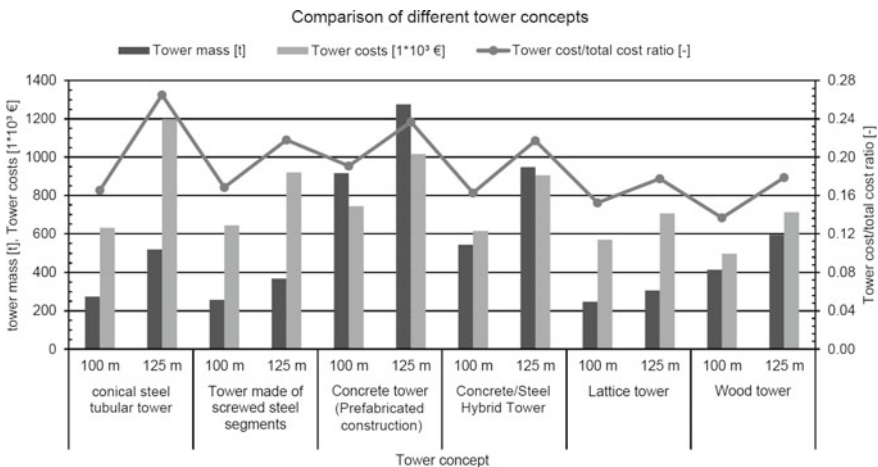
Fig. 13 Comparison of different tower concepts [Data from "Tall Towers for Large Wind Turbines" by Vindforsk, Energimyndigheten, Elforsk [4], edited by WETI]

Vindforsk, Energimyndigheten, Elforsk (2010) [4]. The reference turbine is a theoretical 3 MW turbine, based on the 5 MW turbine from National Renewable Energy Laboratory (NREL). Despite further assumptions and simplifications, the tower masses and costs are realistic in comparison. If the tower concepts are considered individually, there may be some scatter in the results.

The tower masses in this representation include a variety of components, depending on the concept, such as tower shell, flanges, bolts as well as steel reinforcement and concrete. The costs are the result of research work. They consist of the material costs and the working time for the assembly.

As mentioned above, the frequently used tubular steel tower with a height of 100 m can be produced and erected relatively cost-effectively in relation to the total investment of the WTG. However, if the tower height grows to 125 m, the costs necessarily increase as well. This does not happen to the same degree with all the mentioned tower concepts. For example, the cost ratio of tower costs to total costs for the tubular steel tower increases by an above-average of 60%. In contrast, the lattice tower, with the smallest increase in the comparison of just under 17%, remains significantly more cost-effective with an extension to 125 m.

Task for 7

Which structural designs of wind turbine towers do you know? What are the advantages and disadvantages of the different designs?

8 Foundations of Onshore Wind Turbines

The main function of a foundation is to transfer forces and moments from the tower structure into the soil, distributing them as homogeneously as possible. Different solutions have been developed to ensure and implement, depending on the tower structure, the resulting loads and the ground conditions. Most of the foundations are gravity foundations and are made of reinforced concrete. In unfavourable soil conditions, pile foundations are used as well. In principle, all point-symmetrical foundation layouts are conceivable, but are not always economically practical. Seen from above, round and polygonal (hexagonal, octagonal, beam cross) geometries have become established. The entirety of the foundation and the transition to the soil (ground) is called the foundation.

8.1 Foundations and Construction Types

Depending on the condition of the soil and the structure of the wind turbine, a basic differentiation can be made between two types of foundation.

In the case of shallow foundations, the loads are transferred into the ground by means of a foundation that is as large and heavy as possible. In addition, a sufficiently

load-bearing soil is required so that loads can be absorbed and transferred to the soil. The standard solution for shallow foundations is the gravity foundation (see Fig. 14).

If the upper subsoil layers do not have sufficient soil mechanical characteristics, it may be necessary to increase the load-bearing capacity of the foundation. In deep foundations, the load is mainly transferred via piles connected to the foundation in deeper and thus usually more load-bearing soil layers. The piles are used to transfer tensile and compressive forces, which are transmitted into the ground by the mantle resistance and the base resistance (see Fig. 15). The piles are mostly made of reinforced concrete and can be cast on site (in-situ) into pre-drilled holes. Alternatively, the steel piles are prefabricated in the factory and later driven or pressed into the ground.

For uniform soil pressure, it is also important to ensure that the loads are evenly distributed between the foundation and the soil. This transition between foundation
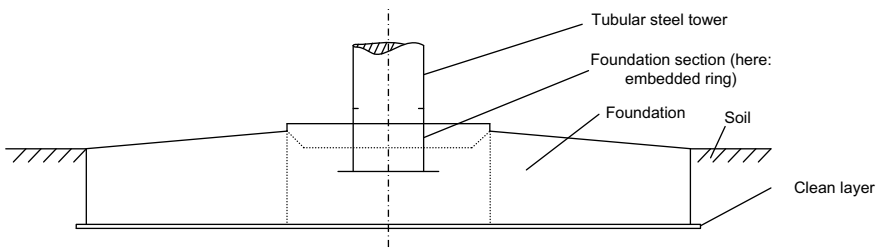
Fig. 14 Construction of a shallow foundation using a beam cross [WETI]
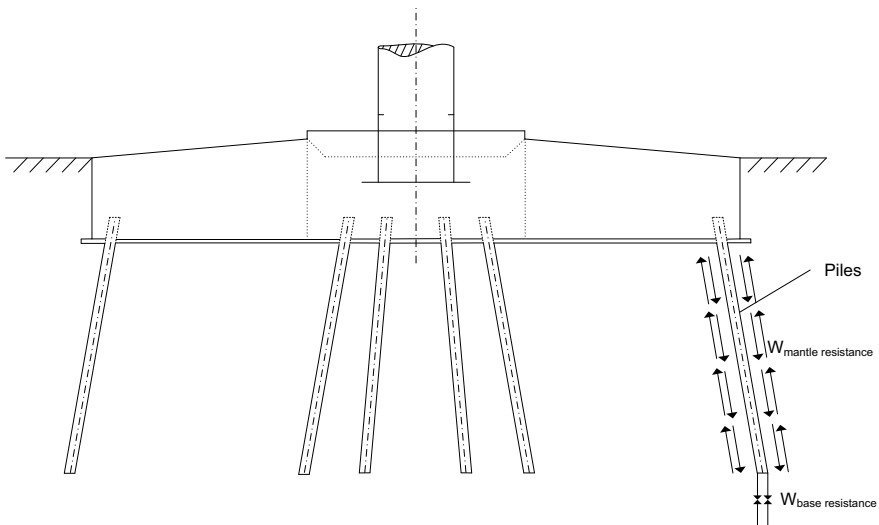
Fig. 15 Structure of deep foundation with piles in beam cross configuration [WETI]
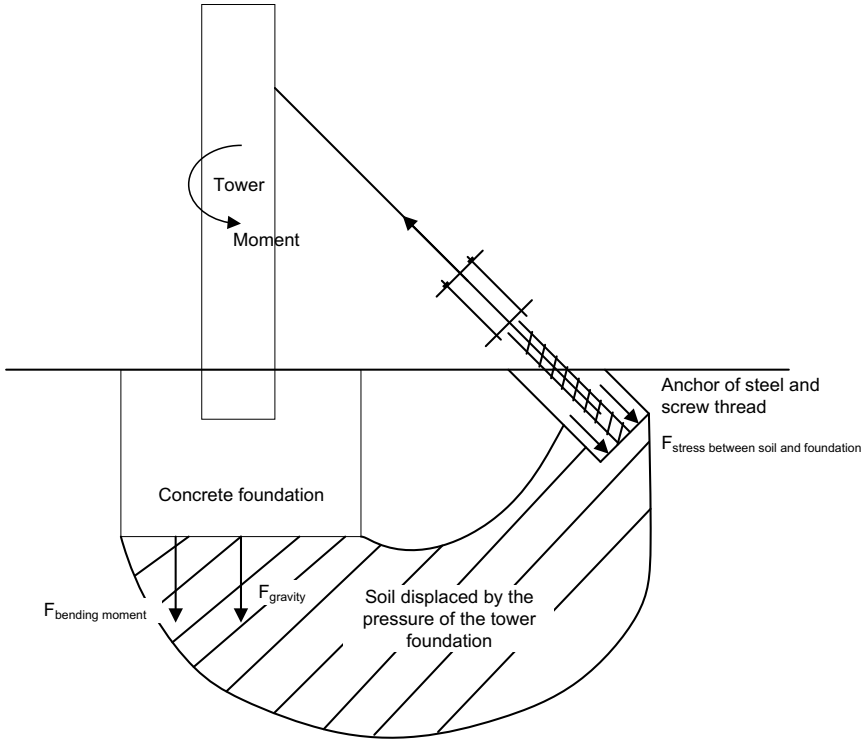
Fig. 16 Force flow: guyed tower with anchorage [WETI]

and soil is created by the so-called clean layer. This is a flat, relatively smooth surface made of concrete of lower strength classes.

For mainly small wind turbine towers, a guyed tower system is sometimes used. In this case, the loads are transferred into the ground by means of ground anchors and prestressed cables (see Fig. 16). This reduces the load on the tower as a load-bearing system, allowing smaller diameters and wall thicknesses to be achieved. A detailed soil analysis is important to ensure stability, otherwise, if the ground is too soft, the load can increase and even lead to structural integrity failure.

8.2 Transition Between Tower and Foundation

The load transfer between tower and foundation is realized by a special anchoring segment. A differentiation can be made between the embedded ring foundation and the anchor cage. The embedded ring foundation consists of an exposed section and a section embedded in reinforced concrete (Fig. 17a, b). The upper exposed steel

(a)   (b)   (c)
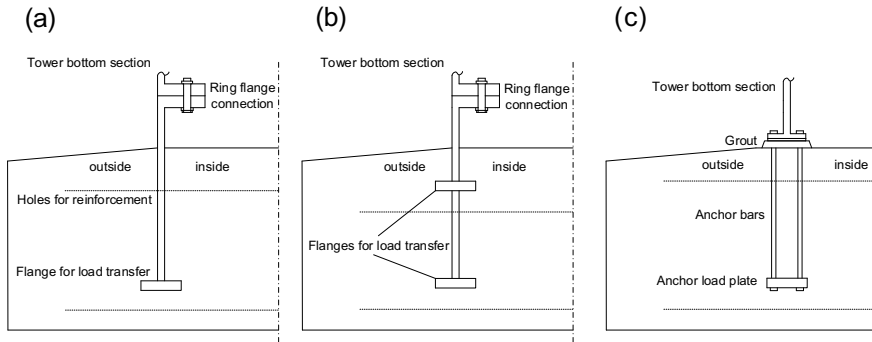
Fig. 17 Different transitions between tower and foundation: **a** embedded ring foundation with one flange for load transfer, **b** embedded ring foundation with two flanges for load transfer, **c** anchor cage [WETI]

cylinder is connected to the tower bottom section by means of a ring flange connection. The lower part transfers the occurring tensile and compressive forces as well as the bending moments into the foundation. These loads are transmitted through one (Figure 17a) or two load introduction flanges (Figure 17b), depending on the design of the embedded ring foundation. The transmission of horizontal forces is realized by reinforcement inserted into a hole in the steel cylinder below the concrete surface.

In the case of the anchor cage (Fig. 17c), an upper flange with anchor bars is connected to a load plate located further down. The anchor bars are prestressed and then cast in concrete. The compressive forces are transferred to the foundation via a pressure-resistant special grout. In contrast, the tensile forces are absorbed by the anchor load plate.

8.3 Verification of the Foundation

Influencing criteria for the design of a foundation are predominantly dead and extreme loads, such as from the rotor thrust, tower head eccentricity and the dynamic wind pressure on the tower. Various soil conditions, such as a varying groundwater level, can also have a major influence on the distribution of base pressure and thus on the stability of the foundation.

When designing reinforced concrete foundations, the internal and external load-bearing capacity must be verified. In the ultimate limit state of the internal load-bearing capacity, the relevant stress verifications and the verification against fatigue must be performed. If a common reinforced concrete flat foundation is involved, the limits of the verification methods commonly used in civil engineering are quickly exceeded. When calculating the fatigue strength, for example, the force flow calculation with an analogous truss model, in which the concrete is allowed to crack, is no longer permissible under a tensile and compression alternating load. On the other

hand, in the case of cyclically dynamically loaded piles, the tensile forces must be examined particularly critically, since only limited experience is available in this area.

In addition to the limit state of the internal load-bearing capacity, verifications must also be carried out in the limit state of the external load-bearing capacity. The interaction between foundation and soil shall be analysed. This includes the verifications against tilting (no gaping joint), ground failure, sliding, uplift and settlement.

For all design modifications, the replacement ground spring also varies depending on the foundation. The influence on the stiffness of the respective wind turbine must then be checked, since the natural frequency and thus the system behaviour (control) and also the loads can change.

Solutions

Section 1: 210 m, up to 33%.

Section 2:

- "Guideline for Wind Turbines, Actions and Stability Verifications for Tower and Foundation" by Deutsches Institut für Bautechnik (DIBt)
- "Guideline for the Certification of Wind Turbines" by DNV (formerly Germanischer Lloyd)
- "Wind turbines—Part 1: "Design requirements" by International Electrotechnical Commission (IEC 61,400)

Section 4:

Calculation of H_A:

$$H_A = F + W_t \text{ mit } W_t = w_t \cdot D \cdot h - c_w$$
$$H_A = F + W_t$$
$$H_A = 2000 \text{ kN} + 748.8 \text{ kN} = 2748.8 \text{ kN}$$

Calculation of V_A:

$$V_A = G + A_{\text{Cross section}} \cdot h - \rho_{\text{steel}} \cdot g \text{ mit } A_{\text{Cross section}} = \frac{\pi}{4}\left(D^2 - (D - 2 - t)^2\right)$$
$$V_A = 1000 \text{ kN} + 0.9852 \text{ m}^2 \cdot 80 \text{ m} - 7750\frac{\text{kg}}{\text{m}^3} \cdot 9.81\frac{\text{m}}{s^2} = 6992 \text{ kN}$$

Calculation of M_A:

$$M_A = M + W_T \cdot \frac{h}{2} + F \cdot h$$
$$M_A = 40000 \text{ kN} + 748.8 \text{ kN} \cdot \frac{80 \text{ m}}{2} + 1000 \text{ kN} - 80 \text{ m} = 229952 \text{ kNm}$$

Calculation of the moment of inertia I:

$$I = \frac{\pi}{64}\left(D^4 - (D - 2t)^4\right)$$
$$I = \frac{\pi}{64}\left((4 \text{ m})^4 - (4 \text{ m} - 2 \cdot 0.08 \text{ m})^4\right) = 1.89 \text{ m}^4$$

Calculation of the deflection δ_{max}:

$$\delta_{\text{Rotor thrust}} = \frac{F \cdot h^3}{3 - E - I}$$

$$\delta_{\text{Rotor thrust}} = \frac{1000 \text{ kN} \cdot (80 \text{ m})^3}{3 \cdot 210000000 \frac{\text{kN}}{\text{m}^2} \cdot 1.89 \text{ m}^4} = 0.43 \text{ m}$$

$$\delta_{\text{Moment of rotor+nacelle}} = \frac{M \cdot h^2}{3 \cdot E \cdot I}$$

$$\delta_{\text{Moment of rotor+nacelle}} = \frac{40000 \text{ kN} \cdot (80 \text{ m})^3}{3 \cdot 210000000 \frac{\text{kN}}{\text{m}^2} \cdot 1.89 \text{ m}^4} = 0.32 \text{ m}$$

$$\delta_{\text{Wind load tower}} = \frac{W_T \cdot D \cdot h^4}{8 \cdot E \cdot I}$$

$$\delta_{\text{Wind load tower}} = \frac{748.8 \text{kN} \cdot 4 \text{ m} \cdot (80 \text{ m})^4}{8 \cdot 210000000 \frac{\text{kN}}{\text{m}^2} \cdot 1.89 \text{ m}^4} = 0.12$$

$$\delta_{max} = 0.87 \text{ m}$$

- The system is subjected to strong oscillations due to the resonance and begins to oscillate. The excitation by the rotor frequency (1P) and the blade passing frequency (3P) must not be in the range of the natural frequencies of the tower and the rotor blade.
- The natural frequencies of the components and/or the operating range can be varied. The natural frequency of the rotor blade would have to be increased by harder material, stiffer cross-section or the operating range would have to be lowered. The natural frequency of the tower would have to be lowered by softer material, stiffer cross-section or the operating range would have to be increased (see also Fig. 18).
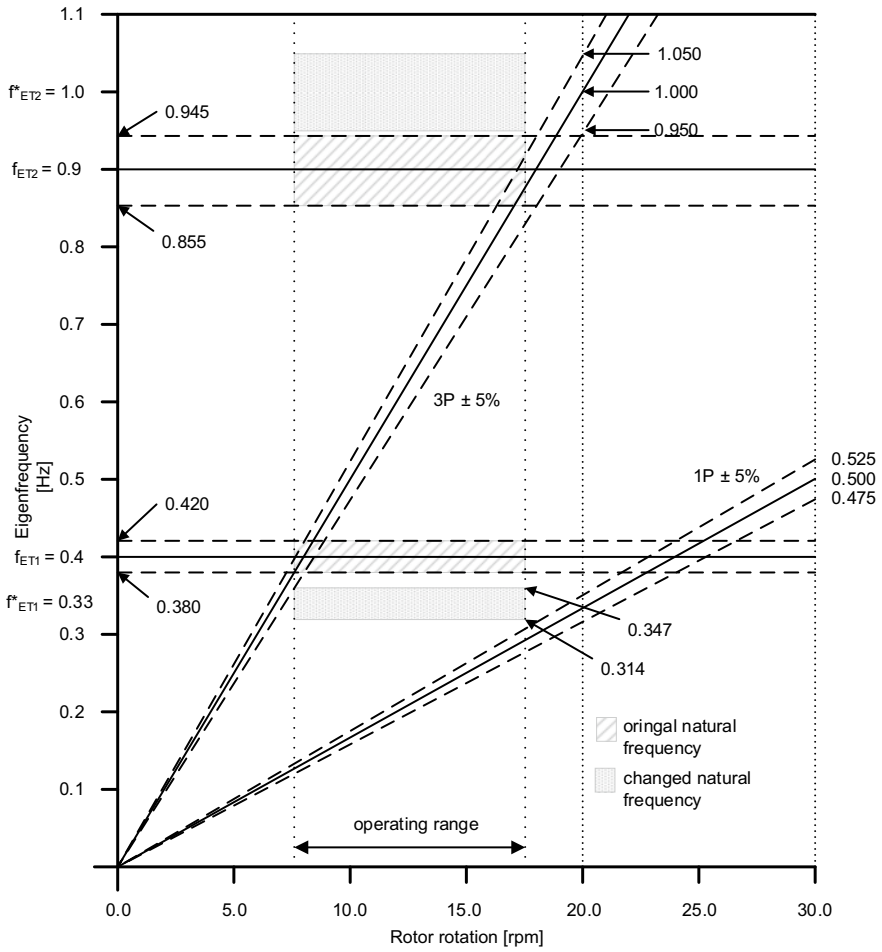
Fig. 18 Campbell diagram

Section 6:

Steel

Positive:

- high degree of prefabrication
- relatively favourable
- quick and easy installation on site.

Disadvantage:

- limitation of the diameter due to transport

- welding of the tower shell at the construction site only possible under certain conditions.

Concrete

Positive:

- hardly any limitation in size (individual segments can be put together)
- hardly any/no corrosion or stability problems
- good damping behaviour.

Disadvantage:

- more expensive to erect for in-situ concrete
- diameter limitation for prefabricated segments.

Wood

Positive:

- wood as a pure natural product is CO_2 neutral
- almost 100% recyclable at the end of the service life of a wind turbine
- transport in 40 foot containers possible without heavy transporter.

Disadvantage:

- connecting means between tower sections little researched.

GRP

Positive:

- high resistance
- low weight.

Disadvantage:

- high costs
- difficult fabrication
- no or few experience.

Section 7:

Tubular steel tower

Positive:

- point-symmetric cross-section
- resistance to load is the same in all directions
- circular cross-section is the most torsionally stiff cross-section
- high degree of prefabrication
- installation on site is simple and fast.

Disadvantage:

- limitation of the diameter due to transport
- uneconomical from heights of approx. 100 m.

Lattice tower

Positive:

- due to lightweight construction and final structure that can be assembled from small parts, there are no transport limits due to size
- high degree of prefabrication.

Disadvantage:

- high degree of maintenance due to the high number of bolt connections as well as components
- great effort of construction on site due to the many components
- elasticity of the tower in relation to the torque can also be critical.

Guyed tower

Positive:

- force reduction that allows for a smaller diameter of the tower
- material can be saved and transport is facilitated.

Disadvantage:

- anchoring the tension cables in the ground is problematic
- exact analysis of the soil structure is time-consuming and expensive.

Literatures

1. Deutsche WindGuard GmbH, Status des Windenergieausbaus an Land in Deutschland—Jahr 2020. https://www.windguard.de/jahr-2020.html?file=files/cto_layout/img/companies/wind-energy-statistics/2020/Status%20des%20Windenergieausbaus%20an%20Land%20-%20Jahr%2020.pdf. Accessed 28 Sep 2021
2. Deutsches Institut für Bautechnik (DIBt), Guideline for Wind Turbines - Actions and Verification of Stability for Tower and Foundation, Department I 8, Bautechnisches Prüfamt, Grundlagen der Standsicherheit, Berlin, Version October 2012 - Corrected Version March 2015
3. DKE German Commission for Electrical, Electronic & Information Technologies in DIN and VDE, IEC 61400-1:2019 (2019)
4. Engström S, Lyrner T, Hassanzadeh M, Stalin T, Johansson J (2010) Tall towers for large wind turbines, Elforsk rapport 10:48, Vindforsk, Energimyndigheten, Elforsk, Stockholm, Sweden

Prof. Dr.-Ing. Torsten Faber Since 1 November 2010, has headed the Wind Energy Technology Institute (WETI) at Flensburg University of Applied Sciences. Prior to this, he gained more than 10 years of professional experience at DNV GL (formerly: Germanische Lloyd Industrial Services GmbH) in the department of rotor blades and construction technology for wind turbines.

Power Electronic Generator Systems for Wind Turbines

Friedrich Wilhelm Fuchs

Abstract This chapter deals with the electrical components of the variable speed wind turbine. These are the generator, the frequency converter, the control for generator and converter, the transformer, the mains filter and other electrical components. The various power electronics generator concepts currently used in newly installed wind turbines are introduced. The procedure is such that the equations of the components, mainly in steady state but with an outlook on dynamic operation and control, are briefly derived. From this, diagrams are developed which show the operating behavior of the components. These diagrams are interpreted and analyzed. This should give the reader an idea of the operating behavior of the drive train and the grid feed-in. In each case, these are the basic variants. Special designs are not considered. The power electronic generator system must fulfill the requirements of the higher-level plant control or system control, as described in Chap. 9, the requirements of grid integration, which are shown in Chap. 10. Exemplarily it is shown how these requirements influence the design of the power electronic generator system. Exercises are added to deepen the understanding of the power electronics generator system.

1 Introduction

Mechanical power obtained from the wind with the aid of the rotor of a wind turbine is converted into electrical energy by means of a generator and fed into electrical grid.

Various suitable concepts are available for this purpose [1, 2]. Often, a gearbox is interposed for the conversion of speed and torque in order to be able to select the base rotational speed of the rotor and generator to the optimum, independently of the wind speed. On the electrical side, the power electronic generator system must be able to take up the mechanical power, convert it into electrical power and feed in into the mains. Generator voltage amplitude and frequency must be adapted to the mains, usually via frequency converter and transformer.

F. W. Fuchs (✉)

Christian-Albrechts-University in Kiel, Christian-Albrechts-Platz 4, 24118 Kiel, Germany
e-mail: fwf@tf.uni-kiel.de

The power acquired from the rotor of the wind turbine and transferred to the shaft of the generator depends on the velocity of the wind and the rotational speed of the rotor, as shown in Fig. 1. The curves with the speed increasing at low rotor rotational speeds and decreasing at higher rotor rotational speeds show a clear maximum. The curves are valid for constant blade pitch angle.

When operating a three-phase AC generator directly connected to the grid, the rotor feeds directly into the grid with its fixed frequency and the rotor of the generator rotates at a fixed rotational speed proportional to this grid frequency. In the case of the synchronous machine, the speed of revolution is fixed exactly to the grid frequency; in the case of the induction machine or, in other words, asynchronous machine, small deviations from the synchronous speed occur depending on the load.

An extension of the previous explained concept of the fixed rotational speed generator is called the "Danish concept" and was widely used in the 1980s [3]. Here, a second generator or a second winding is additionally used in the first generator in order to achieve a second generator speed by switchover.

Due to the non-optimal energy yield when feeding the grid with directly coupled asynchronous AC generators, due to the high loads in the drivetrain and due to the difficulty to achieve reactive power requirement, this concept is hardly used today [3]. The exception is in systems with the smallest output power. This non-optimal energy yield is shown by the vertical line at 7 1/min in the power-rotational speed
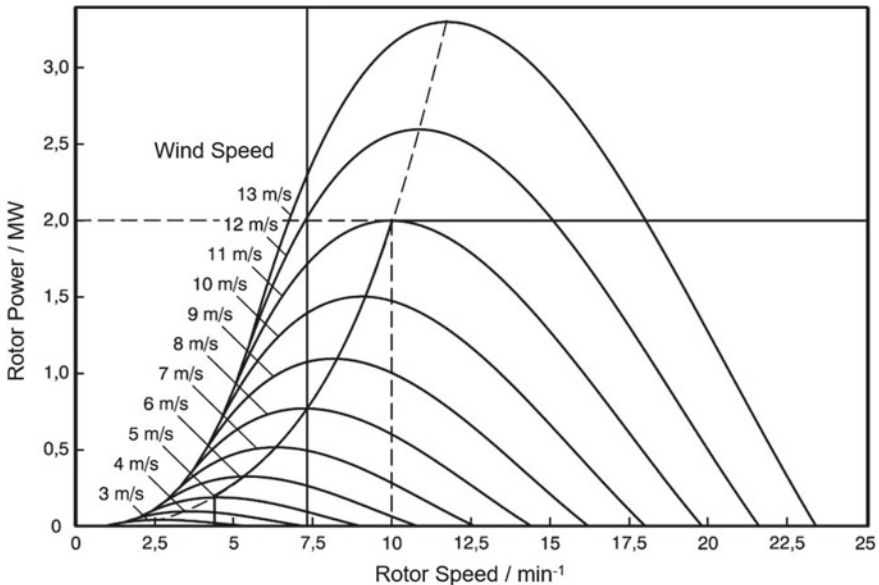
Fig. 1 Power-speed revolution diagram of a rotor arrangement of a wind turbine (optimum pitch angle) and the characteristic curve of a generator at fixed (vertical line at about 7,5 m/s) and variable, optimum frequency (starting at about 4 m/s); example of a 2 MW turbine; parameterization: wind speed; pitch angle constant, from 10 m/s power constant of 2 MW

diagram (Fig. 1). At fixed rotational speed, the optimum power, in the maximum of the power curve, can only be obtained at wind speeds of 7–8 m/s.

As a result, today the concept of a variable rotational speed generator is state of the art. The rotational speed is controlled depending on the wind in such a way that the optimum power is extracted from the wind. In the power-rotational speed diagram (Fig. 1) this is represented by the line intersecting the maxima of the power curves. It means always driving the rotational speed of the generator to the value at which the maximum power is located at the respective wind speed. The rotor rotational speed and thus the generator rotational speed must therefore be varied depending on the wind speed. The pitch angle (angle of the rotor blades turned out of the rotation area) is kept constant, at the optimum power yield, so long as the nominal power is not reached. This range below the rated power is called the power optimization range. If the wind is too strong and thus the nominal power is exceeded, the rotor blade is turned out of the wind by changing the pitch angle (power limitation range, horizontal line in Fig. 1 at 2 MW) and thus the power yield is limited.

The ability to control the rotational speed of the generator and thus also of the mechanical rotor is achieved by connecting a frequency converter between the generator and the grid. On the grid side, it is operated with AC grid voltage of fixed amplitude and frequency and, on the generator side, can generate voltage of variable amplitude and frequency, as required for variable rotational speed operation.

The structure and the components of the drive train as well as the grid feed-in of a wind turbine with converter-fed generator are shown in Fig. 2. Here a wind turbine is shown which is equipped with a fully rated converter. The converter converts the full power of the generator.

The rotor of the wind turbine converts the power of the wind into mechanical power. Often a gearbox is used so that the low speed of revolution of the rotor can be adapted to a then higher base speed of the generator. The generator converts the mechanical power into electrical power. There are two systems with a fully rated frequency converter, which converts the frequency of the variable-speed generator into the fixed grid frequency and feeds the power into the grid via a transformer, grid filter, contactors and fuses. One system is equipped with asynchronous generators with squirrel-cage rotors, and the other system with synchronous generators. In addition to the systems with fully rated converters, systems with partially rated
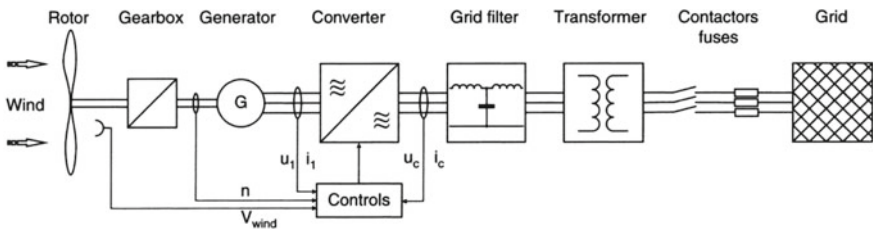
Fig. 2 Structure and components of the drive train and grid feed-in of a wind turbine with a fully rated converter

power converters are in use, as system three. In this case, the asynchronous machine with a slip ring rotor is used. Here, the stator of the generator is directly connected to the grid and the rotor is connected via converter to the grid.

2   Single Phase AC Voltage and Three Phase AC Voltage Systems

As an introduction, some basics of electrical engineering shall be presented, so as to improve the understanding of this chapter for people not familiar with the subject. First of all, the alternating voltage system and the three-phase voltage system are introduced.

Stationary conditions and sinusoidal or cosinusoidal electrical quantities of one frequency are assumed here.

Electrical power is generated by the electrical quantities, current and voltage. These quantities, e.g. the voltage, written $U(t)$ or $u(t)$, have a fixed amplitude $\widehat{U}$ and change cosinusoidally with time t proportional to the angular frequency $\omega = 2\pi f$ of the voltage:

$$U(t) = \sqrt{2}\tilde{U} \cdot \cos(\omega t + \varphi_U) = \widehat{U} \cdot \cos(\omega t + \varphi_U) \tag{1}$$

$\widehat{U}$: Peak value, $\tilde{U}$: RMS value, ω: angular frequency, φ_U: phase angle; each of the voltage.

Here, a phase shift φ_U of the voltage different from zero is assumed for the general case. For higher power, in Germany above 3.7 kW (16 A) in 230 V/400 V grids, a three-phase AC grid is used, with a neutral conductor generally also present. Wind turbines are connected to such AC three-phase grids. Such a grid has three-phase voltages, these are sinusoidal, symmetrical voltages. In this case, the voltages in the three phases have the same amplitude $\widehat{U} = \sqrt{2} \cdot \tilde{U}$ and angular frequency ω and have a phase offset of 120° between the phases. The equations listed for the phases named R, S, T or a, b, c or L1, L2, L3 describe such voltages, here as star voltages. Figure 3 represents the time course of the voltages with phase shift in Phase a equal to $\varphi_{Ua} = 0°$.

$$U_a(t) = \sqrt{2}\tilde{U}_{Star}\cos(\omega t)$$

$$U_b(t) = \sqrt{2}\tilde{U}_{Star}\cos\left(\omega t - \frac{2\pi}{3}\right)$$

$$U_c(t) = \sqrt{2}\tilde{U}_{Star}\cos\left(\omega t - \frac{4\pi}{3}\right) \tag{2}$$
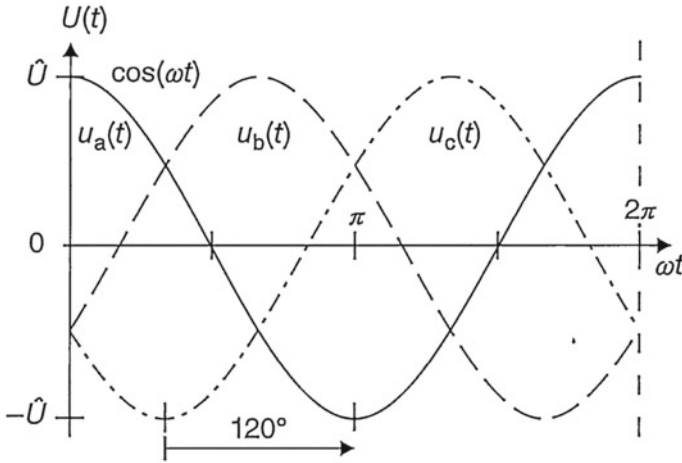
Fig. 3 Variation in time of the voltages of a sinusoidally symmetrical three-phase AC system with $\varphi_{\mathrm{ua}} = 0°$

If these grids with their generators and loads are absolutely symmetrical, then the calculation in one phase is sufficient, since the values of the other phases are the same and thus known, but with a dedicated phase shift of 120° or 240°.

These AC and three-phase grids and generators and transformers are calculated with the aid of a complex AC calculation, also called the phasor calculation. The complex alternating voltage quantities or phasors are marked with an underscore, thus. $\underline{U}$:

$$\underline{U} = \frac{1}{\sqrt{2}}\hat{U} \cdot e^{j\varphi_{\mathrm{U}}} = \frac{1}{\sqrt{2}}\hat{U}(\cos(\varphi_{\mathrm{U}}) + j\sin(\varphi_{\mathrm{U}})) \tag{3}$$

It is to be noted, that the angular frequency is not included in these formulas. The complex values can be displayed in diagrams in the complex plane. Here the diagrams are aligned in such a way that the real axis always points upwards and the imaginary axis points to the left (procedure as used in power engineering, see Fig. 4). In addition, the consumer arrow system is generally used in this chapter, i.e. power consumption results in positive active power.

The variation in time can be determined with the knowledge of the angular frequency of the complex value:

$$\begin{aligned}
U(t) = U_{\mathrm{Star}}(t) &= Re\left\{\sqrt{2}\underline{U} \cdot e^{j\omega t}\right\} \\
&= Re\left\{\sqrt{2}\frac{1}{\sqrt{2}}\hat{U} \cdot e^{j\varphi_{\mathrm{U}}} \cdot e^{j\omega t}\right\} \\
&= Re\left\{\hat{U} \cdot (\cos(\omega t + \varphi_{\mathrm{U}}) + j\sin(\omega t + \varphi_{\mathrm{U}}))\right\} \\
&= \hat{U} \cdot \cos(\omega t + \varphi_{\mathrm{U}}) \tag{4}
\end{aligned}$$

Fig. 4 Selected position of
the axes of the complex
variables
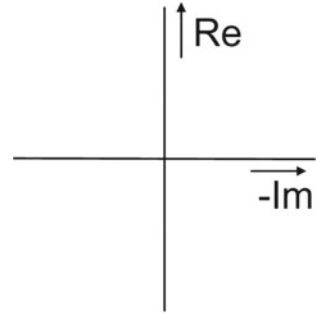
The power and its terms are important for the characterization of wind turbines. The power in such three-phase AC symmetrical systems and grids is calculated for the active power P, which can perform work, the reactive power Q and the apparent power S according to the following equations. The star voltage is used and it is assumed that both voltage and current have a phase shift (φ_U and φ_I). RMS values of voltage and current are also represented in the following by the respective letters (U, I) without further identification.

$$\underline{U}_{Star} = U_{Star} \cdot e^{j\varphi_U} = U_{Re} + jU_{Im} = U_{Star} \cdot (\cos\varphi_U + j \cdot \sin\varphi_U) \tag{5}$$

$$\underline{I} = I \cdot e^{j\varphi_I} = I_{Re} + jI_{Im} = I \cdot (\cos\varphi_I + j \cdot \sin\varphi_I) \tag{6}$$

$$\underline{I}^* = I \cdot e^{-j\varphi_I} = I_{Re} - jI_{Im} \tag{7}$$

$$P = 3 \cdot U_{Star} \cdot I \cdot \cos(\varphi_U - \varphi_I) = 3 \cdot \text{Re}\{\underline{U}_{Star} \cdot \underline{I}^*\} \tag{8}$$

$$Q = 3 \cdot U_{Star} \cdot I \cdot \sin(\varphi_U - \varphi_I) = 3 \cdot \text{Im}\{\underline{U}_{Star} \cdot \underline{I}^*\} \tag{9}$$

$$\underline{S} = P + jQ = 3 \cdot \underline{U}_{Star} \cdot \underline{I}^* \tag{10}$$

$$S = |\underline{S}| = 3 \cdot U_{Star} \cdot I \tag{11}$$

To calculate the power, the conjugate complex value $\underline{I}^*$ *of* the current I is needed.

3   Transformer

The transformer is used to transform voltages to a higher or lower amplitude or to perform potential separation or both as in wind power stations. In the following introduction to the basics, the following is assumed:

- saturation is neglected,
- constant ohmic resistors,
- symmetrical design for three-phase transformers,
- steady-state operation, cosinusoidal voltages.

For more in-depth coverage of the area, the reader is referred to the technical literature (e.g., [4]).

3.1   Principle, Equations

In the simplest case, the transformer consists of an iron core with good magnetic conductivity, on which two coils are mounted, primary coil 1 and secondary coil 2, as shown in Fig. 5. To simplify the illustration, coils with only two turns on both sides are shown here. Primary and secondary windings are well coupled by the main bundle fluxes in the iron core (ϕ_{12} by means of coil 1 into coil 2, ϕ_{21} correspondingly by means of coil 2 into coil 1). Small flux components do not reach the opposite winding and are called stray bundle fluxes ($\phi_{1\sigma}$, $\phi_{2\sigma}$).

Both coils are flown through by the same main bundle flux. The number of turns of the coil windings are w_1 on the primary side and w_2 on the secondary side. This results in the primary and secondary induced voltages U_{i1} and U_{i2} generated by the common primary and secondary main bundle flux (ϕ_{1h}, ϕ_{2h}):
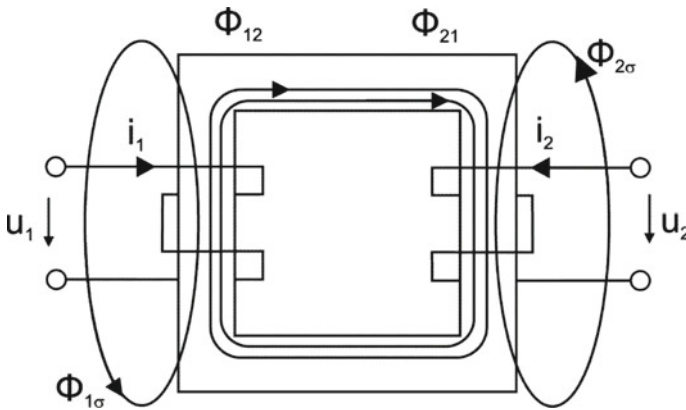
Fig. 5   Single-phase transformer, structure and fluxes

$$U_{i1}(t) = w_1\left(\frac{d\phi_{1h}}{dt}\right); \quad U_{i2}(t) = w_2\left(\frac{d\phi_{2h}}{dt}\right); \quad \phi_{1h} = \phi_{2h} \tag{12}$$

It can be seen that via the number of turns ratio w_1/w_2, the voltage ratio of the internal voltages from the secondary to the primary side can be set:

$$\frac{U_{i1}}{U_{i2}} = \frac{w_1}{w_2} \tag{13}$$

Induced voltages are now written as the product of main inductance and current. They are brought into complex representation:

$$w_1\left(\frac{d\phi_{1h}}{dt}\right) = L_{1h} \cdot \frac{di_1}{dt}; \quad \text{complex} : j\omega L_{1h}\underline{I}_1 \tag{14}$$

$$w_2\left(\frac{d\phi_{2h}}{dt}\right) = L_{2h} \cdot \frac{di_2}{dt}; \quad \text{complex} : j\omega L_{2h}\underline{I}_2 \tag{15}$$

To complete the effects, the voltage drops at the primary and secondary ohmic resistances (R_1, R_2) and the voltage drops on the magnetic leakage paths at the corresponding leakage inductances ($L_{1\sigma}$ and $L_{2\sigma}$) are additionally included. This gives the voltage equations, now presented in the usual form as a complex equation:

$$\underline{U}_1 = R_1\underline{I}_1 + j\omega L_{1\sigma}\underline{I}_1 + j\omega L_{1h}\left(\underline{I}_1 + \underline{I}_2'\right) \tag{16}$$

$$\underline{U}_2' = R_2'\underline{I}_2' + j\omega L_{2\sigma}'\underline{I}_2' + j\omega L_{1h}\left(\underline{I}_1 + \underline{I}_2'\right) \tag{17}$$

Here, the secondary voltage, the secondary current and the secondary resistances have additionally been related (multiplied) to the primary side by the turns ratio $\ddot{u} = w_1/w_2$ or its reciprocal, which is marked with a line behind and over the letter ($\underline{I}_2'$). This leads to the fact that the last terms in both equations are the same. This is based on the following ratios:

$I_2' = \frac{1}{\ddot{u}} \cdot I_2$	Secondary current referred to primary side
$U_2' = \ddot{u} \cdot U_2$	Secondary voltage referred to primary side
$\underline{I}_\mu = \underline{I}_1 + \underline{I}_2'$	Magnetizing current
$L_{1\sigma}$	Primary leakage inductance
$L_{1h} = L_{2h}' = \ddot{u}^2 \cdot L_{2h}$	Primary main inductance equal to secondary main inductance referred to the primary side
$R_2' = \ddot{u}^2 \cdot R_2$	Secondary ohmic resistance referred to the primary side
$L_{2\sigma}' = \ddot{u}^2 L_{2\sigma}$	Secondary leakage inductance referred to the primary side
R_1	Primary side resistance
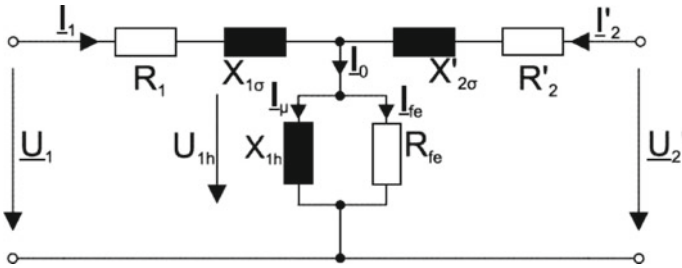
Fig. 6 Single-phase transformer; complete equivalent circuit diagram for power engineering use

3.2 Equivalent Circuit Diagram, Phasor Diagram

Relating the secondary values to the primary values results in equal induced voltages in the equations for the primary and secondary ($U_{1h} = U'_{2h}$). Therefore, a connected equivalent circuit of the primary and secondary side of the transformer can now be created from the primary and secondary side for power engineering use, as shown in Fig. 6. It allows a graphical analysis of both voltages, which generally have very different magnitudes, in one equivalent circuit diagram.

In addition to the ohmic losses in the primary and secondary circuits, there are also losses in the iron. These can be well approximated by a resistance R_{fe} parallel to the main inductance.

A common phasor diagram of the primary and secondary sides of the transformer in the complex plane can be drawn from the voltage equations. An example is shown in Fig. 7. It should be noted, that the ohmic and stray voltage drops are shown relatively large in size here, compared to their real value, to make them clear in the picture.

This equivalent circuit does not include the true potential separation between the primary and secondary sides. This can be inserted by adding an ideal transformer in series, which only realizes the voltage transformation ($w_1 = w_2$, $R = 0$, $L_\sigma = 0$, $L_h \gg \infty$), but is not shown here.

3.3 Simplified Equivalent Circuit Diagram

For simplified considerations, in particular for the short-circuit behavior of the transformer or when regarding the transformer as a component in the network, a simplified equivalent circuit diagram is used. It is called short-circuit equivalent circuit diagram. This takes advantage of the fact that the transverse or shunt impedances are much greater than the longitudinal impedances; transverse or shunt impedances are neglected:

$$R_1, R'_2, X_{1\sigma}, X'_{2\sigma} \ll R_{Fe}, X_{1h} \tag{18}$$

Fig. 7 Single-phase
transformer; phasor diagram,
iron resistance R_{fe} neglected,
ohmic and stray voltage
drops greatly magnified
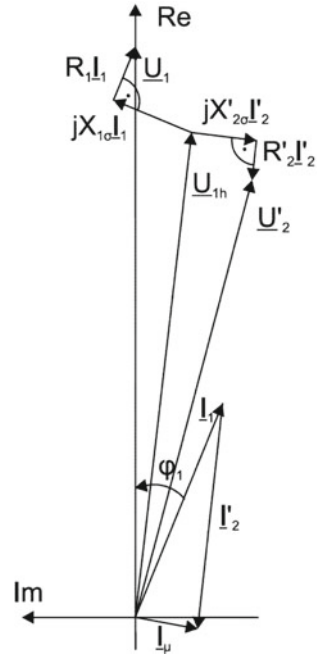
This results in the equivalent circuit as shown in Fig. 8. This is a simple series
R-X network. The following applies:

$$\underline{I}_1 = -\underline{I}'_2 = \underline{I} \tag{19}$$
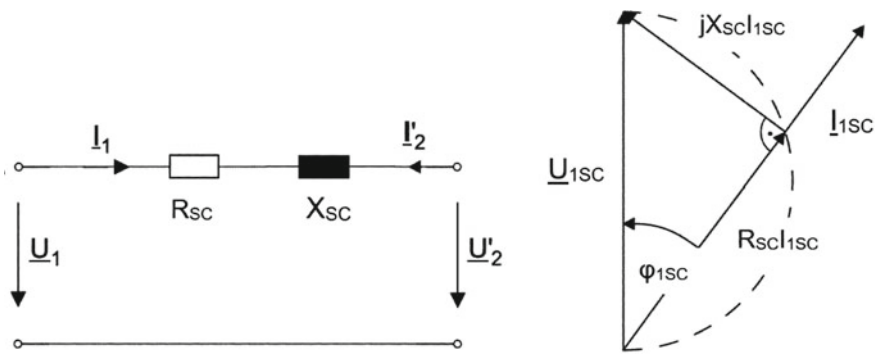
Fig. 8 Simplified equivalent circuit of the transformer (left, U'_2 freely selectable); phasor diagram
of the transformer in short circuit representation (right, $U'_2 = 0$; $I_1 = I_{1SC}$; $U_1 = U_{1SC}$; SC: short
circuited, also called short circuit diagram)

$$Z_{SC} = R_{SC} + jX_{SC}; \quad R_{SC} = R_1 + R_2'; \quad X_{SC} = X_{1\sigma} + X_{2\sigma}' \tag{20}$$

For the characterization of the transformer, the performance in short circuit and the short-circuit voltage U_{SC} are used. To determine this, the simplified equivalent circuit in short circuit representation is used. The transformer is short-circuited on the secondary side. The primary voltage is increased until the rated primary current flows. The resulting primary rated short-circuit voltage is determined according to:

$$\underline{U}_{1SCN} = \underline{Z}_{SC} \cdot \underline{I}_{1N} \tag{21}$$

This voltage represents the voltage drop across the transformer impedances at the rated current. It is considerably smaller than the primary rated voltage. Putting the rated short-circuit voltage in relation to the rated voltage, results in a relative value written u_{SC} that describes the longitudinal impedances in a meaningful way, irrespective of the voltage class of the transformer. It is called relative short-circuit voltage. The value is usually given as a percentage:

$$u_{SC} = \frac{U_{1SCN}}{U_{1N}} \cdot 100\% \tag{22}$$

$$\underline{u}_{SC} = \frac{\underline{U}_{1SCN}}{U_{1N}} = \frac{R_{SC}I_{1N}}{U_{1N}} + j\frac{X_{SC}I_{1N}}{U_{1N}} = u_{1SCR} + ju_{1SCX} \tag{23}$$

The value of short-circuit voltage of power transformers is between around 4–12 %, depending on power and design. Depending on the power, certain values are economical, and higher or lower values can be achieved by suitable design and manufacturing, but generally lead to increased costs.

3.4 Three-Phase Transformers

Three-phase transformers are used to transform three-phase electrical systems. The use of three single-phase transformers would be possible but this is uneconomical and has some technical disadvantages. The three individual transformers are combined into one transformer. A typical design of three-phase transformers, a three leg transformer as used in wind turbines, is shown below in Fig. 9.

The core consists of a rectangular basic shape with two rectangular cut-outs. The vertical parts are called legs, the horizontal parts yokes. On each of the three legs, the primary and secondary windings are applied for one phase of the three-phase system. Depending on the design, these three windings, both primary and secondary, are for example connected in a star (wye) or in a delta connection. (Star: one end parts connected together, other ends result in phase connection; delta: beginning of one and end of the other windings are connected and at the same time phase tapping). Due to the good non-uniform load capacity and the cancellation of certain harmonics,
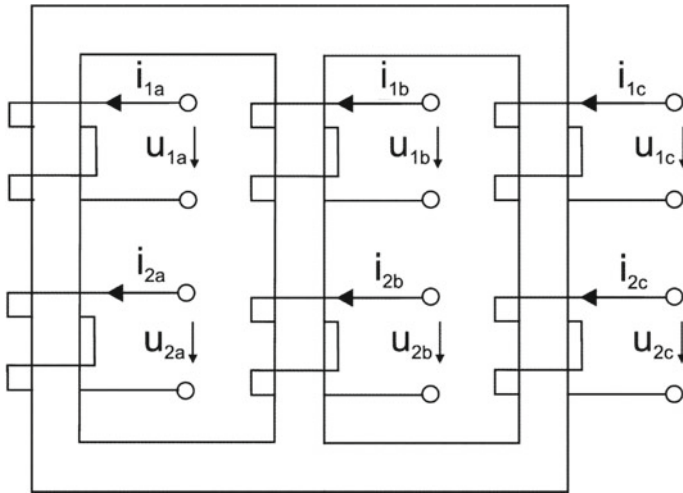
Fig. 9 Three-phase three leg transformer, core structure form, structure of the windings, exemplary representation

interconnections of the windings as a combination of star on one side and delta on the other are common.

The designation of the connection of the windings is made via the abbreviations *D* for delta connection, *Y* for star (wye) connection and *Z* for zigzag connection. An uppercase letter indicates the primary connection, a lowercase letter the secondary connection. The phase shift of the voltages between the primary and secondary windings is given as a number: 12 corresponds to 360°. A common transformer design is the one in delta to star connection with neutral conductor, which has a phase shift primary to secondary of 150°. It is given the abbreviated designation: Dyn5. The designation n indicates that it is a loadable neutral conductor on the secondary side. Typical switching connections are shown in Table 1.

With regard to an unbalanced load, which should, however, hardly occur in wind turbines with three-phase connections, different types of vector groups have different suitability [4]. Star-star circuits (Yyn) with a neutral conductor on the secondary side without a compensating winding in the usual structure designs (three-leg, sheath (mantle), five-leg) are only suitable for low single-phase loads or feed-in of up to

Table 1 Vector groups of three-phase transformers

Vector group or winding connection	Transformation ratio	Phase displacement in multiples of 30°
Yy0	w_1/w_2	0
Dy5	$w_1/\sqrt{3}w_2$	5
Yd5	$\sqrt{3}w_1/w_2$	5
Yz5	$2w_1/\sqrt{3}w_2$	5

10% of the rated power. The other circuit types are fully suitable for three-phase load or supply. The Dyn5 and Yzn5 circuit types are frequently used.

There are also characteristic differences between the circuit types with regards to the transformation or cancellation of harmonics. However, since this concerns the cancellation of low-frequency harmonics (fifth, seventh, etc.) [7], this is not of particular importance for wind turbines with pulse width modulated converters.

Transformers that are connected directly to the power electronics converters, as is the case with wind turbines of not too low power, are referred to as converter transformers. Due to operation at the power electronics converters, these transformers are stressed by converter typical current and voltage harmonics. This leads to increased losses in the iron core due to increased hysteresis and eddy current losses and in the copper due to current displacement at higher frequencies to eddy current losses. The transformers must be designed for this operation.

Three-phase transformers usually behave relatively symmetrically in the individual phases. For this reason, it is permissible for normal considerations to reduce the transformer electrically to its single-phase equivalent circuit and to use the single-phase representation. The voltage equations are given here again:

$$\underline{U}_1 = R_1 \underline{I}_1 + j\omega L_{1\sigma} \underline{I}_1 + j\omega L_{1h}\big(\underline{I}_1 + \underline{I}_2'\big) \tag{24}$$

$$\underline{U}_2' = R_2' I_2' + j\omega L_{2\sigma}' \underline{I}_2' + j\omega L_{1h}\big(\underline{I}_1 + \underline{I}_2'\big) \tag{25}$$

4 Generators for Wind Turbines

Generators in wind turbines are used for the conversion of mechanical power into electrical power. In order to optimize the energy yield of this wind power to electric power conversion, they are used in current installations with variable speed of revolution and therefore fed into the electrical grid via frequency converters (power electronics converter). In addition to the function of controlling the speed of the generator, the frequency converter also has the function of enhanced controllability, both with regards to the generator and the grid feed in.

Various types of power electronic generator systems are used in current wind turbine installations [4, 5]:

- asynchronous machine with squirrel cage rotor, converter on the stator;
- separately excited synchronous machine, converter on the stator;
- permanently excited synchronous machine, converter on the stator;
- doubly-fed asynchronous machine, converter on the rotor.

The different generator types are introduced in this section in the order as shown before.

Prerequisites for the following analyses of the generators are:

- stationary operation;
- neglecting of saturation;
- symmetrical structure;
- constant ohmic resistances.

For more in-depth coverage of the area, the reader is referred to further literature (e.g. [6]).

4.1 Asynchronous Machine with Squirrel Cage Rotor

The asynchronous or induction machine with squirrel-cage rotor is the most widely used machine in industry. It is considered to be very robust and is sometimes also found in the wind industry. Its power range extends from a few watts for small drives to the 10 MW range for boiler feed pumps, for example. In wind turbines, supply voltages of 690 V in the lower MW range and of several kV in the 5 MW and above range are common.

4.1.1 Structure

The induction machine, as shown in Fig. 10, consists of a stator, with a cylindrical hole, in which the rotor, with a cylindrical volume, rotates. Between stator and rotor there is an air gap with a size in the range of millimeters to centimeters. The stator has slots in which the current-carrying windings are inserted with their turns. Machines with three-phase supply are considered here, i.e. fed with sinusoidal voltages of the same amplitude with a phase offset of electrically 120° between the phases. The winding systems are mechanically offset by 120° per pole pair for each phase. Forward and return conductors of the current occur at the circumference $(U - U', V - V', W - W')$. There are several slots per phase in real machines, generally several turns in each slot. In the figure, only one slot per phase is drawn for better clarity. This winding arrangement $(U - U', V - V', W - W')$ can be arranged several times per circumference of the machine. Accordingly, the magnetic poles, outgoing and incoming magnetic fluxes, then occur multiple times around the circumference. This then corresponds to pole pair number count greater than 1 (pole pair number 2: same winding arrangement arranged twice on the circumference, each individual in 180° region).

Like the stator, the rotor can be designed with a three-phase winding, as shown in Fig. 10. In the case of the induction machine with squirrel-cage rotor, the rotor winding is designed as a short-circuit winding which is shorted in the rotor. In the case of the short-circuit winding, the winding does not have to be designed as a three-phase winding. Instead of that, as a common design, bars are equally distributed around the circumference of the rotor and short-circuited at the ends via short-circuit rings. This is called a rotor cage.
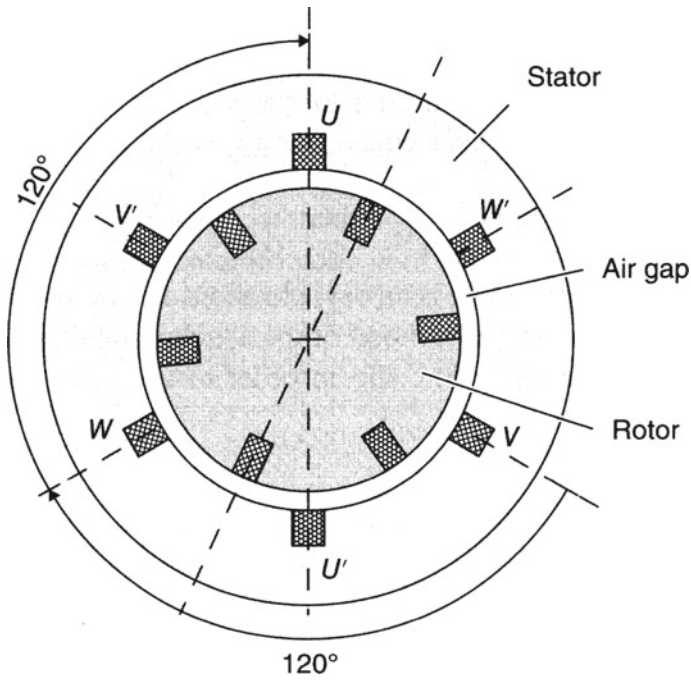
Fig. 10 Structure of a two-pole induction machine with three-phase winding in stator and rotor; number of pole pairs $p = 1$, number of slots $N = 6$ in rotor and stator

4.1.2 Basic Function

A machine with three-phase winding in stator and rotor is considered. The rotor winding is short-circuited. The stator is supplied with a sinusoidal symmetrical three-phase voltage system of frequency f_1. This produces a circumferential moving magnetic field in the machine. The field rotates at the synchronous speed n_{Sync} by one pole pair for each period of the mains frequency. With pole pair number 1 this means the whole circumference per period of the stator frequency, with pole pair number p only the p-th part of the circumference:

$$n_{Syn} = \frac{f_1}{p} \qquad (26)$$

The stator is placed in a stationary position, the rotor rotates with the speed of revolution N, which is, under load, unequal to the synchronous speed and thus unequal to the rotational speed of the stator field. Due to the rotation of the field of the stator in relation to the rotor, a voltage is induced in the rotor and currents are formed in the squirrel-cage rotor. This voltage is proportional to the rotor frequency. The rotor frequency f_2 is proportional to the difference between the stator field speed of revolution n_{Syn} and the rotor speed of revolution n.

$$f_2 = p \cdot (n_{\mathrm{Syn}} - n) = s \cdot f_1 = \frac{n_{\mathrm{Syn}} - n}{n_{\mathrm{Syn}}} \cdot f_1 \qquad (27)$$

The rotor frequency is also given as the product of stator frequency f_1 and slip s. The slip indicates how much the speeds of the rotor and of the stator rotating field deviate from each other in relative terms.

The magnetic rotating field, which rotates at the synchronous speed, and the current induced in the rotor create forces on the rotor winding and thus a torque. This drives the rotor, in motor operation, in the direction of rotation of the rotating field. It tries to reduce the differential speed, to weaken the effect of induction (Lenz's rule). So, the machine is trying to get into synchronism. There, however, no voltage would be induced into the rotor, and no rotor current and no momentum would be produced. The behavior of the machine is thus characterized by the fact that asynchronous operation is required to generate a torque:

$$\text{for } n \neq n_{\mathrm{Syn}} \text{ there is } \quad T \neq 0 \qquad (28)$$

In practical operation, a rotor speed close to the synchronous speed is required to keep the losses small, i.e.:

$$n_{\mathrm{Syn}} - n \ll n_{\mathrm{Syn}}; s = \frac{n_{\mathrm{Syn}} - n}{n_{\mathrm{Syn}}} = \frac{f_2}{f_1} \ll 1; \text{this means} : f_2 \ll f_1 \qquad (29)$$

4.1.3   Voltage Equations

The equations for the machine voltages of the rotor quantities are derived (not shown here) starting from those for a stationary stator and for a rotating rotor in the representation as they would be measured in the rotor. Then the rotor equation is related to the stator (multiplication by w_1/w_2, related values indicated by a superscript) and divided by the slip $s = f_2/f_1$. After this conversion the main voltage parts (at the main inductance) are equal in stator and rotor and make it possible to draw a common circuit diagram as well as a phasor diagram of stator and rotor. After the transformation, the equations for the stator voltage $\underline{U}_1$ and the rotor voltage $\underline{U}_2'$ are obtained in the commonly used form and in complex phasor notation to:

$$\underline{U}_1 = R_1 \underline{I}_1 + j\omega_1 L_{1\sigma} \underline{I}_1 + j\omega_1 L_{1h} (\underline{I}_1 + \underline{I}_2') \qquad (30)$$

$$\frac{\underline{U}_2'}{\frac{f_2}{f_1}} = \frac{f_1}{f_2} R_2' \underline{I}_2' + j\omega_1 L_{2\sigma}' \underline{I}_2' + j\omega_1 L_{2h}' (\underline{I}_1 + \underline{I}_2') \qquad (31)$$

$$L_{1h} = L_{2h}' = \ddot{u}^2 \cdot L_{2h} \qquad (32)$$

R_1: stator resistance; R_2: rotor resistance; $L_{1\sigma}$, $L_{2\sigma}$: stator and rotor leakage inductance.; L_{1h}: stator-related main inductance

The conversion to the stator is carried out with the following equations:

$$\underline{U}_2' = \frac{w_1}{w_2}\underline{U}_2; \quad \underline{I}_2' = \frac{w_2}{w_1}\underline{I}_2; \quad R_2' = \left(\frac{w_1}{w_2}\right)^2 R_2; \quad L_{2\sigma}' = \left(\frac{w_1}{w_2}\right)^2 L_{2\sigma} \tag{33}$$

In order to bring the resulting induced voltages of the stator and rotor to equal values the rotor voltage has to be additionally divided by $\frac{f_2}{f_1}$.

$$\underline{U}_{i1} = j\omega_1 L_{1h}\left(\underline{I}_1 + \underline{I}_2'\right); \quad \frac{\underline{U}_{i2}'}{\frac{f_2}{f_1}} = j\omega_1 L_{2h}'\left(\underline{I}_1 + \underline{I}_2'\right) \tag{34}$$

The stator voltage equation is exactly the same as that for the primary side of the transformer, and the ratios are also the same. The rotor equation is very similar to that for the secondary side of the transformer. Induced voltage components at main and leakage inductances and ohmic voltage drops appear in both equations. A striking feature is the frequency-variable rotor-side resistance $(f_1/f_2)R_2'$ in the rotor equation, which represents the essential difference in these equations to the transformer. Additionally there is the special expression for the rotor voltage $(f_1/f_2)\underline{U}_2'$ characteristic for the peculiarity of the induction machine.

4.1.4 Equivalent Circuit Diagram

The equivalent circuit diagram of the induction machine (Fig. 11) can be set up by means of the equations of the previous section. It corresponds in structure to that of the transformer, although it differs in value in the variable rotor-side resistance $(f_1/f_2)R_2'$ and the rotor voltage $(f_1/f_2)\underline{U}_2'$. As an example, for a squirrel cage rotor, the rotor is short circuited and thus the rotor voltage is set to zero. For consideration of iron losses the iron resistance R_{fe} could be inserted parallel to the main inductance, as in the case of a transformer, but is deleted here.

4.1.5 Phasor Diagram

From the equations of the induction machine in complex notation, a phasor diagram for the voltages and currents can be created in the complex plane, an example is shown in Fig. 12. A phasor diagram is valid for only one operating point.

The stator voltage has been placed in the real axis. The induction machine behaves predominantly inductively, so that the stator current lies in the right half-plane in this representation. From the stator voltage to the induced voltage ($U_{\text{h}} = U_{\text{i}}$) is a voltage drop at the ohmic stator resistance and at the stator leakage inductance. In the induction machine with a squirrel-cage rotor considered here, the rotor-side
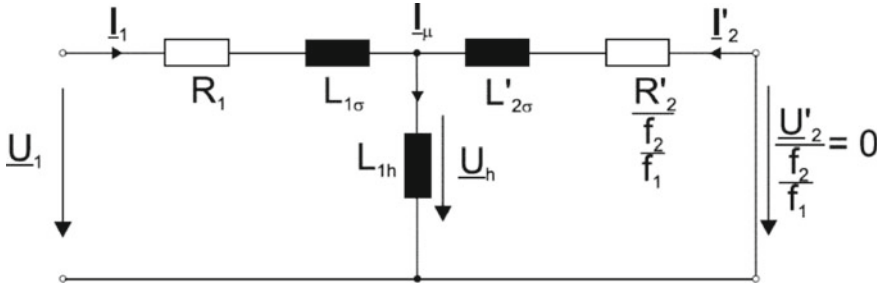
Fig. 11 Single-phase equivalent circuit diagram of the asynchronous machine with squirrel-cage short-circuit rotor

Fig. 12 Phasor diagram of the induction machine with squirrel-cage short-circuit rotor (U_h in the diagram equal to U_i in the equations)
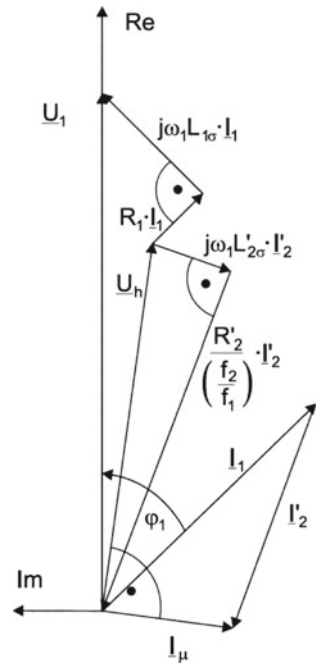
main voltage is generated solely by the voltage drop of the rotor current at the rotor resistance and the stray inductance on the rotor side.

4.1.6   Current Locus Curve - Heyland Diagram

For the consideration and analysis of the operating points of the asynchronous machine with squirrel-cage rotor, the locus curve of the stator current is used. It is called the Heyland circle or Heyland diagram. This circle can be derived from the

voltage equations. For the created equivalent circuit, the complete voltage equation can be set up on the stator side:

$$\underline{U}_1 = \underline{Z}_1 \underline{I}_1 = \left[R_1 + j\omega_1 L_{1\sigma} + \frac{j\omega_1 L_{1h}\left(\frac{R_2'}{\left(\frac{f_2}{f_1}\right)} + j\omega_1 L_{2\sigma}'\right)}{j\omega_1 L_{1h} + \frac{R_2'}{\left(\frac{f_2}{f_1}\right)} + j\omega_1 L_{2\sigma}'} \right] \underline{I}_1 \quad (35)$$

and from this the stator current can be exempted. With the simplification $R_1 = 0$ and $L_1 = (L_{1\sigma} + L_{1h})$; $L_2' = (L_{2\sigma}' + L_{1h})$ this results in the following:

$$\underline{I}_1 = \frac{\left[R_2' + j\frac{f_2}{f_1}\omega_1 L_2'\right]\underline{U}_1}{jR_2'\omega_1 L_1 + \frac{f_2}{f_1}\left((\omega_1 L_{1h})^2 - \omega_1^2 L_1 L_2'\right)} \quad (36)$$

From this simplified ($R_1 = 0$) equation the current locus curve of the asynchronous machine can be developed, as Fig. 13 shows. The equation represents a mathematical expression of the form describing a circle in the complex plane. The construction of the locus of the curve of the current has been exemplified in the figure. The Heyland circle lies with its center on the negative imaginary axis. With knowledge of the smallest stator current $\underline{I}_{10}$ at no-load ($s = 0$, index 0) as well as the largest stator current $\underline{I}_{1\infty}$ ($s \to \infty$, index ∞), which corresponds to a purely theoretical operating point, or the short-circuit current $\underline{I}_{1SC}$ ($s = 1$, index SC), the circle can be drawn.

From the equation for the stator current, the values for special characteristic currents, also drawn in the Heyland circle, can be easily determined. For the no-load current $\underline{I}_{10}$ at $s = 0$ follows (in each case $R_1 = 0$):

$$\underline{I}_{10} = \frac{1}{j\omega_1 L_1} \cdot \underline{U}_1; \quad \left(\sphericalangle(\underline{U}_1, \underline{I}_{10}) = 90^\circ\right) \quad (37)$$

For the ideal short-circuit current $\underline{I}_{1,\infty}$ holds for $s \to \infty$:

$$\underline{I}_{1\infty} = -\frac{j}{\sigma\omega_1 L_1} \cdot \underline{U}_1; \quad \left(\sphericalangle(\underline{U}_1, \underline{I}_{1\infty}) = 90^\circ\right) \quad (38)$$

$$\sigma = \frac{L_1 L_2' - L_{1h} L_{2h}'}{L_1 L_2'} = 1 - \frac{1}{(1 + \sigma_1)(1 + \sigma_2)} \quad \text{(leakage coefficient)} \quad (39)$$

For the starting current or short-circuit current with $n = 0$ and $s = 1$ applies:

$$\underline{I}_{1SC}(s = 1) = \frac{R_2' + j\omega_1 L_2'}{R_2' + j\sigma\omega_1 L_2'} \cdot \frac{1}{j\omega_1 L_1} \cdot \underline{U}_1 \quad (40)$$
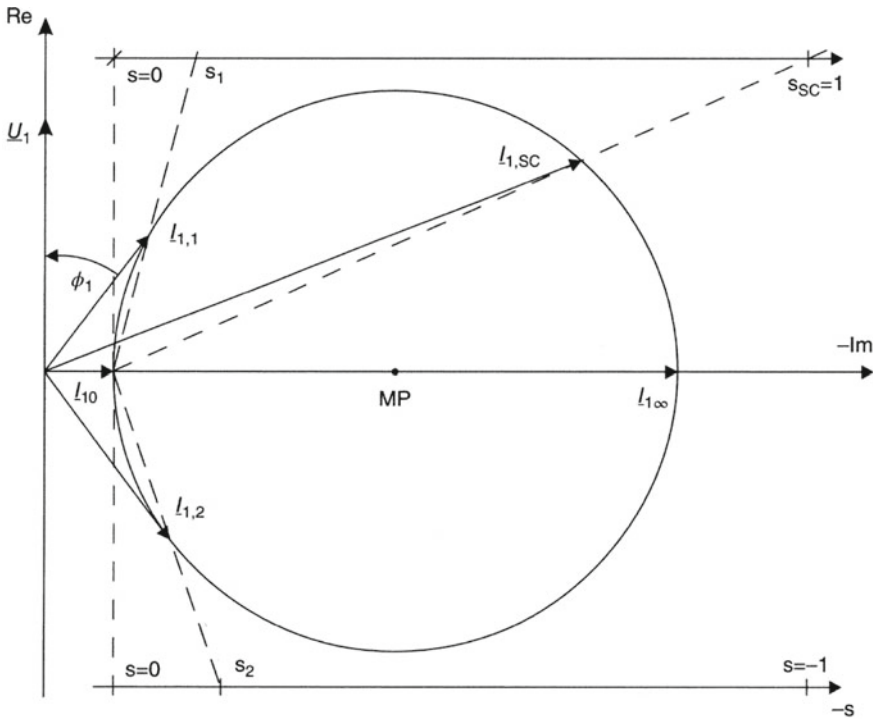
Fig. 13 Heyland circle (current locus curve) of the asynchronous machine with squirrel-cage rotor ($R_1 = 0$)

In addition, two further, freely selected operating points (1, 2) are indicated in Fig. 13 as an example in the Heyland circle diagram. A parameterization of the operating points with the slip can be carried out linearly as shown via the slip line ($s = 0$, $s_{sc} = 1$). The intersection of the straight line through the end point of the phasor $\underline{I}_{10}$, not through the zero current point, and through the end point of the respective current phasor with the vertical slip line results in the slip value (e.g. $= s_{sc} 1$), dashed.

A special point in operation is the optimum point, the point with the largest displacement factor $\cos\varphi_{opt}$ and smallest displacement angle φ_{opt} of the stator current towards the stator voltage. The rated operating point of the machine is often close to this point (I_{11} in Fig. 13). For this operation point it can be derived as (not derived here):

$$I_{1,opt} = \frac{1}{\omega_1 L_1 \sqrt{\sigma}} \cdot U_1; \quad \cos\varphi_{opt} = \frac{1-\sigma}{1+\sigma} \tag{41}$$

This operating point is also very characteristic in the Heyland circuit, since the stator current here forms a tangent to the Heyland circuit.

4.1.7 Power

The power in the machine is made up of the power of the rotating field P_{RF}, the power transmitted to the rotor via the rotating field, from the stator to the rotor. For the assumption made here, $R_1 = 0$, it is equal to the stator power P_1 and is calculated for a three-phase machine with the aid of the star voltage $U_{1,\text{Star}}$ or the phase-to-phase or delta or interlinked voltage $U_{1,\Delta}$:

$$P_D = 3 \cdot U_{1,\text{Star}} \cdot I_1 \cdot \cos \varphi_1 = 3 \cdot U_{1,\text{Star}} \cdot \text{Re}\{\underline{I}_1\} = \sqrt{3} \cdot U_{1,\Delta} \cdot I_1 \cdot \cos \varphi_1 \quad (42)$$

It should be noted here that nameplate data normally represent the value of the phase-to-phase voltage. The horizontal part of the stator current phasor of the Heyland circle, the real part of the complex stator current, represents the active part I_{1a} of the current (see Fig. 14):

$$I_{1a} = \text{Re}\{\underline{I}_1\} \quad (43)$$

The machine always behaves inductively as the stator current has a negative imaginary component.

The rotating field active power P_{RF} can be split into several parts. If the iron losses are neglected, the full power is transferred to the rotor. There it is converted in total in the resistance $(f_1/f_2)R_2'$ on the rotor side. Thereby ohmic losses occur as power losses $P_{2\text{loss}}$ only in the natural resistance R_2' while the remaining power $P_{RF} - P_{2\text{loss}}$ is equal to the mechanical power P_{mech}. It can be expressed by the product of torque T and speed of revolution n.

$$P_{RF} = 3 \cdot \frac{R_2'}{s} \cdot I_2'^2 \quad (44)$$

$$P_{2\text{loss}} = 3 \cdot R_2' \cdot I_2'^2 = s \cdot P_{RF} \quad (45)$$

$$P_{\text{mech}} = P_{RF} - P_{2\text{loss}} \quad (46)$$

Fig. 14 Heyland circuit for $R_1 = 0$, highlighted: Active current component I_{1a} and reactive current component I_{1r} of the stator current
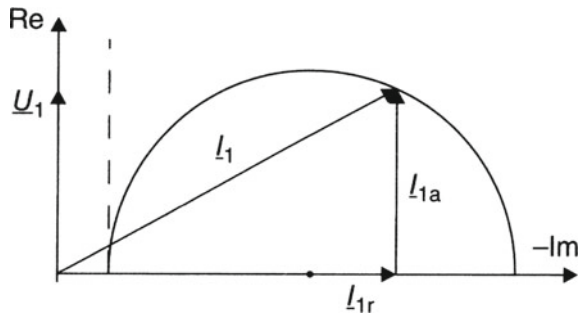
$$P_{\text{mech}} = (1 - s) \cdot P_{\text{RF}} = 2\pi \cdot n \cdot T \tag{47}$$

4.1.8 Torque

The torque can be calculated from the rotating field power.

$$P_{RF} = \frac{\omega_1}{p} \cdot T = 2\pi \cdot n_{\text{syn}} \cdot T = 3 \cdot \frac{R_2'}{s} \cdot I_2'^2; \, n_{\text{syn}} = \frac{\omega_1}{2\pi p} \tag{48}$$

This is done by determining the rotor current as a function of the stator voltage from the equations and inserted in the above formula, not derived here. This results in the Kloss formula:

$$\frac{T}{T_{\text{stall}}} = \frac{2}{\frac{s_{\text{stall}}}{s} + \frac{s}{s_{\text{stall}}}} \tag{49}$$

$$T_{\text{stall}} = \frac{3}{\frac{\omega_1}{p}} \cdot \frac{1 - \sigma}{(1 + \sigma_1) \cdot \sigma \cdot 2 \cdot \omega_1 L_{1h}} U_1^2; \quad s_{\text{stall}} = \frac{R_2'}{\sigma X_2'} \tag{50}$$

Here σ_1 and σ_2 are the primary and secondary leakage coefficients. They indicate how large the leakage inductance, which generates the leakage flux not connecting the stator and rotor sides, is in relation to the main inductance. The main inductance generates the flux connecting both sides.

$$\sigma_1 = \frac{L_{1\sigma}}{L_{1h}}; \quad \sigma_2 = \frac{L_{2\sigma}'}{L_{1h}} \tag{51}$$

The stalling torque T_{stall} indicates the highest value of the torque, this occurs at the stalling slip s_{stall}. The course of the torque curve over the speed is the typical characteristic curve of a machine and is shown in Fig. 15. In the right part of the diagram motor operation takes place, in the left part generator operation.

At no load, the machine is in synchronous operation at the synchronous speed n_{syn}. In motor operation, the speed is below the synchronous speed, the slip and the torque are positive. In regenerative operation, the speed is above the synchronous speed, the slip and the torque are negative. In load operation, the speed deviates from the synchronous speed according to the required torque. Continuous operation is possible with the machine up to the nominal slip, in which case, depending on the design, approximately 30–50% of the breakdown or stalling torque is reached.

In the range of speeds above the positive or below the negative stalling slip, the machine is statically unstable. For motor operation, for example, an increasing load torque would result in a falling machine torque and thus a drop in speed and the machine would come to a standstill.
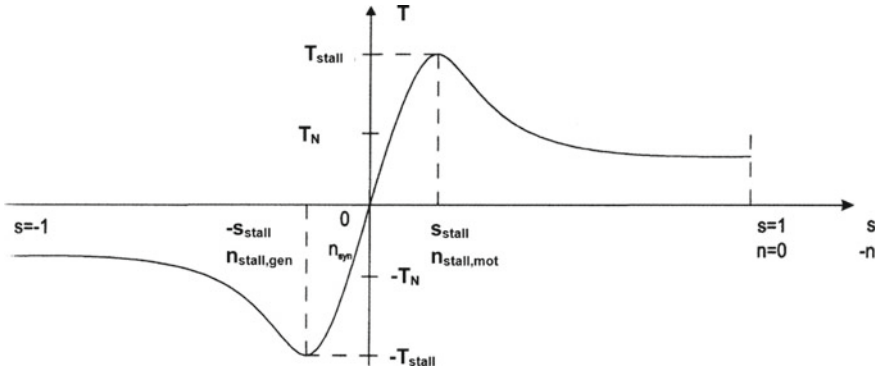
Fig. 15 Torque-speed diagram of the asynchronous machine with squirrel-cage rotor at fixed stator frequency

At start-up, the machine starts with slip one and runs on the characteristic torque-slip curve shown to the point with the required torque. For wind turbines according to the "Danish principle", the characteristic curve from Fig. 15 would be the operating characteristic curve of the generator.

4.1.9 Speed Control of the Asynchronous Machine with Squirrel Cage Rotor

Neglecting the stator resistance, the stator voltage is equal to the derivative of the stator flux linkage. If the voltage is sinusoidal, the result is:

$$U_1(R_1 = 0) = \hat{U}_1 \cos \omega_1 t = -\frac{d\Psi_1}{dt} = \omega_1 \hat{\Psi}_1 \cos \omega_1 t \tag{52}$$

The torque of the machine is formed from the flux in the machine and the electrical loading, the current distribution over the airgap. In addition, a corresponding mutual angular position between both is assumed. The flux is generally kept constant (control to constant flux), usually to the nominal value, at variable speed operation and the torque is set via the stator current. For this constant stator flux linkage Ψ_1 with nominal value (index N) in the machine, neglecting the stator resistance, results, in cosinusoidal quantities:

$$\Psi_1 := \Psi_{1N} = \frac{U_1}{\omega_1} = \frac{U_{1N}}{\omega_{1N}} = \text{const.} \tag{53}$$

Thus, a simplified control law for variable speed operation applies. It states that the stator voltage must be adjusted proportional to the stator angular frequency or stator frequency. This is shown by Fig. 16. However, in the range of small stator frequency ($\omega_1 < \omega_{1min}$), the resistive component increases sharply in relative terms,
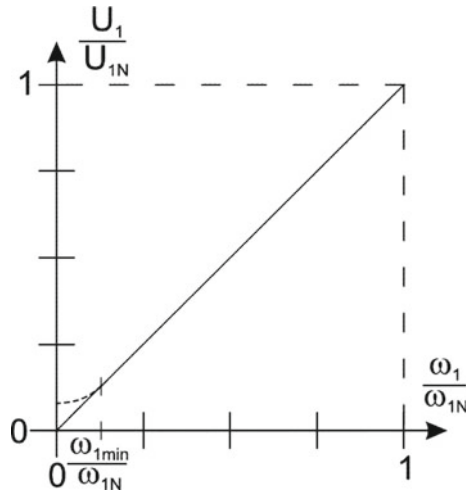
for motor operation. For this range, it would have to be included and the characteristic curve shown in the dashed line results, exemplarily.

In the following, the effect of this control on the torque behavior will be shown. In the equation for the stalling torque (Kloss' formula 50) one finds the term $(U_1/\omega_1)^2$, which under the condition of $R_1 = 0$ is equal to Ψ_1^2, i.e. the stator flux linkage, as the only dependence on operating point-dependent variables. By controlling to constant stator flux, this term is controlled to be constant as described. Thus, the stalling torque remains at its value and thus also the torque equation under speed control conditions as in fixed frequency operation, independent of the level of the selected stator frequency. This has the consequence that for any stator frequency Kloss' formula applies in the same way, here written as a function of rotor frequency ω_2 in place of the slip.

$$T = T_{\text{Stall}} \cdot \frac{2}{\frac{\omega_2}{\omega_{2\text{Stall}}} + \frac{\omega_{2\text{Stall}}}{\omega_2}}; \quad \omega_{2\text{Stall}} = \frac{R_2'}{\sigma L_2'} \tag{54}$$

This results in the speed-torque characteristics curve according to Fig. 17. Here the characteristic curves are plotted against the speed, i.e. reversed as in the original torque-slip diagram. Thus, the machine can be operated in the range from zero speed to the rated speed with a maximum torque in the value of the rated torque ($T_{\text{rat}} = T_N$), operated as a motor ($T > 0$) or operated as a generator ($T < 0$). Continuous speed control with full torque capability is possible based on the machine behavior fed from a frequency converter.

For the rotating field power $P_{\text{RF,vs}}$ at rated stator current I_{1N} for variable speed operation (Index vs), the following applies for this control under the condition $R_1 = 0$, here using the phase-to-phase voltages (cs: constant speed):
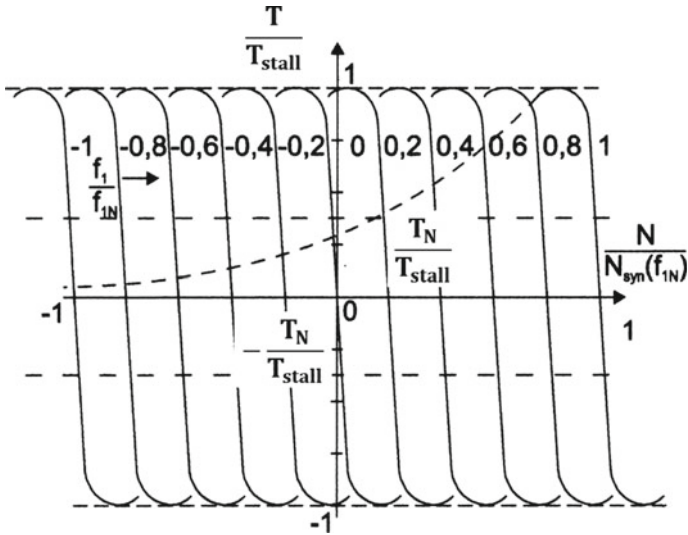
Fig. 17 Torque-speed curves of the asynchronous machine with squirrel-cage rotor for control to constant stator flux linkage Ψ_{1N}

$$P_{RF,vs}(I_{1N}) = \sqrt{3} \cdot U_{1\Delta} \cdot I_{1N} \cdot \cos \varphi_{1N} = \sqrt{3} \frac{\omega_1}{\omega_{1N}} U_{1\Delta N} I_{1N} \cos \varphi_{1N}$$

$$= \frac{\omega_1}{\omega_{1N}} \cdot P_{RFN,cs} \tag{55}$$

Thus, with constant stator current, the power depends proportionally to the stator frequency. According to the results of the derivations, this operating range is also called: Constant torque region, full flux region, region of active power proportional to stator frequency.

A basic implementation of such a control in its simplest form is shown in Fig. 18. The asynchronous machine with squirrel-cage rotor is fed via a frequency converter. On the input side, this is connected to the mains with a fixed voltage amplitude and frequency. Towards the machine, the amplitude and frequency of the voltage can be adjusted as required. The converter is operated via a control system in such a way that the specifications according to the above derivation are adhered to, namely $(U_1/\omega_1) = $ constant. This is done by giving the frequency converter the set value of the stator frequency, approximately proportional to the set value of the speed. The stator setpoint voltage must be specified with a corresponding factor proportional to the stator frequency. This is done in a characteristic curve block (doubly surrounded in the figure). If the stator resistance is to be included, necessary especially at low stator frequencies, the rotor frequency f_2 is required as a further input variable. It represents an equivalence to the torque and the stator current. Depending on the rotor frequency, the characteristic curves are to be shifted slightly upwards or downwards (dashed lines).
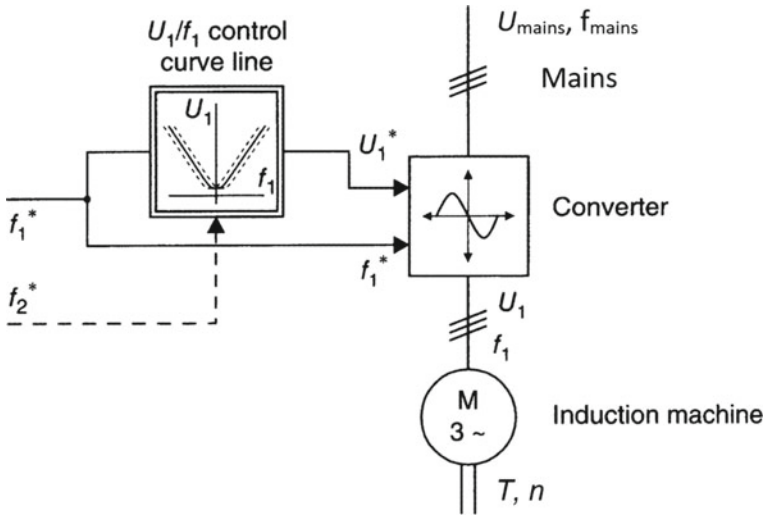
Fig. 18 Overview structural diagram for feeding an asynchronous machine with squirrel-cage rotor via a frequency converter with characteristic curve for flux control

This structural diagram of the speed control serves to clarify the concept. Today's control systems are usually implemented differently, generally as field-oriented control, with much better dynamic behavior.

4.2 Asynchronous Machine with Slip Ring Rotor

Asynchronous machines with slip ring rotor are mainly used for high power applications where asynchronous machines with squirrel cage rotors cannot be built. This is, for example, the motor/generator in pumped storage power plants with outputs up to over 100 MW. From the 1990s onwards, they were increasingly used for smaller outputs below and above 1 MW, namely in variable-speed wind turbines.

The asynchronous machine with slip ring rotor has a special advantage when used in the wind turbine. When used as a speed-controllable generator, in contrast to the other variants with a converter on the stator, as shown in the introduction, here the stator is connected directly to the grid and only the rotor is connected via a frequency converter, as Fig. 19 shows. Thus, the term "doubly-fed asynchronous machine" is used for this.

The frequency converter must only be designed for the required speed range, which corresponds to the power range. In the case of wind turbines, the converter must be designed for approximately 30 % of the rated power. This leads to a partial power converter, which is reflected in lower costs. Converters which are connected to the generators on the stator side in the other systems must be designed for full power,
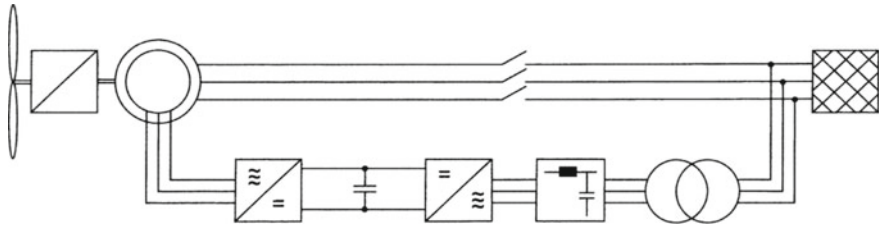
Fig. 19 Block diagram of the asynchronous machine with slip ring rotor and converter in the wind turbine

they are named full power converters. The disadvantage of asynchronous machines with slip ring rotors, however, is that the slip rings require high maintenance and that the machine is directly connected with the stator to the mains. Due to the direct stator coupling with the mains, the behavior when passing through mains short-circuits is difficult to control. The behavior of the stator of the machine at the mains can only be controlled indirectly via the rotor side converter. With a full-power stator-side converter in the other systems mains side control is easier to realize.

4.2.1 Structure

As in all three-phase machines considered here, the stator of the asynchronous machine with a slip ring rotor is built up of three-phase windings. The coils of the three phases $(U - U', V - V', W - W')$ are mechanically offset from each other by 120° and arranged on the circumference of the stator for each pole pair. The windings are positioned in the required number of slots (see Fig. 20).

The rotor is equipped with a three-phase winding of the same type as the stator. At the figure, because of simplicity of presentation, only one slot is shown per phase and pole. The rotor-side windings are accessible from the stator via slip rings. Slip rings consist of rotating copper rings, at least one per phase, which are electrically insulated and fixed to the rotor. They rotate with the rotor and are connected to the rotor windings. On the stator side, carbon brushes are used to tap the current. These are attached to the stator and are pressed onto the slip rings by means of springs.

4.2.2 Basic Function

The stator and the rotor of the asynchronous machine with slip ring rotor are equipped with a three-phase winding. The stator is connected to a cosine-shaped, symmetrical three-phase voltage system of frequency f_1, the rotor to one of frequency f_2. A rotating field is generated by both winding systems. This results in a cosine-shaped magnetic field distributed over a pair of poles, which circulates in proportion to the respective supply frequency.
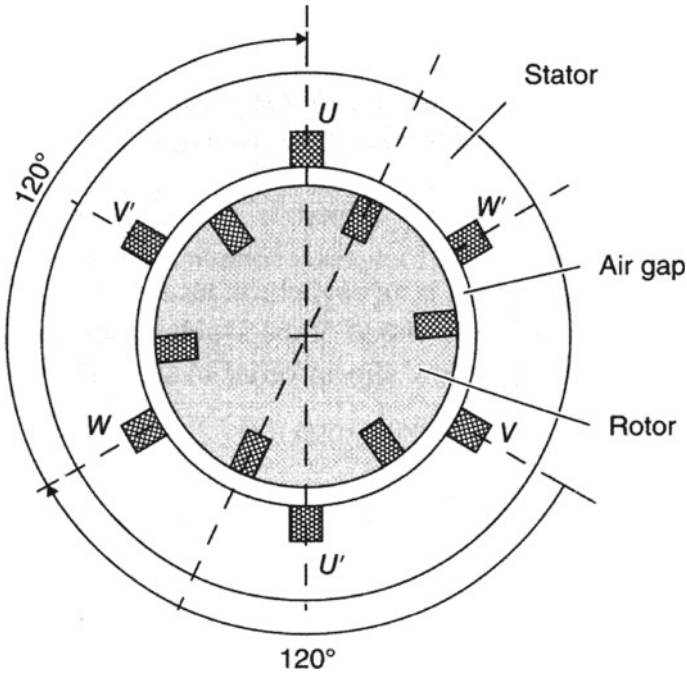
Fig. 20 Design of an asynchronous machine with slip ring rotor (number of pole pairs $p = 1$; number of slots $N = 6$ in rotor and stator); access to the rotor via slip rings

The stator field rotates at the speed n_{1syn}, during a period of the stator frequency the field rotates over one pole pair.

$$n_{1syn} = \frac{f_1}{p} \tag{56}$$

The rotor rotates at speed n. The rotor field is generated by the rotor frequency f_2 and therefore rotates at speed f_2/p in relation to the rotor. A constant torque is only generated if the field of the rotor and that of the stator rotate at the same speed. This is the case if the following applies:

$$n_{1syn} = \frac{f_1}{p} = n + \frac{f_2}{p} \tag{57}$$

$$n = n_{1syn} - \frac{f_2}{p} \tag{58}$$

This equation thus represents the operating condition of the asynchronous machine with slip ring rotor. For a given, fixed stator frequency f_1 the speed of revolution of the rotor n is obtained by subtracting the controllable rotor frequency f_2/p, which

is specified via the rotor-side converter, from the synchronous speed $n_{1\text{syn}}$. If the rotor frequency is selected to be zero, the speed is equal to the rotational speed of the stator rotating field, the synchronous speed. This corresponds to a DC supply in the rotor. The behavior is then that of a separately excited synchronous machine fed with direct current in the rotor. If the rotor frequency is selected different from zero, the speed can be controlled to other values, above or below the synchronous speed.

4.2.3 Voltage Equations

The voltage equations are the equations of the asynchronous machine with voltage at the rotor, the derivation of which was sketched for the asynchronous machine with squirrel-cage rotor (Sect. 4.1.3):

$$\underline{U}_1 = R_1\underline{I}_1 + j\omega_1 L_{1\sigma}\underline{I}_1 + j\omega_1 L_{1\text{h}}\left(\underline{I}_1 + \underline{I}_2'\right) \tag{59}$$

$$\frac{\underline{U}_2'}{\frac{f_2}{f_1}} = \frac{R_2'}{\frac{f_2}{f_1}}\underline{I}_2' + j\omega_1 L_{2\sigma}'\underline{I}_2' + j\omega_1 L_{2\text{h}}'\left(\underline{I}_1 + \underline{I}_2'\right) \text{ mit } L_{2\text{h}}' = L_{1\text{h}} \tag{60}$$

U_1: stator voltage; U_2: rotor voltage; I_1: stator current; I_2: rotor current; ω_1: stator angular frequency; R_1: stator resistance; R_2: rotor resistance; $L_{1\sigma}$, $L_{2\sigma}'$: stator and rotor leakage inductance; L_{1h}: stator-related main inductance.

The conversion of the rotor values to the stator, marked by a superscript (X'), is carried out as for the asynchronous machine with squirrel-cage rotor with the following equations via the number of windings w_1 and w_2:

$$\underline{U}_2' = \frac{w_1}{w_2}\underline{U}_2; \quad \underline{I}_2' = \frac{w_2}{w_1}\underline{I}_2; \quad R_2' = \frac{w_1^2}{w_2^2}R_2; \quad L_{2\text{x}}' = \frac{w_1^2}{w_2^2}L_{2\text{x}} \tag{61}$$

The similarity with the equations of the transformer is obvious. Again, as in the transformer, induced voltage components at main and leakage inductance and ohmic voltage drops appear in both equations. Remarkable is the frequency-variable, rotor-side resistance $(f_1/f_2)R_2'$ and the rotor voltage multiplied by the frequency ratio $(f_1/f_2)U_2'$. For feeding with variable rotor voltage by means of the converter, the latter expression becomes the characteristic variable. The equations thus $(U_2 \neq 0)$ deviate strongly from those of the asynchronous machine with squirrel-cage rotor.

4.2.4 Equivalent Circuit Diagram

With the aid of these equations, the single-phase equivalent circuit of the asynchronous machine with slip ring rotor according to Fig. 21 can be created. It corresponds to the asynchronous machine with squirrel cage rotor except for the peculiarity
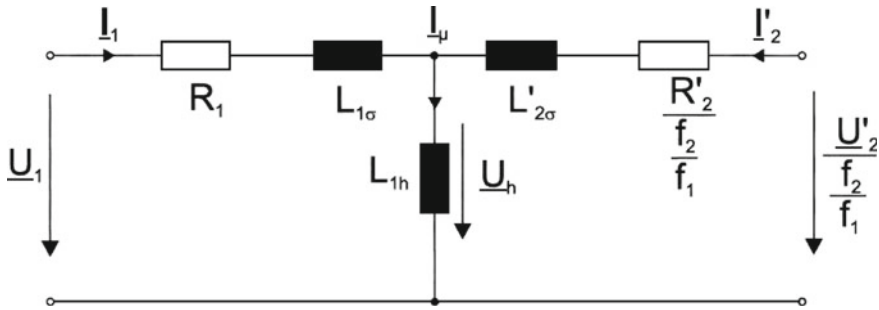
Fig. 21 Equivalent circuit diagram of the asynchronous machine with slip-ring rotor
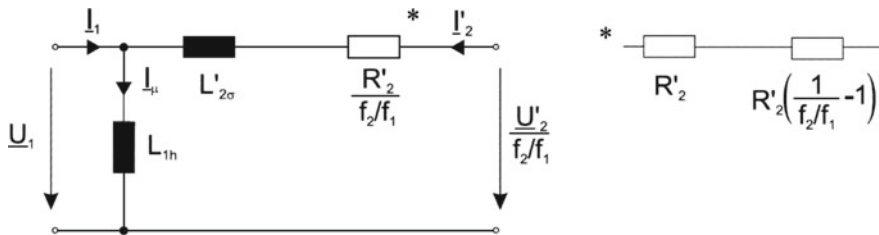
Fig. 22 Simplified equivalent circuit diagram of the asynchronous machine with slip ring rotor, with $R_1 = L_{1\sigma} =: 0$

that here the rotor voltage is different from zero. In order to take the iron losses into account, the iron resistance R_{fe} could be inserted parallel to the main inductance.

To enable a formula description of this system with limited effort, a very simplified equivalent circuit is used, where the stator resistance R_1 and the stator leakage inductance $L_{1\sigma}$ are neglected, as shown in Fig. 22. Nevertheless, the accuracy is reduced. In the separate figure on the right side, the rotor resistance is exemplarily divided into part R_2, which generates losses, and a part which contributes to the mechanical power as is shown below.

By another more complicated conversion, therefore see [7], this structure could also be developed from the equivalent circuit with stator-side leakage inductance included where only the stator resistance is neglected.

4.2.5 Phasor Diagram and Current Locus Curve

The formulas for the behavior of the asynchronous machine with slip ring rotor with rotor supply by means of a frequency converter are derived here step by step. The derivation is performed on a very simplified equivalent circuit ($R_1 = L_{1\sigma} =: 0$), see Fig. 22. This enables an interpretation of the behavior with limited effort, but on the other hand it leads to reduced accuracy.

The rotor current is determined from the equivalent circuit with the aid of the voltage drop across the longitudinal impedances:

$$\underline{I}_2' = \frac{\frac{\underline{U}_2'}{\frac{f_2}{f_1}} - \underline{U}_1}{j\omega L_{2\sigma}' + \frac{R_2'}{\frac{f_2}{f_1}}} \tag{62}$$

If the stator voltage is placed in the real axis and the rotor voltage is divided into an active component (Index a) in the real direction and a reactive component (Index r) in the imaginary direction, then the following applies:

$$\underline{U}_1 = U_1; \quad \underline{U}_2' = U_{2a}' + jU_{2r}' \tag{63}$$

and the rotor current follows:

$$\underline{I}_2' = \frac{\left[\frac{U_{2a}'}{\frac{f_2}{f_1}} + \frac{U_{2r}'}{\frac{f_2}{f_1}}\right] - U_1}{j\omega L_{2\sigma}' + \frac{R_2'}{\frac{f_2}{f_1}}} \tag{64}$$

Expanding the denominator conjugate complex to get a real value, multiplying the numerator by the same value, and then breaking down the numerator, we get the following equation for rotor current:

$$\underline{I}_2' = \frac{-U_1 \frac{R_2'}{(f_2/f_1)} + U_{2a}' \frac{R_2'}{(f_2/f_1)^2} + \omega_1 L_{2\sigma}' \frac{U_{2r}'}{(f_2/f_1)} + j\omega_1 L_{2\sigma}' U_1 - j\omega_1 L_{2\sigma}' \frac{U_{2a}'}{(f_2/f_1)} + jU_{2r}' \frac{R_2'}{(f_2/f_1)^2}}{R_2'^2/(f_2/f_1)^2 + \omega_1^2 L_{2\sigma}'^2} \tag{65}$$

The equation contains six terms in the numerator, two of which depend only on the stator voltage, the other four only on the rotor voltage. This allows the phasor diagrams to be drawn for different operating points.

The phasor diagram of the asynchronous machine with slip ring rotor in Fig. 23 for different operating points characterizes its behavior. In part (a) the state of the rotor current zero by means of equal voltages is illustrated, the active power is equal to zero. In parts (b) and (c) the amplitude and the phase position of the rotor voltage are controlled in a different way, and it can be clearly seen how thereby the rotor current can be set. If the magnetizing current is neglected, the rotor current referred to the stator would be I_2' and would be equal to the stator current. With the inclusion of the magnetizing current, the stator current is obtained equal to $\underline{I}_1$ as shown.

If the stator resistance is neglected, the active rotating field power P_{RF} becomes equal to the active stator power P_1. In the following, star voltages are used.

$$P_{RF} = P_1 = 3U_1 I_1 \cos\varphi_1 \tag{66}$$

The real power losses in the rotor are:
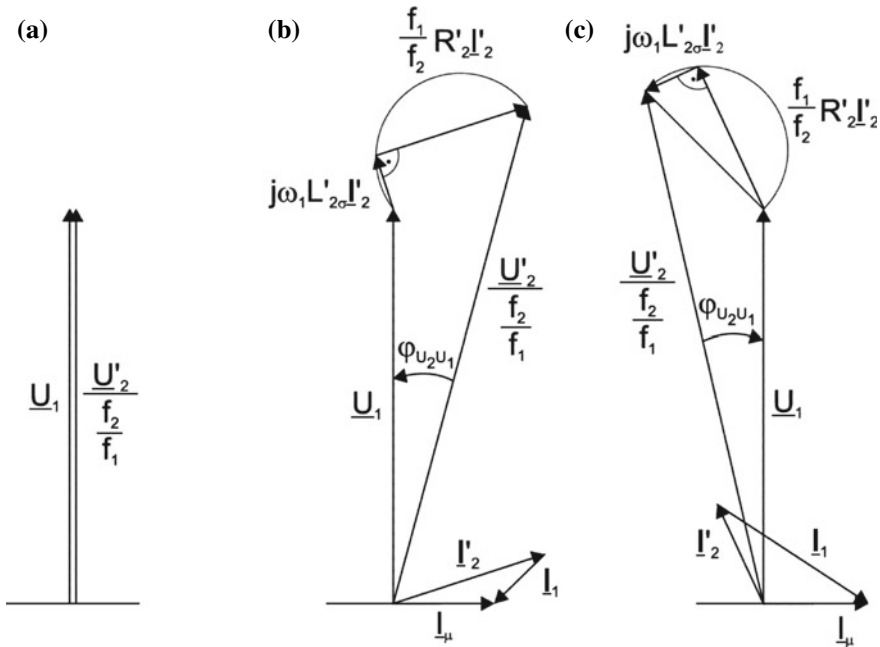
Fig. 23 Phasor diagrams of the asynchronous machine with slip ring rotor and rotor supply: **a** $U_1 = U_2' \frac{f_1}{f_2}$, $P = 0$; **b** $U_2' \frac{f_1}{f_2} > U_1$, angle > °; **c** $U_2' \frac{f_1}{f_2} > U_1$; angle < 0

$$P_{2loss} = 3R_2' I_2'^2 = 3R_2 I_2^2 \tag{67}$$

and the power fed into the rotor by the converter:

$$P_{conv} = 3U_2' I_2' \cos \varphi_2 \tag{68}$$

This results in the mechanical power P_{mech} as the sum of the rotating field power and the power fed in via the converter, subtracting the rotor power losses. It depends in another relation of the rotor frequency, which can be positive or negative.

$$P_{mech} = P_{RF} + P_{conv} - P_{2loss} = \left(1 - \frac{f_2}{f_1}\right) P_{RF} \tag{69}$$

$$P_{2loss} - P_{conv} = \frac{f_2}{f_1} P_{RF} \tag{70}$$

With the previous equations, active power as part of the rotating field power and additionally the torque and subsequently the mechanical power can be determined. Star voltages are assumed in each case.

$$P_{RF} = \text{Re}\{3\underline{U}_1\underline{I}_2'^*\} = 3U_1 \frac{-U_1 \frac{R_2'}{(f_2/f_1)} + U_{2a}' \frac{R_2'}{(f_2/f_1)^2} + \omega_1 L_{2\sigma}' U_{2r}' \frac{1}{(f_2/f_1)}}{\frac{R_2'^2}{(f_2/f_1)^2} + \omega_1^2 L_{2\sigma}'^2} \tag{71}$$

$$T = \frac{P_{RF}}{\omega_1} = 3\frac{U_1}{\omega_1} \frac{-U_1 \frac{R_2'}{(f_2/f_1)} + U_{2a}' \frac{R_2'}{(f_2/f_1)^2} + \omega_1 L_{2\sigma}' U_{2r}' \frac{1}{(f_2/f_1)}}{\frac{R_2'^2}{(f_2/f_1)^2} + \omega_1^2 L_{2\sigma}'^2} \tag{72}$$

$$P_{mech} = 2\pi n \cdot T \tag{73}$$

The reactive power as part of the rotating field power is determined by means of the imaginary part:

$$Q_{RF} = \text{Im}\{3\underline{U}_1\underline{I}_2'^*\} = 3U_1 \frac{-\omega_1 L_{2\sigma}' U_1 + \omega_1 L_{2\sigma}' \frac{U_{2a}'}{(f_2/f_1)} - \frac{R_2'}{(f_2/f_1)^2} U_{2r}'}{\frac{R_2'^2}{(f_2/f_1)^2} + \omega_1^2 L_{2\sigma}'^2} \tag{74}$$

At fixed rotor frequency, i.e. fixed speed, it can be seen from these equations that by varying the components of the rotor voltage (U_{2a}', U_{2r}'), the power and torque can be controlled.

The total power P_{tot} absorbed from the grid via the rotor and stator, which is composed of the stator-side rotating field power P_{RF} and the rotor-side terminal power or converter power P_{conv}, assuming that the converter on the rotor operates without losses, is:

$$P_{tot} = P_{grid} = P_{RF} + P_{conv} = \begin{cases} \eta \cdot P_{mech} & \text{in generator operation} \\ \frac{1}{\eta} \cdot P_{mech} & \text{in motor operation} \end{cases} \tag{75}$$

The total active power P_{tot} is equivalent to the mechanical power in case of neglecting the losses. An efficiency factor has to be added, including the losses, depending on generator operation (η) or motor operation ($1/\eta$).

Due to many components in the equations, it is not easy to obtain an overview of the power flow. This can be well illustrated for different operating points by a power flow diagram.

In Fig. 24 the usual operating ranges of the under- and over-synchronous generator operation for wind turbines are shown. In generator operation, the power is absorbed by the shaft and fed into the grid. For example, sub-synchronous operation would, for wind turbines, be a common speed range of $n_{min} = 1150\,\text{min}^{-1}$ to $n_{nom} = 1500\,\text{min}^{-1}$ for a 2-pole-pair machine on the 50 Hz grid. In super-synchronous operation, power P_{RF} from the stator-side rotating field and P_{conv} from the rotor are fed into the mains via the converter. The mains power is greater than the stator power by the value of the rotor power. For sub-synchronous operation, this is done analogously, but with subtraction of the rotor power from the stator power to the mains power. In the figure, the stator and rotor losses (P_{1loss}, P_{2loss}) are also included.
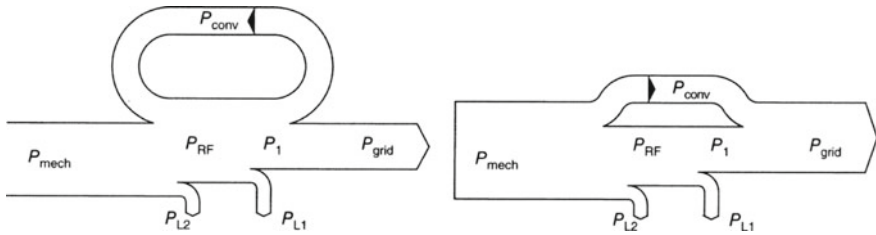
Fig. 24 Power flow in the asynchronous machine with slip ring rotor in generator operation (doubly-fed asynchronous machine; left: sub-synchronous operation; right: super-synchronous operation) (P_{conv}: converter power; P_{L1}, P_{L2}: stator and rotor power loss; P_{RF} rotating field power)

4.2.6 Speed Control

The speed of the doubly-fed asynchronous machine is controlled by feeding the rotor by means of a frequency converter. This converter controls the rotor voltage in the amplitude U_2 and the rotor frequency f_2 to the setpoint, regarded in steady state of view.

To evaluate the behavior, at first the no load point is regarded. It is assumed, that the reactive part I'_{2r} of the rotor current (see Eq. 65) is zero. Setting the remaining active part I'_{2a} of the rotor current to zero gives the following equation. For the rotor frequency f_2 the expression f_{20} is chosen as for no-load rotor idling frequency.

$$\frac{f_{20}}{f_1} = \frac{U'_{2a}/U_1}{1 - \frac{U'_{2r}/U_1}{f_{2SC}/\omega_1}}; \quad f_{2SC} = \frac{R'_2}{L'_{2\sigma}} \tag{76}$$

In case where the rotor reactive voltage U'_{2r} is also controlled to zero, the no-load rotor idling frequency becomes:

$$\frac{f_{20}}{f_1} = \frac{U'_{20}}{U_1} \tag{77}$$

It can be seen, that for this no-load case, with a fixed stator frequency and fixed stator voltage, equal to that of the mains, the rotor voltage U'_2 is to be controlled as a function of the rotor frequency f_2 or vice versa. The rotor frequency indicates the deviation from the synchronous speed. In case of synchronism, the rotor rotates at the speed of the stator rotating field, the rotor frequency and thus the rotor open-circuit voltage are zero. Outside synchronism, the magnetic field of the stator turns with a speed of revolution different from that of the rotor. Thus, the rotor has to be fed with the difference frequency $f_2 = \omega_1/2\pi - p \cdot n$. For no-load operation Eq. 77 is applied. The rotor voltage has to be controlled linearly to the rotor frequency.

Corresponding to the operating range in wind turbine applications, which typically extends from -30 to $+30\%$ around the base speed, there is an equal voltage range
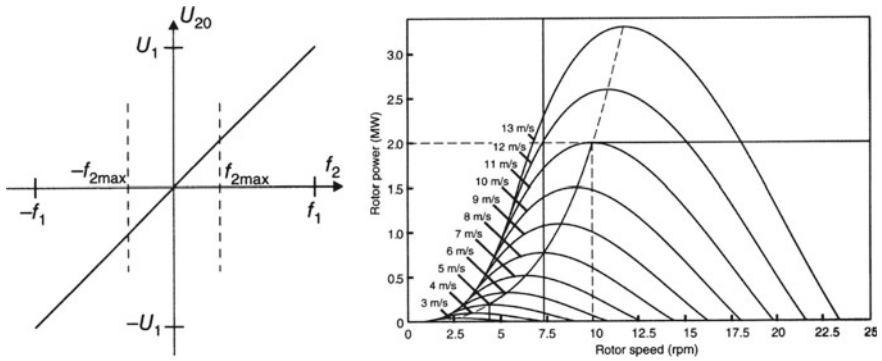
Fig. 25 Variable speed operation of the asynchronous machine with slip ring rotor (doubly-fed asynchronous machine), example; left: control characteristic curve for rotor voltage at no-load with $U'_{2r} = 0$, right: operating range in power-speed diagram, curve through maxima; typical range for wind turbines: $-0.3 \, f_1 < f_2 \ < +0.3 \, f_1$; 4 m/s $< v_{wind} \ < 12$ m, limit 20 m/s; 4 min^{-1} $< n \ < 10$ min^{-1}... 18 min^{-1}

for the rotor open-circuit voltage U_{20}. Under load, additional voltage components need to be added to allow the current to flow across the rotor.

This results in a voltage control characteristic curve at the rotor for this operation of the asynchronous machine with slip ring rotor (doubly-fed asynchronous machine), which is shown in Fig. 25. The curve is fully linear. Typical for wind turbines is an operating range of the rotor frequency from $-0.3 \, f_1$ to $+0.3 \, f_1$.

This results in torque-speed characteristic curves as with the synchronous machine, given in the next chapter. For a fixed rotor supply frequency, a fixed speed results. At this freely selectable speed, any torque within the permissible range can be controlled. As the derivation of the torque equation can only be done by means of a comprehensive derivation it is not given here.

5 Synchronous Machines

Synchronous machines are used in various fields. They can be built up to the highest power in the GW range. They have the property of being able to feed in reactive power in a controlled manner, for example for grid stabilization. For these reasons, they are generally used in power plants. On the other hand, this type of machine is also used in the area of low power, for example in machine tools or in devices for the entertainment industry or printers.

The synchronous machine has been used in wind turbines for a long time; in the former past only the externally fed version, today also with permanent magnet excitation.

5.1 General Function

The introduction of the machine is based on the variant with external excitation. The rotor of this variant of the synchronous machine is equipped with a DC winding and is fed with DC current. This is done via a converter which regulates the field current. The current is transferred to the rotor via slip rings. This results in a DC field in the rotor, which is fixed to the rotor. This field can also be generated by permanent magnets instead.

The stator is equipped with a three-phase winding as used in the asynchronous machine. This is fed with a cosinusoidal, symmetrical three-phase voltage system. The winding systems of the three phases are 120° mechanically offset from each other in one pole pair. A sinusoidal magnetic rotating field is generated by the current in the stator windings, which rotates in proportion to the supply frequency. For each period of the stator frequency, the field continues to run around one pole pair.

$$n_{1syn} = \frac{f_1}{p} \tag{78}$$

A constant torque can be generated when the field of the rotor and the stator rotate at the same speed. The slip is then equal to zero.

$$n = n_{1syn} \leftrightarrow s = \frac{\omega_2}{\omega_1} = 0 \; \rightarrow \; T \neq 0 \text{ possible} \tag{79}$$

This is shown in Fig. 26. For the machine on the mains with fixed frequency there is only one speed operating point.

A further prerequisite for the generation of a torque is that the field directions of the rotor and stator have an angular offset to each other. This is comparable to two bar magnets mounted rotatably on an axis, which exert forces on each other when they are displaced against each other. The machine on the grid thus generates

Fig. 26 Rotor frequency-speed of revolution behavior of the synchronous machine at the mains of fixed frequency f_1 ($f_2 = 0$)
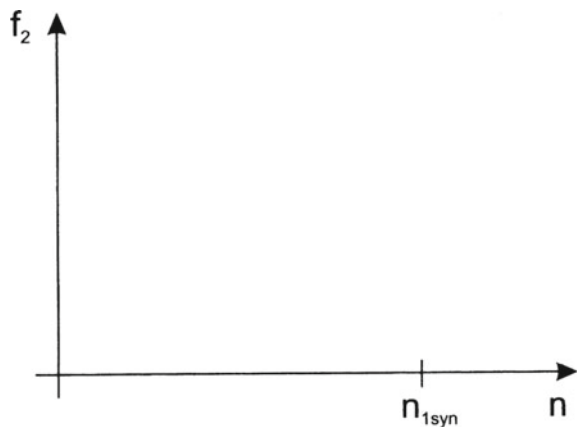
a torque only at a fixed speed, the synchronous speed, and at a phase displacement of the rotating fields or the rotor relative to the stator rotating field.

5.2 Voltage Equations and Equivalent Circuit

The stator with its three-phase winding represents electrically from the supply side the same conditions as the primary side of the transformer or the asynchronous machine. The voltage equation can be taken from there.

$$\underline{U}_1 = R_1 \cdot \underline{I}_1 + j \cdot X_{1\sigma} \cdot \underline{I}_1 + j \cdot X_{1h}\big(\underline{I}_1 + \underline{I}'_f\big) \tag{80}$$

The rotor equation is an equation for a direct current circuit, which only serves to determine the current in the rotor, the direct current I_f. It is given here but will not be used further on in the chapter.

$$U_2 = R_2 \cdot I_f \tag{81}$$

The important determining equation for the synchronous machine is thus the stator voltage equation. There, the effect of the DC rotor current in the turning rotor must be included. Its function to the stator is equal as an alternating current in the stator. The rotor current I_f, for including into the stator voltage equation, is referred to the stator side and stator winding at stator frequency and is named $\underline{I}'_f$. It induces a voltage in the stator, nominated $\underline{U}_P$. Its position results from the position of the rotor in relation to the rotating field of the stator. This voltage caused by the rotor current, as part of the stator voltage, is designated separately as the pole wheel voltage $\underline{U}_P$.

$$\underline{U}_P = j \cdot X_{1h} \cdot \underline{I}'_f \tag{82}$$

Thus, the stator voltage is written in a different form, and with $X_1 = X_{1\sigma} + X_{1h}$:

$$\underline{U}_1 = R_1 \cdot \underline{I}_1 + j \cdot X_1 \cdot \underline{I}_1 + \underline{U}_P \tag{83}$$

From this equation, the equivalent circuit diagram of the synchronous machine is determined according to Fig. 27. It consists of three elements, of which the stator resistance can often be neglected with a good approximation.

From the voltage equation and from the node rule for the current in the machine, we obtain the phasor diagram of the synchronous machine in Fig. 28. The stator voltage $\underline{U}_1$ is composed of the pole-wheel voltage $\underline{U}_P$ and voltage drops across the reactance X_1 and the ohmic resistance R_1. The sum of the stator current $\underline{I}_1$ and the rotor current referred to the stator $\underline{I}'_f$ gives the magnetizing current $\underline{I}_\mu$. Due to the formation of the voltages at inductances there are some right angles: between $\underline{I}_\mu$ and $\underline{U}_i$, between $\underline{U}_P$ and $\underline{I}'_f$ and between $j\omega L_{1\sigma}\underline{I}_1$ and $R_1\underline{I}_1$. The angle between the pole wheel and stator voltage is called the pole wheel angle ϑ. The current is formed due
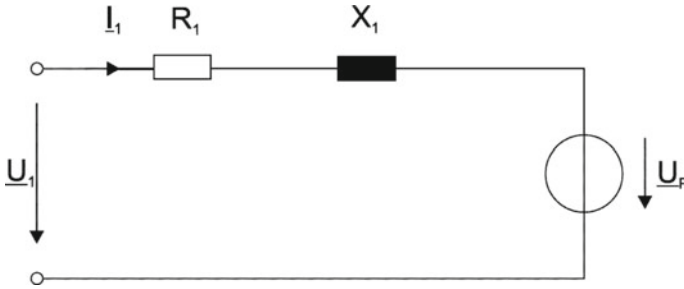
Fig. 27 Equivalent circuit diagram of the synchronous machine
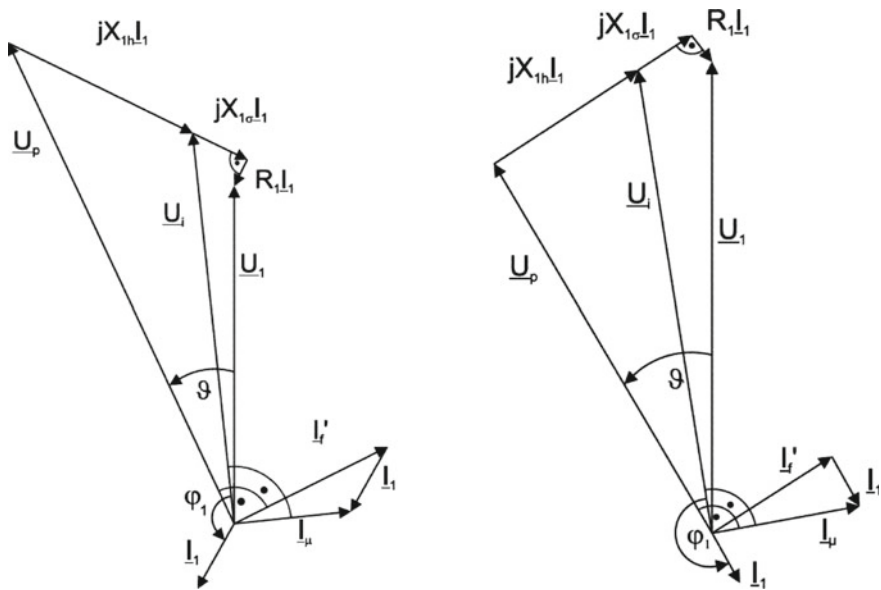
Fig. 28 Phasor diagram of the separately excited synchronous machine, left: generator operation, overexcited ($\vartheta > 0$, $P < 0$, $\cos\varphi < 0$, $Q > 0$, capacitive); right: generator operation, underexcited ($\vartheta > 0$, $P < 0$, $\cos\varphi < 0$, $Q < 0$, inductive)

to different amplitudes as well as different phase angles of the stator and the pole wheel voltage.

In Fig. 28 the operation as a generator is shown. On the left side, over-excited operation is depicted, which is characterized by the fact that the projection of the pole wheel voltage onto the stator voltage is greater than this. The result is a capacitive component in the stator current. On the right side, the under-excited operation is shown. In this case, the projection of the pole wheel voltage onto the stator voltage is smaller than this and the stator current has an inductive component. The diagram is constructed in the load arrow system (defined as in motor operation $P > 0$).

5.3 Power and Torque

The machine takes up power on the stator side, the stator power P_1. If the stator resistance and stator stray inductance are neglected, this is equal to the rotating field power P_{RF}, which is transferred to the rotor in the air gap and which, in the case of the synchronous machine, is converted into mechanical power inside the synchronous machine. Here star voltages are used.

$$P_1 = P_{RF} = 3 \cdot U_1 \cdot I_1 \cdot \cos\varphi_1 \text{ for } R_1 = 0 \tag{84}$$

By transforming the equation via relations which can be derived from the phasor diagram, another notation of the stator active power P_1 *is* obtained which is typical for the synchronous machine. The same can be done with the reactive power Q_1. The following equations apply to star voltages in each case.

$$P_1 = -3 \cdot U_1 \cdot \frac{U_P}{X_1} \cdot \sin\vartheta \tag{85}$$

$$Q_1 = 3 \cdot U_1 \cdot I_1 \cdot \sin\varphi_1 = -3 \cdot U_1 \left(\frac{U_P}{X_1}\cos\vartheta - \frac{U_1}{X_1} \right) \tag{86}$$

The power is determined from the stator and pole wheel voltage and the pole wheel angle. Torque is determined from the active power as:

$$T = -T_{stall} \cdot \sin\vartheta \quad \text{(using the relation } P_1 = 2\pi n_1 T \text{ for } R_1 = 0) \tag{87}$$

$$T_{stall} = \frac{3 \cdot U_1 U_P}{2\pi n_1 X_1} \tag{88}$$

As can be seen from the formula, the torque also depends on the stator and the pole wheel voltage and the angle between them, the pole wheel angle. If both voltages are fixed, the moment depends sinusoidally on the pole wheel angle alone (see Fig. 29). The torque has a maximum value which is called the stalling torque T_{stall}. For reasons of static stability, only angular ranges of the pole wheel angle up to 90° can be driven; in practice, the range is considerably more restricted due to the machine design.

The synchronous machine at a fixed stator frequency, such as on the mains, can only be operated properly at the synchronous speed n_{syn} proportional to the grid frequency, since only then a uniform torque can be generated. At this speed, however, the machine can generate any torque within the permitted range. Accordingly, a torque-speed-diagram of the mains-fed machine results according to Fig. 30.
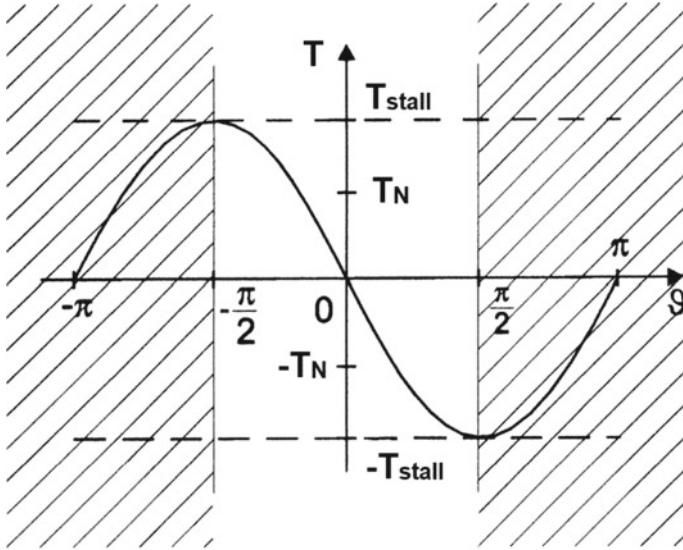
Fig. 29 Torque versus pole wheel angle diagram of the synchronous machine; non-permitted operating range of the pole wheel angle hatched
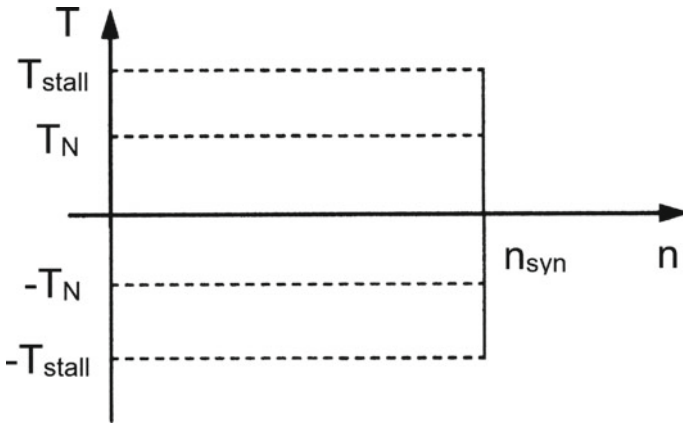
Fig. 30 Torque versus speed diagram of the synchronous machine at fixed stator frequency (solid line)

5.4 Embodiment of Separately Excited Synchronous Machines

The operation mode of the synchronous machine is presented in the previous section for the variant with external excitation. External excitation means excitation with

direct current in the rotor, which is supplied via slip rings. Here, too, there are sub-variants.

The machine considered so far has been assumed to be symmetrical at the circumference of the rotor and stator. The rotor has a cylindrical shape, the air gap is equal at the circumference. This form of rotor is called a drum rotor or solid pole rotor, the machine is called a full-pole machine or turbo machine. It is built for smaller numbers of pole pairs and used in this design for wind turbines when operating at higher speeds, i.e., when using a gearbox.

However, variants without gearboxes are also of interest for wind turbines, the name of the drive system with this type is, for example, direct drive. The machine has a high number of pole pairs, 50 or more, and is then slow running, with machine speeds for nominal operation of, for example, less than 100 min^{-1}. These machines are generally built as salient-pole machines. The poles are manufactured individually and afterwards mounted on the rotor core. The air gap under the poles, in the area of the flux paths, is designed with the usual small air gap thickness. Outside the poles, the air gap usually is larger. The machine therefore has a magnetic saliency; in the pole direction and in the pole gap, different inductances result due to the different air gaps. The course of the torque over the pole wheel angle thus changes somewhat compared to that for the full pole machine.

5.5 Permanently Excited Synchronous Machines

Permanently excited synchronous machines are increasingly being used for wind turbines. Until now, their field of application was mainly in the area of servo motors with outputs below 100 kW. For some time now, however, such machine variants have also been successfully used in wind turbines in the megawatt range.

Permanently excited synchronous machines differ from separately excited ones in that the magnetic excitation is generated by permanent magnets. Permanent magnets with a large coercive field strength are required to be able to run the machines with limited magnetic material. Field strengths of up to $H_C = 1000 \text{ kA/m}$ and remanence inductions of up to $B_R = 1.5 \text{ T}$ are achieved [7]. The materials used are rare earth metals such as samarium-cobalt and neobdymium-iron-boron. An important requirement for use is that the magnets maintain their magnetic properties during heating and during possible opposing fields, for example in the event of faults in the power supply such as short circuits. The manufacturing of the machines and especially the installation of the rotors in the stator must be carried out with special care because of the strong magnetic fields and attractive forces.

For the determination of the electrical and mechanical operating behavior, the derivations for the separately excited synchronous machine can be used. The equations listed there apply. It is to be taken in account that the magnetization originating from the rotor is constant if the saturation, as assumed here, is disregarded. The permanent magnet (PM) pole wheel voltage $U_{P,PM}$, in the voltage equation for the permanently excited machine arises from the permanent magnet magnetization.

$$\underline{U}_1 = R_1 \cdot \underline{I}_1 + j \cdot X_1 \cdot \underline{I}_1 + \underline{U}_{\text{P,PM}} \tag{89}$$

The same applies to the torque equation.

$$T = -T_{\text{stall}} \cdot \sin \vartheta \quad \text{with } T_{\text{stall}} = \frac{3 U_1 U_{\text{P,PM}}}{2 \pi n_1 X_1} \tag{90}$$

It should be noted here that in contrast to the separately excited synchronous machine the magnitude of the pole wheel flux is fixed, and, at a fixed speed, the amplitude of the pole wheel voltage is also fixed, in accordance with the design of the machine. Accordingly, the design also determines whether the machine tends to be over-excited or under-excited at its operating points.

The phasor diagrams and speed-torque characteristics of the separately excited synchronous machine also apply here accordingly.

5.6 Variable Speed Operation of the Synchronous Machine

Variable speed operation is realized by feeding the machine via a converter with stator voltage of variable amplitude and frequency. For variable-speed operation, the flux in the machine is typically to be kept constant and the torque is to be set via the stator current. If the stator flux linkage Ψ_1 is to be kept at its nominal value, then follows, neglecting the stator resistance R:

$$\Psi_1 := \Psi_{1\text{N}} = \frac{U_1}{\omega_1} = \frac{U_{1\text{N}}}{\omega_{1\text{N}}} = \text{const.} \tag{91}$$

A simplified control law therefore applies for the variable speed permanently excited synchronous machine. It states that the stator voltage must be set proportionally to the stator frequency. This is shown in Fig. 31. In the range of low supply frequencies, the ohmic component of the stator resistance has a greater effect and must be considered by increasing the voltage (for motor operation) while decreasing it (in generator operation).

In the equation for the torque there are, in the stalling torque, the terms U_1/ω_1 and $U_{\text{P, PM}}/n_1$ documenting the dependency of the stator voltage and stator frequency and of the pole wheel voltage. Since the first term is to be controlled constantly, it remains constant. The pole wheel voltage U_P changes with the stator frequency, as it is induced by the rotor with the speed $n_1 = n_{1\text{syn}} = f_1/p$. Accordingly, the quotient $U_{\text{P,PM}}/n_1$ also remains constant. Thus, the torque equation is independent of the speed for this type of speed control. The torque solely depends on the pole wheel angle ϑ.

$$T = \frac{3 U_1 \frac{U_{\text{P,PM}}}{\omega_1 L_1}}{2 \pi n_1} \sin\vartheta \tag{92}$$

Fig. 31 Control of the stator voltage of the synchronous machine to constant stator flux linkage for variable speed operation (dashed: required voltage increase for motor operation)
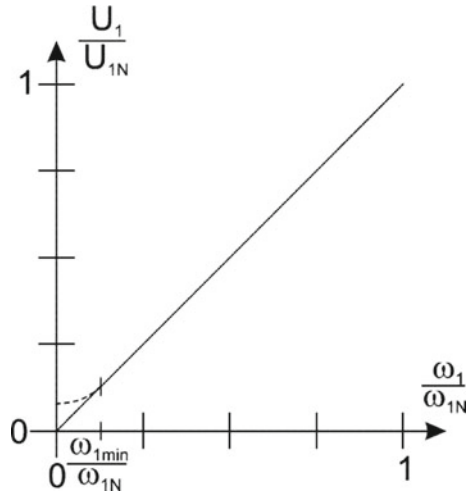
Torque-speed curves of the variable-speed synchronous machine are drawn based on this equation and shown in the Fig. 32. These are vertical lines in the torque versus speed of revolution diagram, and some of these are shown. The conclusion is that continuous speed control is realized.
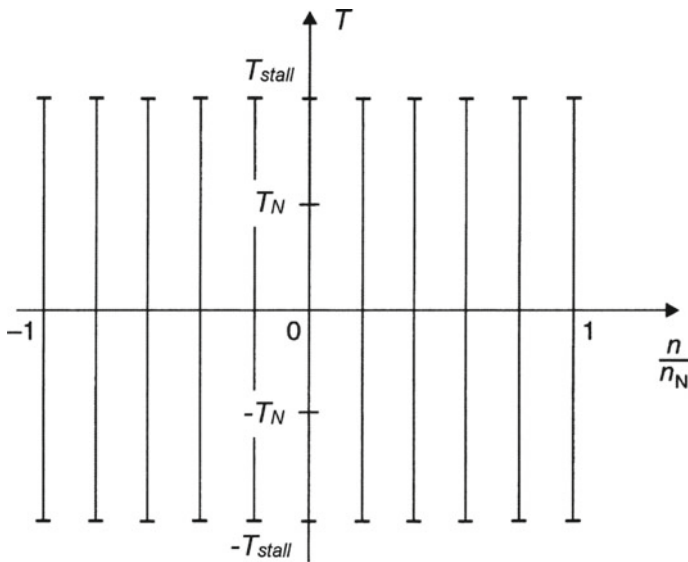
Fig. 32 Torque versus speed curves of the synchronous machine with speed control (exemplarily, discrete torque versus speed curves shown)

6 Converter Systems for Wind Turbines

State-of-the-art wind turbines are generally equipped with variable-speed generators. The system achieves speed control capability by feeding the electrical power of the generator into the electrical grid via an intermediate frequency converter. The frequency converter is operated on the generator side with the variable frequency of the generator, and on the mains side with the mains frequency of 50 or 60 Hz. The task of the frequency converter is to convert the frequency and amplitude of the voltage appropriately between the two systems [1, 2, 8]. At the same time, the frequency converter is equipped with a control system that regulates the power flow and realizes special control requirements on the grid and generator side, such as control of reactive power. Only the standard versions are presented here, as overall in this chapter, in hardware and control. Moreover, there are many variants.

6.1 General Function

The amplitude and frequency conversion are realized in the frequency converters by switching the current or voltage on and off within short time intervals in the range of less than milliseconds [6, 8–10]. The amplitude and frequency of the output variable are controlled by the ratio of the switch-on time to the total switch sector time. The switching is realized by suitable power semiconductors implemented.

In today's converters IGBTs (Isolated Gate Bipolar Transistors) and IGCTs (Integrated Gate Commutated Thyristors) based on silicon are predominantly used. These can block voltages up to the kilovolt range and conduct currents up to the kiloampere range. The IGBT is a combination of MOSFET input and bipolar output stage. Power semiconductors with other materials are on the market and could be used in future.

Due to the ability of these power semiconductors to turn the current on and off by themselves, this type of converter is called self-commutated. These power converters are also called pulse-width modulated converters because of the formation of the output variables by voltage pulses.

There are a variety of circuits for these converters. In the area of wind turbines with outputs below about 5 MW, the variant two-level converter is currently predominantly used. This circuit and its function are presented here. For wind turbines with an output of more than 5 MW, circuits of the three-level converter variant or others are used. These are briefly described.

The circuits of power electronics contain certain components for which ideal conditions are assumed here for clear consideration, as is generally the case. This means:

- ideal power semiconductors, i.e., forward voltage and reverse current zero, no switching delay, switching time zero,
- ideal inductive and capacitive elements, i.e., no losses, reactors with constant inductance, capacitors with constant capacitance.

6.2 Frequency Converter in Two-Level Topology

6.2.1 Topology

Figure 33 shows a frequency converter for converting the power from one three-phase system into another three-phase system. In the case of the wind turbine it converts the power of the generator with variable voltage frequency and amplitude to feed into the electrical grid with fixed voltage amplitude and frequency.

   The frequency converter for feeding the electrical power of the variable-speed generator into the electrical grid of constant frequency consists of two parts. The left-hand part of the converter on the generator side, as a three-phase/direct current AC/DC converter, is connected to the generator terminals in the three-phase mode. Like the other part of the converter, it consists of two power semiconductors for each phase that can be switched on and off, here identified by the symbol of an IGBT, and antiparallel diodes for freewheeling in each case. It generates a DC voltage on the output side from the frequency-variable three-phase voltages of the generator. This is smoothed with capacitors. This connection and decoupling part between the two partial inverters is called an intermediate circuit. A DC/AC converter part is connected to this DC voltage, the grid-side partial converter. It generates a three-phase voltage with suitable grid frequency, amplitude and phase shift from the DC voltage to enable power feed into the grid.

   Both components are carried out here in the same circuit, the two-level topology. The dimensioning regarding voltage and current is slightly different. However, with the aim of standardization, converters of the same dimensioning can be used on both sides.

   Converting voltage amplitude and frequency is carried out by means of a suitable control of the switching of the power semiconductors, called pulse width modulation, as well as a suitable control of the currents and superordinate variables.
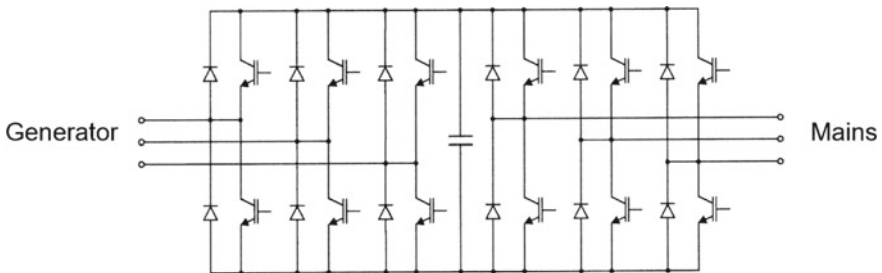
Fig. 33 Frequency converter in a two-level topology for converting voltage amplitude and frequency from the generator to the grid for wind turbines

6.2.2 Pulse Width Modulation

Pulse width modulation for the basic circuit of a DC to three phase AC frequency converter in a two-level topology is considered here in more detail. The circuit is shown in Fig. 34 again in more detail, also for defining values for the formula derivation. This derivation applies to both the machine-side and the mains-side partial inverter.

The circuit generates an amplitude- and frequency-variable three-phase voltage from the DC voltage at the input. For this purpose, the power semiconductors are required, for example the power semiconductors for phase 1 as V_1, V_1', V_4, V_4' . The circuit consists of six power semiconductors that can be switched on/off, which are shown here with the symbol of an IGBT power semiconductor. Antiparallel to each controllable power semiconductor, diodes are installed, for example V_1', which are necessary for the operation of the circuitry, to conduct inductive current components.

At the input is the DC voltage U_d, smoothed by means of capacitors in the DC link. For reasons of comprehensibility, the derivation is shown in two parts, each with the magnitude of half the voltage ($U_d/2$). At the three-phase side additional chokes are necessary, not drawn here, which serve to reduce the pulsations of the three-phase current.

The frequency conversion is performed by pulse width modulation. The function of the conversion from DC voltage to three-phase AC voltage is illustrated in Fig. 35, by the example of a sinusoidal triangular modulation for one phase. The sine wave setpoint voltage of adjustable amplitude and frequency, shown here in terms of the modulation function $m(t)$, is compared with a higher-frequency triangular signal $d(t)$, which determines the switching frequency. At the intersections the switching takes place.

From the comparison of both functions, the information sine wave value greater than the triangle value or sine value less than the triangle value is used. If the sine value
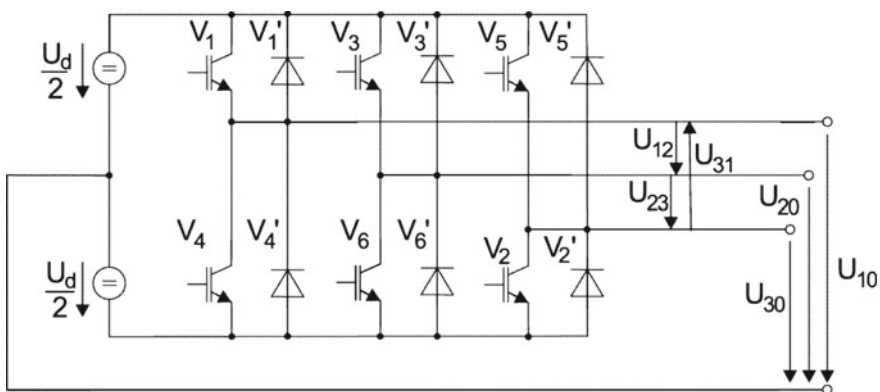
Fig. 34 DC/AC three phase voltage frequency converter in two-level topology, part of the total converter
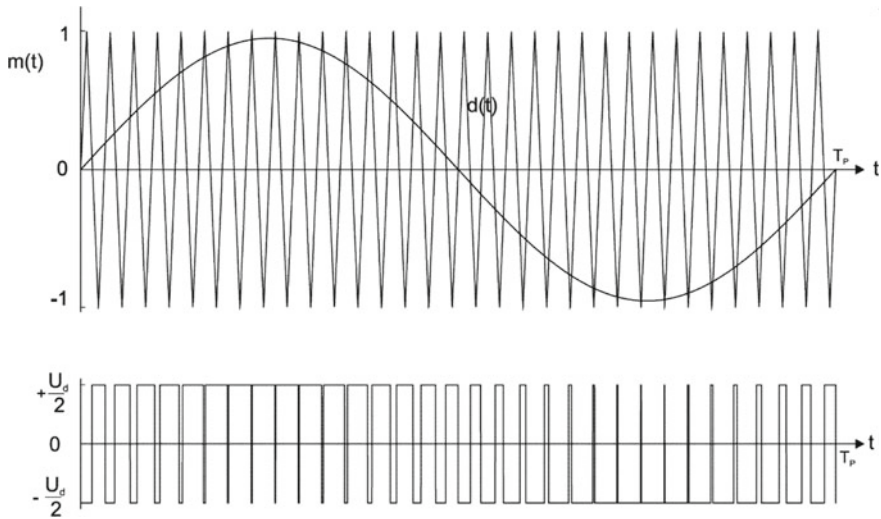
Fig. 35 Pulse width modulation by sine wave to delta curve comparison for one phase of the DC/AC three-phase voltage converter; top: sine wave setpoint reference voltage and triangular function; bottom: resulting pulse train, AC voltage U_{10}, sinusoidally modulated

is greater than the triangle value, the upper switch of the respective phase is switched on, e.g. V_1 for phase 1, and the lower switch, V_4, is switched off. Thus, voltage $U_{10} = U_d/2$ lies between the output point of phase 1 and the midpoint of the DC link (0), regardless of the current flow. If this is positive, it flows via the controllable power semiconductor V_1, in the other case via the antiparallel diode V_1'. If the sine value is smaller than the triangle, the lower controllable power semiconductor V_4 is switched on, the upper one is switched off, the output voltage is negative $U_{10} = -U_d/2$. Also independent of the direction of current flow, either via V_4 or V_4'. The phase can therefore generate two voltage values, hence the name two-level circuitry.

Both power semiconductors of one phase must not be switched on at the same time, as this will lead to a short circuit of the DC link voltage. To ensure that no short circuit occurs, a blocking time must be inserted between the switching on of the upper and the switching on of the lower power semiconductor. This is usually in the order of microseconds for converters in the power range around one megawatt and above.

The resulting output voltage of a phase is shown in the lower diagram in Fig. 35. The sinusoidally modulated pulse widths are clearly visible. The moving average forms the required sinusoidal waveform, proportional to the curve $d(t)$. The other two phases are controlled in the same way, whereby the sine setpoint is shifted by 120° and 240° respectively.

To achieve higher voltage values, the sine function can also be chosen to be larger than the delta function. This is referred to as overmodulation. A more distorted voltage results, so it is well to be checked if to apply.

The phase-to-phase voltages U_L result from the difference of two voltages against point 0. Here they are derived (Eq. 93) as an example for switching state 1 (SZ1, explained below) with valves V_1, V_6 and V_2 switched on. This results in three voltage levels for the phase-to-phase voltage.

$$
\begin{aligned}
U_{\text{L12}} &= U_{10} - U_{20}; \quad \text{for switching state 1}: \quad U_{\text{L12}} = \tfrac{U_d}{2} - \left(-\tfrac{U_d}{2}\right) = U_d \\
U_{\text{L23}} &= U_{20} - U_{30}; \quad \text{for switching state 1}: \quad U_{\text{L23}} = -\tfrac{U_d}{2} - \left(-\tfrac{U_d}{2}\right) = 0 \quad (93) \\
U_{\text{L31}} &= U_{30} - U_{10}; \text{ for switching state 1}: \quad U_{\text{L31}} = -\tfrac{U_d}{2} - \left(+\tfrac{U_d}{2}\right) = -U_d
\end{aligned}
$$

The ratio of the amplitude of the sine wave reference value to the amplitude of the delta shaped carrier function (for half of the DC voltage) is called the modulation depth m. In pulse width modulation, the three-phase voltage, for example phase-to-phase voltage U_{L12}, is proportional to the modulation depth up to its value 1.0 and inversely proportional to the DC voltage for linear modulation, without overmodulation (Eq. 94).

$$
m = \frac{\widehat{U}_{\text{Star}}}{U_d/2}; m = 0 \ldots 1, 0 \, (\ldots 1, 15) \tag{94}
$$

Value $m = 1.15$ applies if, instead of the pure sinusoidal setpoint function, one with an additional component of three times the frequency and 1/6 of the amplitude is used for the modulation (sine wave reference wave: $\sin \omega t + (1/6) \cdot \sin 3\omega t$). In systems without a neutral conductor, the additionally generated voltage components fed in have no negative effects.

The sine-triangle pulse width modulation was used to illustrate the method of controlling the AC voltage. However, another widely used method of voltage control today is space vector modulation, which is also well suited as a basis for implementation on control hardware with microcontrollers or programmable logic circuits. Space vectors, for example $\underline{U}(t)$ of the voltage, represent as complex, time-dependent quantities the characteristics of a three-phase voltage or current system or other quantities. They contain information about amplitude, phase and frequency even under dynamically changing conditions. The real component U_α and the imaginary component U_β of the space vector of the three-phase voltage system for switching state 1 are determined according to:

$$
U_\alpha = \frac{2}{3} U_{\text{L12}} + \frac{1}{3} U_{\text{L23}}; \text{ for switching state 1 } (U_{\text{L12}} = U_d, U_{\text{L23}} = 0): U_\alpha = \frac{2}{3} U_d \tag{95}
$$

$$
U_\beta = \frac{\sqrt{3}}{3} U_{\text{L23}}; \text{ for switching state 1 } (U_{\text{L23}} = 0) : U_\beta = 0 \tag{96}
$$

The space vector is composed of real and imaginary components:

$$\underline{U}(t) = U(t) \cdot e^{j(\omega(t)t)} = U_\alpha(t) + jU_\beta(t) = U(t)(\cos(\omega(t)t) + j\sin(\omega(t)t)) \tag{97}$$

An understanding of the property of the space vector gives the following example for stationary operation: The space vector of a sinusoidally symmetrical three-phase system at constant frequency is a phasor in the complex plane that circulates with constant amplitude and frequency and describes a circle.

In pulse width modulation, discrete space vectors are switched due to the various switching states of the converter. Table 2 shows the switching states for all possible switching combinations of the power semiconductors of the circuitry of a two-level converter. Columns four to six indicate which valves are switched on (1: on, 0: off). Columns one to three indicate the respective value of the phase to midpoint voltage of the DC link. Column seven numbers the switching states and columns eight to eleven indicate the values of the space phasor.

There are six active space vectors (1, 2, 6, 5, 4, 3) and two zero space vectors (7, 0). Zero space vectors with zero amplitude occur when all upper or all lower valves are switched on. Two switched-on valves in one phase are not allowed, as this creates a short circuit. The switching states can be traced on the circuit diagram of the converter.

The switching states can be clarified in a vector diagram in the complex α, β-plane as space vectors, cf. Fig. 36. The conversion equation to the space pointer has been given earlier. The six active space vectors (1…6), leading to the outer corners of the hexagon, and the two zero space vectors (0, 7), at the center of the hexagon, are clearly distinguishable.

The space vector, for example for sinusoidally symmetrical three-phase voltages with constant amplitude and frequency or for the pulse-type output voltage of the sine-wave pulse converter, can be generated by rapid sequential switching of the respective nearby basic space vectors. In the respective sector in which the target space vector is located, the right, the left and the zero space vectors are to be switched on each for a suitably long time to get with the mean value the effect of the setpoint value. For the first sector between base space vectors 1 and 2 this is shown in Fig. 37

Table 2 Switching states for the two-level DC/AC three-phase inverter

U_{L10}	U_{L20}	U_{L30}	V_1V_4	V_3V_6	V_5V_2	No	$\frac{U_\alpha}{U_d}$	$\frac{U_\beta}{U_d}$	$|\underline{U}|$	Arc $(\underline{U})$
$+U_d/2$	$-U_d/2$	$-U_d/2$	10	01	01	1	2/3	0	2/3	0°
$+U_d/2$	$+U_d/2$	$-U_d/2$	10	10	01	2	1/3	$\sqrt{3}/3$	2/3	+60°
$+U_d/2$	$-U_d/2$	$+U_d/2$	10	01	10	6	1/3	$-\sqrt{3}/3$	2/3	+60°
$+U_d/2$	$+U_d/2$	$+U_d/2$	10	10	10	7	0	0	0	0°
$-U_d/2$	$-U_d/2$	$-U_d/2$	01	01	01	0	0	0	0	0°
$-U_d/2$	$-U_d/2$	$+U_d/2$	01	01	10	5	$-1/3$	$-\sqrt{3}/3$	2/3	$-120°$
$-U_d/2$	$+U_d/2$	$+U_d/2$	01	10	10	4	$-2/3$	0	2/3	$-180°$
$-U_d/2$	$+U_d/2$	$-U_d/2$	01	10	01	3	$-1/3$	$\sqrt{3}/3$	2/3	+120°

Fig. 36 Basic voltage space vectors, their switching states and exemplary reference space vector of a two-level converter in the complex plane
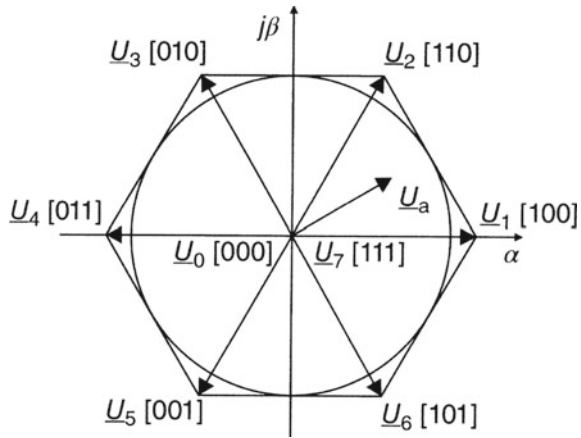
as an example for the reference space vector $\underline{U}(t)$, and the resulting equations are compiled. For the other sectors this applies accordingly.

The nth pulse in one period with a pulse period T_P with the time of a fraction of the period T of the reference sine function of the voltage is considered. The base space vectors 1, 2 and the zero space vectors 7 or 0 are to be switched on for a certain period T_{on1}, T_{on2}, T_{on7} or T_{on0} and together give the setpoint voltage $\underline{U}(n)$ for the nth pulse:

$$\underline{U}(n) = \frac{T_{on1}}{T_P} \cdot \underline{U}_1 + \frac{T_{on2}}{T_P} \cdot \underline{U}_2 + \frac{T_{on0,7}}{T_P} \cdot \underline{U}_{0,7} \tag{98}$$

Fig. 37 Formation of the setpoint space vector $\underline{U}(t)$ or $\underline{U}(n)$ out of the base space vector (example; (1) and (2) base space vectors)
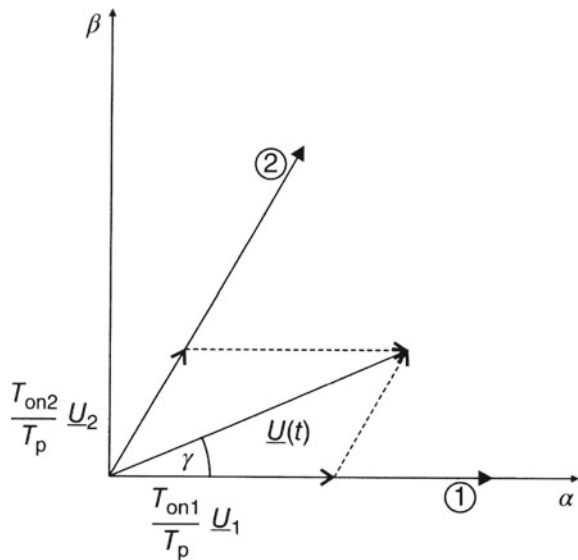
For the calculation the phase position γ of the reference space vector to the real α-axis, shown for example for sector 1 in Fig. 37, is used. The switch-on times of the space pointers 1, 2 and 7 or 0 can be derived out of the diagram by means of the sine theorem for sector 1 and are then given by:

$$\frac{T_{on1}}{T_P} = \sqrt{3} \cdot \frac{U(n)}{U_d} \cdot \sin\left(60° - \gamma\right) \tag{99}$$

$$\frac{T_{on2}}{T_P} = \sqrt{3} \cdot \frac{U(n)}{U_d} \cdot \sin(\gamma) \tag{100}$$

$$\frac{T_{on0,7}}{T_P} = \frac{T_P - T_{on1} - T_{on2}}{T_P} \tag{101}$$

These equations are also used in the implementation on microcontrollers. In the control, the setpoints of amplitude $U(n)$ and phase angle $\gamma(n)$ of the voltage are determined and specified. With the frequency of the pulse frequency f_P and the reciprocal value pulse period T_P, switch-on times are determined according to the voltage setpoint. For implementation in microcontrollers, counters are used to count the turn-on/turn-off times, and the switching signals are then given to the valves. The switching frequencies for converters in wind turbines are in the kHz range (e.g., 2.5 kHz) or lower for large powers.

There are many different variations of pulse width modulation in use.

6.3 Frequency Converter with Multi-level Circuitry

For wind turbines with larger converter power in the higher megawatt range, converters with power semiconductors in series or parallel connection are used. For this case, the variants of the inverter in multi-level connection have also proven to be favorable. This is a special series connection of power semiconductors. However, these are not switched simultaneously, but the switching is staggered. Using this method, it is possible to create finer voltage steps to the output and thus to reduce the required filtering effort.

A very common variant is the three-level converter in the neutral point clamped (NPC) topology [12]. The circuit diagram is shown in Fig. 38. The converter again consists of three identical phases. In each phase, the upper and lower arms are almost identical in structure. Two power semiconductors, here shown as IGBTs, each with an antiparallel freewheeling diode are connected in series in each arm. The phase tap is connected between the two branches.

Since within the series connection of the power semiconductors of a branch a connection to the midpoint of the DC link is given via additional diodes, each individual phase can generate the output voltage $U_d/2$, 0 and $-U_d/2$ towards midpoint 0. To generate for phase 1 the output voltage $U_{10} = +U_d/2$, *for* example, the power
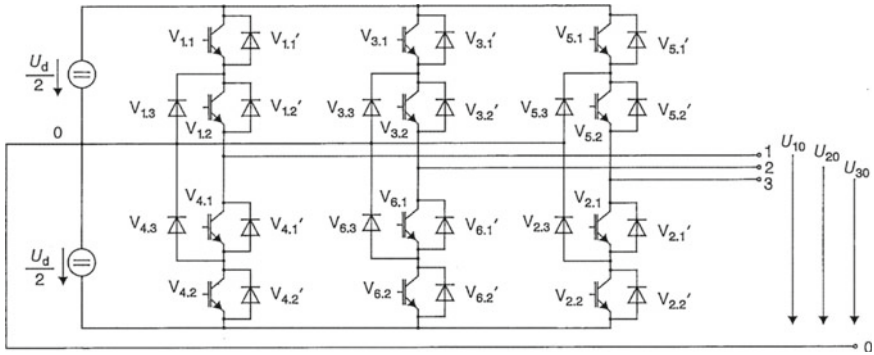
Fig. 38 Three-level frequency converters, mains or generator side part, neutral point clamped topology

semiconductors $V_{1,1}$ and $V_{1,2}$ are to be switched on. To achieve the output voltage $U_{10} = 0$, the power semiconductors $V_{1,2}$ and $V_{4,1}$ are to be switched on. The state $U_{10} = -U_d/2$ is reached with switches $V_{4,1}$ and $V_{4,2}$ switched on. Three voltage levels thus can be generated by each phase, which has led to the designation three-level inverter. In Fig. 39 the phase-to-phase output voltage of a three-level inverter is shown. The combination of the three voltage values of the two phases forming the phase-to-phase voltage results in a five-level shape.
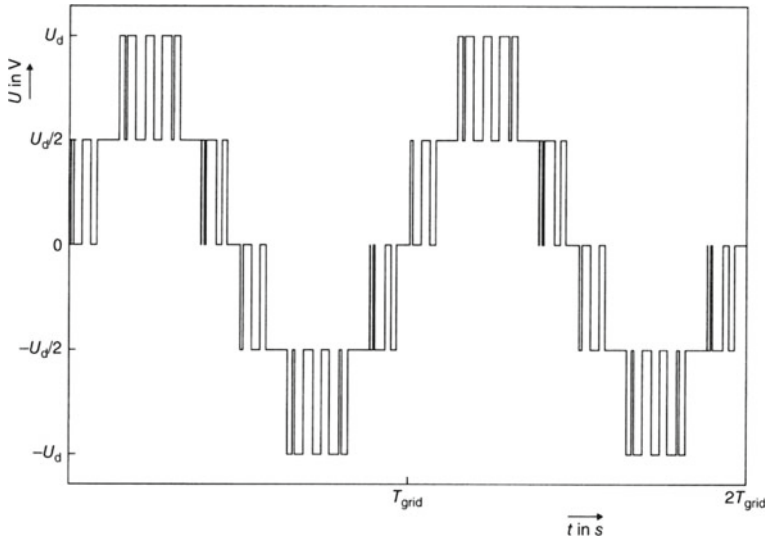
Fig. 39 Three-level frequency converter; course of the phase-to-phase AC output voltage

7 Control of Variable Speed Converter-Generator Systems

At present, there are essentially four different variants of variable-speed generators for wind turbines in new installations. These are, on the one hand, the variants with a squirrel-cage asynchronous machine, with a permanently excited and separately excited synchronous machine, in each case with full converter. The structure is shown in the upper part of Fig. 40. On the other hand, there is the variant with a doubly-fed asynchronous machine, i.e. an asynchronous machine with slip-ring rotor, here with a part power rated converter in the rotor circuit, as shown in the lower part of Fig. 40.

With the aid of control systems [13, 14], designed specifically for each of the different power electronic generator variants, the generator speed is controlled according to the specifications from the operational management and feeds power into the DC link and into the grid. The first function is usually performed by the converter part on the generator side, the second function by the converter part on the grid side.

The control on the generator-side converter regulates the speed of the generator, this is done indirectly via the torque and thus the power extraction from the wind. The control for the grid-side converter regulates the power to be supplied into the electrical grid. The latter is done indirectly by regulating the voltage in the DC link
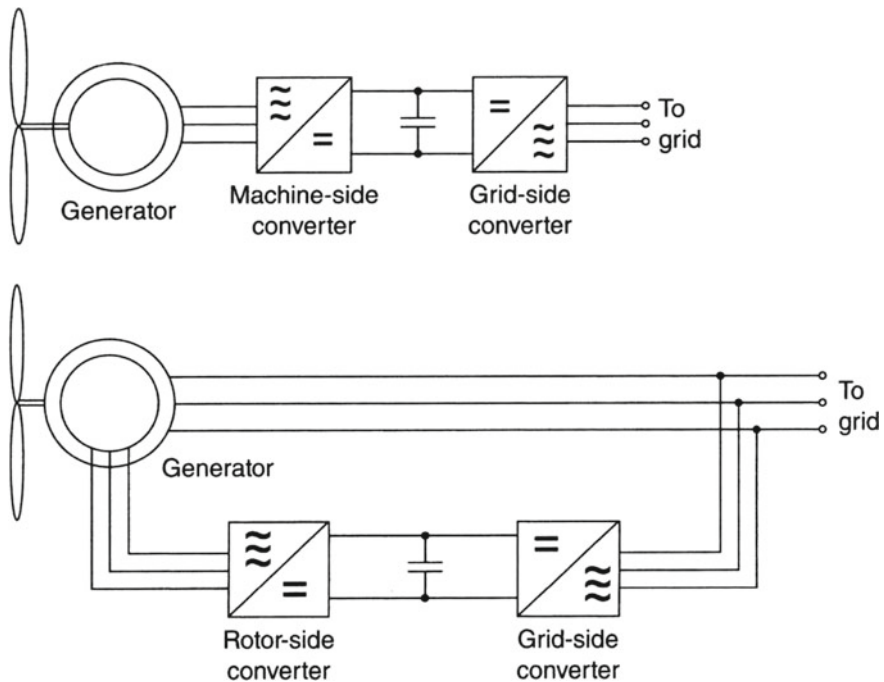
Fig. 40 Structure of electrical drive trains state-of-the-art in wind turbines; top: Generator with fully converter, below: Generator with slip ring rotor and converter on rotor, with part power converter

to a constant value via power output to the grid. Without control, it would rise or fall depending on the higher or lower power feed-in from the generator. These two control tasks are carried out separately, the coupling takes place via the system, the power flow at the connection point of both converters, in the DC link, realized via the capacitors.

Versions of the control systems are also used in which the line-side converter controls the speed, and the machine-side converter controls the DC link voltage, i.e. the functions are distributed inversely.

In the variants with full power converters, the entire power flow is provided and controlled via the converter [11]. In the case of the partly power rated converter variant, only a part of the total power runs via the converter on the rotor side, but via this the total power of the rotor and stator is controlled [12].

In the following, the control of the asynchronous generator, representative for a generator control, as well as the control of the grid-side converter are presented as examples. The controls of the other generator variants are briefly outlined.

7.1 Control of the Converter-Fed Asynchronous Generator with Squirrel-Cage Rotor

Commonly, a field-oriented control for an asynchronous generator with squirrel-cage rotor is employed and presented here examplarily. In Fig. 41 a structural diagram of the control is shown. The control system is structured in two channels.
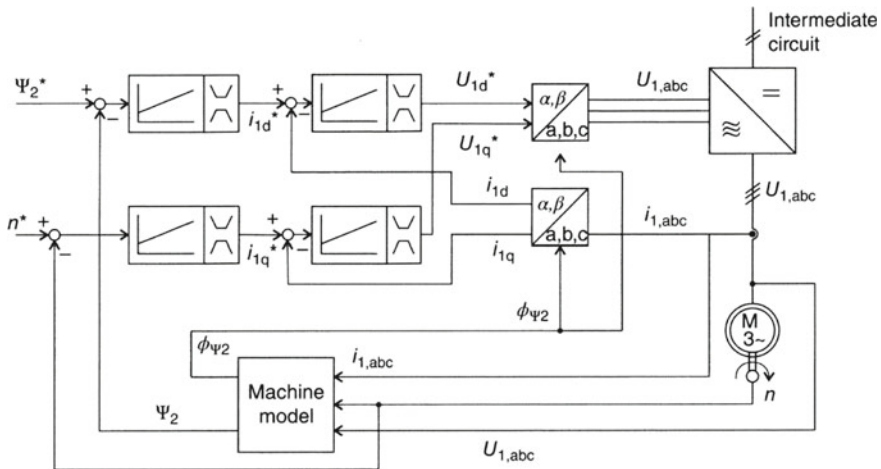
Fig. 41 Structural diagram of the control of an asynchronous generator with squirrel-cage rotor (field-oriented control of rotor flux linkage and speed, with speed sensor)

The concept comprises one channel in which the flux in the machine, for example the rotor flux linkage Ψ_2, is controlled, and one channel in which the speed n or, alternatively, the torque T is controlled. Moreover, the control in both channels is designed in a cascaded manner by using a subordinate current control. This has advantages in that the respective controllers can be adjusted to the respective sections of the system, and, in addition, it is possible to limit the current in order to protect the converters. The limiters are shown as vertical blocks on the controllers. They are also present in the following controller structures but are not shown further on there.

The operation is described in brief. The actual value of the rotor flux linkage Ψ_2 and its setpoint value Ψ_2^* are compared and the difference is passed to the flux controller of PI-type. The PI flux controller has the task of influencing the system via its output in such a way that the setpoint and actual value are aligned. The output of the flux controller is the setpoint for the flux-forming part i_{1d}^* of the stator current. This can be limited, as shown by the special symbol behind the controller block in Fig. 41. It is compared with the measured actual value i_{1d} and the difference is passed to the PI controller for the flux-forming current and controlled. Its output value is the flux-forming setpoint U_{1d} of the stator voltage.

The channel for speed control is set up accordingly. Input quantities are the signals speed setpoint n^* and measured actual value n. The intermediate stage behind the speed controller is the torque-forming current setpoint i_{1q}^* and measured actual value i_{1q} and the output variable is the torque-forming component U_{1q}^* of the stator voltage.

The two voltage components U_{1d} and U_{1q} are combined to form the total voltage and specify the stator voltage setpoint in magnitude and angle as input for the pulse width modulation of the converter on the generator side. In the pulse width modulator, which is seen here as a component of the inverter and is not depicted individually in the figure, the switching patterns for the inverter are calculated to provide the required output voltage value.

The actual measured values required for the control are the stator current, the stator voltage and the speed. Internal variables of the machine that are required for the control, such as the rotor flux linkage in the amount Ψ_2 and its angle as $\phi_{\Psi2}$ as well as the torque T, if required, are calculated using a machine model. This contains the dynamic equations of the machine. By means of this method a problematic measurement of the flux or the torque is avoided.

In the field of drives, proportional-integral (PI) controllers are commonly used and are capable of controlling the system deviation, the difference between the setpoint and the actual value, to zero. Their equation is:

$$y = K_p \cdot x + \frac{1}{T_I} \int x dt \tag{102}$$

$$G(s) = \frac{y(s)}{x(s)} = K_p \frac{s T_I + 1}{s T_I} \tag{103}$$

In this equation, x is the input variable of the controller, thus the difference between setpoint and actual value, and y is the output variable, thus the actuating variable.

$G(s)$ represents the frequency transfer function of the controller, the ratio of output to input versus frequency. K_p is the proportional gain, and T_I is the integration time constant of the controller. These two parameters are, respectively, to be designed towards the controlled section and other conditions for the controller [13]. In drive engineering, the controllers are designed usually according to two standard strategies, namely the technical optimum and the symmetrical optimum. This generally gives good results in terms of dynamics, overshoot and robustness. The adjustment rules can be found, for example, in [13].

In order to determine the parameters for the controllers, the system to be controlled, the generator, must be modeled for dynamic operation, see for example in [13]. Often, as also shown in Fig. 41, the system is represented and controlled in space vectors, frequently in a special dq coordinate system, circulating with the rotor flux. This is in short form derived here.

Therefore, a conversion must be carried out from the three-phase abc real system to the two-phase dq space vector system for the input quantities and in the opposite direction for the output quantities. Therefore, the modeling is performed in the space vector representation as already introduced for the inverters. A space vector is a complex quantity that equivalently represents any three-phase system whose quantities are linearly dependent. The real α-component $U_\alpha(t)$ and the imaginary β-component $U_\beta(t)$, here written for the voltage, are determined from the three-phase quantities according to the following equations, where it is assumed that no zero-sequence system is present:

$$\underline{U}^{\alpha\beta}(t) = \frac{2}{3}\left(U_\mathrm{a}(t) + U_\mathrm{b}(t) \cdot e^{j2\pi/3} + U_\mathrm{c}(t) \cdot e^{j4\pi/3}\right) \tag{104}$$

$$U_\alpha(t) = \mathrm{Re}\left(\underline{U}^{\alpha\beta}(t)\right) = \frac{2}{3}\left(U_\mathrm{a}(t) - \frac{1}{2}U_\mathrm{b}(t) - \frac{1}{2}U_\mathrm{c}(t)\right) \tag{105}$$

$$U_\beta(t) = \mathrm{Im}\left(\underline{U}^{\alpha\beta}(t)\right) = \frac{2}{3}\left(0 \cdot U_\mathrm{a}(t) + \frac{\sqrt{3}}{2}U_\mathrm{b}(t) - \frac{\sqrt{3}}{2}U_\mathrm{c}(t)\right) \tag{106}$$

The superscript $\alpha\beta$ in the formulas denotes that the voltage is represented in this coordinate system. The reverse transformation from the space vector representation in fixed coordinates to the abc three-phase quantities runs according to the following equation:

$$\begin{pmatrix} U_\mathrm{a}(t) \\ U_\mathrm{b}(t) \\ U_\mathrm{c}(t) \end{pmatrix} = \begin{pmatrix} 1 & 0 \\ -\frac{1}{2} & +\frac{\sqrt{3}}{2} \\ -\frac{1}{2} & -\frac{\sqrt{3}}{2} \end{pmatrix} \cdot \begin{pmatrix} U_\alpha \\ U_\beta \end{pmatrix} \tag{107}$$

The aforementioned control of electrical machines in a coordinate system rotating with electrical quantities, for example the flux, named dq, can simplify the analysis

and is derived here. The space vector equations are converted into a rotating dq coordinate system oriented, here for example, to the rotor flux. The system has the time-dependent angle $\theta = \theta(t)$ with respect to the fixed $\alpha\beta$-system. The transformation is done with the rotary operator $e^{j\theta}\left(\underline{U}_{\mathrm{dq}}; \underline{U}_{\alpha\beta}\right)$.

$$\underline{U}^{\mathrm{dq}}(t) = \underline{U}^{\alpha\beta}(t) \cdot e^{-j\theta\left(\underline{U}_{\mathrm{dq}}; \underline{U}_{\alpha\beta}\right)} = U_{\mathrm{d}}(t) + jU_{\mathrm{q}}(t) = \underline{U}^{\alpha\beta}(t)(\cos\,(-\theta) + j\sin\,(-\theta)) \tag{108}$$

$$U_{\mathrm{d}}(t) = U_{\alpha}(t)\cos\theta + U_{\beta}(t)\sin\theta \tag{109}$$

$$U_{\mathrm{q}}(t) = -U_{\alpha}(t)\sin\theta + U_{\beta}(t)\cos\theta \tag{110}$$

The reverse transformation with the inverse rotary operator reads:

$$U_{\alpha}(t) = U_{\mathrm{d}}(t)\cos\theta - U_{\mathrm{q}}(t)\sin\theta \tag{111}$$

$$U_{\beta}(t) = U_{\mathrm{d}}(t)\sin\theta + U_{\mathrm{q}}(t)\cos\theta \tag{112}$$

The peculiarity of the representation in a rotating coordinate system becomes clear at Fig. 42. The three-phase equations for the stator current $\underline{I}_1$ are first transformed into the complex space vector equation for the stator fixed $\alpha\beta$-coordinate system for this representation. Next, the rotor flux-oriented coordinate system in which the control is to be performed is selected. In this case, the d-component is placed on the rotor flux $\underline{\Psi}_2$. The rotor flux lies, as shown in Fig. 42, in the d-axis of the second coordinate system. The stator current is transformed into this coordinate system. Accordingly, it can be divided into the components $i_{1\mathrm{d}}$, $i_{1\mathrm{q}}$ in both axes, i.e., the longitudinal component in the direction of the rotor flux and the transverse component perpendicular to it. This is a very convenient representation for control, since the longitudinal component of the stator current forms the flux and the transverse component forms the torque, as shown by the torque Eq. 120 which follows later. These values can be used directly in the control and form the two channels already shown.

It is of great advantage that for control in rotating coordinate systems, the quantities in steady-state operation are constant quantities, making control easy to implement. An example of this are fluxes and currents in Fig. 42 for the rotor flux-oriented coordinate system. However, controls for three-phase machines can also be realized in differently oriented coordinate systems, for example related to the stator flux linkage. A representation in the stator voltage-related system, i.e. in the $\alpha\beta$-system, can also be used.

The equations for the stator and rotor voltages and the corresponding fluxes when modeling for dynamic behavior of the asynchronous generator can be derived from the known equations of the asynchronous machine [13]. They are transferred directly into the rotating coordinate system and result in:
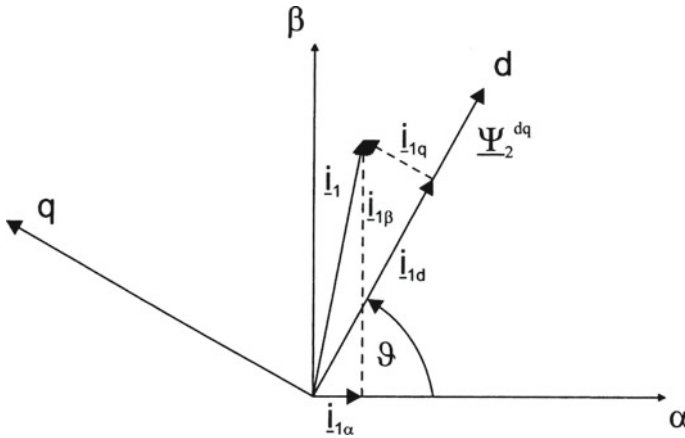
Fig. 42 Rotor flux linkage and stator current in the stator fixed αβ- as well as in the rotor flux oriented dq-coordinate system and partitioning of the stator current into these components ($\theta = \vartheta$)

$$\underline{U}_1^{dq}(t) = R_1 \cdot \underline{i}_1^{dq}(t) + \frac{d}{dt}\underline{\Psi}_1^{dq}(t) + j\omega_{dq} \cdot \underline{\Psi}_1^{dq}(t) \tag{113}$$

$$\underline{U}_2^{dq}(t) = R_2 \cdot \underline{i}_2^{dq}(t) + \frac{d}{dt}\underline{\Psi}_2^{dq}(t) + j\left(\omega_{dq} - p\omega_m\right) \cdot \underline{\Psi}_2^{dq}(t) \tag{114}$$

$$\underline{\Psi}_1^{dq}(t) = L_1 \cdot \underline{i}_1^{dq}(t) + L_h \cdot \underline{i}_2^{dq}(t) \tag{115}$$

$$\underline{\Psi}_2^{dq}(t) = L_2 \cdot \underline{i}_2^{dq}(t) + L_h \cdot \underline{i}_1^{dq}(t) \tag{116}$$

Here, the stator part in the rotor equations has to be referred to the rotor with the winding ratio and vice versa as shown in the sections for basic transformer and machine performance. It is to be noted, that here as in the following this referring is not marked in the formulas as usually done by an apostroph.

These are essentially equations that are similar to the quasi-stationary representation. The voltage equations contain a portion for the ohmic voltage drop and a portion for the voltage generated by the flux derivation, called the transformational component. The respective terms with the factor j result from the mathematical transformation into the rotating coordinate system, in detail by the partial derivation of the respective flux term, called the rotational component.

Resolving the equations into d and q components here for the stator voltage, then they result in the characteristics of these terms:

$$U_{1d}(t) = R_1 \cdot i_{1d}(t) + \frac{d}{dt}\Psi_{1d}(t) - \omega_{dq} \cdot \Psi_{1q}(t) \tag{117}$$

$$U_{1q}(t) = R_1 \cdot i_{1q}(t) + \frac{d}{dt}\Psi_{1q}(t) + \omega_{dq} \cdot \Psi_{1d}(t) \tag{118}$$
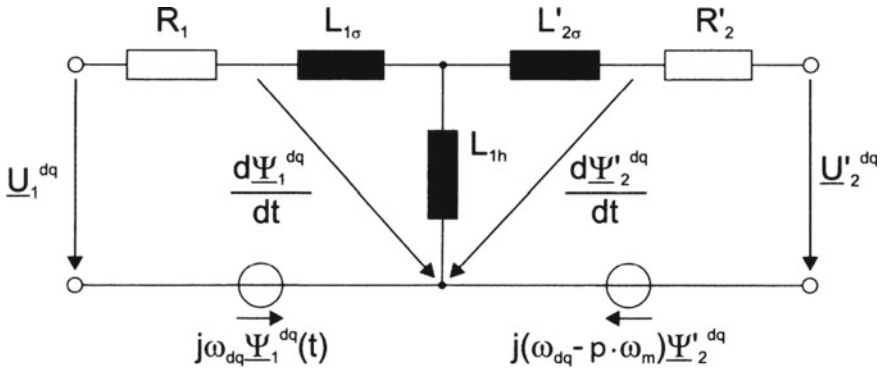
Fig. 43 Equivalent dynamic circuit diagram of the asynchronous machine; referring rotor values to the stator is marked here by an apostrophe (for example U')

The last components in this formula represent the rotational part of the induced voltage (e.g. $\omega_{\mathrm{dq}} \cdot \Psi_{1\mathrm{q}}(t)$, $\omega_{\mathrm{dq}} \cdot \Psi_{1\mathrm{d}}(t)$). Important is to see that the last component in the equations, the rotational component, is a coupling component, that is, the component of the transverse axis (q) acts on the longitudinal axis (d) and vice versa.

The components $i_{1\mathrm{d}}$ and $i_{1\mathrm{q}}$ of the stator current, which appear in the voltage equations, are controlled in the current controller. The system of the machine can be interpreted for the design of these controllers as a first order delay element with the rotor stray time constant. The design according to the technical optimum is used [13].

To these dynamic equations the dynamic equivalent circuit of the asynchronous machine results, as shown in Fig. 43. It is largely similar to the stationary equivalent circuit but is extended by the rotational voltages.

The torque of the machine in representation with rotor flux orientation [13] results due to the orientation of the coordinate system at the rotor flux ($\Psi_{2\mathrm{q}} = 0$) to:

$$T_{\mathrm{Gen}}(t) = \frac{3pL_{\mathrm{h}}}{2L_2} \cdot \left(\Psi_{2\mathrm{d}} \cdot i_{1\mathrm{q}} - \Psi_{2\mathrm{q}} \cdot i_{1\mathrm{d}}\right) = \frac{3pL_{\mathrm{h}}}{2L_2} \cdot \Psi_{2\mathrm{d}} \cdot i_{1\mathrm{q}} \qquad (119)$$

$$\underline{\Psi}_2 = \Psi_{2\mathrm{d}} + j \cdot 0 \cdot \Psi_{2\mathrm{q}} \text{ for rotor flux orientation} \qquad (120)$$

Thus, for the constant rotor flux the torque only depends on the quadrature part $i_{1\mathrm{q}}$ of the stator current.

The variation in time of the rotational speed n or the angular frequency ω_{m} of the mechanical rotation of the generator is formed by the generator torque T_{Gen} and that of the rotor of the wind turbine $\mathrm{T_{Rot}}$, which act on the moment of inertia Θ of the drive train.

$$\frac{d}{dt}\omega_{\mathrm{m}} = \frac{1}{\Theta}(\mathrm{T_{Rot}}(t) - T_{\mathrm{Gen}}(t)) \qquad (121)$$

The speed controller acts on this controlled system. The controlled system has an integral behavior, so that in general a design of the controller parameters according to the symmetrical optimum is selected [13].

In addition, the behavior of the converter must be considered. Power converters are dynamically characterized by a dead time, which is taken into account as a first-order delay element [13].

$$G_{\mathrm{con}}(j\omega) = \frac{1}{1 + s\,T_{\mathrm{con}}} \qquad (122)$$

The time constant T_{con} is determined, depending on the pulse pattern generation (single or double update, immediate pass through of the reference value or not) as a value approximately once or twice times the inverse value of the pulse frequency ($T_{\mathrm{con}} = (1\ldots 2)/f_{\mathrm{pulse}}$ [13]).

Since power electronic generator systems in wind turbines are not operated in the field weakening range, this is not considered here.

7.2 Control of the Doubly-Fed Asynchronous Machine

The structural diagrams of the control of the other power electronic generator systems are presented and explained here in a short way to give an idea of their control methodology [13]. Figure 44 shows the control structure for the doubly-fed asynchronous machine. The d-channel and the q-channel are shown here together in one channel. Its basic structure is the same as that of the squirrel cage asynchronous machine. A speed control and a reactive power control in parallel channels are included as well as a subordinate current control. The speed and by this torque control operates indirect, since only the rotor voltage, not the stator voltage, can be directly influenced. In contrast to the asynchronous machine with squirrel-cage rotor, the flux is not controlled by means of the converter, as it is strongly affected by the mains voltage. Instead of this, in the second channel via stator voltage in magnitude and phase the stator reactive power is controlled by means the rotor current component i_{1q}.

Measured input variables of the control are the stator voltages and currents as well as the speed, in addition the rotor current, which is required for the corresponding current control of the rotor-side converter. Since control is performed in dq coordinates, the corresponding abc/dq and dq/abc transformation blocks are also required here. In addition, a reactive power calculation for the stator side, which has to be carried out dynamically, and a calculation of the angle γ_2 of the rotor flux position for the transformation blocks is required. The phase angle γ_1 of the stator voltage is determined via a phased lock loop (PLL).
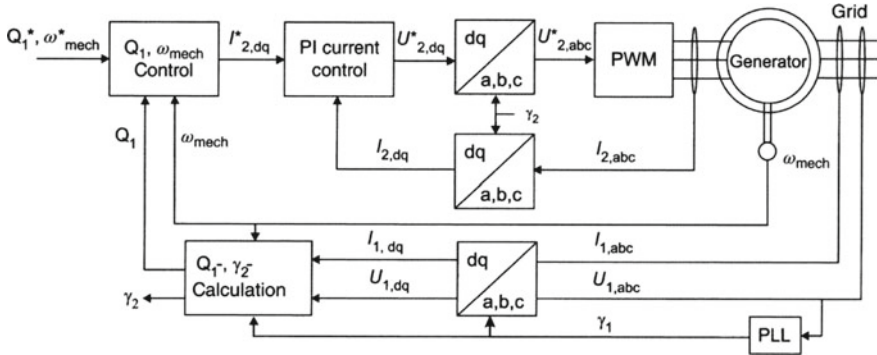
Fig. 44 Structural diagram of the field-oriented control of the doubly-fed asynchronous machine (speed and reactive power control, rotor voltage-oriented control; one line diagram)

7.3 Control of the Synchronous Machine

The control structure of the synchronous machine in both the separately excited and the permanently excited version is structurally very similar to that of the asynchronous machine with squirrel-cage rotor [13]. Speed control and flux control, the latter here implemented as reactive current control, as well as the subordinate current control and calculation of reference values for the converter characterize the structure. In Fig. 45 the control structure for a permanently excited synchronous machine is shown.

The control is usually performed in the dq coordinate system rotating with the rotor, which is similarly oriented in the direction of the rotor flux. In the permanently excited synchronous machine, the rotor flux generated in the rotor is fixed in amplitude by the excitation with the permanent magnets. However, flux components can
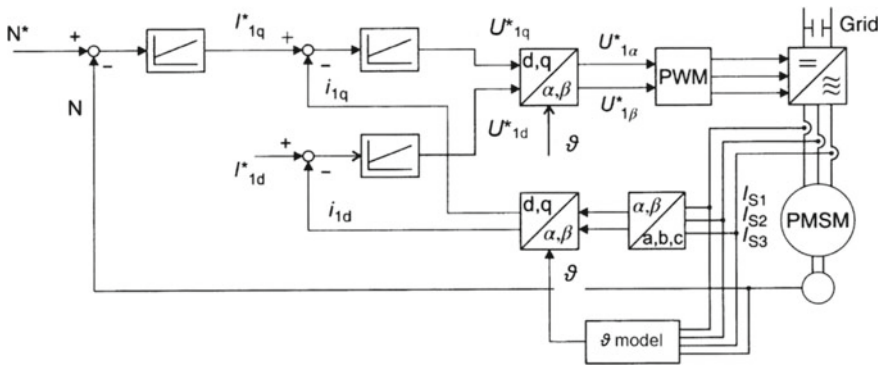
Fig. 45 Structural diagram of the field-oriented control of the synchronous machine (torque or speed and flux or reactive current control, rotor-oriented method)

also be generated here, in this case by currents in the stator winding, in the direction of or against the permanent magnet flux (field weakening or strengthening). The angle of the rotor for the transformation of the quantities is determined by a model or an observer.

In the externally excited machine, in addition to the structure shown in the figure, there is also the excitation winding and the converter for feeding it, which gives another degree of freedom for control. Here, too, there is one control channel for the active component and one for the reactive component.

7.4 Control of the Grid-Side Part Converter

The grid-side converter part is connected to the generator-side converter part via the DC link, consisting of capacitors for decoupling, as shown in Fig. 46. Varying power flow from the generator-side part of the converter, for example, due to fluctuations in wind speed and absorbed power, will charge the capacitors to a greater or lesser extent, leading to an increase or decrease in voltage in the DC link.

The grid-side converter has the task of feeding the power generated by the generator into the grid. This is done indirectly by the fact that it is the task of the control to keep the DC link voltage constant. This ensures that the power delivered by the generator is fed directly and correctly into the grid.

The control structure again corresponds to the basic structures of the other systems [13], as Fig. 47 shows. Superimposed is the control of the DC link voltage, which specifies the d-component $i_{c,d}$ of the inverter current. This ensures an injection into the grid of the power fed in from the generator into the DC link. In the second channel the mains reactive power Q_1 control takes place via the q-component $i_{c,q}$ of the stator current. If no reactive power is to be exchanged with the mains, the setpoint is to be set to zero.

A two-channel mains current control is subordinated, the outputs of which form the setpoints of the converter voltages $U_{c,\mathrm{dq}}$. The control of the grid-side part of the frequency converter is generally carried out in rotating dq coordinates, oriented to the mains voltage. The angle of the mains voltage is determined by a phase locked loop (PLL) [13]. The actual values of the grid currents are transformed from the three-phase system to the corresponding dq system, and the reference voltages for the pulse width modulation are transformed from the dq to the abc system. The

Fig. 46 Machine-side and mains-side converter with DC link intermediate circuit
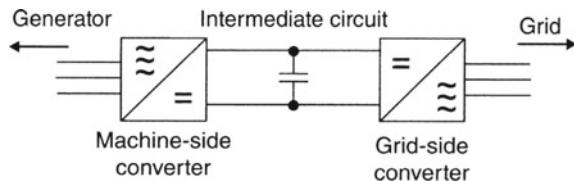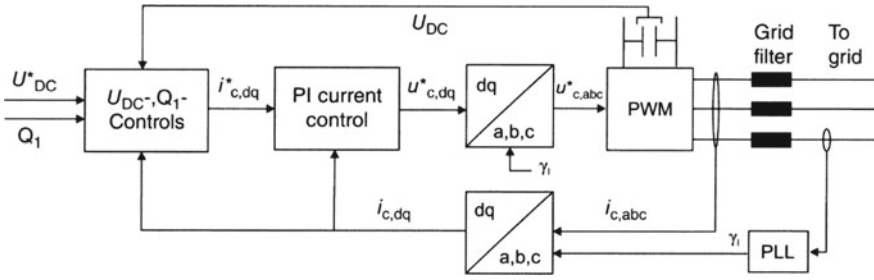
Fig. 47 Structural diagram of the voltage oriented control of the grid-side converter part (control of the DC link voltage and the reactive power; oriented to the mains voltage)
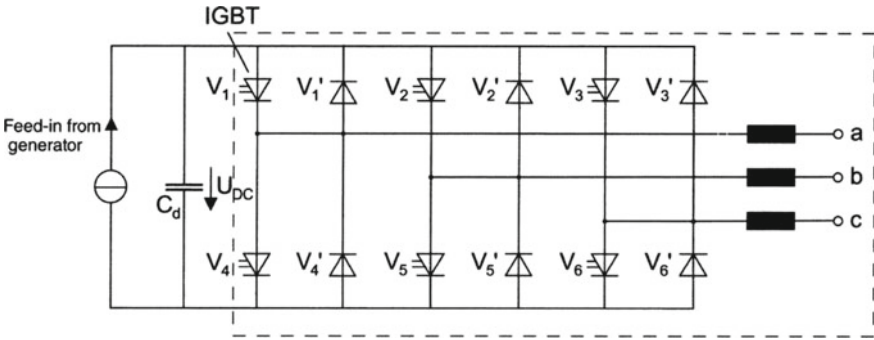
Fig. 48 Direct current/three-phase inverter; circuit and block diagram

PWM block contains the pulse width modulation and the power section of the grid side converter part. (Fig. 48).

Further on, relations concerning the dynamic behavior of the mains feed in, and the DC link are added. They are necessary for the adjustment of the control. The power is fed into the electrical supply network via a mains filter, which is required to comply with the limit values from the standards [15–18] for the harmonics. Here an L-filter is shown. But LCL-filters can also be used, resulting in a reduced filtering effort, but with increased control requirements due to the oscillating filter. In addition, filters are available as suction circuits for the reduction of certain disturbing harmonics.

The dynamic behavior of the controlled system of the mains side frequency converter part is to be illustrated by way of example. The dynamic modeling of the controlled system of the mains pulse width modulated power converter is carried out for the case of an L-filter on the mains side. Here, the total inductance of the filter and the grid is referred to as L_{mains}. In each phase of the three-phase system, the difference between the mains voltage and the converter voltage drops across this inductance. The voltage equation is given by the difference of the mains and the converter voltage, and the voltage drop at the mains filter inductance by the converter current, here for phase a:

$$U_{\text{mains,a}} = L_{\text{mains}} \frac{di_{\text{con,a}}}{dt} + U_{\text{con,a}} \tag{123}$$

and analogously those in phases *b* and *c*. After the transformation into the space vector representation and the transformation of these equations into a coordinate system *d*, *q* rotating with the mains voltage as well as resolution of the differential quotients results:

$$\frac{di_{\text{con,d}}}{dt} = \frac{1}{L_{\text{mains}}} \left(U_{\text{mains,d}} + \omega_{\text{mains}} \cdot L_{\text{mains}} \cdot i_{\text{con,q}} - U_{\text{con,d}} \right) \tag{124}$$

$$\frac{di_{\text{con,q}}}{dt} = \frac{1}{L_{\text{mains}}} \left(U_{\text{mains,q}} - \omega_{\text{mains}} \cdot L_{\text{mains}} \cdot i_{\text{con,d}} - U_{\text{con,q}} \right) \tag{125}$$

This describes the dynamic system of the mains side frequency converter part with regards to the dynamics of the current, which is necessary for the design of the control parameters. Here again a coupling occurs, the effect of, for example, the q-component of the converter current influences its d-component and vice versa. With respect to the control behavior, the effect of the converter voltage U_{con} on the converter current i_{con} in the same axis is important and results in the behavior of an integrator. A PI is adequate to be employed and the controller parameters are to be determined according to the symmetrical optimum [13, 14].

The superimposed regulation of the DC link voltage U_{DC}, which is equal to the voltage U_{Cd} on the DC link capacitor, operates on a path consisting essentially of this DC link capacitor C_{d}. This capacitor is loaded by the current i_{Cd}, equal to the active generator current $i_{\text{Gen,d}}$ minus the active current fed into the mains by the line side part of the frequency converter. This results in the equations:

$$U_{\text{Cd}} = \frac{1}{C_{\text{d}}} \int i_{\text{Cd}} dt + U_{\text{Cd0}} \tag{126}$$

$$\frac{dU_{\text{Cd}}}{dt} = \frac{1}{C_{\text{d}}} i_{\text{Cd}} = \frac{1}{C_{\text{d}}} \left(i_{\text{Gen,d}} - i_{\text{con,d}} \right) \tag{127}$$

Here, again, an integral system behavior can be observed. A PI controller is well suited and a design according to the symmetrical optimum is recommended.

7.5 *Design of the Control*

General requirements such as dynamics, stability and robustness have to be met by the control system, as well as many requirements that are typical for wind turbines, such as:

- smoothed generator torque,
- low voltage pulsations in the DC link,
- smoothed mains power,
- suitable control reaction to harmonics in the mains voltage,

both in steady-state and dynamic operation. The design of the controllers is generally carried out with the rules of the technical optimum and the symmetrical optimum [13], which are common in drive technology, as described briefly for the individual controls.

In addition, the wind turbines and, here in particular, their power electronics generator system must meet the high requirements of system control, see Chap. 9, and grid integration in stationary operation as well as dynamically, for example in the event of voltage dips and outages (low voltage ride through, LVRT), see Chap. 10. This is achieved with special controller design or with additional converter control measures, which are not discussed further here.

8 Grid Integration

The power electronics generator systems must meet special requirements for plant and system control and grid integration and must therefore be designed for this in terms of hardware and control technology. It should be noted that the requirements regarding grid integration have been continuously refined and, in some cases, tightened in the near past with constantly expanding knowledge and experience from operation with decentralized renewable energy feed-in. Ensuring that these requirements are met in terms of control and regulation technology requires special control measures and possibly also a special hardware design, hardware selection or additional hardware. The plant or system control is dealt with in detail in Chap. 9, the grid integration is dealt with in Chap. 10. Here, some requirements and their influence on the power converter hardware and control are presented in an overview.

Mains connection standards with regard to low-frequency electromagnetic emissions must be met, i.e. the permissible harmonics in current and/or voltage. This is done by selecting the appropriate pulse width or space vector modulation in conjunction with suitable L or LCL filters on the mains side and possibly special power converter circuits. If necessary, additional suction circuits can also be used to reduce individual harmonics in the current.

Other important requirements come from the conditions for grid integration [15–18]. One important requirement contained therein is grid support in steady-state operation. The grid connection conditions require active power influencing and reactive power injection, depending on the state of the grid. This must be implemented in the higher-level control system and the power units must have corresponding reserves for the case of an additive reactive power feed-in.
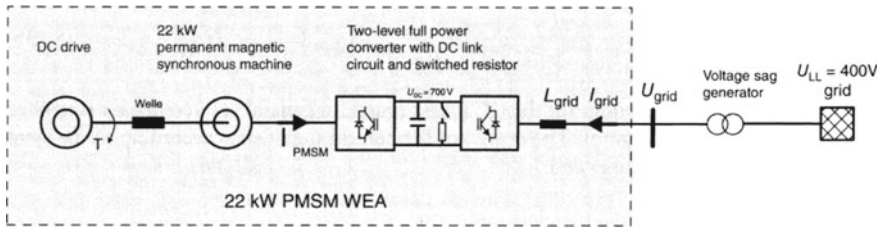
Fig. 49 Structure of the laboratory setup for driving through the grid voltage dip for a wind turbine with frequency converter, permanent magnet excited synchronous machine and voltage sag generator

Another requirement is grid support in dynamic operation. The grid connection rules require, for example, uninterrupted operation in the event of grid voltage fluctuations. If the grid voltage drops, the grid-side converter can no longer feed power into the grid, but it must remain in operation and quickly feed power back in when the grid voltage returns. During the grid voltage drop, the generator produces power which is fed into the DC link via the generator-side converter part. This leads to an increase in the DC link voltage. Protective measures must intervene to protect the converter from damage due to overvoltage [2, 19]. This is generally implemented via a switched resistor in the DC link if control measures are not sufficient.

As an example of such requirements to the converter and how they are fulfilled, the ride-through of a mains undervoltage event, also called low-voltage-ride-through, is considered. There is a requirement that the inverter becomes active again within a very short time after a grid short-circuit and feeds into the grid in order to support the grid or assist in its reconstruction. More details on the requirements are presented in Chap. 10. The passing of the mains undervoltage is presented here as an example by measurements on a 22 kW drive system in the laboratory. In Fig. 49 the used system is shown, with permanently excited synchronous machine and full power converter as shown in one of the previous sections.

The permanently excited synchronous machine feeds into the grid via a two-level pulse width modulated converter and a filter inductor. A resistor with a DC chopper is installed in the DC link of the converter, which becomes active above a certain DC link voltage and absorbs power. A voltage sag generator is connected between the mains and the converter, which creates mains voltage sags. The rotor power equal to drive power is introduced by a DC machine which can reproduce a wind profile. A measurement result for a three-phase fault with voltage sag down to 12% with a duration of 300 ms is shown in Fig. 50. The measured variables were recorded with the hardware and software of a control system (mains voltages, mains currents, DC link voltage, power, stator currents, speed) and visualized accordingly.

In steady-state operation with full mains voltage in the time range from 0 s to about 0.08 s, the mains side converter part feeds a current of $i_{grid} = 6$ A into the mains. At the time 0.08 s, the mains voltage collapses. Transient overcurrents of up to 30 A occur on the mains side. To dissipate the power in the DC link, the mains currents are regulated up to the system limit (here $i_{grid,max} = 10$ A). The generator
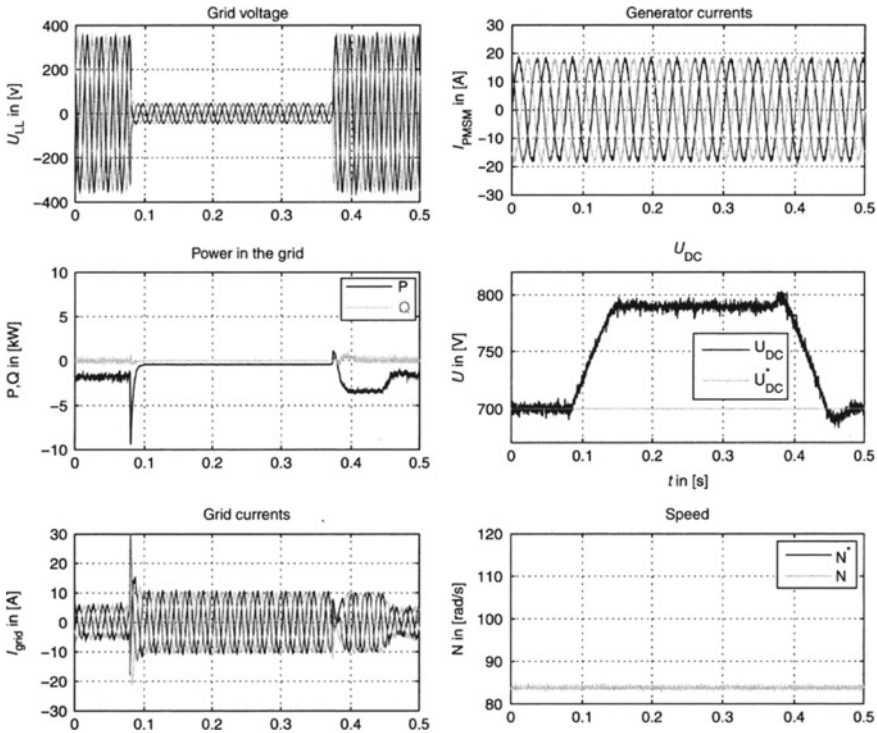
Fig. 50 Sequence of the low-voltage ride-through in the system with permanent magnet excited synchronous machine and full power converter in the laboratory (example; rated power of the drive 22 kW); braking resistor with controller in the DC link; mains sag down to 12% of the rated voltage

currents of the machine and thus the generated power remain constant. Due to the power imbalance, the DC link voltage U_{DC} increases. The resistor in the DC link is activated and limits the voltage there to $U_{DC} = 790$ V. The mains voltage dip is well controlled. At time 0.38 s, the full voltage is switched back on. The mains currents collapse for a short time. In the time range from 0.39 to about 0.46 s, the mains current remains at the limit value of 10 A and discharges the DC link capacitor to its target voltage of 700 V. After this, regular steady-state operation is resumed. This behaviour can also be studied by simulation [20].

9 Further Electrotechnical Components

On the grid side, the permissible voltage or current harmonics are specified in standards or guidelines of the grid operators. The harmonics generated by the converter, depending mainly on the converter circuit, pulse width modulation and operating point, must be kept under these limits by means of suitable pulse width modulation,

of mains filters and the remaining components must be reduced to the permissible level. L-filters (mains reactors), LCL-filters in T-circuit (mains reactors and capacitors) and, if necessary, additional suction circuits (parallel LC-arrangements) are used on the grid side. The permissible limit values for the current harmonic n, here for the medium-voltage grid to which wind turbines of 1 MW or more are generally connected, are specified individually in the countries, for Germany, for example in [3].

Low-power wind turbines could be connected directly to the low-voltage grid. Existing transformers for low-voltage grids have a rated power of approximately 300–1000 kVA, from which the permissible connected load of a wind turbine can be estimated. The wind turbine may generally only use part of the power of the existing grid transformer.

In the case of larger wind turbine output power, these are connected to the electrical grid via their own turbine transformers. Wind turbines in the not too high megawatt range are mainly built with a system voltage of about 690 V or similar. These are connected to the medium-voltage level grid via transformers. In Germany, for example, medium-voltage grids mostly have a voltage of 10, 20 or 30 kV, in the USA for example, mostly 4.16, 12.47, 13.8, 24.9 and 34.5 kV. They must be suitable for power feed-in from the wind turbines, in particular also for the harmonics generated by the converter.

The power electronics generator system, like all other electrical and electronic components of the wind turbine, is connected to the electrical supply network for operation via contactors that can be switched on and off. These contactors are equipped with electronic or thermal overcurrent detectors whose signal is evaluated to open the contactor in the event of overcurrent and protect the system. Depending on the protection concept, additional electrical fuses can be used in series with the mains connection.

In wind turbines according to the state of technique, the angle of the rotor blades with regard to the blade rotating area can be adjusted, it is the angle of attack to the wind, named the pitch angle. This adjustment is carried out hydraulically or electrically. In the latter case, there is therefore an electric pitch drive for each of the, generally, three rotor blades. Here, systems such as geared motors can be used. In order to be able to turn the rotor blades out of the wind into a safe position in the event of a power failure, an emergency power supply is required here.

Additional measuring equipment is also required to operate the wind turbine. On the one hand, this is a wind speed measurement. The wind speed measurement is used to select the operating mode from the actual wind speed value and to specify the setpoint for the speed or power. On the other hand, a device for measuring the wind direction is required to adjust the system into the wind direction based on the measured value.

10 Characteristics of the Power Electronics Generator Systems in Overview

The standard power electronics generator systems used by wind turbines in operation and in production are based on various basic concepts, as presented previously. In addition, there are always manufacturer-specific special features. In Table 3 the essential, basic characteristics of the various standard concepts are compiled, which should be self-explanatory.

An important feature of the characteristics of wind turbines is the gearbox. So far, it has not been discussed in detail, and thus should be explained shortly. In general, roughly outlined, there are currently three variants of gearboxes for wind turbines in the upper megawatt range, with corresponding consequences for the speed of the generator:

- plants with gearboxes with a ratio of about 1:100 and generators with base speeds of about 1500 1/min,
- plants with gearboxes, transmission ratio of about 1:10 and generators with base speeds around 150 1/min as well as
- plants with gearless systems, i.e. gear ratio 1:1 and generators with extremely low base speeds around 15 1/min.

Table 3 Properties of power electronics generator systems in wind turbines

Property	System ASM squirrel cage	System ASM slip ring rotor	System SYM separate excitation	System SYM permanent excitation
Machine design, special features	Standard stator; rotor shorting cage	Standard stator; rotor with winding; slip rings for rotor current	Standard stator; rotor with winding; slip rings for excitation current	Standard stator; rotor with permanent magnets; procurement, costs permanent magnets
Stator current displacement factor in rated operation	Approx. 0.85	Approx. 0,95	Approx. 0,95	Approx. 0,95
Efficiency of the machine	Medium	High	High	High/very high
Converter design, rated apparent power S_N	Standard, full rated converter, approx. 118 % P_N	Standard, partial rated converter, approx. 30 % P_N	Standard, full rated converter, approx. 105 % P_N	Standard, full rated converter, approx. 105 % P_N
Converter efficiency	Less high, due to high reactive current	High and only partial power via converter (lowest losses)	High	High

The selection of the transmission ratio of the gear box and thus the basic generator speed influences the design and the costs to a large extent.

The omission of the gearbox in the latter variant considerably reduces the effort required for the mechanics and leads to cost, volume and weight savings of the mechanics. However, the opposite is the case for electrical engineering: electrical machines with smaller rated speeds become heavier, more voluminous and more expensive.

11 Exercises

Three-phase systems: A wind turbine feeds power into a three-phase grid. The grid voltage is 690 V (effective value of the phase-to-phase voltage). A grid current of 1500 A is fed in with a displacement factor $\cos\varphi = 0.8$ capacitively.

1. Active, reactive and apparent power shall be determined.
2. What reactive power, e.g. from a reactive power converter feeding in parallel, is required to compensate (cancel out) the reactive power fed in.
3. To what value could the grid current be reduced if the active power from part (a) were fed in with optimal $\cos\varphi = 1$?

Transformer: A low-voltage wind turbine feeds into the medium-voltage grid via a three-phase transformer. Transformer data: $S_N = 3$ MVA, $U_{1N} = 10$ kV, $U_{2N} \approx$ 690 V, Dyn5 circuit type; $u_r = 0.03$, $u_x = 0.05$; (u_r resistive, u_x inductive component of the relative short-circuit voltage); $w_1/w_2 = 14.925$. The transformer is operated on the primary side on the 10 kV grid. The simplified short-circuit equivalent circuit diagram is assumed.

4. The transformer is operated at no load on the secondary side. Draw the equivalent circuit diagram. The voltage drop at the primary-side reactances is to be neglected because of the small magnetizing current. Determine the secondary voltage for this no-load point.
5. On the upper voltage side at the transformer, a pure active power of 2 MW at 10 kV is now fed into the grid. What is the required active current?
6. The active current from part 2 is fed via the transformer into the 10 kV grid with a fixed voltage of 10 kV. What voltage drop results at the transformer reactances in magnitude and phase, related to the high voltage side and to the low voltage side. What voltage results on the low voltage side?
7. An additional reactive current of 30% of the active current is fed in, once capacitively, once inductively. What voltage results in these cases on the low-voltage side of the transformer?

The following points are valid: The complete equivalent circuit without an iron resistor is assumed. From the no-load measurement on the primary side, it is known that a current of 2% of the rated current (at U_{1N}) flows.

8. The equivalent circuit is to be drawn. The data of the five impedances are to be determined from the above data. The boundary condition is that the primary and secondary reactances, real and imaginary parts, are equal.

9. Again, 2 MW active power is to be fed into the electrical grid on the primary side. The voltages and currents in the transformer are to be determined with the calculated impedance values. The phasor diagram of the voltages and currents is to be drawn. The losses are to be determined.

Asynchronous generator and converter: In Fig. 51 the measured Heyland circle of an asynchronous machine with squirrel-cage rotor is shown. The machine is fed from a three-phase mains supply with 400 V/50 Hz (phase-to-phase). The stator of the machine is connected in star. The machine has four poles ($p = 2$).

In the following, it is assumed that the primary and secondary leakage coefficients of the machine are identical ($\sigma_1 = \sigma_2$). Furthermore, the ohmic losses of the stator and the iron losses can be neglected. Note: The task parts 1 (10), 2 (11) and the first part of 3 (12) can be solved independently.

10. Calculate the following elements of the single-phase equivalent circuit of the star-connected machine with the aid of the measured Heyland circuit: primary leakage inductance $L_{1\sigma}$, primary main inductance L_{1h} and stator referred secondary leakage inductance $L'_{2\sigma}$. Draw the stator currents used for the calculation in Fig. 52.

11. For the optimum operating point, draw the stator current $I_{1,\text{opt}}$, the phase angle φ_{opt} and the slip s_{opt} in Fig. 51 and determine the values of the three quantities. Then calculate the power factor $\cos\varphi_{\text{opt}}$, the active electrical power $P_{1,\text{opt}}$, the efficiency η_{opt}, the mechanical speed n_{opt}, the mechanical power $P_{\text{mech,opt}}$ and the torque of the machine T_{opt} at this operating point.

12. Determine the stalling slip s_{stall} with the aid of Fig. 51 and calculate the stalling speed n_{stall} and the referred rotor resistance R'_2 of the single-phase equivalent circuit of the machine.

13. Calculate the stalling torque T_{stall} of the given machine.
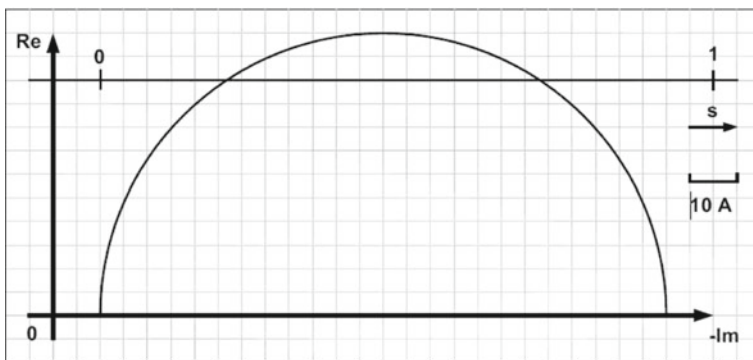
Fig. 51 Measured Heyland circle of the asynchronous machine with squirrel-cage rotor
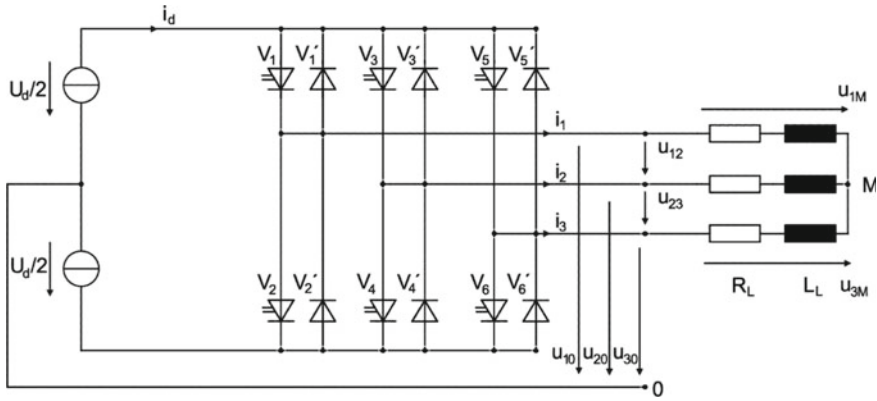
Fig. 52 Three-phase inverter

Converter with space vector modulation: With the aid of a pulse width controlled converter on an electrical load a sinusoidal symmetrical three-phase voltage system is to be simulated as well as possible. The space vector modulation method must be used.

DC link voltage	$U_d = \frac{3}{2} \cdot 400\text{V} \cdot \sqrt{2}$
Load voltage	$\hat{u}_{LM} = 150$ V
Mains frequency	$f_n = 50$ Hz
Pulse frequency	$f_p = 10$ kHz

14. Show in a drawing which basic output voltage space vectors u_i of number i can be generated with the converter and designate them.
15. What is the maximum instantaneous value of the inverter output voltage? Calculate the space vector components u_α and u_β for the switching state [01 10 01] and the magnitude of the corresponding space vector.
16. In this case, into how many discrete angular segments is one revolution of the space pointer divided, and what is the angular range for such a segment?
17. Determine the space vector components u_α and u_β of the load voltage space vector for the 45th angular segment.
18. Determine the on-time of the right, left and zero voltage space vector of the converter required to replicate the space vector of the 45th angular segment and of the corresponding sector.

Wind turbine with squirrel-cage asynchronous machine: A wind turbine with squirrel-cage asynchronous machine is connected to the electrical supply grid via a converter.

System parameters:

$P_N = 2$ MW	Mechanical rated power
$c_p = 0.5$	Power value
$\rho = 1{,}2$	Density of air
$r = 50$ m	Rotor blade length
$n_N = 1800$ 1/min	Rated speed
$p = 2$	Number of pole pairs
$u = 100$	Gear ratio
$U_{grid,N} = 690$ V	Phase-to-phase mains voltage
$\cos\varphi_{grid,N} = 1$	Displacement factor of the grid feed in

19. Is it a fixed speed or a variable speed system? Reason!
20. What wind speed must be given to be able to generate the rated power P_N of the turbine with the rotor blades? ($P = 0.5 c_p \rho A_V v_{wind}^3$; A_V area swept by the rotor)
21. At what rotational speed n do the rotor blades rotate when the generator is operated at rated speed?
22. What is the torque T_N at the rotor of the machine when the plant produces nominal power?
23. Calculate the grid currents, active power and reactive power fed into the grid in the case that the wind turbine generates rated power.
24. Draw the speed-torque diagram of the machine on the mains and mark the rated operating point. How does the diagram change when the stator voltage of the machine is changed in proportion to the speed?
25. Draw the block diagram of the power electronics generator system with generator, converter, gearbox and mains. Why is a gearbox required?
26. Draw the simplified UI characteristic of the inverter and the machine. Mark and name the limits of operation.

Drive train with doubly-fed asynchronous machine: A small wind turbine is equipped with a doubly-fed, four pole-pair asynchronous machine and with a converter in a two-level circuit. Data of the doubly-fed asynchronous machine are shown below. The asynchronous machine is operated on the stator side at the mains and on the secondary side at the converter as well as with constant stator flux linkage.

$P_{1N} = 25$ kW	Rated power
$U_{1N} = 400$ V	Rated phase-to-phase voltage
$R_1 = 0.15\,\Omega$ $0.15\,\Omega$	Stator resistance
$R_2' = 0.12\,\Omega$	Stator referred rotor resistance
$L_1 = L_2' = 50$ mH	Primary and secondary stator referred inductance
$L_{1h} = 49$ mH	Primary main inductance

(continued)

(continued)

$f_{1N} = 50$ Hz	Rated frequency
p = 2	Number of pole pairs

27. The phasor diagram for no-load operation with synchronous speed and with 1.3-times the synchronous speed must be created. In both cases create the phasor diagram when, in addition, in the first case only the active rotor voltage and in the second case only the reactive rotor voltage is increased by 5%.
28. The stator reactive power is to be controlled to zero. The machine outputs 22 kW as the maximum active power to the converter at a speed of 1950 1/min. Determine the torque, slip, speed, stator current, displacement factor, active current, reactive current and stator voltage, rotor current and rotor voltage.

For the following subitems, the data of the converter apply: $U_{DC} = 1, 35 \cdot \sqrt{2} \cdot 400$V.

29. For which rated current, for which rated voltage, for which rated apparent power and for which displacement factor is the inverter to be designed.
30. At what maximum modulation level is the inverter to be operated? Can overmodulation be avoided?

Control of the frequency converter: The grid-side converter part of a wind turbine with rotating field AC three-phase machine and full converter feeds into the grid. The current control is to be designed. The equations for the dynamic behavior of the grid are included in the corresponding chapter. The grid data are:

$U_{mains} = 690$V	Mains phase-to-phase voltage
$u_{SC,mains} = 12\%$	Mains referred short circuit voltage

A proportional-integral controller is to be used:

$$y = K_P \cdot x + \frac{1}{T_I} \int x dt; \quad G(s) = \frac{y}{x} = K_P \frac{sT_I + 1}{sT_I}$$

Design equation for the technical optimum:

$$T_I = T_{max}; K_p = \frac{T_I}{2\sigma_I V_S}$$

T_{max}: largest time constant; σ_I: sum of small time constants; V_S: amplification factor of the controlled system.

The converter operates with a pulse frequency of 2.5 kHz. Two pulse periods are to be assumed as delay by the inverter.

31. The differential equation for the d component of the inverter current is to be taken from the corresponding chapter and the disturbance components (U_{mains}, i_{1q}) must be neglected for the controller design. From the remaining equation the time constant T_{max}, line gain V_S and smallest time constant σ_I are to be determined.

32. Using the equations for parameter determination for the technical optimum, the gain K_p and the time constant T_I are to be determined as controller parameters of the proportional-integral controller.

Control of generators and grid feed in:

33. Draw the phasor diagram of a synchronous machine connected to the mains and operating in phase-shift mode (stator side only capacitive reactive current).

34. Sketch the block diagram of the general type of control loop and designate all subsystems. Name three types of controllers.

35. Draw the complete control loop for field-oriented speed control of the asynchronous machine. Describe the main advantages of the field-oriented control.

36. Which coordinate system is often used as the reference system for field-oriented control? State the reason for this and explain the value for synchronizing the control.

37. Draw the equivalent circuit of the mains side converter and the generator side converter part in the commonly used circuit.

38. Name and describe the steps of controller synthesis. Describe the objective of the controller design "technical optimum".

39. A wind turbine with a permanent-magnet synchronous generator fed via a full rated power converter operates in power-limiting mode. Sketch the control structure. Name all the control loops involved in the power train of the wind turbine and assign tasks to the control loops.

Literatures

1. Liserre M, Cárdenas R, Molinas M, Rodriguez J (2011) Overview of multi-MW wind turbines and wind parks. IEEE Trans Ind Electron 58(4):1081–1095
2. Lohde R, Wessels C, Fuchs FW (2009) Power electronics generator systems in wind turbines and their operational behavior. ETG Congress October 2009, Düsseldorf, Fachtagung 3: Direktantriebe und Generatoren, Düsseldorf, Germany
3. BDEW, German Wind Energy Association; information on the Internet at www.wind-energi e.de
4. Fischer R (2017) Elektrische Maschinen; Hanser, Munich, Vienna
5. Camm EH, Behnke MR, Bolado O, Bollen M, Bradt M, Brooks C, Dilling W, Edds M, Hejdak WJ, Houseman D, Klein S, Li F, Li J, Maibach P, Nicolai T, Patino J, Pasupulati SV, Samaan N, Saylors S, Siebert T, Smith T, Starke M, Walling R (2009) Characteristics of wind turbine generators for wind power plants. In: Power and energy society general meeting, PES'09. IEEE
6. Hagmann G (2019) Power electronics—Fundamentals and applications in electrical drive technology, Aula, Wiesbaden

7. Müller G, Ponick B (2014) Fundamentals of electrical machines, Wiley-VCH, Weinheim
8. Chen Z, Guerrero JM, Blaabjerg F (2009) A review of the state of the art of power electronics for wind turbines. IEEE Trans Power Electron 24(8):1859–1875
9. Mohan N, Undeland TM, Robbins WP (2002) Power electronics: converters, applications, and design. Wiley, New York
10. Schröder D, Kennel R (2021) Elektrische Antriebe: Grundlagen. Springer, Berlin, New York
11. Khan MA, Pillay P (2005) Design of a PM wind generator, optimized for energy capture over a wide operating range. In: 2005, IEEE international conference on electrical machines and drives, pp 1501–1506
12. Mueller S, Deicke M, De Doncker RW (2002) Doubly fed asynchronous generator systems for wind turbines. IEEE Ind Appl Mag 8(3):26–33
13. Schröder D (2015) Elektrische Antriebe: Regelung von Antriebssystemen; Springer, Berlin, New York
14. Teodorescu R, Liserre M, Rodriguez P (2010) Grid converters for photovoltaic and wind power systems. Wiley-IEEE Press
15. BDEW (2008) Technical guidelines for generation plants on the medium-voltage grid; German association of energy and water industries
16. HIEC (2020) International electrotechnical Commission: IEC 61400–21: wind turbines, Part 21: measurement and assessment of power quality characteristics of grid connected wind turbines
17. SDLWindV (2009) Ordinance on system services by wind turbines (Systemdienstleistungsverordnung—SDLWindV, Part I No. 39; issued at Bonn on 10 July 2009; replaced by: NELEV Verordnung zum Nachweis von elektrotechnischen Eigenschaften von Energieanlagen (Elektrotechnisch-Eigenschaften-Nachweis-Verordnung-NELEV); Federal Ministry of Justice and Consumer Protection, 2017; in conjunction with, inter alia, the Medium Voltage Directive [15]
18. Tsili M, Papathanassiou S (2009) A review of grid code technical requirements for wind farms. Renew Power Gener IET 3(3):308–332. ISSN 1752–1416
19. Deng F, Chen Z (2009) Low-voltage ride-through of variable speed wind turbines with permanent magnet synchronous generator. In: 35th Annual conference of IEEE industrial electronics, 2009. IECON '09, pp 621–626
20. Zou Y, Elbuluk M, Sozer Y (2010) A complete modeling and simulation of induction generator wind power systems. In: IEEE industry applications society annual meeting (IAS), pp 1–8

Prof. Dr.-Ing. Friedrich W. Fuchs was head of the Chair of Power Electronics and Electrical Drives at Christian-Albrechts-University in Kiel and is still active in this technical field. An important research focus is the conversion of regenerative energy, especially wind energy. Before that, he spent 14 years in industry, most recently as head of development at CONVERTEAM (then AEG, now GE General Electric Power Conversion).

Control and Automation of Wind Energy Systems

Reiner Schütt

Wind turbines (WT) or several WTs combined in a wind power plant (WPP) are complex systems whose operation requires extensive automation of both the overall system and the subsystems. In this context, wind energy systems (WES) are expected to at least meet the requirements of conventional power plants in terms of reliability, efficiency and operational control system. In contrast to conventional power plants, the supply of energy cannot be influenced but varies strongly and quickly due to the wind speed. For the automatic and safe operation and the large automatic adaptation of the operation of WES to different operating conditions, a complex automation technology is therefore required, which distributes the tasks to different subsystems.

Modern WES feed into the medium or high voltage level of the electrical grid via transformers. In order to optimise the power fed in and limit it to the rated power, WT are used with and without gearboxes with full or partial converters with variable speed and variable blade angles. The automation of WES includes measurement, control, regulation and monitoring of the main parameters within the WT as well as WT and WPP operation control system. It includes remote monitoring and visualisation as well as information and communication technology integrated into other systems, in particular, into the higher level grid control systems. Automation consists of the technical equipment (hardware), the associated programs (software) and the necessary communication systems. Despite the different types of WT, their automation increasingly shows common features, in particular, because in future, WT will have to be integrated into higher level control systems in the same way, irrespective of the manufacturer.

The chapter deals with modern WES and the basic open- and closed-loop control circuits within the WT, the WT and WPP operation control system, the connection of the WT to higher level systems and the so-called SCADA systems. It provides an

R. Schütt (✉)
FH Westküste, Fritz-Thiedemann-Ring 20, D-25746 Heide, Germany
e-mail: schuett@fh-westkueste.de

overview of the essential aspects for the automation of WES, comparable discussions can be found in [4, 6, 7, 10, 15].

1   Fundamental Relationships

The aim of WES automation is the safe and efficient operation of the WT, which is extensively independent of humans. To achieve this, various tasks must be fulfilled, which essentially comprise measurement, control, regulation, monitoring, guidance and visualisation. In English, these individual functions are summarised by the generic term 'control'; in German, the term 'Automatisieren' is used.

To make the content readable, there are some symbols that are not used as usual in English-language publications. The main differences are the wind speed v, the voltage u or U and the torque M.

1.1   Classification of WT Automation

Several hundred physical inputs and outputs must be processed in order to operate a WT. Individual WPP can consist of more than one hundred individual WT and, in addition to the WPP, other generators, consumers and grid resources must also be monitored and coordinated in the grid control system. The large number of automation functions, the requirements for reaction speeds and the data volumes to be processed can only be mastered if the tasks are distributed and arranged in a hierarchy. In plant automation, this hierarchy is represented in the form of an automation pyramid.

Figure 1 shows a frequently used automation pyramid with three main levels, whereby the terms automation or control level have become established for the middle level.

The tasks and requirements for response time and data volumes specified in the figure can also be transferred to the automation of WES. Thus, the switching times of the inverters in the field level are in the µs range, the reaction times of the programmable logic controllers in the automation level are in the ms range and the required response times of the WTs to the requirements for power reduction from the grid control system are in the range of seconds. If only a few analog and digital inputs and outputs are processed by a device in the field level, the data series of all units connected to a supply area, recorded over several years, are stored and evaluated in the management level.

To divide the functions, the three main levels are often subdivided. The division into four to six levels is typical. A uniform naming of the levels has not become established. In Fig. 2, the main subsystems of the WES automation are arranged in six levels. The designations chosen in the following correspond to the main functions of the respective level.
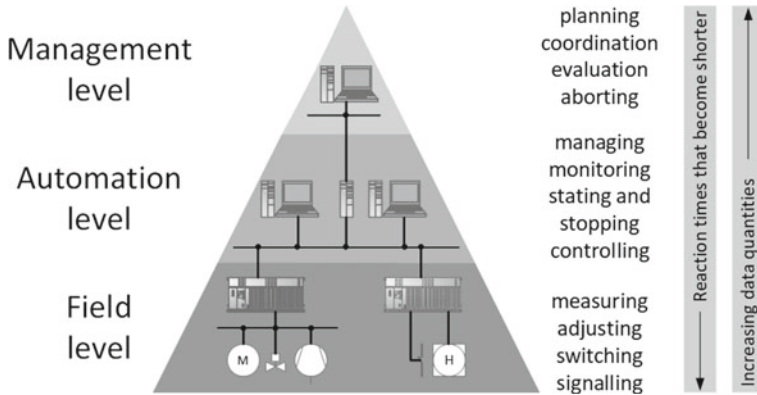
Fig. 1 Three-level model of plant automation with essential functions
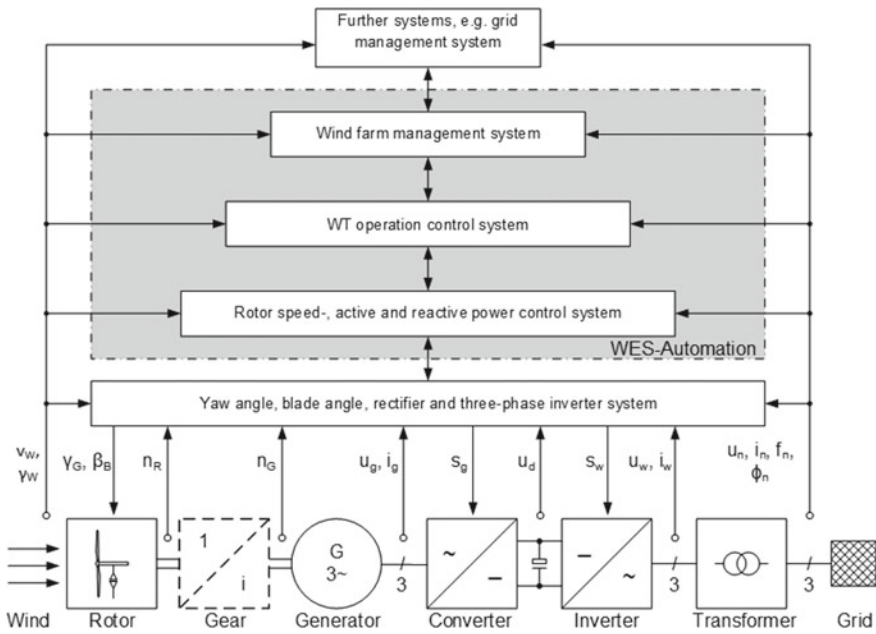
Fig. 2 Arrangement of WT automation in the automation hierarchy

- Sensor-actuator level: The lowest level shows the drive train of the WT with the input variables, wind speed v_W and wind direction γ_W. The characteristic output variables are the three-phase grid voltages u_n and grid currents i_n, the grid frequency f_n and the phase angle φ_n between current and voltage of the three-phase system. The rotor speed n_R is influenced by the variable yaw angle γ_G and the variable blade angles (pitch angles) $\beta = \beta_B$.

Different types of generators are used in WT, essentially the double-fed asynchronous machines (DASM), the separately excited synchronous machines (FSM), the permanently excited synchronous machines (PSM) and the asynchronous machines with squirrel-cage rotors (ASM). They are operated partly with and partly without gears and feed the generator power into the grid either completely or partly via a converter. The figure shows the drive train of a WT with a fully inverter-fed PSM with and without gears.

The mechanical power of the rotor P_R is transmitted via the drive train to the generator with the generator speed n_G. The generator power P_G is fed into the electrical grid via a transformer with the aid of a full converter. The full converter consists of the generator-side rectifier with the generator-side three-phase currents i_G and voltages u_G, the direct current (dc) link with the dc voltage u_d, and the grid-side inverter with the grid-side three-phase currents i_W and voltages u_W. The rectifiers and inverters are designed as six-pulse bridge circuits with IGBTs, each controlled by six control signals s_g on the rectifier side and s_W on the inverter side. With the aid of a transformer, the voltage on the inverter output side is adapted to the mains voltage of the medium- or high-voltage network.

- Adjustment level: The adjustment actuators of the individual drive systems are situated above the sensor-actuator level. The yaw angle actuator, often also called azimuth system, guides the alignment of the nacelle according to the wind direction. The pitch angle setting devices, often called pitch systems, set the pitch angles according to the desired setpoints or reference values. The generator-side electrical power P_G is influenced by the pulse-width-modulated control signals s_G of the pulse rectifier. The inverter-side active electrical power P_W and reactive power Q_W are influenced by the pulse-width-modulated control signals s_W of the pulse inverter. The DC link voltage u_d remains constant if the rectifier-side and inverter-side active powers are identical.

- Closed control loop level: The actual control to the setpoints of the active grid power P_n and reactive grid power Q_n as well as the limitation of the rotor speed takes place in the closed control loop level located above the actuation level. Depending on the operating mode of the WT, different controllers calculate the setpoints for the yaw and pitch angles as well as for the rectifier and the inverter.

- Operation control loop level: The control systems receive their setpoints from the higher level operation control system, which is located in the operation control loop level. Depending on the wind speed, the setpoints from a grid control system or a WPP control system and external specifications, the operational management controls the WT into the required operating state. In addition to specifying the setpoints for the controls, the operational management also controls the other actuators in the WT such as brakes, contactors, heating and ventilation systems or the firing systems and processes additional sensor signals such as temperature, humidity or oil pressure. The plant management system exchanges the information either directly or via a control system with the remote monitoring and control system of the manufacturer or operator as well as with the control system of the grid operator.

- Process control level: If several WTs are operated in a WPP, a WPP control and automation system is superordinate to the individual WT operation control system. The system allocated to the process control level distributes the required power reduction and reactive power fed into the individual WTs in accordance with the setpoints required by the grid operator and ensures the required participation in the short-circuit current in the grid. The WPP control system also ensures an orderly and continuous start-up and shutdown process of the WPP so that no power surges occur.
- Management or planning level: WT operation control or WPP control system receives their setpoints from the management level, also called planning level, and return the actual values of interest back to it. Both the grid control system and the billing systems or the higher level management systems of the plant operators, which are usually oriented towards business management, can be assigned to the top level.

1.2 System Properties of Energy Conversion in WTs

The control, operation and automation systems of the WT aim to optimise the energy conversion from the kinetic energy of the wind to the electrical energy of the grid and to operate the turbine safely in compliance with specified limit values.

Below the nominal wind speed of a WT v_{WN}, the power fed into the grid is maximised for this purpose and above this wind speed it is limited to the nominal power P_N, the nominal electrical power P_{nN} at the grid connection point (GCP). To comply with the grid connection conditions, the WES must limit the active power to the requirements and with rising grid frequency. The reactive power must be changed on demand in case of grid voltage fluctuations. In the event of temporary voltage dips, WES must support the grid by feeding in a specified reactive current.

In order to develop the basic open-loop and closed-loop control functions of a WT, the essential system characteristics of the energy conversion in WTs required for the description are first summarised. Despite the differences in the drive trains (with and without gearbox, high ratio, low ratio), the generator systems (ASM, DASM, FSM, PSM) and the pitch and azimuth drives (hydraulic, electric), the control has fundamental similarities.

Figure 3 shows the block diagram of the energy conversion, in which the subsystems are connected according to their quantities describing the power flow. The DC link, the grid-side inverter and the transformer are combined in one block. This diagram is used to describe the possibilities for influencing the power flow.
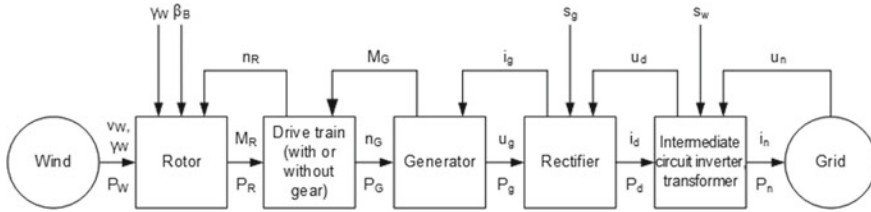
Fig. 3 Schematic representation of the power flow in WTs

1.3 Energy Conversion at the Rotor

Figure 4 shows, using the view of a WT (a), the sectional view of a blade (b) and the plan view (c), the orientation of v_W, n_R, characterising the energy conversion, the rotor diameter D, γ_G and β_B. A good summary of the dependence of the rotor power on these quantities can be found in [15]. At this point, the relationships that are crucial for control and automation are summarised.

In the sectional view, the circumferential speed of the blade u_B and the active speed v_u acting on the blade cross section are shown. The circumferential speed of the blade tip is denoted by u:

$$u = 2 \cdot \pi \cdot n_R \cdot D/2 \tag{1}$$
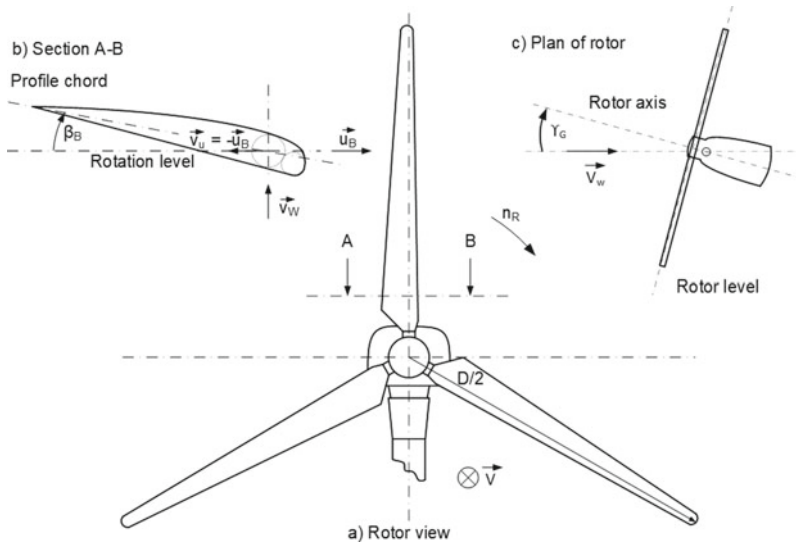
Fig. 4 Characteristic quantities of the rotor for the calculation of the rotor power

The kinetic energy of the undisturbed air flow is partially converted by the rotor into the mechanical energy of the rotor. The ratio of the mechanical power P_R to the power of the wind P_W is called rotor power coefficient or power coefficient c_{pR} for short:

$$c_{pR} = \frac{P_R}{P_W} = \frac{2 \cdot \pi \cdot n_R \cdot M_R}{1/2 \cdot \rho \cdot (\pi \cdot D^2/4) \cdot v_W^3} \tag{2}$$

where ρ is the air density and D is the diameter of the rotor. The power coefficient is determined by the number of blades N, the blade geometry, the pitch angles β_B, the yaw angle γ_G, the wind speed v_W and the rotor speed n_R:

$$c_{pR} = f(N, \text{bladegeometry}, \alpha_G, \beta_B, v_W, n_R) \tag{3}$$

The rotor power becomes maximum when the yaw angle, which indicates the deviation of the wind direction from the orientation of the rotor axis, is zero. As the yaw angle increases, the normal component of the rotor area related to the wind direction becomes smaller, so that the power decreases in first approximation proportional to the cosine of the yaw angle. WTs guide the nacelle according to the wind direction; the influence of the yaw angle on the rotor power is therefore not considered in the following explanations.

The ratio of the blade tip speed u to the wind speed v_W is called the high-speed ratio λ or TSP (tip-speed ratio) and is an essential parameter for performance control:

$$\lambda = u/v_W = (\pi \cdot D \cdot n_R)/v_W \tag{4}$$

For a given number of blades and blade geometry and with a constant yaw angle, the introduction of the tip-speed ratio enables the two-dimensional representation of the power coefficient, the rotor power or the rotor torque. It has been shown that for constant pitch angle, the variation of the power coefficient as a function of the high-speed number shows a maximum. For given blade geometries, the maps $c_{pR} = f(\beta, \lambda)$ can be calculated or measured for implemented WTs.

For replication, the maps are replied by analytical functions, which lead to a satisfactory agreement with measured values by parameter adjustments. Based on the proposal in [1], the following form is used for Figs. 5 and 6:

$$c_{pR} = c_1 \cdot \left(c_2/\lambda_i - c_3 \cdot \beta - c_4 \cdot \beta^x - c_5\right) \cdot e^{-c_6/\lambda_i} \text{ with}$$
$$\frac{1}{\lambda_i} = \frac{1}{\lambda + 0,08 \cdot \beta} - \frac{0,035}{\beta^3 + 1} \tag{5}$$

The constants for the representations are: $c_1 = 0,6$, $c_2 = 116$, $c_3 = 0,4$, $c_4 = 0,001$, $c_5 = 5$, $c_6 = 20$, $x = 2$

The maximum rotor power coefficient occurs for very small pitch angles and is at an optimum tip-speed ratio of 8 for the curves shown. Below the rated wind speed,
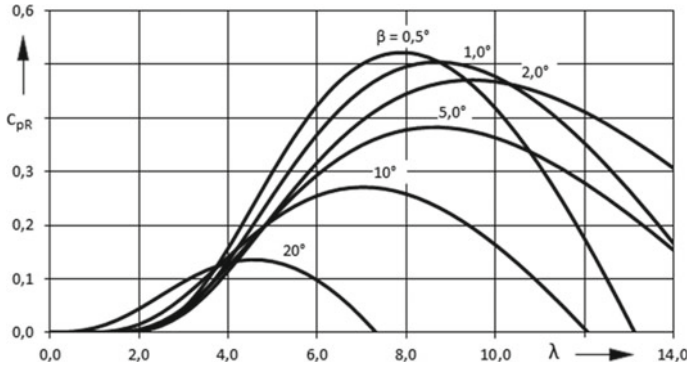
Fig. 5 Curve of the rotor power coefficient at constant pitch angle
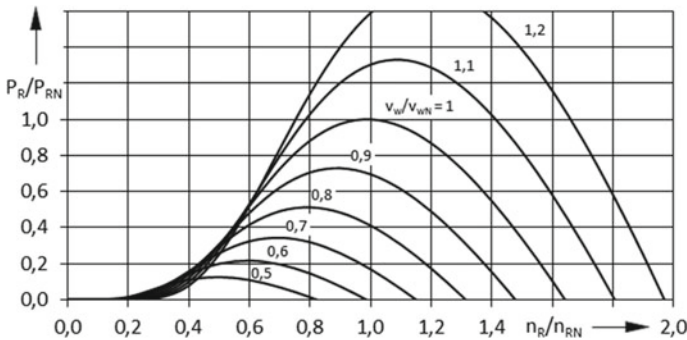
Fig. 6 Curve of the rotor power coefficient at constant wind speed

the rotational speed is adjusted to the changing wind speed in order to convert the maximum power of the wind into rotor power.

For power automation and limitation, it is of interest how the rotor power for the optimum pitch angle is related to the rotational speed of the rotor. The rotor power referenced to the nominal rotor power P_{RN} is surrendered by using the power coefficient in nominal operation c_{pRN} as follows:

$$\frac{P_R}{P_{RN}} = \frac{c_{pR}}{c_{pRN}} \cdot \left(\frac{v_W}{v_{WN}}\right)^3 = \frac{c_{pR}}{c_{pRN}} \cdot \left(\frac{n_R}{n_{RN}} \cdot \frac{\lambda_N}{\lambda}\right)^3 \tag{6}$$

With the power equation and the setpoints characterised by the index N, we obtain the curves shown in Fig. 6 for $\beta = 0.5°$ and $\lambda_N = 8$ for different wind speeds.

The curves show that the optimum rotor speed increases proportionally with increasing wind speed. If the power above the nominal wind speed is limited to nominal power at constant rotor speed, the pitch angle must be increased.

1.4 Energy Conversion at the Drive Train

For the control of the WT, it is crucial how the rotor power P_R is converted into the generator power P_G. The drive train is a complex oscillatory system and can be described in a simplified manner by the two-mass model shown in Fig. 7. The characteristic properties are the mass moment of inertia of the rotor J_R; the stiffness of the shaft k_{shaft}; the damping constant d_{shaft}; the gear translation i, which is equal to one for gearless systems and the mass moment of inertia of the generator J_G. The gears are assumed to be frictionless and massless in this representation. The rotor torque can be determined from the rotor power using Eq. (2) from the rotor power:

$$M_R = c_{pR} \cdot \frac{1/2 \cdot \rho \cdot (\pi \cdot D^2/4) \cdot v_W^3}{2 \cdot \pi \cdot n_R} \tag{7}$$

With the introduction of the torque M_K applied to the generator coupling and the coupling torque M_K' applied to the rotor side, and using the ratio of the ideal gear drive $i = n_R'/n_G = M_K/M_k'$, the following equations for rotor and generator torque are obtained:

$$M_R = J_R \cdot 2 \cdot \pi \cdot \frac{dn_R}{dt} + M_K' \text{ mit } M_K' = d_{\text{Welle}} \cdot 2 \cdot \pi \cdot (n_R - n_G \cdot i)$$
$$+ k_{\text{Welle}} \cdot 2 \cdot \pi \cdot \int (n_R - n_G \cdot i)dt \tag{8}$$

$$M_G = M_K - J_G \cdot 2 \cdot \pi \cdot \frac{dn_G}{dt} \text{ mit } M_K = i \cdot M_K' \tag{9}$$
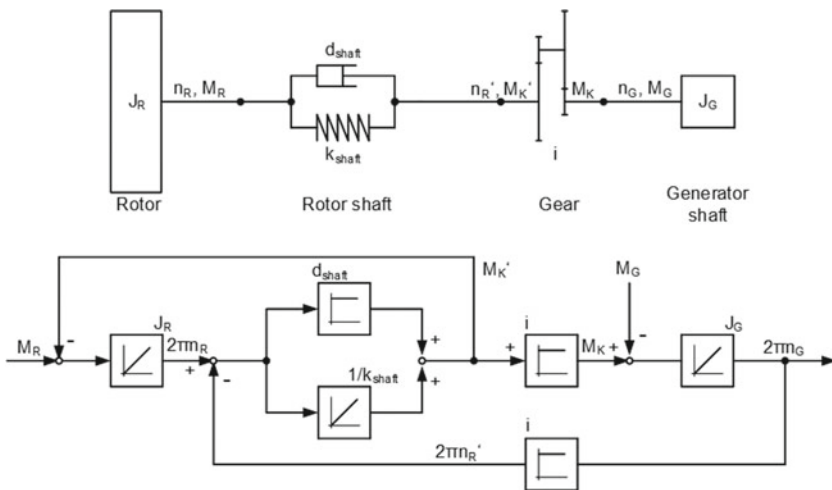
Fig. 7 Two-mass model of the drive train and associated block diagram

Accordingly, for the two-mass model, the block diagram of an oscillatory system is shown in Fig. 7. By large ramp-up times of the WT in the range of seconds and non-instantaneous change of the generator torque, it is achieved that the deviation between start and drive speed remains small. In this case, a rigid shaft can be assumed for simplification, for which only one speed has to be taken into account. For an ideally rigid shaft with $i = n_R/n_G$ the known acceleration equation is obtained as follows:

$$\frac{d\,n_G}{dt} = \frac{1}{i}\frac{d\,n_R}{dt} = \frac{(M_R/i - M_G)}{2\cdot\pi\cdot(J_G + J_R/i^2)} \tag{10}$$

For vibration damping, so-called differential speed controllers are used, which use rotor and generator speed, as known from general drive technology [18].

1.5 Energy Conversion at the Generator-Converter System

The generator-converter system converts the mechanical power at the generator shaft into the electrical power of the grid via several subsystems. To dynamically influence the generator torque and the generator reactive power as well as the grid active power and grid reactive power, it is common to describe the three-phase, electrical quantities by complex time-varying space pointers. A comprehensible introduction can be found in [17].

Detailed descriptions for the individual generator systems can be found, among others, in [14, 16]. For the sake of simplicity, the following explanations refer to the symmetrical cylindrical rotor-SM with restriction to the fundamental frequency behaviour and the copper losses.

Figure 8 shows the simplified equivalent circuit of a PSM and the associated space vector in generator operation. With known rotor position and impressed space vector of the stator voltage $\underline{u}_g$ the angle δ_g to the space vector of the rotor current can be determined. The three stator string currents of the generator are detected and described by the space vector $\underline{i}_S = \underline{i}_g$. The space vector can be transformed to the stationary $\alpha\beta$-components $\underline{i}_{g\alpha\beta} = i_{g\alpha} + j\,i_{g\beta}$ and converted to the rotor-current-oriented dq-components $\underline{i}_{gdq} = i_{gd} + j\,i_{gq}$ using the angle δ_g. The component i_{gd} points in the direction of the permanent magnetic current $\underline{\Psi}_{PM}$ and the component i_{gq} is perpendicular to it.

The absolute value of the space vector of the induced voltage $\underline{u}_{gPM}$ is obtained for a generator with the number of pole pairs p from the induction law:

$$u_{gPM} = 2\cdot\pi\cdot n_G\cdot p\cdot \Psi_{PM} \tag{11}$$

The magnitude of the space vector is determined in such a way that in the stationary case it corresponds to the complex vector of the amplitude of the geometric sum of the string quantities, and it is therefore 2/3 of the geometric sum of the individual
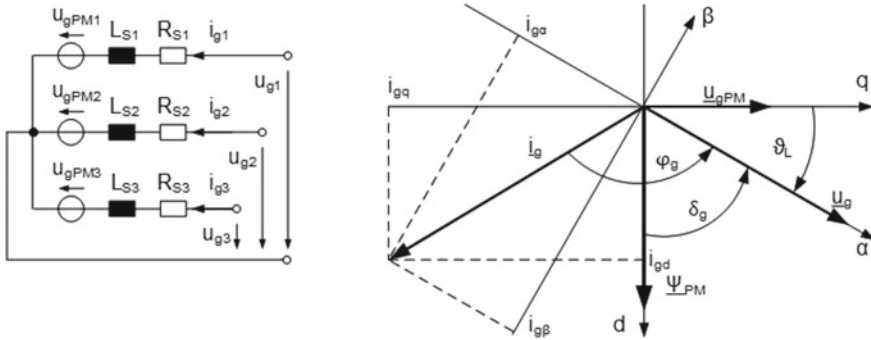
Fig. 8 Simplified equivalent circuit of the PSM and space vector in generator operation

currents. This results in active and reactive power as well as generator power and generator torque as follows:

$$P_g = \frac{3}{2}\left(u_{\mathrm{gd}} \cdot i_{\mathrm{gd}} + u_{\mathrm{gq}} \cdot i_{\mathrm{gq}}\right) \text{ and } Q_g = \frac{3}{2}\left(u_{\mathrm{gq}} \cdot i_{\mathrm{gd}} - u_{\mathrm{gd}} \cdot i_{\mathrm{gq}}\right) \qquad (12)$$

$$P_G = 2 \cdot \pi \cdot n_G \cdot M_G = \frac{3}{2} \cdot u_{\mathrm{gPM}} \cdot i_{\mathrm{gq}} \text{ and } M_G = \frac{3}{2} \cdot p \cdot \Psi_{\mathrm{PM}} \cdot i_{\mathrm{gq}} \qquad (13)$$

Figure 8 makes clear that for the PSM the maximum power occurs at minimum current for $i_{\mathrm{gd}} = 0$. The space vector of the voltage u_g can be influenced by a variable current i_{gd} at constant moment.

The grid-side inverter can be treated in a similar way. For this purpose, the grid-side voltages are transformed to the inverter side. Figure 9 shows the simplified equivalent circuit of the grid referenced to the inverter side and the associated space vector in generator operation. With the aid of a phase-locked loop (PLL), the frequency and phase position of the grid voltage are detected and thus the space vector of the grid
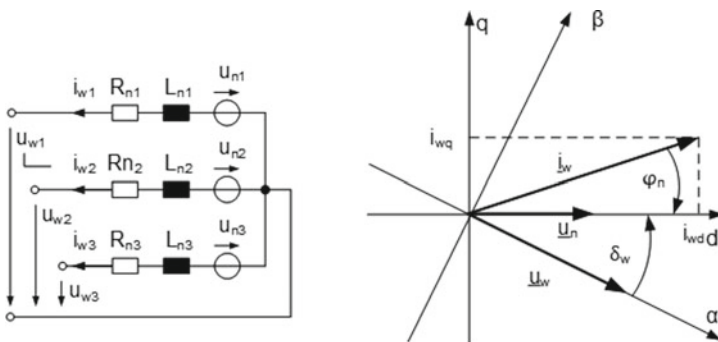
Fig. 9 Simplified equivalent circuit and space vector in generator operation

current is divided into the grid-voltage-oriented d-component and the perpendicular q-component.

If the grid component $i_{nd} = i_{wd}$ points in the direction of the space vector $\underline{u}_n$, then active and reactive power can be influenced in a simple manner with the aid of the current components:

$$P_n = \frac{3}{2}(u_n \cdot i_{wd}) \text{ and } Q_n = \frac{3}{2}\left(u_n \cdot i_{wq}\right) \tag{14}$$

Figure 10 shows the simplified structure of the generator-inverter system for a PSM with full inverter and grid variables transformed to the inverter side. The setpoints transferred by the control system are marked by an *.

Highly dynamic control of generator torque and voltage is possible when the current components are controlled to the setpoints i_{gq}^* and i_{gd}^* with the aid of a controller. The output of the current controller determines the voltage components to be set using pre-control values calculated using a simple generator model. The voltage components are converted into the required control signals of the six-pulse rectifier using pulse width modulation (PWM).

Also, for the grid-side inverter, the setpoints of P and Q can be impressed highly dynamically using the current setpoints i_{wd}^* and i_{wq}^*, the current controllers and the
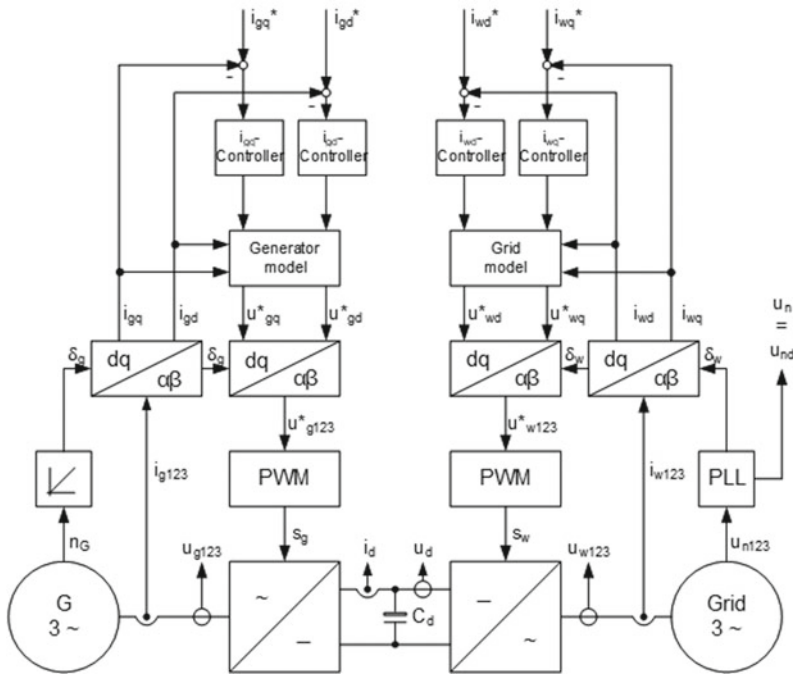
Fig. 10 Simplified structure of the generator-converter system for PSM

PWM of the six-pulse inverter. Here, the pre-control values are determined by the grid model.

The rectifier and inverter are connected by the DC voltage link. The voltage at C_d is determined for lossless assumed rectifier and inverter by integration over the difference of the instantaneous powers $p_g - p_w$ with $p_w = p_n$:

$$C_d \cdot \frac{du_d}{dt} = \frac{p_g}{u_d} - \frac{p_w}{u_d} \quad \text{mit} \quad u_d(t) = \sqrt{u_d(t=0)^2 + \frac{2}{C_d} \cdot \int_0^t (p_g(t^*) - p_w(t^*))dt^*}$$

(15)

If, in the stationary case, the effective generator power and the effective mains power are the same, the DC link voltage does not change.

1.6 Idealised Operating Characteristic Curves of WTs

Based on the system characteristics in the energy conversion of the rotor, four different operating ranges of a WT can be distinguished. These are described on the basis of the idealised sequences with the characteristic variables shown in Fig. 11.

The operating ranges have the following properties:

- Underload (I): Below the cut-in wind speed v_{cin}, the pitch angle is reduced with increasing wind speed so that the WT starts up. The WT does not yet feed into the grid and the rotational speed of the rotor increases.
- Partial load (II): In the range from v_{cin} to v_{wN}, the WT is operated at optimum fast speed by increasing the rotational rotor speed linearly at a constant pitch angle. The power fed into the grid increases cubically.
- Full load (III): Above the nominal wind speed up to the switch-off wind speed (cut-out wind speed v_{cout}), the grid power is limited to nominal power by increasing the
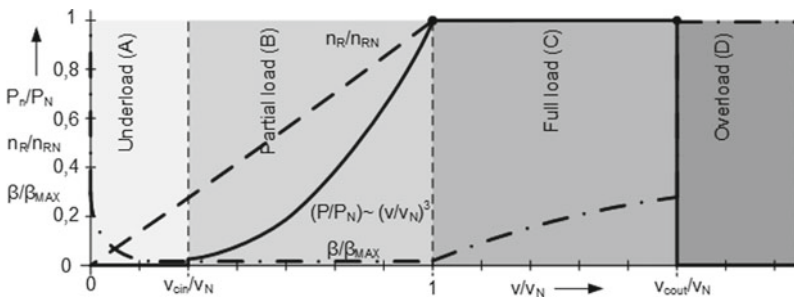
Fig. 11 Idealised operating characteristics of WTGs
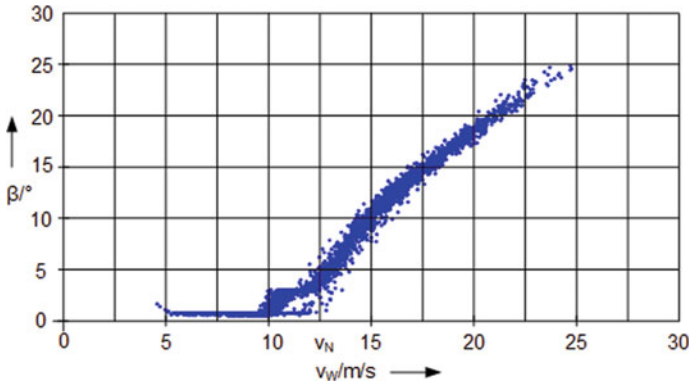
Fig. 12 Measured pitch angle of a WT

pitch angle and thus keeping the rotational rotor speed constant with increasing wind speed.
- Overload (IV): Above the switch-off wind speed, the pitch angle is increased so that the WT decelerates to zero speed. The WT no longer feeds power into the grid.

Throughout the entire operating range, the nacelle tracks the changing wind direction so that the yaw angle is always zero.

In fact, the occurring parameters of the WT deviate from the idealised curves. Short-term changes in wind speed, such as those occur in particular during wind gusts, lead to a change in power, which has an effect on the characteristics depending on the properties of the drive system and the control arrangements.

Figure 12 shows an example of the measured pitch angle of a WT with a cut-in wind speed of 4 m/s, a nominal wind speed of 12.5 m/s and a cut-out wind speed of 25 m/s. The deviations from the idealised characteristic curve at the transition from the partial load to the full load range can be clearly seen. The short-time average over one minute is shown.

The actual operating characteristics, the deviations from the idealised characteristics and the fluctuation range depend essentially on the control systems used and the controller parameterisation.

2 Control Systems of the WT

The control systems used aim to minimise both the dynamic and static deviations of the characteristic variables compared to the idealised curves while complying with the specified limit values of the WT. For this purpose, the control devices of the WT change the yaw angle, the pitch angle, the generator power or the generator torque as well as the active and reactive power fed into the grid.

2.1 Yaw Angle Control

The alignment of the rotor hub actively follows the wind direction. For this purpose, the entire nacelle is adjusted via several frequency converter-controlled geared motors (azimuth drives) and a gear rim attached to the tower. Brakes on the tower ring ensure that the nacelle is fixed when the motors are not driving it. The cut-in times, speeds and direction of rotation of the azimuth drives are controlled and regulated so that, on the one hand, the yaw angle remains low in fluctuating wind directions and, on the other hand, the number of adjustment processes does not become too large.

Figure 13 shows the block diagram of a yaw angle control that optimises the behaviour using parameter adjustment for different wind speed ranges. For tracking, the wind direction Υ_W is acquired and compared with the orientation of the rotor hub or rotor shaft Υ_R.

If the yaw angle $\Upsilon_G = \Upsilon_W - \Upsilon_R$ exceeds a minimum limit value (a few degrees) over a longer period of time, the brakes are opened and the nacelle alignment is regulated. The time for which the deviation must be present decreases with increasing wind speed and with increasing yaw angle. Gain and integration time constant of the PI yaw angle controller are adjusted depending on the wind speed.

At very low wind speeds ($v_W \ll v_{cin}$) the nacelle is not tracked. As the wind speed increases, the speed of the azimuth gears increases with increasing yaw angle. The speed is limited so that the nacelle rotates slowly. Typical maximum speeds are well below one rotation per minute (rpm).

A possibility of parameter adjustment by defining different operating ranges depending on the wind speed and the yaw angle is described in [6]. Due to the fuzzy formulation of the control behaviour, the use of fuzzy controllers is also proposed.
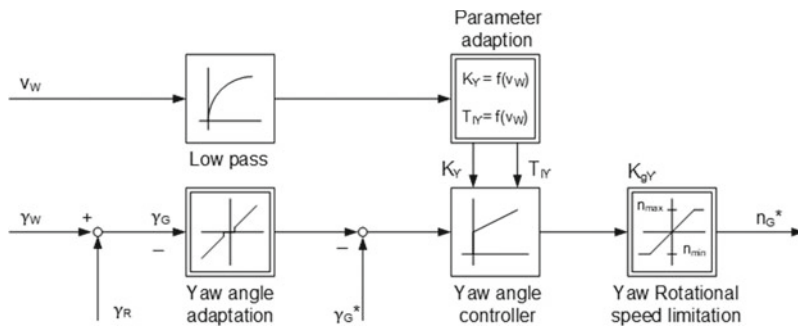
Fig. 13 Block diagram of the yaw angle automation

2.2 Pitch Angle Control

Power and speed limitation in the full load range is achieved by pitch angle automation using electric or hydraulic actuators. The three independent actuators mounted in the hub increase the pitch angle above the rated wind speed in order to keep the rotor power constant with increasing wind power.

In order not to have to react to the fast wind speeds, which can only be determined imprecisely, the deviation of the rotor speed from the nominal rotor speed is used as input of the pitch angle adjustment. In the case of positive deviations, the pitch angle is increased by the PI controller.

The behaviour of the line is non-linear. For small deviations of the wind speed from the nominal wind speed, a large pitch angle change is required to keep the power and thus the speed constant. For large wind speeds, a small pitch angle change is sufficient to limit power and speed. Known controls therefore use a PI pitch angle controller with adjustment of the gain factor (gain scheduling). In this case, the gain factor decreases with increasing pitch angle, so that even at high wind speeds, the control deviations of the speed do not become too large or the closed control loop may even become unstable.

Figure 14 shows a possible pitch angle control structure in which both the pitch angle setpoint and the pitch angle speed are passed to the azimuth drives. Commonly used electric servo-drives then internally use a cascade automation consisting of a superimposed angle control, a speed control and a subordinate torque or current control. Detailed descriptions of the design can be found, among others, in [5, 9].

The speed limitation is designed in such a way that even for an emergency stop the maximum pitch angle of almost 90° is reached in less than 10 s, this means angular velocities of several °/s. This means that the blade angle controller is much slower compared to torque or power control, so that noticeable changes in speed occur with dynamic wind speed changes.

In order to achieve a continuous transition from variable-speed to constant-speed operation, the pitch angle control starts before the rated wind speed and the rated rotor speed are reached. Increasing the gains and decreasing the integration time can
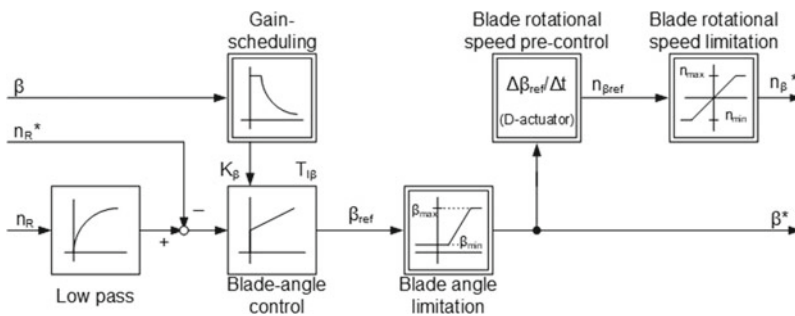
Fig. 14 Pitch angle control with parameter adjustment

reduce the maximum speed deviation. However, such a controller setting leads to a large actuating activity of the pitch angle control, especially during the transition from the variable-speed to the constant-speed range of the WT, which can have the effect of an increased noise level in this wind speed range. The design is therefore often adjusted during test operation. Here, the use of fuzzy controllers is suggested due to the fuzzy formulation of the control behaviour, too.

2.3 Active Power Control

Active power control and limitation is also carried out without direct evaluation of the wind speed measurement. Since the optimum power is achieved in the partial load range at optimum fast speed, the rotational rotor speed is also used for active power control. In partial load mode, it adjusts itself freely according to the difference between drive and generator power.

Control to the maximum achievable power is achieved by specifying the target power P_n^* as a function of the rotor speed via a characteristic curve and setting it by the inverter. If the power specified from the active power characteristic curve is less than the power contained in the wind, the rotor speeds up. If the power specified from the active power characteristic curve is greater than the power contained in the wind for the current wind speed, then the rotor will slow down. In the stationary case, the maximum power coefficient and the optimum rotor speed result for each wind speed in the partial load range.

In Fig. 15, the schematised nominal curve of the power characteristic is plotted in the characteristic diagram of the rotor power coefficient. The cubic curve for low speeds and the constant power for high powers can be seen. The characteristic curves with the specification of power limits by the energy supplier, in this case the typically used 60° and 30° limits, are entered in dashed dot lines.

If the power contained in the wind increases above the limiting characteristics, the increase in rotational speed causes the pitch angle control to kick in, limiting the
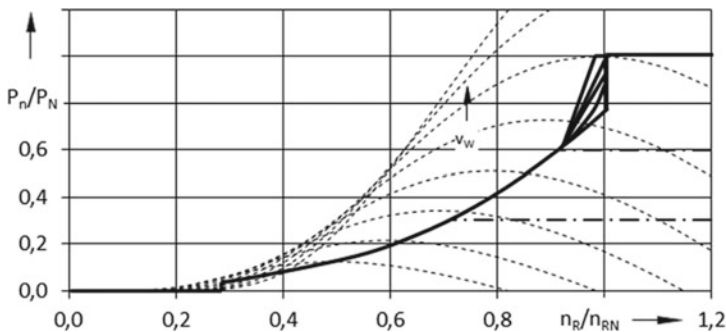
Fig. 15 Schematic setpoint curves of the power

power. Modifications of the characteristic curve are used to optimise the transition between variable and constant speeds, and a detailed description can be found in [3].

In the stationary case and neglecting the losses in the generator-inverter system, the DC link voltage is constant, generator power and active grid power are the same. The generator power or the generator torque can therefore be controlled both directly and via the mains active power if a controller for the DC link voltage ensures that this remains almost constant. Thus, there are two possibilities for active power control:

(a) Control of the grid-side inverter to the maximum achievable power and control of the active power of the rotor-side rectifier so that the DC link voltage remains almost constant.

(b) Control of the rotor-side rectifier to the maximum achievable power and control of the mains active power so that the DC link voltage remains almost constant.

Figure 16 shows the solution for variant (a). Based on the rotor speed, the setpoint value of the active power is specified. According to the deviation between the setpoint and actual value of the grid power P_n, the active power-forming current setpoint i_{wd}^* of the inverter is changed with the aid of a PI controller.

In addition, the active power reductions due to the grid operator's specifications have been added to the figure [21] (BDEW) [2, 19]. On the one hand, this is the gradual reduction of the active power related to the nominal power on demand by means of a control signal to protect against overload of individual grid sections of the transmission grid. On the other hand, it is the continuous reduction of the power available at the time of the request if the grid frequency is too high.

The control of the generator-side currents is shown in Fig. 17. The moment-forming current setpoint i_{gd}^* of the generator-side rectifier is specified in such a way that the DC link voltage remains constant. If the DC link voltage exceeds an upper limit, then the moment-forming current is reduced. If the DC link voltage falls below a lower limit value, then it is increased. The rotor-oriented current i_{gd}^* is either controlled to zero or used to control the optimum stator voltage $u_S = u_g$. If the voltage is too low, the rotor-oriented current is increased accordingly.
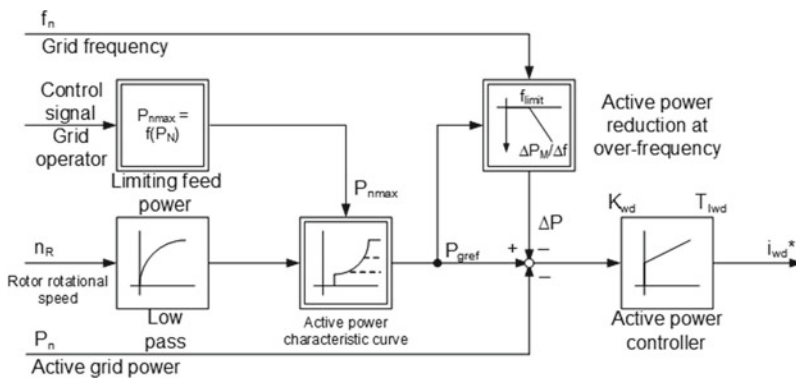
Fig. 16 Active power control by means of the grid-side inverter
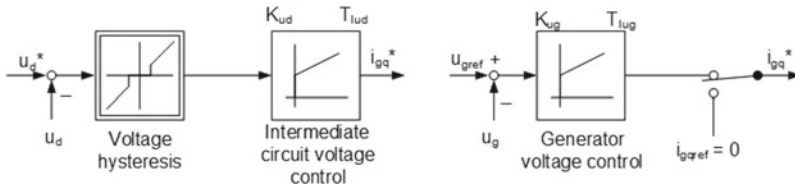
Fig. 17 Control of the generator-side currents

In Sect. 1.4, it is shown that the rotor speed can fluctuate around an average value due to the flexible drive shaft. In [16], it is proposed to damp the oscillations of the rotor speed by prescribing the setpoint of the DC link voltage as a function of the rotational rotor speed deviation in order to impress a moment-forming current which actively damps the oscillations. The voltage hysteresis must then be omitted.

2.4 Reactive Power Control

The grid feed of the WTs is conventionally operated in such a way that the reactive power at the connection node is zero. This means that the active power is fed into the grid at the minimum required grid current. For efficient and safe grid operation, WTs must contribute to voltage regulation both in quasi-stationary operation and dynamically by feeding inductive or capacitive reactive power into the grid. To increase the voltage in the connection node, a capacitive reactive current is usually impressed; the corresponding grid connection guidelines speak of overexcited operation. For voltage reduction, an inductive reactive current is impressed in so-called under-excited operation.

In Fig. 18, a block diagram is shown which enables reactive power control by impressing the reactive power-forming current component $i_{wd}^* = i_{nd}^*$. In order to consider specifications of the grid operator, the block diagram shows a quasi-stationary and a dynamic reactive power feed according to the regulations in BDEW [2, 21].

The specification for the quasi-stationary reactive power feed can be carried out in different ways: the grid operator can directly specify the reactive power to be fed in or the power factor $\cos\phi$ via a control signal. Alternatively, the reactive power can be fed in continuously as a function of the deviation between the actual voltage value and the setpoint value. To limit the required over-dimensioning of the grid-side inverter, the grid operator specifies required limit curves for the reactive power.

When significant dynamic voltage deviations occur, especially in the case of voltage drops due to grid faults, WTs must automatically inject a reactive current to support the voltage. For this purpose, the voltage before the fault is taken as a setpoint and compared with the current grid voltage. Depending on the deviation and a variable amplification factor, the reactive current is corrected accordingly.
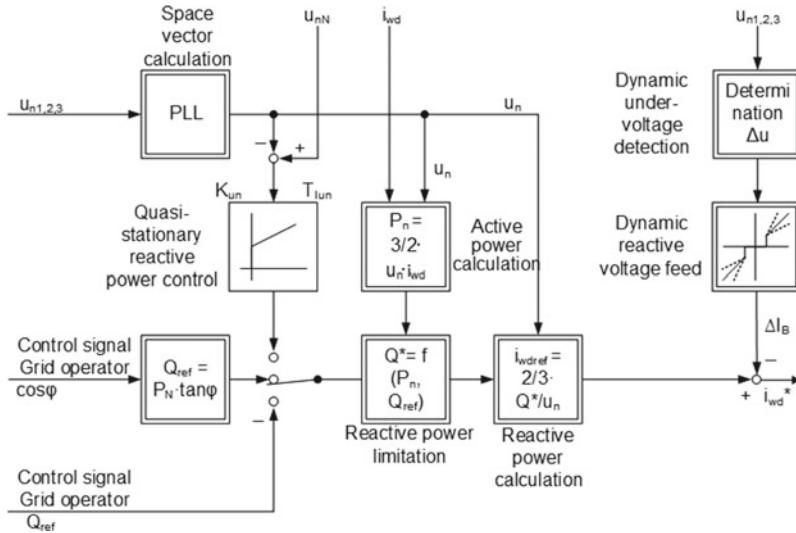
Fig. 18 Quasi-stationary and dynamic control of the mains reactive power

2.5   Summary of the Control Behaviour and Extended Operating Ranges of the WT

The behaviour of the control systems within the WT can be summarised as follows for independent operation without specifications from a grid operator:

- In the entire wind speed range, the nacelle is guided by the azimuth drives according to the wind direction.
- In the entire power range, the generator is operated with optimum current and the grid-side inverter is operated in such a way that no reactive power is fed into the grid.
- The DC link voltage control ensures that the active power of the generator-side rectifier is identical to that of the grid-side inverter in the stationary case.
- Below the rated wind speed, the power is maximised by setting the active power as a function of the rotational rotor speed. The blade adjustment remains constant at its optimum value.
- Above the rated wind speed, the rotational speed and power are kept constant by the pitch angle control.

Speed, blade pitch and power influence each other. Modern WTs have further significant transition areas in addition to the four Fig. 11 marked operating ranges, modern WTs have further significant transition ranges. Figure 19 shows the typical curves depending on the wind speed.

For a continuous transition of the system variables from partial to full load, the control characteristic of the power causes the rotational rotor speed to no longer
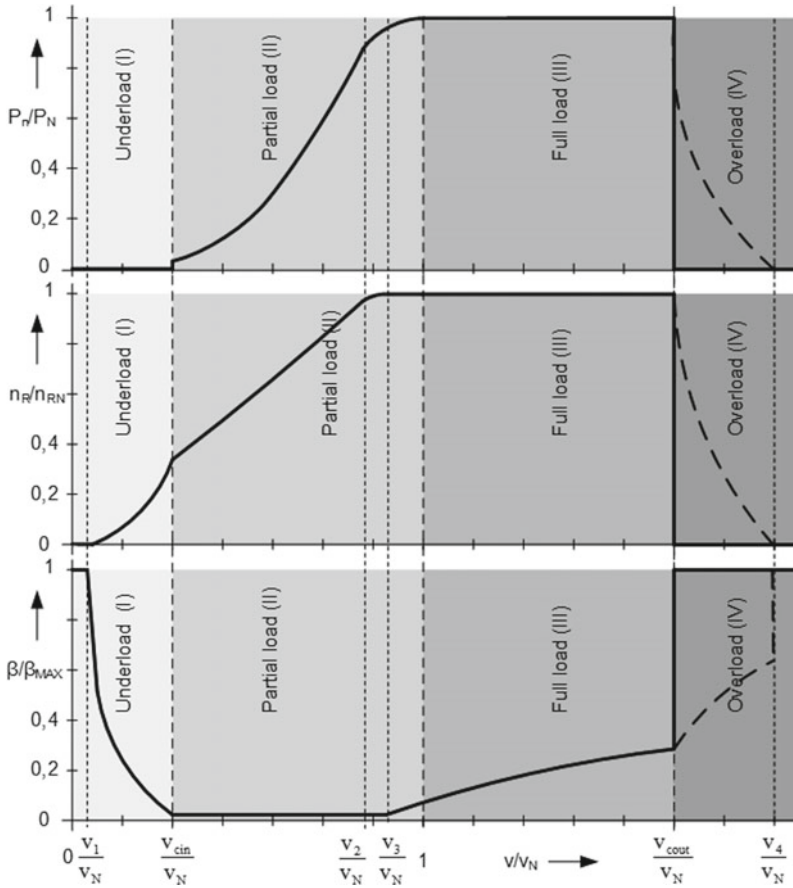
Fig. 19 Extended operating ranges of a WT with operating characteristic curves

increase in proportion to the wind speed even below the nominal wind speed. From v_2 onwards, the WT is therefore no longer operated at the optimum high-speed speed. Blade adjustment control starts at v_3, even if the rated power is not yet fully reached. Thus, the rotor power coefficient decreases additionally. A WT therefore reaches the optimum power coefficient below v_N; when the nominal wind speed is reached, the power coefficient has already dropped noticeably.

3 Operation Control Systems for WTs

The technical operation control system is used to enable the automatic, efficient and safe operation of the WT. It processes the input signals from the WT as well as the signals from the operating equipment and other higher level systems such

as the management system. From these input signals, the operation control system determines the output signals for the WT, for the display devices and the higher level systems. The main tasks of the operation control system include the following:

– the control of the operating sequence and requirements for the setpoints for the WT control systems;
– monitoring critical variables and activating appropriate security measures;
– the collection, storage and exchange of relevant information with higher level systems.

According to these main tasks, the technical operation control system can be divided into three subsystems.

3.1 Control of the Operating Sequence of WTs

With the help of the operating sequence control, the operating state is determined and the transition between the operating states is coordinated. It depends on the selected operating mode (automatic, manual) and the place of operation (remote, local).

In automatic mode, the WT can only be switched on and off; all other functions are specified by the control system. In manual mode, which is required for commissioning, testing, maintenance or service, the change of operating states and the activation of output signals for the WT can also be influenced manually. As a rule, WTs are remotely controlled and monitored via control systems (remote control). Only in manual mode can the WT be controlled on site with the aid of operating equipment (local control). In this case, local control has priority over remote control.

The automatic operating sequence can be displayed with the aid of a sequence chain, whereby a simplified distinction is made between the following essential operating states of the WT:

– Initialise and test the system.
– Start-up of the system without grid feed.
– Operation of the plant in partial and full load mode.
– Shutdown of the plant under normal conditions.
– Quick stop of the system in the event of a fault.

The sequence is clear from the basic structure of Fig. 20. The change from one state to the other takes place depending on the transition condition, which is indicated at the crossbar on the connection.

The five operating states shown and the transitions are described in Fig. 21 taking into account the extended operating ranges from Fig. 19 in detail. The following tasks are to be performed in the steps which are described in detail:

• Initialise: After the system is switched on, all sub-controls initialise and communication between the subsystems and to the higher level controls is established.
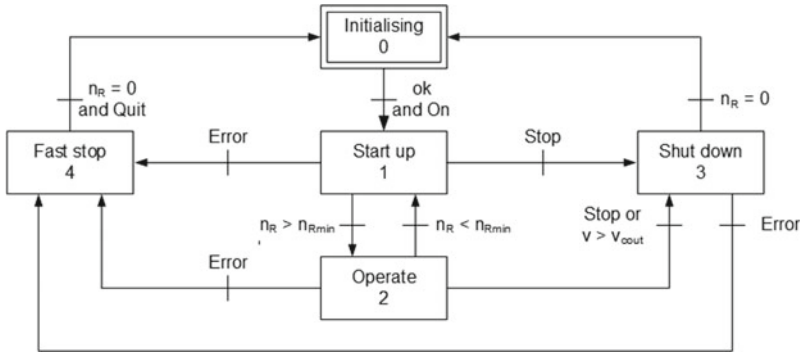
Fig. 20 Simplified basic structure of the sequence control for a WT
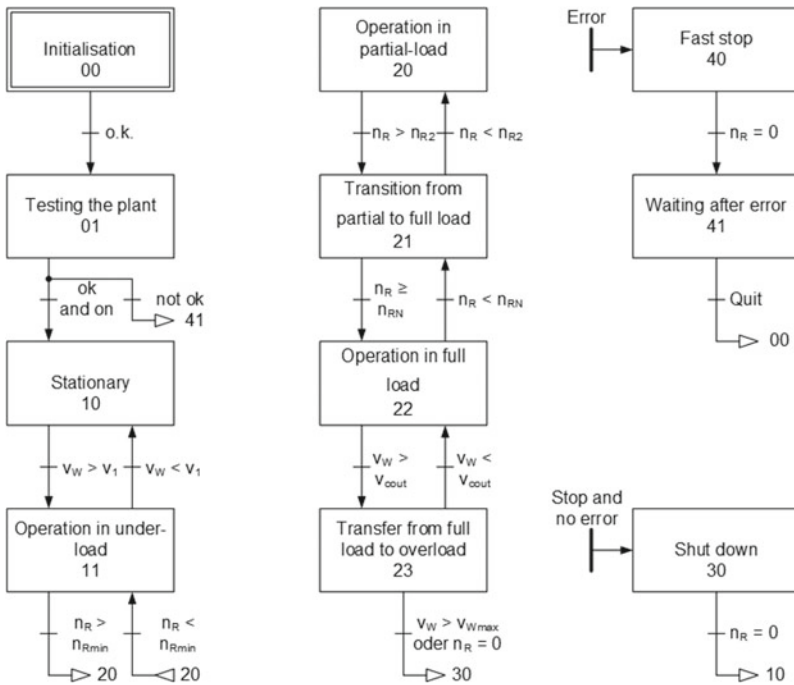
Fig. 21 Sequence control for WTs with extended operating ranges

After the initialisation phase, all status signals and measured values are logged and stored.

- Testing the system: After initialisation, the essential actuators and sensors are tested. Brakes are released and closed again, pitch and yaw drives and their encoders as well as the rotor and generator rotation encoders are tested by a short test run. The ambient conditions such as temperature and humidity, wind

speed and direction as well as the numerous attached vibration and force sensors as well as the current and voltage sensors are checked for compliance with their limit values before the system enters the ready-to-operate waiting state with a stationary rotor.

- Standstill: As long as the wind speed remains lower than the minimum limit value v_1, the WT waits with stationary rotor and the pitch and azimuth drives are not activated. Only when the wind speed exceeds this value the WT switches to the start-up state.
- Operation in underload: For start-up, the turbine is aligned according to the wind direction with the brakes released. The pitch angle is slowly reduced so that the rotor starts to rotate. After exceeding a minimum required rotational rotor speed, the generator-side rectifier builds up torque and the WT starts to feed power into the grid via the converter.
- Operation at partial load: In the partial load range, the active power is maximised by adjusting the rotational speed with an optimum pitch angle. If the wind speed increases to such an extent that the rotor exceeds the characteristic value n_{R2}, the WT switches to the transition range between partial and full load.
- Transition from partial to full load: In this range, the rotor speed and pitch angle are changed. The rotational rotor speed still increases slightly due to the specified power characteristic curve; the power fed into the grid has not yet reached the rated power.
- Operation at full load: Above the rated wind speed, the WT feeds the rated power into the grid. By controlling the pitch angle, the power and rotational speed are kept constant.
- Transition from full load to overload: After exceeding the limit wind speed v_{cout}, the power of the system is continuously reduced to zero (storm control). For this purpose, both the reference power and the reference rotational rotor speed become smaller as a function of the wind speed, so that the pitch angle is increased.
- Transition from full load to overload: For turbines with so-called storm control, the speed and torque are continuously reduced as the wind speed increases. Reference speed and reference power decrease continuously so that the pitch angle increases with a much larger gradient than in full load operation. If the turbine still does not come to a standstill even when a maximum permissible operating wind speed $v_{W\text{max}}$ is exceeded, the WT automatically switches to shutdown mode.
- Shutdown: After exceeding the maximum operating wind speed or on request by a stop signal, the system moves down to zero speed controlled by a ramped, slow increase of the pitch angle. The brakes are then applied again. In the event of a request via the stop signal, the system always switches from the usual operating states to shutdown mode.
- Fast stop: In the event of a fault such as mains voltage failure or very high gust wind speeds, the turbine moves to zero speed in a controlled manner by increasing the pitch angle very quickly. For safety reasons, the rotor brake also engages if the speed is not yet zero after a certain time. From other operating states, the system always switches to fast stop mode if a fault occurs.

- Waiting after error: Automatic restart after a safety-critical error is not possible. A WT that has been slowed down by a quick stop due to a fault can only be restarted, when the cause of the fault has been clarified, is no longer present and can thus be acknowledged.

From the tasks listed here, the output signals for the actuators and the display devices can be derived for each step.

3.2 Safety Systems

In addition to controlling the normal operating sequence, safe operation of the WT must be ensured. The technical operation control system must monitor the operation of the plant and avoid malfunctions, detect faults and changes in the plant at an early stage and automatically initiate safety measures and maintenance work.

Like other installations, WTs must meet basic safety requirements. A good overview of general requirements for the prevention and control of failures as well as technical and organisational requirements for the operation of plants with programmable control systems can be found in [12]. In [10], the basic characteristics of safety systems for WTs are described.

For safe operation, a safety system is superimposed on the technical operation control. So-called failsafe control and switching components are used and additional safety systems are installed that detect the signals independently of the control system and take immediate safety measures.

The control of the operating sequence intervenes at an early stage if limit values, faults or malfunctions are exceeded in order to enable safe operation of the turbine. Even in the event of extraordinary wind speeds, ambient conditions such as the outside temperature, grid supply conditions or unforeseen failure of individual components, for example due to lightning, the WT will be transferred to a safe state.

The following events first lead to a power reduction, before the exceeding of the limit value triggers a quick stop:

- Exceeding threshold values for rotational rotor speed, for forces, torques and vibration amplitudes of tower, blade or drive train.
- Exceeding threshold values for the generator current, for the DC link voltage and for the mains current.
- Exceeding the thermal limits in the nacelle, generator or inverter or the limits of other climatic variables such as humidity.

The following events lead to an immediate quick stop by the blade displacement and the subsequent closing of the rotor brake:

- Failure of the measuring systems for rotational speed, wind speed, current and voltage.
- Failure of individual actuators such as yaw or azimuth drives.

- Failure of the communication systems within the WT between the control system and the actuators.
- Exceeding of mains voltage limits or falling below the limit curves for the permissible mains undervoltage.
- Exceeding the maximum or falling below the minimum mains frequency limit.

In addition, the operating condition of critical technical equipment of the WT is recorded by so-called condition monitoring systems (CMS). These systems automatically initiate the necessary measures, maintenance work or replacement of the equipment at an early stage before damage occurs.

4 WPP Control and Automation Systems

WPPs or wind farms are characterised by the fact that a large number of WTs, distributed over a wide area, are connected to the public grid via a grid connection point (NAP). The connected load of such WPPs exceeds 100 MW and they are often connected directly to the transmission grid.

The WTs in such a WPP often have different outputs. For example, in large WPPs, selected WTs are completely shutdown due to routine maintenance, while in others the power fed in is not identical due to the different wind speed distribution in the WPP. The wind speed of the WT that the wind hits first is much higher than the WT that is on the downwind side of the WPP. In newer large WPPs, the installed capacity of the WPP is greater than the rated connected load, so that it can be fed into the grid even if individual WTs are out of service for maintenance and the wind speed is sufficient.

The individual control of a WT to comply with the grid connection guidelines is now no longer practical. WPP control systems are therefore used which are superordinate to the WT control systems and specify individual setpoints. In detail, these WT control and automation systems have the following tasks:

- controlled increase of power at switch-on with limited dP/dt (switch-on control with presetting of rise time);
- controlled reduction of the power when switched-off with limited dP/dt (switch-off control with presetting of the ramp-down time);
- specification of reserve services;
- compliance with the active power limit specified by the grid operator and quasi-stationary frequency support at the NAP as well as
- compliance with the reactive power specified by the grid operator, quasi-stationary voltage stabilisation and dynamic voltage stabilisation in the event of voltage collapse due to reactive current injection at the NAP.

In Sect. 2, the control systems for individual WTs are described. When used in large WPPs, the tasks of maintaining the grid connection conditions are implemented by a WPP control system. Already in [8, 20] proposals for this were made, which
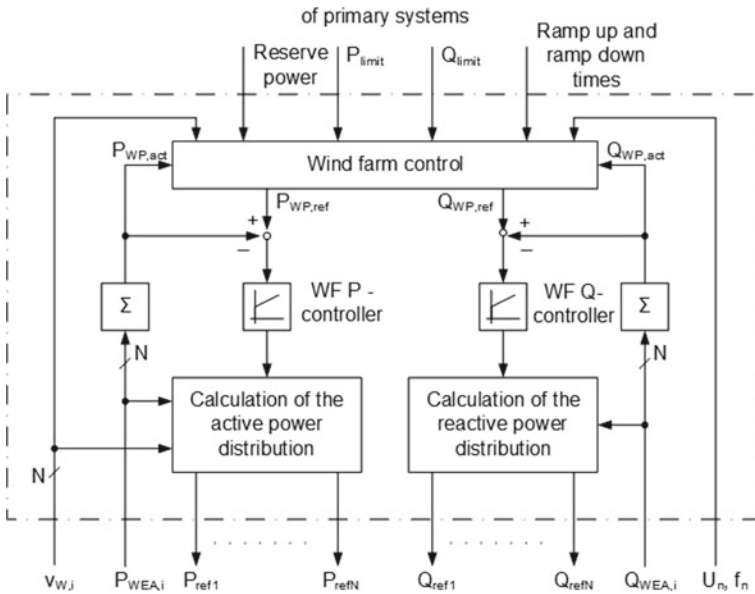
Fig. 22 WPP control system

are now gradually being introduced in new WPP control systems. Figure 22 shows a WPP control system which coordinates the tasks for active and reactive power injection according to the requirements of the grid operator.

The blocks for the distribution of active and reactive power to the individual WTs can be seen. The distribution is optimised by taking into account the WT operating states, the wind speeds and the current actual values of active and reactive power.

Dynamic voltage stabilisation in the event of a voltage drop due to reactive current injection is only possible if the setpoints are transferred quickly and the WTs react correspondingly fast. It may be necessary to add additional units solely for reactive current injection into WPP.

5   Remote Control and Monitoring

Both the data of the technical operation control system and the data of the operating condition monitoring are recorded, processed, displayed, evaluated and stored in modern remote control, maintenance and monitoring systems of WTs. These remote-control systems are abbreviated with the term SCADA for 'supervisory control and data acquisition'. In contrast to operational control system, control and automation, the SCADA system does not intervene directly or in real time in the energy conversion process of the WT.

SCADA systems control not only the individual WT but often all WTs supplied by one manufacturer to different operators or all WTs monitored by one operator from different manufacturers. In addition, the SCADA system also makes selected data available for other applications. For example, selected data is made available to the shareholders for information purposes or the operating companies can integrate selected data into their business data processing systems (billing systems).

The technical tasks of SCADA systems for WT and WPP can be classified as follows:

(a) Control tasks:

- Communication and identification of the WTs: The SCADA system establishes the connection to the WPP and WTs and identifies the location, type and other required plant information.
- Access and types of operating control: The SCADA system controls access to the plant and data depending on usage rights and access controls. It coordinates the switching of local and remote control, the switching of manual mode to automatic mode and the required interlocks.
- Functional testing and parameterisation: With the help of the SCADA system, various actuators can be tested for their function in manual mode. Essential system properties can be re-parameterised via the SCADA system.
- Alarming: The SCADA system automatically triggers warnings, alarms and, if necessary, service calls and spare part procurements via various channels such as email, fax or SMS.

(b) Data collection, analysis and archiving tasks:

- Data acquisition: The SCADA system reads in and stores the relevant measured values of the WT such as wind speed, wind direction, rotational speed, power, current, voltage, frequency, power factor, temperature, humidity, pressure in defined cycles. Operating states, system interventions, maintenance activities are also recorded in this way.
- Data analysis: The SCADA system evaluates the data and determines characteristic parameters such as average values, minimum and maximum values, standard deviations, wind speed distributions, power distributions, production and availability statistics and compiles the information for reporting or event logs.
- Archiving: The SCADA system stores and backs up the data.

(c) Display and operating tasks:

- Display: The SCADA system clearly displays location, time, operating conditions and alarms. It displays wind speed and direction, rotational rotor speed and other WT parameters such as power and energy.
- Visualisation: The SCADA system provides an overview image of WPPs, WTs and WT components in a hierarchical arrangement. It can display significant time histories as time series.

- Operation: The SCADA system offers standard operating options such as start, stop, reset and operating mode selection. Via password-protected login/logout functions, it enables user management and access control.

To fulfil the tasks, the remote-control and monitoring system consists at least of the man-machine interface in the control room (workstation terminal), the actual computer for processing, sending and receiving the data, the data storage, the communication infrastructure and the systems arranged locally in the WT and WPP for interaction with the control room. Different solutions for integration into the communication and automation infrastructure with different communication protocols and data formats are used.

6   Communication Systems for WES

Different communication systems are used in WES and for the exchange of information with the higher level systems, which are essentially determined by the transmission rate, the number of inputs and outputs, the required response times, the distances between the systems and the requirements for the security of the transmission. With the entering of international standards for 'Communication for the monitoring and control of wind turbines' [11] and for 'Communication networks and systems for automation in electrical power supply' [13], the communication structures and protocols for WES are becoming standardised.

Figure 23 shows a typical WT and WPP communication structure and the integration into a grid control system, into the WES remote monitoring and operation as well as further monitoring and diagnostic systems.

Within the WT, the sensors, actuators, WT control and automation exchange the required information via different decentralised communication systems. The different WTs in a WPP are connected to the WES control system via a local WPP bus system, which must meet the real-time characteristics for the time-critical processes. Fibre optic cables are used to achieve high transmission speeds over long transmission distances. External communication then takes place via the TCP-IP network using the standardised protocols and data formats.

In order to be able to integrate the specific information of WTs from different manufacturers into the higher level systems and to be able to control the WTs independently of the manufacturer, both the information exchange process and the representation of the WT information are standardised. Figure 24 shows the WT communication model (a) and the information model of a WT (b) based on [11].

The communication is based on the generally accepted client-server relationship. The WT components exchange the information with the WT information model of a server, which provides it for different clients. Different applications such as a SCADA system can use this data if the client has the appropriate rights. The actual data exchange between client and server takes place via uniform information
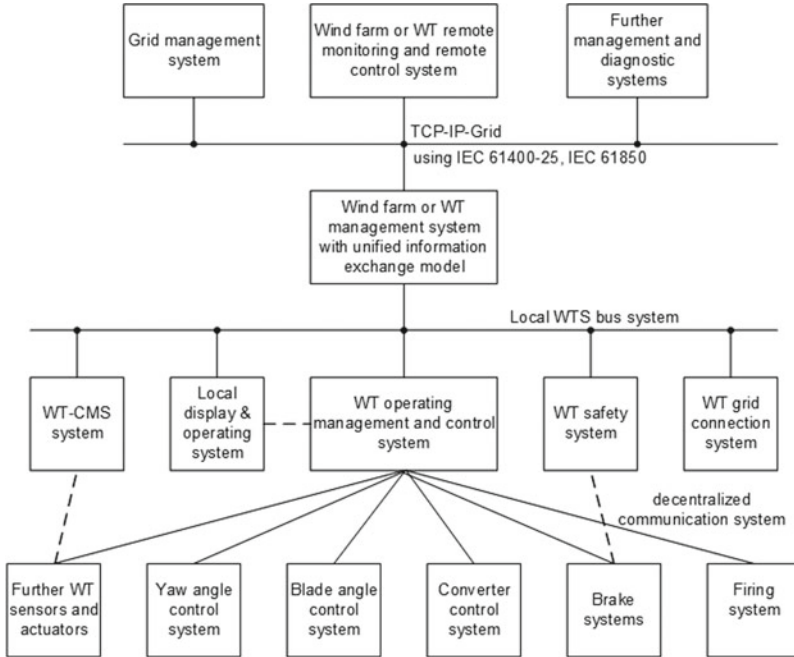
Fig. 23 Schematised WT and WPP communication structure
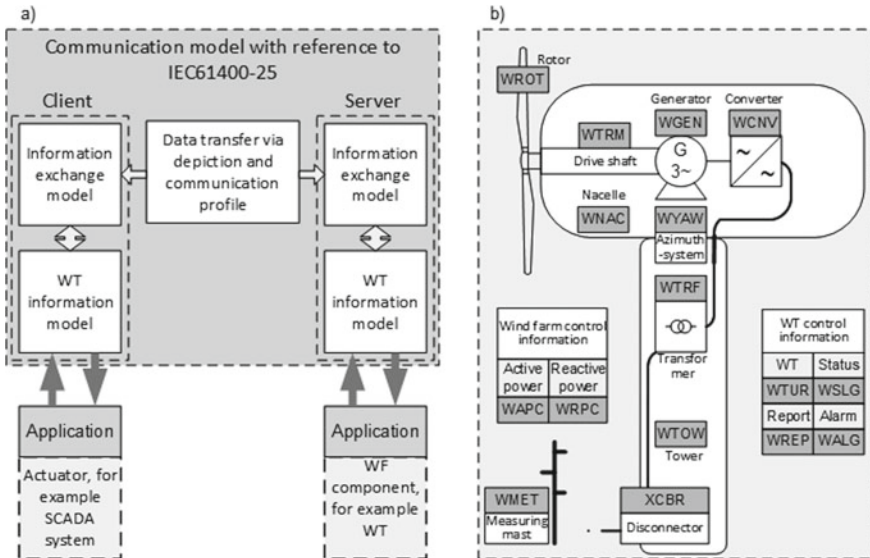
Fig. 24 Unified WT communication model (**a**) and information model (**b**)

exchange models for loading, setting, reporting, controlling or logging and by data transfer using uniform communication profiles for reading and writing.

The WT information model provides the content required for the information exchange between client and server. For this purpose, the components of the real WT write into the unified model of a virtual WT with unified mappings, labels, data types, resolutions and functionalities of the information. Figure 24b shows the main components of the virtual WT. The model is hierarchically organised and includes the information for the drive train with rotor, the power transmission (drive shaft), the generator, the converter and transformer as well as the information of the nacelle, the tower and the azimuth system. In addition, the information on the WT and WPP control system as well as data of the assigned meteorological measuring systems are also described. In Fig. 24b the names of the logical nodes for the components are entered in accordance with [11]. It can be seen that the information of the disconnector already belongs to the group of loops and is therefore coded differently.

With the help of this uniform communication and information model, it is now possible to fulfil different services such as control with the help of a grid management system, the evaluation of data with the help of a condition monitoring system or billing for business management tasks.

Literatures

1. Amlang B et al (1992) Electric power supply with wind turbines. Technische Universität Braunschweig: s.n., 1992. BMFT Research Project 032-8265-B Final Report
2. BDEW Guideline (2008) Technical guideline generation plants on the medium voltage grid. s.l.: Bundesverband der Energie-und Wasserwirtschaft e.V
3. Bianchi FD, De Battista H, Mantz RJ (2007) wind tubine control systems—Principles, modelliong and gain scheduling design. Springer, ondon
4. Gasch R, Twele J (2010) Wind turbines. Wiesbaden: Vieweg und Teubner. GWV Fachverlage GmbH
5. Hansen MH et al (2005) Control design for a pitch regulated, variable speed wind turbine. Roskilde: Risø National Laboratory. Risø-R-1500(EN)
6. Hau E (2003) Wind power systems, 3rd edn. Springer, Berlin Heidelberg
7. Heier S (2009) Wind turbines—System design, grid integration and control, 5th edn. Vieweg und Teubner—GWV Fachverlage GmbH, Wiesbaden
8. Holst A, Prillwitz F, Weber H (2003) Netzregelverhalten von Windkraftanlagen. München : VDI/VDE: 6. GM/ETG Fachtagung "Sichere und zuverlässige Systemführung von Kraftwerk und Netz im Zeichen der Deregulierung"
9. van der Hooft EL (2001) DOWEC Blade pitch control algorithms for blade optimisation purposes. Petten, NL: ECN Wind Energy Report ECN-CX-00-083
10. IEC 61400-1,-3 (2010) IEC DIN EN 61400 61400-1 and -3: Wind turbine design requirements, design requirement for offshore wind turbineit. VDE VERLAG GMBH, Berlin
11. IEC 61400-25 (2007) DIN EN IEC 61400-25: communication for monitoring and control of wind turbines. Beuth-Verlag, Berlin
12. IEC 61508 (2010) Functional safety of safety-related electrical/electronic/programmable electronic systems. VDE VERLAG GMBH, Berlin
13. IEC 61850 (2006) DIN EN 61850: communication networks and systems for automation in electrical power supply. Beuth-Verlag, Berlin

14. Lubosny Z (2003) Wind turbine operation in electric power systems. Springer, Berlin-Heidelberg
15. Manwell JF, McGowan JG, Rogers AL (2008) Wind energy explained—Theory, design and application. Wiley, Chichester
16. Michalke G (2008) Variable speed wind turbines—Modelling, control and impact on power systems. Department of Electrical Engineering and Information Technology, Darmstadt University of Technology. 2008. Dissertation
17. Nuß U (2010) Highly dynamic control of electric drives. VDE-Verlag, Offenbach
18. Riefenstahl U (2008) Electrical drive systems. Teubner Verlag, Wiesbaden, p 2008
19. SDLWindV (2009) Ordinance on system services provided by wind turbines, vol 2009, Part I No. 39, 2009. Published in the Federal Law Gazette, Bonn
20. Soerensen P et al (2005) Wind farm models and control strategies. Risoe National Laboratory Risoe-R-1464(EN), Roskilde
21. TransmissionCode (2007) TransmissionCode 2007 network and system rules of the German transmission system operators. Verband der Netzbetreiber VDN e.V. beim VDEW, Berlin

Prof. Dr. Reiner Johannes Schütt For many years, was Head of Development and Technical Manager at of ENERCON NORD Electronic GmbH in Aurich. Today he teaches and researches in the field of Controls/Electrical Drives and Wind Energy Technology at the West Coast University of Applied Sciences in Heide.

Grid Integration of Wind Turbines

Clemens Jauch

These days, in many grids around the world power system stability relies on the functionalities of modern wind turbines. A modern wind turbine (WT) is usually characterized by a rated power of several megawatts (MW) and its flexibility in operation. Although several MW might seem much for a WT, from a power system's point of view, it means that its generation changes from a few power plants with the size of many hundred MW each to a large number of geographically dispersed individual WTs.

In this chapter, the terms power system (PS) and grid are used as synonyms. Both terms are used in the literature and, hence, for the sake of readability, they are used alternatingly in this chapter.

There is a vast variety of potential interactions between WTs and PSs. Therefore, grid integration of WTs can be approached from many different sides. It is obviously not possible to address all topics related to the grid integration of WTs in this chapter. To give an idea about the complexity of the problem, Fig. 1 shows a selection of related topics in terms of the period lengths of the interactions between wind power and PSs.

The progressing transition to renewable energies has shifted the focus of grid integration of WTs. Consequently, in this chapter emphasis is put on the most important and most recent problems of today's grid integration of wind power.

In the following sections, electric PSs and the different conceivable WT types are briefly introduced. Following that, the historic aspects of grid integration of WTs are briefly touched upon, which then leads to the most dominant problems of today's grid integration of WTs. Subsequently, the grid quantities' voltage and frequency are explained, and each explanation is followed by a section, which discusses how WTs can stabilize the respective grid quantity.

C. Jauch (✉)
Wind Energy Technology Institue, Flensburg University of Applied Sciences, Kanzleistrasse 91-93, 24943 Flensbrug, Germany
e-mail: Jauch@hs-flensburg.de
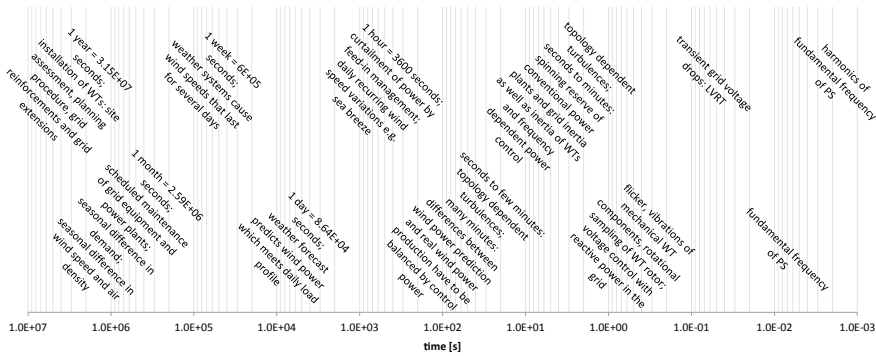
Fig. 1 Logarithmic time scale of mutual effects between wind power and PSs

1 Introduction to Grid Integration of Wind Turbines

It is widely accepted that anthropogenic climate change is mainly caused by greenhouse gases, which result from burning fossil fuels. Therefore, a majority of countries have agreed on reducing greenhouse emissions to limit global warming to less than 1.5 °C above pre-industrial levels [1].

The power sector has been a major emitter of greenhouse gases. Traditionally, electric power has mainly been generated by thermal power plants, which run on fossil fuels. Hence, the necessary decarbonization of the power sector leads to an increasing share of renewable energy generators. One of the most widespread and most widely developed renewable generators are WTs. Therefore, wind power installations, and hence wind power infeed into PSs, grow quickly in many countries all over the world [2, 3]. Due to the increasing share in wind power production, WTs become an indispensable part of a PS. Since WTs replace conventional power plants, they have to be as reliable as conventional power plants. In addition, WTs also have to take over the control functionalities, which have been provided by conventional power plants. Consequently, this chapter focuses on the grid stabilizing functionalities, which have to be provided by WTs. It has to be emphasized, though, that most topics discussed in the section Grid Integration of the first edition of this book remain valid and have to be considered when integrating WTs into PSs [4].

1.1 Introduction to Electric Power Systems

The purpose of electric PSs is to connect the consumers of electric energy with the producers of electric energy. A PS is not only a physical link between the generators and the consumers, but it is also a marketplace for the commodity electricity.

Hence, it is the task of a PS to provide the consumers with the electricity that they buy from the generators. This task has to be performed safely, reliably and with

the least possible losses. Furthermore, the electricity has to be provided in a quality, which is usable for the consumer. Hence, the PS quantities, which are introduced in Sects. 2 and 4, have to be maintained in specific limits.

It is historically grown that large PSs are almost invariably alternating current (AC) systems. One fundamental characteristic of electric AC energy is (unlike other commodities like water, oil and gas) that it cannot be stored. Direct current (DC) can be stored in batteries or capacitors. AC power, on the other hand, has to be generated exactly at the time when it is to be consumed. Traditionally, AC power is generated with rotating generators. Kinetic energy can be stored in the rotation of such generators. However, without the conversion from kinetic energy to electric energy, AC power cannot be produced with rotating generators. Hence, inertia is the only energy storage which can store AC power indirectly, and only in very small amounts. The use of kinetic energy in AC PSs is discussed in detail in Sect. 4.2.

A consequence of this lack of energy storage is that AC power has to be generated simultaneously with its consumption. In other words, generation and demand have to be in balance at all times. The PS frequency is a measure of this balance, which is the topic of Sect. 4.

Since the electricity has to be supplied in a quality, which is usable for the consumer, the producer has little control over the amount that is consumed. Water works could lower the pressure in the water supply network to provide consumers with less water when the demand exceeds the available resources. In an electric PS, the system operator can neither lower the voltage nor the frequency to an effective extent, without making the electricity unusable for the appliances of the consumers. Consequently, the generators have no other choice than to adjust their production to the prevailing demand.

Traditionally, thermal power plants were built in the vicinity of the demand, i.e. close to the load centers. This requires transporting the prime energy to the location of the power plants. The advantage is that the electric power has to be transported over short distances only, which reduces transmission losses. Renewable energy generators, on the other hand, have to be built where natural energy resources are available, irrespective of the location of the electricity demand. In the case of WTs, this means that WTs need to be built where the wind speed is high. The PS has to transport the electricity to the consumers, whose locations are usually not chosen based on wind speeds.

1.1.1 Power System Setup

Most PSs comprise a transmission system, which transports large amounts of power over longer distances, and a distribution system, which distributes the electric power to consumers in geographical proximity. Transmission usually takes place on high voltage (HV) or even extra high voltage (EHV), while distribution usually applies a medium voltage (MV) and low voltage (LV). The higher the voltage, the lower the current at a given power value. Low current means low losses in the lines, which is why transmission over longer distances is done with HV lines.

The nominal voltage ranges of these voltage levels are listed in the following. It has to be noted though that there are no universally applicable definitions of these limits:

$$LV : \leq 1\,kV, \ MV : \ 1 - 60\,kV, \ HV : 60 - 150\,kV, \ EHV : \geq 150\,kV$$

Figure 2 shows a single line (more on this in Sect. 1.1.2) diagram of a typical PS setup. Large generators produce power on the MV level (blue), and their power is transported via HV (red) transmission lines to a MV distribution grid. The power flows via transformers from one voltage level to another. The distribution system transports power over shorter distances. Both larger MV consumers as well as smaller LV (green) consumers are connected to the distribution system. In the LV system, many small consumers run on one single phase only, which leads to a further reduction in voltage; see Sect. 1.1.2. Small generators might also be single-phase appliances, which run on LV; hence, these are also connected to the distribution system.

For redundancy, some connections are ring feeders, which allow the power to flow through two alternative lines. The maximum redundancy is achieved with meshed grids (not shown in Fig. 2), where the power can flow through more than two alternative lines.

A feeder is called radial feeder if the power can flow via a single route only. Radial feeders are simple and cheap, but have the least redundancy. In case a line has a fault, e.g. a short-circuit, circuit breakers on either side of this line can take it out
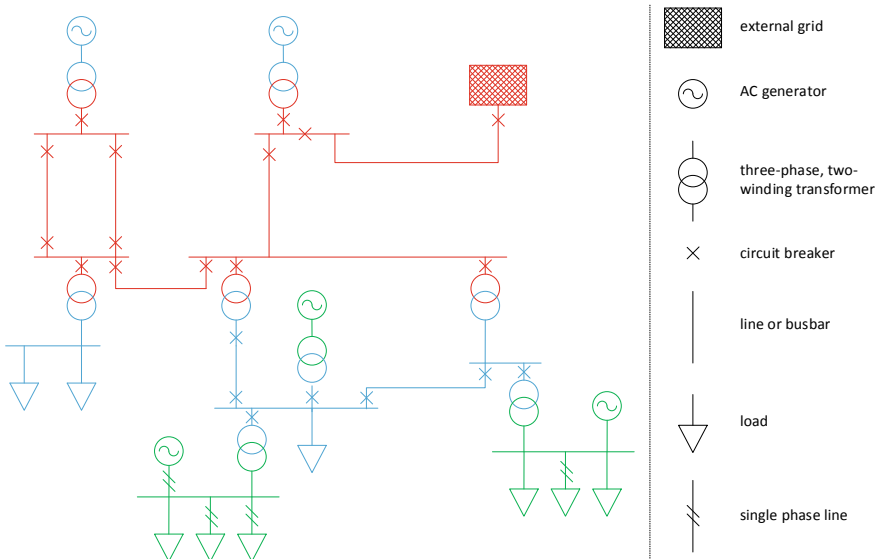
Fig. 2 Left: Single line diagram of a typical three-phase PS comprising HV (red), MV (blue) and LV (green) levels. Right: Legend of the used symbols
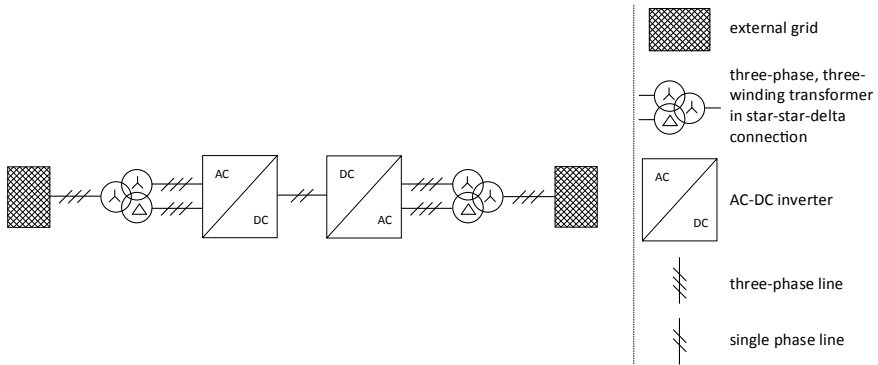
Fig. 3 Left: HVDC link connecting two AC grids. Right: Legend of the used symbols

of operation. By de-energizing a radial feeder, the power has no alternative route to flow.

PSs are usually AC because AC voltages can be easily stepped up and down with transformers. Hence, AC PSs are a well-established technology. However, even in AC PSs also single DC links can be found for varies reasons. Figure 3 shows a typical example, where two AC PSs are connected via a high-voltage DC (HVDC) link. If two AC PSs have different frequencies (50 and 60 Hz), it is inevitable to connect them via DC if power is to be exchanged between them. The same applies if two AC PSs have the same nominal frequency, but are not operated in synchronism, e.g. the British and the Central European PSs.

Even inside an AC PS, DC links might be applied for transporting power over long distances. In such a case, it is an economic decision, whether an AC line or a DC line is built. Looking at Fig. 3, it becomes obvious that DC requires substantial technological effort, as it comprises three-winding transformers and AC/DC inverters on either side of the DC line. However, long AC lines also require substantial technological effort. It is inherent that the instantaneous value of AC voltage varies sinusoidally, i.e. that it is never constant. Hence, electro-magnetic waves propagate through AC lines. If the length of an AC line is in the order of magnitude of the length of these electro-magnetic waves, the voltages along the line are affected by the waves. It is already difficult to maintain voltages inside the tolerance while the line is loaded normally; however, it becomes extremely demanding to avoid too high voltages when the line is only lightly loaded or in no-load condition.

The electro-magnetic waves have the largest impact on the voltage in underground or subsea cables, as opposed to overhead lines. Therefore, many offshore wind farms are connected to the onshore PS via HVDC links. Looking at Fig. 3, one AC grid could be the offshore wind farm, while the other AC grid could be the onshore grid into which the wind farm feeds its power.

The decision of whether an HVDC link is built inside an AC PS is usually taken depending on the voltages that would occur on the alternative AC line. Voltages on AC lines are further discussed in Sect. 2.

1.1.2 Three-Phase System and Single-Phase Representation

AC PSs are usually three-phase systems. Other numbers of phases are conceivable as well, however, three phases are an optimum in the trade-off between benefit and complexity. Multiple phases provide multiple ways to connect generators and consumers to the PS. Figure 4 shows a three-phase transformer, which is connected in the delta on the primary side (*p*) and in a star on the secondary side (*s*). The advantage of the star connection becomes immediately obvious in that there is a fourth "phase": the neutral conductor (*N*), which leads to the star point.

The star point can, but does not need to be, connected to the ground for protection purposes. Therefore, the ground connection is shown in gray in Fig. 4. The star connection provides a division of the voltage. Instead of only the voltage between two phases, in a star connection also the voltage between one phase and neutral is available. Equation 1 gives an example of Fig. 4.

$$V_{abs} = \sqrt{3} \cdot V_{aN\,s} \tag{1}$$

The divided voltages in star connection are advantageous for low-power applications. Low-power appliances are often single-phase, which are therefore connected between phase and neutral. When the three phases in the star connection are loaded differently, the neutral conductor carries the resulting residual current. If one phase is loaded differently from the other two in a delta connection, this has an immediate effect on the current, and hence, the voltages of the other two phases.

In PSs, it is common practice to name nominal voltage as phase-to-phase voltages. Therefore, the voltage ranges for the different voltage levels, mentioned in Sect. 1.1.1, are the root mean square (RMS) values of phase-to-phase voltages (V_{ab}, V_{ac}, V_{bc}).

In a three-phase PS, it is desirable to distribute the load equally among the phases. Hence, in the normal operation of many PSs, the voltages and currents of the three phases are equal. Therefore, in PS analysis it is often unnecessary to deal with the individual phases. Instead, the three phases are aggregated into one phase only: the so-called single-phase equivalent.
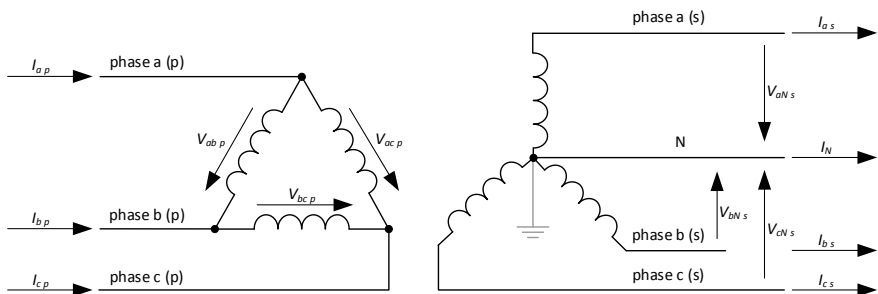
Fig. 4 Three-phase transformer connected in delta on the primary side (*p*) and in star of the secondary side (*s*). The arrows indicate the voltages (*V*) and the currents (*I*)

If the currents are equal ($I_a = I_b = I_c$) and the voltages are equal as well ($V_{aN} = V_{bN} = V_{cN}$), then the powers flowing in the three phases are equal, too: $S_a = S_b = S_c$. Hence, the system can be simplified to a single-phase equivalent, whose power is

$$S = 3 \cdot S_a = 3 \cdot S_b = 3 \cdot S_c \qquad (2)$$

If the voltage in a single-phase equivalent is assumed to be a phase-to-neutral voltage (V_{aN} or V_{bN} or V_{cN}), then the single-phase equivalent current is a current, which cannot be found in the real three-phase system. Instead, the current in the single equivalent phase can be derived from the phase-current of the system in the star connection:

$$I = 3 \cdot I_a = 3 \cdot I_b = 3 \cdot I_c \qquad (3)$$

If the system to be expressed as a single-phase equivalent is not in star connection, a fictive star point has to be calculated with delta-star transformation. The methodology of this transformation can be found in the literature [5], and is hence not elaborated on here.

When considering grid integration of WTs, a balanced system can be assumed in most cases. Exceptions are the analysis of single-phase and two-phase short circuits, which are not elaborated on here. Therefore, in the rest of this chapter there are no more three-phase representations of PSs shown. Instead, only single-phase equivalents are applied for representing three-phase systems.

1.1.3 Per Unit System

In PS analysis, it is common practice to express quantities in per unit (pu) rather than in SI units. Equation 4 shows the concept:

$$\text{value in pu} = \frac{\text{value in SI units}}{\text{base value in SI units}} \qquad (4)$$

There are many reasons why it is advantageous to apply the pu concept:

- If different devices in a PS (e.g. different WTs of different sizes and potentially also of different types) are referred to one basis, they become easily comparable.
- If different devices in a PS (e.g. different WTs) are referred to a system basis (e.g. the rated power of the whole PS), their contribution to the system (e.g. the overall power transmitted through the PS) becomes obvious.
- If a device in a PS is referred to its rated values (e.g. different WTs of different sizes are referred to their rated power values), the loading of each individual device becomes obvious.

- In a PS, multiple MW flow through cables with very small impedances in ohms (Ω): power[6] W flows through impedance^{-3} Ω. Expressing all quantities that are required for PS analysis (voltages, currents and impedances) in terms of pu leads to values that are in the same order of magnitude. Comparable numbers are advantageous for calculations.
- In a PS with different voltage levels, neither the voltages nor the currents in the different voltage levels are directly comparable. In pu representation, the voltage levels seem to disappear and the values become directly comparable. To illustrate this concept, Fig. 5 provides an example.

The example shown in Fig. 5 comprises a radial WT feeder, where a 3 MW WT feeds into a 690 V LV cable. The power is stepped up to 20 kV MV and eventually fed into the 220 kV HV grid. To facilitate comprehensibility, it is assumed that the whole feeder is purely ohmic, i.e. that only energy losses occur along the line; no reactive power occurs. It is further assumed that the transformers are lossless, and hence, only the cables cause ohmic voltage drops and energy losses. The considered operating point of the WT is rated power at rated voltage.

Comparing the currents (I) shown in the middle of Fig. 5, it becomes obvious that they differ grossly, due to the different voltage levels. Also, the cable resistances (R) differ by orders of magnitude. It is impossible to tell the losses that occur from these
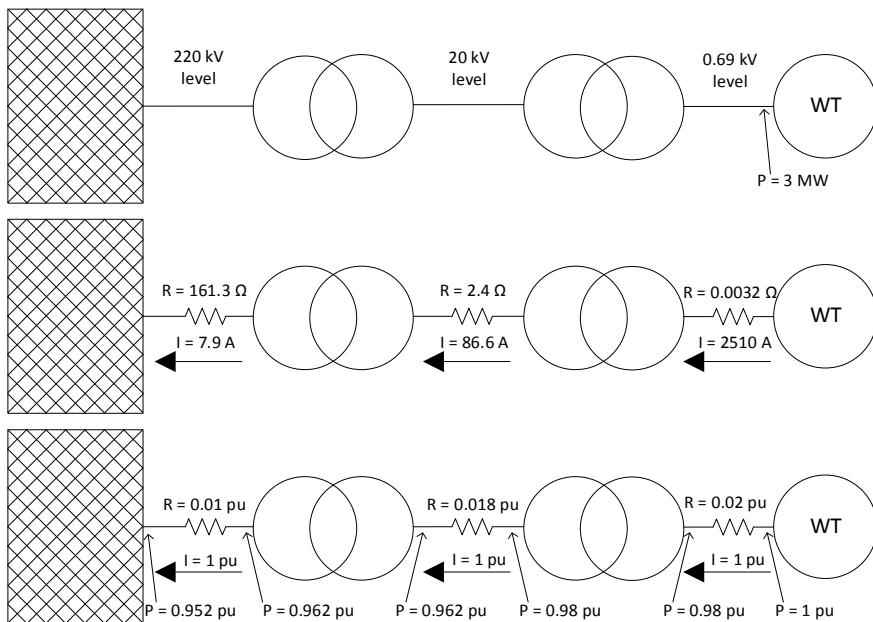
Fig. 5 Simplified WT feeder with three voltage levels (top) with applicable currents in amperes (middle) and with all quantities in pu (bottom)

resistances. In order to translate the system to pu, and in order to let the different voltage levels virtually disappear, base values have to be chosen.

In the example at hand, the base voltage is chosen to be the rated voltage of the WT: $V_{\text{base}} = 690$ V.

The power base is chosen to be the rated power of the WT: $S_{\text{base}} = 3$ MW. (It has to be noted here that for the base power the capital letter S is used, although the active power of the WT is denoted with the capital letter P. This notation is chosen as it is consistent with the notation used in the literature [5]).

With these base values, the applicable base impedance (Z_{base}) can be derived for the applicable voltage level (here the 690 V level to which the WT is connected):

$$Z_{\text{base}} = Z_{\text{base\_LV}} = \frac{V_{\text{base}}^2}{S_{\text{base}}} \tag{5}$$

The impedance base derived in Eq. 5 can be transferred to the other voltage levels with the square of the voltage ratio. Equation 6 shows the transformation from the LV level to the MV level as example:

$$Z_{\text{base\_MV}} = Z_{\text{base\_LV}} \cdot \left(\frac{V_{\text{MV}}}{V_{\text{base}}} \right)^2 \tag{6}$$

Dividing any component impedance by the applicable base impedance leads to a system that looks like everything was on the same voltage level. When dividing a quantity with its base value, which has the same unit as the quantity to be divided, the physical unit cancels out and gets replaced by "per unit" (pu).

With the impedances and the power of the WT in pu, the power along the feeder can be derived. In the bottom of Fig. 5, the system is shown in pu. It can be seen that the pu current is identical in all voltage levels, as there is no path through which the current could flow off. The impedances in pu reveal that the highest voltage level causes the least voltage drop and the least power losses.

Due to the advantages of the pu system, and due to its widespread use in PS analysis, pu notation is used in the following parts of this chapter.

1.1.4 Basic Power System Quantities

Energy sources in PSs are voltage (V) sources. Hence, voltage is the force that drives energy through a PS. Figure 6 shows a WT feeder with LV, MV and HV cables. The WT is the source of V_{WT}, which opposes the voltage in the HV grid, V_{inf}.

V_{inf} is assumed to be independent of the power that the WT feeds into the HV grid. Therefore, the HV grid is called the infinite busbar and, consequently, its voltage is called V_{inf}.

If V_{WT} exceeds V_{inf}, a current, I_{WT}, flows, which in turn causes voltage drops along the feeder. The voltage drops occur in the cables and transformer because all these PS components impede the current flow. Hence, if current flows through these
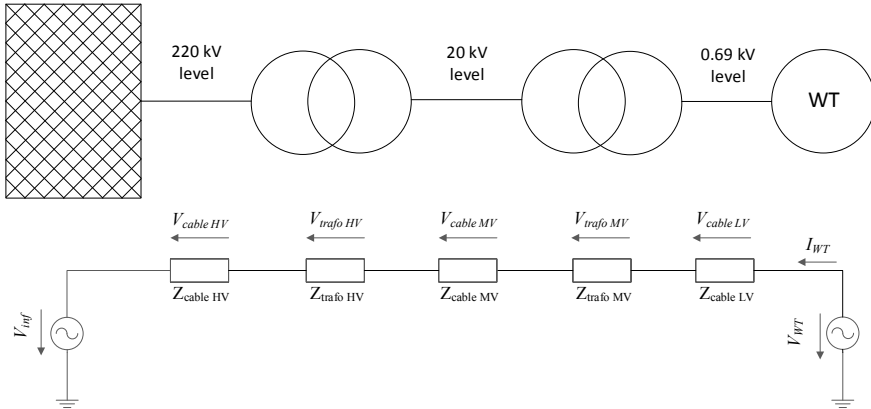
Fig. 6 Single line diagram of WT feeder, with grid plan symbols (top) and with voltage sources and impedances (bottom)

components, their impedances cause a voltage drop. Eventually, for the WT to feed power into the HV grid, it has to produce a voltage, which is large enough to exceed V_{inf} and all voltage drops along the feeder.

Hence, it can be said that the WT produces voltage, which causes a current (I) that is received by the grid. The grid produces a counter-voltage, which is received by the WT. In the following, it is briefly introduced how these PS quantities develop.

In AC PSs, the voltages are sine-waves, which are characterized by their magnitudes, their phase angles and their frequencies. The instantaneous values of the voltages in phases a, b and c are shown in Fig. 7. In PS analysis, it is often assumed that the waveform is sinusoidal at all times, and that the frequency is constant and equal to the rated system frequency (50 or 60 Hz). With these simplifying assumptions, the magnitude and the phase angle are the only variables, which characterize the voltage (and any other PS quantity). Hence, as long as these simplifying assumptions are valid, all PS quantities can be expressed as complex numbers, comprising a magnitude and a phase angle.

It has to be added here that in reality neither the waveform nor the frequency can be considered constant. The waveform can be distorted from harmonics, which is a disturbance with minor consequences. Nonetheless, harmonic distortion is a problem, which is addressed in grid codes. The grid frequency (50 Hz in Fig. 7) is proportional to the speed with which the generators rotate. This speed is a measure of the balance between generation and demand, which is why, in reality, it is hardly ever exactly at its rated value.

Impedances, Z, are complex numbers, which describe how they impede the current flow:

$$\underline{Z} = R + jX \qquad (7)$$

A resistance, R, causes a voltage drop and turns electric energy into heat:
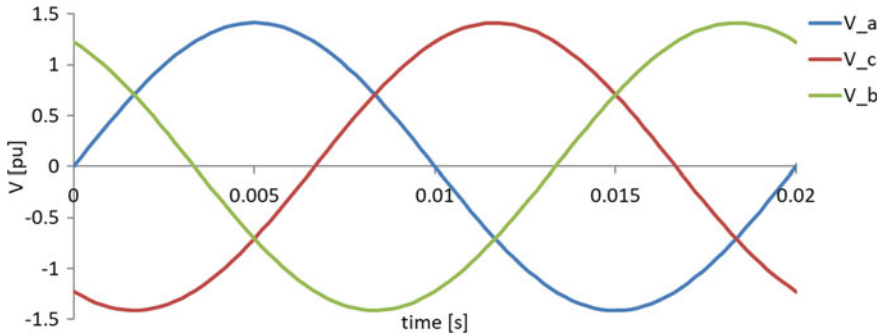
Fig. 7 Instantaneous values of three-phase voltages

$$V = R \cdot I \tag{8}$$

The imaginary part, X, of an impedance, Z, is called reactance. A reactance can be made of a capacitance, C, or an inductance, L. Both capacities and inductances impede the current, but neither of them dissipates energy. Instead, capacities and inductances are energy storages. The degree to which they impede the current, however, depends on the frequency, i.e. it depends on the time available for charging these energy storages. The frequency, which in PS analysis is usually given in Hertz (Hz), has to be turned into an angular frequency, ω, in rad/s:

$$\omega = 2 \cdot \pi \cdot f \tag{9}$$

With ω, the voltage drop, which results when a capacity impedes current, can be calculated. It has to be noted, though, that this voltage drop is a steady state value. That is, this is the voltage drop that results after any transients in the process of charging the capacity have subsided:

$$\underline{V} = \frac{1}{j \cdot \omega \cdot C} \cdot \underline{I} = -j \cdot X_C \cdot \underline{I} \tag{10}$$

The instantaneous voltage drop, which occurs during the charging and discharging of a capacity, can be computed with the following integral equation:

$$v(t) = \frac{1}{C} \int i(t) \cdot dt + v_0 \tag{11}$$

A capacity stores electric energy in the electric field between its poles. To illustrate the effect of the electric energy storage, the above equation is applied to derive the instantaneous voltage when a capacity is charged. To facilitate comprehensibility, a simple DC circuit is applied. However, the effect is directly transferable to AC. In the resistance-capacity (RC) circuit shown in Fig. 8, the capacity, C, is brought to a new
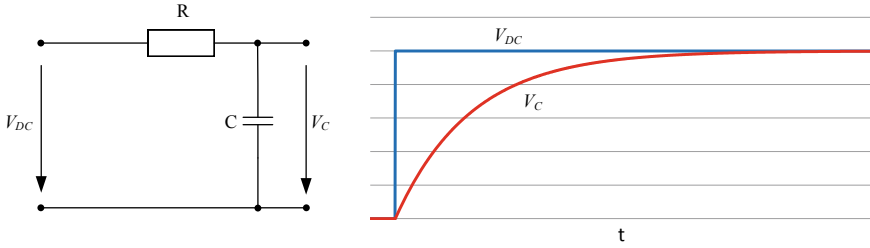
Fig. 8 Capacity, C, stores electric energy when it gets charged with the voltage V_{DC}

state of charge, because the supply voltage, V_{DC}, steps to a new value. The diagram on the right-hand side of Fig. 8 shows a qualitative time trace of the voltages.

The charging or decay time constant, τ, of an RC circuit depends on the capacity and the resistance:

$$\tau = R \cdot C \tag{12}$$

The steady state voltage drop occurring at an inductance is also a complex number:

$$\underline{V} = j \cdot \omega \cdot L \cdot \underline{I} = j \cdot X_L \cdot \underline{I} \tag{13}$$

An inductance stores energy in the magnetic field. Hence, the instantaneous voltage drop caused by charging or discharging the magnetic field is derived with the following differential equation:

$$v(t) = L \cdot \frac{di(t)}{dt} \tag{14}$$

To illustrate the effect of the magnetic energy storages, the above equation is applied to derive the instantaneous voltage when inductance is discharged. Figure 9 shows a resistance-inductance (RL) circuit, which is initially energized to steady state. A short-circuit at the terminals drains the energy from the inductance. The diagram on the right-hand side of Fig. 9 shows a qualitative time trace of the voltage across the resistance. The voltage across the resistance is proportional to the current, which is provided by the inductance.

The charging or decay time constant, τ, of an RL circuit depends on the inductance and on the resistance:

$$\tau = \frac{L}{R} \tag{15}$$
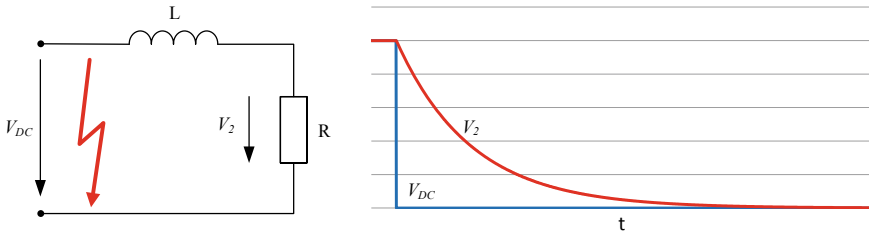
Fig. 9 Inductance, L, is drained of its energy due to a short-circuit at the terminals of the RL circuit

1.1.5 AC Power

Although power is also one of the PS quantities, it is discussed here in a separate subsection, because it is of outstanding importance for grid integration of WTs. Electric power is derived from voltage and current, both in instantaneous values ($s(t)$) and in complex numbers ($\underline{S}$). (Note that the complex power is the complex voltage times the conjugate complex (*) of the current.)

$$s(t) = v(t) \cdot i(t)$$
$$\underline{S} = \underline{V} \cdot \underline{I}^* \tag{16}$$

To approach the problem, the instantaneous power resulting from current flowing through R, C and L (as introduced in Sect. 1.1.4) is shown in Fig. 10. The power of the shown 50 Hz signals is also a sine-wave, however, with double the frequency. In the case of R, the voltage and current are in phase. Hence, power is always a positive value. This means that the power flows in one direction, i.e. it flows into R, where it is turned into heat. Electric power, which can travel and which can be permanently transformed to other types of power, is called active power, P.

In the case of C, the current leads the driving voltage by 90°, while in L it lags the voltage by 90°. Consequently, in both cases the resulting power wave oscillates around zero. This means that the power flows in one direction in one half-wave, while it flows in the opposite direction in the other half-wave. That is, the power does not propagate, but it remains where it is. This kind of power is called reactive power, Q.

Figure 10 further reveals that the sum of all three-phase power sine-waves is a constant value. This is particularly important for rotating three-phase machines, as it means that the torque at their shaft is constant. Constant torque is advantageous because it does not cause mechanical vibrations.

A mixture of active power, P, and reactive power, Q, is the so-called apparent power, S, which can be expressed as a complex number:

$$\underline{S} = P + jQ \tag{17}$$

Figure 11 shows $\underline{S}$ in the complex number plane. P is on the real axis and Q is on the imaginary axis. The angle φ between P and S is also the angle between V and I.
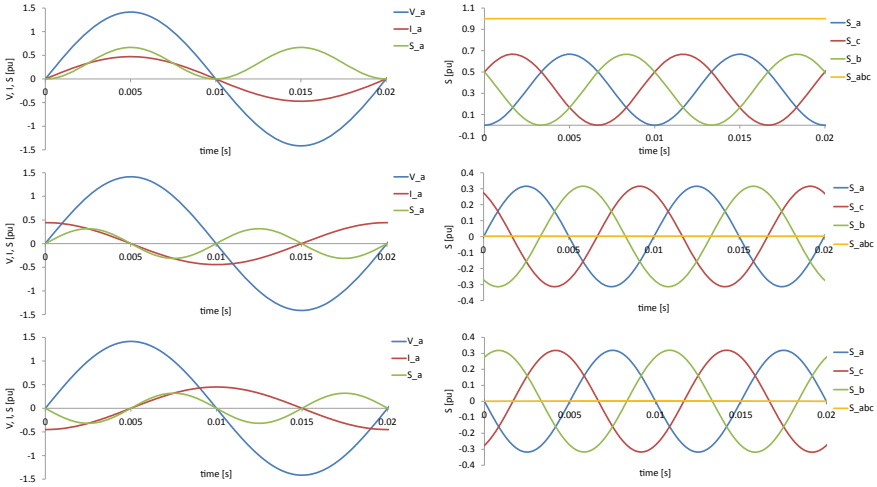
Fig. 10 Instantaneous AC power in a resistance (top), in a capacitance (middle) and in an inductance (bottom). The left column shows how power results from voltage and current in one phase. The right column shows the power in all three phases

Fig. 11 S, P and Q in the complex number plane
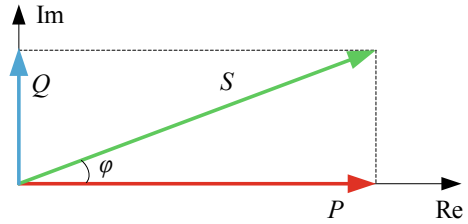
The power factor, $\cos(\phi)$, is a commonly used variable that expresses to what extent apparent power is made of active power:

$$\cos(\varphi) = \frac{P}{S} \tag{18}$$

With the angle ϕ, the apparent power (just like any other complex PS quantity) can also be expressed in angle notation on the polar complex plane:

$$\underline{S} = S\angle\varphi \tag{19}$$

In angular notation, the magnitude $|\underline{S}|$ is the summation of the two orthogonal vectors P and Q:

$$|\underline{S}| = S = \sqrt{P^2 + Q^2} \tag{20}$$
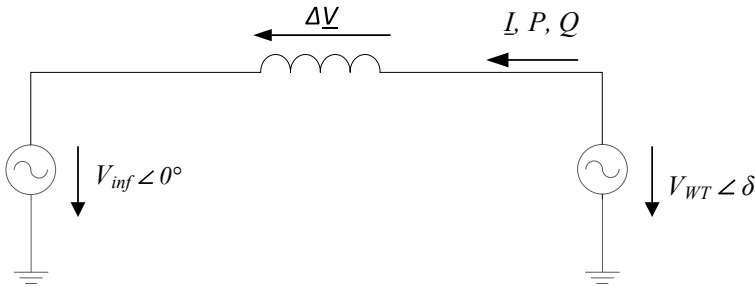
Fig. 12 WT feeder simplified to one lumped inductance only

In the example shown in Fig. 6, it was said that the voltage of the WT, V_{WT}, has to exceed the voltage in the infinite busbar, V_{inf}, for a current to flow. To substantiate this statement, it first has to be defined in what way V_{WT} has to exceed V_{inf}. Since both voltages are complex numbers, they are characterized by their magnitudes and their phase angles. Hence, there are two variables which can be different. In other words, there are two variables in the voltage to control the current, and hence, the power flow.

The WT feeder shown in Fig. 6 is mainly inductive, due to the massive inductance of the two transformers. For the purpose of explaining AC power flow, and for the sake of comprehensibility, the feeder is assumed to consist of an aggregated inductance only; see Fig. 12.

The voltage of the infinite busbar, V_{inf}, is considered the reference. Therefore, its angle is determined to be zero. The WT produces a voltage, which has a magnitude V_{WT} and an angle δ with respect to V_{inf}. (The complex voltages in Fig. 12 are in angle notation).

The voltage difference

$$\underline{\Delta V} = \underline{V_{\mathrm{WT}}} - \underline{V_{\mathrm{inf}}} \tag{21}$$

drives a current through the feeder with its impedance $\underline{Z}$:

$$\underline{I} = \frac{\underline{\Delta V}}{\underline{Z}} \tag{22}$$

This allows computing the apparent power, which the WT feeds into the feeder:

$$\underline{S} = \underline{V_{\mathrm{WT}}} \cdot \underline{I}^* \tag{23}$$

P and Q, shown in Fig. 12, can be derived by decomposing the apparent power into its real and imaginary parts:
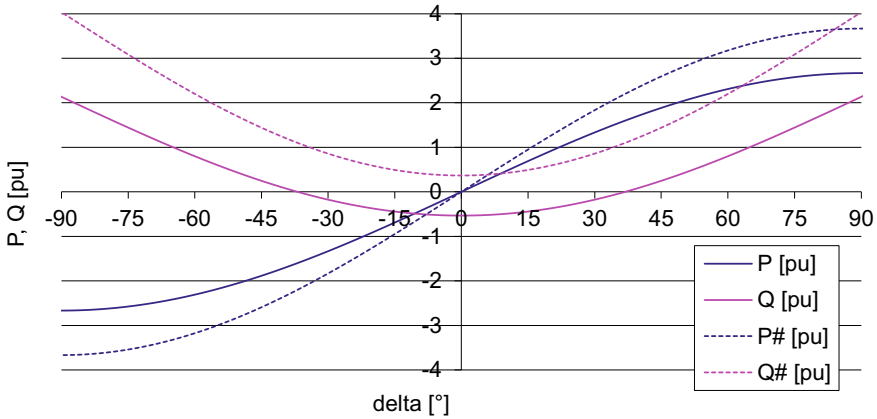
Fig. 13 P and Q as function of angular difference between two voltages (delta), for a difference in voltage magnitudes of -0.2 pu (solid lines) and $+0.1$ pu (dashed lines, $P\#$ and $Q\#$)

$$
\begin{aligned}
P &= \mathrm{Re}\{\underline{S}\} \\
Q &= \mathrm{Im}\{\underline{S}\}
\end{aligned}
\tag{24}
$$

The above equations are used for generating the diagram shown in Fig. 13. In this diagram, $\underline{V}_{\mathrm{inf}}$ is always kept unchanged: $|\underline{V}_{\mathrm{inf}}| = 1.0$ pu, while the magnitude of $\underline{V}_{\mathrm{WT}}$ is either $|\underline{V}_{\mathrm{WT}}| = 0.8$ pu or $|\underline{V}_{\mathrm{WT}}| = 1.1$ pu (#).

This diagram reveals that P is controlled best via the angular difference between the voltages. Q, on the other hand, can be controlled easily by varying the magnitude of one voltage source with respect to the other. This concept is well known from synchronous generators, where P is a function of the load angle (delta in Fig. 13) and Q is controlled with the excitation, which varies the magnitude of the terminal voltage of the synchronous generator.

This concept of controlling P with the angle and Q with the magnitude of a voltage source applies always. It does not matter whether the considered voltage source is a synchronous generator of a conventional power plant, an induction generator of Type I or Type II WT (see Sect. 1.2), a frequency converter of a Type III or Type IV WT or a quadrature booster (phase-shifting transformer).

1.1.6 Power System Stability

PS stability is divided into voltage stability and angular stability. Angular stability (also called synchronous stability) refers to the stability of the AC-connected rotating machines in the system, i.e. the PS frequency.

A PS is stable when it returns to an acceptable operating point, in all locations of the PS, after it has been upset by a disturbance [6]. As an example, Fig. 14 shows the oscillations in the generator speed after this generator has been upset by a transient
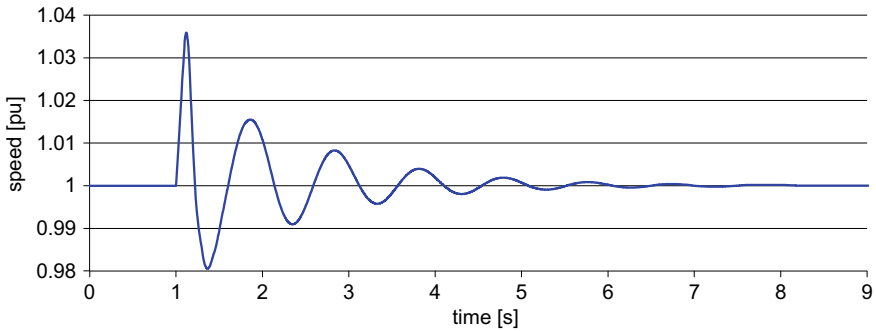
Fig. 14 Stable oscillation of the rotational speed of a generator after it has been upset by a short-circuit in the PS

short-circuit at its terminals. The oscillations subside and the final generator speed is, again, 1 pu. Hence, the system is stable, as the generator returns to an acceptable operating point.

An oscillation is stable when its magnitude decreases with time [7]. An operating point is acceptable when the PS can serve its purpose. This is particularly important in the context of voltage stability. After a voltage collapse at the end of a radial feeder (this is discussed in Sect. 2.3), the voltage might be permanently zero volts, while the rest of the system is in normal operation. Although this is a stable operating point, it is obviously not acceptable.

A comparable example of instability is conceivable when considering the PS frequency. A transient voltage drop can lead to excessive acceleration of a synchronous generator, such that it suffers pole slipping. That is, the rotor accelerates beyond synchronism. In this situation, the protection system will disconnect the generator and bring the prime mover to a standstill. Standstill is surely a stable operating point; however, since power production is impossible in a standstill, it is not an acceptable operating point.

Voltage stability is discussed further in Sect. 2.3, while frequency stability is the topic of Sect. 4.4.

1.2 Introduction of the Different WT Types

Different WT technologies are available on the market and potential technologies are discussed in scientific literature. When considering grid integration of WTs, different technologies have different implications for the grid. WT manufacturers pursue different technologies, but their basic concepts are comparable. Therefore, the different conceivable technologies are usually categorized into so-called WT types to make them independent of particular WT manufacturers [8]. In the following, these types are briefly introduced. In this chapter, only those technologies are considered

which are relevant for grid integrated WTs of considerable size, i.e. which are suitable for MW-size WTs.

Grid code compliance is a driver for technological development. Some of the WT types introduced in the following have disappeared from most markets because it is economically unfeasible to make them comply with some of today's grid code requirements. Other WT types were developed due to emerging grid code requirements.

1.2.1 Type I—Fixed Speed WTs with SCIG

This type of WT is invariably equipped with a squirrel cage induction generator (SCIG), which is directly connected to the AC grid; see Fig. 15. The SCIG is usually driven via a gearbox to achieve a synchronous speed of 3000, 1500 or 1000 RPM when connected to 50 Hz grids. Due to the substantial reactive power (Q) demand for excitation of the SCIG, the synchronization with the grid has to be done with a soft starter. After synchronization is completed, the soft starter is bypassed with a bypass switch. In steady state operation, the reactive power demand of the SCIG is covered by compensation capacitors (C), which are connected and disconnected depending on the voltage (V) or the power factor ($\cos(\phi)$) at the terminals of the SCIG.

Type I WTs can either be passive stall WTs, where the aerodynamic power is not actively controlled. Instead, the stall effect sets in automatically when the ambient wind speed leads to more than rated power. Alternatively, the power can be controlled via the pitch angle (θ) of the rotor blades. Since pitch angle control is not always contained in Type I WTs, the pitch control circuit is shown in gray in Fig. 15. In fixed speed WTs, the power can be controlled with the pitch angle either in the positive direction (pitch to feather) or in the negative direction (pitch to stall).
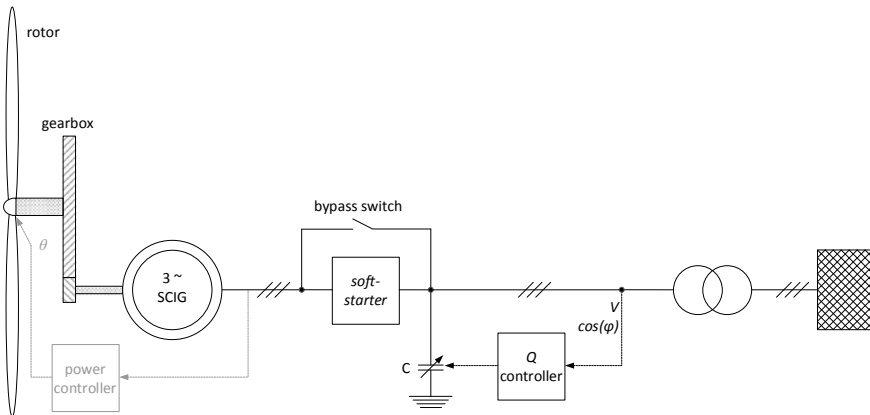
Fig. 15 Type I—fixed speed WT with or without power control via the pitch angle
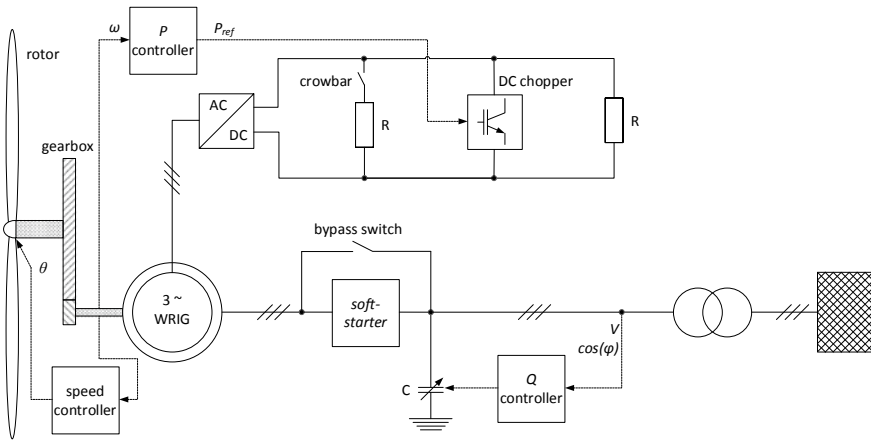
Fig. 16 Type II—semi-variable speed WT with variable rotor resistance connected to a WRIG

1.2.2 Type II—Semi-Variable Speed WTs with WRIG

A semi-variable speed WT is a speed-controlled WT; hence, the rotor speed is controlled with the pitch angle (invariably pitch to feather). In a Type II WT, a wound rotor induction generator (WRIG) is driven via a gearbox, as shown in Fig. 16. Just like in a Type I WT, also in a Type II WT the generator is synchronized with the grid via a soft starter, and the reactive power demand of the generator is compensated with controllable capacitors. Connected to the rotor windings of the WRIG is a variable resistor. Figure 16 shows that this is actually a constant resistor (R), which is bypassed by a DC chopper. The current, which can flow through R or the DC chopper, is the rectified current from the rotor windings. By controlling the current, which bypasses the resistor, it appears to the WRIG as if there were a variable resistor connected to its rotor windings. By controlling the virtual rotor resistance as a function of the rotational speed (ω) of the WRIG, a certain power operating point (P_{ref}) can be realized. However, this speed variability causes reduced efficiency due to heat losses in the resistor (R); see Sect. 1.1.4. The crowbar in the rotor circuit is a safety measure to protect the DC chopper from harmful voltages in case of grid faults.

1.2.3 Type III—Semi-Variable Speed WTs with DFIG

A doubly fed induction generator (DFIG) is a WRIG whose rotor terminals are connected to a back-to-back frequency converter, instead of variable rotor resistance. A Type III WT is basically a Type II WT with a DFIG, instead of a WRIG. The stator terminals of DFIG are directly connected to the grid. Hence, a DFIG behaves like a synchronous generator, where the excitation is controlled via the voltage in the rotor circuit. Whenever the rotational speed (ω) of the DFIG is different from the speed with which the stator field rotates, the frequency converter has to inject the excitation
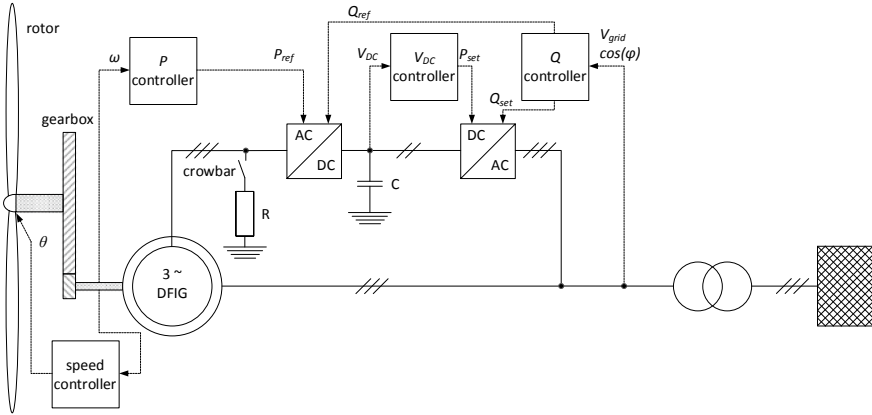
Fig. 17 Type III—semi-variable speed WT with DFIG

current into the rotor not as DC current, but as AC current with the slip frequency. That is, the frequency converter has to offset the difference between the rotational speed of the mechanical rotor and the stator field.

With the machine-side inverter (see Fig. 17), the load angle in the DFIG can be adjusted, i.e. the active power operating point (P_{ref}) can be set, compared with Sect. 1.1.5. The reactive power, which the DFIG feeds via its stator terminals into the grid (Q_{ref}), can be varied by varying the magnitude of the voltage in the rotor of the DFIG. The grid-side inverter controls the DC voltage (V_{DC}) in the DC circuit, by feeding power (P_{set}) into, or extracting P_{set} from, the DC capacitor (C). The grid-side inverter can further exchange reactive power (Q_{set}) with the grid without interfering with the DFIG.

Just like in a Type II WT, the crowbar in the rotor circuit is a safety measure to protect the machine-side inverter from harmful voltages in case of grid faults.

The speed variability of Type III WTs allows for optimizing the energy yield and limiting torque peaks in the mechanical structure of the WT. One of the main advantages of Type III WTs is that the frequency converter is relatively small; see Chap. 8. The consequence of this advantage is, however, that the speed range is limited.

1.2.4 Type IV—Full Variable Speed WTs

Type IV WTs are full variable speed because the generator is entirely decoupled from the grid frequency; see Fig. 18. The generators used in Type IV WTs can be SCIGs, electrically excited synchronous generators or a permanent magnet excited synchronous generators. The choice of generator makes a difference in the control of the excitation of the generator. In the case of an electrically excited synchronous generator, there can be an excitation controller, which varies the DC current in the
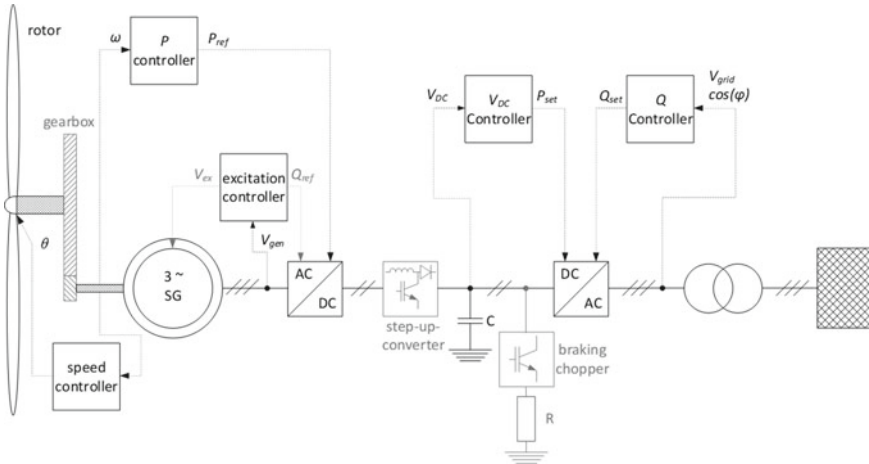
Fig. 18 Type IV—full variable speed WT with full-scale converter

rotor windings. In the case of a permanent magnet, excited synchronous generator or a SCIG the machine-side inverter has to vary the reactive power (Q_{ref}) in the stator of the generator to control the voltage of the stator.

Just like in a Type III WT, also here the machine-side inverter controls the active power, which is extracted from the generator (P_{ref}). The grid-side inverter controls the DC voltage (V_{DC}) in the DC circuit, by feeding power (P_{set}) into, or extracting P_{set} from, the DC capacitor (C). The reactive power, which a Type IV feeds into the grid (Q_{set}), can only be produced by the grid-side inverter.

In the DC link of the frequency converter there might be a step-up converter (shown in gray in Fig. 18) to boost the rectified generator voltage in case of low rotational speed. Also optionally contained in the DC circuit is a braking chopper. The DC chopper might be necessary for dissipating power while the grid voltage is low. This is further discussed in Sect. 3.2.1.

1.2.5 Type V—WTs with Directly Grid-Connected Synchronous Generator

Type V WTs are comparable to Type II WTs. They are of variable speed and the generator stator is AC-connected to the grid. However, the main difference is the generator type. A Type II WT uses an induction generator, which is less advantageous for the PS, because of its reactive power demand. A Type V WT uses an electrically excited synchronous generator; see Fig. 19, which is favorable for the PS, due to the controllability of its reactive power exchange with the grid.

In Type II WTs, the speed variability is achieved with a slip in the generator. In Type V WTs, the speed variability is achieved with mechanical (or rather hydraulic)
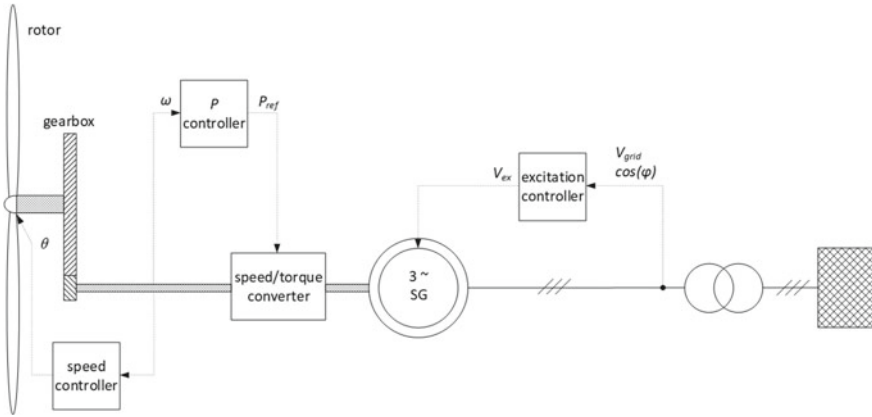
Fig. 19 Type V—variable speed WT with mechanical (hydraulic) torque/speed converter and electrically excited synchronous generator (SG)

slip in the variable transmission stage between the main gearbox and the generator shaft [9].

From a PS's point of view, this WT type is primarily advantageous because of its synchronous generator. It allows the WT to behave like a conventional power plant. The PS protection schemes, which are historically grown to fit synchronous generator-based power production, fit also Type V WTs [10].

1.3 Traditional Aspects of Grid Integration

Connecting a WT to a PS requires a suitable grid connection point. That is, the grid has to be capable of taking on the power from the WT. The suitability of a grid connection point is determined by, among other factors, the short-circuit ratio. The short-circuit ratio can be derived from the short-circuit power of the grid connection point and the rating of the connected wind power installation. The short-circuit power is a measure of the stiffness of the PS and is discussed in more detail in Sect. 2.2.

Physically connecting a WT to a PS does not only require a suitable grid connection point. The correct dimensioning of cables, transformers, switch gear, protection relays and potentially reactive power compensation equipment is premises for safe and reliable operation of the WT. All this equipment has to be selected and parametrized correctly to maintain permissible voltage variations, low flicker and acceptable harmonic distortions during the operation of the WT [4].

However, even perfectly dimensioned grid connection equipment of a WT cannot solve the problem of insufficient power transfer capability of the upstream grid. It is usually the responsibility of the PS operator to facilitate grid connection of WTs.

That is, the short-circuit power at the grid connection point has to be sufficient. If this is not the case, grid reinforcements have to be carried out.

Insufficient power transfer capability can lead to thermal overloading of grid components like lines and transformers, and/or to unacceptable voltages. The thermal time constant of grid components is usually in the range of many seconds to minutes. Hence, thermal overloading is a slow process, which can be responded to in a closed control loop. However, too large power transfer leads to unacceptable voltage drops instantaneously [11].

If WTs are taken into operation although the power transfer capability of the grid is (still) insufficient, the power fed in by the WTs has to be truncated. This so-called feed-in management is usually carried out by the PS operator, who issues maximum power values, which must not be exceeded at the grid connection point of the WTs, i.e. at the point of common coupling. Due to the instantaneous response of the voltage, feed-in management is usually conducted in a precautious manner. Too large power transfer can lead to voltage instability, as discussed in Sect. 2.3, or harmful overvoltages, long before any PS component suffers thermal overloading.

Truncating the power of WTs means lowering the power setpoint of the WTs. Thereby, the energy yield of the WTs is reduced, which means financial losses for the owner of the WTs, unless compensating remuneration is payed. Besides the lower energy yield, feed-in management can also have an impact on the wear and tear in the WT [12]. Hence, it can shorten the service life of the WTs, which is indirectly also a financial loss.

In the beginning of the twenty-first century, many PS operators realized that the share of wind power has increased to an extent, which is no longer negligible. Consequently, WTs had to become reliable sources of power infeed, which meant that they were no longer allowed to disconnect from the grid when a system fault occurred [13]. Short-circuits can occur very frequently in many PSs. Hence, WTs are demanded to remain connected to the grid even in case of short-circuits, i.e. they are demanded to ride through low voltages, which is called "low-voltage ride through" (LVRT). LVRT has been the focus of research and development for a number of years [14].

Since all these aspects have been relevant in the past already, they shall not be discussed in detail in the current edition of this book. Consequently, this edition focuses on the topics, which have been emerging in recent years. These recent topics are introduced in the following section. Although LVRT is nothing new, it is nonetheless discussed in this edition for reasons outlined in Sect. 3.2.

1.4 Overview of Current Challenges of Grid Integration

The transition to renewable energies changes the role of WTs. In the past, they only supplemented the energy production of conventional power plants. These days, wind power is becoming one of the dominating generation technologies. Consequently, WTs have to take over the role of conventional power plants, which also means that

they are becoming responsible for the stability of the PS. Therefore, this chapter focuses on the aspects of grid integration of WTs, which are related to this role reversal.

1.4.1 Grid Topology and Loading of Feeders

For the PS, the change in generation technologies means, primarily, that the number of generators increases dramatically. In the past, the power was produced by a few large power plants. The transition to renewable energies leads to a very large number of geographically dispersed generators. Hence, grid extensions into remote locations, and grid reinforcements of already existing remote feeders, become inevitable.

Since grid reinforcements and grid extensions are usually a lot slower than the installation of WTs, feed-in management will be necessary also in the years to come. To increase the wind energy yield and the degree to which the grid assets are utilized, feed-in management is likely to change. Currently, feed-in management demands WTs to operate at a low power setpoint, which is kept constant for several minutes to hours. In future, the power setpoint is likely to be adapted to the current loading of the grid continuously [11]. Hence, feed-in management will mean continuous power setpoint variations, which makes it comparable to grid frequency stabilization [15]. Consequently, this chapter does not focus on feed-in management as one of the dominant aspects of grid integration. Instead, PS stability with WTs is emphasized.

1.4.2 Power System Stability with Wind Turbines

The definition of PS stability is given in Sect. 1.1.6. It is important to note that the PS has to settle to an acceptable operating point in all locations. This is particularly important when considering the PS voltage. Since WTs are usually installed in remote locations, their grid connection point is often very weak, because the feeders leading to the WT locations are very long. Consequently, it might be difficult for the WTs to feed in their power while maintaining acceptable voltages [16]. The PS voltage is introduced in Sect. 2. The voltage stability at the end of a radial feeder, which is usually the type of feeder used for connecting WTs, is discussed in Sect. 3.

The definition of PS stability does not only apply to the PS voltage but also to the PS frequency. In this context, it is particularly important to note that the PS frequency is a result of the balance between generation and demand. The power consumption usually varies permanently. Increases or decreases in consumption can be anticipated to some extent, but apart from this vague anticipation, the consumption varies without prior warning. Hence, the generation in a PS has to be adapted to consumption. In the case of a PS, which is highly penetrated with wind power, WTs have to be able to adjust their power to the demand. Decreasing the power output of a WT is easy to realize, but increasing the power output, beyond the power in the wind, is only possible with an energy storage. An additional challenge in maintaining the balance between generation and demand with WTs is that the prime energy of WTs, i.e. the

wind, is bound to vary unforeseeably, too. The PS frequency is introduced in Sect. 4 and the capability of WTs to participate in the stabilization of the PS frequency is discussed in Sect. 5.

1.4.3   Inertia Contribution and Short-Circuit Current Contribution

A side effect of the transition to renewable energies is that conventional AC-connected generators are replaced by frequency converters. In the case of state-of-the-art WTs, frequency converters decouple the electromechanical generator from the PS. Hence, the transition to renewable energies leads to a reduction in PS inertia, which makes the control of the PS frequency a difficult task [17].

Another side effect of replacing AC-connected, rotating generators with frequency converters is that the short-circuit current is reduced [18]. Short-circuit current is important for detecting, locating and clearing short-circuits in a PS. Without substantial short-circuit currents, a PS can operate in faulted conditions unnoticed for an indefinite period of time. Synchronous condensers, which are basically electrically excited synchronous generators without prime movers, are proposed as a means of improving the short-circuit contribution of wind farms with Type III and Type IV WTs [19].

Types I, II and V WTs do not cause these problems. However, they are no longer state-of-the-art and are therefore hardly applied in newly built wind farms.

It has to be noted that the focus of this chapter is on the grid integration of WTs. Hence, additional wind farm equipment, like synchronous condensers, is not discussed any further. Alternative WT technologies, which would solve the problem of low PS inertia contribution and low short-circuit current contribution, are proposed in the scientific literature [20]. Such technologies would avoid additional wind farm equipment, but cannot be found on the WT market, and are hence irrelevant for current PSs.

1.4.4   Grid Code Requirements

The requirements for connecting WTs to PSs vary from country to country, but all these requirements have in common that they strive for maintaining PS stability with the help of WTs. Requirements regarding voltage and frequency control and operating ranges, in particular LVRT, have been stipulated in European grid codes for many years [21]. Beyond these requirements also power quality, like flicker and harmonic distortion, communication with WTs and wind power forecasting, as well as requirements specifically for offshore wind farms, exist in many, also non-European, countries [22]. In the United States of America, the requirements for connecting WTs to the grid are different for the different states [23].

If WTs are to participate in balancing generation and demand, it might be inevitable to apply energy storage. Potentially, PS operators consider such energy storage as additional equipment, instead of considering them as being part of a wind

farm. In this case, different requirements might apply specifically to the energy storage and their grid connection infrastructure [24].

Examples of current grid codes, or requirements, which are comparable to these, are mentioned in the context of the grid voltage in Sect. 3 and in the context of the grid frequency in Sects. 4 and 5.

1.4.5   Mechanical Loads Resulting from Grid Services

It has to be noted that the newly emerging grid services have an increasing impact on the mechanical loads on the structure of the WT. Mechanical loads, i.e. wear and tear in the mechanical part of a WT have, strictly speaking, no influence on the capability of WTs to provide grid services. However, mechanical loads can reduce the service life of a WT. As a consequence, the levelized cost of energy from a WT is affected by the mechanical loads. The price per kilowatthour (kWh) has a direct influence on energy trading, which is the basis for the power exchange in the grid. Therefore, also information about the mechanical loads, which result from the considered grid services, is given in the following sections. It has to be noted, though, that neither detailed load analysis nor specific energy costs are mentioned, as this would be beyond the scope of this chapter.

2   Power System Voltage

When a WT feeds its power into a PS, current has to flow through the different grid components before the generated power arrives at the consumer. All grid components are characterized by their impedances, which cause voltage drops when current flows through them. The most important grid components are generators, cables, overhead lines and transformers, as these are mainly responsible for the voltage drops caused by power transfer.

2.1   Equivalent Circuits of Power System Components

An equivalent circuit is a theoretical connection of basic electrical elements, which exhibits the same electrical behavior as the PS component, which it has to represent. Since all PS components impede current, equivalent circuits comprise impedances. However, as already introduced in Sect. 1.1.4, reactances can be expressed in terms of complex numbers if only the steady state is of interest. The instantaneous electrical behavior results from the fact that both inductances and capacities are energy storages. Hence, the integral Eq. 11 and the differential Eq. 14 need to be applied in order to also assess the instantaneous behavior of grid components.

The equivalent circuits of all PS components have to represent the voltage drop that occurs when current flows through them. When a WT is integrated into a PS, the voltages, which result from the power that the WT feeds into the grid, are of interest. Therefore, in the following the relation between current and voltage is considered. This consideration is extended to the relation between power and voltage in Sect. 2.2.

As introduced in Sect. 1.1.2, in PS analysis the three phases are reduced to one equivalent phase, whenever the loading of the three phases is equal enough to consider them identical. Therefore, the equivalent circuits shown here are also single-phase equivalents of the three-phase PS components.

2.1.1 Generators

A WT can, as any other generator, be considered an infinitely stiff voltage source behind an impedance. Infinitely stiff means that the source voltage is not affected by the current, which is drawn from this source. Since this would be unrealistic, there has to be an impedance, which causes a voltage drop as a function of the current; see Fig. 20. Generally, generators in an AC PS behave inductive. Rotating electro-magnetic machines comprise coils for producing the magnetic field, which links the stator and the rotor. Frequency converters comprise filter chokes at their terminals for making their current sinusoidal. Hence, all types of generators that can be found in the different WT types (see Sect. 1.2) behave inductive. Therefore, they can be represented as voltage sources behind inductances; see Fig. 20.

If the operating point of a generator changes, the magnetic energy stored in the inductance changes, too. Transients in the voltage lead to transients in current; see Fig. 9. Hence, when representing the instantaneous behavior of a generator, the voltage across the inductance has to be expressed with the differential Eq. 14. For the sake of simplicity, it is desirable to avoid differential equations in PS analysis whenever possible. In this case, the inductance is expressed as impedance or reactance; see Eq. 13. However, changes in the energy stored in an inductance cannot be represented realistically with steady state impedances. Therefore, as a trade-off,
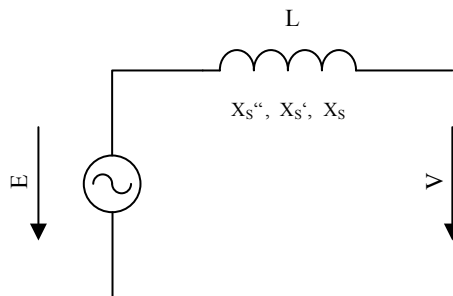
Fig. 20 Voltage source behind an inductance (or impedance) representing the electrical behavior of a generator

the inductance of a generator is represented with different reactances, depending on the state of operation of the generator: subtransient reactance (X_S''—applies initially after the occurrence of a transient event), the transient reactance (X_S'—applies in the transition from transient to steady state) and the synchronous reactance (X_S—applies in steady state operation).

Voltage source frequency converters, which are commonly used in WTs, do not only comprise an inductive filter choke. There is also a DC capacitor as energy storage between the AC/DC inverter and the DC/AC inverter; see Chap. 8. Both energy storages, as well as the inductance of the rotating generator, have substantial charging time constants (Eqs. 12 and 15), which can be in the same order of magnitude as the mechanical time constants of a WT. These energy storages have a bearing on the choice of the reactances in the equivalent circuit. Besides, they are not only of interest for assessing the grid behavior of a WT but also for assessing the dynamic behavior of the WT itself.

2.1.2 Lines and Cables

Overhead lines and underground (or subsea) cables can be represented with the so-called π-model. Figure 21 reveals that power lines are resistive (there is inevitably resistance (R) involved, which dissipates energy), inductive (L) and capacitive (C). Resistance and inductance are in the length path, i.e. they are affected by the current, which flows through the cable. The capacity is in the shunt path and is divided among the two ends of the line. It has to be noted that the π-model is only applicable to short lines. Longer lines are series connections of π-models.

The difference between an overhead line and an underground or subsea cable is the insulation material. Overhead lines use air as insulation material, which is cheap, universally available and self-healing (more about this in Sect. 2.4). Underground cables use plastics, paper and/or oil as insulation material, which have a much higher insulation voltage than air. Therefore, the distance between the conductors in a cable is by orders of magnitude smaller than the distance between conductors in an overhead line.
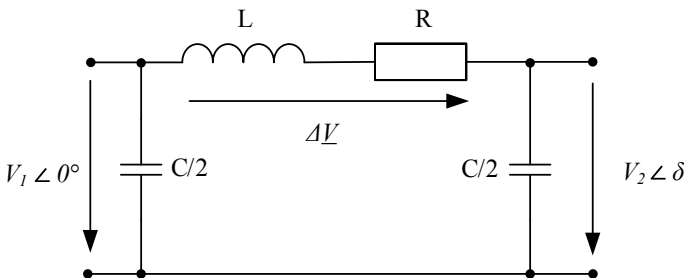
Fig. 21 π-model of an overhead line or an underground cable

The setup of the π-model reveals that the inductance and the resistance cause the voltage drop, $\Delta \underline{V}$, when the line is loaded. The capacity, on the other hand, dominates the behavior when the considered line is only lightly loaded, or even open circuit.

Both the inductance and the capacity are affected by the distance between the conductors (the distance between phase conductors or the distance between phase and ground). Besides the distance, d, also the length, l, the radius, r, of the conductor, as well as the permeability of the insulation material, μ_0, determine the inductance:

$$L = \frac{\mu_0 \cdot l}{2 \cdot \pi} \left(\ln \frac{d}{r} + \frac{1}{4} \right) \tag{25}$$

The capacity is furthermore affected by the dielectric coefficient of the insulation material, ε:

$$C = \frac{2 \cdot \pi \cdot \varepsilon \cdot l}{\ln \frac{d}{r}} \tag{26}$$

Comparing Eq. 25 with Eq. 26 reveals that with increasing distance between the conductors (d), the inductivity increases and the capacity decreases. Consequently, overhead lines are primarily inductive, while underground cables are primarily capacitive.

Looking at the equations Eqs. 10 and 13, it becomes obvious what different effects the capacity in the shunt path and the inductance in the series path of a line have: The inductance causes a voltage drop whenever the line is loaded. The capacity, on the other hand, is a negative reactance when exposed to AC voltage. That is, it generates reactive power. When this reactive power flows through the series impedance of the line, a voltage drop occurs in the negative direction. Hence, when the line shown in Fig. 21 is only lightly loaded or even open circuit on the receiving end, the voltage on this end, V_2, increases. This phenomenon is particularly relevant for offshore wind farms, where the subsea cables are often very long, and where the applied voltage is as high as somehow possible to minimize losses. Therefore, offshore wind farms are often connected via HVDC links to the onshore AC grid. If an AC connection is chosen, inductive reactors need to be installed in the wind farm to absorb the reactive power generated in the cables. Otherwise, the voltage in the wind farm can reach destructive values when the wind farm exchanges only a little power with the onshore AC grid.

2.1.3   Transformers

A transformer is inductive and resistive (losses). In contrast to lines and cables, transformers have no capacity, which is of relevance for PS considerations. Therefore, the equivalent circuit of a transformer looks as shown in Fig. 22.

The task of a transformer is to step the voltage up or down from one voltage level to another. Hence, it might be surprising to see the equivalent circuit of a transformer in
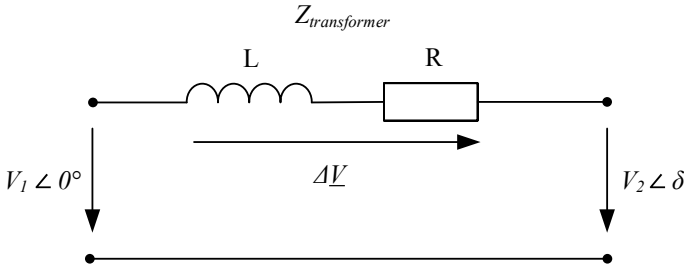
Fig. 22 Transformer model in per unit representation, comprising inductance and resistance

Fig. 22, where the primary voltage, $\underline{V}_1$, and the secondary voltage, $\underline{V}_2$, are identical as long as no current flows. Here, it is important to note that different voltage levels are dealt with best when using the per unit (pu) representation as introduced in Sect. 1.1.3. When applying the pu system, the voltage levels disappear, and the current appears to flow through a transformer like it does when it flows through a line.

2.2 Power System Stiffness and Short-Circuit Power

A PS, where power is produced in generators and transmitted to the loads via lines and transformers, exhibits voltage drops, which depend on the flowing current. The voltages at the terminals of the generators and the loads have to be in particular ranges, as it otherwise might be destructive for the grid equipment and/or unusable for the consumers.

How much the voltage in a PS responds to the current is called the PS stiffness. A stiff PS exhibits rather constant voltages, even when the current varies considerably. The PS stiffness can be quantified by the short-circuit power and the short-circuit ratio.

The short-circuit power is the power, which an infinite busbar feeds into a short-circuit. Figure 23 visualizes the concept. The case shown is the WT feeder already shown in Fig. 6 and simplified to Fig. 12. In Fig. 23, the WT is replaced by a short-circuit, into which the infinite busbar with its voltage, $\underline{V}_{\text{inf}}$, drives the short-circuit current $\underline{I}_{\text{SC}}$.

Hence, the short-circuit power is in single-phase pu representation:

$$\underline{S_{SC}} = \underline{V}_{\text{inf}} \cdot \underline{I}_{\text{SC}}^*$$ (27)

When a short-circuit suppresses the voltage to zero, the whole voltage of the infinite busbar has to drop along the line ($\underline{V}_{\text{inf}} = \Delta \underline{V}$). Therefore, the short-circuit power can also be expressed with the short-circuit impedance, $\underline{Z}_{\text{SC}}$, and the short-circuit current, $\underline{I}_{\text{SC}}$:
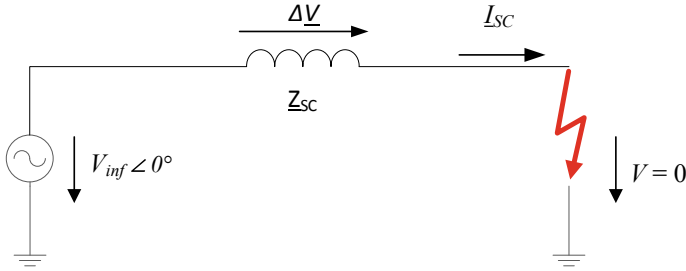
Fig. 23 Short-circuit in a PS

$$\underline{S}_{SC} = \left| \underline{Z}_{SC} \right| \cdot \underline{I}_{SC} = \frac{V_{inf}^2}{\left| \underline{Z}_{SC} \right|} \qquad (28)$$

Unfortunately, the short-circuit power is not easily applicable to a particular WT to be connected to the PS. The short-circuit power has to be put into perspective with the rated power of the WT, $\underline{S}_{WT}$. For this purpose, the short-circuit ratio, SCR, is introduced:

$$SCR = \frac{\left| \underline{S}_{SC} \right|}{\left| \underline{S}_{WT} \right|} \qquad (29)$$

When considering a grid connection point for a WT, the suitability of this connection point can be quantified in terms of the short-circuit ratio. The ranges given in Table 1 are defined by Boemer [16].

In the example in Fig. 5, which is further applied in Fig. 23, the simplification is made that the whole feeder between the infinite busbar and the WT (or the short-circuit) is purely inductive. This is, of course, not entirely true. In reality, there is always some resistance related to any conductor. Therefore, it is more realistic to consider the short-circuit impedance a complex number comprising a real and an imaginary part:

$$\underline{Z}_{SC} = R_{SC} + jX_{SC} \qquad (30)$$

In PS analysis, usually power flow is considered rather than current flow. (Current only becomes indispensable when the voltage is faulted and potentially suppressed

Table 1 Suitability of grid connection points quantified in terms of short-circuit ratio [16]	"Strength" of a grid connection point	Short-circuit ratio at the point of common coupling
	Strong	>10
	Modest	5–10
	Weak	<5

to low values.) Power flow yields immediate insight into the loading of a PS and into the operating points of its components. Therefore, it would be advantageous to have an expression for the voltage drop, ΔV, which comprises active and reactive power, rather than current. The relation between voltage drop and real and imaginary part of the apparent power (i.e. P and Q) can be derived graphically from the phasor diagram of a closed voltage loop. The derivation of this phasor diagram is beyond the scope of this chapter. Applying this graphical methodology to the circuit shown in Fig. 12, and applying Eq. 30 as an expression for the impedance of the conductor, leads to the expression in Eq. 31. (The sending end voltage is V_{inf}.)

$$\Delta V = \frac{P \cdot R_{\text{SC}} + Q \cdot X_{\text{SC}} + P \cdot X_{\text{SC}} - Q \cdot R_{\text{SC}}}{V_{\text{inf}}} \tag{31}$$

However, the phasor diagram would reveal that the part of ΔV, which is projected onto the imaginary axis, is negligibly small. Hence, as a good approximation, the voltage drop, ΔV, can be expressed with the following expression in terms of active power, reactive power and short-circuit impedance:

$$\Delta V \approx \frac{P \cdot R_{\text{SC}} + Q \cdot X_{\text{SC}}}{V_{\text{inf}}} \tag{32}$$

From this relation, it becomes obvious that not only the short-circuit ratio is of interest but also the relation between reactance and resistance. This so-called X over R ratio describes the nature of a PS. Transmission of the active power, P, is the inherent purpose of a PS. Therefore, there is no way ΔV can (or rather should) be controlled with active power. Instead, reactive power, Q, should be used to control the voltage, while the intended active power is transmitted. Consequently, it would be advantageous if the PS was dominated by reactance and if resistance was as small as possible. Small resistance means little power losses, i.e. high efficiency, while large reactance provides good control over the voltage via reactive power. Table 2 summarizes the connection between X/R ratios and voltage levels.

Table 2 Qualitative X/R ratios in different voltage levels

Voltage level	X/R ratio	Reasons, consequences
Low	Small	• Low voltage = large current → comfortable cross section of conductor would be expensive → large R • Low insulation required → smaller distance between conductors → inductance in series path of conductor (see Fig. 21 and Eq. 25) is small → small X
High	Large	• High voltage = small current → small cross section of conductor required, but conductor must not be too thin, as otherwise its mechanical strength would be insufficient → small R • High insulation voltage required → large distance between conductors → inductance in series path of conductor (see Fig. 21) is large → large X

In transmission systems, the X/R ratio is usually between 8 and 10, while in distribution systems it is often well below 6.

2.3 Voltage Stability

Remembering the definition of PS stability (see Sect. 1.1.6), it is particularly important to remember that it applies to any location in the PS. Remembering also that voltage is controlled best with reactive power (see Sect. 2.2) leads to the dedicated definition of voltage stability: *Voltage stability is the ability of a PS to control the voltage, V, with reactive power, Q, in any location of the PS. That is, the V-Q sensitivity has to be positive at every busbar in the PS.*

The problem can be described with a radial feeder, where a generator, e.g. a WT, feeds power into one end and a load receives the power at the other end; see Fig. 24.

The generator end of the line is considered to be the reference. Therefore, the angle of the generator voltage, $\underline{V}_1$, is considered to be 0°. Consequently, the voltage at the receiving end, $\underline{V}_{\text{load}}$, varies in magnitude and angle, δ, according to the voltage drop, $\Delta \underline{V}$, across the line impedance, $\underline{Z}_{\text{line}}$.

The purpose of generators is to provide the consumers with active power. Therefore, the active power flowing into the load impedance is shown on the horizontal axis of the diagram in Fig. 25. The reactive power, on the other hand, is a means of controlling the load voltage at any desired active power operating point. In order to quantify the share of these two power components, the commonly used power factor is applied; see Eq. 18. Figure 25 shows the voltage versus load power for different power factors. Positive power factor means capacitive, i.e. leading power factor, which corresponds to an overexcited operation of a synchronous generator. (In the example of Figs. 12 and 13, this corresponds to a WT voltage, $\underline{V}_{\text{WT}}$, larger than the voltage at the infinite busbar, $\underline{V}_{\text{inf}}$). Negative power factors refer to inductive, i.e. lagging power factors, which corresponds to underexcited operation of a synchronous generator.
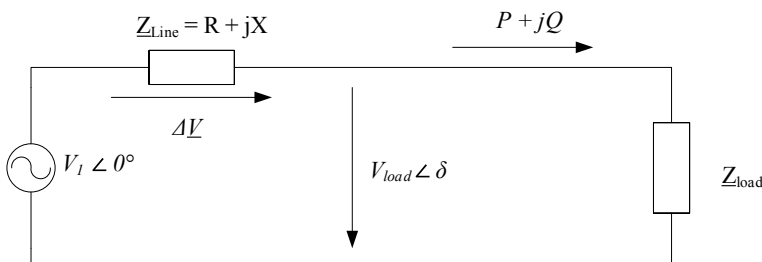
Fig. 24 Radial feeder with line impedance, $\underline{Z}_{\text{line}}$, to which a generator is connected on one end and a load with impedance $\underline{Z}_{\text{load}}$ is connected to the other end
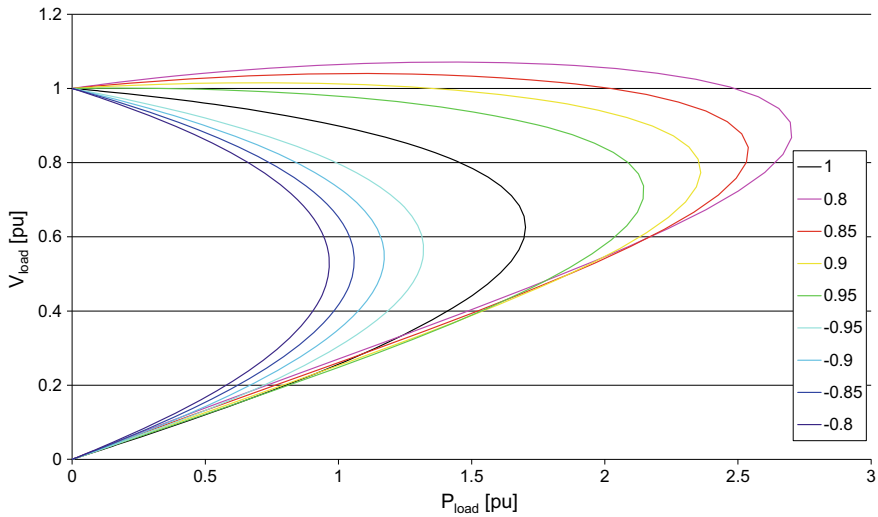
Fig. 25 Receiving end voltage versus active power for different power factors illustrating voltage collapse at radial feeder

Figure 25 shows that active power can be increased to a certain point, beyond which the voltage collapses. Considering neutral power factor ($\cos(\phi) = 1$), i.e. active power transfer only, the load voltage decreases with increasing power. The maximum active power transfer can only be extended by reducing the power factor to capacitive operation. (Inductive (negative) power factors make the situation even worse).

Figure 25 suggests that any arbitrary active power transfer could be achievable if only sufficient reactive power is fed into the feeder. However, Eq. 16 has to be kept in mind, which makes clear that an increase in power comes at the cost of increased current. Eventually, the conductors of the feeder will be overloaded thermally if active and reactive power lead to excessive current.

The above-mentioned definition of voltage stability refers to voltage versus reactive power sensitivity. Therefore, Fig. 26 shows the load voltage as a function of reactive power. (Obviously, not all active power operating points in Fig. 25 can be considered in Fig. 26). Stable operating points are those which are above the voltage collapse point in Fig. 25. In Fig. 26, stable operating points are characterized by positive slopes in the voltage versus reactive power curves. That is, a PS is stable when it can increase the voltage with increased reactive power infeed in all locations, and vice versa.
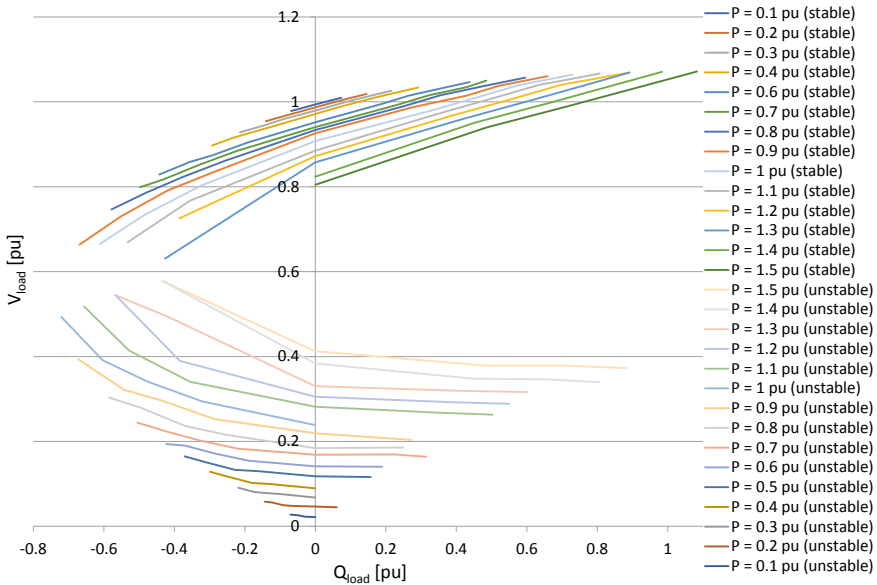
Fig. 26 Receiving end voltage versus reactive power for different active power operating points in Fig. 25

2.4 Transient Voltage Drops

The voltage in a PS is hardly ever constant. As discussed in the previous sections, it varies with the loading of the system. While it is the intention of PS operators to maintain the voltage within certain boundaries, this is not always possible. It has been discussed above that particularly the reactive power has a strong influence on the voltage. In situations where large amounts of reactive power are transmitted through the system, the voltage is bound to vary strongly, too. Connection of large inductive loads, e.g. the magnetization of a large induction machine, can cause local and temporary voltage drops below the lower boundary of the normal voltage range.

Another common cause for transient voltage drops is short-circuits in the system. Conductors, which use air as insulation material, e.g. overhead lines or busbars in substations, are particularly prone to suffer short-circuits. A short-circuit in air causes an arc consisting of ionized air. Hence, an arc is highly conductive. Due to the high conductivity of ionized air, the short-circuit current, which the PS voltage drives into an arc (compare Fig. 23), is very large. Large short-circuit currents cause large voltage drops along the lines in which they flow. Therefore, short-circuits can be sensed as voltage drops, not only in the location of the short-circuit but also in neighboring grid locations.

The disadvantage of using air as an insulation material is that short-circuits can happen quite frequently. Contaminations on insulators or lightning strikes on over-head lines are frequently occurring system disturbances. On the other hand, the

advantage of using air as an insulation material is that it is self-healing. If the current supply to an arc is interrupted, the arc extinguishes and the insulation strength of air recovers within hundreds of milliseconds. Therefore, protection relays in PSs open the circuit breakers on either side of a line, as soon as a short-circuit is detected on this line. After opening the circuit breakers, the protection relays wait for about one second, before they close the circuit breakers again. This so-called auto-reclosure intends to extinguish arcs in anticipation that the initial cause for the short-circuit (e.g. dirt on insulators or lightning strike) has gone. If after closing the circuit breakers the short-circuit re-occurs, the procedure might be repeated once or twice, depending on the resilience of the affected PS components.

Short-circuits can occur between the three phases, between two phases, between three or two phases and earth, or between one phase and earth. These different fault types have different consequences for the PS. Most severe are three-phase short-circuits, however, these occur only rarely. The most common type of short-circuit is the single-phase-to-earth fault.

Short-circuits are perceived as transient voltage drops by consumers and generators, which are connected to the PS in the vicinity of the fault location. Most consumers do not even notice transient voltage drops. If the consumers notice it at all, they might find it a nuisance, e.g. because of flickering light intensity from electric illumination. Hardly any consumer disconnects from the grid, merely because of a transient voltage drop. Hence, the standard is that consumers resume power consumption as soon as the voltage recovers.

In contrast to consumers, for rotating generators, the consequences of transient voltage drops at their terminals are a lot more severe. While the voltage is low, the electric power is potentially low, too. In the extreme, when the voltage is suppressed to zero volts, the electric power has to be zero; see Eqs. 16 and 17. The electric power can drop almost instantaneously. The electric torque of a rotating generator depends on the electric power and the rotational speed. If the electric power drops steeply, also the electric torque has to drop steeply. This means that the electric output torque drops almost instantaneously, while the mechanical driving torque of the generator is still there in unchanged extent; see Fig. 27.

The rotational speed of a generator, ω, is affected by the imbalance between driving torque, T_{mech}, and output torque, T_{elec}, which act on the inertia, J, of a generator.

Fig. 27 Mechanical input torque, T_{mech}, driving the inertia, J, of a generator, which produces the electric output torque T_{elec}
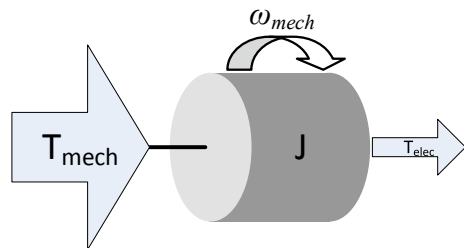
$$\frac{d\omega}{dt} = \frac{T_{\text{mech}} - T_{\text{elec}}}{J} \tag{33}$$

Hence, transient voltage drops invariably lead to the acceleration of rotating generators. However, this acceleration must not lead to the disconnection of the generators, because the consumers stay connected to the grid and resume power consumption despite the transient voltage drop. If generators disconnect because of acceleration, the balance between generation and demand is upset. As a consequence, a local transient voltage drop could lead to system-wide instability in the grid frequency. This is further discussed in Sect. 4.

3 Voltage Stability with Wind Turbines

Favorable locations for WTs are usually determined by the wind potential, and not normally by the location where the electric energy is needed. Therefore, most WT feeders are radial feeders reaching out to the WT locations and bringing the power of the WTs to the PS. Hence, WTs have to be able to maintain acceptable voltages at the end of radial feeders, as discussed in Sect. 2.3.

The radial feeder setup also poses problems in the case of short-circuits near the WT. While the short-circuit is on, the voltage is suppressed and leads to the acceleration problem introduced in Sect. 2.4. However, while the protection relays try to clear the fault, it is likely that the WT is in open-circuit operation. That is, it has no connection to the rest of the PS to export decelerating power, until the auto-reclosure.

3.1 Voltage Support with Wind Turbines

Since WTs are an indispensable part of the generation mix in many PSs, the requirements in terms of voltage support are comparable to the requirements demanded from conventional power plants with synchronous generators. The voltage support requirements are usually stipulated in terms of reactive power at a given active power operating point. Figure 28 shows an example, where the active power, P, is given in pu (referred to the rated active power, P_{rated}) on the vertical axis. The demanded reactive power, Q, is also given per rated active power, P_{rated}. In the example requirement shown in Fig. 28, the blue dashed line is the boundary of the operating range which has to be achievable. This requirement looks similar to the $P - Q$ requirements in many grid codes. It is the worst-case scenario taking the requirements of several countries into account [21]. The WTs, which have to fulfill these requirements, have to be capable of providing reactive power (up to 0.1 kVAr/kW$_{\text{rated}}$ capacitive or inductive), even when the wind does not allow for active power production. During active power production, the capacitive reactive power requirement is slightly more
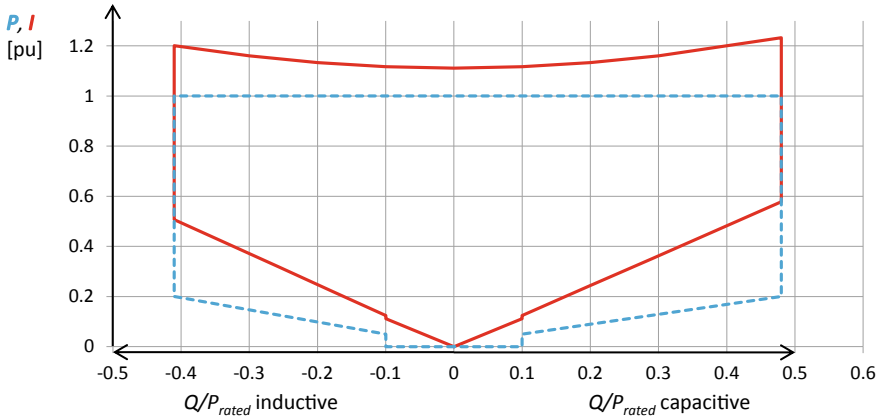
Fig. 28 Exemplary $P - Q$ requirement (blue dashed line) for voltage support with reactive power. The current for fulfilling this requirement (red line) is given for grid voltage $= 0.9$ pu

extensive (reaching up to 0.48 kVAr/kW$_{\text{rated}}$) than the inductive one, because many PSs are mainly inductive. That is, they need reactive power production to compensate for the reactive power demand of lines and transformers.

The demanded reactive power even at full active power ($P = 1$ pu) means that the current rating of the WT has to be considerably larger than what is needed for rated active power only. To illustrate this problem, Fig. 28 also shows the current in pu (on the basis of rated active power and rated voltage) for a slightly suppressed voltage of 0.9 pu. The current is derived with Eqs. 16 and 20. The red current curve in Fig. 28 shows clearly that the grid connection equipment of WTs, which have to fulfill such reactive power requirements, have to be suitable for permanent currents that are about 20% larger than the rated current.

The ability to support the grid voltage is highly dependent on the WT type, i.e. on the generator technology. The comparison of the different WT types in Sect. 1.2 reveals that there are WTs with and without power electronic frequency converters. The beauty of frequency converters is that they can produce reactive power independent of the active power operating point. By varying the magnitude of their source voltage, they can increase or decrease the reactive power production or absorption independently of the active power; compare with Fig. 13. The voltage in the DC circuit and the current rating of the frequency converter are the only limits.

The WT Types I and II have generators, which need to import reactive power for magnetization. These WTs can only compensate the reactive power demand of their generators with additional compensation equipment, e.g. capacitors; see Figs. 15 and 16. These so-called capacitor banks consist of single capacitors, which are connected and disconnected with contactors. The reactive power demand of the induction generator depends on the active power operating point, which varies with the wind speed.

Compensating the reactive power demand of the generator, and at the same time supporting the grid voltage with reactive power, as shown in Fig. 28, requires the installation of large capacitor banks. Hence, grid voltage support is only possible to a limited extent, with limited precision and with limited response speed. If requirements as shown in Fig. 28 are to be fulfilled with Type I or Type II WTs, the effort in additional compensation equipment is substantial. The consequence might be that the economic advantage of these WTs is no longer given.

Type III WTs can provide reactive power via the grid side inverter, or with the machine side inverter via the excitation of the DFIG; see Fig. 17. Fulfilling the requirements shown in Fig. 28 means that either the grid side inverter or the machine side inverter and the generator have to be rated to permanently larger currents.

Type IV WTs have a full-scale converter (see Fig. 18), which can provide any active and reactive power. However, the current rating of this frequency converter has to be chosen to permanently sustain currents larger than rated. The response speed is, as typical for frequency converters, more than sufficient, which is favorable for grid voltage support.

Type V WTs comprise synchronous generators, which are usually electrically excited, and directly connected to the grid; see Fig. 19. The $P - Q$ behavior of such WTs is very comparable to conventional power plants. In part load, the active power, i.e. the load angle, delta, in the synchronous generator varies with the wind speed; see Fig. 13. Varying load angle means that the excitation has to be varied too, if a certain reactive power is to be maintained, as specified in Fig. 28. Electric excitation systems are usually sufficiently quick for varying the reactive power of a synchronous generator, at least as quickly as the load angle varies.

3.2 Low Voltage Ride Through with Wind Turbines

Some of the most demanding grid code requirements revolve around the ability to ride through transient voltage drops. This functionality is called low voltage ride through (LVRT). The LVRT capabilities of the different WT types [14] are discussed in the following, as LVRT has various implications for the grid and for the WTs.

3.2.1 Drive Train Acceleration and Active Power Recovery

As indicated in Sect. 1.3, LVRT is dealt with here, although it has been a state-of-the-art requirement for many years already. From a PS's point of view, LVRT is an important functionality of generators, as outlined in Sect. 2.4, and LVRT with WTs is a game changer for two reasons: (i) In many PSs, the generated power from WTs exceeds the generation from conventional power plants, which are based on AC-connected synchronous generators. (ii) The LVRT capabilities of variable speed WTs are a lot more advantageous compared to those of conventional power plants.

During a transient voltage trough, WTs, like all other rotating generators, accelerate (see Eq. 33), because of the inevitable imbalance between mechanical driving power, P_{mech}, and electric power that can be exported despite the suppressed voltage, P_{elec}:

$$\Delta P = P_{\text{mech}} - P_{\text{elec}} \tag{34}$$

Hence, WTs have to accumulate the excess power, ΔP, for the duration of the voltage trough, t, in the form of kinetic energy, E_{kin}:

$$E_{kin} = \Delta P \cdot t = \frac{1}{2} \cdot J \cdot \left(\omega_{\text{end}}^2 - \omega_{\text{start}}^2 \right) \tag{35}$$

The angular speed ω_{start} is the speed of the WT at the time of the voltage drop, while ω_{end} is the speed at voltage recovery.

The drive train of a WT exhibits substantial flexibility in torsional direction, which is why it can be represented as a spring-mass-oscillator, as depicted in Fig. 29. If such a drive train experiences a voltage drop, i.e. if T_{elec} drops, while the aerodynamic driving torque, T_{rot}, remains unchanged, also the torsional stiffness, k, of the drive train gets unloaded. The twist angle, β, by which the drive train is twisted due to the loading, is reduced. An instantaneous unloading of such a flexible drive train causes the inertia on the low-speed shaft, J_{lss}, and even more so the inertia on the high-speed shaft, J_{hss}, to oscillate against the torsional stiffness. Hence, the drive train accelerates not only because of the accumulation of excess driving power but also because of the oscillations to which it gets excited by the step change in T_{elec}.

Looking at Fig. 15, it becomes obvious that Type I WTs can only perform LVRT if there is a pitch control, which allows reducing the rotor torque with the pitch angle, θ, when the drive train accelerates. Otherwise, the time available before the induction generator has exceeded its breakdown slip is extremely short. After exceeding the breakdown slip, a squirrel cage induction generator provides only little torque, which invariably leads to overspeeding.
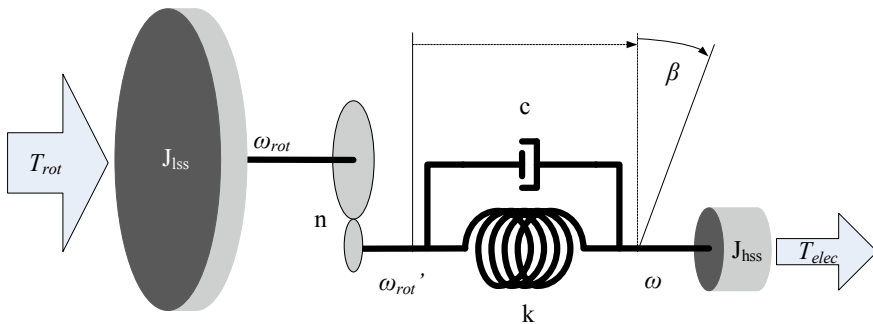
Fig. 29 Mass-spring-damper model of a WT drive train comprising a gearbox
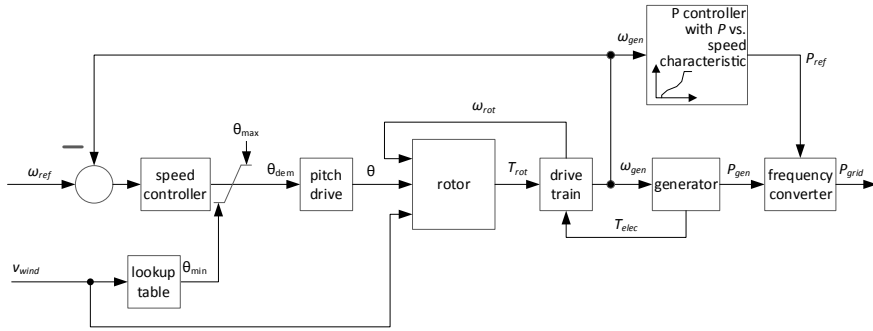
Fig. 30 Simplified control circuit of a variable speed WT with speed control via the pitch angle and power (torque) control via the frequency converter

For the WT structure, the steep power variations, during the voltage drop and the voltage recovery, invariably mean harmful steep torque variations, due to the constant rotor speed. Different solutions to these problems have been proposed in the literature. One of them is the slip-synchronous concept, where the advantages of synchronous generators are combined with the slip variability of induction generators to be used in Type I WTs [25].

All other WT types are of variable speed, which means that they control their speed with the pitch angle; see Figs. 16, 17, 18 and 19. Hence, all these WTs can mitigate the acceleration by reducing the aerodynamic driving torque, although the speed, with which the pitch angle can be varied, is slow (only up to about 10°/s, in the case of small WTs, and less than that in multi-MW WTs).

The simplified control circuit of a variable speed WT, as shown in Fig. 30, comprises the speed control loop and the power control loop. This control circuit applies to the WT Types II, III, IV and to some extent also to Type V. The power is controlled with the power electronic converter (except for WT Type V), depending on the measured generator speed, ω_{gen}. The generator speed is controlled with the speed controller, which varies the pitch angle accordingly.

The control circuit in Fig. 30 reveals that the speed controller responds automatically if LVRT leads to an increase in generator speed beyond rated speed, ω_{ref}. Due to the low response speed of the pitch drive, the speed controller can only respond adequately to longer voltage drops. In case of short voltage drops, too drastic pitch angle variations can lead to undesirable power dips once the voltage recovers. The speed controller has to find a trade-off between overspeed and undershooting the desired speed due to oscillations. Oscillations in the generator speed are normally damped by controlling the electric power, i.e. the generator torque accordingly. This is obviously not possible while power export to the grid is hampered due to low grid voltage. Hence, also generator speed oscillations can lead to undesirable operating points once the grid voltage recovers. When the voltage recovers, the active power infeed is, again, determined by the power controller with the power versus speed characteristic. If the generator speed happens to be on a downswing in its oscillation,
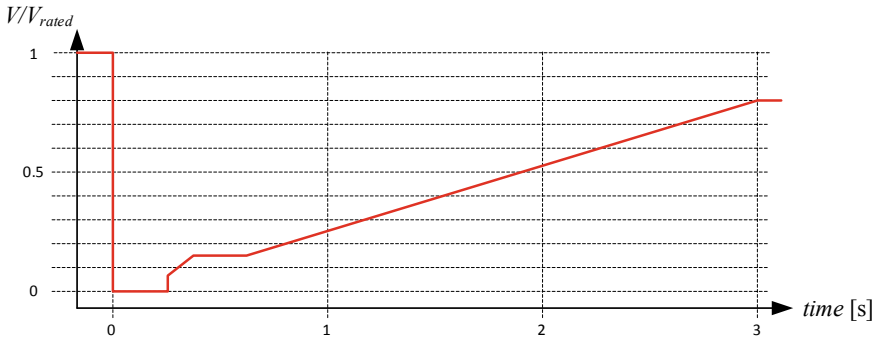
Fig. 31 Exemplary LVRT requirement [21]

or if the pitch angle is too large, in the time the grid voltage recovers, the active power might be too low and needs to be ramped up quickly.

Figure 31 shows exemplary LVRT requirements that span the requirements of different countries [21]. The vertical axis in the diagram in Fig. 31 shows the voltage in pu, while the horizontal axis shows the duration of a transient voltage drop. The time 0 s is the beginning of a transient voltage drop. The red curve contours the operation region, which has to be possible. Operation above the red curve is required without disconnecting the WT from the grid. Below the red curve, i.e. when the voltage drops deeper and/or for longer than what is contoured with the red curve, the WT may disconnect, or has to disconnect from the grid. This is stipulated in the applicable grid codes.

The requirement shown in Fig. 31 reflects the acceleration problem discussed above. The deeper the voltage drops, the less the electric power can be exported to the grid. That is, less electric torque is available in a WT for mitigating the drive train acceleration. Consequently, the deeper the voltage drops, the shorter the time, during which operation has to be sustained. The higher the value to which the voltage drops, the less kinetic energy has to be accumulated, and the less severe the excitation to oscillations. Therefore, longer LVRT is demanded because pitch control can, although it is slow, avoid dangerous overspeeds.

The steep torque variations, resulting from voltage drops and voltage recoveries, pose a burden for the mechanical structure of a WT. The same applies to overspeeds, which can develop during voltage troughs. The acceleration of a WT drive train can be mitigated with quick pitching of the rotor blades. However, this limitation of the rotational speed comes at the price of harmful variations of the aerodynamic thrust, which causes fatigue, mainly in the WT tower [26]. Some Type IV WTs mitigate mechanical loads by applying braking resistors in the DC circuit of the full-scale converter; see Fig. 18. A braking chopper controls the power, which is absorbed from the DC circuit, and dissipates it in braking resistors. These heat losses compensate for some of the electric power, which cannot be fed into the grid while the voltage is low.

3.2.2 Reactive Current Provision

As discussed in Sect. 3.1, WTs have to feed reactive power into the grid in order to support the grid voltage. Voltage support is even more important when the voltage is low due to a fault in the system. In the case of LVRT, it is impracticable to specify the demanded voltage support in terms of reactive power, because power varies with voltage. Therefore, whenever the voltage is outside the tolerance range of normal operation, the voltage support is specified in terms of reactive current. Figure 32 shows an exemplary reactive current requirement. In this requirement, the WT has to feed its rated current in the form of reactive current, already when the voltage has dropped to 50% of the rated voltage. The reactive current only serves the grid voltage. However, if a WT also wants to mitigate its acceleration problem, as discussed in Sect. 3.2.1, it also has to feed active current into the grid. Consequently, the grid connection equipment of a WT has to be designed to temporarily sustain considerably larger currents than rated current.

Type I and Type II WTs are hardly able to provide sufficient reactive current with their compensation capacitors alone. Hence, unless such WTs are supplemented with power electronic reactive current sources like static synchronous compensators (STATCOM), they cannot fulfill common reactive current requirements for voltage support during LVRT. It has to be mentioned, though, that induction generators temporarily feed substantial reactive currents into the grid, when the grid voltage drops. This reactive current results from the fact that the magnetic energy in the coils of the generator gets drained. A comparable effect is shown in Fig. 9. Therefore, this reactive current cannot be sustained. But, even worse, this reactive current has to be imported from the grid when the voltage recovers and the generator needs to get re-magnetized again. Absorbing reactive current (i.e. inductive current) hampers the voltage recovery, and is, therefore, undesirable from a PS's point of view.

Type III and Type IV WTs can provide the required current if their frequency converters are designed to be overloaded temporarily. (More on this problem in the
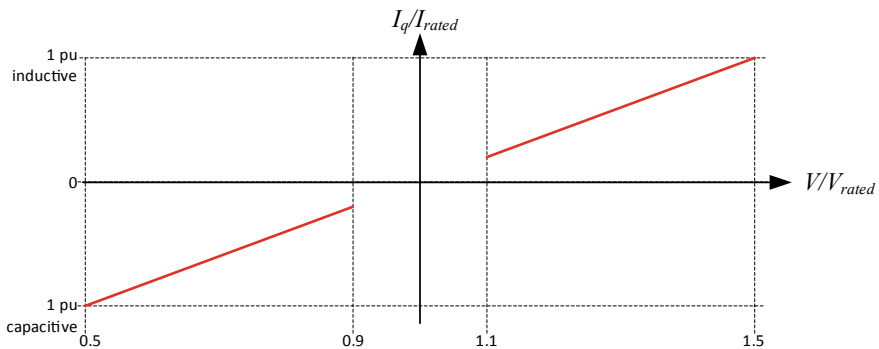
Fig. 32 Exemplary reactive current, I_q, requirement for voltage support. Diagram based on E. ON Grid Code—High and extra high voltage, 1. April 2006

following Sect. 3.2.3). The synchronous generators in Type V WTs can be overloaded quite heavily for several seconds. This is well-known standard technology from conventional power plants.

3.2.3   Short-Circuit Current Provision

Whenever a short-circuit is the cause of a voltage drop, the protection relays in the PS have to detect this fault, they have to locate the fault location and they have to isolate the fault location. For this purpose, it is crucial that short-circuits cause short-circuit currents. In contrast to reactive current provision for voltage support, short-circuit currents are primarily needed at the beginning of a short-circuit. Hence, durable provision of short-circuit current is not needed.

Short-circuit currents can only be provided by generators or energy storages. In a PS, all capacitive and inductive devices are energy storages. A prime example is the induction machine, which is the generator in Type I and Type II WTs, and which is often used as a motor in rotating consumers. As explained in Sect. 3.2.2, induction machines provide a current when they get de-magnetized. This does not only apply when they run as generators but also when they operate as motors. The short-circuit current contribution of different generator types and different WT types is summarized in Table 3.

The short-circuit current provision of the different WT types depends on the short-circuit type (how many phases involved, with or without the involvement of the earth) and on the operating point of the WT prior to the fault [18]. The values given in Table 3 are maximum values.

Synchronous generators, as contained in conventional power plants and in Type V WTs, provide very large short-circuit currents when the voltage at their terminal drops. A further advantage of electrically excited synchronous generators is that they do not absorb reactive current from the grid when the grid voltage recovers. Instead, the excitation system takes care of the re-magnetization.

A Type III WT can provide short-circuit currents larger than rated due to its similarity to squirrel cage induction generators when the crowbar is fired for protecting the frequency converter. This, however, is seldom the case, as LVRT with Type III

Table 3   Short-circuit current contributions of different generator types and WT types, in pu referred to rated current

Generator type	WT type	Maximum short-circuit current (pu)
Squirrel cage induction generator (SCIG)	Type I	≈6
Wound rotor induction generator (WRIG)	Type II	Depending on rotor resistance <6
Doubly fed induction generator (DFIG)	Type III	≈3
Full-scale frequency converter	Type IV	≈1 (independent of generator type used behind full scale frequency converter)
Synchronous generator	Type V	≈8

WTs is normally done with the frequency converter in fully controlled operation. If the crowbar is not fired, a doubly fed induction generator is also similar to a synchronous generator due to its electric excitation from the machine side inverter and due to its directly grid-connected stator terminals. The similarity of these two generators depends on the slip, i.e. on the speed difference between the stator field and the rotor.

The power electronic interface between Type IV WTs and the grid is a strict limitation of short-circuit current. Power electronic frequency converters can hardly be overloaded. Therefore, they need to be over-dimensioned substantially to be able to provide satisfactory short-circuit currents. Alternatively, the short-circuit current of a Type IV wind farm has to be provided by synchronous condensers, which are installed as extra equipment in the wind farm. The red current curve in Fig. 28 shows the minimum current rating for this reactive power requirement in normal operation. If a Type IV WT is dimensioned to fulfill this requirement, its frequency converter has to be able to sustain permanent operation with 1.23 pu current (referred to rated power at rated voltage). This means that this Type IV WT is capable of providing a short-circuit current of a bit more than 1.23 pu for a fraction of a second. An example of how frequency converters adjust their operation to suppressed and potentially unsymmetrical grid voltages is introduced and discussed in Chap. 8.

4   Power System Frequency

The PS frequency is the frequency with which the voltage in the system alternates. In Figs. 7 and 10, the period of the voltage is 0.02 s, i.e. the frequency of the PS, to which these voltages belong, is 50 Hz. An AC PS can be considered a rotating machine. The power is produced with rotating generators, and it is driven through the PS with alternating voltage. The frequency of this AC voltage is proportional to the rotational speed of the generators. Figure 33 visualizes the concept, where two exemplary AC machines are connected to each other via a transmission line. In each machine, the magnetic field links the rotor with the stator. Hence, the rotational speed, ω, of the rotor fields and the stator fields are identical in both machines.

The angular speed, ω in radians per second, can be translated into a frequency in Hertz with Eq. 9, which is the commonly used unit for PS frequency. In the case of a machine with one pole pair, as shown in Fig. 33, this equation translates the mechanical speed into the electrical grid frequency.

4.1   Frequency Control

The speed of a generator, i.e. the frequency of the AC voltage that it produces, is determined by its mechanical prime mover. In the case of multiple AC-connected generators, the speed of the magnetic fields in all generators has to be identical, at least
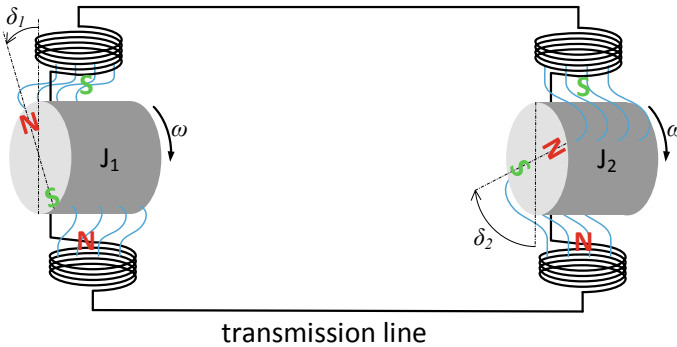
Fig. 33 Two AC machines with their inertias J_1 and J_2 are connected via magnetic fields, with their north (N) and south (S) poles, and a transmission line. Therefore, both rotors rotate in synchronism with the angular speed ω

in steady state. The consumers and the transmission losses absorb the power which the generators produce. If the produced power and the consumed power are in balance, the rotational speed, i.e. the electrical frequency, is constant. If the generated power exceeds the consumption, the frequency rises; and it declines if the consumption exceeds the generation.

Since the grid frequency is directly connected to the balance between generation and demand, PS operators do not need to know the demand precisely in order to adjust the power of the generators. Controlling the electric frequency in the grid by adjusting the generation, such that the frequency is at its desired value, automatically adjusts the generation to the prevailing demand. Obviously, PS operators have to have a vague idea of the demand to be expected. Otherwise, excessively many power plants would need to be connected to the grid in anticipation of potential power demand. Therefore, a large fraction of the consumed power is traded beforehand on the energy market. The consumption of, for example, private households is not known precisely in advance. However, the behavior of the consumers is predictable as it repeats itself according to the so-called load profile. The load profile is historic data of consumption over the hours of a day, over the days of a week and over the weeks of a year. The remaining uncertainty in consumption has to be catered for by control power plants, which adjust their power according to the deviation of the grid frequency from its rated value.

Hence, control power plants can only respond after an imbalance between generation and demand has led to a discrepancy in grid frequency, which implies a delay. However, control power plants cannot respond arbitrarily quickly. Therefore, it is important that an imbalance does not lead to too steep frequency excursions. Otherwise, the limit for acceptable frequency values might be exceeded before the control power plants were able to respond. This is discussed further in Sect. 4.2.

Figure 34 illustrates what happens when the frequency deviates slightly from the rated frequency (which is normal PS operation), and when frequency thresholds are exceeded.
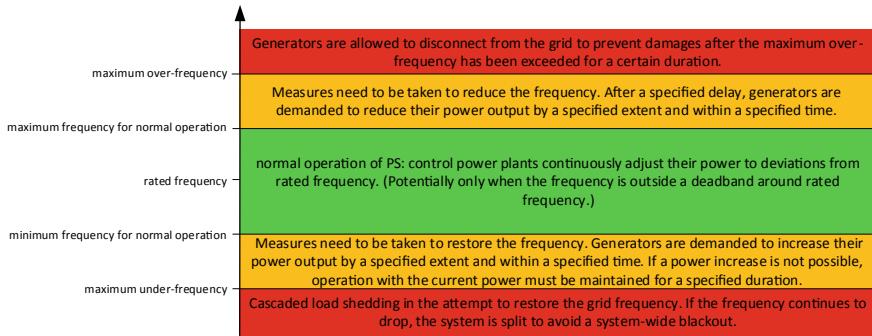
Fig. 34 Operation of a PS in the different frequency ranges

When the frequency deviates from its rated value, there are also some consumers, which help restoring the balance. These so-called frequency-sensitive loads vary their power consumption as a function of the grid frequency. A prime example is fans, which are driven by AC-connected motors. The power of a fan varies with the cube of its rotational speed. The rotational speed of an induction motor is determined by the grid frequency and its loading. Hence, when the grid frequency drops, the speed of the motor drops and this lets the power demand of the fan drop, too. Consequently, the motor absorbs less power from the grid, which is advantageous for the grid, because the decline in frequency indicates that more power should be generated, or, alternatively, less power should be consumed.

4.2 System Inertia

In Sects. 2.4 and 3.2.1, the problem of acceleration resulting from an imbalance between driving power and decelerating power is discussed. Although in these sections the discussion revolves around rotating machines which experience an imbalance because of transient voltage drops, the situation is perfectly comparable to the situation in an AC PS, where the generation does not fit the consumption. Equation 33 describes the acceleration of a rotating machine in general. As shown in Fig. 33, an AC PS is a rotating machine, too. It is further known that power is the product of torque and speed, which is why the electric power in a synchronously rotating machine (or in a whole AC PS) results from the grid frequency (Eq. 9) and the electric torque, T_{elec}:

$$P_{\text{elec}} = \omega \cdot T_{\text{elec}} \tag{36}$$

Knowing that in a PS not only the consumers absorb power (P_{load}) but also the transmission losses (P_{loss}) allows reformulating Eq. 33 to represent the acceleration of the angular velocity in a PS:

$$\frac{d\omega_{\text{elec}}}{dt} = \frac{P_{\text{elec}} - P_{\text{load}} - P_{\text{loss}}}{\omega_{\text{elec}} \cdot J_{\text{sys}}}$$ (37)

The inertia J_{sys} is the system inertia, i.e. the aggregated inertia of all directly AC-connected generators and consumers.

Looking at Eq. 37, it becomes obvious that the speed, with which the grid frequency varies, depends on the inertia in the PS. In other words, the time mentioned in Sect. 4.1, which has to be allowed for control power plants to respond, increases with increasing inertia. Therefore, PS inertia is a premise for the controllability of the grid frequency; i.e. only if a PS behaves inertial, its frequency varies slowly enough to be controllable.

The inertia, J_{sys}, is a value in kgm² and could, in principle, be derived if the geometry of all synchronously connected machines were known. While it might be possible to have the necessary data about the connected generators, it is entirely impossible to acquire this information about the rotating loads, which are connected to the PS at a time. Just like generators, rotating loads contribute to PS inertia, provided that their motors are AC-connected. If there is a frequency converter connected between an electric machine (generator or motor) and the PS, the inertia of this rotating machine does not inherently contribute to PS inertia.

Identifying the inertia contribution from consumers is realistically only possible by analyzing the time traces of the grid frequency in transient events, preferably in small PSs. The system in Great Britain reveals a load inertia share of about 20% of the total system inertia [27]. In a small islanded system in Germany, which resulted from a system split, and which spread only about 55,000 connected consumers, the inertia share of the consumers could be identified to be 21% of the total system inertia [28].

4.2.1   Inertia Constant, H

The inertia in kgm² is not only difficult to identify, but it is also rather useless, as it does not quantify the inertial behavior of a PS in an illustrative manner. However, inertia in motion stores kinetic energy, E_{kin}; see Eq. 35. Simplifying Eq. 35 leads to the overall kinetic energy contained in inertia:

$$E_{\text{kin}} = \frac{1}{2} \cdot J \cdot \omega^2$$ (38)

To get a practicable measure of the inertial behavior of a single rotating machine, like a power plant, or of a whole PS, the following situation is assumed. The considered rotating electric machine runs at rated speed while it is loaded with its rated electric power. Then, the driving torque at its shaft is set to zero instantaneously (this is practically hardly possible, but conceivable for the sake of this theoretical assumption). In order to continue producing rated electric power, the machine can
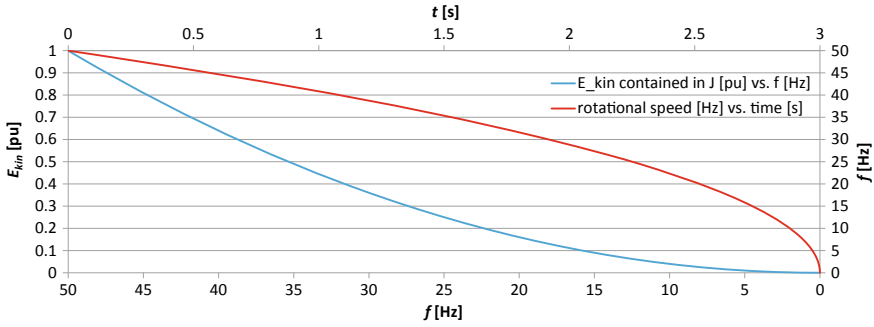
Fig. 35 Kinetic energy is extracted from a mass with $H = 3$ s, which rotates with the frequency f, and which produces rated power from 50 Hz all the way down to standstill

only tap the kinetic energy stored in its inertia (Eq. 38), as this is the source of energy that it is left with.

Dividing the stored kinetic energy, with its unit Watt-seconds (Ws), by the rated power, with the corresponding unit Watt (W), leads to the so-called inertia constant, H:

$$H = \frac{E_{\text{kin}}}{P_{\text{rated}}} = \frac{\text{Ws}}{W} \tag{39}$$

Hence, the inertia constant is the time in seconds, in which the rotating machine can continue producing rated electric power, after it lost its driving torque. Figure 35 visualizes the concept, where an electric machine with inertia constant $H = 3$ s loses kinetic energy because it produces rated power from a rated speed (50 Hz) to a standstill.

This is obviously a theoretical consideration, as rated power at very low speeds is impossible. However, the inertia constant is a very practical measure to quantify the inertia independent of the size of the considered machine. Figure 35 illustrates quite well what Eq. 38 suggests: It is advantageous to operate a PS close to its rated frequency. The lower the frequency gets, the softer the inertia responds, i.e. the quicker the speed drops while maintaining the demanded power.

Table 4 gives an idea of realistic inertia constants of different AC-connected conventional power plants. Inertia constants of state-of-the-art WTs are deliberately omitted, as they do not inherently contribute to the system inertia, which is further discussed in Sect. 5.1. The system-wide inertia constant is derived with Eq. 40 using the inertia constants and rated powers of all AC-connected rotating machines, where i is the counter that runs through all machines:

$$H_{\text{sys}} = \frac{\sum \left(H_i \cdot P_{\text{rated},i} \right)}{\sum P_{\text{rated},i}} \tag{40}$$

Table 4 Inertia constants for different types of power plants [29, 30]

Prime mover type	Inertia constant (s)
Hydro (small scale)	1
Hydro (conventional)	3–4.5
Pump storage	5.5
Nuclear power-driven steam turbines	6.3
Combined cycle turbines	2.5
Open cycle gas turbines	6–6.5
Other thermal prime movers	4

In Eq. 40 also, the values of the AC-connected rotating consumers, as discussed above, have to be considered.

4.2.2 Power from Inertial Response

An imbalance between generation and demand is instantaneously taken care of by the inertia in a PS. This means, for the duration of the imbalance, the missing power is delivered by inertia. Hence, it is of interest how this power is derived and how it is related to the rotational speed of the inertia. The previously introduced Eq. 35 can be applied. It defines the kinetic energy, E_{kin}, when the rotational speed (in this context the speed of the synchronously rotating machines in the grid) varies from an initial grid frequency (ω_{start}—consider Eq. 9) to a final grid frequency (ω_{end}), which is reached until control power plants step in. Hence, with the kinetic energy the instantaneous power from the inertial response can be derived:

$$P_{inertia} = \frac{d}{dt} E_{kin} = J \cdot \omega \cdot \frac{d\omega}{dt} \tag{41}$$

Equation 41 reveals that power from the inertial response is a function of the grid frequency and of the derivative of the grid frequency. The derivative of the grid frequency is commonly referred to as the rate of change of frequency (ROCOF):

$$\text{ROCOF} = \frac{df}{dt} = \frac{1}{2 \cdot \pi} \cdot \frac{d\omega}{dt} \tag{42}$$

Equation 41 is further proof of what is already shown in Fig. 35: The inertial power, which caters to the imbalance between generation and demand, can be easier provided at higher grid frequencies. Hence, the frequency should not sag too deeply but should be kept within tight limits.

Equation 41 further reveals that if the inertia in a PS is low, the ROCOF has to be large to produce the needed power. The inertia in a PS is, as outlined above, largely unknown, but the ROCOF can be measured easily. Hence, the occurring ROCOFs allow characterizing a PS. With the transition to renewable energies, many

power plants of the types listed in Table 4 are replaced by photovoltaic systems or WTs. That is, synchronously connected rotating generators are replaced by frequency converters. While photovoltaic systems do not even possess any rotating masses, WTs of Type III and Type IV do not contribute their inertia to the grid inertia, because of their frequency converters. Consequently, it can be observed that with progressing transition to renewable energies, the ROCOFs increase.

From the perspective of PSs, it is unfortunate that Type III and Type IV WTs are the most commonly used WTs. However, the controls of such WTs can be modified to provide the grid with synthetic inertia, as discussed in detail in Sect. 5.1.

4.3 Damping Sub-synchronous Oscillations

Figure 33 illustrates the situation of AC PSs. Rotating masses are synchronously connected to each other via transmission lines. In this context, it does not matter whether the inertias are single machines, like power plants, or whole grid regions. If two areas in a PS are connected to each other via one tie line, the inertias in each area can be aggregated to one single equivalent inertia. The load angles, δ_1 and δ_2 in Fig. 33, characterize the operating points of the connected machines (or grid regions). The load angles are the angles on the horizontal axis in the diagram in Fig. 13.

Figure 33 further illustrates that the inertias are linked to the transmission line via the magnetic fields (blue lines) in the airgaps between the stator and rotor. Magnetic fields are flexible links between the mechanically rotating mass and the electric power in the transmission line. Elongating the magnetic field lines, i.e. increasing the load angle, δ, requires a torque, T. Hence, the setup shown in Fig. 33 is an electromechanical oscillatory system comprising a mechanical inertia, J, and an electro-magnetic spring. The stiffness, k, of this electro-magnetic spring (in Newton meter (Nm) per radian) is determined by the excitation of the involved machines:

$$k = \frac{T}{\delta} \tag{43}$$

Hence, potential energy is stored in the elongated electro-magnetic spring:

$$E_{\text{pot}} = \frac{1}{2} \cdot k \cdot \delta^2 \tag{44}$$

Obviously, the inertia stores kinetic energy as given by Eq. 38. With these two types of energy, the premise for oscillation is given. If the system shown in Fig. 33 is excited, e.g. by a load change or a transient voltage drop, it oscillates with the frequency ω_{swing}:

$$\omega_{\text{swing}} = \sqrt{\frac{k_{\text{eq}}}{J_{\text{eq}}}} \tag{45}$$

In Eq. 45, the two inertias, J_1 and J_2, behave like equivalent inertia, J_{eq}:

$$J_{eq} = \frac{J_1 \cdot J_2}{J_1 + J_2} \tag{46}$$

Likewise, also the two stiffnesses, k_1 and k_2, of the magnetic fields, can be aggregated to an equivalent stiffness, k_{eq}:

$$k_{eq} = \frac{k_1 \cdot k_2}{k_1 + k_2} \tag{47}$$

In an AC PS, the voltage is desired to oscillate with the fundamental frequency of the PS; i.e. in land-based PSs typically with 50 or 60 Hz. The electromechanical oscillations, however, are undesired sub-synchronous oscillations. The frequency of such electromechanical oscillations can vary in a wide range. They also vary with time, as they depend on the loads and the generators connected to the considered PS. In the study on the Nordic grid, the observed frequencies in the different locations ranged from 0.3 to 0.8 Hz [31]. Tests in the Finnish grid revealed frequencies in the range of 0.6–1 Hz [32]. In general, the frequency of electromechanical grid oscillations is in the range of 0.1–0.7 Hz when considering inter-area oscillations. The frequencies of local grid oscillations can be expected to be above that and in the range of 0.7–2 Hz, while oscillations of single machines are typically with frequencies above 2 Hz [33].

These oscillations are obviously grid frequency oscillations, as the swinging of the rotors, of the considered machines, is superimposed on their rotational speed. Hence, the load angles, δ, of the machines oscillate around their mean value. Figure 13 shows that variations in load angle mean variations in active and reactive power. Considering the situation shown in Fig. 33, these power oscillations mean increases and decreases in the power to be transferred through the transmission line. The danger of such power swings is that the transmission line might get temporarily overloaded and taken out of operation by its protection relays. Hence, sub-synchronous electromechanical oscillations can cause system splits and eventually blackouts. Therefore, they need to be damped before they get out of hand.

Damping sub-synchronous electromechanical oscillations is done with so-called power system stabilizers (PSS). The definition of damping, D, is torque, T, proportional to speed of motion of the oscillation, ω_{swing}:

$$D = T \cdot \omega_{swing} \tag{48}$$

Considering the likely frequencies of sub-synchronous oscillations, as mentioned above, this means that active power variations have to be realized with frequencies between 0.1 and 2 Hz. Such active power variations cannot be realized with the controls of most mechanical prime movers. Therefore, it is realized with the electrical excitation of, for example, synchronous generators, as shown in Fig. 36.
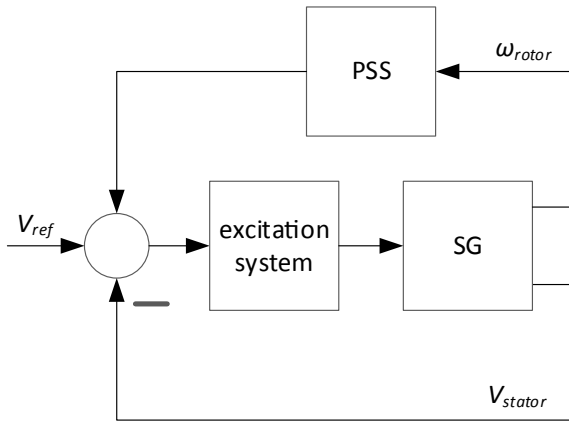
Fig. 36 Block diagram of a synchronous generator (SG) with controls of the electrical excitation system and Power System Stabilizer (PSS) impacting the excitation system

Varying the excitation of a generator varies the voltage at its stator terminals. However, the excitation does not only influence the reactive power, which primarily determines the voltage, but also the active power. Figure 37 shows a fraction of Fig. 13 with arrows indicating the sequence of events that take place when active power needs to be varied rapidly.
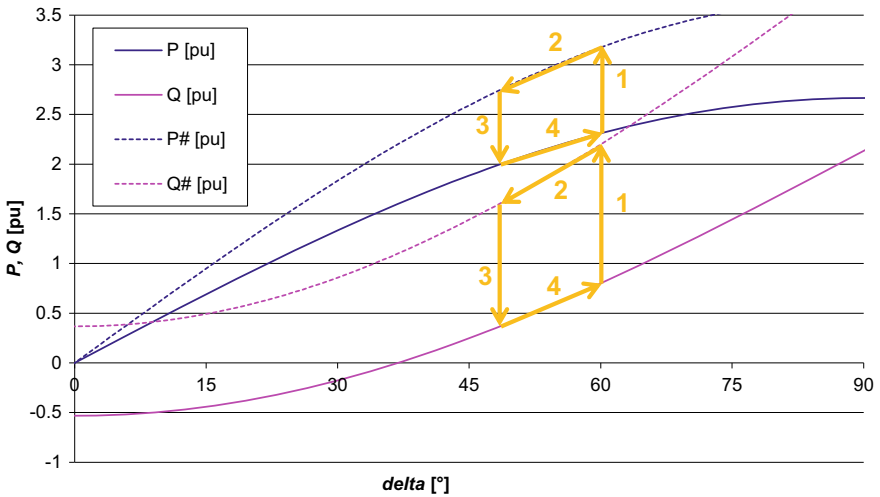
Fig. 37 Different active and reactive power operating points of a voltage source, e.g. a synchronous generator, during power system stabilization at constant mechanical driving power. 1: increase in excitation; 2: excess power generated from kinetic energy → decline in load angle; 3: reduction of excitation → power drops below mechanical driving power; 4: recovery of load angle and power

A transition from one state of excitation to another is shown with arrow 1 in Fig. 37. Not only the reactive power but also the active power is increased because the excitation is increased. If the mechanical driving power remains unchanged, the additional active power is generated from the kinetic energy in the rotor. Consequently, the rotational speed drops (arrow 2), until the excitation is reduced (arrow 3) to allow for the initial operating point to recover (arrow 4).

Such variations in active power can be realized rapidly and also periodically. Hence, periodic rotor speed oscillations (i.e. grid frequency oscillations) can be damped without having to control the mechanical prime mover.

4.4 Frequency Stability

Frequency stability is the ability of an AC PS to maintain an acceptable frequency and synchronism throughout the whole system. This means that it must be possible to maintain the frequency with the mechanisms shown in Fig. 34. Neither a steady state situation nor a transient event must lead to system splits, which would disintegrate a PS into several islands.

Hence, frequency stability is based on the availability of sufficient control power to cater to unforeseeable imbalances between generation and demand (see Sect. 4.1). In order for this control power to be able to respond without violating frequency limits, sufficient inertia is needed in the system as a premise for the controllability of the frequency (see Sect. 4.2). Finally, if transient events excite the system, sufficient damping power is required to avoid those oscillations leading to disconnection of PS components (see Sect. 4.3), which could cascade into a blackout.

5 Frequency Stability with Wind Turbines

Considering the definition of frequency stability in Sect. 4.4, the current section assesses the ability of WTs to contribute to frequency stability.

All WT types introduced in Sect. 1.2 have the ability to control their power output, except for WT Type I in passive stall design. Hence, these WT types can adjust their power output to support the grid frequency. Since the kinetic energy in the wind cannot be stored, WTs can only increase their power output in case of dropping grid frequency if they were in throttled operation beforehand. Power variations can be realized quite rapidly, in particular with WTs of Type II, Type III and Type IV, because these WTs control their power output with power electronics. But even the WT types, which rely on pitch angle control to vary their aerodynamic driving power, are capable of varying their power faster than conventional power plants.

However, irrespective of how the power is controlled, variations in the operating point inevitably excite the structure of the WT to vibrations. Figure 29 illustrates the problem for the WT drive train. However, also other WT components, like the
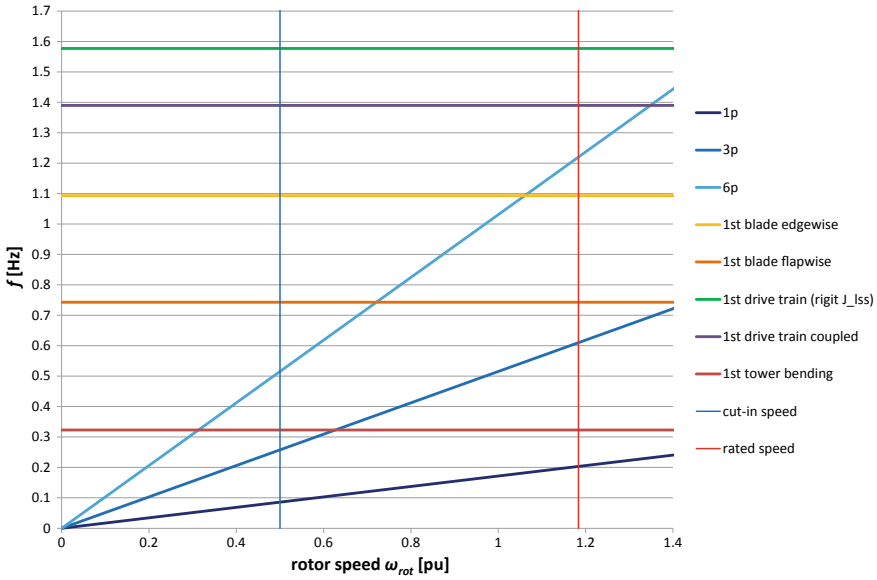
Fig. 38 Campbell diagram with the first eigenmodes of some WT components of the NREL 5 MW reference WT

tower and the rotor blades, are prone to vibrations. As an example, Fig. 38 shows a simplified Campbell diagram of the NREL 5 MW references WT [34], where only the first eigenmodes of the most important WT components are plotted versus the rotational speed in per unit. The basis for the per unit conversion is the synchronous speed of the generator [35].

WTs are continuously excited to vibrations by their rotation and by turbulent wind. Mechanical vibrations can have a direct impact on the active power operating point; see Fig. 30. From the perspective of the PS, oscillating power infeed should be avoided, as this could, potentially, excite electromechanical oscillations in other PS components.

5.1 Inertial Response of Wind Turbines

Any WT, whose generator is AC-connected to the PS, inherently behaves inertial. This means that WTs of Type I and Type V behave inertial, i.e. they provide power from the inertial response, whenever their generators are connected to the grid. WTs of Type II, Type III and Type IV only provide power from the inertial response when their power electronics are deliberately controlled to do so. When such WTs adjust their power to the changes in the grid frequency, i.e. the absolute value of the frequency and the rate of change of frequency (Eq. 41), they behave similar

to synchronously connected rotating machines. Hence, they behave inertial in a controlled manner; i.e. they provide inertia not inherently but synthetically [36]. This emulates real inertia, which is a way for grid operators to maintain controllability of the grid frequency, even in the case of high penetration with wind power [37]. For a WT, this way of controlling its active power means partially decoupling its controls from its available prime energy, i.e. the wind speed.

A technique to make voltage source converters behave similar to synchronous machines is the so-called virtual synchronous machine (VSM). A VSM allows controlling a frequency converter such that it responds to transients in the grid voltage and the grid frequency similarly favorably as synchronous generators do it. In some respects, VSMs even behave more favorably than real synchronous machines, e.g. in terms of damping of sub-synchronous oscillations. In other respects, like short-circuit current contribution, they are tied to the physical constraints of the frequency converter hardware, and hence, perform a lot worse than real synchronous machines [38]. Some general details on how frequency converters in WTs can be controlled are discussed in Chap. 8.

However, irrespective of how a particular active power behavior is achieved with a frequency converter in a WT, this active power has to be drawn from the generator of the WT. Active power in a generator means torque, hence, inertial response has an influence on the rotational speed and on the mechanical structure of the WT. To take the needs of a variable speed WT into account, which is bound to be exposed to varying wind speeds, and at the same time to satisfy the need for reliable inertia provision in the grid, the variable inertia constant (Hvar) controller was proposed [39]. The main advantage of this controller is that it avoids the risk that the WT disconnects from the grid when during low wind speeds a large negative ROCOF (steep drop in grid frequency) requires a large increase in power. A variable speed WT with Hvar controller behaves like a synchronous generator. However, unlike a synchronous generator, the rotational speed of a WT is not constant. In an AC-connected synchronous generator, the rotor speed varies with the grid frequency only. That is, it is almost constant. In a variable speed WT, however, the rotational speed is not determined by the grid frequency, but by the wind speed. Hence, it can vary in a wide range; see the horizontal axis in Fig. 38. Therefore, the Hvar controller varies the inertia constant, which is emulated by the WT, according to the current rotational speed. As shown in Fig. 39, the inertia characteristic of such a WT reaches the demanded inertia constant when the rotor rotates with rated speed. At cut-in speed, the emulated inertia constant is zero. Consequently, the synthetically provided inertia of the WT is a function of the kinetic energy contained in the drive train of the WT.

Comparing the demanded inertia constants shown in Fig. 39 with the inertia constants of conventional power plants listed in Table 4, it becomes obvious that synthetic inertia can exceed real inertia by far. The demanded inertia constant H_dem = 12 s is just an example. Studies have shown that the inertia contribution with this exemplary inertia constant yields good results for the PS and has virtually no impact on the energy yield [15]. The ability of WTs to avoid a blackout has also been tested with simulations of a real blackout scenario [40].
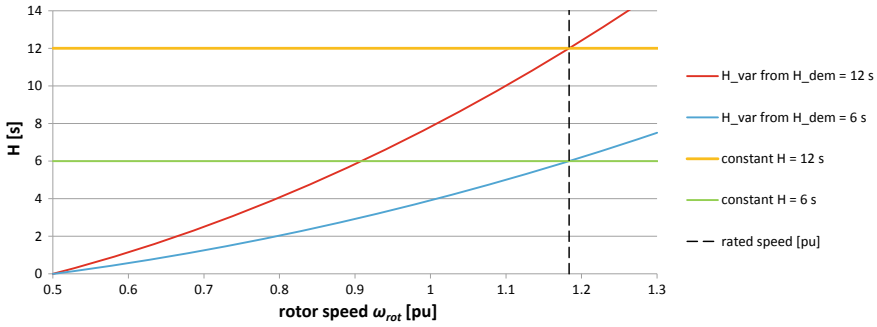
Fig. 39 Inertia characteristic of an AC-connected generator with inertia constant = 6 s (green) and 12 s (yellow). Inertia characteristic of a variable speed WT with Hvar controller and demanded inertia constant H_dem = 6 s (blue) and H_dem = 12 s (red)
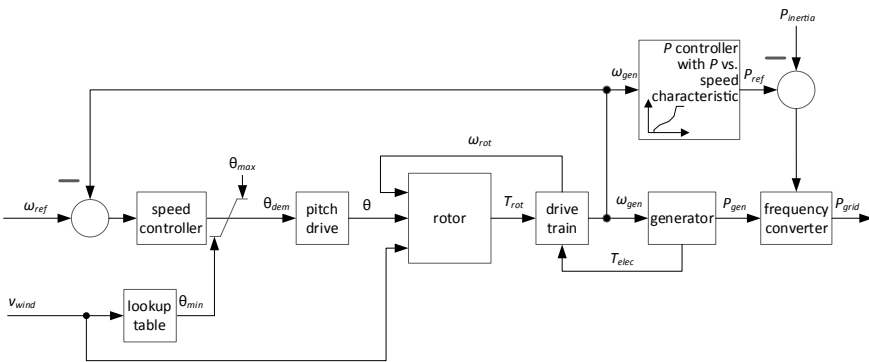
Fig. 40 Simplified control circuit of a variable speed WT with power offset for inertial response realized via the frequency converter

The active power provision from inertial response has an inevitable effect on the torque, and hence, the mechanical structure of the WT. Therefore, the influence of this permanent partial decoupling of the active power control from the prevailing wind speed has been assessed. It was found that WTs can provide synthetic inertia in most operating points, and for most conceivable grid frequency events, reliably, without undue effect on their lifetime [41].

Combining Eq. 41 with Eqs. 38 and 39 while applying Eq. 42 allows deriving the demanded power from the desired inertial response:

$$P_{\text{inertia}} = \frac{2 \cdot H_{\text{var}} \cdot P_{\text{rated}}}{f} \cdot \frac{df}{dt} \tag{49}$$

This power from inertial response enters into the control circuit of a variable speed WT as shown in Fig. 40. It has to be noted that P_{inertia} is added to the power reference

for the frequency converter with a negative sign. That is, a negative ROCOF (df/dt) has to cause the WT to inject extra active power into the grid.

If a WT is to support the grid frequency with inertial response only, the sign of P_{inertia} is bound to alter frequently. Therefore, P_{inertia} is not likely to have a lasting effect on the rotational speed of the WT drive train.

5.2 Fast Frequency Response with Wind Turbines

In this section, the support of the grid frequency with control power from WTs is discussed. It is obvious that any WT type, which can control its power, is suitable for reducing its power output in case of too high grid frequency. Therefore, in the following only power increases, which are necessary when the grid frequency is too low, are discussed.

To avoid confusion, the terminology shall be introduced first. It has to be noted that different, and in some cases contradicting, terminology can be found in the literature. In this chapter, the convention used by Eriksson et al. is applied. Hence, fast frequency response refers to power adaptations based on grid frequency deviations. This is in contrast to the inertial response, as introduced in Sect. 5.1, where the deliberately produced power adaptations, called synthetic inertia, are primarily driven by the rate of change of frequency [36].

As an example, in this section fast frequency response is described according to the requirements stipulated for the Canadian grid in Quebec [42]. It is particularly important to note that in this grid code the response to frequency deviations is called inertial response. To avoid confusion, in the chapter at hand the term fast frequency response is used instead.

Hydro Quebec demands WTs to inject a minimum power for a minimum duration and with minimum ramp rates if the grid frequency drops below a certain threshold. This type of power provision for grid frequency support is particularly suitable for generators with small energy storage. That is, it is suitable for WTs which can access the kinetic energy in their drive trains.

Depending on the rotational speed, variable speed WTs have different amounts of kinetic energy stored in their drive train. Figure 41 shows the power versus speed characteristic of the variable speed WT already discussed in Fig. 38. The green curve is the power versus speed characteristic for normal continuous operation. The red characteristic is for the temporary power increase by 0.1 pu, as demanded in the above-mentioned grid code [42]. Maintaining this power increase in part load for the demanded duration of 10 s causes kinetic energy to be extracted from the drive train and, consequently, the speed to drop as shown by the blue horizontal lines. After the 10 s have elapsed and the power is released again, the power drops back to the normal power versus speed characteristic, but at a lower value, as indicated by the orange vertical lines.
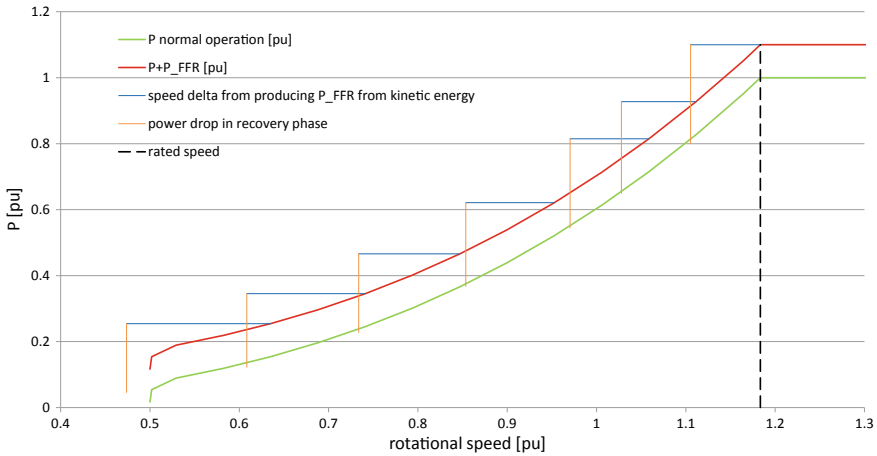
Fig. 41 Power versus speed characteristic of variable speed WT. Power increase by 0.1 pu of rated power for fast frequency response, resulting in speed delta and following power drop

Fast frequency response in full load operation beyond rated wind speed is obviously trivial, as there the wind speed usually contains sufficient kinetic energy; hence, the WT can produce extra power merely from the wind.

The power demand offset called P_FFR in Fig. 41 enters into the control circuit of a variable speed WT as shown in Fig. 40 at the same summation point where $P_{inertia}$ enters; however, P_FFR would be added with a positive sign.

For the purpose of illustrating fast frequency response operation, a part load operating point is simulated. To have a realistic case, the reference incident as defined by ENTSO-E [43] is chosen; see top diagram in Fig. 42. Fast frequency response as required by Hydro Quebec is applied (bottom diagram in Fig. 42); although Hydro Quebec operates a 60 Hz grid, the requirement can be adapted to 50 Hz grids. The threshold for activation of fast frequency response is set to −10 mHz, which also complies with the restrictive grid code of the Irish 50 Hz grid [44]. To improve comprehensibility, the scenario shown in Fig. 42 considers a non-turbulent constant wind speed of 11 m/s. The simulated Type IV WT exhibits the characteristics shown in Figs. 38 and 41.

Figure 42 reveals the major disadvantage of fast frequency response with WTs in part load operation. The extra power can only be provided from kinetic energy in the drive train, as this is the only energy storage available in a state-of-the-art variable speed WT. However, extracting kinetic energy invariably means that the rotational speed drops. Consequently, the power has to be reduced after a few seconds, in order to return to the optimal rotational speed. The period of reduced power and increasing speed is called the recovery phase. This recovery phase comes at a time when the PS is in desperate need of more power, not less, because the grid frequency (top diagram in Fig. 42) has still not returned to its rated value yet.
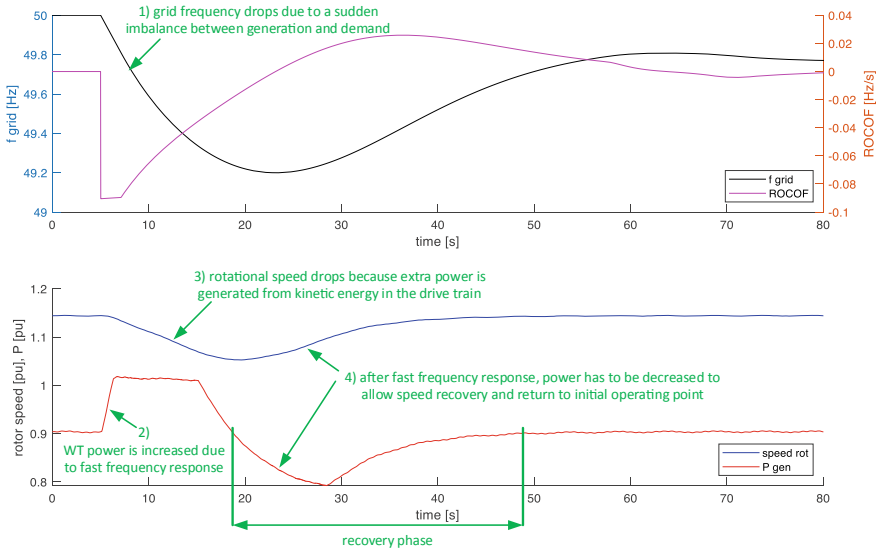
Fig. 42 Fast frequency response of a variable speed WT. (1) Grid frequency drops, (2) WT power is increased beyond its initial part load operating point, (3) the speed drops because kinetic energy is extracted from the drive train and (4) the recovery phase is inevitable for returning to the previous operating point

An alternative approach for supporting the grid frequency with control power from WTs is to apply a droop characteristic. In the case of dropped grid frequency, a droop characteristic calls for a power increase, which is proportional to the depth of the frequency drop and which potentially lasts for a long time. This is the approach commonly applied in conventional primary frequency control power plants. Such long-term extra power provision cannot be sustained from kinetic energy in the drive train of a WT. Instead, precautious down-regulation of the WT is the only way of realizing this kind of control power supply [37]. The downside of this approach is that it potentially leads to very large losses in wind energy yield.

5.3 Power System Stabilization with Wind Turbines

The concept of PS stabilization, as introduced in Sect. 4.3, can be transferred to any generator, also to WTs. It is particularly important to note that the likely frequencies of sub-synchronous oscillations change with increasing shares of frequency converter-based generation. Since frequency converters decouple the inertia of a generator, e.g. a WT, from the PS, the overall inertia in a PS is bound to decrease, as discussed in Sect. 4.2. Consequently, the frequency of sub-synchronous oscillations is bound to increase with progressing transition to renewable energies, as suggested by Eq. 45. It can be expected, though, that this increase in frequency ω_{swing} will be moderate,

because the real inertia is partially substituted by synthetic inertia, as discussed in Sect. 5.1.

Since electromechanical grid oscillations are grid frequency oscillations, it could be suspected that PS stabilization is identical with inertial response or fast frequency response. However, neither is the case as fast frequency response is only active when a certain frequency threshold is exceeded. Grid frequency oscillations can threaten system stability even if their magnitude seems harmless, as discussed in Sect. 4.3. Inertial response, on the other hand, is mainly driven by the derivative of the grid frequency (ROCOF). Hence, its power is 90° out of phase with the grid frequency oscillations; therefore, it does not contribute to damping.

The concept of PS stabilization has been proposed in the past already for the application of Type I WTs, which can vary their power output solely with the pitch angle [45]. The performance of PS stabilization in fixed speed WTs was assessed with simulations of electromechanical oscillations in the Nordic grid [31]. The concept of PS stabilization in a synchronous generator was adapted to Type IV WTs, where the DC capacitor voltage was controlled similar to the excitation control in a synchronous generator [46]. Also, other methods of PS stabilization with WTs are conceivable [33]. However, all these methods have in common that active power is extracted from the grid in case the frequency swings beyond its steady state value, and that extra active power is injected when the frequency swings below its steady state value. Type III or Type IV WTs can emulate PS stabilization by periodically varying the reactive power infeed. The obvious advantage of this approach is that WTs can provide PS stabilization independent of wind speed [32]. Independent of the wind speed means, on the other hand, that the generator is not involved. Therefore, the frequency converter cannot exchange active power, as a synchronous generator does (see Fig. 37), when its reactive power is varied via the excitation. Hence, this method is not comparable to conventional PS stabilization. Instead, the damping effect in the grid is caused by the resistances of lines and cables, which act as braking resistors when the injected reactive power flows through them.

A Type V WT, with its AC-connected synchronous generator and its electrical excitation system, can obviously perform conventional PS stabilization as explained in Sect. 4.3. Type III and Type IV WTs can perform conventional PS stabilization with their frequency converters, as long as their generators are in operation. In this case, the controls of the frequency converter can vary the load angle, δ, as shown in Fig. 37. The resulting active power is then exchanged between the generator of the WT and the PS.

Periodically varying the power of the generator obviously excites the mechanical structure of the WT to vibrations. Comparing the exemplary eigenfrequencies of the 5 MW WT shown in the Campbell diagram in Fig. 38 with the possible frequencies of grid oscillations mentioned in Sect. 4.3 reveals that it is very likely that PS stabilization excites WTs to vibrations. Therefore, PS stabilization is among the most demanding grid services, which is why it is not commonly demanded from WTs, yet.

Literatures

1. UN, United Nations Framework Convention on Climate Change (UNFCCC). https://unfccc.int/. Accessed 02 Aug 2021
2. IEA, Renewables 2020—Analysis. https://www.iea.org/reports/renewables-2020/wind. Accessed 02 Aug 2021
3. Global Wind Energy Council (2021) Global Wind Report 2021. https://gwec.net/global-wind-report-2021/. Accessed 02 Aug 2021
4. Schaffarczyk A (2014) Understanding wind power technology, theory, deployment and optimisation. Wiley, Chichester, UK. ISBN: 978-1-118-64751-6
5. Weedy BM, Cory BJ (1998) Electric power systems, 4th edn. Wiley
6. Kundur P (1994) Power system stability and control. McGraw-Hill, New York, NY, USA
7. Nise NS (2000) Control systems engineering, 3rd edn. Wiley, Hoboken, NJ, USA
8. Yaramasu V, Wu B, Sen PC, Kouro S, Narimani M (2015) High-power wind energy conversion systems: state-of-the-art and emerging technologies. Proc IEEE 103(5):740–788. https://doi.org/10.1109/JPROC.2014.2378692
9. Voith Turbo Wind GmbH & Co. KG, Windstrom einzigartig erzeugen – Die WinDrive-Technologie. https://voith.com/cn/990_d_cr355_de_voith-windrive-fuer-windturbinen.pdf. Accessed 12 Aug 2021
10. Beckhoff Automation GmbH & Co. KG, DeWind mit neuem Antriebssystem für Windkraftanlage D8.2 – Neues Konzept für amerikanischen Markt, PC-Control 02 | 2008. http://www.pc-control.net/pdf/022008/solutions/pcc_0208_dewind_d.pdf
11. Jauch C, Gloe A, Hippel S, Thiesen H (2017) Increased wind energy yield and grid utilisation with continuous feed-in management. Energies 10:870. https://doi.org/10.3390/en10070870
12. Jauch C, Gloe A (2016) Improved feed-in management with wind turbines. In: Proceedings of the 15th wind integration workshop, Vienna, Austria
13. Jauch C, Matevosyan J, Ackermann T, Bolik S (2005) International comparison of requirements for connection of wind turbines to power systems. Wind Energy 8(3):295–306. https://doi.org/10.1002/we.160
14. Hiremath R, Moger T (2020) Comprehensive review on low voltage ride through capability of wind turbine generators. Int Trans Electr Energ Syst 30(10). https://doi.org/10.1002/2050-7038.12524
15. Jauch C, Gloe A (2019) Simultaneous inertia contribution and optimal grid utilization with wind turbines. Energies 12:3013. https://doi.org/10.3390/en12153013
16. Boemer JC (2016) On stability of sustainable power systems-network fault response of transmission systems with very high penetration of distributed generation. Technische Universiteit Delft. https://doi.org/10.4233/uuid:78bffb19-01ed-48f9-baf6-ffb395be68a0
17. Tielens P, Van Hertem D (2016) The relevance of inertia in power systems. Renew Sustain Energy Rev 55:999–1009. https://doi.org/10.1016/j.rser.2015.11.016
18. Muljadi E, Samaan N, Gevorgian V, Li J, Pasupulati S (2010) Short circuit current contribution for different wind turbine generator types. In: IEEE PES general meeting, pp 1–8. https://doi.org/10.1109/PES.2010.5589677
19. Jia J, Yang G, Nielsen AH, Muljadi E, Weinreich-Jensen P, Gevorgian V (2018) Synchronous condenser allocation for improving system short circuit ratio. In: 5th international conference on electric power and energy conversion systems (EPECS), pp 1–5. https://doi.org/10.1109/EPECS.2018.8443358
20. Ockhuis DK, Kamper M (2021) Potential of slip synchronous wind turbine systems: grid support and mechanical load mitigation. Energies 14:4995. https://doi.org/10.3390/en14164995
21. Sourkounis C, Tourou P (2013) Grid code requirements for wind power integration in Europe. In: Conference papers in energy, pp 1–9. https://doi.org/10.1155/2013/437674
22. Wu Y-K, Chang S-M, Mandal P (2019) Grid-connected wind power plants: a survey on the integration requirements in modern grid codes. In: Proceedings of the 2019 IEEE/IAS 55th

industrial and commercial power systems technical conference (ICPS). IEEE, Calgary, AB, Canada, pp 1–9. https://doi.org/10.1109/ICPS.2019.8733382

23. Denholm PL, Sun Y, Mai TT (2019) An introduction to grid services: concepts, technical requirements, and provision from wind. National Renewable Energy Laboratory, Golden, CO, NREL/TP-6A20-72578

24. Luo X, Wang J, Wojcik JD, Wang J, Li D, Draganescu M, Li Y, Miao S (2018) Review of voltage and frequency grid code specifications for electrical energy storage applications. Energies 11(5):1070. https://doi.org/10.3390/en11051070

25. Potgieter JHJ, Kamper MJ (2012) Design of new concept direct grid-connected slip-synchronous permanent-magnet wind generator. IEEE Trans Ind Appl 48(3):913–922. https://doi.org/10.1109/TIA.2012.2191251. Accessed 12 Aug 2021

26. Arbeiter M, Hopp M, Huhn M (2021) LVRT impact on tower loads, drivetrain torque and rotational speed—Measurement results of a 2 MW class DFIG wind turbine. Energies 14:3539. https://doi.org/10.3390/en14123539

27. Bian Y, Wyman-Pain H, Li F, Bhakar R, Mishra S, Padhy NP (2018) Demand side contributions for system inertia in the GB power system. IEEE Trans Power Syst 33(4):3521–3530. https://doi.org/10.1109/TPWRS.2017.2773531

28. Thiesen H, Jauch C (2020) Determining the load inertia contribution from different power consumer groups. Energies 13:1588. https://doi.org/10.3390/en13071588

29. Seneviratne C, Ozansoy C (2016) Frequency response due to a large generator loss with the increasing penetration of wind/PV generation-A literature review. Renew Sustain Energy Rev 57:659–668. https://doi.org/10.1016/j.rser.2015.12.051

30. Ørum E, Kuivaniemi M, Laasonen M, Bruseth AI, Jansson EA, Danell A, Elkington K, Modig N (2015) ENTSO-E Report—Future system inertia. https://www.statnett.no/globalassets/for-aktorer-i-kraftsystemet/utvikling-av-kraftsystemet/nordisk-frekvensstabilitet/future-system-inertia-phase-1.pdf. Accessed 31 Aug 2021

31. Jauch C, Sørensen P, Norheim I, Rasmussen C (2007) Simulation of the impact of wind power on the transient fault behavior of the nordic power system. Electr Power Syst Res 77(2):135–144. https://doi.org/10.1016/j.epsr.2006.02.006

32. De Rijcke S, Hamann N, Harjula A, Seppanen J, Kuusela A, Luukkonen I (2016) Damping power system oscillations by wind power plants. In: In: Conference on Proceedings of the 15th wind integration workshop, Vienna

33. Dominguez-Garcia JL, Gomis-Bellmunt O, Bianchi FD, Sumper A (2012) Power oscillation damping supported by wind power: a review. Renew Sustain Energy Rev 16(7):4994–5006. https://doi.org/10.1016/j.rser.2012.03.063

34. Jonkman J, Butterfield S, Musial W, Scott G (2009) Definition of a 5 MW reference wind turbine for offshore system development. National Renewable Energy Laboratory, Golden, Colorado, USA. https://www.nrel.gov/docs/fy09osti/38060.pdf. Accessed 01 Sep 2021

35. Jauch C (2020) First eigenmodes simulation model of a wind turbine—For control algorithm design. WETI Hochschule Flensburg. https://doi.org/10.13140/RG.2.2.17192.19204

36. Eriksson R, Modig N, Elkington K (2018) Synthetic inertia versus fast frequency response: a definition. IET Renew Power Gener 12(5):507–514. https://doi.org/10.1049/iet-rpg.2017.0370

37. EirGrid; Soni, All Island TSO facilitation of renewables studies. http://www.eirgridgroup.com/site-files/library/EirGrid/Facilitation-of-Renewables-Report.pdf. Accessed 01 Sep 2021

38. Roscoe AJ, Yu M, Dyśko A, Booth C, Ierna R, Zhu J, Urdal HA (2016) VSM (Virtual Synchronous Machine) convertor control model suitable for RMS studies for resolving system operator/owner challenges, In: Conference on proceedings of the 15th wind integration workshop, Vienna

39. Gloe A, Jauch C, Craciun B, Winkelmann J (2019) Continuous provision of synthetic inertia with wind turbines: implications for the wind turbine and for the grid. IET Renew Power Gener 13(5):668–675. https://doi.org/10.1049/iet-rpg.2018.5263

40. Gloe A, Jauch C (2021) Grid support with wind turbines: the case of the 2019 blackout in Flensburg. Energies 14:1697. https://doi.org/10.3390/en14061697

41. Gloe A, Jauch C, Craciun B, Zanter A, Winkelmann J (2021) Influence of continuous provision of synthetic inertia on the mechanical loads of a wind turbine. Energies 14:5185. https://doi.org/10.3390/en14165185
42. Hydro-Québec (2019) Technical requirements for the connection of generating stations to the hydro-Québec transmission system, Decision D-2018-145. http://www.hydroquebec.com/transenergie/fr/commerce/pdf/2_Requirements_generating_stations_D-2018-145_2018-11-15.pdf. Accessed 26 Jan 2021
43. ENTSO-E (2016) Frequency stability evaluation criteria for the synchronous zone of continental Europe—Requirements and impacting factors—RG-CE system protection & dynamics sub group. https://eepublicdownloads.entsoe.eu/clean-documents/SOC%20documents/RGCE_SPD_frequency_stability_criteria_v10.pdf. Accessed 06 Sep 2021
44. EirGrid, Grid Code, Version (2020). http://www.eirgridgroup.com/site-files/library/EirGrid/GridCodeVersion9.pdf. Accessed 06 Sep 2021
45. Jauch C, Cronin T, Sørensen P, Bak-Jensen BA (2007) Fuzzy logic pitch angle controller for power system stabilization. Wind Energy 10(1):19–30. https://doi.org/10.1002/we.205
46. Jauch C (2007) Transient and dynamic control of a variable speed wind turbine with synchronous generator. Wind Energy 10:247–269. https://doi.org/10.1002/we.220

Prof. Dr. Clemens Jauch has been working in the wind energy sector since 1999. After several years as a development engineer at the wind turbine manufacturers Nordex Energy and Suzlon Energy, as well as a doctorate at the Risø National Laboratory (today DTU Windenergy) in Denmark, he has been Professor of Wind Energy Technology at Flensburg University of Applied Sciences since 2012.

Offshore Wind Energy

Christian Keindorf

1 Introduction

1.1 History and Development Trends

The share of offshore wind energy in Europe's electrical power production has increased significantly in recent years. By the end of 2020, a capacity of approx. 25 GW had been fully commissioned in Europe. There are now 116 offshore wind farms in operation, which can be allocated to 12 European countries. A total of 5,402 offshore wind turbines (OWT) have been installed for this purpose, of which approx. 79% are located in the North Sea, 9% in the Baltic Sea and 12% in the Irish Sea. Figure 1 shows on the one hand the accumulated capacity of offshore wind energy in Europe and on the other hand the new installed capacity per year.

Table 1 shows the national shares of capacity for offshore wind energy in Europe.

In Germany, a total of 1,501 offshore wind turbines with a total capacity of 7,689 MW were connected to the grid by the end of 2020. A further 32 OWT had been fully erected by then but were still waiting for grid connection.

Most OWT were supplied and installed by Siemens, which have 68% market share in Europe by the end of 2020, followed by Vestas with 24% and Senvion with 4.4%. Although the BARD group has 1.5% market share, it is no longer active in the wind industry. Furthermore, GE and Alstom's turbines will in future be grouped under GE Renewable Energy, which has the remaining market share.

The average rated power of an OWT installed in 2020 is 8.2 MW. A complete offshore wind farm installed in 2020 has an average capacity of 788 MW. Compared to 2015 with 338 MW, it can be seen that the size of a wind farm has increased significantly.

C. Keindorf (✉)
Kiel University of Applied Sciences, Grenzstr. 3, D-24149 Kiel, Germany
e-mail: christian.keindorf@fh-kiel.de
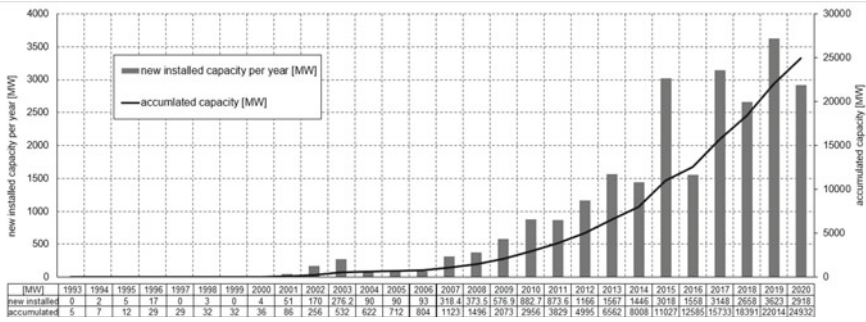
Fig. 1 Development of offshore wind energy in Europe. Data source EWEA

Table 1 Installed capacity of offshore wind energy in Europe until the end of 2020 [EWEA]	Nation	Installed capacity (MW)	Number of turbines	Number of windfarms
	United Kingdom	10 428	2 294	40
	Germany	7 689	1 501	29
	Netherlands	2 611	537	9
	Belgium	2 261	399	11
	Denmark	1 703	559	14
	Sweden	192	80	3
	Finland	71	19	3
	Ireland	25	7	1
	Portugal	25	3	1
	Spain	5	1	1
	Norway	2	1	1
	France	2	1	1
	Total	25 014	5 402	116

The grid connections for German offshore wind farms are listed in Table 2, distinguishing between the North Sea and the Baltic Sea. A total of approx. 8.6 GW of power transmission to the shore is installed and in operation.

Further grid connections must be realized for future offshore wind farms, for which the Offshore Grid Development Plan is the basis. An additional capacity of approx. 20 GW is planned for further grid connections in German sea areas. Thus, a total capacity of approx. 28.6 GW can be expected.

By 2030, offshore wind turbines with a total capacity of 20 GW shall be installed in the German sector of North Sea and Baltic Sea, for which the grid connections must be completed in time. With reference to Table 1 this would require an annual new installation of approx. 1.2 GW. The European Wind Energy Association (EWEA)

Table 2 Grid connections for German offshore wind farms (North Sea and Baltic Sea)

Grid connection	Year of commissioning	Connected offshore wind farms	Capacity (MW)
North Sea			
Alpha Ventus	2010	Alpha Ventus	60
BorWin 1	2010	BARD Offshore 1	400
BorWin 2	2015	Global Tech I Veja Mate	800
BorWin 3	2019	OWP Albatross	900
DolWin 1	2014	Trianel Wind Farm Borkum MEG Offshore I	800
DolWin 2	2015	North Sea One Gode Wind I and II	900
DolWin 3	2017	Borkum Riffgrund I and II	900
HelWin 1	2014	Nordsee Ost Meerwind Süd/Ost	576
HelWin2	2015	Amrumbank West	690
Nordergründe	2016	Nordergründe	111
Riffgat	2014	Riffgat	108
SylWin 1	2014	DanTysk Butendiek Sandbank	864
Baltic Sea			
Baltic 1	2011	Baltic 1	200
Baltic 2	2014	EnBW Baltic 2	400
Total			8 609

has forecast a total capacity of approx. 80–100 GW for Europe by 2030. Future forecasts will be significantly influenced by the European Green Deal. However, 300 GW offshore wind energy should be installed and available by 2050.

The costs must be further reduced in all phases of the supply chain to accelerate the continuous expansion of offshore wind energy. The decisive factors are the levelized costs of energy (LCOE), which are compared in Fig. 2 with other kinds of energy resources in Germany. Compared to conventional power plants, offshore wind energy offers more favourable conditions, although these must be evaluated depending on the site conditions. However, onshore wind energy and photovoltaics still have more favourable LCOE. With regard to the size of turbines, it is expected that the costs for an offshore wind farm (OWF) can be further reduced because with larger turbines a smaller number of units will be required for the same total capacity of the OWF. This will also reduce the number of inner-park cables, as well as the number of foundations. For example, in 2015, 100 turbines were still required for a 400 MW offshore wind farm, if an average rated power of about 4 MW for each turbine is taken into account. In contrast, in 2020, with approximately 8 MW average rated
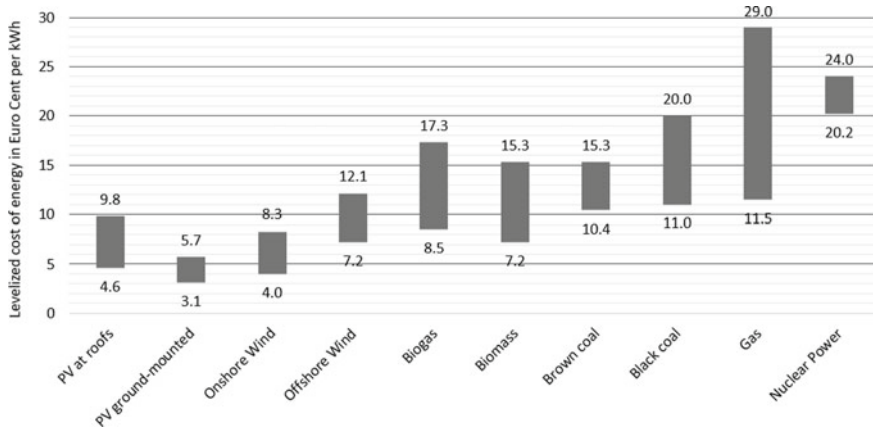
Fig. 2 Levelized cost of energy for renewable and conventional energies in Euro cents per kWh for locations in Germany 2021. Data source Fraunhofer ISE

power, only half the number of turbines (50) were needed to achieve the same size of the OWF. This trend will continue in the future and enable further potential savings in material and finally in costs.

The actual LCOE for offshore wind energy in Germany range from 7.2 to 12.1 Euro cents per installed kW of nominal capacity [data source Fraunhofer ISE], which depends on the site-specific conditions and the environmental conditions as well as the setup of the OWF. However, the offshore wind energy can be classified as competitive compared to conventional energy plants, see Fig. 2.

It is also traceable in Fig. 2 that renewable energy production with photovoltaics and onshore wind enables even lower LCOE as offshore wind energy, because of lower transportation and installation costs. The differences between onshore and offshore wind turbines including the structural components are explained in more detail in the following chapter.

1.2 Differences Between Onshore and Offshore Wind Turbines

Offshore wind turbines are subject to almost the same load actions as onshore wind turbines (wind, ice, temperature, etc.), if components of rotor blades, nacelle and tower are analysed. However, stronger and steadier winds on average (lower turbulence) are observed in OWF. Thus, 4,000–4,500 full operational hours per year were recorded for the first offshore wind turbines in the "Alpha Ventus" research wind farm. In comparison approx. 1,700–2,500 full operational hours per year can be expected for onshore wind turbines, depending on the location.
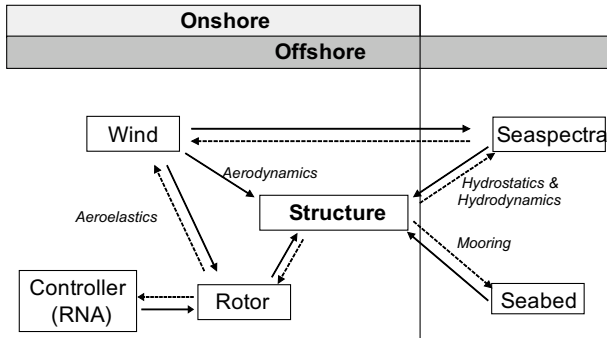
Fig. 3 Differences between onshore and offshore wind turbines

In the case of a larger number of wind farms, the turbines influence each other because they are relatively close together for cost reasons for the cable connections. As a result, stronger turbulences can occur, which also have an effect on the loads (size of the voltage amplitudes and number of load changes).

Offshore wind turbines are subject to additional loads compared to onshore wind turbines. These mainly concern the support structure and the foundation (e.g. wave, current and ice loads). In addition to aeroelastic and aerodynamic effects, hydrostatic and hydrodynamic loads must also be taken into account for OWT. Therefore, coupled load simulations (wind and wave) are required for the structural design, which also include the soil-structure-interaction between the foundation and seabed, see Fig. 3. In addition, mooring lines are required for floating structures, which are designed with so-called mooring analyses.

1.3 Design Basis for Offshore Wind Farms

The design basis for offshore wind farms is the Standard 7005 [1] established by the Federal Maritime and Hydrographic Agency (BSH) which is responsible for the regulations with regard to the German Territorial Sea (SeeAnlV). The BSH Standards describe the minimum requirements for the design of structural components for OWT with regard to their structural integrity [1].

The following project phases are defined by the BSH for an OWF:

1. Development (design basis with site-specific data and metocean conditions)
2. Design (modelling, structural analysis, reports, method statements and drawings)
3. Execution (fabrication, transportation, installation and commissioning)
4. Operation (plant operation, maintenance, repair and monitoring)
5. Decommissioning (planning and execution of deconstruction).

The requirement of compliance with the state of the art or, alternatively, the state of research refers to the completion of the respective project phase or, in the case of

the design phase, of the respective section. Each project phase end with the so-called release by the BSH as approval authority [1].

The Eurocodes are primarily to be applied when designing support structures and foundations for OWT. However, since not all actions, such as wave and current loads, are regulated in these Eurocodes, suitable offshore standards and guidelines may be applied in addition for the structural design or special components. These include DIN EN 61400-3 [2], the ISO, API and NORSOK standards and the guidelines of certification agencies.

In addition to the requirements of DIN EN 61400-1 for onshore wind turbines, further criteria for the assessment of site-specific conditions and metocean conditions are defined in DIN EN 61400-3 [2] for OWT. Furthermore, essential design requirements are specified to ensure the structural integrity of each component for OWT. Compliance with the requirements of this standard provides adequate safety against damage or failure due to extreme load situations and hazards during the operational lifetime.

1.4   Environmental Protection and Safety Requirements

The BSH Standard 7003 [3] must be considered for the investigation of the effects of OWT related to marine environment. The approval authority imposes numerous requirements on OWT to be erected, with the following aspects being reviewed in particular:

- Suitability of the location (adverse effects on shipping and fishing)
- Suitability of the seabed
- Risk analysis for ship collisions
- Influence on birds and marine fauna and flora (fish, marine mammals etc.)
- Noise emissions to the environment
- Distances between OWT within a wind farm and between OWF
- Marking of the installations (optical, acoustic)
- Marking on nautical charts
- Routes of sea cables
- Options for decommissioning.

The verifications must be provided by the applicant for the OWF with the assistance of suppliers and experts. The approval authority reserves the right to impose conditions before approvals are granted for each project phase.

Furthermore, the offshore works have to fulfil more requirements in terms of health and safety compared to constructions works onshore. For example, the transfer from the service vessel to the OWT via so-called boat landing represents a critical phase for the personnel, which must be trained previously so that the suitability of each person can be certified. The BSH standards set the following criteria for the safety requirements for offshore works:

- Measures for health and safety as well as for fire protection must be considered during all project phases
- Limits for electromagnetic emissions must be checked for no interference with the common navigation and communication systems at the sea.

2 Essential Components of an Offshore Wind Farm

An offshore wind farm essentially consists of the following components:

- Foundations in the seabed (foundation elements)
- Support structures (tower and substructure, if applicable, load-bearing components of the operational structure for offshore stations)
- Operational components (nacelle, hub and rotor blades for OWT, topside for offshore stations)
- Sea cables between OWT and interconnection to the offshore substation
- Components for power transmission from the substation via the offshore transformer station to the grid connection at the shore and
- further offshore installations (e.g. measuring mast, residential platform).

Figure 4 shows the major components of an OWF using the example of an OWT with monopile foundation and transformer station with jacket foundation.

2.1 Turbines for Offshore Wind Farms

The turbine, together with the rotor blades, are the operational components of an OWT, cf. Fig. 4. Due to the high investment costs for OWF, turbine sizes tend towards to 12 MW or even 16 MW rated power per turbine in order to obtain the highest possible energy output for one location and to reduce the required number of OWT compared to the 4–8 MW class. As an example, Table 3 shows a comparison between different turbine classes with regard to their key facts. The specific power in W/m^2 is the ratio of the rated power to the swept area of the rotor. The specific nacelle mass in kg/kW is the ratio of the nacelle weight to the rated power. The first prototypes with 16 MW rated power are expected for 2025 together with new challenges for the offshore industry. For example, rotor blades will be more than 115 m long, which have to be manufactured, transported and finally installed. Such components require high-quality manufacturing processes and specialized transportation and installation concepts.

With regard to the technical details for each component of a turbine, reference is made to the previous chapters. For the transition to the support structure, the nacelle has a ring flange at the lower edge to enable a force transfer to the tower top. The different support structures and foundations for OWT are explained more in detail in the following sections.
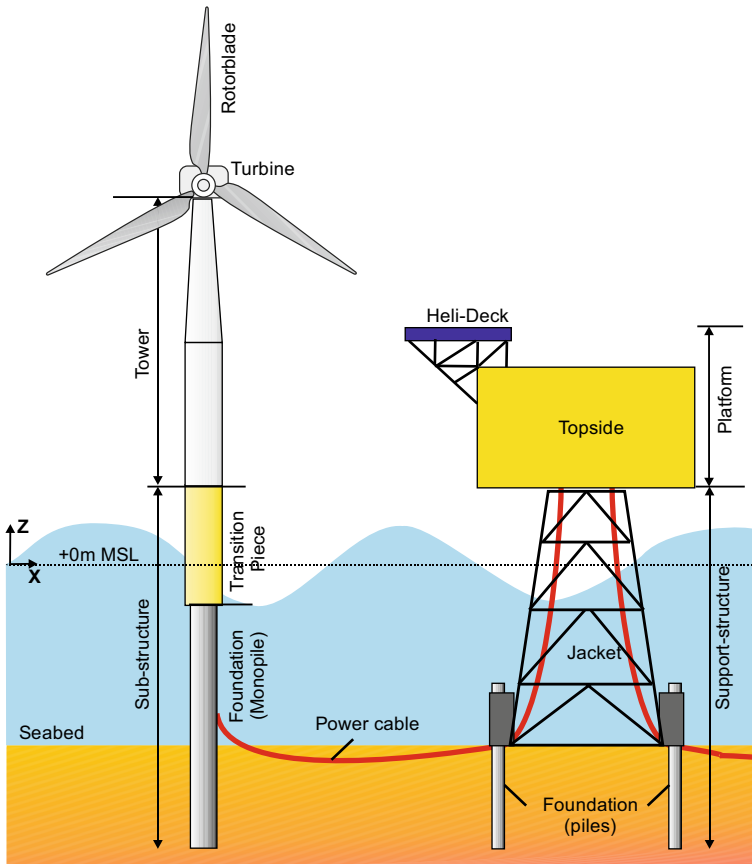
Fig. 4 Major components of an offshore wind farm

Table 3 Turbine classes for offshore wind farms

Turbine class	4 MW	8 MW	12 MW	16 MW
Rotor diameter (m)	130	164	220	242
Swept area of rotor (m^2)	13'273	21'124	38'013	45'996
Hub height above MSL (m)	90 or project-specific	105 or project-specific	110 or project specific	115 or project specific
Tower top mass (kg)	Approx. 240'000	Approx. 500'000	Approx. 685'000	>600'000
Spec. power (W/m^2)	301	379	316	348
Spec. mass of nacelle (kg/kW)	60,0	62,5	57,1	37,5

2.2   Support Structures for Offshore Wind Turbines

The material properties to be used for the structural components of an OWT (concrete, reinforcing steel, prestressing steel, steel, plastics, fibre composites, etc.) must be specified during the design phase. In principle, generally approved building materials in accordance with the list of regulated building products shall be used for the load-bearing components (primary and secondary structure). Exceptions are to be applied for at the BSH via a single case approval.

2.2.1   Tower

The tower of an OWT often consists of tubular steel sections, which are manufactured as conical or cylindrical cans. The steel sections are often assembled at ship yards or workshops near the coast specialized for the offshore industry. Several cans, which are previously cut from heavy steel plates and formed with round roll bending machines. The length or height of a single can is limited by the equipment of the workshop and is usually 3 m. After all longitudinal seams have been welded on the cans, the first can is welded onto a ring flange in circumferential direction. The ring flange ensures the stability for the ongoing assembly so that further cans can be welded to get finally a complete tower section, see Fig. 5.
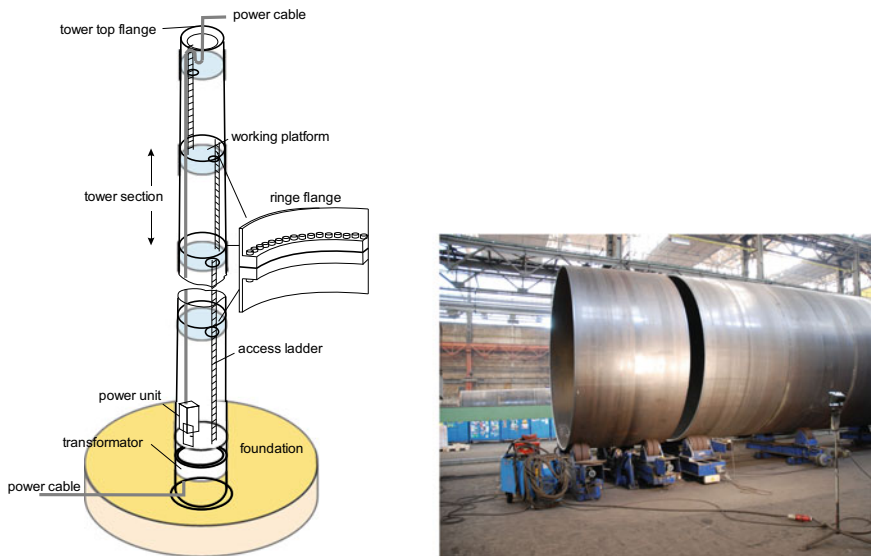
Fig. 5   Structural components and fabrication of tower sections

If the welding process for the tower section is finished, attachments for tower internals (ladder, working platforms, cable shafts, etc.) will be manufactured. Afterwards, a quality check is carried out to ensure that all structural components are free of defects and that all dimensions keep within the given tolerances. Finally, the corrosion protection has been applied for each tower section. Thus, the tower sections can be transported horizontally or vertically by vessels to the location for offshore installation. Vertical transport eliminates the upending procedure, which saves assembly time. However, the slender tower sections must be checked for fatigue due to vortex-induced vibrations (VIV) that can occur during the sea transport.

The tower sections are lifted by a crane and positioned onto the foundation. Afterwards the bolting operation starts at the ring flange connection to ensure the force transfer between the tower and the foundation. High-strength bolts are used with a certain pretension force for these ring flange connections having the steel grade 10.9. The metric size from M39 up to M72 are covered by DASt guideline 021 for the high-strength bolts, whereas smaller sizes are regulated in the Eurocode EN 1993-1-8 in combination with EN 1090-2.

For further details on the tower sections, please refer to the descriptions in Chap. 7, because these structural components are designed very similar to onshore wind turbines.

2.2.2 Transition Piece

A so-called Transition Piece (TP) is arranged between the lowest tower section and the Monopile (MP) to compensate misalignments and imperfections due to the pile driving procedure. The boat landing, the external access platform and the internal working platforms (e.g. air tight deck) are already mounted on the TP so that after its installation the offshore structure is accessible for further installation work on site. A ring flange connection is positioned at top of the TP to ensure the force transfer to the lowest tower section.

The TP has often a so-called skirt to get an overlapped length with the monopile (MP). The vertical position of the TP will be measured and modified with the assistance of hydraulic jacks to minimize the inclination. Afterwards, the annular gap between MP and TP will be filled with a high-strength grout, which is pumped through fixed pipes or flexible hoses. After the grout has hardened, contact pressures and frictional stresses can be transmitted via the grout. This kind of a grouted-connection is one of the non-regulated construction methods in Germany, which is the reason for a single case approval at the BSH.

2.3 Bottom-Fixed Foundations for Offshore Wind Turbines

Typical bottom-fixed foundations are presented in Fig. 6, which are used for OWT.
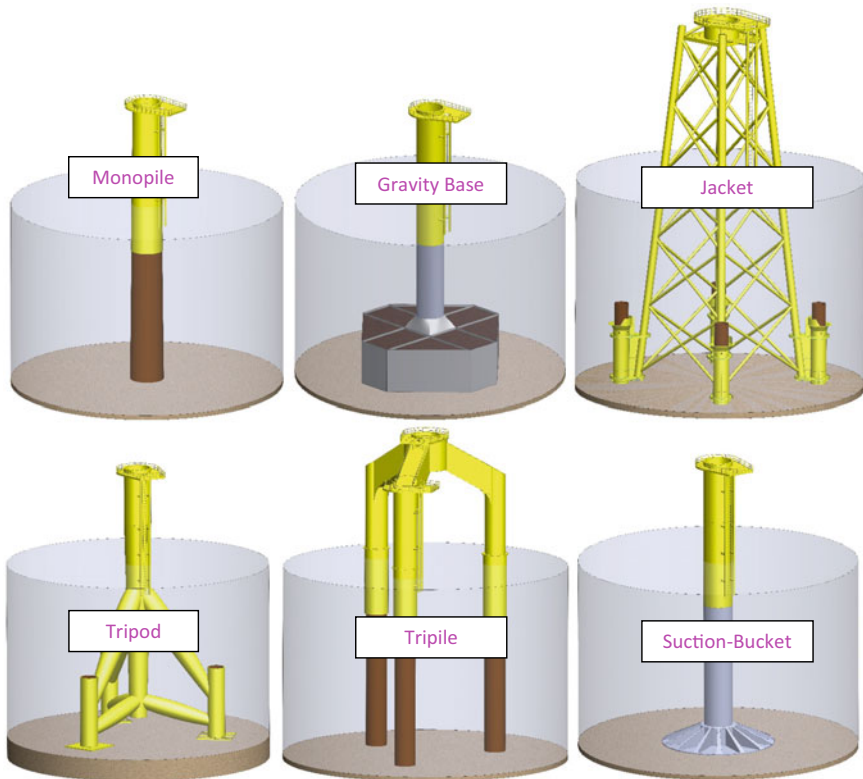
Fig. 6 Fixed bottom foundations for offshore wind turbines [SKI]

The application of bottom-fixed foundations depends on numerous criteria, such as:

- required height h of the foundation depending on the water depth
- maximum stresses (increase with h or h^2)
- Maximum deformations or inclinations of the structure (increase with approx. h^4 or h^3)
- Natural frequencies (decrease with approx. $1/h^2$)
- Location at sea (wave heights, sea spectra, currents, wind conditions)
- Nature of the seabed and bearing capacity of the soil layers
- Required embedded length for piles (e.g. max. pile driving energy)
- Weight of the foundation (manufacturing, transportation, crane capacities)
- Requirements for environmental protection (e.g. noise emission during pile driving).

The market share for foundations in Europe by the end of 2020 is dominated by monopiles, which have a share of 81.2% with 4 681 installations, followed by jackets with 568 installations (9.9%). The 289 gravity-base foundations have a market share

of about 5%. The market share for OWT with 126 tripods (2.2%) and 80 triples (1.4%) will be lower in the future because these types of foundations are no longer considered in actual plans for the next generation of OWF.

The details of the different type of foundations are explained more in detail in the following chapters.

2.3.1 Monopile

A monopile foundation is very often used for OWT, where a single pile is embedded into the soil, cf. Fig. 6. As an alternative to the driving method, vibrating methods can also be used to reduce noise levels. Monopiles with diameters of up to 7 m and lengths of up to 100 m are now state of the art. The installation methods are constantly being further developed so that diameters of 8–10 m will also be possible in the future. With regard to the length of the cans, 3 m is the standard, with current developments taking into account the use of 4 m cans to reduce the number of circumferential welds. The tonnage per MP will exceed 1,000 tons in the future (XXL monopiles), so that installation vessels with larger crane capacities will also be required for this purpose. The so-called floating trapped air concept can be used as an alternative installation method, whereby the MP will be sealed with cover plates and towed to the offshore location. During the upending procedure, the full weight of the MP does not have to be lifted because the buoyancy force assists the crane force.

The developments for pile driving technology have led to lower tolerances for inclinations, so ring flange connections between MP and TP are used as an alternative solution compared to grouted connections. Too large inclinations would cause negative effects for operation of the turbine and its rotor blades. However, fatigue loading must be considered for driven monopiles with ring flanges. The load cycles due to pile driving have to be accumulated with those from the operational phase to evaluate the accumulated damage value for the fatigue limit state of certain notch details. Compared to the grouted-connection, a ring flange connection can be installed independently of the temperature and accelerates the dismantling process, because the bolts of the ring flange can be released very quickly with torque tools.

The advantages and disadvantages of a monopile foundation are listed below.

Pros:

- simple static system
- simple and cost-effective fabrication
- no preparation of the seabed required.

Cons:

- high single weight
- high pile driving energies and noise mitigation measures required
- dismantling of the full length of the monopile is difficult or even impossible.

Recent developments consider it to not be a TP anymore. Thus, the ring flange of the MP is directly connected with the ring flange of the lowest tower section.

2.3.2   Gravity Base Foundation

A gravity foundation is not one of the bottom-fixed foundations, because it is only settled on the seabed and does not have a certain embedment or foundation elements into the soil layers. Gravity base foundations transfer forces and moments due to permanent load actions (e.g. weight) and variable load actions (e.g. wind and wave loads) via friction stresses and contact pressures to the seabed. The load-bearing behaviour is similar to that of a shallow foundation for onshore turbines, so that the geotechnical verifications, e.g. ground failure, soil pressure, overturning and sliding must also be checked for this kind of foundation. Steel or concrete structures that are lowered and ballasted are often used for gravity base foundations, see Fig. 6.

In Danish offshore wind farms, for example, gravity base foundations were used, which were installed at water depths of up to about 10 m. The advantages and disadvantages of this kind of foundation are listed as follows.

Pros:

- Cost-effective fabrication directly at the quay or dry dock (outside a workshop)
- low noise emissions during installation (no pile driving required)
- high load bearing capacity in icy conditions
- complete decommissioning possible.

Cons:

- high investment costs for the production line (partly outside halls)
- high single weights
- larger footprints required (preparation of the seabed may be necessary)
- higher expenditure for scour protection.

2.3.3   Jacket

A jacket foundation is a lattice structure composed of legs and braces made of tubular steel members. The braces can be positioned horizontally and/or diagonally to provide stiffening as well as to reduce the flexural buckling of the legs. The tubular members are connected to each other with welded or cast-iron joints, see Fig. 6.

The forces and moments are transmitted into the seabed via piles which are guided by sleeves next to the jacket legs. A stiff connection between the pile and sleeve is ensured by grouted pile-sleeve connections, which have to be carried out completely under water with the assistance of pumping equipment. In this process, the grout material pumped via fixed pipes or flexible hoses and pumped upwards via inlet valves into the annular gap between the pile and sleeve.

It is possible to use suction buckets instead of piles. Jackets are state of the art over several decades and can be classified as suitable foundations for offshore platforms in the oil and gas industry at water depths of up to 400 m. The advantages and disadvantages of a jacket foundation are:

Pros:

- low weight along the height of structure
- higher stiffness due to the lattice structure
- smaller pile diameters possible, but more pieces of them required.

Cons:

- Higher welding effort for tubular joints
- Higher effort for inspection and maintenance
- Lower safety against ship collision than with monopiles.

2.3.4 Tripod

Tripods have three legs connected with a centre tube, cf. Fig. 6. The connection to the piles is made by grouted pile-sleeve-connections. Compared to jackets, fewer tubular joints are required, but the dimensions of the tubular joints are significantly larger and require more effort of welding. The top of the central tube is positioned at the interface with tower bottom (TB), where the connection also has a ring flange with high-strength bolts.

Pros:

- lower number of tubular joints compared to jackets
- higher stiffness than monopile
- smaller number of different tubular members than jackets.

Cons:

- large tubular joints required with high welding effort
- higher risk for scour effects
- higher single weight compared to jackets for the same OWT.

2.3.5 Tripile

A tripile foundation has three piles below a centre structure with three radial beams, cf. Fig. 6. The centre structure has three pins, which will be lowered by a crane into the piles, which were previously driven into the seabed. A grouted connection is provided between each pin (inner steel tube) and the pile (outer steel tube) in order to be able to compensate fabrication and installation tolerances. The diameters of the driven piles can be smaller compared to monopiles, so the size of the required installation equipment is still moderate. So far, tripile foundations have only been

installed and commissioned in serial production for the offshore wind farm "BARD Offshore 1".

Pros:

- only driven piles are located in the corrosive splash zone
- smaller diameters and lower weights for the piles compared to monopile foundations.

Cons:

- high effort for the fabrication of the centre structure
- high bending moments and axial forces at each pile
- low torsional stiffness due to missing braces (no lattice structure).

2.3.6   Suction-Bucket

A suction bucket has often a cylindrical shape with a watertight cover plate on the top and an open end, cf. Fig. 6. The bucket will initially push itself a certain depth into the seabed by self-weight. Pump hoses are then connected to the top cover so that the generated suction is used to suck the chamber into the seabed. The relative difference of pressure inside and outside the bucket causes this additional effect as driving force. As a further support for the penetration process, cutting nozzles can also be located at the lower edge of the bucket in order to flush out soil particles directly below the tip of the bucket.

The gravity force in addition with the driving force due to suction must greater as the sum of friction forces and bearing pressure between the steel surfaces and the soil. The forces that occur due to the relative suction during installation must not be taken into account when verifying the stability during operation, as the difference in pressure will be eliminated after the pumps will be stopped and the water will flow into the chamber (bucket).

In principle, this type of foundation replaces driven piles and can be designed as a mono-bucket or multiple-bucket. It has been demonstrated in single offshore campaigns, that a ratio between length (L) and diameter (D) can achieve a value of nearly $L/D = 1$. Especially for locations in the North Sea it could be practically possible, where non-cohesive soil layers (e.g. sand) are dominant. The total soil mass enclosed by the bucket contributes to the stability of the foundation. In addition to the lower installation effort and relatively simple equipment (pumps, valves and hoses), the dismantling by reversing the installation principle (overpressure) should also be mentioned as an advantage for suction buckets. Up to now, suction buckets have been used primarily for oil and gas platforms and for measuring masts. A first OWT with buckets was installed as a prototype in the offshore wind farm "Borkum Riffgrund 1" in August 2014, whereby a bucket was connected at the bottom of each leg of the jacket. This prototype was used by the involved parties to investigate the interaction between the structure and the soil under cyclic loads.

Estimation of the circumferential stress of a cylinder due to external or internal pressure:

$$\sigma = \frac{p \cdot R}{t} \tag{1}$$

Estimation of the critical buckling pressure of a cylinder due to external pressure (according to EBNER [4]):

$$p_{\text{krit}} = \frac{\pi \cdot E \cdot R}{9 \cdot l} \left(\frac{t}{R} \right)^{5/2} \cdot \sqrt[4]{\frac{36}{\left(1 - v^2 \right)^3}} \tag{2}$$

with p_{krit} = critical buckling pressure = maximum permissible pressure difference outside/inside; E = modulus of elasticity of the material; v = Poisson ratio; R = radius of the cylinder; l = length of the cylinder; t = wall thickness

The advantages and disadvantages of a suction bucket as foundation are listed below.

Pros:

- very low noise emissions (no pile hammer equipment required)
- controlled penetration process without pile driving fatigue and misalignments
- complete decommissioning possible (reversal of the principle—generate over-pressure)
- relatively low tonnage.

Cons:

- limited penetration depths, as not suitable for every soil type without restrictions
- increased risk of buckling of the cylinder shell due to the difference in pressure
- low stability for cyclic loads and lifting forces
- extra effort for scour protection.

2.4 Floating Structures for Offshore Wind Turbines

The potential of offshore wind energy is significantly greater if locations with water depths greater than 50 m are also taken into account. Many coastal regions in Europe have coasts with deep water, such as Norway, France and Portugal. Thus, floating structures for offshore wind turbines are being more and more considered in these countries. There are also initial projects and prototypes in America and Japan pushing floating offshore wind. Experiences from the oil and gas industry, which have already implemented floating structures, are considered. The floating structures for OWT, which were predominantly used for the first prototypes are:

- Spar Buoy
- Tension Leg Platform
- Semi-Submersible Platform

These basic variants are described more in detail in the following chapters.

2.4.1 Spar Buoy

A so-called "Spar Buoy" can be considered as a floating structure for water depths of 200 m and more, see Fig. 7. The Spar Buoy is a vertical tubular section, where the centre of gravity (CoG) is significantly below the centre of buoyancy (CoB) to ensure a stabilizing moment. The additional buoyancy is compensated by tension forces in the mooring lines and ballast materials. This will stabilize the vertical position of the floating foundation. Due to the high effort of tonnage for the Spar Buoy and the moorings as well as the complex installation, the LCOE are higher as for bottom-fixed foundations. However, Spar Buoys allow the use of areas with deep water and the LCOE can be reduced when large wind turbines will be considered. The length of the mooring lines made of steel are several hundred meters and requires hundreds of tons. However, as the development of OWT goes on (cf Table 3), the higher effort for materials will be more economical in the future.

Fig. 7 Spar Buoy for a floating offshore wind turbine [SKI]

The first commercial OWT with a floating foundation was installed in Norway in 2009 with a Spar Buoy (Hywind project). The shaft above the mean seawater level is of steel shaft and below MSL a concrete shaft, taking into account a draft of nearly 90 m. In addition, approx. 3,500 tons of ballasting were necessary to keep the 2.3 MW turbine from Siemens in stable position. Further possible applications for this type of floating foundations are currently investigated, e.g. at the coasts of Scotland.

2.4.2 Tension Leg Platform (TLP)

A Tension Leg Platform are provided with large excess buoyancy when fully submerged. This is compensated for by tension legs with high pretension forces to hold the floater completely below the water line. The shape of the platform is often triangular or quadrangular. The tower sections are preferably connected in the centre of the floater, see Fig. 8.

When the platform is heeled by wind and wave loads, the pretension forces of the legs will be increased on the side facing the wind (luv) and reduced on the side facing away from the wind (lee), depending on the orientation of the system to the wind direction. The changed forces in the tendons or ropes cause a restoring or stabilizing moment on the platform. As long as the stabilizing moment is greater than the heeling moment, the OWT remains buoyant. The tensile forces must be large enough to compensate the heeling moment due to operational and environmental loads of the OWT in all directions.

Due to the high effort of material including the tension legs and the floater, such foundations are only to be considered as an alternative to bottom-fixed foundations, if the water depth achieves more than 60 m and large wind turbines will be considered.

Fig. 8 Tension Leg Platform for a floating offshore wind turbine [SKI]
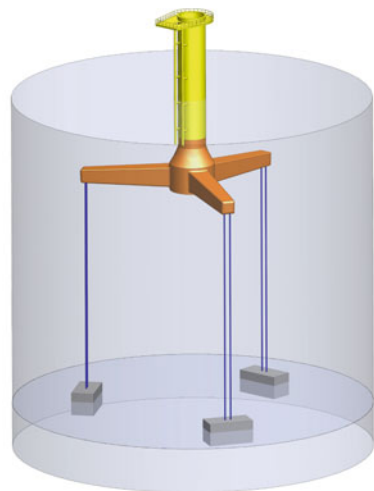
Tension Leg Platforms cannot be recommended for shallow waters due to economic reasons.

2.4.3 Semi-Submersible Platform

A floating OWT can be also realized with a Semi-Submersible Platform anchored to the seabed with mooring lines as steel chains or polyester ropes, cf. Fig. 9. The restoring forces are not prestressing forces as in the TLP variant, but self-weights of the mooring lines and friction forces between the chain and the seabed. The tower sections are connected either in the middle of the floater or at one edger, as is the case for example with the prototypes of Principal Power in Portugal. Due to the large steel columns, it is also possible to install an active ballast system, whereby ballast water is pumped from one column to the other to compensate heeling effects.

Another advantage is the floating capability of the turbine during transportation and installation, so that no crane vessel is required. During the transportation phase, the complete system including the rotor blades can already be assembled. Disadvantage are the long mooring lines, which can be several hundred meters similar to the mooring lines for a Spar Buoy.

Table 4 gives an overview of realized prototypes for floating OWT in Europe until the end of 2020.

Fig. 9 Semi-Submersible Platform for a floating offshore wind turbine [SKI]
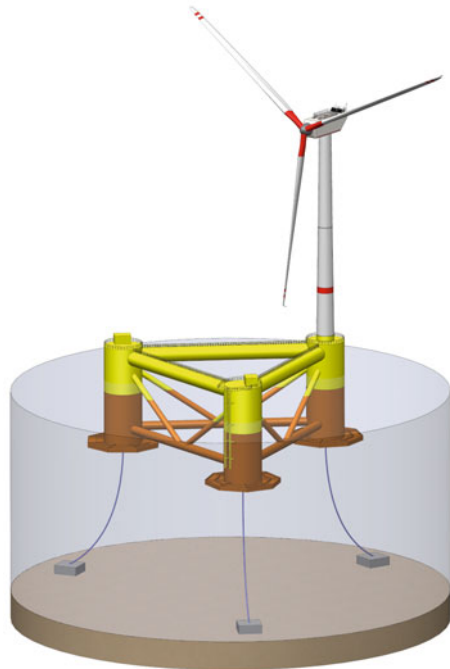
Table 4 Realized prototypes for floating offshore wind turbines in Europe

Year	Country	Name of project	Type of foundation	Type of turbine	Capacity (MW)
2007	Italy	Blue H technologies	TLP	Two-Blades 0.08 MW	0.08
2009	Norway	Hywind demonstrator	Spar Buoy	Siemens 2.3 MW	2.3
2011	Portugal	WindFloat Phase 1	Semi-submersible	Vestas 2.0 MW	2.0
2011	Norway	Sway	Spar Buoy	Sway A/S	0.015
2017	UK	Hywind Scotland	Spar Buoy	Siemens 6.0 MW	30.0
2020	Portugal	WindFloat Atlantic	Semi-submersible	Siemens 8.4 MW	25.2
2021	UK	Kincardine	Semi-submersible	Vestas 9.6 MW	48.0

There are many other activities worldwide for the development of floating foundations, mainly in USA, Japan, South Korea, Taiwan and China, but these activities are not included in the table.

Further and larger commercial projects for floating OWT are expected in Europe for the next few years. A selection of the upcoming projects is shown in Table 5.

Based on the capacity per project, it can be seen that the commercial phase of floating structures for OWT has begun and the size of wind farms will be increased. In future, floating wind farms are expected to contribute significantly to the generation of green electricity worldwide.

Table 5 Planned projects for floating offshore wind turbines in Europe

Year	Country	Name of project	Type of foundation	Type of turbine (MW)	Capacity (MW)
2022	Spain	Flocan 5 Canary	Semi-submersible	Gamesa 5.0	25.0
2022	Norway	Hywind Rope	Spar Buoy	Siemens 8.0	88.0
2022	France	Eoliennes Flottantes de Groix	Semi-submersible	Vestas 9.5	28.5
2023	France	EFGL	Semi-submersible	Vestas 10.0	30.0
2023	France	EolMed	Barge	Vestas 10.0	30.0
2023	France	Provence grand large	TLP	Siemens 8.4	25.2

2.5 Offshore Stations

A converter platform with technology for high-voltage direct current transmission (HVDC) or an offshore substation with technology for alternate current (AC) within a wind cluster are classified as offshore stations according of BSH Standard 7005 [1]. These offshore stations basically consist of an operational structure (topside), a support structure and foundation elements, cf. Fig. 4.

The electrical energy from each OWT is transmitted via submarine cables to an offshore substation within the wind farm. The alternating current is transformed to a higher voltage level (often to 155 kV) at these substations.

Figure 10 shows how the electrical energy is transported via further submarine cables to a converter station, where the alternating current (AC) is converted into direct current (DC). The voltage level of the direct current is usually 320 kV.

The advantage of converting to direct current is that with high-voltage direct current (HVDC) transmission, high power can be transmitted over long distances without compensations. The losses of energy for this HVDC technology is significantly lower than those of HVAC systems for power transmission. The power is converted back at the shore into AC so that it can used for the existing power grid in Germany.

The converter stations often have the names of the windcluster for grid connections (cf. Table 2). Many of these offshore stations are significantly larger and heavier than the substations in a single OWF. Some converter stations, such as DolWin beta, are so heavy (approx. 20 000 t) that no crane could have lifted the entire station. In such cases, self-floating construction methods are used or transport barges that can be lifted and lowered with the help of ballast tanks.
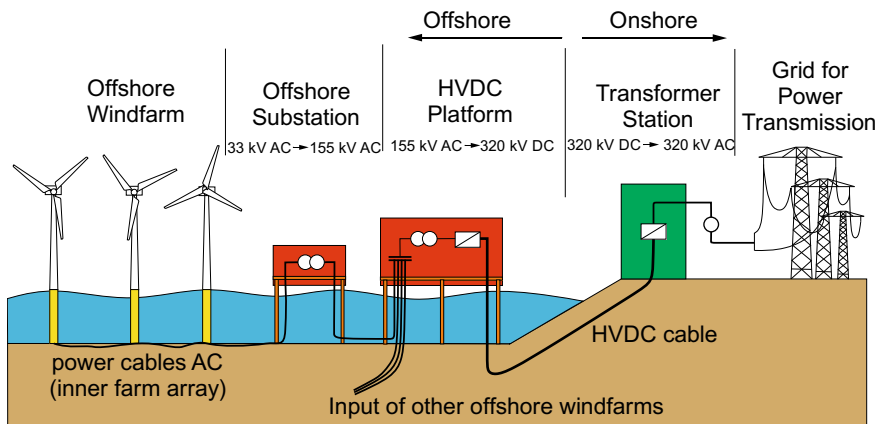
Fig. 10 Power transmission from offshore windfarms to the shore
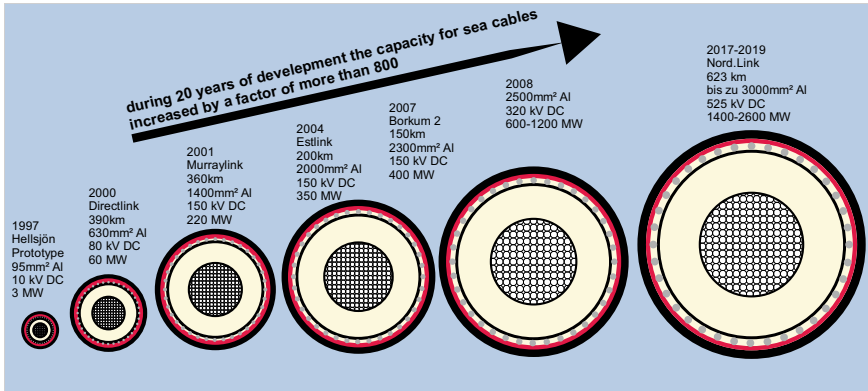
Fig. 11 Development of power cables for offshore applications. Data source ABB

2.6 Power Cables

A so-called inner farm cabling is required for an OWF to connect each OWT with the substation. These submarine cables are buried in the seabed to avoid damage from ship anchors. Power cables for offshore wind energy are divided into:

- the inner farm cabling between the single turbines and the substation,
- the power transmission line (alternating current) from the offshore-substation to the converter-platform and
- the power transmission line (direct current) from the converter-platform to the shore.

Particularly in the case of power transmission via direct current transmission (DC cables), many innovative developments have been made in recent years for the high-voltage range, which have enabled a significant increase in performance in terms of the transmission capacity per cable, see Fig. 11.

For test requirements and proof of suitability, the technical regulations of the VDE must be observed for an alternating current transmission (AC cable) with plastic-insulated low, medium and high voltage cables. However, the recommendation of CIGRE must be considered for DC cables.

2.7 Research Platforms

In addition to the offshore wind farms, several research platforms were installed in the North Sea and Baltic Sea. Therefore, three platforms (FINO 1, FINO 2 and FINO 3) are available, see Fig. 12.

The research platforms are used for numerous oceanographic and meteorological studies and measurement campaigns, some of which are listed below:

Fig. 12 Research platforms in the North Sea and Baltic Sea (FINO 1, 2 and 3)

- Measurements of wind speed, wind direction and turbulence depending on the height
- Measurements of wave height, wave period and wave propagation
- Measurements of ocean currents
- Temperature and solar radiation measurements
- Measurements at the seabed (e.g. scour effects)
- Flash measurements.

The meteorological and oceanographic data are archived in the FINO database at the BSH. In addition, accompanying ecological research on issues such as population of birds and marine animals takes place on these research platforms.

The research results should help to clarify remaining uncertainties regarding the technical design of the turbines and to close the gaps in knowledge about the biotopes in these areas and their changes during the installation and operation of OWF.

Furthermore, project-specific measuring masts were installed in the early phase of some OWF to obtain an improved forecast for the wind speed and other meteorological data before the construction phase for the project started. A further issue was the evaluation of the energy yield and its optimization within the array of the OWF. Since the measuring masts are in principle no longer needed after the installation phase of the OWF, alternative measuring methods were developed to avoid the expenditure for these measuring masts, in particular for the dismantling. In the meantime, wind measurements via floating lidar systems installed on sea buoys are favoured. Wind speed measurements at several measuring heights simultaneously up to about 250 m above the water surface should be possible. The measuring accuracy is comparable to that of fixed measuring masts, because the movements of the buoy are eliminated or compensated by a correction algorithm.

3 Load Actions for Offshore Wind Turbines

Numerous standards must be considered for the approval of OWT. In Germany, the BSH Standard 7005 [1] is the design basis for structures of OWF. This standard lists in hierarchical order further standards to be used as a basis for load actions on offshore structures. The Eurocodes are predominantly used for offshore-projects in Germany. Eurocode 1 (DIN EN 1991 Parts 1–9) defines the load actions, as follows:

- permanent load actions (G):

    – self-weight (G)
    – pretension (P)
    – earth pressure (G_E)
    – static fluid pressure, hydrostatic (G_H)

- variable load actions (Q):

    – pay loads and live loads (Q)
    – wind loads (W)
    – snow and ice loads (S)
    – temperature induced loads (T)
    – settlements (Δa)
    – dynamic fluid pressure (Q_H)

- accidental load actions (A):

    – impact loads
    – explosion loads
    – earthquake loads.

However, not all relevant load actions are regulated in Eurocode 1991, so that supplementary standards for offshore structures must be also considered. In addition to the inertial and gravity loads, the aero- and hydrodynamic loads as well as functional loads (e.g. starting and stopping processes) of an OWT must also be taken into account. Furthermore, DIN EN 61,400-3 [2] lists actions that must additionally be considered depending on the type of turbine and site-specific conditions (e.g. skewing, prestressing forces, thermal effects, ice loads, earthquakes etc.), see Fig. 13.

Different types of loads are listed in Table 6 related to their duration of time and their nature.

The periodic loads are of particular importance with regard to the design of the support and foundation structure, since the rotational speed of the rotor and multiples of this frequency are often in the range of the first and second tower natural frequencies. In particular, the 1P and 3P frequencies can lead to large resonance effects. In the following, the basics of hydrostatic and hydrodynamic loads are explained, which additionally have to be considered for offshore wind turbines compared to onshore wind turbines.
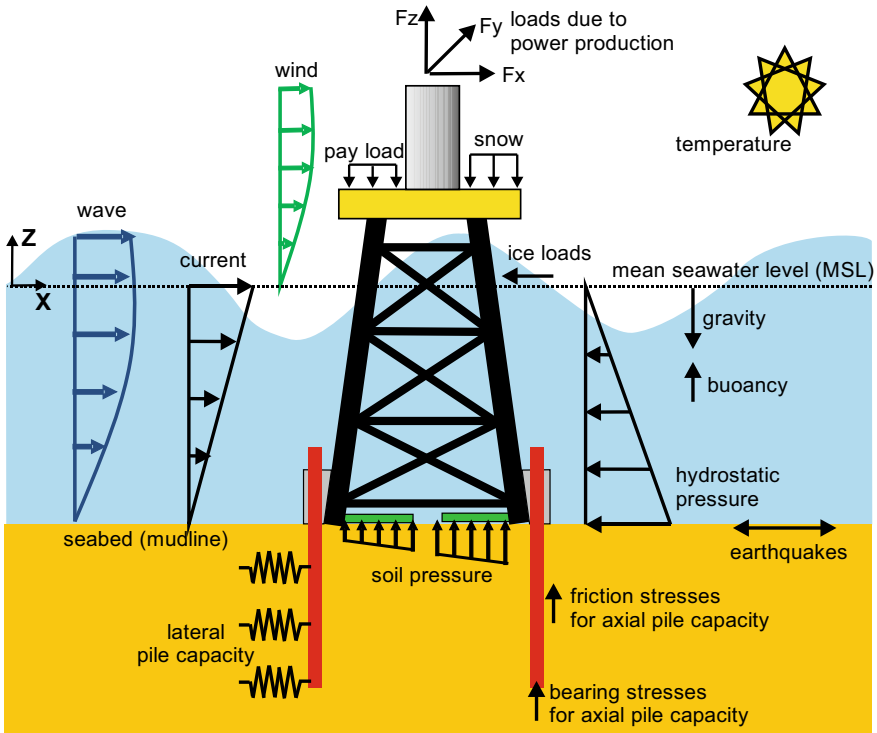
Fig. 13 Load actions on support structures for offshore wind turbines

Table 6 Differentiation of the types of stress according to time course and cause

Duration	Type of load action	Physical reason	Condition of the system
Constant (stationary)	Self-weight, centrifugal forces, lift, mean wind force, current	Gravity, rotation of the rotor, mean wind speed	Normal design situation, e.g. power production
Periodic	Unbalanced forces, aerodynamic forces	Inertia effects, blade passage at the tower	Normal design situation
Stochastic	Aero- and hydrodynamic forces	Wind turbulence, wave	Extreme and normal design situation
Transient	Impact loads, emergency stop, earthquake	Ship collision, emergency shutdown of turbine, horiz. acceleration due to earthquake	Extreme and accidental situation

3.1 Permanent Loads

The self-weight of an OWT results mainly from the rotor, nacelle, tower and foundation, which are components of the so-called primary structure. In addition, self-weight for attachments (access platform, boat landing etc.) and internals (cables, platforms, ladders etc.) must also be taken into account, which are considered as a secondary structure. In addition, electrical equipment's, such as transformers and ventilation systems, have significant weights and must also be included in the design basis for permanent loads.

Due to mass inertias, the gravity loads must be known for dynamic analyses so that the inertial forces during the (oscillatory) structural response can be correctly recorded.

3.2 Aerodynamic Loads

The aerodynamic loads depend on the site-specific wind speed, for which statistical data must be available. In DIN EN 1991-1-4 [5], the effects due to wind are normatively regulated for German regions, so that statistically validated values are available for corresponding return periods (e.g. 50-year wind and 50-year gust).

On the one hand, the wind loads on the rotor blades have to be determined and on the other hand, wind forces also act on the tower, which have to be taken into account for structural analyses. For further details on the aerodynamic loads, please refer to Chaps. 3 and 4.

3.3 Hydrostatic Loads

In addition to aerostatics (static equilibrium of gases) and aerodynamics (dynamic equilibrium of gases), hydrostatics (static equilibrium of water) and hydrodynamics (dynamic equilibrium of water) are also important for the design of OWT because the seawater will cause load actions on the structure.

Normal stresses in fluids (here seawater) are always compressive stresses, since tensile stresses cannot generally be transmitted. Static equilibrium means that there is no opposite displacement between the fluid particles, which is why no shear stresses occur in this state.

The hydrostatic pressure on the surfaces of the components must be taken into account. This pressure at depth h below the water level is equal to the pressure above the water level and the weight force per area of the water column above.

Furthermore, the buoyancy force must be considered, which, according to the ARCHIMEDES principle, is equal to the weight of the displaced water volume. The

following case distinction must therefore be observed in the calculations for offshore structures:

- non-flooded members or components with chambers under water
- flooded members.

As a general rule, the buoyancy force of non-flooded members, e.g. braces of a jacket, is significantly greater compared to flooded members with same dimension. These differences must be considered not only in the case of different water levels in the operational phase, but also during the installation phase, such as the launching of a jacket, where the jacket is pushed into the sea from a transport barge. Therefore, the buoyancy conditions must be recorded very precisely so that the jacket remains buoyant on the water surface to continue the installation phase with the upending.

The steps for launching and upending a jacket can be seen in Fig. 14. Different hydrostatic conditions have to be taken into account during these installation steps. In addition to the hydrostatic loads, the effects of ocean currents and waves must be considered for various phases of the launching due to safety reasons (e.g. seabed clearance).

Ballasting the launch end of barge
Step 1

Moving jacket along skid beams
Step 2

Jacket pivots on rocker arms
Step 3

Floating in water
Step 4

Upending with derrick barge
Step 5

In place
Step 6
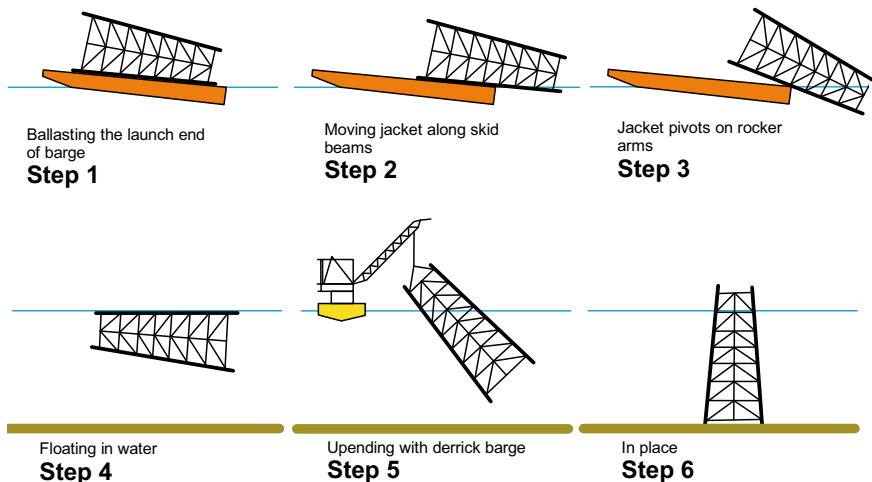
Fig. 14 Launching and upending of a jacket

3.4 Hydrodynamic Loads

3.4.1 Currents

Ocean currents can cause significant static and dynamic loads on foundations of OWT. Thus, these environmental loads must be considered for the structural analysis. The ocean currents are divided into:

- constant ocean currents (so-called thermo-saline currents)
- tidal currents
- wind-induced currents.

The loads due to currents are treated as quasi-static loads, since the periods of change (e.g. tide, period approx. 12.5 h) are much larger than the periods of oscillation of OWT components.

For tidal currents, a power approach is generally used (u_{T0} = current velocity at the water surface ($z = d$)), according to DNV-GL, e.g. $n = 7$ is to be selected:

$$u_T(z) = u_{T0} \cdot \left(\frac{z}{d}\right)^{1/n} \tag{3}$$

A linear approach over the depth z is often used for wind-induced currents:

$$u_{Wi}(z) = u_{Wi}(d) \cdot \frac{z}{d} \tag{4}$$

The velocity at the water surface $u_{Wi}(d)$ is assumed according to the following approximation (U_{1h} = wind speed at a height of 10 m, averaged over one hour):

$$u_{Wi}(d) = 0,02 \cdot U_{1h} \tag{5}$$

Several measurements are available for tidal currents, but only a few for ocean currents. For u_{Wi}, the value of 2 kn[1] is often used. Thus, for the current velocity u_c (c for current) over depth, one obtains the Eq. 6. The directions of the two current components can differ by the angle α.

$$u_c(z) = u_{T0} \cdot \left(\frac{z}{d}\right)^{1/n} + \cos \alpha \cdot U_{Wi} \cdot \frac{z}{d} \tag{6}$$

---

[1] 1 kn (knots) = 1 sm/h (nautical mile/h) = 1.852 km/h = 0.5144 m/s.

3.4.2 Loads Due to Currents

If currents act on a submerged body, drag forces are generated, which stress the offshore foundations. A distinction is made between wave-induced and friction-induced forces. The wave-induced forces only arise at the interfaces between two media of different density, such as water and air (Fig. 15).

The drag forces are proportional to the current velocity in square. If model tests will be carried out for verifications the REYNOLDS number of the real structure and the model must be the same. The REYNOLDS number is defined as follows:

$$\text{Re} = D \cdot u / v \ [-] \tag{7}$$

with: $u = $ inflow velocity; $D = $ diameter of the body flowed around; $v = $ kinematic viscosity of the medium.

Example $u = 2$ kn; $D = 5$ m; $v_{\text{Seew.15°C}} = 1{,}19 \times 10^{-6}$ m^2/s; $\Rightarrow$ Re $= 4{,}3 \times 10^6$ [$-$].

If components of offshore structures are loaded by currents in a certain angle to vertical axis the load is divided into a lift component and a drag component perpendicular to the axis.

The drag force is defined as:

$$F_{\text{D}} = -1/2 \cdot \rho \cdot \int_2 (\text{L})c_{\text{D}} \cdot |u| \cdot u \cdot A \cdot dz \tag{8}$$

and the lifting force:
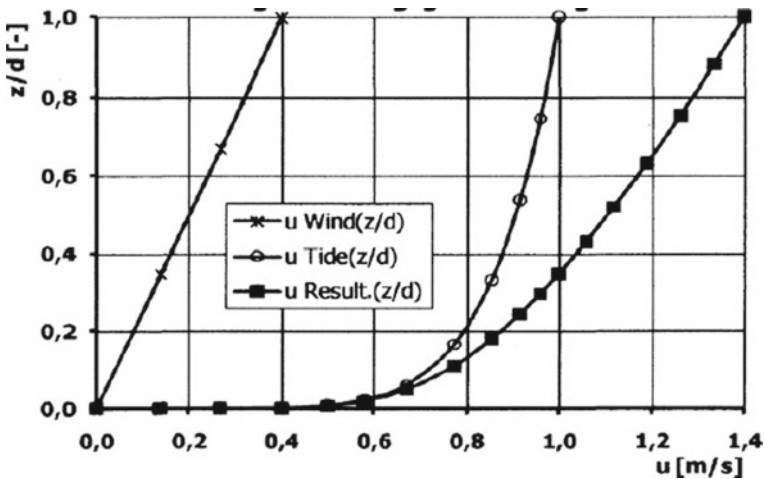
Fig. 15 Wind-induced current and tidal current

$$F_L = -1/2 \cdot \rho \cdot \int_{(L)} c_L \cdot |u| \cdot u \cdot A \cdot \mathrm{d}z \tag{9}$$

where c_D = dimensionless drag coefficient of the cross-section; c_L = dimensionless lift coefficient; ρ = specific density of the medium (e.g.1025 kg/m³ for seawater); A = projected area of the body; L = length of the body in submerged area.

The coefficients c_D (D for drag) and c_L (L for lift) depend on the shape of the body, e.g. cylinder or rectangle, and on the current velocity as well as the REYNOLDS number (laminar or turbulent flow). The expression u^2 must be split into $|u| \cdot u$ to obtain the sign or direction of the forces, since these always act in the opposite direction to the flow direction. Specific values for the drag and lift coefficients can be found in HAPEL [6] or ECK [7] for example.

Since the dimensions and shape of the cross-section as well as the current velocity and thus also the coefficients can vary over the depth, the forces per unit length must be determined and integrated over the length of the component.

$$f_D(z) = -1/2 \cdot \rho_{\text{Wasser}} \cdot c_D(z, A, \text{Re}) \cdot D(z) \cdot |u(z)| \cdot u(z) \tag{10}$$

Thus, the drag force is the integral depending on the z-level:

$$F_D = -1/2 \cdot \rho_{\text{Wasser}} \int_{(L)} c_D(z, A, \text{Re}) \cdot D(z) \cdot |u(z)| \cdot u(z) \cdot \mathrm{d}z \tag{11}$$

The calculation of the lift force can be done analogously.

Example The drag force of a pile (cylinder as cross section) in seawater subjected to a wind-induced current is to be determined as follows:

Given: $D = 5.0$ m; $d = 30$ m (water depth); $\rho_{\text{Seew.}} = 1025$ kg/m³; wind speed u_{1h} = 15 m/s.

Result: current velocity at the water surface $u_{\text{Wi}} = 0{,}3$ m/s; Re = $1{,}25 \times 10^6$; c_D $\approx 0{,}35$; $\rightarrow F_D = 1210$ N.

Note: 1 N = 1 kg m/s² [Force].

3.4.3   Waves

The waves of the water surface induced by the wind are so-called gravity waves. Due to the friction of the wind currents and the turbulence in the boundary layer between air and water, the water particles are accelerated in addition to the gravity. The water particles move on orbitals harmoniously in theory. To describe the dynamics of the waves, a vortex-free, incompressible and frictionless fluid is assumed for the following wave theories.
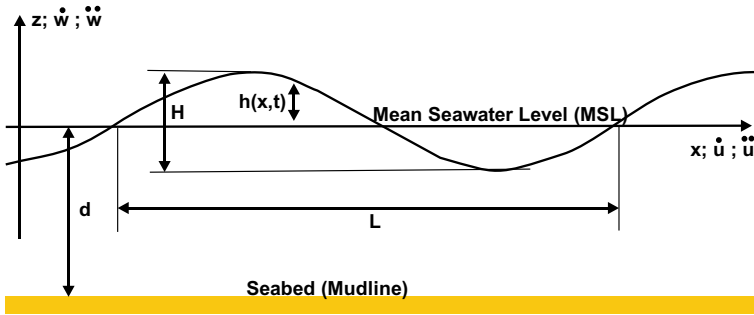
Fig. 16 Description for linear wave theory according to AIRY

Different wave theories were defined according to AIRY, GERSTNER, STOKES, FENTON as well as the stream function, solitary waves and elliptical waves etc. The application of a certain wave theory depends on water depth, wave length, wave height and wave period.

These theories describe the movement of a single wave in the *x–z-plane*, movements in *y-direction*, i.e., transverse to the wave direction do not take place. More details about the wave theories can be found in the literature HAPEL [6] and CLAUSS [8] for example.

The most important definitions of a wave are given in Fig. 16: $h(x, t) =$ local wave height at location *x* at time *t*; $H = wave$ height; $L =$ wavelength; $T = wave$ period; $c = wave$ propagation velocity; $\omega =$ wave frequency $= 2\text{-}\pi/T$; $k =$ wave number $= 2 - \omega/L$.

The BERNOULLI equation (one of the two basic equations of fluid mechanics besides the continuity equation) can be linearized and the kinematic and dynamic boundary conditions can be fulfilled.

The following two equations can be used for incompressible, vortex and frictionless fluids:

$$\frac{(\dot{u})^2}{2} + \frac{p}{\rho} + g \cdot z = \text{const.} \tag{12}$$

$$aQ = A \cdot \dot{u} = \text{const.} \tag{13}$$

with $u° =$ flow velocity $= du/dt$; $p = pressure$ in the flow; $\rho =$ specific density of the medium; $z =$ height; $Q =$ volumetric flow; $A =$ cross-section through which the medium flows

If a two-dimensional time-dependent potential of velocity $\Phi(x, z, t)$ is implemented, the potential equation is obtained from the continuity equation:

$$\Delta\Phi(x, z, t) = \frac{\partial^2\Phi}{\partial x^2} + \frac{\partial^2\Phi}{\partial z^2} = 0 \tag{14}$$

If the velocity potential is known, the velocities $u°$ in the *x-direction* and $w°$ in the *z-direction* are obtained by derivations. The accelerations are calculated by second derivations (according to the time or the coordinates x and z):

$$\dot{u}(x, z, t) = \frac{dx}{dt} = \frac{\partial \Phi}{\partial x}; \quad \dot{w}(x, z, t) = \frac{dz}{dt} = \frac{\partial \Phi}{\partial z} \tag{15}$$

$$\ddot{u}(x, z, t) = \frac{d^2 x}{dt^2} = \frac{\partial^2 \Phi}{\partial x^2}; \quad \ddot{w}(x, z, t) = \frac{d^2 z}{dt^2} = \frac{\partial^2 \Phi}{\partial z^2} \tag{16}$$

If the velocities are put into Eq. 12, the intransient BERNOULLI equation (EULER equation of motion) for vortex-free fluids can be derived:

$$\frac{\partial \Phi}{\partial t} + \frac{1}{2} \cdot (\text{grad}\Phi)^2 + g \cdot z = 0 \tag{17}$$

$$\text{with grad } \Phi(x, z, t) = \frac{\partial^2 \Phi}{\partial x^2} + \frac{\partial^2 \Phi}{\partial z^2} \text{ (two−dimensional)} \tag{18}$$

Equation 17 is a nonlinear partial differential equation of second order, which can be solved for the following boundary conditions:

- at the seabed ($z = -d$) the velocity of the water particles perpendicular to the horizontal seabed is equal to zero.

$$\dot{w}(x, z = -d, t) = \frac{\partial \Phi}{\partial z} = 0 \tag{19}$$

- at the surface of the wave at $z = h(x, t)$ the pressure p is constant. The pressure can be arbitrarily set to zero. Thus, Eq. 17 is used to get the following criteria.

$$\frac{\partial \Phi}{\partial t} + \frac{1}{2} \cdot (\text{grad}\Phi)^2 + g \cdot z = 0 \tag{20}$$

- for the velocity $w°$ at the surface $z = h(x, t)$ andwith Eq. 19 the result is:

$$\dot{w}(x, z = h(x, t), t) = \frac{\partial \Phi}{\partial z} = \frac{\partial z}{\partial t} = \frac{\partial h(x, t)}{\partial z} \cdot \frac{\partial x}{\partial t} = \frac{\partial h}{\partial z} \cdot \dot{u} + \frac{\partial h}{\partial t} \tag{21}$$

Since Eqs. 20 and 21 are nonlinear, a closed solution of the differential Eq. 17 is not possible. Only approximations can be given for it.

3.4.4   Linear Wave Theories

The most common theory for linear waves was defined by AIRY, who linearizes the equations and assumes a simple sinusoidal form of the wave. In contrast, the non-linear wave theories according to STOKES consider terms with regard to a power series.

The wave theory according to AIRY considers a sine or cosine form plus phase shift (depending on the selected coordinate origin) for the wave form based on the following conditions:

- the water depth d is greater than half of the wave length L (deep water)
- the wave height H is small compared to the wave length (low wave steepness)
- the water surface is undisturbed.

In comparison to the real nature of waves, which are described more precisely with nonlinear theories, the most important wave effects can be represented approximately with AIRY's theory.

The approach for the wave height according to AIRY is defined for wave crest at $x = 0$ and $t = 0$:

$$h(x, t) = \frac{H}{2} \cdot \cos\left(2 \cdot \pi \cdot \left[\frac{x}{L} - \frac{t}{T}\right]\right) = \frac{H}{2} \cdot \cos(k \cdot x - \omega \cdot t) \qquad (22)$$

The nonlinear terms in Eqs. 17 and 20 have smaller magnitudes than the linear terms and can therefore be neglected for first assumptions. Furthermore, the boundary conditions in Eqs. 20 and 21 for the local wave elevation $h(x, t)$ can be replaced by the constant value $h = 0$.

An analytical solution of the Eq. 17 with the approach according to Eq. 22 is possible for the assumptions and the velocity potential Φ can be calculated as follows:

$$\begin{aligned}\Phi(x, z, t) &= \frac{H}{2} \cdot \frac{g}{\omega} \cdot \frac{\cosh[k \cdot (z + d)]}{\cosh[k \cdot d]} \cdot \sin(k \cdot x - \omega \cdot t) \\ &= \frac{H}{2} \cdot \frac{g}{\omega} \cdot \eta(z) \cdot \sin(k \cdot x - \omega \cdot t)\end{aligned} \qquad (23)$$

The expression $\eta(z)$ represents the depth depending on the velocity potential.

Based on Eq. 21 the dispersion equation can be derived, which describes the relations between wave frequency ω, wave number k and water depth d.

$$\omega^2 = g \cdot k \cdot \tanh(k \cdot d) \qquad (24)$$

It can be written for the wave length in the case of deep water:

$$L = \frac{g \cdot T^2}{2 \cdot \pi} \cdot \tanh\left(2 \cdot \pi \cdot \frac{d}{L}\right) \qquad (25)$$

and for the wave period:

$$T = \sqrt{\frac{2 \cdot \pi \cdot L}{g} \cdot \frac{1}{\tanh(2 \cdot \pi \cdot d/L)}} \tag{26}$$

as well as for the velocity of wave propagation (celerity):

$$c = \frac{L}{T} = \frac{\omega}{k} = \sqrt{\frac{g \cdot L}{2 \cdot \pi} \cdot \tanh\left(2 \cdot \pi \cdot \frac{d}{L}\right)} = \sqrt{\frac{g}{k} \cdot \tanh(k \cdot d)} \tag{27}$$

The velocity components are obtained from the partial derivatives of the potential in Eq. 23 depending on the coordinates x or z and the accelerations from the second derivatives with respect to time:

$$\dot{u}(x, z, t) = \frac{\partial \Phi}{\partial x} = \frac{g \cdot k}{\omega} \cdot \frac{\cosh[k \cdot (z + d)]}{\cosh[k \cdot d]} \cdot \frac{H}{2} \cdot \cos(k \cdot x - \omega \cdot t) \tag{28}$$

$$\dot{w}(x, z, t) = \frac{\partial \Phi}{\partial z} = \frac{g \cdot k}{\omega} \cdot \frac{\sinh[k \cdot (z + d)]}{\cosh[k \cdot d]} \cdot H \cdot \sin(k \cdot x - \omega \cdot t) \tag{29}$$

The trajectories of the water particles are obtained by integrating the velocities according to Eqs. 28 and 29 over time, which are:

$$u(x, z, t) = \frac{H}{2} \cdot \frac{g \cdot k}{\omega^2} \cdot \frac{\cosh[k \cdot (z + d)]}{\cosh[k \cdot d]} \cdot \sin(k \cdot x - \omega \cdot t) \tag{30}$$

$$w(x, z, t) = \frac{H}{2} \cdot \frac{g \cdot k}{\omega^2} \cdot \frac{\sinh[k \cdot (z + d)]}{\cosh[k \cdot d]} \cdot \cos(k \cdot x - \omega \cdot t) \tag{31}$$

The trajectories form circles in deep water ($d \to \infty$) and ellipses with the semi-axes in shallower water ($d < \approx L/2$):

$$\frac{H}{2} \cdot \frac{g \cdot k}{\omega^2} \cdot \frac{\cosh[k \cdot (z + d)]}{\cosh[k \cdot d]} \quad (\text{in } x\text{-direction}) \tag{32}$$

$$\frac{H}{2} \cdot \frac{g \cdot k}{\omega^2} \cdot \frac{\sinh[k \cdot (z + d)]}{\cosh[k \cdot d]} \quad (\text{in } z\text{-direction}) \tag{33}$$

The radii of the circles of ellipses decrease with increasing water depth according to the hyperbolic functions. The values become zero at the seafloor, so that the water particles move only forward and backward in horizontal direction (boundary layer).

Thus, velocities and accelerations with $\cosh(\alpha \cdot x) = (e^{\alpha \cdot x} + e^{-\alpha \cdot x})/2$ and $\sinh(\alpha \cdot x) = (e^{\alpha \cdot x} - e^{-\alpha \cdot x})/2$ will result from the Eqs. 28 to 33 for the following trajectories:

$$u(x, z, t) = -H/2 \cdot e^{k \cdot z} \cdot k \cdot \sin(k \cdot x - \omega \cdot t) \tag{34}$$

$$w(x, z, t) = H/2 \cdot e^{k \cdot z} \cdot k \cdot \cos(k \cdot x - \omega \cdot t) \tag{35}$$

$$\dot{u}(x, z, t) = H/2 \cdot \omega \cdot e^{k \cdot z} \cdot k \cdot \cos(k \cdot x - \omega \cdot t) \tag{36}$$

$$\dot{w}(x, z, t) = H/2 \cdot \omega \cdot e^{k \cdot z} \cdot k \cdot \sin(k \cdot x - \omega \cdot t) \tag{37}$$

$$\ddot{u}(x, z, t) = H/2 \cdot \omega^2 \cdot e^{k \cdot z} \cdot k \cdot \sin(k \cdot x - \omega \cdot t) \tag{38}$$

$$\ddot{w}(x, z, t) = H/2 \cdot \omega \cdot e^{k \cdot z} \cdot k \cdot \sin(k \cdot x - \omega \cdot t) \tag{39}$$

Finally, the linear wave theory is defined with the Eqs. 24–39.
For **deep water** with $d \to \infty$ is obtained with Eq. 24:

$$\omega^2 = g \cdot k \tag{40}$$

Deep water is assumed in practice for: $d < L/2$.
If the approximations $\tanh(k \cdot d) \approx 1$ and $\sinh(k \cdot d) \approx \cosh(k \cdot d) \approx e^{k \cdot d/2})$ will be used, the following relationships can be written for deep water:

$$\text{length of wave: } L = \frac{g \cdot T^2}{2 \cdot \pi} \tag{41}$$

$$\text{frequency of wave : } \omega^2 = (2 \cdot \pi/T)^2 = g \cdot k \tag{42}$$

$$\text{celerity (wave propagation) : } c = \frac{L}{T} = \frac{\omega}{k} = \sqrt{\frac{g \cdot L}{2 \cdot \pi}} = \sqrt{\frac{g}{k}} \approx 1,25 \cdot \sqrt{L} \tag{43}$$

The parameters H and L or H and T are required for an analysis according to AIRY to describe a harmonic wave in deep water.
Shallow water is assumed when: $d < L/20$.
In shallow water, because of $\tanh(k \cdot d) \approx \sinh(k \cdot d) \approx k \cdot d$ and $\cosh(k \cdot d) \approx 1$ the celerity is:

$$c = \frac{\omega}{d} = \sqrt{g \cdot d} \tag{44}$$

The celerity of the wave is only dependent on the water depth and the frequency.
Transition range is assumed for: $L/2 > d > L/20$.
The radius r of the wave orbitals decreases with increasing the water depth:

$$r = r(z) = H/2 \cdot e^{2 \cdot \pi \cdot z/L} \tag{45}$$

with z = distance from the water surface (z downwards negative).

For a water depth of $z = -L/2$, the radius is $r \approx 0,043 \cdot H/2$ and for $z = -L$, the radius is $r \approx 0,0019\,H/2$, i.e. negligibly small.

If waves run into shallower water, the wave heights also change. With the assumption that the waves are not yet broken, energy considerations result in wave heights H in shallow water (H_0 = height in deep water) as follows (Figs. 17 and 18):

$$\frac{H}{H_0} = \left[\frac{1}{\tan(k \cdot d) \cdot \left\{ 1 + \frac{2 \cdot k \cdot d}{\sinh(2 \cdot k \cdot d)} \right\}} \right]^{1/2} \tag{46}$$

The ratio for "shallow water" will be:
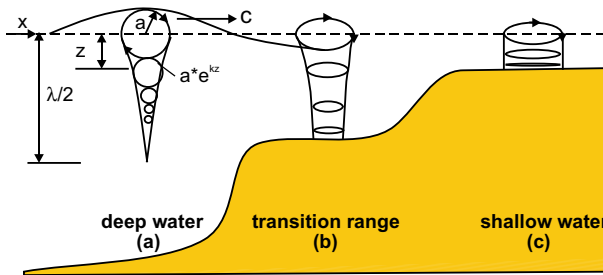
Fig. 17 Movements of water particles at different water depths, **a** for deep water, **b** for the transition range and **c** for shallow water
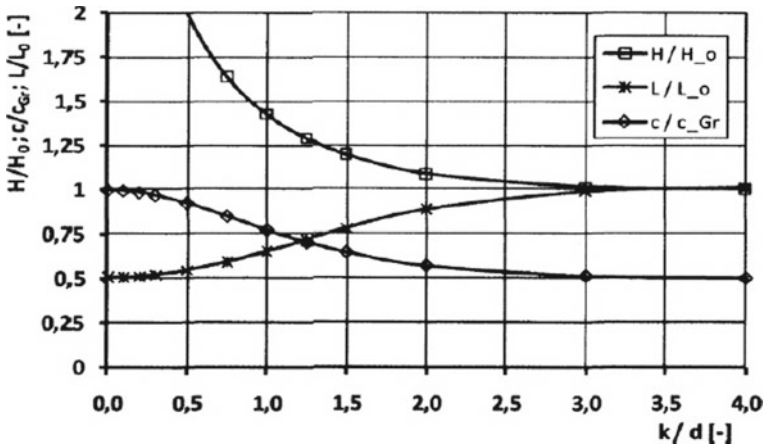
Fig. 18 Changes in wave heights, wave lengths and celerity's when a wave get into shallow water

$$\frac{H}{H_0} = \left[\frac{\sqrt{g \cdot T}}{4 \cdot \pi \cdot \sqrt{d}}\right]^{1/2} \approx 0,5 \cdot \sqrt{\frac{T}{\sqrt{d}}} \tag{47}$$

Velocity of wave groups

A sea state is called "regular" if it consists of randomly superimposed harmonic waves of similar frequency, length and direction (wave group). The wave group propagates with the velocity of the "envelope", the group celerity c_{Gr}, which is defined as:

$$c_{Gr} = \frac{c}{2} \cdot \left[1 + \frac{2 \cdot k \cdot d}{\sinh(2 \cdot k \cdot d)}\right] \tag{48}$$

In deep water, the group celerity becomes smaller because of the term for $\sinh(2 \cdot k \cdot d)$, which increases with the water depth d:

$$c_{Gr} = c/2 \tag{49}$$

For shallow water, the group celerity is (Fig. 19):

$$c_{Gr} = c \tag{50}$$

Wave energy

The energy of a moving, undamped system with a certain mass can be described with a potential and a kinetic component. A volume of fluid is considered, which is bounded in the *x–z plane* by $x = 0$ and $x = L$ and by $z = h(x, t)$ and $z = -d$. In addition, a constant width of 1 is assumed in the *y-direction*.

The potential energy is:

$$V(t) = \iiint\limits_{(Vol.)} m(x, y, z) \cdot g \cdot z(t) \cdot dx \cdot dy \cdot dz \tag{51}$$

with: m = mass/volume
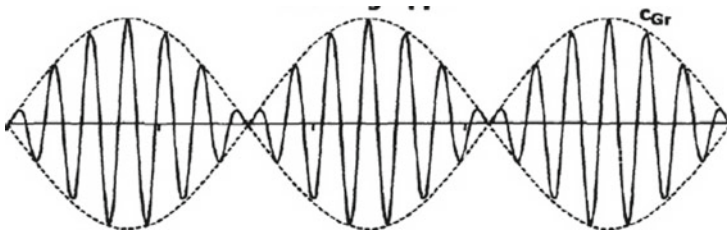
Fig. 19 Group of waves

By choosing a suitable reference frame for z, it can be achieved that the potential energy is greater than zero. Thus, the potential of wave energy can be written as:

$$
\begin{aligned}
V &= g \cdot \rho_{\text{Seew.}} \cdot \int_{(A)} z \cdot dA = \cdots \\
&= -\frac{1}{2} \cdot \rho_{\text{Seew.}} \cdot g \cdot d^2 \cdot L + \frac{1}{4} \cdot \rho_{\text{Seew.}} \cdot g \cdot \left(\frac{H}{2}\right)^2 \cdot L
\end{aligned}
\tag{52}
$$

The first term of Eq. 51 gives the potential energy of the still water, if the still water level is chosen as reference level for the potential energy. This is an arbitrary constant with respect to the wave energy and can therefore be omitted. Thus, a wave with a height H, a length L and a width of 1 can be described as potential energy:

$$
V = \frac{1}{4} \cdot \rho_{\text{Seew.}} \cdot g \cdot \left(\frac{H}{2}\right)^2 \cdot L
\tag{53}
$$

The kinetic energy is obtained according to:

$$
T = \frac{1}{2} \cdot \int \int \int_{(\text{Vol.})} m(x, y, z) \cdot \left[\underline{r}^{\circ}(x, y, z, t)\right]^2 \cdot dx \cdot dy \cdot dz \geq 0
\tag{54}
$$

with: $\underline{r}^{\circ} = $ vector of velocity

It is always ≥ 0 because of the square of the velocity $\underline{r}^{\circ} = dr/dt$.

Thus, the kinetic energy of all water particles for the given volume is:

$$
\begin{aligned}
T(t) &= \frac{1}{2} \cdot \rho_{\text{Seew.}} \cdot \int \int \int_{(V)} \left[\underline{\dot{r}}(x, y, z, t)\right]^2 \cdot dx \cdot dy \cdot dz \\
&= \frac{1}{2} \cdot \rho \cdot \int_{(A)} \left[u^2 + w^2\right] \cdot dA = \cdots \\
&= \frac{1}{2} \cdot \rho_{\text{Seew.}} \cdot g \cdot \int_{x=0}^{L} h(x) \cdot dx \\
&= \frac{1}{4} \cdot \rho_{\text{Seew.}} \cdot g \cdot \left(\frac{H}{2}\right)^2 \cdot L \geq 0
\end{aligned}
\tag{55}
$$

The sum of the energy components is divided by the wave length L. The average energy of a wave is obtained as follows:

$$
E = \frac{T + V}{L} = \frac{1}{8} \cdot \rho_{\text{Seew.}} \cdot g \cdot H^2
\tag{56}
$$

The energy transport takes place with the celerity of the wave group according to Eq. 48.

Based on the AIRY-theory, the water particles perform an orbital or circular movement, i.e. there is no mass transport, but only an energy transport. According to the non-linear wave theories as well as in real waves, this is not the case. While single water particles have the same height $=$ *z-coordinate* after passing through a wave, a propagation of the water particles takes place in the *x-direction*, since the velocity of the water particles depends on the water depth. The forward transport velocity in the wave crest is greater than the backward velocity in the wave trough, since the water particles have a smaller *z-coordinate* $(z = -H/2)$, i.e. the circles or ellipses are no longer closed.

The vertical velocity of the water particles is in the direction of wave progress:

$$\dot{u}(z) = \left(\frac{\pi \cdot h(z)}{L}\right)^2 \cdot c \tag{57}$$

It decays with water depth because of $h(z)$.

3.4.5 Nonlinear Wave Theories

The non-linear wave theories are required for the more accurate analyses of the velocities and accelerations of the water particles when waves pass through offshore structures, since they can be used to determine the resulting forces more accurately. Furthermore, the resulting forces are generally higher than those according to the linear wave theory. Since these forces represent one of the main loads of offshore structures, the knowledge is important for the optimization of structural elements.

In contrast to AIRY's theory, the non-linear theories do not consider sinusoidal curves, but different lengths and shapes for wave crest and wave trough. Furthermore, AIRY's theory only applies to small wave heights. However, the waves of a natural sea-spectra have a much larger ratio of H/L, so that non-linear theories must be used for a more accurate description.

A trochoid (a special form of cycloid or roll-off curves) is often assumed as a good approximation for surface waves in deep water, e.g. for analysis of ships according to GERSTNER [9].

To create a trochoid, a wheel of radius R is unrolled on a straight line, see Fig. 20. The result is a trajectory of the point P at radius $r < R$. The circumference of the wheel of radius R is equal to the wave length L. A water particle at the surface performs a circular motion on the radius r. If R and r are equal, the classical cycloid is obtained.

$$\text{wave crest at } L/2: \quad x = R \cdot \alpha + r \cdot \sin \alpha; \quad z = -r \cdot \cos \alpha \quad (0 \leq \alpha \leq 2 \cdot \pi) \tag{58}$$

$$\text{wave trough at } L/2: \quad x = R \cdot \alpha - r \cdot \sin \alpha; \quad z = r \cdot \cos \alpha \tag{59}$$
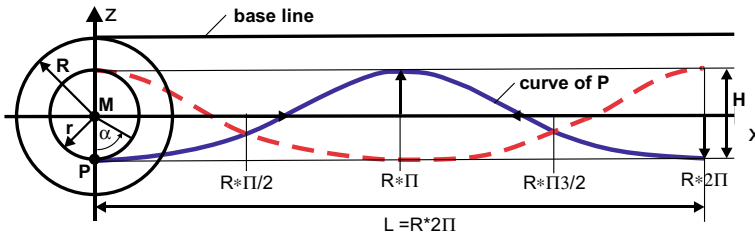
Fig. 20 Trochoidal wave according to GERSTNER

with $R = L/(2 - \pi)$; $L = wave\ length$; $r = H/2$; $H = wave\ height$.

It can be observed that the wave trough is longer than the wave crest ($l_{WT} = L/2 + 2 \cdot H$; $l_{WB} = L/2 - 2 \cdot H$). The larger the ratio H/L is, the longer the wave trough will be. This corresponds to the real characteristics of waves in nature.

Wave steepness

The measure of wave steepness is the ratio H/L (wave height to wave length). At a steepness of more than 1/7, the wave theoretically becomes unstable and breaks even in deep water. In real sea sates, waves break at a steepness of about 1/10, losing a large percentage of energy. In shallow water, the ratio of wave height to water depth is decisive; the waves break at $H/d \geq 0.78$ in such locations.

The AIRY theory applies only to waves with small steepness $H/L < \approx 1/50$, but real waves have much higher values ($H/L \approx 1/30\text{–}1/10$). Thus, wave theories must consider the ratios between water depth, wave length, wave frequency and wave height for accurate analysis of offshore structures. The wave profiles according to the different theories are shown in Fig. 21. Special software tools are used for the analysis of non-linear waves and resulting forces on structures.

If waves hit large bodies or if the water depth decreases, e.g. in coastal areas, the propagation of the waves is disturbed. The following effects can occur:

- **Shoaling** If the wave get in contact with the seabed ($d < L/2$) the celerity is reduced, the wave length decreases, the wave height increases (shoaling factor K_S).
- **Refraction** Waves that are not perpendicular to the front of the seabed will continue to move towards the coast until their crests are parallel to the depth contours. The wave heights can thereby become larger or smaller than those of the initial waves. Such an effect is considered by the refraction coefficient K_R.
- **Diffraction** Waves that hit a large body, move around it and enter into the wave shadow behind it. The wave heights generally decrease as a result.
- **Reflection**: If a massive body blocks the propagation of waves in deep water, they are reflected (angle of incidence = angle of reflection). The wave heights remain the same.
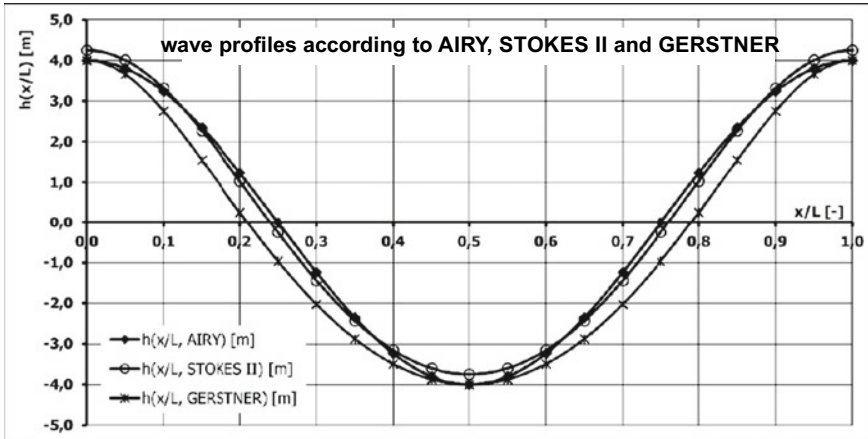
Fig. 21 Wave profiles of different theories

3.4.6 Loads Due to Waves

The loads on an offshore structure due to waves are influenced by the ratios of wave length to structure size and wave height or wave length to water depth. The size of the structure relative to the wave height is described by the dimensionless KEULEGAN-CARPENTER number KC.

$$KC = \pi \cdot \frac{H}{2 \cdot D} \tag{60}$$

with H = *wave height*; D = structure dimension transverse to the wave front

A difference must be considered between slender and massive offshore structures. Slender structures with $D/L < 0.2$ or $KC < 0.4$ are referred to as "hydrodynamically transparent", assuming that the wave is not significantly changed when passing through the structure. Drag and inertia forces due to the wave have approximately the same magnitude before and after passing the offshore structure.

Massive or large structures with $D/L > 0.5$ are called "hydrodynamically compact". Here, the wave is disturbed by the offshore structure and the inertia force dominates with increasing value of D/L.

The support structures of OWT are classified as hydrodynamically transparent. On the other hand, some oil or gas production platforms are so large (hydrodynamically compact) that the waves are influenced or even diffracted. In such cases, the wave forces must be calculated according to the diffraction theory, see e.g. CLAUSS [8].

Slender structures of OWT can be calculated by the superposition method (drag and inertia forces) according to MORISON [10]. It is the most commonly used method to calculate wave forces on slender offshore structures.
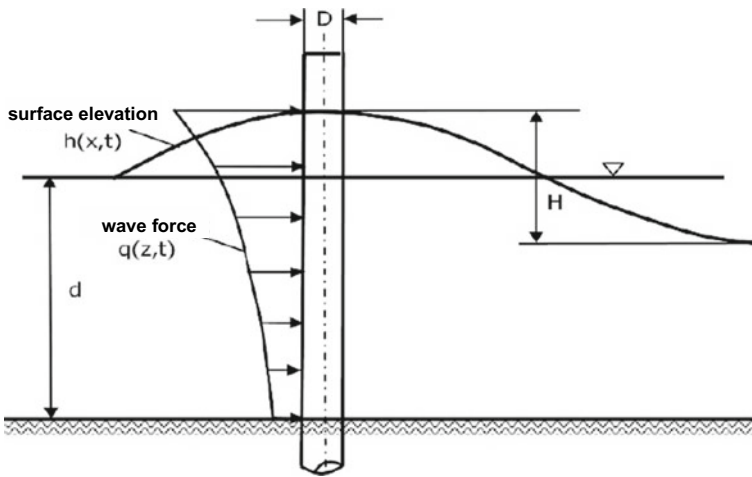
Fig. 22 Wave profile and wave forces at a vertical cylinder (pile)

Method according to MORISON

The forces on a body surrounded by a wave are divided into two components according to the MORISON method:

- inertia force F_M
- drag force F_D.

The force components are calculated separately and afterwards superimposed. The maxima of the two force components occur at different time steps according to the determining variables (velocity $u°$ or acceleration $u°°$). They are shifted against each other by a quarter of the wave period T. The horizontal velocity of the water particles corresponds to the effective flow, and the horizontal velocity of the water particles correlates to the effective acceleration (Fig. 22).

The drag force along the height is according to MORISON:

$$q_D(z, t) = \frac{1}{2} \cdot C_D(z, \text{Re}) \cdot \rho_{\text{Seew.}} \cdot D(z) \cdot \dot{u}(z, t) \cdot |\dot{u}(z, t)| \tag{61}$$

and the inertia force:

$$q_M(z, t) = C_M(z) \cdot \rho \cdot A(z) \cdot \dot{u}(z, t) \tag{62}$$

where $C_D(z, \text{Re})$ = drag coefficient of the cross-section; ρ = specific density of water; $D(z)$ = diameter of the cross-section at the considered depth; $A(z)$ = cross-section at the considered depth; $u°(z, t)$ = horizontal velocity of water particles; $u°°(z, t)$ = horizontal acceleration of water particles; $C_M = 1 + C_a$ = mass coefficient of inertia;

$C_a = m_a/m_0$ coefficient of hydrodynamic mass of cross section; $m_a(z)$ = added mass; $m_0(z)$ = displacement of the body (submerged volume * density of the water).

The superimposed wave force along the height is:

$$q_W(z, t) = q_D(z, t) + q_M(z, t) \tag{63}$$

Hydrodynamic mass or added mass

If a submerged body is accelerated by waves, the surrounding water must also be accelerated. This co-moving mass is called hydrodynamic mass or added mass. The magnitude of the added mass depends on the shape of the body, but nearly independent of the velocity or acceleration. It must be considered for analyses in the time-domain or frequency-domain.

If the hydrodynamic masses are calculated, it is assumed that a certain component of the surrounding water gets the same acceleration as the body. Helpful values for the hydrodynamic mass are listed, for example, in HAPEL [6].

Using AIRY's linear wave theory for a vertical cylinder in water (e.g. pile), the following terms can be calculated according to the MORISON equations:

$$
\begin{aligned}
q_D(z, t) =& \frac{1}{2} \cdot C_D \cdot \rho \cdot D \cdot \left(\frac{H}{2}\right)^2 \cdot \omega^2 \\
&+ \left\{ \frac{\cosh[k \cdot (z + d)]}{\cosh(k \cdot d)} \right\}^2 \cdot |\cos(\omega \cdot t)| \cdot \cos(\omega t) \\
=& \frac{1}{8s} \cdot C_D \cdot \rho \cdot D \cdot H^2 \cdot \omega^2 \cdot \eta^2(z) \cdot |\cos(\omega \cdot t)| \cdot \cos(\omega t)
\end{aligned}
\tag{64}
$$

$$
\begin{aligned}
q_M(z, t) =& C_M \cdot \rho \cdot \frac{\pi \cdot D^2}{4} \cdot \frac{H}{2} \cdot \omega^2 \cdot \frac{\cosh[k \cdot (z + d)]}{\cosh[k \cdot d]} \cdot \sin(\omega \cdot t) \\
=& \frac{1}{8} \cdot C_M \cdot \rho \cdot \pi \cdot D^2 \cdot H \cdot \omega^2 \cdot \eta(z) \cdot \sin(\omega \cdot t)
\end{aligned}
\tag{65}
$$

The resulting forces in the direction of the wave $\Rightarrow Q_x\,(z, t)$ acting on the offshore structure are obtained by integrating the total wave forces $q_W(z, t)$ along the height z (water depth).

$$Q_x(z = z_0, t) = -\int_{z=0}^{z_0} [q_D(z, t) + q_M(z, t)] \cdot dz = -\int_{z=0}^{z_0} qw(z, t) \cdot dz \tag{66}$$

The bending moment around the y-axis $\Rightarrow M_y\,(z, t)$ is the product of the wave force per height multiplied with distance to the mudline (seabed).

$$M_y(\overline{z}_0, t) = -\int_{z=0}^{z_0} q_W(\overline{z}, t) \cdot \overline{z} \cdot dz \quad (\overline{z} = \text{mudline}) \tag{67}$$

For a vertical cylinder with constant values for D and C_D over z, the integral of Eq. 66 can be evaluated as follows:

$$Q_x(z = d, t) = -\int_{z=0}^{d} [q_D(z, t) + q_M(z, t)] \cdot dz$$

$$= -F_D(d, t) - F_M(d, t) \tag{68}$$

$$F_D(t) = \frac{1}{8} \cdot C_D \cdot \rho \cdot D \cdot H^2 \cdot \omega^2 \cdot d \cdot \frac{\sinh(2 \cdot k \cdot d) + 2 \cdot k \cdot d}{k \cdot d \cdot [\cosh(2 \cdot k \cdot d) - 1]} \cdot \cos^2(\omega \cdot t) \tag{69}$$

$$F_M(t) = \frac{1}{8} C_M \cdot \rho \cdot A \cdot H \cdot \omega^2 \cdot \frac{1}{k} \cdot \sin(\omega \cdot t) \tag{70}$$

The function of the bending moment according to Eq. 67 must be integrated numerically.

Example Loads on a monopile due to regular waves (according to MORISON equations).

Water depth $d = 25$ m; pile diameter $D = 5$ m; wave length $L = 75$ m; wave height $H = 4$ m; drag coefficient $C_D = 0.7$; mass coefficient $C_M = 2.0$; density of water $\rho = 1.025$ kg/m³; $\Rightarrow$ ratios $d/L = 0.3333 \Rightarrow$ transition range shallow/deep water $\Rightarrow k = \frac{2 \cdot \pi}{L} = 0,08377$ m⁻¹ $T = \sqrt{\frac{2 \cdot \pi \cdot L}{g \cdot \tanh(2 \cdot \pi \cdot d/L)}} = 7,037$ s; $\omega = \frac{2 \cdot \pi}{T} = 0,8929$ s⁻¹.

The coordinate z is measured from the mean sea water level.

Maximum velocity of water particles	$\dot{u}_{max}(z = 0) = 1,841$ m/s
Maximum acceleration of water particles	$\ddot{u}_{max}(z = 0) = 1,595$ m/s²
Drag force	$q_{D,max}(z = 0) = 6.078$ kN/m
Inertia force	$q_{M,max}(z = 0) = 66.161$ kN/m
Total drag force	$F_{D,max}(t = 0) = 39.68$ kN
Total inertia force	$F_{M,max}(t = T/4) = 766.14$ kN
Bending moment of the pile at the seabed	$M_{y,max}(z = d) = 42.430$ kNm

The bending moment at the seabed was determined with the assumption of a fixed-bottom. However, the actual bending moment along the pile is higher, since the effective embedded length of the pile in the seabed (weakness of the soil layers near the mudline).

The functions for the velocity and acceleration of the water particles as well as the wave loads along the pile shall be determined as a function of the depth ratio z/d.

The roughness k of the surfaces of structure has an influence on the wave forces and can vary on corrosion effects and marine growth. The roughness is given by the ratio k = grain size to structural diameter (new steel material: $k \approx 0.02$–0.1; concrete material: ≈ 0.5–1.0). The drag coefficient C_D increases with increasing roughness and the mass coefficient C_M decreases.

Superposition of waves and constant current

If a constant current is present in the same direction of wave propagation, the drag forces increase in the wave crest (quadratically with the velocity) and decrease correspondingly in the wave trough. The inertia forces remain unchanged due to a superposition with a constant current. However, it should be noted that waves and currents can have different directions.

Loads due to breaking waves

Breaking waves are non-linear events. Therefore, it is assumed that inertia forces are low compared to the drag forces. The water particles hit the offshore structure with high values of velocity.

The wave height of breaking waves is H_B (depending on the water depth). The horizontal velocity of the breaking wave corresponds approximately to the celerity of the wave in shallow water:

$$u_{\max^\circ} \approx \sqrt{g \cdot H_B} \tag{71}$$

The so-called slamming forces are determined as follows (Note. Equation 72 is not dimensionally neutral, i.e. the arguments must be used with the units given below):

$$F_S = C_5 \cdot \frac{1}{2} \cdot \rho \cdot D \cdot |\dot{u}_{\max}| \cdot \dot{u}_{\max} \cdot \lambda \cdot h_B \tag{72}$$

where F_S = slamming force [kN], C_S = slamming coefficient $\approx 2 \cdot \pi$ [−]; ρ = density of water [kg/m^3]; D = pile diameter [m]; λ = "curling" factor ≈ 0.5 [−]; h_B = maximum height of breaker above the still water level (about $0.7 \cdot H_B$) [m]; $u_{\max}^\circ$ = maximum horizontal velocity of the water particle [m/s].

3.4.7   Regular Sea State

Sea waves are primarily caused by the effect of wind along the water surface. When air particles pass over the initially calm water surface, the friction between air and water as well as air turbulence cause first small waves. In the initial phase, low and short waves are created, the so-called ripple waves. As the wind acts over a longer time period, these waves grow up and become faster.

The "regular" sea state is assumed to consist only of waves with similar lengths and heights.

If the wind blows with constant velocity and direction (fetch time) over a longer distance (fetch length), waves of almost the same length, height and direction dominate in deep water. This applies to larger wind forces with correspondingly long and high waves, e.g. in the North Atlantic, Arctic Ocean and Indian and Pacific Oceans south of the 40° of latitude. Regular sea states can be observed at relatively low wind velocities in North Sea and Baltic Sea.

3.4.8 Irregular or Natural Sea State

In addition to the waves caused by the wind in one direction can be overlaid with waves from other directions. Such superimposed waves are referred to as "natural sea state".

When describing a sea state, a distinction is made between:

- "long-crested" sea state: Only harmonic waves are superimposed with similar lengths and frequencies. They have all the same direction.
- "short-crested" sea state: Waves can have different directions, lengths and frequencies, i.e. a directional distribution is added. The frequencies generally have a GAUSS distribution, the wave heights a RALEYGH distribution.

The sea state can be described by a FOURIER integral. FOURIER integrals are analogous to FOURIER series developments, in which the frequencies are no longer integer multiples of a base frequency, but are continuously distributed (notice: the integral must be finite).

3.4.9 Spectra of Sea States

The distribution of parameters describing the natural or irregular sea state, such as wave heights, frequencies or lengths, can no longer be described by the wave theories mentioned above, but only by statistical methods.

A suitable method is:

GAUSS distribution or normal distribution: This is used, for example, to describe the wave frequencies of the natural sea state. The frequency distribution of the GAUSS distribution of a random process is (s = scatter):

$$f(x) = \frac{1}{s \cdot \sqrt{2 \cdot \pi}} \cdot \exp\left[-\frac{x^2}{2 \cdot s^2}\right] \tag{73}$$

The statistical distribution of probability results in:

$$F(x_0) = \int_{-\infty}^{x_0} f(x) \cdot \mathrm{d}x = \frac{1}{s \cdot \sqrt{2 \cdot \pi}} \cdot \int_{-\infty}^{x_0} \exp\left(-\frac{x^2}{2 \cdot s^2}\right) \cdot \mathrm{d}\xi \tag{74}$$

WEIBULL distribution: The WEIBULL distribution represents an extreme function, related to an expected minimum of a random process. It is used in particular for distribution of wind speeds. If the parameters are changed, it can be adapted to many different distributions. The equation of the WEIBULL distribution is:

$$f(x) \begin{cases} = \frac{m}{x_0} \cdot \left(\frac{x-x_u}{x_0}\right)^{m-1} \cdot \exp\left[-\left(\frac{x-x_\mu}{x_0}\right)^m\right] & \text{for } x \geq x_u \\ = 0 & \text{for } x < x_u \end{cases} \tag{75}$$

where x_0 = nominal value of the investigated parameter; x_u = lower value of the parameter; m = WEIBULL modulus (the larger the modulus, the "sharper" or the steeper the distribution of the probability). Thus, the distribution of probability can be written as follows:

$$F(x) = \int_0^x f(x) \cdot dx = \begin{cases} 1 - \exp\left[-\left(\frac{x-x_u}{x_0}\right)^m\right] & \text{for } x \geq x_u \\ 0 & \text{for } x < x_u \end{cases} \tag{76}$$

RAYLEIGH distribution: The RALEIGH distribution describes certain random processes, such as the distribution of wave heights of a natural sea state. It is a special case of the WEIBULL distribution with the WEIBULL module $m = 2$ and the lower limit $x_u = 0$.

The RAYLEIGH distribution is:

$$f(x) = \left\{ \frac{x \cdot \pi}{x_M \cdot 2} \cdot \exp\left[-\frac{\pi}{4} \cdot \left(\frac{x}{x_M}\right)^2\right] \quad \text{for } x \geq 0 \right. \tag{77}$$

with x_M = reference value (e.g. mean wave height or mean wind speed)

The distribution of probability results in:

$$F(x) = \left\{ 1 - \exp\left[-\frac{\pi}{4} \cdot \left(\frac{x}{x_M}\right)^2\right] \quad \text{for } x \geq 0 \right. \tag{78}$$

The moments from the distributions are obtained according to:

$$m_0 = \int_0^\infty f(x) \cdot dx; \quad m_n = \int_0^\infty x^n \cdot f(x) \cdot dx \tag{79}$$

with $f(x)$ = function of distribution; m_0 = moment of 0th order, the moments of higher order (n) are determined analogously) (Fig. 23).

The wave heights of an irregular sea state can be represented by the following FOURIER integral.
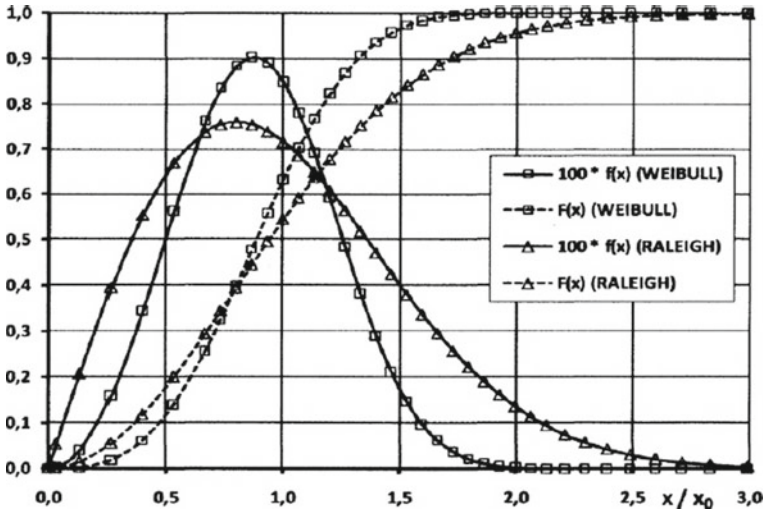
Fig. 23 Statistical distributions according to WEIBULL ($m = 3$) and RALEYGH

$$h^2(t) = \int_{\omega=0}^{\infty} S_h(\omega) \cdot d\omega < \infty \tag{80}$$

where $h(t)$ = surface elevation of water at time t; ω = frequency of sea state; $S_h(\omega)$ = spectra of the sea state.

If Eq. 80 is multiplied by the factor $\rho \cdot g/2$, the wave energy is estimated, which has the sea state.

A long-crested sea state is presented and it is assumed that all waves have the same direction. The sea state can be treated as a two-dimensional problem.

To describe a short-crested sea state, the spectra of the long-crested sea state must be multiplied by an additional term for the wave direction, to get a formula for a three-dimensional problem.

$$S_h(\omega, \mu) = S_h(\omega) \cdot G(\omega, \mu_e) \tag{81}$$

where $G(\omega, \mu)$ = function of wave propagation; μ = angle of the major direction with respect to a fixed coordinate system; μ_e = angle of each single wave depending on the major direction.

The distribution of wave directions can be described as:

$$\int_{\mu=-\pi/2}^{\pi/2} G(\omega, \mu_e) \cdot d\mu_e = 1 \tag{82}$$

Assuming that this distribution is independent of the direction of travel of the frequency, the following equation is often used:

$$G(\mu_e) = \begin{cases} k_n \cdot \cos^n(\mu_e) \text{ for } -\frac{\pi}{2} \leq \mu_e \leq +\frac{\pi}{2} \\ 0 \qquad\qquad\qquad \text{otherwise} \end{cases} \tag{83}$$

with the assumed values: $n = 2$ or $n = 4$

The consideration of the distribution for wave directions leads to lower stresses (number of load cycles and stress amplitudes) of foundations for OWT compared to uni-directional equations, since the maximum stresses occur at different locations around the structure. Thus, lower wall thicknesses for the piles are possible if the fatigue limit state is the design driver. The same effect can be considered for the distribution of the wind directions.

The general spectra of a sea state can be written according to **BRETSCHNEIDER**:

$$S_h(\omega) = \alpha \cdot \omega^{-5} \cdot \exp\left(-\beta \cdot \omega^{-4}\right) \left[\text{m}^2 \cdot \text{s}\right] \tag{84}$$

where $S_h(\omega) =$ spectral density of the sea state; $\omega =$ frequency of the sea state; $[\text{s}^{-1}]$; $\alpha =$ coefficient $[\text{m}^2/\text{s}^4]$; $\beta =$ coefficient $[\text{s}^{-4}]$.

The **PIERSON-MOSKOWITZ spectrum** (P-M spectrum) can be used for a dominant wind sea (so-called long-crested sea state with wind speed u).

$$S_h(\omega) = 0,0081 \cdot g^2 \cdot \omega^{-5} \cdot \exp\left[-0,74 \cdot \left(\frac{g}{u \cdot \omega}\right)^4\right] \tag{85}$$

with $\alpha = 0,0081 \cdot g^2$ and $\beta = 0,74 \cdot (g/u)^4$

The coefficients α and β determined by observations and measurements of sea states in the North Atlantic. These two-parameters modify the P-M spectra. The "modified" P-M spectra or **ISSC spectra** (ISSC = International Ship Structure Conference) is also often used. This spectrum can also be used for other sea states, i.e. fetch length is not sufficient to generate a dominant wind sea (example: storm conditions at the North Sea or Baltic Sea). Therefore, several values must be defined to characterize such a sea state.

These are: $H_{1/3} =$ mean height of waves higher than 2/3 of all waves (also called "significant" wave height H_S); T_0 (zero crossing period ($h(t) = 0$) or T_m (mean wave period) or T_P (period of maximum of spectra).

The $H_{1/3}$ and T parameters must be determined from statistics for sea states. The ISSC spectra is:

$$S_h(\omega) = 173 \cdot H_{1/3}^2 \cdot T_m^2 \cdot \omega^{-5} \cdot \exp\left[-692 \cdot \left(\frac{1}{T_m \cdot \omega}\right)^4\right]$$

$$= 124 \cdot H_{1/3}^2 \cdot T_0^2 \cdot \omega^{-5} \cdot \exp\left[-496 \cdot \left(\frac{1}{T_0 \cdot \omega}\right)^4\right] \tag{86}$$

The relations between the different periods are valid for the P-M spectra and ISSC spectra:

$$T_m = 0,7716 \cdot T_P = 1,0864 \cdot T_0 \tag{87}$$

If a wind speed of $u = 20$ m/s is assumed, the following can be derived from Fig. 13 for ω_P or T_P:

$$\Rightarrow \omega_p = 0,43\text{s}^{-1} \Rightarrow T_P = 2 \cdot \pi/\omega_p = 14,6\text{s};$$
$$T_0 = 0,7102 \cdot T_P = 10,4\text{s}; \quad T_m = 11,3\text{s}$$

The significant wave height $H_{1/3}$ is obtained from the value for m_0 according to the Eq. 62 by integration of the sea state spectra.

$$H_{1/3} \approx 4 \cdot \sqrt{m_0} = 4 \cdot \sqrt{\int_0^\infty S_h(\omega) \cdot d\omega} \tag{88}$$

It results for $u = 20$ m/s: $H_{1/3} = 9.89$ m.

However, these are only theoretical values, since a wind speed of 20 m/s $\approx$ 39 kn would require a fetch length of more than 4 000 km for a dominant wind sea.

If the fetch length is limited and the influence of the water depth is present (transition between deep and shallow water), the so-called **JONSWAP spectra** (Joint North Sea Wave Project) is used.

$$S_h(\omega) = \alpha \cdot g^2 \cdot \omega^{-5} \cdot \exp\left[-1,25 \cdot \left(\frac{\omega}{\omega_P}\right)^{-4}\right] \cdot \gamma^p \tag{89}$$

where α = "PHILLIPS" constant (cf. Eq. 91 as fixed value of 0.0081); γ = magnification factor with respect to the P-M spectra (between 1 and 7). The mean value γ = 3.3 is used for the standard JONSWAP spectra.

$$p = \exp\left[-\frac{(\omega - \omega_p)^2}{2 \cdot \sigma^2 \cdot \omega_p^2}\right] \tag{90}$$

$$\sigma = \begin{cases} \sigma_a \text{ for } \omega \leq \omega_p \text{ (value for spectra left of } \omega_P) \\ \sigma_b \text{ for } \omega > \omega_p \text{ (value for spectra right of } \omega_P) \end{cases}$$

$$\sigma_a = 0,07; \quad \sigma_b = 0,09 \text{ (common values)}$$

The parameters σ and ω_P are dependent on the effective fetch length x. It was determined with measurement that:

$$\alpha = 0,076 \cdot \overline{x}^{(-0,22)}; \quad \omega_P = 0,557 \cdot \frac{g}{\overline{u}_{10}m} \cdot \overline{x}^{(-0,33)} \tag{91}$$

$$\text{mit } \overline{x} = \frac{g}{\overline{u}_{10}} \cdot x^2; \quad \overline{u}_{10} = \text{wind speed at 10 m height} \tag{92}$$

With the values for $\alpha_{JONSWAP} = \alpha_{P-M} = 0.0081$ and $\omega_{PP-M} = \omega_{PJONSWAP}$ (see above for values), for comparison, the two spectra are shown in Fig. 24. The magnification factor of a JONSWAP spectra compared with a PIERSON-MOSKOWITZ spectra with the same values for α und ω_P is obtained for the ratio of the maxima of the two spectra:

$$\gamma^P = \frac{S_{h\,max}^{JONSAWP}}{S_{h\,max}^{P-M}} \approx 2,7 \tag{93}$$

The wave loads at an offshore structure result can be estimated with these spectra. If the natural frequencies of the structures is known, the structural response can be calculated taking into account the damping effects. Finally, the stresses can be calculated depending on the wave loads and accumulated for the fatigue assessment considering all load cycles (see HAPEL [6] or CLAUSS [8]).
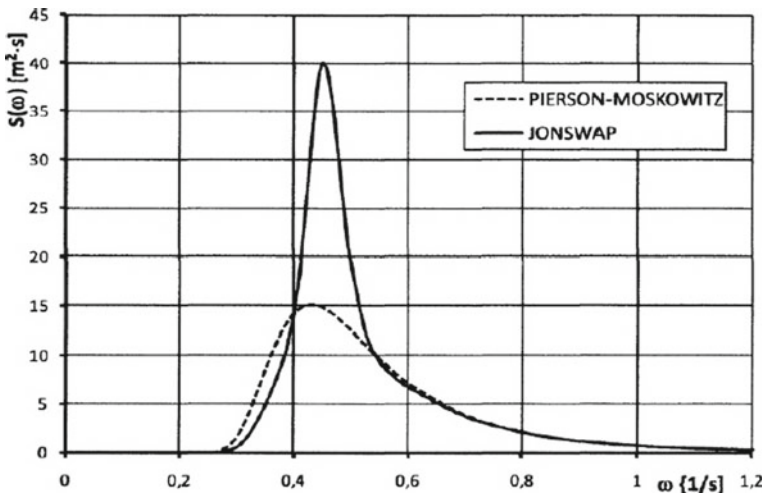
Fig. 24 PIERSON-MOSKOWITZ and JONSWAP spectra (wind speed = 20 m/s, α and ω_P equal)

3.5 Effects Due to Temperature

Load actions induced by a change in temperature are classified as variable and indirect actions. DIN EN 1991-1-5 [11] specifies the characteristic values for temperature actions that can be used for the design of structures subjected to daily and seasonal temperature changes. It shall be verified for all components structures to avoid failure caused by deformations induced by temperature changes. Concrete support structures must be distinguished as follows:

1. No consideration of deformations from one-sided solar radiation (combination coefficient $\psi_{0,T} \to 0$ if superposition with wind loads).
2. Temperature gradient in the tower shell due to different climatic conditions: $\Delta T = \pm 15$ K.

   This results in a thermal strain gradient: $\varepsilon_T = \pm\alpha_T\cdot\Delta T/2$.
   If no specific data are available, normal environmental conditions shall be assumed for OWT as follows:

- ambient temperatures between -20 and $+50\,°C$. The uniform temperature change shall be assumed to be: $\Delta T_N = \pm 35\,°C$ with respect to an average temperature of $+15\,°C$
- power production must be possible between -10 and $+40\,°C$ ambient temperature
- relative humidity up to 100%
- unpolluted sea atmosphere
- intensity of solar radiation 1 000 W/m^2
- air density 1.225 kg/m^3
- water density 1025 kg/m^3
- salinity of water 3.5%.

   The lowest seawater temperature may be assumed to be 0 °C. Special assumptions shall be made for sites with extreme temperature changes or ice conditions.

3.6 Effects Due to Ice

If the proposed location of an OWT may also have ice conditions, the following specifications and statistical data shall be used:

- dimensions, form, surfaces and stiffness of the structure
- size, form, thickness of the ice and it's drift
- type of ice and ice formation (ice floes, drift ice, ice ridges/walls)
- temperature and salinity of the ice
- angle of impact of the ice on the structure
- mechanical properties of the ice (compressive strength, flexural strength)
- velocity of ice loading.

For the design of offshore structures, the following ice forms must be distinguished: Closed ice cover, ice floes, pack ice fields, press ice ridges and icebergs. The different ice forms are created by environmental conditions such as wind, currents, waves and local site conditions.

Ice loads are to be assumed with the same direction of action as the wind loads, whereby either the high water or low water level with the required return period is considered. The combination with the more unfavourable effects or internal forces is decisive for the respective component.

The ice thickness is an essential parameter to be assumed on the basis of site-specific and statistical data. The strength values depend on ice temperature, salinity and air bubbles. The following values can be assumed for the compressive strength of ice at 0 °C:

North Sea	1.5 MPa (1 Megapascal $= 10^6$ N/m^2 $= 1$ N/mm^2)
Baltic Sea	1.8 MPa
Freshwater	2.5 MPa

The compressive strength increases by approx. 0.25 MPa per degree lower ice temperature. The ice behaves like a brittle material when it breaks. A design formula for the line load acting horizontally on the structure at the waterline (according to KHORZAVIN) is:

$$F_H = k_K \cdot k_F \cdot D \cdot h \cdot \sigma_0 \tag{94}$$

where F_H = horizontal force on the structure; k_K = contact coefficient (ice/structure); k_F = shape coefficient (shape of the structure); D = structure width; h = ice thickness; σ_0 = uniaxial ice compressive strength.

Example Ice loading on a vertical structure in the Baltic Sea with the following data: Ice temperature $T_{ice} = -10$ °C; $k_K = 0,33$; $k_F = 1, 0$; $D = 5,0$ m; $h = 0,5$ m $\rightarrow \sigma_0 \approx 2,0 + 10 \cdot 0,25 = 4,5$ MPa $\rightarrow F_H = 0,33 \cdot 1,0 \cdot 5,0 \cdot 0,5 \cdot 4,5 = 3,7$ MN.

A foundation in the Baltic Sea can be designed, for example, with an ice cone in order to be able to break the ice due to bending effects. The design of an ice cone can be optimized, if its slope will be chosen steep enough so that the ice load does not exceed the design wave load. In an "inverted" ice cone, the ice is forced under the waterline. The lower edge of such a cone should be below the water level (at design low water) by at least the dimension of the ice thickness. Further regulations for ice loads can be found, for example, in the DNV-GL guidelines.

3.7 Functional Loads

Functional loads can occur, for example, during installation or maintenance of an OWT. Typical load actions in these conditions can be:

- weight loads of equipment for installation or repair
- crane loads during lifting operations
- landing of a helicopter on the heli-deck
- mooring and fendering forces when ships are moored.

3.8 Accidental Loads

Accidental loads on an offshore structure may include:

- impact load
- explosion load
- earthquake load.

The action due to earthquakes shall be dynamically analysed as a load case combination with normal wind and sea state conditions. A calculation in the time domain or frequency domain is recommended according to EN 1998. A return period of 500 years shall be applied for the reference peak value of the horizontal ground acceleration, which can be taken from the national annexes of EN 1998 for the corresponding region or earthquake zone.

4   Design of Offshore Structures for Wind Energy

Support structures for wind turbines are mostly designed as slender structures with a heavy top mass. Thus, they are very prone to vibrations, whereby the most varied types of vibrations can be caused by the described actions. These actions are classified into constant, cyclic, stochastic, transient and structure-induced loads depending on time duration, cf. Table 6. The dynamic behaviour of the overall system consisting of turbine, tower and foundation has a significant influence on the structural loads. This influence mainly determines the design of the primary structural members.

4.1 Design Basis

The design rules for offshore wind turbines or offshore stations are summarized in the design basis and submitted to the relevant approval authority. All essential site conditions and project data are collected in the design basis. Thus, all parties of the project get the same in formations. The normative standards and guidelines as well as their hierarchy for the implementation planning of the offshore structure are to be clearly defined. It must be demonstrated which set of rules is to be applied for the respective verification. The hierarchy of normative standards for the fabrication and installation phase must be also defined for the project. Furthermore, the technical

specifications and requirements for the primary and secondary support structures of wind turbines and platforms shall be defined.

Basically, the planning of an offshore wind farm can be classified into the following phases:

- Pre-Design
- Basic Design
- Detail design

The operational life time should be at least 20 years for OWT and 30 years for offshore stations.

4.2   Site Conditions

The design of offshore structures must be based on the representative environmental conditions of the location. These include meteorological and oceanographic effects (so called metocean conditions) as well as the geotechnical details of the seabed. All site-specific and environmental conditions must be included in the design basis.

4.2.1   Meteorological and Oceanographic Conditions

The following meteorological and oceanographic conditions shall be provided as minimum:

- Water levels,
- Scatter plots of significant wave heights,
- Wind, wave and possibly ice parameters,
- Correlation of wind, wave and possibly ice,
- Ocean currents,
- Bathymetry,
- Seawater characteristics (density, salinity, temperature range, etc.),
- Scour-influencing conditions,
- Marine growth and
- Corrosion effects.

The metocean data can be collected from long-term statistics and must be supplemented during the early phase of the investigations for the location.

4.2.2   Geotechnical Investigation for the Seabed

The nature of the seabed with its different soil layers has a decisive influence on the structural integrity of the foundations. The soil must withstand the forces and moments from wind, waves, currents, etc. that act on the foundations. The bearing

behaviour of the soil layers play an essential role. Therefore, knowledge of the soil properties is necessary and must be explored with suitable measures/methods as part of the soil investigation.

The soil properties are collected in a random sampling manner at selected locations of a wind farm at least up to the planned penetration depth of the foundations, e.g. by drilling single bore holes and cone penetrations tests (CPT). The type and number of investigations depend on the size of the wind farm and the changes in soil properties within a wind farm. The procedure for site investigation and the number of samples required are specified for the German EEZ by the BSH in Standard No. 7004 [12].

Geotechnical and geophysical methods can also be used to determine soil properties.

The stratifications of the soil layers and their properties can be very different in the North Sea and the Baltic Sea. In general, a distinction is made between cohesive and non-cohesive soils. While both soil types can transfer relatively large compressive stresses and/or shear stresses, the transfer of tensile stresses in non-cohesive soil types is not possible in dry conditions and almost zero in the wet conditions (example: dry and wet sand). Cohesive soils can transfer small tensile stresses. The cohesion is described by the cohesion factor c'.

Cohesive soil types are loam, clay, silt, boulder clay, marl or peat. They generally have a plate-like structure and small grain sizes of approx. $0.001 \div 0.06$ mm. Their density in water ranges from 1 (peat) to 12 kN/m^3 (marl).

Non-cohesive soil types are sand and gravel with a roundish structure and grain sizes ranging from 0.06 mm (sand) to 65 mm (gravel). Densities in water range from 10 (gravel) to 11 kN/m^3 (dense sand), according to EAU [13]. Other soil types include rock and organic silt, as well as mixtures of the above soil types.

Depending on how compacted the soils are, a distinction is made between loose, medium-dense, dense and very dense soils. The pores between the grains are filled with water or air.

The following mechanical parameters of soils are necessary to determine the bearing capacity of a foundation (numerical values according to EAU [13]):

- Compressive strength σ
- Shear strength τ
- Internal friction angle φ' (similar to angle of repose): in water approx. 30°–40° for non-cohesive soils, approx. 15°–25° for cohesive soils.
- Cohesion factor c': approx. 0–8 kN/m^2 for non-cohesive soils, approx. 5–25 for cohesive soils.
- Secant modulus $_{ES}$: approx. 20–300 MN/m^2 for non-cohesive, approx. 0.5–100 for cohesive soils
- Permeability k: approx. 5×10^{-5} m/s for loose sand, approx. 10^{-3} for dense clay
- Permeability (water permeability) indicates how fast water flows through the soil type. Under dynamic loads, e.g. vibrations or passing waves, the water pressure in the soil changes over time. If the permeability is too low and does not adapt quickly to the surrounding static pressure, an overpressure or suction occurs (the so-called pore water pressure). The temporal change of the pore water pressure is

described by its gradient *p(t).* If this value exceeds the yield point of the soil, the shear strength becomes zero, i.e. the soil loses its bearing capacity completely, it "liquefies". This effect is not fully understood and is currently the subject of research projects.

- The investigations of soil properties are mostly done experimentally, e.g. by seismic methods or by laboratory tests on samples from the local boreholes. A proven method is the investigation with the "triaxial device". This allows the most important soil properties to be determined by varying the parameters (stresses in the three directions (triaxial), pore water pressure, wet or dry condition). More details on the laboratory tests and their evaluations can be found, for example, in SCHMIDT [14] (Fig. 25).

Permanent alternating load actions lead to a reduction of bearing capacity and stiffness of the soil. If a soil layer is overloaded, the soil deforms permanently. Procedures for determining the ultimate limit state of a soil type (plastic failure, fracture) can also be found in SCHMIDT [14].

The load actions of an offshore foundation must be transmitted into the soil layers. For example, the weight of the OWT causes vertical forces, the wind and wave loads cause horizontal forces. If these horizontal forces are multiplied with the distance to the seabed (mudline), bending moments also result. Due to the turbulence of the wind, the rotor blades have different load situations, so that torsional moments can occur in relation to the tower axis, which must be also transferred into the foundation and finally into the soil layers.

The sum of the forces and moments from the load actions must be in equilibrium with the resistances in of the soil layers to ensure the structural integrity of the foundation.

Different effects occur on the soil depending on the type of foundation, cf. Fig. 26:

- Monopile foundations: The bending moments and horizontal forces are in equilibrium with the passive earth pressure as resistance. The lateral bearing capacity of the pile is significantly determined by the soil parameters (*p-y curves* according to API). The vertical forces of an offshore structure are transferred by skin friction
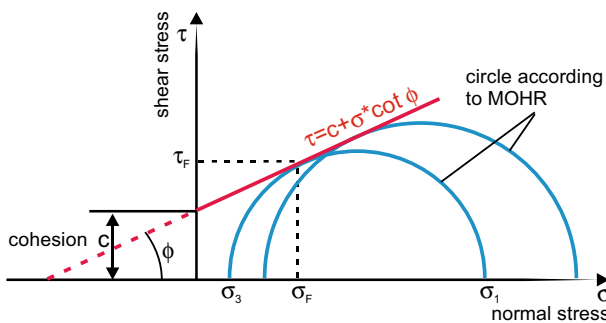
Fig. 25 Stress conditions in soil layers (MOHR-COULOMB boundary condition)
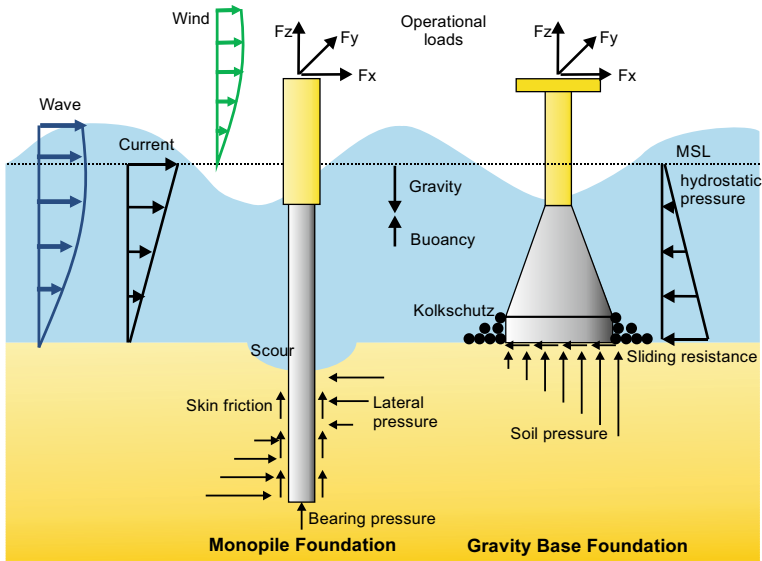
Fig. 26 Load transfer for monopile and gravity base foundations

along the pile shaft and bearing pressure at the pile tip (*t-z curves* according to API). The maximum bending moment in the pile is below the seabed due to elastic embedment and possible scour effects below the seabed.

- Tripod and jacket foundations: The moments and forces are transmitted with axial and lateral capacity of the single piles, whereby the bending moments can be substituted by a couple forces.
- Gravity base foundations: Vertical forces and bending moments are absorbed by soil pressures distributed over the footprint. Thereby, the bending stresses are captured by a linear increase of the soil pressures, which increase towards the leeward side. Torsional moments and horizontal forces are transmitted by frictional and sliding resistances at the bottom edge of the foundation.
- Suction buckets: The forces and moments are primarily absorbed by skin friction on the inside and outside of the bucket and bearing pressure at the tip. If the gap between the lid of the bucket and the seabed has been filled with grout (under base grouting), bottom pressures can also be activated as resistance for the bending moments.

The axial and lateral bearing capacity of the piles is modelled by multiple linear and/or nonlinear springs (see Fig. 27). The spring characteristics are described by stress-displacement or force-displacement curves of each soil layer depending on the depth. The so-called *p-y curves* are used for the lateral pile capacity, which describe the soil deformation in horizontal direction due to the acting compressive stresses (pressure) *p*. In contrast, the *t-z curves* describe the soil deformations in the vertical *z-direction* due to shear or tangential stresses *t*, which are used for the axial pile

Fig. 27 Spring-Damper model of a single pile foundation
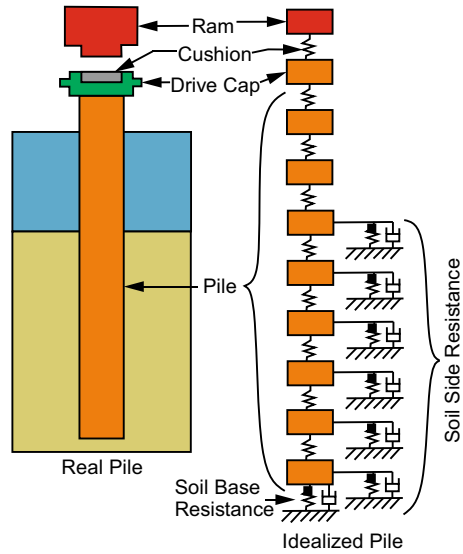
capacity. Tensile stresses or forces cannot be transmitted by the springs in order to represent the real soil bearing behaviour.

Each soil layer must be represented by the corresponding curves or spring characteristics. This allows the stresses and deformations of a pile to be calculated like a beam with linear (elastic) or nonlinear effects, e.g. using FE methods.

4.2.3 Scour Effects at the Seabed

Scours effects occur when single soil particles are loosened and eroded by turbulence effects of the current around a pile foundation. The velocity of the current will be increased and eddies will be generated if the water particles pass flow around the surface of the pile. As a result, scour occurs around the foundation as shown in Fig. 28. The reason for currents can be ocean, tidal, wind induced and wave currents. Depending on the nature of the seabed and the velocity of the current, scour can generate quickly in so-called non-cohesive soils, while the development of scour can take longer in cohesive soils.

Scour effects and suitable measurements for scour protection must be considered during the design phase of foundations for offshore structures. Scour effects can influence the load-bearing and operational behaviour of the OWT as follows:

- The stresses in the foundation become higher (the "cantilever beam" of foundation plus tower becomes longer).
- The load on the seabed increases (the embedded length of the foundation below the seabed become shorter, thus the forces to be transmitted into the soil layers increase).
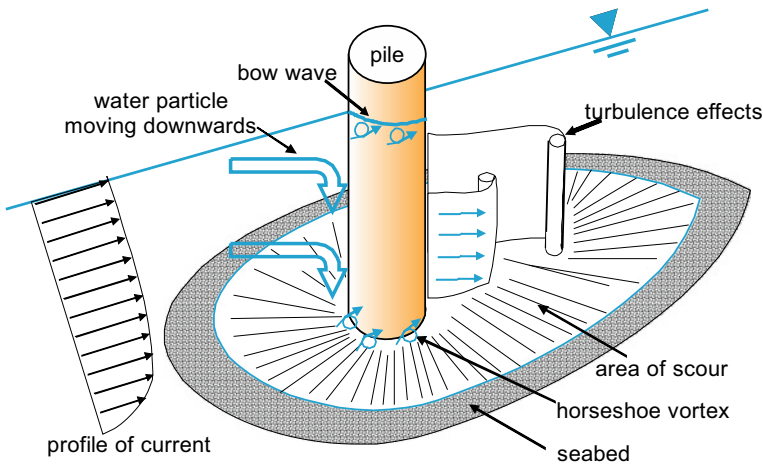
Fig. 28 Scour effects around a pile foundation at the seabed

- Natural frequencies of the overall system become smaller, thus also changing the operational conditions of OWT (possible shift into critical frequency ranges).
- These effects can reduce the fatigue life time of single components of the primary structure.
- The contact area can be reduced by scouring in the case of gravity base foundations, so that the stability of the system is reduced.

Therefore, it is necessary either to consider a maximum scour depth when dimensioning the foundations or to implement measurements for scour protection (e.g. several layers of different stone sizes, synthetic seagrass mats, etc.). Scour protection shall be provided either prior to installation of the foundation or afterwards. If scour protection measures are provided, they must also be checked and possibly improved during the operational life time of the wind farm.

In particular, the sea cables for power transmission must be protected in such a way that they are not exposed under any circumstances, as they are generally not designed for the resulting loads caused by waves and currents.

Some formulas are available for small pile diameters, e.g. for bridge piers, which are also partly experimentally verified. The above-mentioned scour effects are still in the scope of research projects for offshore wind turbines. The formulas developed so far provide very different results. According to these, scour depths of 0.3–$3 \cdot D$ are obtained [15]. The DNV-GL assumes a scour depth of $2{,}5 \cdot D$ with D for the pile diameter. Due to the wide scattering of the results, the empirical methods and equations must be validated for practical use.

4.2.4   Icing

Water freezes at 0 °C (fresh water) and at −1.8 °C with a salt content of approx. 3.5% (North Sea), depending on the salt content. With sustained frost, the salt content in the ice is reduced and the strength of the ice increases. The strength depends on the salinity, the ice temperature and the velocity of the icing process.

Ice that does not melt during the warm season is called multi-year ice, and ice that forms anew in winter is called first-year ice. The strength of multi-year ice is generally higher than that of one-year ice, as the salt content in the ice slowly decreases.

The risk of ice formation is low in the North Sea because of the influence of the Gulf Stream. In contrast, ice formation must generally be expected in the Baltic Sea.

For non-rotating components of an OWT, an all-round ice cover of 30 mm thickness shall be assumed with an ice density of 900 kg/m³. If spray water from the sea is added, a thicker ice cover shall be considered. If no specific data are available, an ice thickness of 100 mm shall be assumed.

For icing of rotor blades, a mass distribution can be assumed which increases linearly from zero at the hub to the value μ_E at half length of the blade and remains constant from there to the blade tip. More detailed information for μ_E can be found in [16].

4.2.5   Marine Growth

Structures that are in the water for a long time are colonized by numerous animals and plants. The vegetation influences not only the dynamic behaviour, but also the static behaviour of the structures. A distinction is made between:

1. "soft" marine growth such as algae, kelp, sea anemones, etc.: It causes an increase in flow resistance and wave forces by increasing the cross-sections and roughness. An increase in the static and hydrodynamic masses occurs only to a small extent, since the soft fouling only partially follows the movements of the structures. The density of the soft marine growth is approx. 1000 kg/m³.
2. "hard" marine growth such as mussels, barnacles, tubeworms, etc.: This marine growth increases the drag coefficient and the related forces on an offshore structure by increasing the cross-sections and roughness. In addition, the static masses and in the case of oscillatory processes, the hydrodynamic masses are increased, since the marine growth performs the same movements as the structures. The density of the hard marine growth is approx. 1300–1400 kg/m³.

The strength of the marine growth is influenced by the following effects:

- Water depth: The greater the water depth, the lower the rate of marine growth. At a water depth of 0–10 m the mass of marine growth can be approx. 250–300 kg/m², at a depth of >50 m up to approx. 20 kg/m².

Fig. 29 Marine growth

- Distance from the coast: the greater the distance to the shore, the development of marine growth is smaller and slower.
- Current velocity: The higher the current velocity, the more difficult it is for algae, barnacle or mussel larvae, etc. to attach to the structures.
- Temperature: Higher temperatures accelerate the marine growth.
- Water clarity: The clearer the water, the deeper the sunlight reaches and the more it encourages the growth of algae, etc., reaching greater depths.
- Nutrient content of the water: The higher the nutrient content of the water, the better the growth conditions for algae, mussels, etc. (Fig. 29).

4.2.6 Corrosion

Seawater is one of the most aggressive media, especially in combination with intensive solar radiation, high humidity and frequent dew point (condensation with salt concentrations). For this reason, special attention must be paid to adequate corrosion protection for offshore constructions over the service life time of approx. 20 years with limited accessibility. Defects will sooner or later affect the availability of the turbines and are often quickly visible on the external surfaces. The corrosive effect of the salty and humid air extends to the nacelles of the OWT.

Corrosion is the generic term for material changes in components. These can be material erosion (thickness reductions) or changes in material properties (chemical or metallurgical).

The main types of corrosion are:

- Oxidation: In steel, it leads to rust formation (transformation of iron into iron oxide with completely different material properties) and thus to a reduction in the load-bearing material thicknesses. In this process, oxygen access is required at the surface. In the case of aluminium, an oxide layer forms there which is impermeable to oxygen and thus protects the material. If this layer is destroyed, e.g. by mechanical stress, a new layer forms immediately. In seawater, this protective layer is generally not resistant.
- Galvanic or contact corrosion: If two electrically conductive materials with different electrical potentials (e.g. steel and aluminium) are wetted by an electrically conductive liquid such as seawater, material erosion occurs in the material

with the lower electrical potential, in this case aluminium. The greater the potential difference between the materials, the greater the galvanic corrosion.

- Other types of corrosion are: Pitting, crevice, stress corrosion cracking, vibration cracking and biochemically induced corrosion.

Welding can considerably reduce the corrosion resistance of otherwise corrosion-resistant steels in the area of the weld seam (increased tendency to stress corrosion cracking due to internal tensile stresses in the weld seam area, segregation of the alloy constituents).

The design rules of the certification bodies provide for corrosion allowances for components at risk. They are intended to ensure that a component still has sufficient material thickness or strength even after prolonged operation, during which "rusting", i.e. reductions in material thickness, cannot be avoided.

Depending on the corrosive stress (seawater) and maintenance, it can be assumed that in the case of steel components protected by paint coatings, a reduction in material thickness occurs due to a corrosion rate of approx. 0.1 mm per year, in the case of unprotected components approx. 0.3 mm, and in the alternating air/water zone (splash zone) up to approx. 0.5 mm per year.

There are numerous standards and guidelines for corrosion protection. The most important standards for offshore constructions are:

- DIN EN ISO 12944 "Corrosion protection of steel structures", 1998
- NORSOKM501 "Surface Preparation and Protective Coating", 1999.

There are different strategies for corrosion protection, which are to be differentiated on the one hand according to the locality (atmosphere, splash water, water change, underwater) and on the other hand according to material properties including the type of processing, such as:

- Coating only,
- Coating in combination with cathodic corrosion protection (CCP),
- External power systems and/or.
- Corrosion allowance, usually in combination with the above three processes.

The DIN EN ISO standard differentiates between several categories of corrosion stress, which can be taken from Table 7.

The atmospheric categories for onshore wind turbines are "C3 moderate" to "C5-M very strong" depending on the site conditions (offshore or nearshore with saline atmosphere). The components in the ground or in the water get the categories "Im1" to "Im3". The category "C5-M very strong" is provided for the atmospheric area and the categories "Im2" to "Im3" are provided for zones with permanent water pollution (splash zone).

The Norwegian NORSOK standard M-501 [17] has been prepared for offshore structures in the oil and gas industry. It describes the corrosion protection to be provided for such applications in detail and can also be used for OWT.

Table 7 Corrosion zones

Zone	Corrosive areas	According to DIN EN ISO 9223 and Din EN ISO 12944-2
4	Atmosphere (inside)	C4
3	Atmosphere (outside)	C5/CX
2	– Splash zone (SpWZ) – Water exchange zone (WWZ) – Low Water Exchange Zone (NWZ)	lm2/CX
1	Underwater zone (inside and outside)	lm2/lm4
	Seabed (inside and outside)	lm3/lm4

C5 currently corresponds to C5-M; lm4 = lm2 or lm3 each with KKS

4.3 Semi-Probabilistic Safety Concept

DIN EN 1990 [18] specifies principles and requirements for the structural integrity, serviceability and durability. It describes the basics of structural design, including the verifications, which must also be considered for offshore structures in addition to special standards and guidelines for such applications.

The structures shall be designed and constructed in such a way that during construction phase and during the service life time, it is possible with reasonable reliability and economy to

- withstand the possible impacts and influences and
- maintain the required performance characteristics.

In order to be able to demonstrate adequate reliability, a safety concept is required, which is defined in normative standards. A safety concept makes it possible to prove that these requirements are met and that the limit states of the structure will be not exceeded. Thus, the structure must be designed for the following requirements:

- Load bearing capacity
- Serviceability and
- Durability.

4.3.1 Partial Safety Factors

A scatter in material properties (resistance) or environmental conditions (load actions) must be covered by safety factors. Instead of a global safety factor, partial safety factors are used separately for the load actions (index F for Forces) and for the material resistances (index R for Resistance):

γ_F Partial safety factor for load actions.
γ_R Partial safety factor for material resistance.

4.3.2   Characteristic Values for Load Actions

The characteristic values (index k) for load actions are defined in DIN EN 1991 (Parts 1–9. The permanent load actions (G_k) have only a small deviation based on the mean value (μ). On the other hand, the characteristic value of a variable load action (Q_k) corresponds either to the upper value which must not be exceeded during a certain reference period with a given probability or to a nominal value of the statistical distribution for a load action. The 98% fractile value is often used for time-dependent variable action, which means that this value is not exceeded with a probability of 98% during the reference period of one year or is only once reached during 50 years (return period). Thus, the term 50-year wind or 50-year wave is also used for the structural design of offshore constructions. If the characteristic value is multiplied by the partial safety factor, the design value (index d) of a certain load action is obtained:

$$F_d = \gamma_F \cdot F_k \text{ or in general } E_d = \gamma_F \cdot E_k \tag{95}$$

If several load actions must be considered simultaneously, the variable load actions are multiplied by a combination factor ψ_i in order to capture the probability of occurrence of several actions at the same time. It is assumed that the maximum values of independent variable load actions, such as wind and wave, do not occur simultaneously. Thus, a dominant variable action is applied and the remaining variable actions are included in the load combination in a reduced form by multiplication with the combination factor. The following representative values are defined in the Eurocodes for this purpose:

Q_k	Characteristic value
$\psi_0 \cdot Q_k$	Combination value
$\psi_1 \cdot Q_k$	Frequent value
$\psi_2 \cdot Q_k$	Quasi-permanent value

The correlations between the representative values of a load action (F) as a function of time (t) are shown in Fig. 30.

4.3.3   Characteristic Values for Resistance of Materials

The properties of the materials are also defined by characteristic values (index k), often using the lower 5% fractile value of a statistical distribution (e.g. for the tensile strength of steel). Generally, this value is referred to as the material resistance R_k. If R_k is divided by the partial safety factor γ_R, the design value R_d for the material resistance is obtained:

$$R_d = \frac{R_k}{\gamma_R} \tag{96}$$
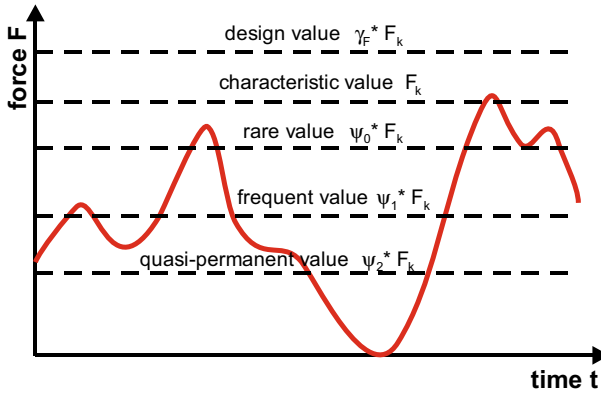
Fig. 30 Representative values and design values for variable load actions

The partial safety factors depend on the type of material and are specified in the respective Eurocodes for different limit states.

4.3.4 Design Methods

When designing a structure or its components, it must always be verified that the design value of the action E_d is less than or at most equal to the design value of the material resistance R_d

$$\gamma_F \cdot E_k = E_d \leq R_d = \frac{R_k}{\gamma_R} \tag{97}$$

The equation above is based on the semi-probabilistic safety concept, which was established using probabilistic methods according to the Eurocodes. The statistical distribution of load actions and material resistances is recorded via the partial safety factors in order to be able to ensure adequate reliability. However, this implies a certain probability of failure, which must be tolerated by society. Figure 31 shows an example for the probability of failure of a tension rod, if all characteristic values and safety factors are correctly considered. The tension rod has a statistical distribution for its material resistance R and is loaded by a tension force E, which has also a statistical distribution. The small area enclosed below the two distributions corresponds to the probability of failure P_f.

The accepted probability of failure for offshore wind turbines is $P_f = 10^{-4}$ per year according to the offshore guidelines of DNV-GL.
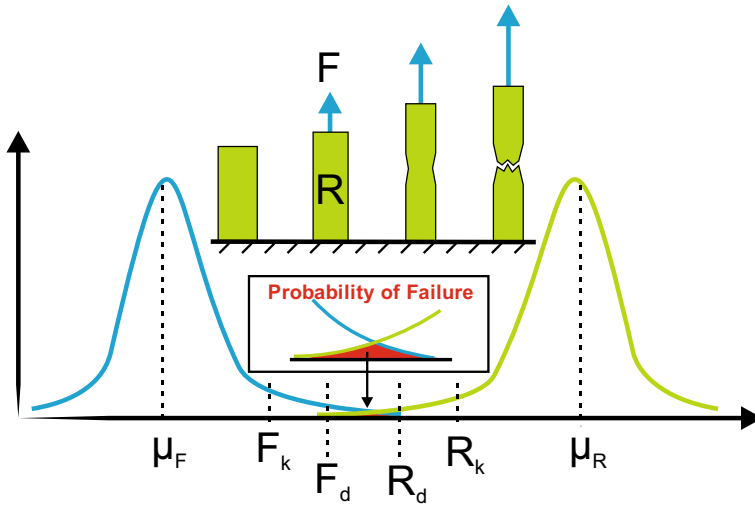
Fig. 31 Semi-probabilistic safety concept

4.4 Design Load Cases and Load Case Combinations

The actions are considered in DIN EN 61,400-3 [2] in various design load cases (DLC) and are divided into the following groups or conditions:

1. Power production
2. Power production and occurrence of a failure
3. Start
4. Normal shutdown
5. Emergency shutdown
6. Parking (standstill or idle)
7. Parking and fault condition
8. Transport, assembly, maintenance and repair.

Compared to the design of onshore wind turbines, additional effects, such as waves, ocean currents and ice must be considered for offshore wind turbines. Thus, more parameters must be included in the design load cases (DLC). As an example, the required calculation parameters for the first two load cases (DLC1.1 and 1.2) according to DIN EN 61400-3 are listed in Table 8.

The abbreviations in the Table 8 are described in DIN EN 61400-3. Based on the parameters, it becomes clear that complex calculations must be carried out for an OWT, whereby aero- and hydrodynamic effects must be considered simultaneously. Furthermore, control-related effects have to be considered during the analysis in the time domain. Therefore, special software tools have been developed for offshore wind energy. The requirements on these load simulations are explained in the following section.

Table 8 Extract for the design load cases of OWT according to DIN EN 61,400-3

Design condition	DLC	Wind	Waves	Orientation of wind and waves	Ocean currents	Water level	Type of analysis
(1) Power production	1.1	NTM vin < vhub < vout	NSS Hs = E[Hs Ivhub]	COD, UNI	NCM	MSL	U
	1.2	NTM vin < vhub < vout	NSS	COD, MUL	None	NWLR or $\geq$ MSL	F
	1.3	..	..	..	..	..	..

4.5   Analysis Methods for Structural Design

Special features must be considered for the analysis of an OWT compared to conventional constructions. Simulations in the time-domain are necessary to include effects like turbulence of wind or the orbital movements of water particles in waves. Figure 32 demonstrates the design procedure for offshore wind turbines.

In general, the forces and moments of each structural component are determined by a coupled load simulation including permanent and variable load actions. In addition to the inertial and gravitational loads, the aero- and hydrodynamic loads must be considered [2]. The procedure is comparable to the time-history analysis, which are nowadays carried out for simulations of slender large bridges. However, a simplified calculation may also be carried out if the natural frequencies of the supporting structure have a sufficient distance to frequencies of the turbine. A range of ±5% is specified as a sufficient distance.

The simplified method is sometimes used during the pre-design phase as well as for the intermediate steps of the iterative procedure. The advantage of the simplified method is the comparatively low computational effort, which is achieved by decoupling the main components of the overall system by defining an interface between the support structure and the turbine. Usually, the tower top (TT) or the tower bottom (TB) is chosen as an interface between the submodels.

4.6   Limit States of Structrual Design

The equilibrium, the serviceability and the durability must be verified for structures of an OWT. The verifications are based on the semi-probabilistic safety concept according to DIN EN 1990 [18] and include the limit states to be investigated for:

- the ultimate limit state (ULS)
- the fatigue limit state (FLS)
- the serviceability limit state (SLS)
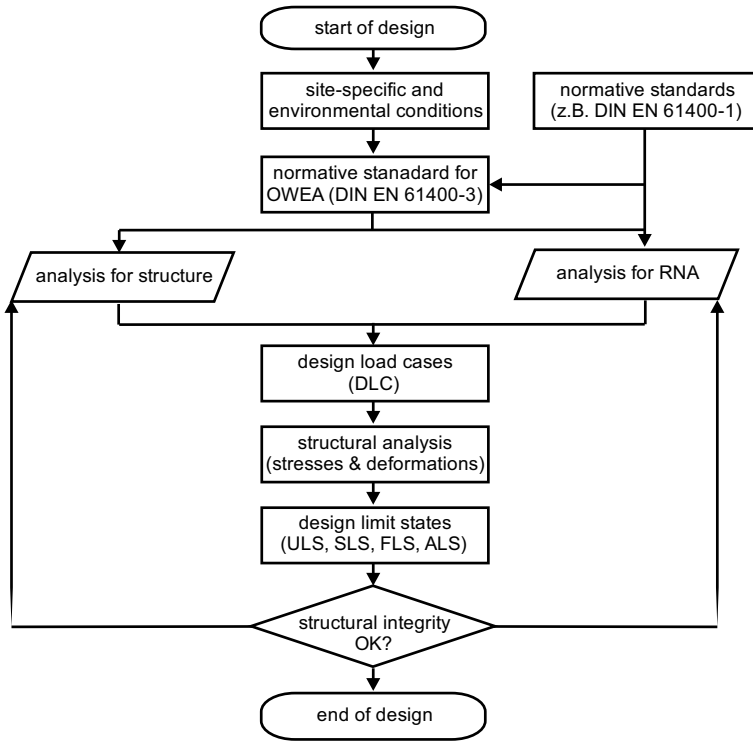
Fig. 32 Procedure for structural design of support structures for offshore wind turbines

- the accidental limit state (ALS).

Structural engineering must be performed not only for the operational condition (in-place analyses), but also for all relevant fabrication, transportation and installation phases.

4.6.1 Ultimate Limit State (ULS)

The required verifications in the ultimate limit state are mainly:

- Strength and stability verifications for each component, verifications for connections (STR)
- Equilibrium (EQU)
- Ground failure (GEO)
- Structural fire protection.

The relevant normative standards and guidelines for the design are to be used as a basis for the verification depending on the type of material and kind of structural component.

4.6.2 Fatigue Limit State (FLS)

As part of the structural design, fatigue analyses (FAT) must be carried out for the load-bearing components if these are to be classified as dynamically loaded components. Site-specific conditions and environmental conditions, such as use in the seawater, under free must be taken into account by suitable measures in the design of the offshore wind farms.

The fatigue assessment can be carried out at the level of:

- time series with stress cycles,
- stress ranges for each load level.
- damage-equivalent values.

in combination with suitable methods for accumulation of fatigue effects. Therefore, the stresses of a time series are classified in several stress ranges and collected in a set of n blocks. The fatigue life time is then computationally predicted by means of accumulation of the damage components from all single load cycles of each block.

The fatigue strength of the material especially for the notch details must be considered according to normative standards or literature [19]. Alternatively, to experimental investigations, the following methods are available for the fatigue assessment:

- Nominal stress concept
- Structural stress concept (hot spot concept)
- Notch stress concept
- Notch strain concept
- Crack propagation concept (fracture mechanics).

The International Institute of Welding (IIW) has defined the so-called detail categories (fatigue classes) for components made of steel or aluminium. The reference stresses are corrected by factors, e.g. for the type of welding process, thickness of the component or mean stress, etc.

There are several methods for the analysis of the fatigue life time, e.g. the linear damage accumulation according to PALMGREN-MINER [20, 21]. This method assumes that each closed hysteresis of a load cycle causes a partial damage in the notch of the material. The load cycle n_i on a certain level (index i) of a stress range $\Delta\sigma_i$ is determined as a partial damage, when the ratio n_i/N_i is calculated with the allowable load cycles N_i. Finally, all partial damage values are accumulated linear to the total damage D.

$$D = \frac{n_1}{N_1} + \ldots + \frac{n_j}{N_j} = \sum_{i=1}^{j} \frac{n_i}{N_i} \leq 1.0 \tag{98}$$

N_i is the number of allowable load cycles associated with the stress range $\Delta\sigma_i$ for the S-N-curve according to WÖHLER. Fatigue failure occurs if the sum of all partial damages n_i/N_i reaches the value $D = 1.0$.

4.6.3 Serviceability Limit State

The serviceability of an offshore structure is checked for the required functions of each component (fit for purpose). For example, the support structure of an offshore wind turbine must be checked for natural frequencies to avoid resonance effects during power production of the turbine. In principle, it must be verified that frequencies of the turbine and natural frequencies of the structure have a sufficient distance from each other. Therefore, the following criteria must be checked:

$$\frac{f_R}{f_{0,1}} \leq 0.95 \tag{99}$$

where f_R = max. rotational frequency of the rotor power production and $f_{0,1}$ = first natural frequency of the supporting structure and

$$\frac{f_{R,m}}{f_{0,n}} \leq 0.90 \text{ or } \geq 1.05 \tag{100}$$

with $f_{R,m}$ = blade frequency of the m rotor blades and $f_{0,n}$ = n-th natural frequency of the support structure

If the criteria cannot be fulfilled and power production shall keep unchanged the additional criteria must be checked for serviceability limit state:

- Limitation of deformations, velocities and accelerations,
- Limitation of the concrete compressive stresses, the concrete or prestressing steel stresses.
- Limitation of concrete crack widths.

4.6.4 Accidental Limit State

Earthquake is as an example of an accidental case, for which calculations must also be carried out if the OWT is located in an earthquake zone. Other accidental loads may include hurricanes and typhoons in other oceans of the world, which may also affect an OWT.

The objective of analyses for ALS shall be to ensure that

- human life is protected,
- damages remain limited and
- important structures for the protection of people remain functional.

4.6.5   Additional Load Cases

Additional load actions must be provided for the durability of offshore structures, including in particular corrosion protection. Furthermore, the stability of the foundation soil can be important, e.g. for temporary installation phases as the on-bottom stability analysis for unpiled jackets on the seabed. Based on this example it becomes clear that for an offshore structure not only the operational condition but also temporary transportation and installation condition can be critical. Therefore, appropriate design methods must be considered. However, variety of additional verifications and method statements during the transport and installation phase cannot be fully addressed in this chapter. Thus, reference is made to further literature, normative standards and guidelines for offshore wind energy.

Literatures

1. BSH: Standard No. 7005 (2021) Minimum requirements for the design of offshore structures in the exclusive economic zone (EEZ)
2. DIN EN 61400-3 (2010) Wind turbines—Part 3: design requirements for offshore wind turbines (IEC 61400-3:2009), Beuth-Verlag
3. BSH: Standard No. 7003 (2013) Investigation of the impact of offshore wind turbines on the marine environment (StUK 4)
4. EBNER (1967) Strength problems of submarines. Schiffstechnik 14(74)
5. DIN EN 1991-1-4 (2010) Actions on structures—Part 1–4: general actions—Wind loads, Eurocode 1, Beuth Verlag
6. Hapel K-H (1990) Strength analysis of dynamically stressed offshore structures. Vieweg Verlag, Stuttgart
7. Eck B (1966) Technische Strömungslehre. Springer, Berlin
8. Clauss G et al (1988) Meerestechnische Konstruktionen. Springer, Berlin
9. Gerstner FJ (1809) Theory of waves. Annalen der Physik
10. Morison et al (1950) The force exerted by surface waves on piles. Trans AIME 189
11. DIN EN 1991-1-5 (2004) Actions on structures—Part 1–5: general actions—Temperature actions, Eurocode 1, Beuth Verlag
12. BSH: Standard No. 7004 (2014) Subsoil investigation for offshore wind farms
13. EAU (2004) Recommendations of the working group on shore edging. Ernst & Sohn, Berlin
14. Schmidt H-H (2006) Grundlagen der Geotechnik. Teubner Verlag, Wiesbaden
15. Richwien W, Lesny K (2004) Can scour at offshore wind turbines be calculated, BAW-Workshop Boden-und Sohl-Stabilität
16. DNV-GL (2014) Design of offshore wind turbine structures (DNV OS-J101), Oslo
17. NORSOK (2004) Standard M-501, surface preparation and protective coating
18. DIN EN 1990 (2002) Fundamentals of structural design, Eurocode 0, Beuth Verlag
19. Haibach E (2006) Structural durability—Methods and data for component calculation. VDI Verlag, Düsseldorf

20. Palmgren A (1924) The service life of ball bearings. Verein Deutscher Ingenieure 68:339–347
21. Miner MA (1945) Cumulative damage in fatigue. J Appl Mech 12:159–164

Prof. Dr.-Ing. Christian Keindorf studied civil engineering at the Technical University of Braunschweig and did his doctorate on tower constructions for wind turbines at Leibniz University Hanover in 2009. Since 2009, he has been a founding partner of SKI Ingenieurges. mbH, which specialises in, among other things, with support structures for renewable energy systems. At the beginning of 2015, he accepted the professorship for offshore plant engineering at Kiel University of Applied Sciences and is and works there at the Institute for Shipbuilding and Maritime Technology. In 2015, he was also by the Lower Saxony Chamber of Engineers as an expert for support structures of onshore and offshore wind turbines.

Index